Se Won Suh
Room 839

AsCA'09 Beijing

Joint Conference of the Asian Crystallographic Association and Chinese Crystallographic Society

Program Book

October 22-25, 2009 • Beijing, China

AsCA'09 Beijing

Joint Conference of the Asian Crystallographic Association and Chinese Crystallographic Society

Program Book

October 22-25, 2009 • Beijing, China

Dear Colleagues,

You are cordially invited to Beijing for the Joint Conference of the Asian Crystallographic Association and Chinese Crystallographic Society, AsCA'09, from October 22-25 2009.

This conference is devoted to crystallography in Asia. The meeting aims to cover all aspects of crystallography, ranging from inorganic and organic small molecules to macromolecular proteins, viruses, and membrane proteins; from crystal growth to protein engineering; from structural chemistry and material science to nanoscience and nanotechnology; from crystal structure, proteomics, and genomics, to drug design; from diffraction physics and ray optics to the applications of electron, neutron, and synchrotron X-ray photons for structural investigations, and so on.

Beijing, the host city of the 2008 Olympic Games, is the political, educational and cultural capital of China. It offers an exciting and stimulating blend of rich cultural heritage and thoroughly modern facilities. The city is home to many beautiful historic sites, including the Great Wall, the Forbidden City, the Temple of Heaven, and the Summer Palace.

The AsCA'09 meeting will be held in Jingyi Hotel, an elegant conference facility opened prior to the 2008 Olympic Games. Boasting excellent meeting, recreation and health facilities, Jingyi Hotel is located 6 km from downtown Beijing and 40 km from Beijing International Airport. It is within easy reach of many cultural sights, either via taxi or by subway from two nearby subway stations.

We look forward to welcoming you to Beijing in 2009. With your participation, we have every confidence that AsCA'09 will be a successful meeting, both scientifically and socially.

Zihe Rao
Chairman, AsCA'09
President of Nankai University

Jianhua Lin
Chairman, AsCA'09
Vice President of Peking University

International Program Committee

Chairman: Peter Colman (Australia)

Jacqui Gulbis (Australia)	Pinak Chakrabarti (India)	Shigeyuki Yokoyama (Japan)
Altaf Hussain (Bangladesh)	Ashwini Nangia (India)	Junje Cho (Korea)
Jianhua Lin (China)	Seiki Kuramitsu (Japan)	Se Won Suh (Korea)
Zihe Rao (China)	Kunio Miki (Japan)	Peter Metcalfe (New Zealand)
Ian Williams (HK, China)	Masaki Takata (Japan)	Haiwei Song (Singapore)
Chwan-Deng Hsiao (Chinese Taipei)		

Local Organizing Committee

Chairman: Zihe Rao (Nankai University), Jianhua Lin (Peking University)

Zhi-Jie Liu (Executive, IBP/CAS)	Shixiong Liu (Fuzhou U)	Jiyang Wang (Shandong U)
Xiaodong Su (Executive, Peking U)	Yang Lv (IMM/CAMS)	Mu Wang (Nanjing U)
Jijie Chai (NIBS)	Zhenhong Mai (IOP/CAS)	Zheming Wang (Peking U)
Xiaolong Chen (IOP/CAS)	Liwen Niu (USTC)	Yicheng Wu (TIPC/CAS)
Xiaoming Chen (SYS U)	Feng Pan (Tsinghua U)	Ruiming Xu (IBP/CAS)
Jiangping Ding (SIBS/CAS)	Lianmao Peng (Peking U)	Ze Zhang (BUT)
Weimin Gong (IBP/CAS)	Yigong Shi (Tsinghua U)	Weitao Zheng (Jilin U)
Luhua Lai (Peking U)	Dacheng Wang (IBP/CAS)	

International Advisory Committee

Honorary Chairman: Hikaru Shimura (President & CEO of Rigaku)

Dong-Cai Liang	Institute of Biophysics, CAS
Haifu Fan	Institute of Physics, CAS
Bi-Cheng Wang	University of Georgia, USA
Mitchell Guss	President of AsCA
Jules Hendrix	President & CEO of Marresearch GmbH

Secretariat (China)

Secretary-general: Mark Bartlam

Deputy Secretary-general: Shunyi Wei, Xiaoke Xia, Neil Shaw

Secretariat: Ke Chen, Yue Wang, Wenli Xu, Chongyun Cheng, Ping Shan, Weihong Zhou

Scientific Program

	Thursday, October 22	Friday, October 23	Saturday, October 24	Sunday, October 25
09:00	Registration 09:00-21:00 Workshop 1 09:00 - Meeting Room 1	**Plenary Lecture** Hongkun Park Grand Ball Room	**Keynote-1** by Joel Sussman Meeting Room 1 **Keynote-2** by Matthew Rosseinsky Meeting Room 6	**Keynote-3** by David Owen Meeting Room 1 **Keynote-4** by Thomas Mak Meeting Room 6
09:50		Conference photo	Tea Break	Tea Break
10:00	Workshop 1 - 12:00 Meeting Room 1	**MS-1**: Structural Biology in disease Grand Ball Room **MS-2**: Inorganic and nano-materials Meeting Room 1 **MS-3**: Neutron and synchrotron sources and applications Meeting room 6	**MS-7**: Membrane proteins Meeting room 1 **MS-8**: Organic crystal engineering and structure Meeting room 6 **MS-9**: Small angle scattering and soft materials crystallography Meeting room 7	**MS-13**: Hot structures Meeting room 1 **MS-14**:Superconductivity and crystal properties Meeting room 6 **MS-15**: Electron microscopy and diffraction Meeting room 7
12:00		Rigaku Lunchon Seminar	Lunch, AsCA Council Meeting	Lunch, CCrS Council Meeting
13:30	Workshop 2 13:30-17:00 Meeting Room 1 Workshop 3 13:30-17:00 Meeting Room 6	**Poster Session** (Odd Number)	**Poster Session** (Even Number)	**Rising Stars Symposium** Grand ball room
15:45				
16:00		**MS-4**: Macromolecular assemblies Meeting room 1 **MS-5**: Charge density studies Meeting room 6 **MS-6**: Advanced X-ray/neutron/ electron imaging techniques Meeting room 7	**MS-10**: New tools for macromolecular crystallography Meeting room 1 **MS-11**: Metal-organic crystal engineering Meeting room 6 **MS-12**: Powder diffraction Meeting room7	**Plenary Lecture** by Yoshinori Fujiyoshi Grand ball room
18:00	Opening Ceremony and **IUCr Plenary** Ted Baker			6:30 Rigaku
19:00	Welcome Reception	dinner ticket	Conference Banquet	dinner reception (~100 people only)

Thursday, October 22

09:00-12:00 **Meeting Room 1 (2nd floor)**

Workshop 1: *Macromolecular crystallization, data collection and data processing techniques*

13:30-17:00 **Meeting Room 1 (2nd floor)**

Workshop 2: *Direct-method SAD phasing and dual-space model completion*

13:30-17:00 **Meeting Room 6 (2nd floor)**

Workshop 3: *Publication of Small Molecule Structures in IUCr Journals*

18:00-19:00 ***Opening and Welcome*** *– IUCr Plenary* (Grand Ball Room, 2nd floor)

Celebrating Crystallography
Ted Baker
Chair: Jianhua Lin

Friday, October 23

09:00-09:50 **Grand Ball Room**
Plenary 1
Vertical Nanowire Arrays: a Universal Platform for Interfacing with Living Cells
Hongkun Park
Chair: Jing-Tai Zhao

09:50-10:10 **Conference Photo**

October 23, 10:00-12:00 (Grand Ball Room)

MS-1 Structural Biology in disease

Chairs: Michael Parker, Xiao-Dong Su

10:00-10:25 **Arms race between host and pathogen**
Jijie Chai

10:25-10:50 **Structural studies of the Glutathione Transferases and their involvement in resistance to chemotherapy treatment.**
Lorien J Parker, Paul J Dyson, Mario Lo Bello, Michael W Parker

10:50-11:15 **Structural Study of PA subunit from an Avian Influenza Virus RNA polymerase**
Yingfang Liu

11:15-11:40 **Ligand recognition by the TLR4-MD-2 complex**
Jie-Oh Lee

11:40-12:00 **Scaffold-based discovery of a novel selective inhibitor of oncogenic B-Raf kinase with potent anti-melanoma activity**
Kam YJ Zhang

October 23, 10:00-12:00 (Meeting Room 1, 2nd floor)

MS-2 Inorganic and nano-materials

Chairs: Ian Williams, Stephen S-Y Chui

10:00-10:30 **Metal Organic Frameworks for Proton Conduction and CO2 Uptake**
Jeff Hurd, Ramanathan Vaidhyanathan, Jared Taylor, Simon Iremonger, Karl Dawson, George Shimizu

10:30-11:00 **Homoleptic Metal Organothiolate and –selenolate Coordination Polymers $[M(SR)_n]_\infty$ (n = 1–3): Structural Determination using Powder X-ray Diffraction and Their Materials Properties**
Stephen Sin-Yin Chui, Kam-Hung Low, Roy VAL, Chi-Ming Che

11:00-11:20 **Ionothermal Synthesis of Metal Organic Framework Materials**
Zhuojia Lin, Linna Huang, Ming-Liang Tong, Russell E Morris

11:20-11:40 **To bridge or not to bridge – carbonyl ligand configurations in some phosphine and arsine substituted tricobalt carbon cluster systems**
Jim Simpson, C John McAdam, Brian H Robinson, Roderick G Stanley

11:40-12:00 **Crystal Engineering of Chiral Metal Organic Frameworks (MOFs) from Tartrates and N-Donor Spacer Ligands**
Pokka K-C Pang, Herman H-Y Sung, Ian D Williams

October 23, 10:00-12:00 (Meeting Room 6, 2nd floor)

MS-3 Neutron and synchrotron sources and applications

Chairs: Richard Garrett, Hongjie Xu

10:00-10:20 **Current status and future development of neutron scattering at China Advance Research Reactor**
Dongfeng Chen, Yuntao Liu, Hongli Wang, Kai Sun, Meimei Wu

10:20-10:40 **Current Status of Shanghai Synchrotron Radiation Facility**
Jianhua He, Zhentang Zhao, Hongjie Xu

10:40-11:00 **Crystallography and Materials Science at the J-PARC pulsed spallation neutron facility**
Takashi Kamiyama

11:00-11:20 **The Current Status of Taiwan Photon Source**
Yu Wang, Mau-Tsu Tang, Gwo-Huei Luo, Yaw-Wen Yang, Keng S Liang

11:20-11:40 **Cold Neutron Research Facility at HANARO**
Kye Hong Lee, Young Ki Kim

11:40-12:00 **New Facilities for Australian Research: The Australian Synchrotron and the OPAL Research Reactor**
Richard F Garrett

October 23, 12:00-13:30 Rigaku Lunchon Seminar (Grand ball room)

October 23, 14:00-16:00

14:00-16:00 **Poster Session 1** (Poster room and corridor on the 2nd floor)

October 23, 16:00-18:30 (Meeting room 1)

MS-4 Macromolecular assemblies (viruses, proteins, protein-nucleic acid complexes)

Chairs: Peter Metcalf, Tomitake Tsukihara

16:00-16:30 **Structure of the bacterial flagellum and the mechanism of its self-assembly**
Katsumi Imada

16:30-17:00 **Understanding cytokine receptor signaling**
Guide Hansen, Tim R Hercus, Jack Kng Scott, Angel F Lopez, Michael W Parker

17:00-17:30 **Effector recognition of Rab and Arf family small G proteins in vesicle transport and membrane remodelling**
Soichi Wakatsuki

17:30-17:50 **Structural Basis of Transcription: Backtracked RNA Polymerase II**
Dong Wang, Roger D Kornberg

17:50-18:10 **Structure of RNA-guided RNA Modification Enzymes**
Keqiong Ye, Ling Li, Jingqi Duan, Ru Jia, Jinzhong Lin, Minghua Ju, Jin Peng, Anbi Xu, Liman Zhang

18:10-18:30 **RNA-protein interactions in the core domain of spliceosomal U4 snRNP**
Adelaine K W Leung, Jade Li, Kiyoshi Nagai

October 23, 16:00-18:30 (Meeting Room 6)

MS-5 Charge density studies

Chairs: Masaki Takata, Yu Wang

16:00-16:30 **Recent Progress in X-ray Charge Density Studies of Advanced Materials**
Bo B Iversen

16:30-16:55 **Non-linear Optical Properties and Spin Densities from X-ray Charge Density Measurements**
Dylan Jayatilaka

16:55-17:20 **Exploring Halogen -Halogen interactions via charge density analysis**
Guru Row

17:20-17:45 **Challenge to Atomic Orbital Visualization by 0.2A Resolution Synchrotron Radiation Single Crystal Experiment**
Hiroshi Sawa, Eiji Nishibori, Shinobu Aoyagi

17:45-18:10 **MEM Electrostatic Potential Imaging**
Hiroshi Tanaka

18:10-18:30 **Photo-induced Structure Determination and Electron Density Study by MEM of Spin Crossover Complex [Fe(abpt)2(NCS)2]**
Che Hsiu Shih, Chou Fu Sheu, Kunihisa Sugimoto, Jungeun Kim, Kenichi Kato, Yu Wang, Masaki Takata

October 23, 16:00-18:30 (Meeting Room 7, 2nd floor)

MS-6 Advanced X-ray/neutron/electron imaging techniques

Chairs: Steve Wilkins, Mau-Tsu Tang

16:00-16:30 **Recent Developments in Coherent Diffractive Imaging Instrumentation and Applications**
Andrew G Peele

16:30-17:00 **Visualization of Bio-Structures Using Coherent X-Ray Diffraction**
Yoshinori Nishino, Kazuhiro Maeshima, Naoko Imamoto, Ryuta Hirohata, Eiichiro Matsubara, Yukio Takahashi, Tetsuya Ishikawa

17:00-17:30 **Phase imaging using a liquid cell in a transmission x-ray microscope**
Gung-Chian Yin

17:30-17:50 **Improved Accuracy Laue Neutron Diffraction**
Ross Piltz, Alison Edwards

17:50-18:10 **Development and Application of Neutron 2D-Counter for Crystal and Magnetic Structure Analysis**
Y Noda, C-H Lee, M-K Moon, S-A Kim, Y Ishikawa, H Kimura, R Kiyanagi

18:10-18:30 **State-of-the-art Multilayer Optics for Modern X-ray Analysis**
J Wiesmann, T Samtleben, C Michaelsen, B Hasse, J Graf, F Hertlein

Saturday, October 24

09:00-09:50 **Meeting Room 1**
Keynote 1
Proteopedia - a Scientific 'Wiki' Bridging the Rift Between 3D Structure and Function of Biomacromolecules
Joel Sussman
Chair : Jenny Martin

09:00-09:50 **Meeting Room 6**

Keynote 2
Reactivity and flexibility in metal-organic frameworks: amino-acid based and post-synthetically functionalised materials

Matthew Rosseinsky
Chair: Gautam Desiraju

October 24, 10:00-12:00 (Meeting Room 1)

MS-7 Membrane proteins

Chairs: Jacqui Gulbis, Kenji Inaba

10:00-10:25 **Structure and mechanism of an amino acid antiporter**
Yigong Shi

10:25-10:50 **The structure of human connexin 26 gap junction channel**
Shoji Maeda, So Nakagawa, Michihiro Suga, Eiki Yamashita, Atsunori Oshima, Yoshinori Fujiyoshi, Tomitake Tsukihara

10:50-11:15 **The role of AmtB-GlnK complex in nitrogen regulation**
Xiao-Dan Li, Fritz Winkler, Mike Merrick

11:15-11:40 **Structure and function of A-ATPase: combining electron microscopy and X-ray crystallography to study a transmembrane rotary motor complex**
Lawrence K Lee, Alastair G Stewart, Mhairi Donohoe, Olga Esteban, Ricardo A Bernal, Daniela Stock

11:40-12:00 **Crystal Structure of Bacterial Nitric Oxide Reductase, a Key Enzyme in the Respiratory Evolution**
Yushi Matsumoto, Shingo Nagano, Yoshitsugu Shiro

took only 1 year B. Stearothermophilus

October 24, 10:00-12:00 (Meeting Room 6)

MS-8 Organic crystal engineering and structure

Chairs: VR Pedireddi, Suresh Valiyaveettil

10:00-10:10 Introduction by Chairs

10:10-10:35 **Engineering Organic Crystals using Arene-Perfluoroarene Interactions**
Todd B Marder

10:35-11:00 **Proton Dynamics in Hydrogen-bonded Organic Solids - from Protonic Dielectrics to Proton-motor**
Tadashi Sugawara, Kentaro Suzuki

11:00-11:20 **Structure-property correlations: mechanical properties of molecular crystals**
C Malla Reddy, Michael T Kirchner, K Anantha Padmanabhan, Gautam R Desiraju

11:20-11:40 **Polymorph and pseudo-polymorph of co-crystal; controlling formation and structural transition**
Miao Du, Xiu-Juan Jiang, Min Tang

11:40-12:00 **Towards knowledge-based design and control of pharmaceutical crystal forms**

Colin R Groom, Peter T A Galek, Peter A Wood

October 24, 10:00-12:00 (Meeting Room 7)

MS-9 Small angle scattering and soft materials crystallography

Chairs: Naoto Yagi, Monnhor Ree

10:00-10:30 **A small/wide-angle X-ray scattering instrument for structural characterizations with soft matter, nanomaterials, and air-liquid interfaces**
U-Ser Jeng, Chiu Hun Su, Chun-Jen Su, Kuei-Fen Liao, Wei-Tsung Chuang, Ying-Huang Lai, Je-Wei Chang, Yi-Jiun Chen, Yu-Shan Huang, Ming-Tao Lee, Kuan-Li Yu, Din-Goa Liu, Zia-Fung Chang, Chin-Yen Liu, Chien-Hung Chang, Keng S Liang

10:30-11:00 **Surface and flow ordering of complex fluids**
WA Hamilton, L Porcar, PD Butler, GG Warr

11:00-11:30 **Intimate Relationship between Micro-phase Separation and Crystalline Phase Transitions in Polyethylene- Poly(ethylene Oxide) Diblock Copolymer as Viewed by Synchrotron SAXS/WAXD and IR/Raman Measurements**
Kohji Tashiro, Weiyu Cao, Makoto Hanesaka, Hiroyasu Masunaga, Sono Sasaki, Masaki Takata

11:30-11:45 **The Quokka Small Angle Neutron Scattering Instrument at OPAL**
Richard F Garrett, Elliot P Gilbert, William A Hamilton, Kathleen Wood

11:45-12:00 **The effect of interface on the crystallization behavior of poly(3-hydroxybutyrate) ultra-thin film revealed by grazing incident X-ray dffraction**
Xiaoli Sun, Harumi, Sato, Yukihiro Ozaki, Shouke Yan, Isao Takahashi

October 24, 12:00-13:30 AsCA Council Meeting (Meeting room 3)

October 24, 14:00-16:00

14:00-16:00 **Poster Session 2 (Poster room and corridor on the 2nd floor)**

October 24 16:00-18:30 (Meeting Room 1)

MS-10 New tools for macromolecular crystallography (including structural genomics)

Chairs: Kunio Miki, Joel Sussman

16:00-16:25 **Tracking ligand migration pathways in carbonmonoxy myoglobin at cryogenic temperatures**
Shin-ichi Adachi

16:25-16:50 **Exploring the conformational energy landscape of acetylcholinesterase by kinetic crystallography**

Jacques-Philippe Colletier, Benoît Sanson, Didier Fournier, Joel L Sussman, Israel Silman, Dominique Bourgeois, Martin Weik

16:50-17:10 **Structure of HIV-1 Protease in Complex with Inhibitor KNI-272 Determined by Neutron Crystallography**
Motoyasu Adachi, Ryota Kuroki

17:10-17:30 **Taking the edge off: The softer side of in-house SAD phasing**
Joseph D. Ferrara, James W. Pflugrath, Cheng Yang

17:30-17:50 **Reductive methylation of surface lysines assists crystallization of proteins**
Neil Shaw, Chongyun Cheng, Zhi-Jie Liu

17:50-18:10 **Improvement of a new rotation function for molecular replacement by designing new scoring functions such as relative entropy and dynamic correlation coefficient**
Fan Jiang, Wei Ding

18:10-18:30 **New and Underused Methods for X-ray Crystallography at Low Resolution**
Yong Xiong

October 24, 16:00-18:30 (Meeting Room 6)

MS-11 Metal-organic crystal engineering

Chairs: Ian Williams, Jing-tai Zhao

16:00-16:30 **Thermoelectric Zintl Compounds in R-T-Sb (R = Ca, Sr, Ba, Eu, Yb; T = Zn, Cd) Systems**
XJ Wang, H Zhang, MB Tang, XX Yang, HH Chen, ZY Man, U Burkhardt, Y Grin, JT Zhao

16:30-17:00 **Solid-state photochemical reactivity of coordination polymers and metal complexes containing trans-1,2-bis(4-pyridyl)ethylene**
Jagadese J Vittal, Mangayarkarasi Nagarathinam, Abdul Malik Puthan Peedikakkal

17:00-17:25 **Anatomy of a void in an aluminium-copper-tin alloy**
Laure Bourgeois, Matthew Weyland, Philip NH Nakashima, Barry C Muddle

17:25-17:45 **SMART X2S - Chemical Structures at the Touch of a Button**
Eric Hovestreydt, Michael Ruf, Holger Ott

17:45-18:00 **Rational Design, Synthesis and Properties of Layered Compounds LnOZnSb (Ln=La, Ce, Pr, Nd)**
Kai Guo, Hao-Hong Chen, Zhen-Yong Man, Mei-Bo Tang, Xin-Xin Yang, Xiang-Xin Guo, Jing-Tai Zhao

18:00-18:15 **Cation···Cation Supramolecular Interactions in Zinc–Imidazole–Oxovanadate Compounds**
Samroeng Krachodnok, Kenneth J Haller, Ian D Williams

18:15-18:30 **Synthesis and X-ray Structures of Diorganotin Complexes with *Tris*{(hydroxymethyl)aminomethane Schiff base**
See Mun Lee, Hapipah Mohd Ali, Kong Mun Lo

October 24, 16:00-18:30 (Meeting Room 7)

MS-12 Powder diffraction

Chairs: Xiaolong Chen, Takashi Ida

16:00-16:25 **Precise Structure Analysis of Ceramic Materials up to 1830 K**
Masatomo Yashima

16:25-16:50 **Structural analysis of zeolites and related functional materials**
Yingxia Wang

16:50-17:10 **Spinner-Scan Method for Evaluation of Particle Statistics in Powder Diffractometry**
Takashi Ida, Taishi Goto, Hisashi Hibino

17:10-17:30 **Structural and magnetic properties of doped wide bandgap semiconductors**
Gang Wang

17:30-17:50 **Vanadium substituted potassium tungsten bronzes – synthesis and characterization**
A M Abdullah, A Hussain

17:50-18:10 **Charge density study from high resolution powder diffraction data**
Eiji Nishibori, Shinobu Aoyagi, Hiroshi Sawa

18:10-18:30 **Interplay between the crystalline and magnetic structures in lightly Cr-doped $Bi_{0.37}Ca_{0.63}Mn_{0.96}Cr_{0.04}O_{2.9}$**
Wen-Hsien Li, Chun-Chuen Yang, Chun-Ming Wu, Jirong Sun, Jeffrey W Lynn

Sunday, October 25

09:00-09:50 **Meeting Room 1**
Keynote 3
Cargo recognition during clathrin-coated vesicle formation
David Owen
Chair: Soichi Wakatsuki

09:00-09:50 **Meeting Room 6**
Keynote 4
Crystalline silver(I) complexes containing all-carbon and carbon-rich anionic ligands
Thomas Mak
Chair: JJ Vittal

October 25, 10:00-12:00 (Meeting Room 1)

MS-13 Hot structures

Chairs: Se-Won Suh, Yigong Shi

10:00-10:25 **The structure of rat liver vault**
Hideaki Tanaka, Koji Kato, Eiki Yamashita, Tomoyuki Sumizawa, Yong Zhou, Min Yao, Kenji Iwasaki, Masato Yoshimura, Tomitake Tsukihara

10:25-10:50 **Recognition of Nuclear Export Signal by CRM1**
Yuh Min Chook

10:50-11:15 **NEMO regulates NF-κB activation by specific recognition of linear ubiquitin chains**
Simin Rahighi, Fumiyo Ikeda, Masato Kawasaki, Masato Akutsu, Nobuhiro Suzuki, Ryuichi Kato, Tobias Kensche, Tamami Uejima, Stuart Bloor, David Komander, Felix Randow, Ivan Dikic, Soichi Wakatsuki

11:15-11:40 **The atomic structure of granulovirus polyhein at 1.8Å resolution**
Elaine Chiu, Shin-Mei Yeh, Richard Bunker, Clemens Schulze-Briese, Peter Metcalf

11:40-12:00 **Crystal structure of human REV7 in complex with REV3 fragment**
Kodai Hara, Toshiyuki Shimizu, Yoshiki Murakumo, Shunsuke Kobayashi, Toshiaki Kogame, Satoko Akashi, Satoru Unzai, Tomo Hanafusa, Haruo Ohmori, Shunichi Takeda, Mamoru Sato, Hiroshi Hashimoto

October 25, 10:00-12:00 (Meeting Room 6)

MS-14 Superconductivity and crystal properties

Chairs: Mohana Yethiraj, Xian-Hui Chen

10:00-10:40 **High Pressure Synthesis and Superconducting Properties of Oxygen-deficient Oxypnictide Superconductors *Ln*FeAsO$_{1-y}$**
H Eisaki, K Miyazawa, M Nakajima, S Ishida, M Ishikado, K Kihou, P M Shirage, C H Lee, N Takeshita, R Kumai, Y Tomioka, H Kito, K M Kojima, T Ito, S Shamoto, S Uchida, A Iyo

10:40-11:20 **Diffraction Study of the Fe-based High Temperature Superconductors**
Wei Bao

11:20-11:40 **Electric Polarisation Flop and Magnetic Phase Transition Induced by Magnetic Field in Multiferroic RMn_2O_5 (R=Tm, Yb)**
Hiroyuki Kimura, Yuma Sakamoto, Mamoru Fukunaga, Yukio Noda, Nobuyuki Abe, Kouji Taniguchi, Taka-hisa Arima, Shuichi Wakimoto, Kazuhisa Kakurai

11:40-12:00 **Effect of Ga^{3+} Substitution for Mn^{3+} on Magnetic and Dielectric Properties in Multiferroic YMn_2O_5**
Yuma Sakamoto, Hiroyuki Kimura, Satoru Horio, Arno Fey, Mamoru Fukunaga, Ryoji Kiyanagi, Yukio Noda, Hiraka Haruhiro

October 25, 16:00-18:30 (Meeting Room 7)

MS-15 Electron microscopy and diffraction

Chairs: Laure Bourgeois, Koh Saitoh

10:00-10:30 **Electron Microscopy of Low-Dimensional Nanomaterials**
Fangfang Xu

10:30-11:00 **3 Dimensional Coherent Electron Diffractive Imaging of a Nanoparticle**
Fu-Rong Chen, Roman Dronyak, Keng S Liang

11:00-11:30 **High Resolution Structural Analysis of Membrane Proteins by Electron Crystallography**
Kaoru Mitsuoka

11:30-11:45 **Strain Mapping near Si/SiGe Interfaces Using HOLZ Line CBED Patterns**
Koh Saitoh, Maiko Hamabe, Nobuo Tanaka

11:45-12:00 **Visualisation of the Orbital-ordered State of $FeCr_2O_4$ using the CBED Method**
Daisuke Morikawa, Kenji Tsuda, Shintaro Ohtani, Takahisa Arima

October 25 –12:00-13:30 CCrS Council Meeting (Meeting room 3)

October 25 -13:30-16:35 (Grand Ball Room)

13:30-15:30 **Rising Stars Symposium**
Chair: Mitchell Guss

15:45-16:35 Plenary 2
Structural physiology based on electron crystallography
Yoshinori Fujiyoshi
Chair: Zhi-Jie Liu

General Information

Conference Venue

The AsCA'09 conference, including poster presentations and company exhibitions, will be held on the 2nd floor of the Jing-Yi hotel from Oct. 22 to 25, 2009. The Jingyi Hotel is located 11 km from downtown Beijing and 30 km from Beijing International Airport. It is within easy reach of many cultural sights, either via taxi or by subway from two nearby subway stations.

Registration Desk

The registration desk will be located in the lobby of Jingyi hotel on Oct. 22. From Oct. 23–25, the registration and information desk will be moved to the 2nd floor near the Grand Ball Room. The registration desk will be open during the following days and times:

Oct. 22 (Lobby of the Jingyi Hotel): 9:00 – 21:00

Oct. 23 – 25 (2nd floor, near the grand ball room): 09:00-11:30, 13:30-17:30

Any inquiries about the registration, social events, tours, etc. may be answered by approaching any of the staff at the registration desk. Participants may pick up their Conference kits, badges and invitations/tickets at the registration desk.

On-site Registration Fees

Full Registration	USD $500 or RMB3410
Full-time Student Registration	USD $350 or RMB2387
Accompanying Person	USD $200 or RMB1364
One Day Registration	USD $150 or RMB1023

Payment On-site

Cash and credit cards (Master, Visa and American Express) are acceptable. No personal check and traveler's check are accepted for the payments. All bank charges will be borne by the participant.

Instructions for Presentations

①Presentation facilities:

Powerpoint presentations are encouraged for oral presentations. Laptop Computers and data projectors will be made available in the meeting rooms. If you would like to use your own computer, please send it to our staff at least 20 minutes before the session of your speech.

②Speakers' Information Desk

There will be a designated computer located at the Speakers' Information Desk. This desk will be somewhere near the registration desk. The speakers are encouraged to copy their files to the computer at your earliest convenient time, or are kindly requested to copy your presentation files into this computer at least 20 minutes before the session of your speech. Speakers are advised to preview their presentations before the start of each session.

③Poster session:

1) A display board measuring 90cm wide by 120cm high will be provided for each poster. Poster boards are numbered according to the same numbering scheme in the abstract book.

2) The poster presentations will be in the room next to the grand ball room on the second floor. The posters will be divided into two sessions during the conference. **The first session of the posters with odd numbers** are requested to be set up in the afternoon of Oct. 22 and its presentation is scheduled at ***13:30-15:30 on Oct. 23***. **The second session of the posters with even numbers** are requested to be set up in the same poster room at 20:00-21:30 on Oct. 23 and the poster presentation is scheduled at ***13:30-15:30 on Oct. 24***.

   1) During the two poster displays, presenters are requested to remain in front of their poster boards to meet with other attendees.

   2) Please note that the first session of the poster presenters are advised to take down the posters before 19:00 on Oct. 23 and the second session of the poster presenters should take down the posters before 12:00 on the Oct. 25.

      All posters left uncollected at the end of its session will be disposed of by the staff.

   3) The schedule for poster presentation:

      A. **Rising Star Symposium**: 13:30-15:30 on Oct. 25
      The candidates of Rising Star Award are advised to prepare a 15 minutes talk. Six of the candidates will be selected for presentations in the Rising Star Symposium.

      B. Posters of first session:

      The time for setting up poster: from 14:00 on Oct. 22

      Poster Presentation: 13:30-15:30 on Oct. 23

      C. **Posters of second session**: Oct. 23-24

      The time for setting up poster: 20:00-21:30 on Oct. 23

      Poster Presentation: 13:30-15:30 on Oct. 24

Exhibition

A scientific exhibition will be held during the AsCA''09 to highlight recent developments in technology and to demonstrate new products for the crystallography research and related fields. The exhibition will be on the 2nd floor, where is in front of the grand ball room and near the poster session area. The exhibition will be open from 9:00-18:00 from Oct. 23 –25.

Tea breaks

Morning and afternoon tea breaks will be served daily adjacent to the grand ball room where mineral water, tea, coffee and snacks will be provided..

Internet

Internet access is available in each guest room of the Jingyi Hotel with free of charge.

Meals

①Lunches:

1) There are three restaurants and two bars inside Jingyi Hotel. A few more restaurants are within walk distance from hotel.

. 2) Lunchon Seminar: Rigaku Corporation will organize a seminar at lunch time on Oct. 23. The participants are welcome to attend and the lunch will be provided. ***The seminar vouchers are available at the registration desk or Rigaku's exhibition booth.***

②Dinners:

The dinners for registered participants will be provided in the Chinese Restaurant and Rose Cafe located on the first floor of Jingyi hotel on Oct. 23 and Oct. 25. The coupons will be placed in your registration package.

③Welcome reception and conference banquet

The welcome reception (Oct. 22) and conference banquet (Oct.24) will be held in the grand ball room of the second floor. The coupons will be placed in your registration package.

Breakfast:

7:30 – 8:30

Participants who stay in Jingyi hotel will have breakfast on the 1st floor of the hotel. Please remember to show your room card when having breakfast.

Smoking

Please be advised that smoking is not permitted inside the meeting rooms.

Social Events

Oct. 22nd (Thursday):

9:00-12:00: Workshop 1: *Macromolecular crystallization, data collection and data processing techniques*

Meeting room 1 (2nd floor)

13:30-17:00: Workshop 2: *Direct-method SAD phasing and dual-space model completion*

Meeting room 1 (2nd floor)

14:00-17:00: Workshop 3: *Publication of Small Molecule Structures in IUCr Journals*

Meeting room 6 (2nd floor)

18:00 –19:00: Opening Ceremony & IUCr Plenary Lecture

Grand Ball Room (2nd floor)

19:00 –20:30: Welcome Reception for registered participants

Grand Ball Room (2nd floor)

Oct. 23rd (Friday):

09:50-10:10: Picture taking for all participants will be in the lobby of the hotel. ***Please don't miss it!***

12:00-13:30: Lunchon Seminar by Rigaku Corporation

Oct. 24th (Saturday):

19:00 –21:00: Conference Banquet for registered participants

Awards Ceremony: AsCA Travel Awards, IUCr Travel Awards, Rising Star and Poster Awards

Grand Ball Room (2nd floor)

Oct. 25th (Sunday):

13:30 –15:30: Rising Star Symposium

Grand Ball Room (2nd floor)

Business Meetings

Oct. 22nd (Monday):

09:00 –18:00: Rigaku Corporation Meeting

Meeting room 3 (2nd floor)

Oct. 24th(Saturday):

12:30 –13:30: AsCA Council Meeting

Meeting room 3 (2nd floor)

Oct. 25th (Sunday):

12:30 –13:30: CCrS Council Meeting

Meeting room 3 (2nd floor)

Weather

The optimal season to visit Beijing is Autumn. Late October in Beijing is sunny and comfortable with a little bit cold. The average daily temperature is about 12 °C /53°F, with highs of around 18°C /64°F and lows of around 6°C /43°F. It is an ideal time for tourists to enjoy the beautiful sites of Beijing.

Name Badges

Please do wear your Conference name badge at all times. In addition, tickets issued in your registration package must be presented for all social events.

Participants:	Blue
Exhibitors:	Green
Accompanying persons:	Light blue
Host staff:	Orange

Public Transportation

Transportation in Beijing is convenient, with buses and subway/light rail.

- **Bus:** The bus ride in Beijing costs about 1 yuan - 3 yuan depending on distance. Most city buses run from 5:30 ~ 22:00.
- **Subway/Light rail:** The full fare is about 3 yuan.

Taxis

Taxis are everywhere in the city and is the most convenient way to get around. Taxis charge 2.0 yuan per kilometer for the first 10 km, and then 2.4 yuan for every additional kilometer. Toll fees are an extra. It costs around 100 yuan from the airport to the Jingyi hotel and about 35 yuan to downtown.

Secretariat

If you need help or have any requirements during AsCa'09, please contact the conference secretariat at the registration desk from Oct. 23 – Oct. 25 during daytime hours. Alternatively, the conference secretariat can be reached in the Jingyi Hotel in the evening. The room number and telephone number of the staff will be available on the information board either in the lobby of the Jingyi hotel or on the information desk near the meeting room area.

Or you can contact the staffs below by cell phone if needed

Mr. Xiaoke Xia:	13601365704
Ms. Shunyi Wei:	13011058198
Ms. Ke Chen:	15901483571

Attention

1. All participants are advised to wear name badge during the conference.
2. Please note that all participants are requested to present the corresponding ticket for the meals during the conference, including Welcome Reception and Conference Banquet.
3. The local organizing committee of AsCA'09 will set up receiving stations for the participants both in Terminal No. 2 and Terminal No.3 of the Beijing International Airport on Oct. 22. The participants are advised to look for the **AsCA'09** sign near the exit doors. The staff will escort you to the taxi stand.

. **Taxi service:** The cost of the taxi from the airport to the Jingyi Hotel is about RMB 100 yuan. Please show the Taxi Direction Note and map below to the taxi drivers.

Please be advised *that you should not accept a taxi service offer anywhere other than at the* **taxi stand** *of the airport.*

TAXI NOTE

Please take me to the Jingyi Hotel. Thank you!

请 送 我 到 京 仪 大 酒 店， 谢 谢

Address of Jingyi Hotel: 北京海淀区大钟寺东路 9 号

电话(Tel)：010-62165588

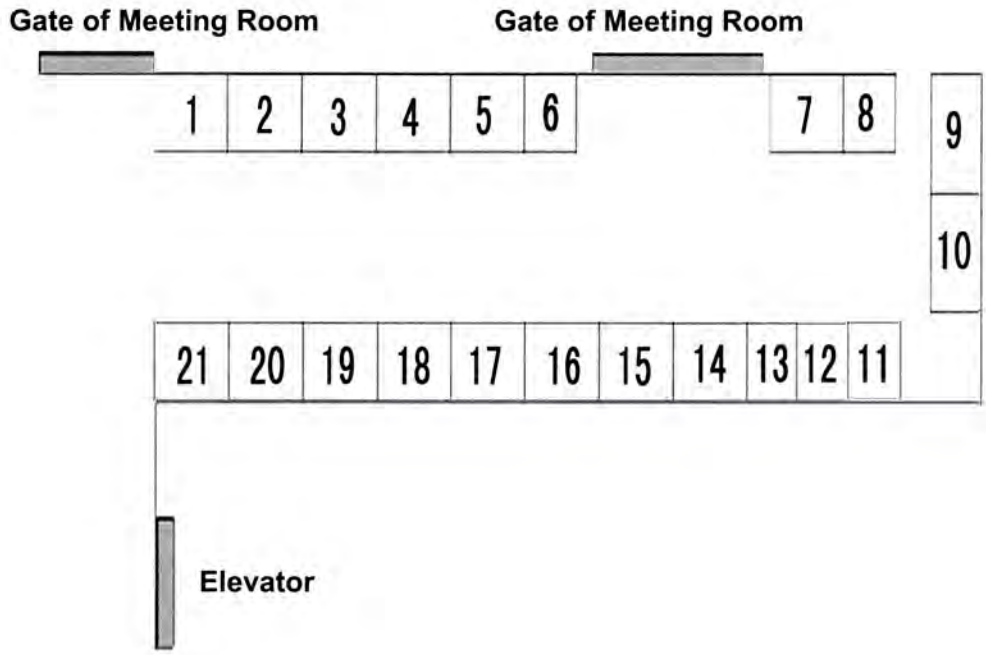

Booth Number	Exhibitor Name	Booth Number	Exhibitor Name
1+2	Rigaku Corporation	11	PDBj: Protein Data Bank Japan
3	Area Detector Systems Corporation	12	GN Biosystems, Inc.
4	Rayonix LLC	13	Seajet Scientific Inc
5	Marresearch GmbH	14+15	Oxford Diffraction
6	Oxford Cryosystems LTD	16	Microlytic
7	Thermo Fisher Scientific (China) Co. , Ltd	17	Bioray Instruments Limited / XtalQuest Corp
8	Hamilton Bonaduz AG Shanghai Rep. Office	18	Cambridge Crystallographic Data Centre
9	International Union of Crystallography	19	Bruker AXS GmbH
10	Dawning Information Industry Co., Ltd	20	TTP LabTech Ltd China Office
		21	GE Healthcare

Sponsors

Rigaku Corporation
Thermo Fisher Scientific (China) Co. , Ltd
Marresearch GmbH
GE Healthcare

Exhibitors

Oxford Diffraction
Cambridge Crystallographic Data Centre
Rayonix, LLC
TTP LabTech Ltd China Office
Bioray Instruments Limited / XtalQuest Corp.
Bruker AXS GmbH
Area Detector Systems Corporation
Microlytic
International Union of Crystallography
Oxford Cryosystems LTD
Dawning Information Industry Co., Ltd
PDBj: Protein Data Bank Japan
GN Biosystems, Inc.
Hamilton Bonaduz AG Shanghai Rep. Office
Seajet Scientific Inc.

AsCA'09 Beijing

Joint Conference of the Asian Crystallographic Association and Chinese Crystallographic Society

Abstract Book

October 22-25, 2009 • Beijing, China

Abstracts

Ted Baker CV and Abstract

Professor Ted Baker began his career in protein crystallography as a Postdoctoral Fellow at Oxford University, working with Professor Dorothy Hodgkin on the structure of insulin. He then led the establishment of structural biology in New Zealand, and has made international contributions in many areas, including protein structure refinement, hydrogen bonding, and the function of metalloproteins and bacterial toxins. In other international roles, he served as President of the International Union of Crystallography (1996-1999), and is a member of the Scientific Advisory Boards of several international bodies, including the Worldwide Protein Data Bank. He is currently Distinguished Professor of Structural Biology at the University of Auckland. Professor Baker is a Fellow of the Royal Society of New Zealand, winner of the Rutherford Medal (New Zealand's foremost science honour) and the Hector Medal, and was an International Research Scholar of the Howard Hughes Medical Institute. His current research interests focus on experimental protein structure analysis and its applications to functional genomics, structure-based drug design, and the microbial pathogenesis.

Celebrating Crystallography

PL-1

Edward N. Baker
Maurice Wilkins Centre for Molecular Biodiscovery and School of Biological Sciences, University of Auckland, Private Bag 92019, Auckland, New Zealand
(ted.baker@auckland.ac.nz)

Crystallography provides a unique window on the natural world. Its ability to "see" the atomic and molecular structures of materials, whether from biology, chemistry or other areas of science, can give new insights into how things are and present wonderful opportunities for creativity and applications. This lecture will trace the historical development of crystallography, celebrating its contributions to understanding the world around us.

Crystallography was initially the province of philosophers and mathematicians who marvelled at the beauty and symmetries of crystals and speculated about what these might mean. The idea gradually developed that external form must reflect internal structure, with Louis Pasteur providing one of the first and most important demonstrations of this idea. The discovery of X-ray diffraction in the early 1900s changed crystallography radically, with a series of great pioneers such as William and Lawrence Bragg, Dorothy Hodgkin, J. D. Bernal, Linus Pauling, Max Perutz, Francis Crick and others showing how crystallography could help reveal the mysteries of chemistry and biology. Subsequent generations of crystallographers have also led the way in showing how knowledge of atomic and molecular structures can be usefully applied in areas such as the development of new therapeutics or novel materials. Finally it is also apparent that the structures themselves carry connections between biology, chemistry mathematics and even art and architecture.

These are all good reasons to celebrate the ways in which crystallography provides such a stimulating and satisfying discipline.

Hongkun Park CV and Abstract

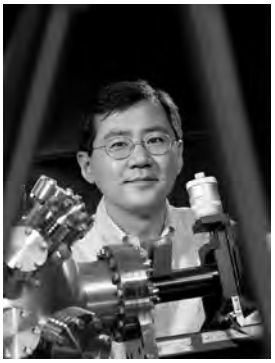

Professor of Chemistry and of Physics, Harvard University
Contact:
12 Oxford Street, Cambridge, MA 02138
Tel: 617-496-0815
Fax: 617-384-7998
E-mail: hongkun_park@harvard.edu
WWW: www.people.fas.harvard.edu/~hpark/index.html

Curriculum Vitae

- 2004 – present: Full Professor Chemistry and of Physics, Harvard University
- 2003 – 2004: John L. Loeb, Associate Professor of the Natural Sciences, Harvard University
- 2003 – 2004: Associate Professor of Chemistry, Harvard University
- 1999 – 2003: Assistant Professor of Chemistry, Harvard University
- 1996 – 1999: Postdoctoral fellow, Lawrence Berkeley National Laboratory
- 1991 – 1996: Ph.D., Physical Chemistry, Stanford University
- 1986 – 1990: B.S., Chemistry, Seoul National University

Selected Awards and Honors

- NIH Director's Pioneer Award (2008)
- Fellow, The World Technology Network (2004)
- Ho-Am Prize for Science (2003)
- Visiting Miller Research Professorship, University of California, Berkeley (2003)
- Camille and Henry Dreyfus Teacher-Scholar Award (2003)
- Alfred P. Sloan Foundation Research Fellowship (2002)
- David and Lucile Packard Foundation Fellowship for Science and Engineering (2001)
- National Science Foundation CAREER Award (2001)
- Research Corporation Research Innovation Award (1999)
- Camille and Henry Dreyfus New Faculty Award (1999)
- Franklin Veatch Memorial Fellow, Stanford University (1993)
- Presidential Prize and Valedictorian: Seoul National University (1990)

Research Interests

Nanometer-sized materials represent a natural size limit of the miniaturization trend of current technology, and they exhibit physical and chemical properties significantly different from their bulk counterparts. Hongkun Park is developing cutting-edge experimental methods to incorporate individual molecules and nanostructures into electronic, optoelectronic, and plasmonic devices. Using these methods, he is characterizing their behaviors in detail to gain insights about their behavior and exploring the potential of these devices for future technological applications.

He is also using his nanoscience expertise to develop new nano- and microelectronic tools that can interface with live cells, cell networks, and living organisms. Specifically, he is investigating vertical nanowire arrays as a platform to perturb cellular functions in a massively parallel, arrayed fashion, and patch-clamp and nanowire arrays for recording real-time dynamics of *in vitro* and *in vivo* neuronal ensembles. These tools will impact a broad range of high-throughput discovery efforts in biology and help scientists to unravel the design principles of complex cellular networks.

PL-2

Vertical Nanowire Arrays: a Universal Platform for Interfacing with Living Cells

Hongkun Park
Department of Chemistry and Chemical Biology and Department of Physics, Harvard University, 12 Oxford Street, Cambridge, MA 02138
(hongkun_park@harvard.edu)

At the heart of all investigations into cellular function lies the need to induce specific and controlled perturbations to cells. A variety of tools are now available to accomplish this in a rational and directed fashion by delivering various biological effectors (small molecules, DNAs, RNAs, peptides, and proteins). These options, however, are often limited to either particular molecules or certain cell types due to the lack of a general strategy for transporting polar or charged molecules across the plasma membrane. In this presentation, we show that vertical silicon nanowires (NWs) can serve as a universal platform for delivering virtually any type of molecule into a wide variety of cells in a format that is compatible with live-cell imaging and microarray technology. The platform's simplicity and generality stem from the direct physical access to the cells' interiors that NW penetration affords, thereby enabling efficient introduction of numerous biological effectors without chemical modification or viral packaging. Furthermore, this NW-based system is fully compatible with standard microarray printing techniques, allowing large collections of biomolecules to be co-delivered into live cells in a parallel and miniaturized fashion.

Yoshinori Fujiyoshi CV and Abstract

Contact: Department of Biophysics, Graduate School of Science, Kyoto University, Oiwake, Kitashirakawa, Sakyo-ku, Kyoto, 606-8502, Japan
Tel: +81-75-753-4215,
Fax; +81-75-753-4218
E-mail; yoshi@em.biophys.kyoto-u.ac.jp

Education:

1982	Kyoto University, Ph. D. (Chemistry)
1976	Kyoto University, M. Sc. (Chemistry)
1971	Nagoya University, B. Sc. (Chemistry)

Employment:

1996-	Molecular Biophysics, Department of Biophysics, Faculty of Science, Kyoto University, **Professor**
1994-1996	International Institute for Advanced Research, Matsushita Electric Industrial Co., Ltd., **Research Director**
1987-1994	Protein Engineering Research Institute, **Senior research Scientist** (1987-1988); **Research Director** (1988-1994)
1980-1987	Institute for Chemical research, Kyoto University, **Research Assistant** (1980-1984); **Instructor** (1985-1987)

Other Activities and Awards:

2008	Japan Academy Prize, The Japan Academy
2007	Medal with Purple Ribbon, Government of Japan
2006	The Shimadzu Prize, Shimadzu Science Foundation
2005	The Keio Medical Science Prize, Keio University Medical Science Fund
2005	The Yamazaki-Teiichi Prize, Foundation for Promotion of Material Science and Technology of Japan
2005	DOCTOR HONORIS CAUSA of the "Iuliu Hatieganu" University of Medicine and Pharmacy of Cluj-Napoca
2005	Minister of Science and Technology Policy Award for the Industry-Academia-Government Collaboration Contributor Awards
2000-2004	Japan Biological Information Research Centre, Structural Genomics team leader
2003-2006	RIKEN Harima Institute, MD group leader
1999-2003	RIKEN Harima Institute, MD group, Multisome team leader
1988	Setoh Prize, the Japanese Society of Electron Microscopy
1979-1980	Kyoto University, Fellow of the Japan Society for the promotion of Science

PL-3 Structural physiology based on electron crystallography

Yoshinori Fujiyoshi
Department of Biophysics, Graduate School of Science, Kyoto University, Oiwake, Kitashirakawa, Sakyo-ku, Kyoto 606-8502, JAPAN
(yoshi@em.biophys.kyoto-u.ac.jp)

A biological cell, such as a nerve cell, regulates cell signaling mainly by ion channels. Water permeation through biomembranes should therefore be strictly separated from the movement of ions. This means water channels must be highly specific and effective for water to prevent any ions. One water channel can permeate 3 billion water molecules in a second without proton permeation. When water molecules rapidly cross the membrane channel, they form a continuous unbroken column and their hydrogen-bond chain conducts protons as domino toppling with great efficiency. The pore has to prevent proton passage and the hydrogen-bond separation is required while such requirement increases energy barrier reducing the water permeation speed. For answering these questions, structure of aquaporin-1 was analyzed at a resolution of 3.8 Å by electron crystallography [1]. For accomplishing the effective water channel functions, the structure showed peculiar structural determinants including an unusual fold, for which we named aquaporin fold [1]. Based on the structure of aquaporin-1, we proposed H-bond isolation mechanism by which we could explain a mechanism of high speed water permeation without transfer of protons. However, the resolution was limited and we could observe no water molecules in the structure analysis of aquaporin-1. By analyzing structure of aquaporin-0 at a resolution of 1.9 Å, we could clearly observed water molecules in the channel [2]. However, the structure was at closed state of the channel and only three water molecules ware discriminated. By improving the resolution of fast water permeation channel, aquaporin-4, whose structure was analyzed at 3.2 Å resolution [3] and showed 8 water molecules in the channel, we confirmed the H-bond isolation mechanism [4].

The aquaporin-4 molecule acquired two very important functions in cell biology, cell adhesive and channel functions. We named this type channels as "Adhennel" family [3]. Gap Junction channel is a typical Adhennel family protein and we analyzed structure of a mutant of Cx26 which was related with hearing loss. Based on the structure of the mutant Cx26 channel, we proposed a plug gating model [5]. We also published a structure of wild type Cx26 at open state analyzed by X-ray crystallography, and explained a gating mechanism by transjunctional voltage [6]. Although the gating mechanisms of gap junction channels are complicated, electron crystallography enables us to elucidate structural and functional relationship of such membrane proteins based on their structures in membrane.

By focusing on multifunctional channels like Adhennels, I would like to introduce recent results in structural physiology based on electron crystallography of membrane proteins by utilizing our cryo-electron microscopes with helium cooled specimen stages [7].

References

[1] K. Murata et al., Nature 407, 599-605 (2000)

[2] T. Gonen et al., Nature 438, 633-638 (2005)

[3] Y. Hiroaki et al. J. Mol. Biol. 355, 628-639 (2006)

[4] K. Tani et al. J. Mol. Biol. 389, 694-706 (2009)

[5] A. Oshima et al. PNAS 104, 10034-10039 (2007).

[6] S. Maeda et al., Nature 458, 597-602 (2009)

[7] Fujiyoshi Y., Adv. Biophys. 35, 25-80 (1998)

Joel L. Sussman CV and Abstract

Prof. Joel L. Sussman is the Morton and Gladys Pickman Professor of Structural Biology at the Weizmann Institute of Science, and the Director of the Israel Structural Proteomics Center (ISPC, http://www.weizmann.ac.il/ISPC) He is a member of the European Molecular Biology Organization (EMBO) and a member of the Executive Board, Int'l Structural Genomics Org (ISGO) and on the editorial board for the journals: *Proteins*, *PEDS* & *PLoS ONE*. He is Chairman of the Israel Council of Higher Education Bioinformatics Committee and the Coordinator of the *Forum for European Structural Proteomics*. He is an Honorary Professor of the Chinese Academy of Sciences, received the Bergmann Prize for Outstanding Research in Chemistry in Israel (1979), the U.S. Army Science Conference Award for Outstanding Research (1991), the Elkeles Prize for Outstanding Scientist in Medicine in Israel (2005), the Teva Founders Prize for Breakthroughs in Molecular Medicine (2006) and. From 1994 -1999 he was the director of the Brookhaven Protein Data Bank (PDB). He obtained his B.A. at Cornell University in 1965, and his Ph.D. in biophysics at MIT in 1972. His research group, at the Weizmann Institute, is studying the 3D structure/function of nervous system proteins, such as b-secretase, acetylcholinesterase, cholinesterase-like adhesion molecules (CLAMs), b-glucosidase (the enzyme that is defective in Gaucher disease) and paraoxonase (a key enzyme that helps rid the arteries of plaque-forming clumps of LDL ("bad" cholesterol) that can lead to arteriosclerosis). The goal of his research is to use the 3D structures of proteins that his group is determining as a basis for new leads for treating neurological disorders, such as Alzheimer's Disease, autism, and in developing new therapies for Gaucher and arteriosclerosis. He is also studying *intrinsically unfolded* proteins as well as how proteins adapt to extreme environments, *e.g. halotolerant* proteins. Most recently he and his colleagues have developed *Proteopedia*, the free, collaborative 3D encyclopedia of proteins & other molecules (http://www.proteopedia.org).

Proteopedia - a Scientific 'Wiki' Bridging the Rift Between 3D Structure and Function of Biomacromolecules

KN-1

Joel L Sussman[1,2], Eran Hodis[3], Jaime Prilusky[1,4], Israel Silman[1,5], John Moult[6] & Eric Martz[7]

[1]The Israel Structural Proteomics Center, [2]Departments of Structural Biology, [3]Computer Science & Applied Math, [4]Biological Services Unit, [5]Neurobiology, Weizmann Institute of Science, Rehovot 76100 ISRAEL; [6]CARB, Univ of MD Biotechnology Institute, Rockville, MD 20850; [7]Department of Microbiology, Univ of MA, Amherst, MA 01003

Rather than relying just on printed text to provide the basis for the understanding of

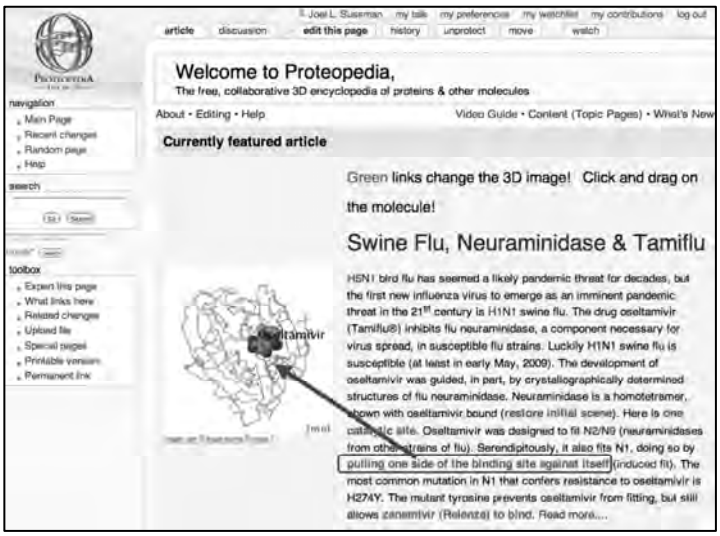

biomacromolecular structures, a collaborative website called ***Proteopedia*** is a new resource for linking written information and 3D structural information. ***Proteopedia*** (http://www.proteopedia.org) displays protein structures and other biomacromolecules interactively, i.e. can be rotated and zoomed (see figure). These interactive images are surrounded by text with hyperlinks that change the appearance of the 3D structure to reflect the concept explained in the text. This makes the complex structural information readily accessible and comprehensible, even to non-structural biologists. Using ***Proteopedia***, anyone can easily create descriptions of biomacromolecules linked to their 3D structure, *e.g.*:

β2-Adrenergic Receptor - http://www.proteopedia.org/wiki/index.php/Hoelzer_Sandbox
Proton Channels: http://proteopedia.org/wiki/index.php/Proton_Channels
HIV-1 protease: http:/proteopedia.org/wiki/index.php/HIV-1_protease
Lac repressor: http://proteopedia.org/wiki/index.php/Lac_repressor
AChE/Aricept complex in Chinese: http://www.proteopedia.org/wiki/index.php/1eve (Chinese)

Aside from content added by the more than 500 registered users of ***Proteopedia***, pages on each of the more than 60,000 entries in the PDB have been automatically created, and are primed for expansion by users. Members of the scientific community are invited to request a user account to edit existing pages and to create new ones. For details, see: Hodis, Prilusky, Martz, Silman, Moult & Sussman (2008) *Genome Biol* **9**, R121.

Matthew Rosseinsky CV and Abstract

Matthew Rosseinsky obtained a degree in Chemistry from the University of Oxford and a D. Phil under the supervision of Professor P. Day, FRS in 1990. He was a Postdoctoral Member of Technical Staff at A.T.&T. Bell Laboratories in Murray Hill, New Jersey where his work with D.W. Murphy led to the discovery of superconductivity in alkali metal fullerides. In 1992, he was appointed University Lecturer at the Inorganic Chemistry Laboratory, University of Oxford, where he remained until 1999 when he moved to the University of Liverpool as Professor of Inorganic Chemistry. He was awarded the inaugural de Gennes Prize for Materials Chemistry by the RSC in 2009. He was elected a Fellow of the Royal Society in 2008.

His work has spanned several fields, but is unified by the development of synthesis coupled with detailed characterisation to control the functional behaviour of materials in a chemically understandable manner. He has demonstrated the new materials properties that arise from the construction of microporous materials from molecular components, focussing on differences from the highly thermally stable aluminosilicate systems and emphasising flexibility of response to guests and chiral sorption, most recently through the construction of open frameworks from amino acid and peptide components. He has developed the metal fullerides into the best model systems for correlated electron high temperature superconductivity. He has worked extensively on transition metal oxide chemistry, developing hydride ion reduction to access novel reduced materials with high ionic mobility and recently extending this work to the identification of a new class of interstitial-based oxide ion conductor. To enable a more direct relationship between the design of complex oxide structures and real synthetic procedures, he has used layer-by-layer pulsed laser deposition to access metastable inorganic solids as thin films by sequential assembly of unit cells of the structural components. His work has been characterised by extensive collaboration with many academic and industrial colleagues.

KN-2 Reactivity and flexibility in metal-organic frameworks: amino-acid based and post-synthetically functionalised materials

M.J. Rosseinsky
Department of Chemistry, University of Liverpool

The precisely defined interior cavities of porous metal-organic frameworks with a high degree of chemical diversity are attractive for selective sorption. We describe a family of amino-acid based open frameworks (1) which display chirally selective sorption that is highly specific to the functional group disposition within the sorbed molecules. The nature of the interaction between the framework and sorbate is revealed by computational approaches used in protein-ligand docking.

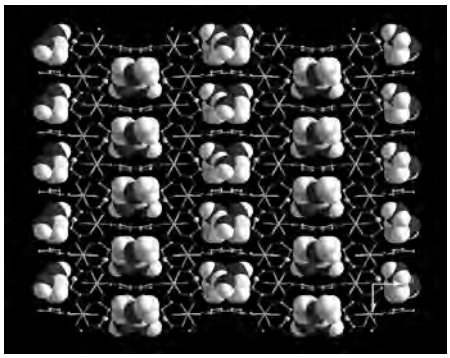

The cavities within metal-organic framework materials are also attractive hosts for the observation of chemical reactions with atomic-scale resolution by crystallography, permitting the observation of co-operative involvement of the surrounding solid in accommodating the changes at the reacting centre (2). This motivates the development of post-synthesis chemistry to introduce catalytically active centres into metal-organic frameworks, which in turn opens up the possibility of reactive sites and reaction chemistry that are inaccessible outside the metal-organic framework environment. (3)

References

[1] Vaidhyanathan, R., Bradshaw, D., Rebilly, J. N., Barrio, J. P., Gould, J. A., Berry, N. G., and Rosseinsky, M. J., *Angew. Chem. Int. Ed. Engl.*. **45**, 6495 (2006); Ingleson, M. J., Bacsa, J., and Rosseinsky, M. J., *Chemical Communications* (29), 3036 (2007); Barrio, J. P., Rebilly, J. N., Carter, B., Bradshaw, D., Bacsa, J., Ganin, A. Y., Park, H., Trewin, A., Vaidhyanathan, R., Cooper, A. I., Warren, J. E., and Rosseinsky, M. J. *Chemistry-a European Journal* **14** (15), 4521 (2008); Rebilly, J. N., Gardner, P. W., Darling, G. R., Bacsa, J., and Rosseinsky, M. J., *Inorganic Chemistry* **47** (20), 9390 (2008). J.N. Rebilly, J. Bacsa, M. J. Rosseinsky *Chemistry – an Asian Journal* **4**, 892-903, (2009)

[2] D. Bradshaw *et al. Science* **315**, 977 - 980, 2007.

[3] Ingleson, M. J., Barrio, J. P., Bacsa, J., Dickinson, C., Park, H., and Rosseinsky, M. J., *Chemical Communications* (11), 1287 (2008); Ingleson, M. J., Barrio, J. P., Guilbaud, J. B., Khimyak, Y. Z., and Rosseinsky, M. J., *Chemical Communications* (23), 2680 (2008). M. J. Ingleson, J. Perez Barrio, J. Bacsa, A. Steiner, G. R. Darling, J. T. A. Jones, Y. Z. Khimyak, and M. J. Rosseinsky *Angew. Chemie., Int. Ed.,* **48**, 2012, *(*2009).

David Owen CV and Abstract

Following a degree in biochemistry and a D.Phil with Professor Dame Lousie Johnson on the structure and function of protein kinases, both at the University of Oxford, David Owen moved to the MRC LMB in Cambridge in 1995. Here he carried out structure/function studies on protein involved clathrin coated vesicle formation under the sponsorship of Dr Philip Evans. In 2000 he was awarded a Wellcome Trust Senior Research Fellowship in Basic Biomedical Science to start a small group in the Cambridge Institute for Medical Research in Medical School at the University of Cambridge to carry on this work.

KN-3 Cargo recognition during clathrin-coated vesicle formation

David Owen

Transmembrane proteins are moved between organelles in transport vesicles. Once cargo has been sorted into a forming vesicle, the vesicle buds from the donor membrane and is then transported to and fuses with its target membrane. Many steps in post-Golgi transport is mainly mediated by clathrin-coated vesicles (CCVs), whose coats are composed of an outer clathrin scaffold linked to the membrane by clathrin adaptors including AP complexes, GGAs, epsins and ARH. Clathrin adaptors have folded domains that bind to membrane phospholipid headgroups and in some cases simultaneously bind to transmembrane cargo thereby selecting the cargo for incorporation into a CCV. The remainder of the proteins are extended, flexible regions that connect contain multiple short motifs, which bind to clathrin and the appendages of major clathrin adaptors, the APs and GGAs. Standard cargo possesses short, transplantable, linear motifs such as YxxΦ, [DE]xxxLL and FxNPxY or are poly or multiply monoubiquitinated so enabling the cargo to bind directly to the folded domains of clathrin adaptors and so be recruited as cargo into forming CCVs. For clathrin mediated endocytosis from the cell's limiting membrane, YxxΦ motifs are bound by the μ2 subunit of the AP2 adaptor complex and [DE]xxxLL motifs by the σ2 subunit.

The SNAREs are type II integral membrane proteins, which are present on both transport vesicles and target membranes. They form highly specific trans hetero tetrameric complexes thus bringing the vesicle and its correct target into close apposition and so provide the specificity and at least part of the mechanical driving force for the fusion of a transport vesicle with its target. In addition to the SNARE helix that is common to all SNAREs and through which SNARE complexes are formed, many SNAREs also small folded regulatory N-terminal domains. We have very recently shown that there are highly specific, fold-dependent, extensive surface patch mediated interactions between the N-terminal domains of two SNAREs (vti1b and Vamp7) with two different CCV components (epsinR and Hrb respectively) by determining the structures of the complexes formed by the two SNARE/adaptor pairs. In both cases disruption of the interactions by single point mutations abolishes the interactions between the pairs of proteins *in vitro* and and alters the steady state distribution of the SNAREs *in vivo*. These data, along with other published work, suggest that non-motif mediated recognition of SNARE N-terminal folded domains by CCV components is a general feature of the trafficking of individual SNAREs and SNARE complexes.

Taken together, these two pieces of work suggest that there are at least two distinct cargo recognition systems that function in parallel without competing with each other during CCV formation. This talk will present some of the molecular mechanisms behind these different types of clathrin adaptor: CCV cargo interactions.

Thomas Mak CV and Abstract

BSc (Hon. Chem & Phy) 1960, PhD (Chem) 1963,

The University of British Columbia

Wei Lun Research Professor and Professor Emeritus, The Chinese University of Hong Kong

Member of Chinese Academy of Sciences

Ten Representative Publications

[1] X.-D. Chen, C.-Q. Wan, H. H.-Y. Sung, I. Williams and T.C.W. Mak***:** Control of Channel Size for Selective Guest Inclusion with Inlaid Anionic Building Blocks in a Porous Cationic Metal-organic Host Framework. *Chem. Eur. J.* **15**, 6518-6528 (2009).

[2] L. Zhao, C.-Q. Wan, J. Han, X.-D. Chen and T.C.W. Mak* . Ancillary Ligands and Spectator Cations as Controlling Factors in the Construction of Coordination and Hydrogen-bonded Networks with the *tert*-Bu–C≡C⊃Ag_n (n = 4, 5) Supramolecular Synthon. *Chem. Eur. J.* **14**, 10437-10444 (2008).

[3] J. Han, C.-W. Yau, C.-K. Lam and T.C.W. Mak***.** Designed Supramolecular Assembly of Anionic Hydrogen-bonded Rosette Layers. *J. Am. Chem. Soc.* **130**, 10315-10326 (2008).

[4] S.-Q. Zang, L. Zhao and T.C.W. Mak*. Diverse Intermolecular Interactions in Metal-Organic Frameworks Constructed with New Supramolecular Synthon Ag_n-L-Ag_n (n = 4 or 5) (H_2L = 2,2'-bis-prop-2-ynyloxy-biphenyl). *Organometallics* **27**, 2396-2398 (2008).

[5] T.C.W. Mak,* X.-L. Zhao, Q.-M. Wang and G.-C. Guo. Synthesis and structural characterization of silver(I) double and multiple salts containing the acetylenediide dianion. *Coord. Chem. Rev*. 251, 2311-2333 (2007).

[6] L. Zhao, X.-L. Zhao and T.C.W. Mak. Assembly of Infinite Silver(I) Columns, Chains, and Bridged Aggregates with Supramolecular Synthon Bearing Substituted Phenylethynides". *Chem. Eur. J.* **13**, 5927-5936 (2007).

[7] L. Zhao and T.C.W. Mak*: Assembly of Polymeric Silver(I) Complexes of Isomeric Phenylenediethynides with the Supramolecular Synthons Ag_n⊂ C_2—R—C_2 ⊃Ag_n (R = *p*-, *m*-, *o*-C_6H_4; n = 4, 5). *J. Am. Chem. Soc.* **127**, 14966-14967 (2005).

[8] C.-K. Lam, F. Xue, J.-P. Zhang, X.-M. Chen and T.C.W. Mak*. Hydrogen-Bonded Anionic Rosette Networks Assembled with Guanidinium and C_3-Symmetric Oxoanion Building Blocks. *J. Am. Chem. Soc.* **127**, 11536-11537 (2005).

[9] L. Zhao and T.C.W. Mak*. Silver(I) Butadiynediide and Two Related Silver(I) Double Salts Containing the C_4^{2-} Dianion. *J. Am. Chem. Soc.* **126**, 6852-6853 (2004).

[10] Q.-M. Wang and T.C.W. Mak*. Elliptic Column Consolidated by Acetylide Dianion, Cyanide and Trifluoroacetate in a Novel Quadruple Salt of Silver(I). *J. Am. Chem. Soc.* **123**, 1501-1502 (2001).

Books

T.C.W. Mak and G.-D. Zhou, "Crystallography in Modern Chemistry: A Resource Book of Crystal Structures", Wiley-Interscience, New York, 1992; Professional Paperback Edition, 1997.

W.-K. Li, G.-D. Zhou and T.C.W. Mak, "Advanced Structural Inorganic Chemistry", Oxford University Press, Oxford, 2008.

KN-4

Crystalline Silver(I) Complexes containing All-carbon and Carbon-rich Anionic Ligands

Thomas C. W. Mak
Department of Chemistry and Center of Novel Functional Molecules,The Chinese University of Hong Kong, Shatin, Hong Kong SAR,, China (tcwmak@cuhk..edu.hk)

In the context of supramolecular chemistry, the coordination concept as commonly applied to metal ions has been extended to polyatomic anionic species.[1] In the designed construction of coordination networks, it is of interest to determine the highest ligation number (HLN) of simple inorganic polyatomic anions, namely the largest number of coordination bonds that a particular anion can form with neighboring metal centers in its complexes.[2]

Over a decade ago, we embarked on a systematic study on the HLN of small inorganic anions such as the pseudohalides CN^-, SCN^-, N_3^- and $SeCN^-$ using the silver(I) ion as an ideal probe. Such a choice is favored by the tendency of Ag(I) to form multinuclear aggregates through the d^{10}–d^{10} metallophilic interaction.[3] By dissolving each silver(I) pseudohalide in a concentrated aqueous solution containing one or more water-soluble silver(I) salts, a series of new double and triple silver(I) salts were obtained, and their crystal structures were determined by single-crystal X-ray diffraction.

We subsequently investigated the all-carbon diatomic ligand ethynediide (also named acetylenediide, C_2^{2-}), an isoelectronic structural analog of CN^-, N_2 and NO^+. In the resulting double, triple and quadruple silver(I) salts, the dumbbell-like $^-C{\equiv}C^-$ species was found to be invariably encapsulated in a polyhedral silver(I) cage of 6-10 vertices, and each C-terminal has significant σ, π, and mixed (σ, π) interactions with only four or five vertices. We then expanded the scope to synthesize silver(I) complexes of 1,3-butadiyne-1,4-diide ($^-C{\equiv}C{-}C{\equiv}C^-$) and related ethynide species $R{-}C{\equiv}C^-$ (R = alkyl, aryl), thereby establishing the identity and utility of the multi-nuclear metal-ligand supramolecular synthons $Ag_4{\subset}C{\equiv}C{-}C{\equiv}C{\supset}Ag_4$ and $R{-}C{\equiv}C{\supset}Ag_n$ (n = 4,5) for the construction of multi-dimensional coordination networks. Several factors of influence, including the choice of counter anions, the presence of ancillary spectator molecules, and variation of aromatic ring substituents on the self-assembly of silver-ethynide supramolecular synthons in crystallization have been systematically explored. Our work up to 2007 has been summarized in two reviews,[4] and some recent advances will be presented here.

***Acknowledgements**: This work is supported by Hong Kong Research Grants Council GRF CUHK 402405 and 402408.*

References

1. (a) *Supramolecular Chemistry of Anions*, ed. Bianchi, A.; Bowman-James, K.; and Garcia-Espańa, E. Wiley-VCH, New York, 1996. (b) Beer, P. D.; Smith, D. K.; *Prog. Inorg. Chem*. **1997**, *46*, 1–96.
2. Guo, G.-C.; Mak, T. C. W. *Chem. Commun*. **1999**, 813–814.
3. Pyykkö, P. *Chem. Rev.* **1997**, *97*, 597–636.
4. (a) Mak, T. C. W.; Zhao, X.-L.; Wang, Q.-M.; Guo, G.-C. *Coord. Chem. Rev*. **2007**, *251*, 2311–2333. (b) Mak, T. C. W.; Zhao, L. *Chem. Asian J.* **2007**, 2, 456–467.

MS1-1 Arms race between host and pathogen

Jijie Chai
National Institute of Biological Sciences, Beijing 102206,China (chaijijie@nibs.ac.cn)

Molecular mimicry is a common strategy utilized by pathogens for manipulating host cellular signaling to their own benefit. Here we first present an example where a large family bacterial effector protein functions as GEFs mimics rather than GTPase mimics as previously proposed. Our data define a novel mechanism underlying the selection of host substrates by bacterial GEF mimics, which is consistent with pathogenic diversity observed in numerous bacterial infectious agents. We then present evidence that host can also employ a mimicking strategy to counter against the invading pathogens. Coupled with genetic and biochemical studies, the crystal structure of a plant pathogen effector protein AvrPto in complex with its host Pto kinase suggests that Pto may act as a 'decoy' by mimicking a kinase that is targeted by pathogens for their pathogenesis. Collectively, our results suggest that the interplay between pathogen and host features a process of dynamic evolution.

MS1-2 Structural studies on the Glutathione Transferases and their involvement in resistance to chemotherapy treatment

Lorien J. Parker[1,4], Paul J. Dyson[2], Mario Lo Bello[3] and Michael W. Parker[4]
1. RIKEN Systems and Structural Biology Center, 1-7-22 Suehiro-cho,Tsurumi-ku, Yokohama City, 230-0045, Kanagawa, Japan (parker@ssbc.riken.jp)
2. Institut des Sciences et Ingénierie Chimiques, Ecole Polytechnique Fédérale de Lausanne, 1015 Lausanne, Switzerland (paul.dyson@epfl.ch)
3. Department of Biology, University of Rome Tor Vergata, Via della Ricerca Scientifica snc, Rome 00133 Italy (lobello@uniroma2.it)
4. St. Vincent's Institute of Medical Research, 9 Princes St, Fitzroy, Melbourne, Victoria, 3065, Australia (mparker@svi.edu.au)

The clinical efficacy of anti-cancer drugs is often limited by the emergence of drug resistance in cancer cells. The Pi class GST enzyme, GSTP1-1, is believed to be an important factor in resistance and its overexpression has been reported in a number of different human malignancies. Changes in the levels of GSTs have repeatedly been correlated with resistance to anti-cancer agents, presumably through accelerated detoxification of drugs by conjugation with glutathione[1]. More recent evidence, described below, suggests GSTs also contribute to resistance through covalent or non-productive binding of some compounds, highlighting the potential in targeting GSTs for inhibitor drug design.

To elucidate the mechanism behind drug deactivation by GSTs crystal structures of GSTP1-1 with numerous anti-cancer drugs were determined. Cisplatin, an extensively used anti-cancer drug, was expected to bind in the active site where it was presumed to be deactivated by GSH conjugation, thus explaining the resistance suffered by patients undergoing treatment with this compound. Surprisingly, the drug bound at dimer interface rather than the active site as predicted. This is the first GSTP1-1 ligand identified to bind at the dimer interface, an important discovery for drug design since, to date, all efforts targeting inhibition of GSTs have focused on inhibiting the active site. The results from this structure indicate a necessary

shift towards targeting the dimer interface, in addition to the active site, when developing potent and specific inhibitors for use as adjuvants in chemotherapy treatment.

The structure of the GST-ethacraplatin complex, (an inhibitor based on cisplatin designed by our collaborators) reveals the compound also binds at the dimer interface. In concordance with these findings, collaborators in Switzerland designed a ruthenium-based drug to target both sites simultaneously. This compound has been shown to successfully inhibit enzymatic activity. The structure of the complex confirms the compound is able to bind at both sites of the enzyme[2].

The structure of GSTP1-1 in complex with phenyl-arsine oxide, a membrane-permeable phosphotyrosine phosphatase inhibitor, has been determined. Again the compound binds at the dimer interface as well as at the active site. Furthermore, this structure reveals that each of the molecules bound at the two separate sites also interact with each other. This structure provides a scaffold for design of an inhibitor that binds simultaneously to both sites.

Taken together, these novel findings suggest that GSTP1-1 plays a role, other than classical detoxification, in contributing to the development of drug resistance. Surprisingly, the metal-based drugs bind at the dimer interface rather than the active site, thus revealing a new mechanism of resistance whereby the enzyme can sequester the drug from the cellular milieu. Collectively, this information, in conjunction with findings from *in-silico* screening, have lead to crystallographic fragment based screening methods. Information gained from these techniques will be used for the design of optimal drug candidates by medicinal chemists in the near future.

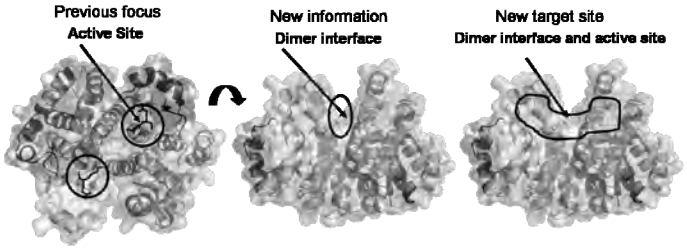

Figure depicting progress of GSTP1-1 drug targeting. Initial efforts targeted the active site. Results from our work identified the dimer interface as important for metal-based inhibitors. Thus, current strategies focus on targeting both sites. **1**.*Journal of Molecular Biology* (2008) **380**(1): 131-144. **2.***Angewandt Chemie Internat. Ed* (2009) **48**: 3854-7

MS1-3 Structural Study of PA subunit from an Avian Influenza Virus RNA polymerase

Yingfang Liu[1], Zihe Rao[2]
1.Institute of Biophysics, Chinese Academy of Sciences, Beijing, China
2.IBP/Nankai University/Tsinghua University

Structural study of Influenza viral proteins especially its RNA polymerase proteins is critical for elucidation the underlying mechanisms of viral life cycle and for development of anti-influenza virus drugs. The influenza RNA-dependent RNA polymerase (RdRp) complex,

consisting of PA, PB1 and PB2 subunits, plays crucial roles in viral RNA replication and transcription. Recently, we have determined crystal structures of PA subunit from an avian influenza A virus H5N1 by splitting it into two individual domains. Our results have not only revealed some previously uncharacterized functional roles of PA, but also provided an ideal target for novel anti-influenza therapy.

MS1-4 Ligand recognition by the TLR4-MD-2 complex

Jie-Oh Lee
Department of Chemistry, KAIST, Daejeon 305-701, Korea (jieoh.lee@kaist.ac.kr)

TLR4 and MD-2 form a heterodimer that recognizes LPS from Gram negative bacteria. Eritoran is a candidate anti-sepsis drug that antagonizes LPS activity by binding to the TLR4-MD2 complex. We determined the crystal structures of the TLR4-MD-2-Eritoran and LPS complexes. TLR4 is an atypical member of the LRR family and is composed of N-terminal, central and C-terminal domains. The ˛ sheet of the central domain shows unusually small radii and large twist angles. MD-2 binds to the concave surface of the N-terminal and central domains. Agonistic LPS induced the formation of an "m"-shaped receptor multimer composed of two copies of the TLR4-MD-2-LPS complex arranged in a symmetrical fashion. LPS interacts with a large hydrophobic pocket in MD-2 and directly bridges the two components of the multimer. Eritoran bind to the LPS pocket in MD-2 and blocks LPS binding and TLR4 heterodimerization. Five of the six lipid chains of LPS are buried deep inside the pocket and the remaining chain is exposed to the surface of MD-2, forming a hydrophobic interaction with the conserved phenylalanines of TLR4. The F126 loop of MD-2 undergoes localized structural change and supports this core hydrophobic interface by making hydrophilic interactions with TLR4. Comparison with the structures of tetraacylated antagonists, Eritoran and Lipid Iva, bound to MD-2 indicates that two other lipid chains in LPS displace the phosphorylated glucosamine backbone towards the solvent area by ~5 angstrom. This structural shift allows phosphate groups of LPS to contribute to receptor multimerization by forming ionic interactions with a cluster of positively charged residues in TLR4 and MD-2. The TLR4-MD-2-LPS structure illustrates the remarkable versatility of the ligand recognition mechanisms employed by the TLR family, which is essential for defense against diverse microbial infection.We propose that formation of the TLR dimer brings the intracellular TIR domains close to each other to promote dimerization and initiate signaling.

MS1-5

Scaffold-Based Discovery of a Novel Selective Inhibitor of Oncogenic B-Raf Kinase with Potent Anti-Melanoma Activity

Kam Y.J. Zhang[*], James Tsai, John T. Lee[1], Weiru Wang, Jiazhong Zhang, Hanna Cho, Shumeye Mamo, Ryan Bremer, Sam Gillette, Jun Kong[1], Nikolas K. Haass[1], Katrin Sproesser[1], Ling Li[1], Keiran S.M. Smalley[1], Daniel Fong, Yong-Liang Zhu, Adhirai Marimuthu, Hoa Nguyen, Billy Lam, Jennifer Liu, Ivana Cheung, Julie Rice, Yoshihisa Suzuki, Catherine Luu, Calvin Settachatgul, Rafe Shellooe, John Cantwell, Sung-Hou Kim[¶], Joseph Schlessinger[$], Brian West, Ben Powell, Gaston Habets, Chao Zhang, Prabha N. Ibrahim, Peter Hirth, Dean R. Artis, Meenhard Herlyn[1], Gideon Bollag

Plexxikon, Inc., 91 Bolivar Drive, Berkeley, CA 94710;

[*]Advanced Science Institute, RIKEN, 2-1 Hirosawa, Wako, Saitama, 351-0198, Japan (kamzhang@riken.jp).

[1]Department of Molecular and Cellular Oncogenesis, The Wistar Institute, 3601 Spruce Street, Philadelphia, PA 19104;

[¶]220 Calvin Laboratory, University of California, Berkeley, CA 94720;

[$]Department of Pharmacology, Yale University School of Medicine, 333 Cedar Street, New Haven, CT 06520

$BRAF^{V600E}$ is the most frequent oncogenic protein kinase mutation known. The $BRAF^{V600E}$ gene is found in approximately 70% of malignant melanomas and a large number of colorectal and thyroid tumors. Furthermore, inhibitors targeting "active" protein kinases have demonstrated significant utility in the therapeutic repertoire against cancer. Therefore, we pursued the development of specific kinase inhibitors targeting B-Raf – and the V600E allele in particular. Here, we present a novel scaffold targeting protein kinases, and we report the elaboration of this scaffold into a potent and selective inhibitor of "active" B-Raf. PLX4720, a 7-azaindole derivative that inhibits $B\text{-}Raf^{V600E}$ with an IC_{50} of 13 nM, defines a novel class of kinase inhibitor with marked selectivity in both biochemical and cellular assays. PLX4720 preferentially inhibits the "active" $B\text{-}Raf^{V600E}$ kinase compared to a broad spectrum of other kinases, and potent cytotoxic effects are also exclusive to cells bearing the V600E allele. Consistent with the high-degree of selectivity, ERK phosphorylation is potently inhibited by PLX4720 in $B\text{-}Raf^{V600E}$-bearing tumor cell lines but not in cells lacking oncogenic B-Raf. In melanoma models, PLX4720 induces cell cycle arrest and apoptosis exclusively in $B\text{-}Raf^{V600E}$-positive cells. In $B\text{-}Raf^{V600E}$-dependent tumor xenograft models, orally-dosed PLX4720 causes significant tumor growth delays – including tumor regressions – without evidence of toxicity. We describe here the entire discovery process, from initial identification through structural and biological studies in animal models, to a promising personalized therapeutic for testing in cancer patients bearing $B\text{-}Raf^{V600E}$-driven tumors.

MS2-1 Metal Organic Frameworks for Proton Conduction and CO_2 Uptake

Jeff Hurd, Ramanathan Vaidhyanathan, Jared Taylor, Simon Iremonger, Karl Dawson, George Shimizu
Department of Chemistry, University of Calgary, Calgary, Alberta, Canada (gshimizu@ucalgary.ca)

Two families of compounds will be presented in this talk, proton conducting MOFs and, MOFs with amine-lined pores for carbon dioxide sorption. MOFs are well studied for gas sorption and the notion to include amine functionalities in pores has been pursued by several groups. Recent results from our group concerning high heats of CO_2 adsorption attained with a zinc aminotriazolate/oxalate system will be presented.[1] On a separate theme, some recent work on proton conducting MOFs prepared in our group will be shown.[2] Beyond showing that a crystalline MOF material can function to conduct protons in an anhydrous environment at 150°C, the illustration will be made that the "PCMOFs" can function as gas separators.

References

1. R. Vaidhyanathan, S. S. Iremonger, K. W. Dawson, G. K. H. Shimizu, *Chem. Commun.*, **2009**, 5230 - 5232.
2. J. A. Hurd, R. Vaidhyanathan, V. Thangadurai, C. I. Ratcliffe, I. Moudrakovski, G. K. H. Shimizu, *Nature-Chem.* accepted for publication.

MS2-2 Homoleptic Metal Organothiolate and Organoacetylide Coordination Polymers: Structural Determination using Powder X-ray Diffraction and Their Materials Properties

Stephen Sin-Yin, CHUI[1], Kam-Hung, LOW[1], Roy V. A. L.[2], Chi-Ming CHE[1]
[1] *Department of Chemistry, The University of Hong Kong, China (chuissy@hkucc.hku.hk)*
[2] *Department of Physics and Materials Science, The City University of Hong Kong, China.*

In this presentation, several insoluble homoleptic metal organothiolate $[M(S\text{-}aryl)_n]_\infty$ (M = Cu(I), Ni(II), Pd(II), Pt(II) and Ru(III) and Co(III)) and organoacetylide complexes $[M(C\equiv C\text{-}R)]_\infty$ (M = Cu, Ag, Au, R = aryl and n-alkyl) will be reported. All these complexes have been structurally determined and refined by powder X-ray diffraction data. They are found to adopt either 1-D or 2-D coordination polymers with different topologies. For $[Cu(SR)]_\infty$, these 1-D polymers grew along the long axes of the rod-like nano-crystals and their crystallite morphology is significantly affected by the substituents of the thiolate ligands. Fabrication of the respective bottom-contacted field-effect transistors using such nano-rod crystals, uses of single-source precursor from $[M(SR)_n]_\infty$ and magnetic properties of some $[M(SR)_3]_\infty$ polymers and photoluminescence of the $[Cu(C\equiv C\text{-}R)]_\infty$ will be discussed.

References

1. S. S. Y. Chui, M. F. Y. Ng, C. M. Che, *Chem. Eur. J.* **2005**, *11*, 1739–1749.
2. C. M. Che, C. H. Li, S. S. Y. Chui, K. H. Low, V. A. L. Roy, *Chem. Eur. J.* **2008**, *14*, 2965–2975.

MS2-3

Ionothermal Synthesis of Metal Organic Framework Materials

Zhuojia Lin[1], Linna Huang[1], Ming-Liang Tong[1] and Russell E. Morris[2]
[1] *MOE Key Laboratory of Bioinorganic and Synthetic Chemistry, School of Chemistry and Chemical Engineering, Sun Yat-Sen University, Guangzhou 510275, China (linzhjia@mail.sysu.edu.cn)*
[2] *EaStChem School of Chemistry, University of St. Andrews, St Andrews, Fife, Scotland, UK KY16 9ST (rem1@st-and.ac.uk)*

Ionothermal synthesis, the use of an ionic liquid as solvent and structure directing agent in the synthesis of crystalline materials, offers many advantages over traditional materials synthesis methods. Here we report the use of ionothermal synthesis to prepare new metal organic framework materials based on the copper, cobalt, nickel and manganese trimesate (TMA) systems and discuss some interesting chemistry happened in ionic liquids.

A series of novel materials can be prepared simply by changing the metal used (Co/Ni) or the organic cation of the ionic liquid, showing the template effect of ionic cations in the ionothermal synthesis of metal organic frameworks. The anions in ionic liquids play a significant role in solvent polarity and hydrophibicity, which in turn control the structures of materials formed in the ionothermal synthesis. More surprisingly changing the anion from bromide to the enantiometically pure anion L-aspartate allows a chiral induction effect that results in a chiral framework that does not occlude the L-aspartate anion and is composed of only non-chiral building blocks. This is, we believe, the first time such an effect has been seen in materials synthesis. We also found that a highly porous copper-TMA metal organic framework with an unusual chemical composition displaying copper-chloride bonds on the internal surface of the pores is accessible using ionothermal approaches. Such a material is impossible to prepare using hydrothermal approaches. Finally hydrogen bonding directing effect in the ionothermal synthesis will be discussed. This work shows the great potential to adjust the structures and properties of metal organic framework materials via the control of the structures and composition of ionic liquids.

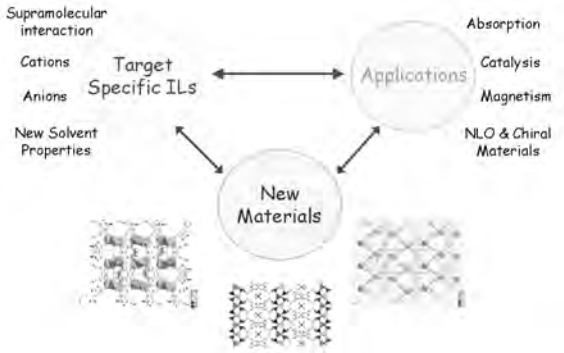

References

1. **Z.-J. Lin**, D. S. Wragg, P. Lightfoot and R. E. Morris* *Dalton. Trans.* **2009**, 5287.
2. **Z. Lin***, Y. Li, A. M. Z. Slawin and R. E. Morris *Dalton. Trans.* **2008**, 3898.

3. **Z. Lin**, A. M. Z. Slawin and R. E. Morris* *J. Am. Chem. Soc.* **2007**, 129, 4880.
4. **Z. Lin**, D. S. Wragg, J. E. Warren and Russell E. Morris* *J. Am. Chem. Soc*. **2007**, *129*, 10334.
5. **Z. Lin**, D. S. Wragg and R. E. Morris* *Chem. Commun*., **2006**, 2021.

MS2-4 To bridge or not to bridge – carbonyl ligand configurations in some phosphine and arsine substituted tricobalt carbon cluster systems

Jim Simpson , C. John McAdam, Brian H. Robinson, and Roderick G. Stanley.
Department of Chemistry, University of Otago, P.O. Box 56, Dunedin, 9054, NEW ZEALAND. (jsimpson@alkali.otago.ac.nz)

In simple methinyltricobaltnonacarbonyl clusters, $RCCo_3(CO)_9$, six of the carbonyl ligands occupy equatorial sites, close to the plane of the triangle of cobalt atoms with the the other three carbonyl groups approximately orthogonal to that plane in axial positions. Monodentate or bidentate phosphine or phosphite ligands almost invariably substitute carbonyl groups from equatorial sites [**1**,**2**]. Furthermore, the remaining equatorial carbonyl ligands generally adopt terminal conformations. A search of the Cambridge Database [**3**] reveals that carbonyl bridging of the Co—Co bonds is unusual and is generally found only in situations where the apical substituent R, or the substituting ligands, significantly increase the electron density on the CCo_3 cluster core.

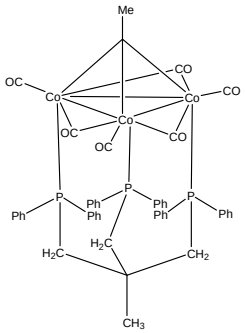

We have prepared a number of derivatives of methinyltricobaltnonacarbonyl clusters with the potentially tridentate 1,1,1-tris(diphenylphosphinomethyl)-ethane, $CH_3C(CH_2PPh_2)_3$, (triphos) ligand. In all cases, the resulting compounds have bridging carbonyl ligands. This paper will report the structure of these complexes and examine the factors that influence carbonyl bridging in these and related cluster systems. Crystal packing in methinyltricobaltnonacarbonyl clusters will also be discussed.

Acknowledgements*: We thank the New Economy Research Fund; Grant No. UOO-X0808 for support of this work and the University of Otago for purchase of the diffractometer*

References

[1] Matheson, T.W., Robinson, B.H. & Tham, W.S. (1971) *J Chem Soc A* 1457-1464.
[2] Downard, A.J., Robinson, B.H. & Simpson, J. (1986) *Organometallics* **5**, 1122—1131.
[3] Allen, F. H. (2002). *Acta Cryst.* B**58**, 380—388.

MS2-5 Crystal Engineering of Chiral Metal Organic Frameworks (MOFs) from Tartrates and N-Donor Spacer Ligands

Pokka K-C. Pang, Herman H-Y. Sung, Ian D. Williams
Department of Chemistry, Hong Kong University of Science and Technology, Clear Water Bay, Kowloon, Hong Kong, China (pokka@ust.hk)

Ten new crystalline phases have been structurally characterized with formulae related to [Cu(4,4'-bipy)(L-Tar)]. These fall into two isostructural series one is tetragonal with space group $P4_12_12$ and the other is triclinic, with space group P1 or P-1 depending on whether the tartrate is homo-chiral or not. The structures are open, 3D network polymers, which in the case of L-tartrate or L-malate lead to chiral MOFs. The 1D channels in the triclinic family are slightly expanded and can contain water, acetic acid or 4,4-bipyridine. The copper II centers are all square pyramidal with two trans N-donors and three O donors from the carboxylates. Tartrates are all in μ_3,κ^3 bridging coordination mode, which form CuTar sheets with different topological arrangements for the tetragonal and triclinic families. The channels can be enlarged by several angstrom by using more extended N-donor bridges than 4,4-bipy, and the channel wall functional groups can be altered by varying tartrate stereochemistry from L-Tar to DL-Tar and meso-Tar, as well as L-or DL-Malate analogues. This varies the extent and spatial location of hydroxyl functionalities pendant to the channel walls and which affect the channel hydrophilicity. Several phases also show two different channel types with guest molecule differentiation. Finally the structures are surprisingly robust to ca 150^{o}C and survive loss of channel solvent. Selective and enantioselective sorption studies are now being conducted on these promising MOF materials.

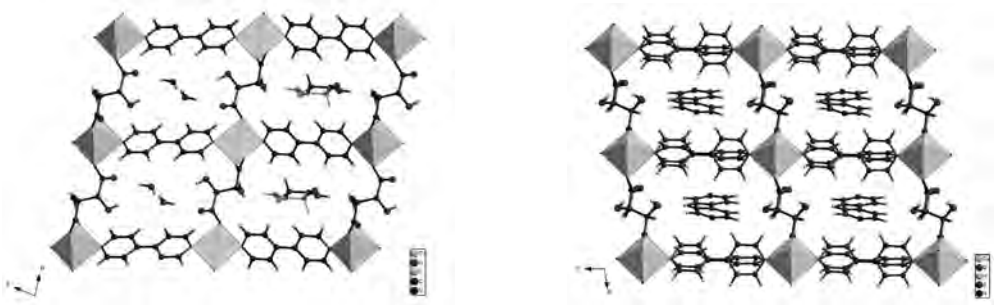

***Acknowledgements**: The Research Grant Council of Hong Kong is gratefully acknowledged for financial support of this work (grant 603307)*

MS3-1 Current status and future development of neutron scattering at China Advance Research Reactor

Dongfeng Chen, Yuntao Liu, Hongli Wang, Kai Sun, Meimei Wu
China Institute of Atomic Energy, P. O .Box 275-80, Beijing, 102413, P. R. China (dongfeng@ciae.ac.cn)

Presently, both neutron and X-ray techniques are well developed internationally. For example, America, Europe and Japan have both the world-class synchrotron sources, such as APS、ESRF/ DIAMOND、SPRING8，and the world-class neutron sources, such as SNS/HFIR、

ILL/ISIS、J-PARC/JRR3. In China, although synchrotron facilities have been built and properly developed in Beijing, Hefei and Shanghai, neutron scattering research is not well developed due to lack of an advanced neutron source. However, the completion of the China Advanced Research Reactor (CARR) will push the neutron scattering technique developing in a quick way.

The construction of the 60-MW China Advanced Research Reactor (CARR), a 7.7B¥RMB, 9-year project at the China Institute of Atomic Energy (CIAE), is scheduled to complete with the reactor reaching criticality at the end of 2009. The Neutron Scattering Laboratory (NSL) of CARR is responsible for the development of a user facility which initially consists of at least 7 beamlines and endstations. The power of CARR will be 60 MW and $8x10^{14}n/(cm^2.s)$ unperturbed thermal neutron flux make it standing on an international advanced level.

A suite of instruments, including powder, single crystal, residual stress neutron diffractometers and a neutron imaging facility will be opened for international and domestic users from 2009. NSL will focus on following aspects: (A) the methodology study of neutron scattering technique; (B) the neutron scattering study on the relation between the structures and properties of novel function materials. (C) studies of the residual stress distribution in engineering components and the methodology of neutron imaging.

References

1. D.F. Chen et al., Physica B 385-386, 966(2006)
2. D.F.Chen et al., J Phys : Condens Matter. 10 , 255-260 (1998)
3. Z.H.Cheng et al., Physical Review B,57(22) 14299-14309(1998)

MS3-2 Current Status of Shanghai Synchrotron Radiation Facility

Jianhua He, Zhentang Zhao and Hongjie Xu
Shanghai Institute of Applied Physics, Chinese Academy of Sciences, Shanghai, 201800, China (hejh@sinap.ac.cn)

The Shanghai Synchrotron Radiation Facility (SSRF) is a third generation light source of 3.5GeV electron energy, aimed at producing very brilliant X-ray and soft X-ray beams to facilitate the researches in life science, material science, earth and environmental sciences, and many other fields. The construction of SSRF started in December of 2004 and was completed by the end of April 2009. During the commissioning stage, the main parameters of accelerators and beamlines were measured with the conclusion that all the design specifications of accelerators have been met and all the beamlines have reached the requirements for user operation. The user operation of SSRF started in May of 2009 and it will provide more than 2000 hours beamtime to over 300 user groups this year.

At present, seven beamlines have been built on SSRF as the phase I beamlines:

1) Macromolecular Crystallography Beamline
2) X-ray Diffraction Beamline
3) X-ray Absorption Fine Structure Beamline
4) Hard X-ray Micro-focusing Beamline

5) X-ray Imaging and Biomedical Applications Beamline
6) Soft X-ray Spectromicroscopy Beamline
7) Small Angle X-ray Scattering Beamline

In this talk, an overview of SSRF construction and the commissioning of SSRF Phase I beamlines will be introduced. Some preliminary experimental results obtained since the user operation will be shown and the future beamline programs will be introduced as well.

MS3-3 Crystallography and Materials Science at the J-PARC pulsed spallation neutron facility

Takashi Kamiyama
J-PARC Center / High Energy Accelerator Research Organization, KEK Tokai Campus, 2-4 Shirakata Shirane, Tokai, Naka, Ibaraki 319-1195, Japan
(takashi.kamiyama@kek.jp)

The first spallation neutron beam was successfully delivered to 5 neutron instruments on May 30, 2008. At present (June, 2009), 12 instruments are carrying out neutron beam experiments, among which 8 of them accepts general users. We have four polycrystalline diffractometers: a super high resolution powder diffractometer (SuperHRPD), a 0.15 %-resolution powder diffractometer of Ibaraki prefecture (iMATERIA), an engineering diffractometer (Takumi), and a high intensity S(Q) diffractometer (NOVA). In addition, the high-pressure community as well as the battery community are planning to construct dedicated polycrystalline diffractometers. A macromolecule single crystal diffractometer has started commissioning from last year and accept the general user program. Another single crystal diffractometer for solid-state sciences is proposed. A reflectometer with horizontal sample geometry has been constructed and commissioning was started with the instrument used at the KENS facility. We also have three chopper spectrometers with different S(Q,w) range and resolution. The layout of the experimental hall is shown in Fig. 1(left).

SuperHRPD has recorded the world best resolution with $\Delta d/d = 0.035$ %, which is compatible with the best SR diffractometer. Figure 1 (right) shows the comparison of two Bragg peaks measured by the SuperHRPD as well as the KENS Sirius diffractometer; FWHM is three time improved in SuperHRPD and the tail of each Bragg peak observed in Sirius was not observed in SuperHRPD resulting in 10 times improvement in 1/10-width. This characteristics is rather effective in both precise crystal structure analyses of complicated materials with large unit cells as well as detection of tiny structural distortion.

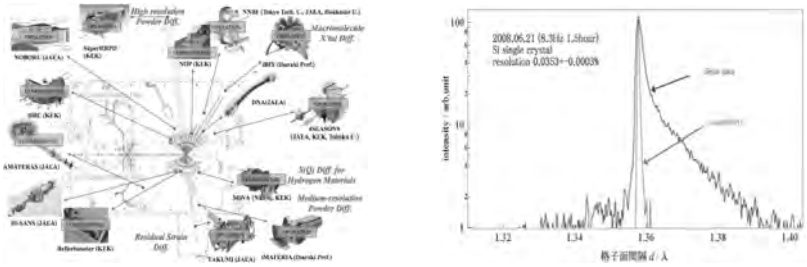

Fig.1 (left) The layout of MLF experimental hall. (right) The measured Bragg reflection at d = 1.36 Å.

MS3-4 The Current Status of Taiwan Photon Source

Yu Wang[2], Mau-Tsu Tang[1], Gwo-Huei Luo[1], Yaw-Wen Yang[1] and Keng S. Liang[1]
[1] *National Synchrotron Radiation Research Center, 101 Hsin-Ann Road, Hsinchu Science Park, Hsinchu 30076, Taiwan, (mautsu@nsrrc.org.tw)*
[2] *Department of Chemistry National Taiwan University, No. 1, Sec. 4, Roosevelt Road, Taipei, 10617 Taiwan (wangyu@ntu.edu.tw)*

A new synchrotron project proposed by NSRRC several years ago, the Taiwan Photon Source, has obtained government approval in June 2007 with a total budget of ~ US$215M for civil and accelerator constructions. The project is aimed to build a low-emittance 3 GeV storage ring for future X-ray research in nano and bio medical sciences. After extensive soil studies and ground vibration survey, among other infrastructure considerations, the current site of NSRRC, which houses the 1.5 GeV Taiwan Light Source, has been chosen for the new synchrotron. The project has now reached some major millstones. The layout of the civil construction is completed and detail architect design is in progress. The major machine parameters have been fixed: a circumference of 518.4 m with a concentric booster, 24 DBA cells with six 12m straights and eighteen 7m straights, a lattice with an emittance of 1.6 nm-rad at high-dispersion and 4.9 nm-rad at zero-dispersion mode. The NSRRC is also soliciting domestic and international scientific proposals for the first-phase beamlines to be built at TPS. In our current schedule, the commissioning of TPS is aimed for late 2013.

MS3-5 Cold Neutron Research Facility at HANARO

Kye Hong LEE[1], Young Ki KIM[1]
[1] *Korea Atomic Energy Research Institute, 1045 Daedeok-daero, Yuseong-gu, Daejejon 305-353, Korea (khlee@kaeri.re.kr)*

The cold neutron research facility (CNRF) project is facing the last year of the project. The cold source has been installed in the reactor core last June and the performance test of He refrigerator has been completed. The process system for cold source has been installed and the first cold neutron beam will be produced this September. The neutron guide in the reactor hall has been installed and aligned and the one in the guide hall is being manufactured and installed before this September so that the neutron instruments can start the performance tests. 8m SANS has been detached from the beam port in August last year so that the cold neutron guide in-pile plug, the primary shutter, and the removable shielding have been installed in high radiation environment in October last year. REF-V will be disassembled at the end of this year and be relocated to the guide hall. The procurement request of in-beam motor part and sample table for Bio-REF will be submitted in July this year. For 40 m SANS, the collimator and vacuum chamber for detectors have been installed and aligned. The dance floor for Cold-TAS is under construction in the guide hall. The chopper and detector tank for DC-ToF is being manufactured. The guide bunker in the guide hall has been completed. Hr SANS is being designed by KIST and will be completed by 2010.

Currently, 7 neutron beam instruments are operating. Thermal-TAS and Bio-diffractometer are being installed in the reactor hall. Hence, there will be 16 neutron beam instruments in 2012 while DC-ToF has a budget problem to secure 352 PSD and detector circuits. The international HANARO Symposium will be held in November 2010 to celebrate the

completion of CNRF project.

Fig. CNRF Project Group in the guide hall

MS3-6 New Facilities for Australian Research: The Australian Synchrotron and the OPAL Research Reactor

Richard F. Garrett
ANSTO, Private Mail Bag 1, Menai, NSW, 2234, Australia

The last 2 years have seen unprecedented new opportunities for Australian science with the opening of two world class major user facilities: the Australian Synchrotron and the OPAL research reactor. Both facilities opened in 2007 have been quickly embraced by the Australian and international research communities with both having well over one thousand registered users.

The Australian Synchrotron is a 3 GeV third generation facility, located in Melbourne, Victoria. Its initial suite of nine beamlines include dedicated Protein Crystallography, EXAFS, powder diffraction, SAXS/WAXS, micro-beam Infra-red and soft X-ray spectroscopy beamlines. A high energy beamline dedicated to imaging and medical therapy is under construction. The OPAL research reactor is a 20 MW swimming pool design reactor with a very compact core delivering high neutron flux. It is located at ANSTO in Sydney, New South Wales, and is designed not only for neutron beam research, but also for radioisotope production and irradiation services. It currently operates 7 instruments on thermal and cold sources beams dedicated to powder diffraction, single crystal diffraction, residual stress and strain, SANS, reflectivity and triple axis inelastic scattering, with two additional instruments under construction.

The capabilities of these two new facilities and plans for future beamlines and instruments will be presented. Some research highlights will also be shown.

MS4-1 Structure of the bacterial flagellum and the mechanism of its self-assembly

Katsumi Imada
Graduate School of Frontier Biosciences, Osaka University, 1-3 Yamadaoka, Suita, Osaka 565-0871, Japan (kimada@fbs.osaka-u.ac.jp)

Gram-negative bacteria, such as *E. coli* and *Salmonella*, swim by rotating a helical filamentous organelle called the flagellum. The flagellum rotates at a speed of 200 to 300 Hz driven by a reversible rotary motor embedded in the cell membrane at the base of the filament. The motor is powered by the electrochemical potential difference of proton across the cell membrane. The torque is generated by rotor-stator interactions coupled with proton translocation through the channel within the stator composed of MotA and MotB. About ten stators are assembled around the rotor and anchored to the peptidoglycan (PG) layer, about 100 Å away from the hydrophobic surface of the cell membrane, by the peptidoglycan-binding (PGB) domain of MotB. The stators dynamically assemble to and disassemble from the functional motor, and proton translocation is activated only when the stator is installed.

The flagellum is a huge molecular assembly made of 20 to 30 thousands of subunits of about 30 different proteins. The rotational part of the flagellar structure can be divided into two classes, the basal body rings and the tubular axial structure. Since the axial structure extends from the cytoplasmic membrane, its component proteins must be exported from the cytoplasm. The protein subunits are synthesized in cytoplasm, are translocated into the central channel of the growing flagellum by the flagellar type III protein export apparatus, which is composed of six transmembrane proteins (FlhA, FlhB, FliO, FliP, FliQ, FliR) and three soluble components (FliH, FliI, FliJ), and then travel through the channel to the growing end for their self-assembly.

Recent structural studies on the stator proteins have provided a possible molecular mechanisms of the motor activation coupled with the stator assembly. The structural studies on the flagellar type III protein export apparatus have demonstrated a remarkable similarity between the the flagllar export apparatus and F_0F_1-ATP synthase. I will show the recent progress of the structural study of the bacterial flagellum and discuss the molecular mechanisms of flagellar self-assembly and the motor activation.

MS4-2 Understanding Cytokine Receptor Signalling

Guido Hansen[1], Tim R. Hercus[2], Jack King-Scott[1], Angel F. Lopez[2], Michael W. Parker[2]
[1] *St. Vincent's Institute of Medical Research, 9 Princes Street, Fitzroy, Melbourne, Victoria 3065, Australia (mparker@svi.edu.au)*
[2] *Division of Human Immunology, Centre for Cancer Biology, Hanson Institute, Adelaide, South Australia 5000, Australia*

The GM-CSF, IL-3 and IL-5 family of cytokines regulates the survival, proliferation, differentiation and functional activation of hematopoietic cells. [1] These same cytokines have also been implicated in multiple pathologies resulting from the excessive or aberrant

expression of the cytokine or their receptors, in conditions such as arthritis, asthma, autoimmunity and leukaemia. The receptors for these cytokines are expressed on the surface of hematopoietic cells and comprise a cytokine-specific alpha subunit and a beta subunit that is common to all three receptors. The alpha subunit binds cytokine with low affinity forming a complex that is able to recruit the beta subunit, converting the binding to a high affinity state. This promotes dimerisation of both subunits which in turns leads to receptor activation although the mechanisms of receptor activation are still quite poorly understood.

We have recently determined the structure of a GM-CSF:receptor ternary complex, representing the first structure of an "activated" receptor of this family of cytokines.[2] Inspection of the structure reveals exciting insights into the mechanism of receptor activation and provides a unifying molecular explanation for the diverse functional properties of related cytokine:receptor systems.

References

1. Hercus, T.R., Thomas, D., Guthridge, M.A., Ekert, P.G., King-Scott, J., Parker, M.W. & Lopez, A.L. (2009) The GM-CSF receptor: linking its structure to cell signaling and its role in disease. *Blood*, in press.
2. Hansen, G., Hercus, T.R., McClure, B.J., Stomski, F.C., Dottore, M., Powell, J., Ramshaw, H., Woodcock, J.M., Xu, Y., Guthridge, M., McKinstry, W.J., Lopez, A.F. & Parker, M.W. (2008) The structure of the GM-CSF receptor complex reveals a distinct mode of cytokine receptor activation. *Cell*, 134, 496-507.

MS4-3 Effector recognition of Rab and Arf family small GTPases in vesicle transport and membrane remodeling

Soichi.Wakatsuki
Photon Factory, IMSS, KEK, Tsukuba, Japan (soichi.wakatsuki@kek.jp)

Vesicle transport is orchestrated by a network of dynamic protein-protein interactions which present as challenging targets for structural biology. Rab and Arf family proteins are involved in various stages of vesicle transport by interacting with effectors which are often multi domain proteins whose domains make specific but transient interactions. The small GTPases are activated by guanine nucleotide exchange factors (GEF). Crystallographic studies on complexes between plant Rab5 GTPases (Ara6&7) and their GEF, Vps9a, in various stages of GDP recognition and its release reveal the atomic details of the activation mechanism. In particular, there is a pivoting motion of the plant Rab5 by about 20 degrees when the complexes are superimposed on Vps9a, which might account for the release of GDP by Vps9a. By inspecting the binding mode of the nucleotide and the available space between the two proteins in the complex structures, a high throughput screening method has been established. Some 14,000 compounds have been screened for activation or inhibition of the GEF function, which yielded dozens of candidates and further investigation is underway.

Once activated, the GTP-bound Arf or Rab can interact with a number of effectors for specific functions such as cellular localization, control of vesicle budding or fusion, and membrane remodeling. The effector/small GTPase specificities are achieved in most cases by the surface

area including Switches I/II and interswitch antiparallel beta sheet. This will be illustrated using crystallographic examples: (1) Arf1 in complex with the N-terminal GAT domain of GGA, (2) Rab11 in complex with the Rab11-binding domain (RBD) of FIP3/Arfophlin-1, dual effector for Rab11 and Arf5/6, and (3) Rab27a with Exophilin4/Slp2-a, a Rab27 effector responsible for melanosome and secretory granules. In these cases, the interswitch beta sheet align parallel to the helices of the effectors, which will orient the effector helices perpendicular to the membrane to reach other partner proteins in the cell. On the other hand, there are cases where the interswitch beta sheet and effector helices lie orthogonal to each other. One remarkable example is a complex between a GTPase and a BAR domain. The complex structure shows a curved surface ideally shaped for bending the target membrane using both the concave surface of the BAR domain as well as the small GTPase itself.

MS4-4 Structural Basis of Transcription: Backtracked RNA Polymerase II

Dong Wang, Roger D. Kornberg
Department of Structural Biology, Stanford University School of Medicine, Fairchild Bldg. D117, 299 Campus Dr. West, Stanford, CA 94305-5126 (dongwang@stanford.edu)

Transcription is the first step of gene expression. During transcription, RNA polymerases oscillate between three stable states, two of which, pre- and post-translocated, were previously subjected to X-ray crystal structure determination. Here we report the crystal structure of RNA polymerase II in the third state, the reverse translocated, or "backtracked" state, which completes the picture of the transcribing enzyme [1].

Backtracking enhances the fidelity of transcription by enabling proofreading of the nascent transcript. It is frequently caused by encountering a DNA lesion or incorporating a mismatched nucleotide. The defining feature of the backtracked structure is a binding site for the first backtracked nucleotide. This binding site is occupied in case of nucleotide misincorporation in the RNA or damage to the DNA, and is termed the "P" site, because it supports proofreading. Defined stable structure of RNA polymerase II backtracked by one residue supports the idea that there is an equilibrium between forward and backward motion during transcription. It also confirms that backtracking by one residue is favorable whereas going back over several residues is not.. The work we present here provides a structural framework for understanding the essential transcription proofreading process.

References

[1] Wang, D., Bushnell, D. A., Westover, K. D., Huang, X. H., Levitt, M. & Kornberg, R. D. Structural basis of transcription: Backtracked RNA polymerase II at 3.4 Å resolution. Science, 324, 1203-1206 (2009)

Structure of RNA-guided RNA Modification Enzymes

MS4-5

Keqiong Ye, Ling Li, Jingqi Duan, Ru Jia, Jinzhong Lin, Minghua Ju, Jin Peng, Anbi Xu, and Liman Zhang
National Institute of Biological Sciences, Beijing 102206, China
(yekeqiong@nibs.ac.cn)

Over one hundred types of chemical modification are introduced at specific sites of cellular RNAs after their transcription. These modifications, which greatly increase the chemical diversity of RNA, are generally beneficial and sometimes even critical for the structure and function of host RNAs. RNA modifications are normally carried out by individual protein enzymes. However, an exception is the large number of pseudouridine and 2'-O-methylated nucleotides in rRNAs, snRNAs, and tRNAs that are synthesized by H/ACA and C/D RNA-protein complexes (RNPs), respectively. In each such complex, a distinct guide RNA belonging to the H/ACA or C/D RNA family determines the substrate specificity by base-pairing with the substrate around the modification site. We are trying to understand the molecular mechanism by which guide RNAs direct RNA modification, with the main goal to determine the crystal structure of H/ACA and C/D RNP and their complex with substrate RNA.

We previously solved the structure of an entire substrate-free H/ACA RNP from *Pyrococcus furiosus* to 2.3 Å (1). The RNP complex comprises a 65-nucleotide H/ACA RNA, pseudouridine synthase Cbf5 and accessory proteins L7Ae, Gar1 and Nop10. In the RNP structure, the H/ACA RNA directly associates with Cbf5, Nop10 and L7Ae and places the bipartite guide sequences, in a flexible conformation, near the active site. Gar1 does not bind RNA, yet sequesters a thump loop of Cbf5. To understand the enzyme in action, we also recently determined the crystal structure of H/ACA RNP with a 14-nt substrate bound at the active site cleft, revealing the mechanism of substrate recruitment (2). Substrate binding leads to a reorganization of a preset pseudouridylation pocket and an adaptive movement of the PUA domain and the lower stem of the H/ACA RNA. Moreover, the thumb loop flips from the Gar1-bound state in the substrate-free RNP structure to tightly associate with the substrate. Mutagenesis and enzyme kinetics analysis suggest a critical role of Gar1 and the thumb in substrate turnover, particularly in product release.

In archaea, a C/D RNA assembles with L7Ae, Nop5, and the methyltransferase fibrillarin into a specific modification enzyme. We have determined the crystal structure of an archaeal C/D RNP composed of all three core proteins and an engineered half guide RNA to 4 Å, as well as two Nop5 protein substructures at higher resolution (3). The C/D RNP structure reveals that the C-terminal domains of Nop5 in the dimeric complex provide symmetric anchoring sites for two L7Ae-associated kink-turn motifs of the C/D RNA. A prominent protrusion in Nop5 appears to be important for guide RNA organization and function, and for discriminating the structurally related U4 snRNA. Multiple conformations of the N-terminal domain of Nop5 and its associated fibrillarin in different structures indicate the inherent flexibility of the catalytic module, suggesting that a swinging motion of the catalytic module is part of the enzyme mechanism. Our results provide insight into the overall organization and mechanism of action of C/D RNA-guided RNA methyltransferases.

References

1. Li, L. and Ye, K. Crystal structure of an H/ACA box ribonucleoprotein particle. Nature 443, 302-307 (2006).
2. Duan, J., Li, L., Lu, J., Wang, W. and Ye, K. Structural mechanism of substrate RNA recruitment in H/ACA RNA-guided pseudouridine synthase. Mol Cell. 34:427-439 (2009)
3. Ye K., Jia R., Lin J., Ju M., Peng J., Xu A. and Zhang L. Structural organization of box C/D RNA-guided RNA methyltransferase. PNAS (In press).

RNA-protein interactions in the core domain of spliceosomal U4 snRNP

MS4-6

Adelaine K.W. Leung[1, 2], Jade Li[1], Kiyoshi Nagai[1]

[1]*Medical Research Council Laboratory of Molecular Biology, Hills Road, Cambridge, CB2 0QH, U.K. (jl@mrc-lmb.cam.ac.uk)*

[2]*Department of Neurobiology, Harvard Medical School, 220 Longwood Avenue, Boston, MA, 02115, USA (Adelaine_Leung@hms.harvard.edu)*

The spliceosome responsible for processing pre-mRNA to mRNA is assembled from U1, U2, and U4/U6-U5 snRNPs (small nuclear ribonucleoprotein particles). The core domain of the U1, U2, U4 and U5 snRNPs is formed when seven Sm proteins (B/B', D1, D2, D3, E, F and G) are assembled into a ring around the Sm site sequence within the particular snRNA. Particle-specific proteins are added to this core to produce mature snRNPs.

The Sm proteins share a conserved sequence motif in two segments, called Sm1 and Sm2, joined by a linker of variable length. We have reconstituted and crystallised the human U4 snRNP core domain comprising the U4 snRNA Sm site with flanking helices and the seven Sm proteins. Crystals belong to space group $P3_1$ with 12 copies of the core domain per asymmetric unit, related by approximate *222* rotational ncs and 3-fold translational ncs in the *a,b*-plane. Using MAD with SeMet labelling of the EFG proteins, the structure was solved initially in $P6_122$ in a reduced unit cell containing one copy per asymmetry unit, by approximating the non-crystallographic symmetries as crystallographic. A partial model was built and used for molecular replacement into the true cell.

The structure at 3.6Å resolution shows the seven Sm proteins forming a closed ring through H-bonding across the Sm1, Sm2 motifs all the way round, and the snRNA threaded through the central pore. In the central pore the seven bases of the U4 Sm site (AUUUUUG) are splayed out, each base bound in a unique pocket formed primarily by one protein. RNA helices flanking the Sm site are located on opposite faces of the ring; the 5' RNA is on the face with the N-terminal protein helices, while the 3' RNA after passing through the ring makes sequence-non-specific interactions with the Sm1-Sm2 linker loops. Compared with the U1 snRNP structure at 5.5Å resolution [1], peripheral regions of the Sm proteins show RNA-dependent conformational differences. These differences, in addition to the snRNA sequence, may provide selectivity for the addition of particle-specific proteins.

References

[1] D A Pomeranz Krummel, C Oubridge, A K W Leung, J Li & K Nagai (2009) *Nature* 458: 475-480. Crystal structure of human spliceosomal U1 snRNP at 5.5 Å resolution.

MS5-1 Recent Progress in X-ray Charge Density Studies of Advanced Materials

Bo Brummerstedt Iversen
Centre for Materials Crystallography, Centre for Energy Materials and iNANO, Department of Chemistry, University of Aarhus, DK-8000 Århus C, Denmark (bo@chem.au.dk)

During the last decade the X-ray charge density method has been revitalized due to major advances in the experimental methods with the availability of area detectors, intense short wavelength synchrotron radiation and stable helium cooling devices. The use of area detectors has greatly increased the data collection speed, and this has made the technique a generally applicable analytical tool. Furthermore, comparative ED studies between related materials are now possible, which may provide insights that cannot be obtained in single system studies. While area detectors primarily produce speed, the latter two developments, synchrotrons and helium cooling devices, produce significant improvements in data accuracy. However, the intense short wavelength synchrotron radiation also has made it possible to tackle experimental charge density studies on complex molecular systems containing heavy atoms and on weakly diffracting microcrystals. The talk will illustrate the application of charge density methods in studies of magnetic coordination polymers [1], polynuclear transition metal systems [2] and photomagnetic systems [3].

References:

[1] (a) Clausen, H. F.; Overgaard, J.; Chen, Y. S.; Iversen, B. B., J. Am. Chem. Soc. 2008, 64, 7988-7996. (b) Poulsen, R. D.; Jørgensen, M. R. V.; Overgaard, J.; Larsen, F. K.; Morgenroth, W.; Graber, T.; Chen, Y.; Iversen, B. B. Chem. Eur. J. 2007, 13, 9775 – 9790. (c) Poulsen, R. D.; Bentien, A.; Chevalier, M.; Iversen, B.B., J. Am. Chem. Soc. 2005, 127, 9156-9166
[2] (a) Overgaard, J.; Schulman C. J.; Stasch. A.; Iversen, B. B. J. Am. Chem. Soc. 2009, 131, 4208–4209. (b) Poulsen, R. D; Overgaard, J.; Schulman, A.; Østergaard, C. D.; Murillo, C. A.; Spackman, M. A.; Iversen, B. B. J. Am. Chem. Soc. 2009, 131, 7580–7591. (c) Overgaard, J.; Clausen, H. F.; Platts, J. A.; Iversen, B. B. J., J. Am. Chem. Soc. 2008, 130, 3834-3843. (d) Overgaard, J.; Larsen, F. K.; Schiøtt, B.; Iversen, B. B. J. Am. Chem Soc. 2003, 125, 11088-11099
[3] Svendsen, H.; Overgaard, J.; Chevallier, M.; Collet, E.; Iversen, B. B. Angew. Chem. Intl. Ed. 2009, 48, 2780-2783

MS5-2 Non-linear Optical Properties and Spin Densities from X-ray Charge Density Measurements

Dylan Jayatilaka[1], P. Munshi[2], M.J. Turner[1], J.A.K. Howard[3], M.A. Spackman[1]
[1] *University of Western Australia, Perth, Western Australia (dylan.jayatilaka@uwa.edu.au)*
[2] *Universite Henri-Poincare, Nancy, France*
[3] *Durham University, Durham, United Kingdom*

According to the Hohenberg-Kohn theorem, the electron density determines the electronic energy and hence all electronic properties of a system. But, in practice, how do we use the electron density to get these properties?

In the X-ray constrained wavefunction approach, a model wavefunction is constrained to

reproduce the X-ray structure factors from a charge density measurement. Electronic properties can then be calculated from this "fitted" wavefunction. The constrained wavefunction approach combines *ab initio* quantum chemistry and X-ray diffraction techniques.

In this talk I will describe the results for obtaining refractive indices, non-linear optical properties [1], and even spin densities from the X-ray constrained wavefunctions [2] applied to molecular crystals. The properties will be compared to measurements from independent electro-optical and polarised neutron diffraction experiments.

References

1. D. Jayatilaka, P. Munshi, M.J. Turner, J.A.K. Howard, M.A. Spackman, *Phys. Chem. Chem. Phys.* **11**, 7209-7218 (2009)
2. D. Jayatilaka, *Phys. Rev. Lett.* **80**, 798-801 (1998); D.J. Grimwood and D. Jayatilaka, *Acta. Cryst* **A 57**, 76-86 (2001); D. Jayatilaka and D.J. Grimwood, *ibid*, 87-100 (2001)

MS5-3 Exploring Halogen -Halogen Interactions via Charge Density Analysis

T. N. Guru Row
Solid State and Structural Chemistry Unit, Indian Institute of Science, Bangalore 560012,India (ssctng@sscu.iisc.ernet.in)

The presence of halogen…halogen intermolecular interactions and their capability in generating supramolecular assemblies has been studied extensively in recent years. The interactions are represented as C-X_1···X_2-C moieties (where X_1 and X_2 are halogens and the geometry is defined as type I, type II and type III based on the values of the angles θ_1=C-X_1···X_2 and θ_2=X_1···X_2-C; distance R_{ij}=X_1···X_2)[1]. These contacts are classified as either attractive or repulsive based on the geometry. However interactions involving organic fluorine have remained controversial issue. Experimental[2] and theoretical[3] charge density analysis will provide the necessary inputs to the understanding of the nature of such halogen…halogen contacts. Several recent examples of charge density analysis on some molecular crystals which display all three types of Halogen –Halogen interactions, in particular C-Cl…Cl -Cand C-F…F-C will be presented in this talk bringing out the evaluation of the nature of such interactions in terms of electron density related properties like net charges, dipole moments and other one electron properties.

References

1. (a) K. Gnanaguru, N. Ramasubbu, K. Venkatesan, and V. Ramamurthy, *J. Org.*Chem., **1985**, 50, 2337.
(b) G. R. Desiraju and R. Parthasarathy, *J. Am. Chem.Soc.* **1989**, 111, 8725.
(c) N. Ramasubbu, R. Parthasarathy, and P. Murray-Rust, *J. Am. Chem. Soc.*, **1986**, 108, 4308.
2. A. Volkov, P. Macchi, L. J. Farrugia, C. Gatti, P. Mallision, T. Richter and T. Koritsanszky, *XD2006,* **2006**.
3. R. Dovesi, V. R. Saunders, C. Roetti, R. Orlando, C. M. Zicovich-Wilson, F. Pascale, B. Civalleri, K. Doll, N. M. Harrison, I. J. Bush, Ph D'Arco and M. Linuell, *CRYSTAL06*, University of Torino, **2006**.

MS5-4 Challenge to Atomic Orbital Visualization by 0.2A Resolution Synchrotron Radiation Single Crystal Experiment

Hiroshi Sawa, Eiji Nishibori, Shinobu Aoyagi
Department of Applied Physics, Nagoya University, Nagoya, 464-8603, Japan
(z47827a@cc.nagoya-u.ac.jp)

An ultimate goal of the structure analysis is determination of the charge density distribution in the unit cell of crystal. There are various types of accurate structural analysis method, the multi-pole refinement, anharmonic thermal factor refinement, Bader topological analysis, and maximum entropy method. If you use these analyses, common attention to experimental conditions of X-ray diffraction is necessary. Those conditions are high statistical accuracies and high Q resolution in diffraction data.

The high stability of X-ray is obtained by the Top-up driving mode in SPring-8. Almost constant ring current produces extremely steady X-ray to the diffraction experimental system because the thermal loading of an optical component may become constant. A new large cylindrical camera was set up as an X-ray diffractometer for a single crystal at the beamline, BL02B1/SPring-8. In conceptual design, the image plate (IP) was selected as the detector, because IP detector not only takes care until high 2θ angle for one shot but also statistically observe the reliable data.

The functional transition metal complexes are currently attractive in the investigation of degree of freedom of *d*-orbital and charge. The statistically reliable and high resolution data is demanded to lead the exact orbital resolution of *d*-electron configuration. The resolution of 0.2A is necessary to determine the *d*-orbital that differs from *p*-orbital and occupies a narrow range of the space. These conditions are achieved by the high stability and parallel of a synchrotron radiation X-ray.

Recently, we have carried out various types of accurate structural studies. The main targeted materials are strong correlated transition metal oxides, organic conductors, endohedral fullerenes, and so on. The single crystal data of multiferroic transition metal oxide has been observed using high energy X-ray enough for order resolution of *d*-electron configuration. The method of orbital resolution was developed by the combination of maximum entropy method and multi-pole analysis.

MS5-5 MEM Electrostatic Potential Imaging

Hiroshi Tanaka
Dept. of Materials Science, Shimane University 1060, Nishi-kawatsu-cho, Matsue, Shimane, 690-8504, Japan
(h.tanaka@riko.shimane-u.ac.jp)

Recently, we developed a new method evaluating the electrostatic potential from x-ray diffraction data by using the MEM (Maximum Entropy Method) [1]. In this method, electrostatic potential is divided into the contribution from nuclear charge and that from electron charge. The former is estimated by ordinary Ewald's method, while the later is

evaluated by the MEM charge density in the reciprocal lattice (structure factor). It is a key point that we can soundly extrapolate the structure factor by MEM up to the reciprocal lattice points needed for the convergence of the calculation.

The electrostatic potential is sensitive to the number of valence electrons and/or electron polarization at atomic level. Then, our method is useful for the analysis of ionic crystals such as ferroelectric [1], charge transfer[2], and charge ordering materials [3].

For example, Fig. 1 shows the isosurface of charge density for $Nd_{0.5}Sr_{0.5}MnO_3$ colored by the amplitude of electrostatic potential in gray scale. It is known that this material shows charge order transition at 150K. After the transition, the Mn ions are separated into the Mn^{3+} ions and the Mn^{4+} ions. It is clearly shown in the figure that the electrostatic potential is higher around the Mn^{4+} ions than around Mn^{3+} ions corresponding to the difference in the valence between the two ions.

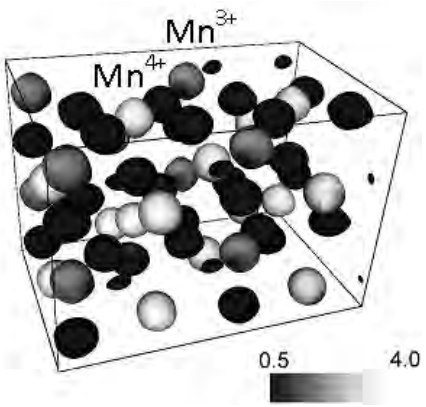

Fig.1 Isosurface of charge density for Nd0.5Sr0.5MnO3 colored by the amplitude of electrostatic potential in gray scale from 0.5 e/Å (black) to 4.0 e/Å (white).

Acknowledgements: *This work was financially supported by the X-ray Free Electron Laser Utilization Research Project and by a Grant-in-Aid for Scientific Research from the Ministry of Education, Culture, Sports, Science and Technology, Japan.*

References

[1] H. Tanaka, Y. Kuroiwa, and M. Takata, Phys. Rev. B74, 172105 (2006).
[2] K. Katoh, et al., J. Phys. Soc. Jpn. 76, 123602 (2007).
[3] K. Katoh, et al., Phys. Rev. B77, 081101 (2008).

MS5-6 Photo-induced structure determination and electron density study by MEM of Spin Crossover complex $[Fe(abpt)_2(NCS)_2]$

Che Hsiu Shih[1,2], Chou Fu Sheu[3], Kunihisa Sugimoto[2,4], Jungeun Kim[2,4], Kenichi Kato[2,4], Yu Wang[3], Masaki Takata[1,2,4]
1. University of Tokyo, 7-3-1 Hongo Bunkyo-kyu, Tokyo, Japan. 113-8654.
2. RIKEN, Harima, Japan.
3. National Taiwan University, Taipei Taiwan.
4. Japan Synchrotron Radiation Research Institute (JASRI)/SPring-8.
(karu@spring8.or.jp)

Molecular multi-stability has attracted an increasing interest in the context of functional materials. To study the relationship between crystal structure and functions allows gaining new insights into novel material design. Spin Crossover (SCO) materials are one of light-switchable molecular system. We have investigated the photo-induced (PI) switching process in SCO complex $Fe(abpt)_2(NCS)_2$ (abpt = 4-amino-3,5 bi(pyridine) 1,2,4-triazole) through the crystal structure determination and its charge density study by Maximum Entropy Method (MEM). For the precise structure analysis of photo-induced phase transition, we collected the high resolution data at BL02B1/SPring-8. The PI spin transition of $Fe(abpt)_2(NCS)_2$ was taken place under 532nm green light laser irradiation from low spin (LS) to high spin (HS) at cryogenic temperature. We could hold sufficiently stable HS state by PI at 35 K using helium gas flower cooling device during data collection. The single crystal data was collected on the maximum resolution of 0.6 Å (R_{int}=3.49%) using high brilliant and stable synchrotron radiation X-ray source and large cylindrical Image Plate camera, and the data was refined to R_1=3.35% , GOF =1.054 for 13094 unique observed reflections. The Light Induced Excited Spin State Trapping (LIESST) effect gives the extension of the Fe-N bond length by ~0.2 Å based on electronic configuration transition $e_g^0\ t_{2g}^6$(LS) → $e_g^2\ t_{2g}^4$ (HS). The results of SQUID and infrared spectroscopy are reasonable with precise structure analysis. The difference of electron density distribution between ground state and PI meta-stable state could be directly visualized by MEM. In our presentation, we will show the direct observation of electron density distribution by MEM and discuss about the electron configuration between GS and PI meta-stable states.

Keywords: LIESST, photo-induced single-crystal-single-crystal-transformation. MEM charge density

MS6-1 Recent Developments in Coherent Diffractive Imaging Instrumentation and Applications

Andrew G. Peele[1,2]
[1] Department of Physics, La Trobe University, 3086, Australia (a.peele@latrobe.edu.au)
[2] Australian Research Council, Centre of Excellence for Coherent X-ray Science

Coherent diffractive imaging (CDI) has the potential to become an important high resolution microscopy technique. Potential applications include projection and 3D imaging of biological and advanced materials samples. While much of the impetus for the development of CDI has come from the promise of high brightness from a new generation of x-ray source – the x-ray

free electron laser – there are many applications possible at 3rd generation synchrotron sources.

Keyhole FCDI image of a fusebay region in an integrated circuit with resolution at 20 nm. Image from B. Abbey et al "Quantitative Coherent Diffractive Imaging of an Integrated Circuit at a Spatial Resolution of 20 nm" Appl. Phys. Lett. 93, 214101, (2008)

CDI relies on the detection of photons scattered to relatively high angles (at least in a small angle scattering sense). At a 3rd generation source, where long exposures are required to collect sufficient high angle photons, it is important to develop very efficient data collection and analysis methods. In terms of analysis methods relevant problems include overcoming stagnation issues in the iterative solution methods used to phase the measured diffraction patterns and overcoming the requirement for the sample to be small and isolated.

Introducing phase curvature into the illumination alters the nature of the diffraction pattern by removing the translational invariance seen in the far field diffraction pattern for plane wave illumination. In this "Fresnel" CDI method we have been able to show that stagnation is greatly ameliorated. In addition, the known illumination function can be used to define an isolated region within a larger sample – allowing "Keyhole Fresnel CDI" to be used to mosaic an image of extended objects. A further advantage includes the ability to compete against the degrading effects of poor spatial coherence by using appropriately chosen illuminating curvature. We also describe our results dealing with the case of illumination that is not simply monochromatic, as can be seen in a single XFEL pulse.

The application of these methods requires the development of a new class of instrument with extremely strict tolerances on the relative stability between the optics producing the phase curvature in the illumination and the sample. We describe the dedicated endstation at beamline 2-ID-B at the Advanced Photon Source that has been developed to meet these needs.

We demonstrate our successful application of our instrumentation and methods to the imaging of biological and materials samples and discuss the implications of our results for imaging protein structures.

MS6-2

Visualization of Bio-Structures Using Coherent X-Ray Diffraction

Yoshinori Nishino[1], Kazuhiro Maeshima[2], Naoko Imamoto[3], Ryuta Hirohata[4], Eiichiro Matsubara[4], Yukio Takahashi[5], Tetsuya Ishikawa[1]
[1]*RIKEN SPring-8 Center, 1-1-1 Kouto, Sayo-cho, Sayo-gun, Hyogo 679-5148, Japan (nishino@spring8.or.jp, ishikawa@spring8.or.jp)*
[2]*Structural Biology Center, National Institute of Genetics, Shizuoka 411-8540, Japan (kmaeshim@lab.nig.ac.jp)*
[3]*Cellular Dynamics Laboratory, RIKEN, Saitama 351-0198, Japan (nimamoto@riken.jp)*
[4]*Department of Materials Science and Engineering, Kyoto University, Kyoto 606 8501, Japan (e.matsubara@materials.mbox.media.kyoto-u.ac.jp)*
[5]*Graduate School of Engineering, Osaka University, Osaka 565-0871, Japan (takahashi@prec.eng.osaka-u.ac.jp)*

We report our studies on X-ray diffraction microscopy (XDM) for biological samples. XDM requires no lenses, and a sample image is directly reconstructed from the coherent diffraction data. It is ideal X-ray phase-contrast imaging with no contrast degradation due to lenses. XDM is especially useful for observing internal structures of thick objects, such as cells or cell organelles, thanks to high penetrating power of X-rays.

The first biological application of XDM was for Escherichia coli bacteria cells [1]. The internal distribution of the proteins stained with manganese oxide was two-dimensionally imaged. In the image reconstruction, the Fourier transform of a lower-resolution sample image observed under a full-field soft X-ray transmission microscope was used to make up for missing coherent X-ray diffraction data near-forward direction. The missing data problem was later solved by improvements of microscope instruments to reduce parasitic scattering noise [2,3] and also by improvements of the phase retrieval algorithm, e.g. the iterative normalization algorithm [4]. These improvements have made it possible to reconstruct a sample image only from the coherent diffraction data.

Recently, we succeeded in observing an unstained human chromosome in three dimensions [5]. This is the first three-dimensional electron density mapping of a cell organelle by using hard X-rays. It is important because XDM is directly connected with X-ray crystallography, which is currently the most powerful method of the atomic structure analysis for proteins. The observed images reveal an axial structure with high electron-density in the chromosome, which other microscopic methods have been unable to visualize under unstained condition. Such mesoscopic-scale structures as cell organelle have been difficult to be observed, although molecular structures of their components like DNA and histone proteins could be studied by X-ray crystallography or electron microscopy. Our result experimentally demonstrates the high imaging ability of coherent X-ray diffraction for unstained biological specimens, which are almost transparent to X-rays, opening a novel and strong means of exploring cellular structures.

References

[1] Miao J., Hodgson K.O., Ishikawa T., Larabell C.A., LeGros M.A., Nishino, Y., Proc. Natl. Acad. Sci. USA **100**, 110 (2003).
[2] Nishino Y. et al., IPAP Conference Series, Proceeding of 8th International Conference on X-Ray Microscopy **7**, 386 (2006).

[3] Nishino Y. et al., IPAP Conference Series, Proceeding of 9th International Conference on X-Ray Microscopy, to be appeared.
[4] Nishino Y., Miao J., Ishikawa T., Phys. Rev. **B 68**, 220101 (2003).
[5] Nishino Y., Takahashi Y., Imamoto N., Ishikawa T., Maeshima K., Phys. Rev. Lett. **102**, 018101 (2009).

MS6-3 Phase imaging using a liquid cell in a transmission x-ray microscope

Gung-Chian Yin

MS6-4 Improved Accuracy Laue Neutron Diffraction

Ross Piltz, Alison Edwards
Bragg Institute, ANSTO, PMB 1, Menai NSW 2234, Australia (rop@ansto.gov.au)

Koala is a neutron Laue diffractometer designed for rapid data collection from single crystals with primitive cell lengths up to 30Å. The high speed is achieved using a cylindrical image-plate detector with 3-π coverage and a white beam via super-mirror guides from a thermal moderator. While the use of image-plates and a white beam ensures rapid data collection, it also creates several problems in obtaining accurate intensities for structure refinement. Structure refinements using this technique commonly have wR2 about 15% due to systematic errors via inadequately corrected intensity data.

An improved set of intensity corrections has been devised based on the wavelength, spatial, and time dependent behavior of neutron-sensitive image-plates. The intensity correction also includes wavelength dependent absorption and extinction effects. The result is a 50% reduction in wR2 for model systems, greater accuracy for atomic parameters, and greater ability to distinguish between competing structural models.

A comparison of structural refinements will be presented for well characterized samples as well as a selection of user program samples. The latter provide a snap shot of current Koala experiments: resolving oxidation states potentially misassigned due to the presence of hydride; hydrogen position and motion for supramolecular framework compounds; superlattice structure of $BiRe_2O_6$; comparison of the $Ba(Re,Y,Tb)Co_4O_x$ family of materials.

MS6-5 Development and Application of Neutron 2D-Counter for Crystal and Magnetic Structure Analysis

Y. Noda[1], C-H. Lee[2], M-K. Moon[2], S-A. Kim[2], Y. Ishikawa[1], H. Kimura[1] and R. Kiyanagi[1]
[1] *Institute of Multidisciplinary Research for Advanced Materials, Tohoku University, 2-1-1 Katahira, Aobaku, Sendai 980-8577, Japan (ynoda@tagen.tohoku.ac.jp)*
[2] *HANARO, Korea Atomic Energy Research Institute, 150 Deokjin-dong, Yuseong-gu, Daejeon 305-353, Korea (leech@kaeri.re.kr)*

Neutron single crystal structure analysis is very powerful tool to investigate accurate position of light atoms such like Oxygen and Hydrogen. Neutron is also very sensitive for magnetic

structure. Thus, neutron single crystal experiment is indispensable for crystal and magnetic structure analysis for complicated magnetic system in multiferroics. The only difficulty is the lack of efficiency of the measuring time. Usually it requires long beam time, and sometimes, it is impossible to carryout.

In order to overcome such low efficiency on single crystal neutron experiments, we have developed a large two dimensional position sensitive neutron counter (2D-PSD), and applied to structure analysis. We have started from the small size of a flat 2D-PSD for evaluation study, and extended the size until 1m x 0.5m of the active area. Fig.1 shows the 2D-PSD installed at KAERI-HANARO. As the test experiment, standard samples NaCl and $Tb_3Fe_5O_{12}$ (TbIG) are used. In Fig.2, the result of the structure analysis for TbIG is shown, as the comparison of $|Fcal|^2$ vs $|Fobs|^2$. The rotation speed of the crystal is 0.4 degree/min, and 120 degree is covered. Exposure time is 5 hours. TbIG is a body centered cubic lattice with the lattice constant 12.44A. Within this short time measurement, 962 Bragg points are covered including 181 absent Bragg reflections by symmetry.

This work has been supported by a Grant-In-Aid for Scientific Research (A) No. 21244051, from the Ministry of Education, Culture, Sports, Science and Technology, and also by National Research Foundation and Ministry of Education, Science & Technology, Korean government through its National Nuclear Technology R&D Program.

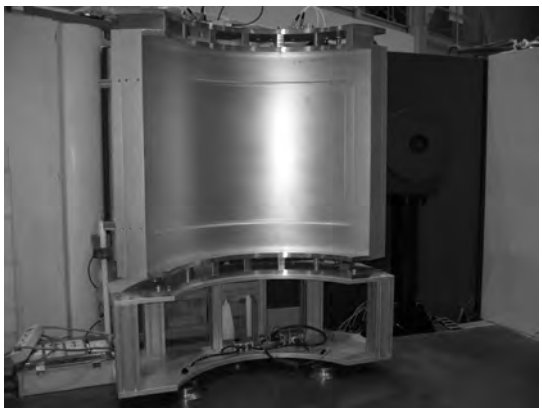

Fig.1 Neutron 2D-PSD

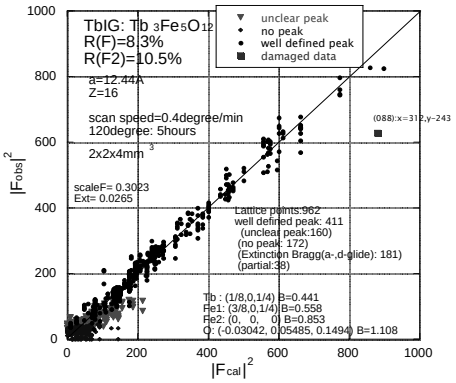

Fig.2 Result for TbIG

MS6-6 State-of-the-art Multilayer Optics for Modern X-ray Analytics

J. Wiesmann, T. Samtleben, C. Michaelsen, B. Hasse, J. Graf, F. Hertlein
Incoatec GmbH, Max-Planck-Straße 2, D-21502 Geesthacht, Germany (administration@incoatec.de)

In this contribution, we give an overview on current developments of multilayer optics for diffractometry in the lab as well as for synchrotron applications. We explain the manufacturing process of the optics, summarize the different types of optics and give some examples of typical applications which benefit from the new possibilities, especially in combination with modern microfocus X-ray sources for diffractometry.

The optics consist of bent substrates with shape tolerances below 100 nm, upon which multilayers are deposited with single layer thicknesses in the nanometer range and up to several hundreds of layer pairs. The multilayers were designed with lateral thickness gradients within ± 1% deviation of the ideal shape. We use sputtering technology for deposition, optical profilometry in order to characterize the shape and X-ray reflectometry in order to characterize the multilayer thickness distribution both laterally and as in-depth. The microstructure is investigated by transmission electron microscopy. The beam parameters like monochromaticity, flux, brilliance and divergence demonstrate the quality of the multilayer optics used for different applications in the home-lab as well as at synchrotrons.

We will present actual results of a combination of our new microfocus source IμS with a new type of 2-dimensional beam shaping multilayer optics. These so called Quasar Optics are now developed for different wavelengths like Cu, Mo, Ag and Cr. They shape a focused or a collimated beam with a very high flux density as well as an adequate divergence directly at the sample position. Optics are also available, which focuses in one dimension and collimates in the other. This delivers a line-shaped beam profile. Some applications realized with an IμS are (GI)SAXS, texture, stress analysis, μ-diffraction or single crystal diffractometry to name but a few.

MS7-1 Structure and Mechanism of An Amino Acid Antiporter

Xiang Gao, Feiran Lu, Lijun Zhou, Jiawei Wang, and Yigong Shi
Center for Structural Biology, School of Life Sciences, Tsinghua University, Beijing 100084, China

Virulent enteric pathogens such as *Escherichia coli* strain O157:H7 rely on acid resistance (AR) systems to survive acidic environment in the stomach. A major component of AR is an arginine-dependent arginine:agmatine antiporter that expels intracellular protons. Here we report the crystal structure of AdiC, the arginine:agmatine antiporter from *E. coli* O157:H7 and a member of the amino acid/polyamine/organocation (APC) superfamily of transporters a. The overall fold is similar to that of several Na^+-coupled symporters. AdiC contains 12 transmembrane segments, forms a homodimer, and exists in an outward-facing, open conformation in the crystals. A conserved, acidic pocket opens to the periplasm. Structural and biochemical analysis reveals the essential ligand-binding residues, defines the transport route, and suggests a conserved mechanism for the antiporter activity.

MS7-2 The structure of human connexin 26 gap junction channel

Shoji Maeda[1], So Nakagawa[1], Michihiro Suga[1], Eiki Yamashita[1], Atsunori Oshima[2], Yoshinori Fujiyoshi[2], Tomitake Tsukihara[1,3]
[1] *Institure for Protein Research, Osaka University, 3-2 Yamadaoka, Suita, Osaka-fu, Japan (maesyou@protein.osaka-u.ac.jp)*
[2] *Dept. of Biophysics, Graduate School of Science, Kyoto University, Oiwake, Kitashirakawa, Sakyo-ku, Kyoto, 606-8502, Japan*
[3] *Picobiology Institute, Graduate School of Life Science, University of Hyogo, Kamigohri, Akoh, Hyogo 678-1297, Japan*

Gap junctions consist of arrays of intercellular channels between adjacent cells that permit the exchange of ions and small molecules. Here, we report the crystal structure of the gap junction channel formed by human connexin-26 (Cx26) at 3.5 Å resolution and discuss structural determinants of solute transport through the channel (Figures). The density map revealed the two membrane-spanning hemichannels and the arrangement of the four transmembrane helices of the six protomers forming each hemichannel. The hemichannels feature a positively charged cytoplasmic entrance, a funnel, a negatively charged transmembrane pathway, and an extracellular cavity. The pore is narrowed at the funnel, which is formed by the six N-terminal helices lining the wall of the channel, which thus determining the molecular size restriction at the entrance of the channel. The structure of the Cx26 gap junction channel also has implications for the gating of the channel by the transjunctional voltage.

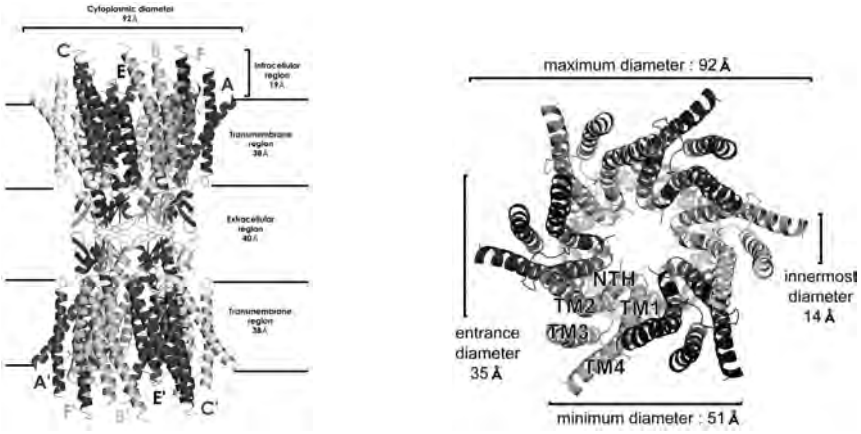

Figure. Structure of the Cx26 gap junction channel. The corresponding protomers in the two hemichannels are shown in the same color. (left) Side view of the Cx26 gap junction channel. (right) Top view of the Cx26 gap junction channel showing the arrangement of the transmembrane helices.

MS7-3 The role of AmtB-GlnK complex in nitrogen regulation

Xiaodan Li*[1], Fritz Winkler[1], Mike Merrick[2]
[1] *Paul Scherrer Institute, 5232 Villigen, Switzerland (xiao.li@psi.ch)*
[2] *Department of Molecular Microbiology, John Innes Centre, Norwich NR4 7UH, United Kingdom.*

Ammonia is an important nitrogen source for bacteria, fungi and plant, therefore its regulation in the cell is essential and important. Ammonia exists in two forms at physiological condition,

namely as ammonia gas (NH_3) and ammonium ion (NH_4^+). Under nitrogen deficiency condition, the gene encodes the ammonia channel protein (AmtB) from *E. coli* and is strictly subjected to nitrogen control. AmtB is expressed and inserted into membrane in order to make sure that the bacteria get enough nitrogen for their growth. Once the bacteria have enough nitrogen, the expression of AmtB protein will stop and also the existing AmtB will be blocked by the de-uridylylated regulation protein GlnZ. We have solved the structure of AmtB as well as AmtB-GlnZ complex structures at atomic resolution and have studied the function of AmtB protein and relevant mutants. From our structural and functional studies, we conclude that AmtB protein works as an ammonia channel with an ammonium binding site and both conserved histidines are essential for optimum substrate conductance. The de-uridylylated GlnZ interacts with AmtB via a long surface loop containing Y51 (T-loop), the tip of the T-loop inserts deeply into the cytoplasmic pore exit of AmtB, blocking ammonia conduction. GlnK interacts with AmtB almost exclusively via a long surface loop containing Y51 (T-loop), the tip of which inserts deeply into the cytoplasmic pore exit, blocking ammonia conduction. Y51 of GlnK is also buried in the pore exit, explaining why uridylylation of this residue prevents complex formation.

MS7-4 Structure and function of A-ATPase: combining electron microscopy and X-ray crystallography to study a transmembrane rotary motor complex

Lawrence K. Lee[1], Alastair G. Stewart[1], Mhairi Donohoe[1], Olga Esteban[2], Ricardo A. Bernal[3] & Daniela Stock[1]

[1] *Victor Chang Cardiac Research Institute, 405 Liverpool St, Darlinghurst NSW 2010, AUSTRALIA (d.stock@victorchang.edu.au)*

[2] *MRC Laboratory of Molecular Biology, Hills Rd, Cambridge CB2 2QH, UK*

[3] *Department of Chemistry, The University of Texas at El Paso, 500 West University, El Paso, Texas 79968, U.S.A.*

Proton translocating ATPases are central to biological energy conversion. While eukaryotes contain specialised F-ATP synthases for ATP synthesis and V-ATPases for proton pumping, eubacteria and archaea typically contain only one enzyme for both tasks. Although many eubacteria contain H^+-ATPases of the F-type, some eubacteria and all known archaea contain ATPases of the A-type. A-ATPases are closely related to eukaryotic V-ATPases, but simpler in design and thus more amenable for structural studies. We are using a low-resolution 3D reconstruction from electron micrographs as an envelope to build a composite model of the intact A-ATPase from high-resolution X-ray structures of individual subunits. We have now fitted eight of the nine different subunits, which has given us ample insights into the function of this intricate molecular machine.

References

1. Ricardo A. Bernal & Daniela Stock (2004) "Three Dimensional Structure of the Intact *Thermus thermophilus* H^+-ATPase/Synthase by Electron Microscopy" *Structure* **12**, 1789-1798.
2. Hisayoshi Makyio, Ryota Iino, Chiyo Ikeda, Hiromi Imamura, Masatada Tamakoshi, Momi Iwata, Daniela Stock, Ricardo A. Bernal, Elisabeth P. Carpenter, Masasuke Yoshida, Ken Yokoyama & So Iwata (2005) "Structure of a central stalk subunit F of prokaryotic V-type ATPase/synthase from *Thermus thermophilus*" *EMBO J.* **24**, 3974-3983.

3. Ingmar Schäfer, Susanne M. Bailer, Monika G. Düser, Michael Börsch, Ricardo A. Bernal, Daniela Stock & Gerhard Grüber (2006) "Crystal Structure of the Archaeal A_1A_O ATP Synthase Subunit B from *Methanosarcina mazei Gö1*: Implications of Nucleotide-binding Differences In the Major A_1A_O Subunits A and B" *J. Mol. Biol.* **358**, 725-740.
4. Olga Esteban, Ricardo A. Bernal, Mhairi Donohoe, Hortense Videler, Michal Sharon, Carol V. Robinson & Daniela Stock (2008) "Stoichiometry and localisation of the stator subunits E and G in *T. thermophilus* H^+-ATPase/synthase." *J. Biol. Chem.* **283**, 2595-2603.

MS7-5 Crystal Structure of Bacterial Nitric-oxide Reductase, a Key Enzyme in the Respiratory Evolution

Yushi Matsumoto[1,2], Shingo Nagano[1], Yoshitsugu Shiro[1]
[1]*Division of Protein Chemistry, Post-genome Science Center Medical Institute of Bioregulationm Kyushu University, Japan, (ymatsumoto@bioreg.kyushu-u.ac.jp)*
[2] *RIKEN SPring-8 Cente, Japan*

Nitrous oxide (N_2O), a major non-carbon dioxide greenhouse gases, is mainly produced in soils through microbial processes. Nitric oxide reductases (NORs) produce N_2O from nitric oxide (NO) and are involved in nitrate respiration and denitrification where stepwise reduction of nitrate (NO^{3-}) to molecular nitrogen is coupled to energy production1. Cytochrome oxidase and NOR belong to the same superfamily of heme-copper oxidases and NOR is generally considered to be the evolutionary progenitor to cytochrome oxidases. To date, several crystal structures of cytochrome oxidase have been solved, but there is no known crystal structure of NOR thereby limiting our understanding of nitrate respiration, denitrification, and molecular evolution of respiratory enzymes. Here we report the first crystal structure of *Bacillus stearothermophilus* NOR and its complex with an electron donor analogue 2-heptyl hydroxyquinoline *N*-oxide (HQNO) at 2.5- and 2.7-Å resolution, respectively. The overall structure of the transmembrane region and the position of the metal centers are similar to those of cytochrome oxidase clearly indicating an evolutionary relationship. However, a His-Tyr covalent linkage in the binuclear center found in cytochrome oxidases is not found in NOR. In addition, two highly conserved Glu residues not present in cytochrome oxidase may provide protons required for NO reduction. These differences create a relatively larger substrate binding pocket capable of binding two NO molecules. In contrast to previous predictions1, there is no obvious proton transfer pathway from the extracellular side to the active site. These and other structural similarities and differences provide new insight into NO reduction and suggest how this enzyme evolved for O_2 reduction, which was essential step in the evolution of respiration.

MS8-1 Engineering Organic Crystals Using Arene-Perfluoroarene Interactions

Todd B. Marder
Department of Chemistry, Durham University, South Road, Durham, DH1 3LE, UK (todd.marder@durham.ac.uk)

Arene-arene interactions play a critical role in a number of important areas of chemistry, biology and materials science including, for example, influencing protein structures, charge

transport in organic field effect transistors (OFETs), light emission from aromatic luminophores, etc. The main motifs arise from face-to-face or edge-to-face interactions, with edge-to-edge interactions often being neglected. Interestingly, whilst benzene and hexafluorobenzene (HFB) exhibit similar crystal structures dominated by alternating edge-to-face stacking, and both compounds have melting points of ca. 5°C, in 1960, Patrick and Prosser showed[1] that a 1:1 mixture of the two compounds melts at ca. 24 °C. It was subsequently shown that a 1:1 co-crystal is formed comprising alternating face-to-face stacks of the C_6H_6 and C_6F_6 molecules, although there is a lateral slippage of the rings. Thus, the ring centroids are not directly 'on top' of one another, i.e., the vector connecting the ring centroids is not normal to the ring planes. Whilst subsequent studies focused predominantly on co-crystals of HFB with other 6-membered arenes, we have concentrated our efforts on the following areas: (1) controlling the solid-state organization of mono-disperse phenylene-ethynylene oligomers; (2) examining the influence of arene-perfluoroarene interactions on liquid crystal phase behaviour; and (3) exploring the limits of the use of such interactions as synthons with respect to the sizes and shapes of the two components in binary co-crystals, and the incorporation of substituents with various steric and electronic properties. The latter issues are important for potential applications involving 'molecular recognition' effects in which the fluoroarene might be required to be tethered to another group. The talk will address these issues with examples[2-9] drawn from our work on conjugated rigid-rods, disk-like polycyclic aromatics and heterocycles, and will discuss potential applications as well as current thinking on the nature of the interaction.

References

1. C. R. Patrick and G. S. Prosser, *Nature*, **187**, 1021, 1960.
2. C. Dai, P. Nguyen, T. B. Marder, A. J. Scott, W. Clegg, and C. Viney, *Chem. Commun.*, 2493, 1999.
3. J. C. Collings, K. P. Roscoe, R. Ll. Thomas, A. S. Batsanov, L. M. Stimson, J. A. K. Howard, and T. B. Marder, *New J. Chem.*, **25,** 1410, 2001.
4. J. C. Collings, K. P. Roscoe, E. G. Robins, A. S. Batsanov, L. M. Stimson, J. A. K. Howard, S. J. Clark, and T. B. Marder, *New J. Chem.*, **26**, 1740, 2002.
5. C. E. Smith, P. S. Smith, R. Ll. Thomas, E. G. Robins, J. C. Collings, C. Dai, A. J. Scott, S. Borwick, A. S. Batsanov, S. W. Watt, C. Viney, J. A. K. Howard, W. Clegg, S. J. Clark, and T. B. Marder, *J. Mater. Chem.*, **14**, 413, 2004.
6. S. W. Watt, C. Dai, A. J. Scott, J. M. Burke, R. Ll. Thomas, J. C. Collings, C. Viney, W. Clegg, and T. B. Marder, *Angew. Chem. Int. Ed.*, **43**, 3061, 2004.
7. J. C. Collings, A. S. Batsanov, J. A. K. Howard, D. A. Dickie, J. A. C. Clyburne, H. A. Jenkins and T. B. Marder, *J. Flourine Chem.,* **126**, 515, 2005.
8. I. A. I. Mkhalid, D. N. Coventry, D. Albesa-Jové, A. S. Batsanov, J. A. K. Howard, R. N. Perutz, and T. B. Marder, *Angew. Chem. Int. Ed. Engl.*, **45**, 489, 2006.
9. A. S. Batsanov, I. A. I. Mkhalid, and T. B. Marder, *Acta Crystallogr.*, **E63**, o1196, 2007.

MS8-2 Proton Dynamics in Hydrogen-bonded Organic Solids from Protonic Dielectrics to Proton-motor

Tadashi Sugawara[1], Kentaro Suzuki[1]
Dept. of Basic Science, Graduate School of Arts and Science, University of Tokyo, Japan (suga@pentacle.c.u-tokyo.ac.jp)

The tautomerization of 3-hydroxyenones in the solid state is generally frozen at lower temperatures due to the anti-parallel ordering of dipolar moments of individual tautomers.

However we found that such tautomerization of 5-bromo-9-hydorxyphenalenone in the crystal was not suppressed even at 4 K due to the quantum proton-tunneling in the symmetrical double well of the proton potential on the basis of the symmetrical crystal environment [1, 2].

These findings prompted us to measure the temperature and frequency dependence of the ac dielectric permittivity of single crystals of bisquaric acid (**H_2BSQ**). This hydrogen-bonded crystal exhibited dielectric response ($\varepsilon' = 180$ at 800 Hz at 290 K) due to the movement of protonic solitons along the intermolecular hydrogen bond [3].

More distinct dielectric property was observed in a hydrated crystal of bis(squaryl)biphenyl (**BSQB**·4H_2O). The squaryl group and four water molecules form a hybrid 1D-hydrogen bonded chain. The dielectric permittivity showed a distinct frequency dependence ($\varepsilon' = 4.7 \times 10^4$ at 340 K and 1 kHz), suggesting that the proton-rely transmitted along the infinite hydrogen-bonded chain in crystal [4]. Proton transfer along this artificial system provides important insight into the mechanism of the active proton transport that membrane proteins exhibit.

Recently we found that oleic acid formed multilamella tubular vesicle of a helical structure in a buffered water solution at pH = 8.0. Surprisingly this helix spontaneously rewound in water, associating with the movement of the kink that is a movable boundary between helical domains [5]. If the mode of undulation of the membrane due to the local stress, which is caused by the difference in the effective volumes of oleic acid and oleate, is transmitted in phase, macroscopic dynamics, such as winding and unwinding a helix, will emerge. The dynamics could be regarded as a molecular motor in a sense that the local undulation is converted to the rational motion promoted by the concerted exchange of protons and counter anions (Na^+) between facing oleic acid and oleate across a thin water layer between bilayer membranes.

References

1) T. Mochida, A. Izuoka, T. Sugawara, et al., *J. Chem. Phys*., 101, 7971-7974 (1994)
2) R. Kiyanagi, A. Kojima, H. Kimura, Y. Noda, et al. *J. Phys. Soc. Jpn*., 74, 613-620 (2005)
3) I. Takasu, T. Sugawara, T. Mochida, *J. Phys. Chem. B,* 108 (48), 18495-18499 (2004)
4) H. Terao, T. Sugawara, Y. Kita, N. Sato, et al., *J. Am. Chem. Soc.*, 123, 10468-10474 (2001)
5) M. Ishimaru, T. Toyota, K. Takakura, T. Sugawara, Y. Sugawara, *Chem. Lett.,* 34(1), 46-47 (2005)

MS8-3 Structure–Property Correlations: Mechanical Properties of Molecular Crystals

C. Malla Reddy,[1, 2] Michael T. Kirchner,[2] K. Anantha Padmanabhan,[3] Gautam R. Desiraju[2]
[1] *Indian Institute of Science Education and Research, Kolkata, Nadia, West Bengal; 741 252 (cmreddy@iiserkol.ac.in)*
[2] *School of Chemistry, University of Hyderabad, Hyderabad 500046*
[3] *Department of Mechanical Engineering, Anna University, Chennai 600025*

The typical organic crystal is generally known to be brittle and is susceptible to deformation or breakage on application of a mechanical stress. In our study, it was found that some of the organic crystals may be sheared through crystal layers like pack of cards, and some other bent

plastically.[1-2] A survey of over 60 molecular crystals helped us to establish a causative correlation between the mechanical properties and crystal packing.[3] Based on the observed mechanical properties and the crystal structures, the crystals divided into three categories; (1) shearing, (2) bending and (3) brittle. Crystals with parallel layered (4 or 8 Å) structure having strong *intra*layer and weak *inter*layer interactions could be sheared on application of a mechanical stress. Bending occurs when the strength of intermolecular interactions in orthogonal directions is significantly different. Isotropic crystals with comparable intermolecular interactions in the three orthogonal directions are "cross-linked" and do not bend; they are hard and brittle.

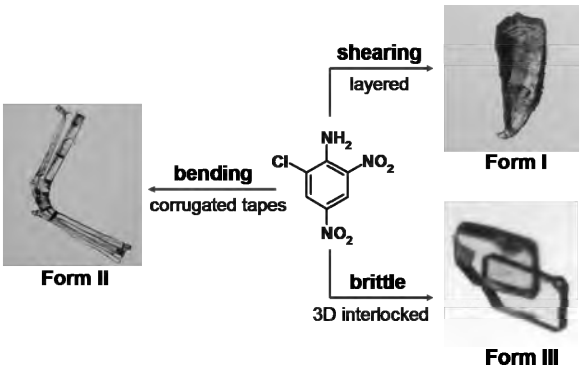

References

1. C.M. Reddy, S. Basavoju, and G.R. Desiraju, *Chem. Commun.*, (2005) 2439.
2. C.M. Reddy, R.C. Gundakaram, S. Basavoju, M.T. Kirchner, K.A. Padmanabhan and G.R. Desiraju, *Chem. Commun.*, (2005) 3945.
3. C.M. Reddy, K.A. Padmanabhan, and G.R. Desiraju, *Cryst. Growth Des.*, **6** (2006) 2720.

MS8-4 Polymorph and Pseudopolymorph of Co-crystal: Controlling Formation and Structural Transformation

Miao Du,* Xiu-Juan Jiang, Min Tang
College of Chemistry and Life Science, Tianjin Key Laboratory of Structure and Performance for Functional Molecule, Tianjin Normal University, Tianjin 300387, P. R. China (dumiao@public.tpt.tj.cn)

Both co-crystal and polymorphism are attractive topics in crystal engineering of organic supramolecular solids. In the past years, ee have made a systematic investigation on the co-crystal system of different carboxylic acids and bent dipyridyl tectons with an oxadiazole spacer.[1] In this course, hydrothermal technique that is widely used in synthesizing inorganic and inorganic-organic hybrid crystalline materials, has been demonstrated to be a suitable approach in preparation of such co-crystals. On the other hand, further studies indicate that polymorph of co-crystal may be readily obtained under different synthetic conditions when related dipyridyl building blocks with multiple H-bonding sites are applied.[2] In our recent continuous effort, controlling formation of several polymorph and pseudopolymorph of a co-crystal system as well as the salt-co-crystal continuum has been well realized by adjustment of the crystallizing temperature. In addition, possible structural transformation between these multi-component complexes will also be presented.

References

1. (a) M. Du, Z.-H. Zhang, X.-J. Zhao, *Cryst. Growth Des.* **2005**, 5, 1199–1208. (b) M. Du, Z.-H. Zhang, X.-J. Zhao, *Cryst. Growth Des.* **2005**, 5, 1247–1254. (c) M. Du, Z.-H. Zhang, X.-J. Zhao, H. Cai, *Cryst. Growth Des.* **2006**, 6, 114–121. (d) M. Du, Z.-H. Zhang, X.-J. Zhao, *Cryst. Growth Des.* **2006**, 6, 390–396.
2. (a) M. Du, Z.-H. Zhang, X.-G. Wang, H.-F. Wu, Q. Wang, *Cryst. Growth Des.* **2006**, 6, 1867–1875. (b) M. Du, X.-J. Jiang, X. Tan, Z.-H. Zhang, H. Cai, *CrystEngComm* **2009**, 11, 454–462.

***Acknowledgements**: This work was supported by the National Natural Science Foundation of China, Program for New Century Excellent Talents in University and Tianjin Normal University.*

MS8-5 Towards knowledge-based design & control of pharmaceutical crystal forms

Colin R. Groom, Peter T. A. Galek, Peter A. Wood
Cambridge Crystallographic Data Centre, Cambridge, UK (groom@ccdc.cam.ac.uk)

The pharmaceutical industry is becoming increasingly concerned with better control of the solid form of drugs due to the financial risks represented by possible polymorphism and the potential improvements in physicochemical properties that could be afforded by utilising co-crystallisation. The Cambridge Structural Database (CSD, [1]) now contains half a million crystal structures and the wealth of information this provides is highly relevant to all aspects of Crystal Engineering and the understanding of intermolecular interactions at a fundamental level. The accessibility and application of relevant data is of prime importance when investigating issues like polymorphism and co-crystal design.

Recent software advances [2] have broadened the opportunities for using the CSD in the design and control of crystal forms. Analysis of a large family of pharmaceutical co-crystals containing a consistent API component [3] utilising this software has provided a great deal of insight into intermolecular interactions in general as well as co-crystal design in particular. Further specific work exploring the propensity for hydrogen-bond formation [4] has highlighted the importance of the CSD in estimating the relative stabilities of pharmaceutical polymorphs.

References

1. Allen, F. H. A; *Acta Cryst. B*, 2002, 58, 380-388.
2. Macrae, C. F.; Bruno, I. J.; Chisholm, J. A.; Edgington, P. R.; McCabe, P.; Pidcock, E.; Rodriguez-Monge, L.; Taylor, R.; van de Streek, J.; Wood, P. A.; *J. Appl. Cryst.*, 2008, 41, 466-470.
3. Childs, S. L.; Wood, P. A.; Rodriguez-Hornedo, N.; Reddy, L. S.; Hardcastle, K. I.; *Cryst. Growth Des.*, 2009, 9, 1869-1888.
4. Galek, P. T. A.; Fábián, L; Motherwell, W. D. S.; Allen, F. H. A; Feeder, N; *Acta Cryst. B*, 2007, 63, 768-782.

MS9-1 A small/wide-angle X-ray scattering instrument for structural characterizations with soft matter, nanomaterials, and air-liquid interfaces

U-Ser Jeng,[1] Chiu Hun Su,[1] Chun-Jen Su,[1] Kuei-Fen Liao,[1] Wei-Tsung Chuang,[1] Ying-Huang Lai,[2] Je-Wei Chang,[2] Yi-Jiun Chen,[2] Yu-Shan Huang,[1] Ming-Tao Lee,[1] Kuan-Li Yu,[1] Din-Goa Liu,[1] Zia-Fung Chang,[1] Chin-Yen Liu,[1] Chien-Hung Chang,[1] Keng S. Liang[1]

[1] *National Synchrotron Radiation Research Center, 101 Hsin-Ann Road, Hsinchu Science Park, Hsinchu 300,Taiwan, (usjeng@nsrrc.org.tw)*

[2] *Department of Chemistry, Tunghai University, Taichung, 407, Taiwan*

At the National Synchrotron Radiation Research Center (NSRRC) a small/wide-angle X-ray scattering (SAXS/WAXS) instrument has been installed to the BL23A beamline with a superconducting wiggler insertion device. With the two monochromators incorporated into one rotating cradle for fast exchange, the X-ray beam can be monochromatized either by the double Si(111) crystal monochromator (DCM) for high energy resolution ($\Delta E/E \approx 2\times10^{-4}$) in the energy range of 5-23 keV, or by the double Mo/B_4C multilayer monochromator (DMM) for 10-30 times higher photon flux of ~2×10^{11} photons/s in the 6-15 keV range. A plane Si mirror is especially installed to selectively deflect the beam downwards with an appropriate incident angle for grazing-incidence SAXS (GISAXS) with air-liquid/liquid-liquid interfaces. Synchronized SAXS and WAXS measurements are achieved via a data acquisition protocol that can integrate two linear gas detectors for WAXS and an area detector (gas type or MAR165 CCD) for SAXS; the protocol also incorporates sample change and temperature control for programmable data collection. The post-sample section is comprised of the vacuum bellow system, beamstop system, and detector systems, all situated on a motorized optical bench for motion in 6 degrees of freedom. In particular, the 4-m vacuum bellow system of 260 mm inner diameter provides convenient and continuous changes of the sample-to-detector distance under vacuum. The performance of the instrument is illustrated via the measurements of several on-going projects of different classes, including (1) simultaneous SAXS/WAXS and differential scanning calorimetry for polymer crystallization, (2) structural evolution with a large ordering spacing of ~200 nm in a supramolecular complex, (3) SAXS for polymer blends under in situ drawing, (4) SAXS and anomalous SAXS for unilamellar lipid vesicles and metalloprotein solutions, (5) anomalous grazing incidence SAXS (GISAXS) for oriented membranes of Br-labeled lipids embedded with peptides, and (6) GISAXS for silicate films in situ formed at the air-water interface.

MS9-2 Surface and flow induced ordering of complex fluids

W.A. Hamilton[1], L. Porcar[2], P.D. Butler[3] and G.G. Warr[4]

[1] *Bragg Institute, Australian Nuclear Science and Technology Organisation, Lucas Heights, NSW 2234, Australia (wha@ansto.gov.au)*

[2] *Large Scale Structures Group, Institut Laue-Langevin, Grenoble, France*

[3] *National Institute of Standards and Technology, Center for Neutron Research, Gaithersburg, MD 20899, USA*

[4] *School of Chemistry, University of Sydney, Sydney, NSW 2006, Australia*

Over the last few decades an ever increasing number of soft matter systems have been shown (or engineered) to exhibit a degree of ordering and symmetry traditionally associated with

inorganic crystals – most obviously in the self-assembly of controlled polymer systems. Another area in which more order exists than might have been expected is in colloid systems. The name itself means gluelike (from the Greek "κόλλα") and was given to the class by the father of colloid science, English physicist Thomas Graham, to distinguish the inchoate characteristics of its members from those of the more obviously ordered "crystalloids". Over the last ten years or so using both small angle neutron scattering and reflectometry our group has probed the response of complex fluid colloidal structures to anisotropic ordering conditions – either under flow or constrained by a proximate surface - or in Poiseuille flow a combination of both. In a number of cases we have found that the increased order imposed under such conditions does result in a more regular arrangement of some rather flexible and extended self-assembled structures than is observed under static conditions, and that the responses of these systems to these conditions can reveal some of the finer details of their dynamics.

MS9-3 Intimate Relationship between Micro-phase Separation and Crystalline Phase Transitions in Polyethylene- Poly(ethylene Oxide) Diblock Copolymer as Viewed by Synchrotron SAXS/WAXD and IR/Raman Measurements

Kohji Tashiro[1], Weiyu Cao[1], Makoto Hanesaka[1], Hiroyasu Masunaga[2], Sono Sasaki[2] and Masaki Takata[2]

[1] *Department of Future Industry-oriented Basic Science and Materials, Toyota technological Institute, Tempaku, Nagoya 468-8511, Japan (ktashiro@toyota-ti.ac.jp)*

[2] *Japan Synchrotron Radiation Institute (SPring-8)*

Among the various kinds of diblock copolymers, the crystalline-crystalline diblock copolymers should show complicated behaviors since there occur two types of structural changes: (i) the structural changes in the crystalline lattices of each polymer domains and (ii) the morphological changes in higher-order structure of these domains (micro-phase separation). In the present paper we describe the details of these structural changes (i) and (ii) for polyethylene-poly (ethylene oxide) (PE-*b*-PEO) diblock copolymer [$H(CH_2CH_2)_m(OCH_2CH_2)_nOH$, EmEOn], one of the most typical crystalline diblock copolymers. There have been reported quite limited papers so far, in which only the order-disorder change of lamellar structure was described (L.Sun *et al*. *Polymer* **2004**, *45*, 8181; R. V. Castillo *et al*., *Macromolecules* **2008**, *41*, 879). We have found out the complicated morphological changes between lamella-(perforated lamella)-gyroid-cylinder-sphere phases in the heating and cooling processes on the basis of simultaneously-measured synchrotron SAXS/WAXD data. At the same time the infrared and Raman spectral data revealed the phase transition of PE phase between orthorhombic-hexagonal-melt phases (W-Y Cao *et al.*, *J. Phys. Chem. B*, **113,** 2338, 8495 (2009)). For example, Figure 1 shows the intimate relationship between the structural changes (i) and (ii) clarified for E39EO86 sample. One of the most noticeable points is that the lamella-to-gyroid transition occurs even when the PE parts are still in the orthorhombic crystal phase (PEO parts are already melted). It is difficult in general to imagine such a

remarkable morphological change as long as the crystalline component remains in the sample. The temperature dependent Raman spectral measurement clarified that the PE chains experience thermally-activated motion even in the orthorhombic phase. In this way the thermal motion of chain segments is found to be one important factor for the mesoscopic phase transition phenomenon. In the case of E131EO171 sample with longer chain segments, the morphological transition did not occur at all and only the order-disorder transition was observed in the lamellar phase. The quantitative analysis of SAXS data revealed that the PE chain segments are once folded on the lamellar surface. The Raman measurement told us that the thermal motion was not active even at high temperature. Therefore, it may be reasonably said that the existence of folded chain structure depresses the thermal motion of PE chains, prohibiting the morphological changes from the lamellar structure. In this way the micro-phase transition phenomena of PE-*b*-PEO diblock copolymers are governed by such important factors as thermal mobility and folded structure of PE chain segments in addition to the conventionally-discussed volume ratio between PE and PEO segmental parts. This new idea of "folded chain structure" as one important factor helps us to understand the reason why the general crystalline diblock copolymer with relatively long chain segments does not show any complicated transitions from lamella to gyroid and cylinder phases.

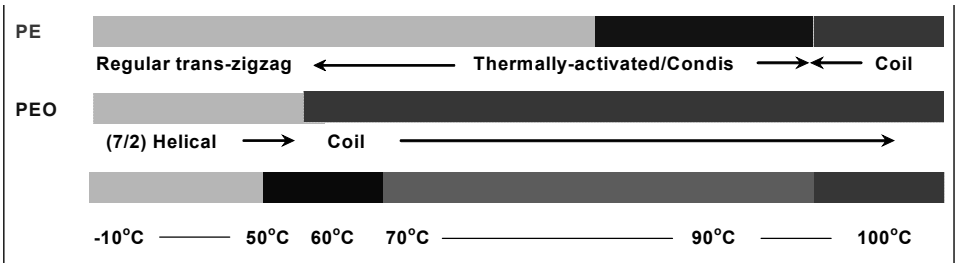

MS9-4 The Quokka Small Angle Neutron Scattering Instrument at OPAL

Richard F. Garrett, Elliot P. Gilbert, William A. Hamilton and Kathleen Wood
ANSTO, Private Mail Bag 1, Menai, NSW, 2234, Australia

Quokka is a 40m small angle neutron scattering instrument installed on the cold source of the OPAL research reactor operated by ANSTO. The source – sample distance is selectable from 1 – 20 metres via a series of neutron super-mirror guides, and the sample to detector distance is continuously variable over the same range. Coupled with a standard operating neutron wavelength of 5Å, this produces a q range of .0008 to 0.8 $Å^{-1}$. The heart of the instrument is a $1m^2$ 2-D wire detector with 5mm pixels. In addition to the standard 20-position automatic sample changer, a wide range of sample environment equipment is available including variable temperature cryostats and furnaces, cryo-magnets capable of fields up to 11T, a rapid heat/quench cell, and standard shear and stirring cells.

Quokka is one of the flagship instruments at OPAL and is attracting users from a wide range of research disciplines, from polymers/soft matter to complex fluids and condensed matter physics. In the Australian context it is a key instrument for a number of food science

projects investigating proteins, polymers and emulsions. Construction and commissioning of Quokka was completed in the first half of 2009, and the instrument was made available to general users for the first time in the May 2009 proposal round. It attracted intense interest from the Australian and international research community with instrument time requests far exceeding the available time.

The capabilities and performance of Quokka will be presented, along with highlights from the first experiments.

MS9-5 The effect of interface on the crystallization behavior of Poly(3-hydroxybutyrate) ultra-thin film revealed by grazing incident X-ray dffraction

Xiaoli Sun,[1, 2] Harumi, Sato,[1] Yukihiro Ozaki, [1]Shouke Yan, [2*]Isao Takahashi[1*]
1 Faculty of Science and Technology, Kwansei-Gakuin University, Sanda, Hyogo 6691337, Japan (suikyo@kwansei.ac.jp)
2 State Key Laboratory of Chemical Resource Engineering, Beijing University of Chemical Technology, Beijing 100029, China. (skyan@mail.buct.edu.cn)

Poly(3-Hydroxybutyrate) (PHB) is one of the most intensively studied crystalline biodegradable polymers. In the present study, crystallization behavior of PHB ultra-thin film with different interface was investigated by the out-of-plane grazing incident X-ray diffraction (GIXD). On the substrate of Si(100) wafer capped by natural oxide, only (020) Bragg reflection is observed at $2\theta = 13.56°$. The orientation of b-axis in the thin PHB film is leaded by the mobile surface layer in the polymer-air interface. However, on the surface of hydroxyl Si, another Bragg reflection around 23.05° appears in the GIXD profile. This may be induced by the hydroxyl group which has an interaction with the C = O group in the PHB helical chains. When polystyrene (PS) is covered on the surface of PHB (i.e. sandwiched structure of Si-oxide/PHB/PS), crystallization of PHB was not significantly affected. However, the sandwiched structure of hydroxyl-Si/PHB/PS, (020) Bragg reflection disappears and only the reflection around 23.05° is observed.

References

1. Mori,K.; Mukoyama, S.; Zhang, Y.; Sato, H.; Ozaki, Y.; Terauchi, H.; Noda, I.; Takahashi, I. Macromolecules 2008, 41, 1713
2. Capitan, M. J.; Rueda, D. R.; Ezquerra, T. A. Macromolecules 2004, 37, 5653
3. Toney, M. F.; Russell, T. P.; Logan, J. A.; kikuchi, H.; Sands, J. M.; Kumar, S. K. Nature, 374, 709

MS10-1 Tracking ligand migration pathways in carbonmonoxy myoglobin at cryogenic temperatures

Shin-ichi Adachi
Photon Factory, KEK, 1-1 Oho Tsukuba, Ibaraki, 305-0802, Japan (shinichi.adachi@kek.jp)

In general, protein crystallography reveals static structures of proteins. However, in order to explore the mechanism of protein function, it is also crucial to unveil their dynamic structures. For example, myoglobin (Mb) is a small oxygen storage protein in muscle, which reversibly binds gas ligands (O_2, CO, NO etc.) at the heme iron site deeply inside the protein matrix. Ligand dissociation can be easily triggered by photo-irradiation [1], and the ligand binding reaction in Mb has been studied by using various techniques. In particular, the photolysis of carbonmonoxy myoglobin (MbCO) in crystal has been extensively studied by X-ray diffraction experiments (e.g. Laue diffraction at room temperature and monochromatic X-ray diffraction at cryogenic temperatures [2, 3]). Although many details are known regarding gas ligand molecules trapped in internal hydrophobic cavities in Mb, there exists no direct evidence to show the dynamic properties of migration pathways connecting these cavities. In order to explore these pathways in Mb, we have carried out cryogenic X-ray crystallographic investigations of native sperm whale MbCO under photo-irradiation. Our method of continuous illumination of MbCO crystals with pulsed laser light at cryogenic temperatures has allowed the production of a movie of ligand migration in Mb on the time scale of several hours [4]. The whole data collection was done at beamline NW14A at the PF-AR, KEK [5]. The experimental details and the dynamic nature of the ligand migration pathways will be discussed.

References

[1] Q. H. Gibson, *J. Physiol.*, **134**(1956)112.
[2] F. Schotte *et al.*, *Science*, **300** (2003) 1944.
[3] T. Y. Teng *et al.*, *Nature Struct. Biol.*, **1** (1994) 701.
[4] A. Tomita *et al.*, *Proc. Nat. Acad. Sci. USA*, **106** (2009) 2612.
[5] S. Nozawa *et al.*, *J. Synchrotron Rad.*, **14** (2007) 313.

MS10-2 Exploring the conformational energy landscape of acetylcholinesterase by kinetic crystallography

Jacques-Philippe Colletier, Benoît Sanson, Didier Fournier, Joel L. Sussman, Israel Silman, Dominique Bourgeois and Martin Weik.
[1] *Institut de Biologie Structurale, CEA/CNRS/UJF 41 rue Jules Horowitz, 398027 Grenoble, France (colletier@ibs.fr; benoit.sanson@ibs.fr; dominique.bourgeois@ibs.fr; weik@ibs.fr)*
[2] *Institut de Pharmacologie et de Biologie Structurale, CNRS, 218 Route de Narbonne, 31400 Toulouse, France (didier.fournier@ipbs.fr)*
[3,4] *Departments of Structural Biology and Neurobiology, Weizmann Institute of Science, 76100 Rehovot, Israel (joel.sussman@weizmann.ac.il; israel.silman@weizmann.ac.il).*

Acetylcholinesterase (AChE) is a very rapid enzyme, essential in the process of nerve impulse transmission at cholinergic synapses [1]. It is the target of most currently approved anti-Alzheimer drugs [1] and further progress in the modulation of its activity requires

structural as well as dynamical information. The set of conformations accessible to AChE for the formation of complexes [2] indeed pre-exists in the conformational energy landscape of the native enzyme [3], a point of particular interest in the quest for "tailor-made", more efficient drugs [4].

Three experimental approaches will be outlined, which have allowed gaining structural insights into the dynamics of this captivating enzyme. We will first describe a steady-state approach for determining atomic-resolution structures of enzyme/substrate complexes, which has allowed to structurally follow the traffic of substrates within the active site of AChE [5,6]. Shall then be described a new kinetic-crystallography strategy in which a photolabile precursor of the enzymatic product is cleaved in-crystallo by means of UV-laser irradiation, and the molecular motions necessary for the expulsion of photolysis-products to occur triggered and quenched by temperature-controlled X-ray crystallography [7]. Last, we will present a novel yet extremely simple approach for following in "real-time" the traffic of enzymatic products in crystalline enzymes, and discuss the results obtained on AChE [8].

The relevance of these results as to permit a detailed description of the traffic of substrates and products within acetylcholinesterase will be discussed, as well as the provided insights into its conformational energy landscape[9].

References

1. Silman I and Sussman JL. (2005) ***Curr Opin Pharmacol***, **5**, 293-302.
2. Colletier J.P., Sanson B., Nachon F., Gabellieri E., Fattorusso C., Campiani G. and Weik M. (2006) ***J Am Chem Soc***, **128**, 4526-4527.
3. Xu Y., Colletier J.P., Weik M., Jiang H., Moult J., Silman I. and Sussman J.L. (2008) ***Biophys J***, **95**, 2500-2511.
4. Xu Y., Colletier J.P., Jiang H., Silman I., Sussman J.L. and Weik M. (2008) ***Protein Science***, **17**, 601-605.
5. Stojan J., Brochier L., Alies C., Colletier J.P. and Fournier D. (2004) ***Eur J Biochem***, **271**, 1364-1371.
6. Colletier J.P., Fournier D., Greenblat H.M., Sussman J.L., Zaccai G., Silman I. and Weik M. (2006) ***EMBO J***, **25**, 2746-2756.
7. Colletier J.P., Royant A., Sanson B., Specht A., Nachon F., Masson P., Zaccai G., Sussman J.L., Goeldner M., Silman I., Bourgeois D. and Weik M. (2007) ***Acta Crystallogr D***, **63**, 1115-1128.
8. Colletier J.P., Bourgeois D., Fournier D., Silman I., Sussman J.L. and Weik M. (2008) ***Proc Natl Acad Sci USA***, **105**, 11742-11747.
9. Colletier J.P and Weik M. (2007) ***Ann Pharm Fr***, **65**, 108-118

MS10-3 Structure of HIV-1 protease in complex with inhibitor KNI-272 determined by neutron crystallography

Motoyasu Adachi[1], Ryota Kuroki[1]

[1] *Japan Atomic Energy Agency, Tokai, Ibaraki, 319-1195, Japan (adachi.motoyasu@jaea.go.jp)*

Neutron crystallography will provide us important structural information to elucidate catalytic mechanism of enzymes through observation of hydrogen atoms in catalytic residues. We have recently determined a crystal structure of HIV-1 protease by neutron crystallography. HIV-1 protease is a dimeric aspartic protease that cleaves the nascent polyproteins of HIV-1 and plays an essential role in viral replication. Althogh the development of HIV-1 protease

inhibitors is regarded as a major success of structure-based drug design and contributes to establish highly active anti-retroviral therapy for AIDS, the catalytic mechanism of HIV-1 protease has still been a matter of some devate. To further understand the catalytic mechanism of HIV-1 protease, we have determined the crystal structure of HIV-1 protease in complex with a transition state mimetic tripeptide inhibitor, KNI-272 to 1.9 Å resolution by neutron crystallography in combination with 1.4 Å resolution X-ray diffraction data (Figure 1) [1]. Our results indicates that the carbonyl group of allophenylnorstatine (Apns) in KNI-272 forms a significant hydrogen bond with protonated Asp 25, and the hydrogen atom from the hydroxyl group of Apns forms a remarkable hydrogen bond with the deprotonated Asp125 (Figure 2). These results show direct evidence that Asp25 provides a proton to carbonyl group of substrate and Asp125 contributes to activate the attacking water molecule as a nucleophile.

Figure 1. Tertiary structure of HIV-1 protease determined by neutron diffraction

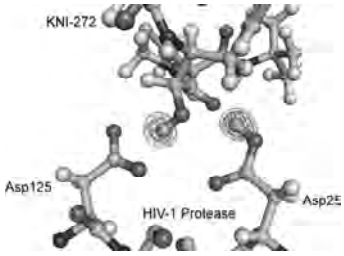

Figure 2. Nuclear Density of the hydrogen atoms seen in the catalytic site of HIV-1

Reference

M. Adachi et al. Proc. Natl. Acad. Sci. USA, 106, 4641-4646 (2009).

MS10-4 Taking the edge off: The softer side of in-house SAD phasing

Joseph D. Ferrara, James W. Pflugrath, Cheng Yang
Rigaku Americas Corporation, The Woodlands, Texas, USA
(joseph.ferrara@rigaku.com)

The phase problem in macromolecular crystallography has been mitigated dramatically in recent years by advances in methodology and instrumentation. SAD phasing has now become the primary *de novo* phasing method. A search of the PDB of structures released in 2007 reveals the number of structures solved by SAD phasing exceeds those solved by MAD for the first time. A number of these examples of successful S-SAD and Se-SAD phasing used Cr radiation (λ = 2.29 Å), which can double the anomalous signal of sulphur and selenium compared to Cu radiation.

This report reviews recent results from phasing with the enhanced anomalous signal provided by Cr radiation to demonstrate this longer wavelength can be used to solve *de novo* structures. Selenium, as the heavy atom, with Cr radiation can provide sufficient anomalous scattering for routine phasing. Cr radiation opens a new path to extracting the weak anomalous signal from sulphur to phase native protein data. With the addition of Cr radiation to the crystallographer's toolkit, in-house X-ray sources can routinely provide at least two

wavelength options. The combination of diffraction data collected using both Cu (λ = 1.54 Å) and Cr radiation can improve the electron density tremendously. Anomalous scattering from sulphur can also assist in molecular replacement solutions. Finally, the data collected with Cr radiation can be used to refine a structure. Ultimately, this makes it possible to solve a protein structure with a single data set.

This in-house phasing approach we describe has been given the label "**know before you go**" by John Rose and B.C. Wang at the University of Georgia. This method improves the efficiency of the solution of macromolecular crystal structures and usage of the synchrotron beam time.

MS10-5 Reductive methylation of surface lysines assists crystallization of proteins

Neil Shaw, Chongyun Cheng, Zhi-Jie Liu
National Laboratory of Biomacromolecules, Institute of Biophysics, Chinese Academy of Sciences, Beijing 100101, China

A pure, homogenous protein sample may not guarantee a 3D structure. Often the side chains of surface residues like lysines and glutamic acids are dis-ordered and hinder the formation of a crystal or interfere in the packing of the molecules in the lattice. Chemical modification of a protein using a reductive methylation protocol[1, 2], results in the addition of 2 methyl groups to the side chain amine nitrogen of lysine residues. The methyl groups have been observed to physically bridge the distance between the amine nitrogen and carboxyl group of glutamic acids, resulting in the formation of cohesive (NZ)CH…O contacts[3]. (NZ)CH…O contacts help localize the side chains and make the protein compact. Analytical ultracentrifugation analysis and thermal denaturation studies reveal a more compact protein structure with better solvent exclusion of buried tryptophan residues in the folded state of the methylated protein, assisting crystallization[3].

Examples of proteins that have been successfully crystallized in our laboratory by methylating the side chain amine nitrogen of lysine residues will be discussed.

References

1. Neil Shaw, Chongyun Cheng, and Zhi-Jie Liu. Procedure for reductive methylation of protein to improve crystallizability. *Nature Protocols* DOI: 10.1038/nprot.2007.287 (2007).
2. Rayment, I. Reductive alkylation of lysine residues to alter crystallization properties of proteins. *Methods in Enzymology* 276, 171-179 (1997).
3. Neil Shaw, Chongyun Cheng, Wolfram Tempel, Jessie Chang, Joseph Ng, Xin-Yu Wang, Sarah Perrett, John Rose, Zihe Rao, Bi-Cheng Wang, Zhi-Jie Liu. (NZ)CH...O Contacts assist crystallization of a ParB-like nuclease. *BMC Struc. Biol.* 7, 46-58 (2007).

MS10-6 Improvement of a new rotation function for molecular replacement by designing new scoring functions such as relative entropy and dynamic correlation coefficient

Fan Jiang, Wei Ding
Institute of Physics, Chinese Academy of Sciences, 8 South St. No.3, Zhong Guan Cun, Haidian District, Beijing, 100190, China (fjiang@aphy.iphy.ac.cn)

As structural genomics progresses, automatic structure determination using molecular replacement method has becoming increasingly important. This has spurred more development of both the search engine and the automatic intelligent pipeline for molecular replacement, such as AMORE, MOLREP, PHASER, Mr.Bump and so on.

Previously we have introduced a new rotation function for the rotation search of the molecular replacement method [1]. In this new method, the atomic coordinates of the search model is directly matched with the Patterson map of the target crystal. The goodness of matching is measured by several scoring functions such as product of atomic and map weights, correlation coefficient of atomic and map weights, relative R-factor of atomic and map weights, and so on. The signal-to-noise ratio of the matching is enhanced by first averaging the peaks of all possible matches and then optimizing a set of weights by linear regression method to obtain a combined score of all the individual matching functions. We have found that the set of weights optimized from local search around the correct solution can be generalized to global search with reasonably good results. This set of weights should at least applicable for a given model and a target crystal with known space group and cell parameters. We also found the set of weights optimized depends on the crystal form. This will greatly limit the applicability of our new rotation function when applying to an unknown target crystal form.

In this work, we propose a new method of calculating the correlation coefficient for each rotation angle sampled in the rotation function search, and this "dynamic" correlation coefficient is used as the value of our new rotation function. So the set of weights are optimized dynamically and locally instead of globally for a given target crystal, this will reduce the dependence of the weights on the crystal form. In addition, we add two new matching scoring functions: the relative entropy between the model weights and the Patterson map weights, and the mean-square residue between the model weights and the map weights. The relative scales between the model and map weights are such to minimize their differences in distribution. We found that our new rotation function was applicable to a number of crystal structures extracted PDB with experimental diffraction data.

References

1. Fan Jiang (2008) A new rotation function for molecular replacement by using both the self and cross Patterson vectors. Acta Cryst. D64, 561-566.

MS10-7 New and Underused Methods for X-ray Crystallography at Low Resolution

Yong Xiong
Department of Molecular Biophysics and Biochemistry, Yale University, New Haven, CT 06511, USA

The challenge for X-ray crystallography at low resolution. While crystals of many important macromolecules/complexes are often obtained, they frequently only diffract to low resolutions, leading to a large amount of available data unused. For example, structural genomic centers produced 11547 unique crystals in the past four years; however, only 3417 have resulted in structures, all at a resolution higher than 3.5 Å [1]. Similarly, only the most experienced structural biology labs will use only low-resolution data to pursue structure determination. Of the greater than 13,000 unique crystal structures deposited in the PDB to date, only about 150 structures have been determined at a resolution lower than 3.5 Å, fewer than 10 of which are lower than 4 Å.

Theoretically, detailed amino acid side chain information exists even in the range of 3.5-5 Å resolutions. We have demonstrated in practice that the theoretical limit is achievable with adequate treatment of the computation factors affecting the resolution [2]. These general but underused techniques can have an immediate impact on structural analysis of macromolecular complexes.

Sharpening, is an effective method to correct the electron density blurring caused by motion or displacement of molecules in the crystal, with a typical symptom of high B-factors. Despite its proven success, it is practiced only by a small number of research groups. Our survey of the PDB depositions shows that the vast majority of crystal structures determined at a resolution lower than 3 Å could have been sharpened to produce an electron density map with enhanced details, which is crucial for atomic model building by reducing the uncertainty of main chain connectivity and side chain assignment. However, even in 2009, few published structures have used the sharpening technique. We have implemented a correlation-based method to standardize the procedure and determine the optimal sharpening factor. In addition, we are extending capability of the technique to perform domain-wise sharpening. The optimized sharpening method will significantly increase the likelihood and accelerate the pace for structure determination of macromolecular complexes at low resolution.

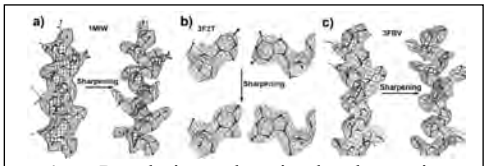

Fig. 1 Resolution-enhancing by sharpening.

A general use of multi-crystal averaging, perhaps the most powerful phase improvement technique. To date, use of this technique has been limited to when more than two crystal forms of the same molecule are available. We have demonstrated the use of this method between crystals that contain many common components, such as crystals of a molecular complex at different functional stages, crystals of a complex and its individual components, or crystals of different complexes that have any common protein/nucleic acid component. Significantly, we have successfully extended its use to crystals of homologous, but not identical molecules [5]. These much more general applications of this powerful technique means that the large amount

of structural information in PDB can be harvested through multi-crystal averaging to aid the determination of new structures.

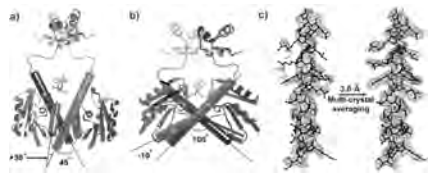

Fig. 2 a) and b) Two functional structures of resolvase [3]. c) Effect of multi-crystal averaging. The improvement is an unbiased overall phase improvement as the helix is not included in the averaging.

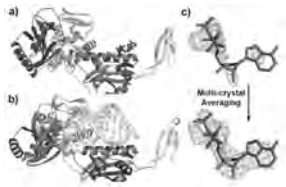

Fig. 3 Structures of a) CCA-adding enzyme and b) its ternary complex with RNA and ATP [4]. c) Effect of multi-crystal averaging. ATP is not included in averaging.not included in the averaging.

References

1. http://olenka.med.virginia.edu/mcsg/phtml/progress_viewer.phtml.
2. Lomakin, I.B., Y. Xiong & T.A. Steitz (2007). *Cell* **129**, 319-32.
3. Li, W., et al. (2005). *Science* **309**, 1210-5.
4. Xiong, Y. & T.A. Steitz (2004). *Nature* **430**, 640-5.
5. Fang, Y., et al. (2009). *Nature* (Advance online publication).

MS11-1

Thermoelectric Zintl Compounds in R-T-Sb (R = Ca, Sr, Ba, Eu, Yb; T = Zn, Cd) Systems

X.J. Wang[a], H. Zhang[a], M.B. Tang[a], X.X. Yang[a], H.H. Chen[a], Z.Y. Man[a], U. Burkhardt[b], Y.Grin*[b], J.T. Zhao*[a]

[a] *Key Laboratory of Transparent and Opto-Functional Inorganic Materials of Chinese Academy of Sciences, Shanghai Institute of Ceramics, Shanghai 200050, P.R. China;*
[b] *Max-Planck Institute for Chemical Physics of Solids, Dresden, Germany*
(jtzhao@mail.sic.ac.cn)

Recently many new promising thermoelectric (TE) materials have been found in a special category of intermetallic compounds, i.e. Zintl phases. The classical Zintl phases are semiconductors with narrow band gap and many have complex crystal structures containing "rattle" heavy atoms to produce low lattice thermal conductivities. In our systematic investigations of potential TE materials in intermetallic compounds with polar character, ternary Zintl phases $R_xT_yS_z$(R=Ca, Sr, Ba, Yb and Eu; T=Transition elements; S= Semi-metal elements) showed to be promising. Based on first principle calculations on electronic structures and crystal structure analyses, the pnictide candidates such as $BaZn_2Sb_2$, $YbCd_2Sb_2$ and $EuCd_2Sb_2$ were synthesized and their thermal and electrical transport properties were characterized. These compounds show promising TE properties with considerably high figure of merit (e.g. ZT~1at 700K for $YbCd_2Sb_2$). The solid solution system $YbCd_xZn_{2-x}Sb_2$ (x = 0, 0.4, 0.8, 1, 1.2, 1.6 and 2) were synthesized and their TE properties were also characterized. The results revealed that Zn substitution of Cd in $YbCd_2Sb_2$ can easily tune carrier concentration and decrease thermal conductivity, which resulted in improvement of ZT value (e.g. ZT ~1.2 at 700K for x = 0.4).

References

1. X.J. Wang, M.B. Tang, H.H. Chen, X.X. Yang, J.T. Zhao, U. Burkhart, Yu. Grin, *Appl. Phys. Lett.* 94 (2009) 092106

2. H. Zhang, J.T. Zhao, Yu. Grin, X.J. Wang, M.B. Tang, Z.Y. Man, H.H. Chen, X.X. Yang, *J. Chem. Phys.* 129 (2008), 164713.
3. H. Zhang, L. Fang, M.B. Tang, H.H. Chen, X.X. Yang, X.X. Guo, J.T. Zhao, Yu. Grin, *Intermetallics-D-08-00373R1* (2009).

MS11-2 Solid-state photochemical reactivity of coordination polymers and metal complexes containing *trans*-1,2-bis(4-pyridyl)ethylene

Jagadese J. Vittal, Mangayarkarasi Nagarathinam, Abdul Malik Puthan Peedikakkal
Department of Chemsitry, National University of Singapore, 3 Science Drive 3, Singapore 117543 (chmjjv@nus.edu.sg)

The criteria for solid-state photochemical [2+2] cycloaddition reactions have been well established, however, it is still a challenge to stack a pair of C=C bonds in the crystal lattice by design. A number of weak interactions have been serendipitously discovered to align the double bonds in the crystal lattice congenial for the photochemical dimerization reactions. The strength and directionality of the hydrogen bonds have been elegantly exploited to align the double bonds in 4,4'-bipyridylethylene (bpe) with considerable success. Such photochemical reactions have also been carried out in the inorganic compounds containing ligands with C=C bonds in their backbones. For example, coordination polymers with ladder-like structures provided an interesting possibility to align the photoreactive double bonds in the solid-state. In another example, a 1D coordination polymer was found to reorganize to form ladder structure on desolvation which undergoes [2+2] cycloaddition under UV irradiation quantitatively. However, hydrogen bonded metal complexes have not been used to align the C=C bonds for photochemical cycloaddition reactions. Different strategies used to align the C=C bonds in the author's laboratory will be discussed and the challenges for the coordination chemist in utilizing this rational approach to orient the coordination polymers will be highlighted with reference to *trans*-1,2-bis(4-pyridyl)ethylene (bpe).

MS11-3 Anatomy of a Void in an Aluminium-Copper-Tin Alloy

Laure Bourgeois[1,2], Matthew Weyland[1], Philip N.H. Nakashima[2], Barry C. Muddle[2]
[1]Monash Centre for Electron Microscopy and Department of Materials Engineering, Monash University, Victoria 3800, Australia
[2]Australian Research Council Centre of Excellence for Design in Light Metals and Department of Materials Engineering, Monash University, Victoria 3800, Australia

Under certain conditions voids are able to nucleate and grow in association with precipitate phases in an aluminium-copper-tin alloy. This alloy, of composition Al-1.7at.%Cu-0.01at.%Sn, constitutes a model system for the study of the mechanisms by which some trace alloying additions like Sn are able to efficiently promote the nucleation of strengthening phases, in this case the phase θ' of composition Al_2Cu [1]. Since vacancies are a key element in nucleation and growth mechanisms of precipitates, the presence of voids, or giant vacancy clusters, associated with Sn and θ' nano-particles, is of great interest.

The present work is a detailed structural study of large voids (~50 nm in diameter) in a

Al-1.7at.%Cu-0.01at.%Sn alloy, using several transmission electron microscopy (TEM) techniques: high-resolution scanning (S)TEM and phase-contrast TEM imaging, energy-dispersive X-ray (EDX) mapping, electron tomography, and convergent beam electron diffraction (CBED).

Fig. 1 shows a typical example of a void associated with a precipitate each of θ' and tin; the latter was found to be the β-Sn phase. Viewed along the [100] direction of the α-Al matrix phase, the void-matrix interface displays clear facetting parallel to the $\{200\}_\alpha$ planes, together with 2 Å steps corresponding to the $\{200\}_\alpha$ interplanar distance. A three-dimensional electron tomographic reconstruction of another such void-tin-θ' group confirmed the distinct facetting of the void surface (Fig. 2). In combination with high resolution TEM, the crystallographic characteristics of the β-Sn- and θ'-void interfaces could be determined; the latter is particularly useful information given that the θ' phase is always found embedded in α-Al. CBED revealed the total absence of strain in the void-matrix region, suggesting that the void acts as strain relief for the β-Sn and θ' precipitates in contact with it. Although EDX failed to detect any content in the void, one cannot discount the presence of trace impurities such as oxygen at the void surface, which might reduce its surface energy.

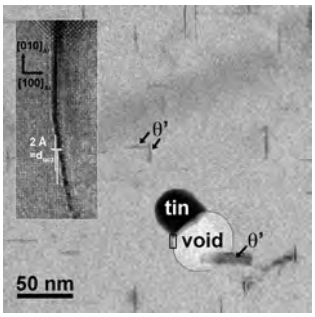

Fig. 1: TEM image along $[100]_\alpha$ of a void-tin-θ' group. There is distinct $\{200\}_\alpha$ facetting and 2 Å steps at the void-matrix interface.

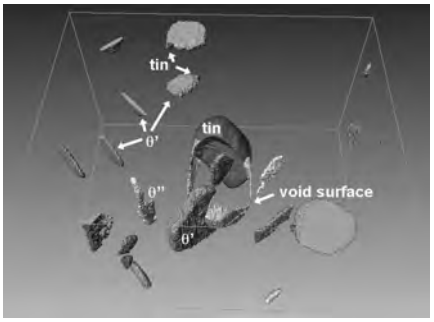

Fig. 2: Electron tomographic reconstruction of another void-tin-θ' group, revealing the 3-D void morphology, including the clear facetting exhibited by the β-Sn and θ' precipitates-void interfaces.

Reference

L. Bourgeois, J.F. Nie, B.C. Muddle, 2005, Phil. Mag. 85, 3487.

SMART X2S - Chemical Structures at the Touch of a Button

MS11-4

Eric Hovestreydt[1], Michael Ruf[2], Holger Ott[1]
[1] *Bruker AXS GmbH, Oestliche Rheinbrueckenstrasse 49, D 76181 Karlsruhe, Germany (info@bruker-axs.de)*
[2] *Bruker AXS Inc., E. Cheryl Parkway 5, MADISON, WI 53711-5373, United States of America (info@bruker-axs.com)*

Modern research moves at breakneck speed. The newly introduced SMART X2S produces 3-D structures at the touch of a button in your own laboratory! The compact and economical SMART X2S has a couple of unique features, such as fully automated operation from sample loading and alignment through data collection and structure solution which will be addressed

in detail.

Its compact air-cooled benchtop design that requires only standard single-phase AC power, allowing the instrument to be easily placed anywhere. Cost of ownership will be compared to standard instruments. The SMART X2S is an expert system that allows chemists to do routine

publication quality crystal structures in a few hours. The SMART X2S automatically loads and aligns your sample, acquires a complete crystallographic dataset, and then solves and refines the 3-D structure, completely without user intervention! The user-friendly software, operated from a touch-screen, combines an expert knowledge of structural chemistry with the power of industry-standard SHELXTL data processing engines for structure solution and refinement. A number of examples will be shown during the talk. Additional applications of the SMART X2S, e.g. as a crystallographic teaching tool, will be presented.

MS11-5 Rational Design, Synthesis and Properties of Layered Compounds LnOZnSb (Ln=La, Ce, Pr, Nd)

Kai Guo[1, 2], Hao-Hong Chen[1], Zhen-Yong Man[1], Mei-Bo Tang[1], Xin-Xin Yang[1], Xiang-Xin Guo[1], Jing-Tai Zhao[1]

[1] *Key Laboratory of Transparent Opto-functional Inorganic Materials of Chinese Academy of Sciences, Shanghai Institute of Ceramics, Shanghai 200050, PR China* (*jtzhao@mail.sic.ac.cn*)

[2] *Graduate School of Chinese Academy of Sciences, Beijing 100039, PR China*

The rational design of new inorganic compounds perplexes solid-state chemists while serendipity still plays important role to explore new material. However, controlling the microcosmic structures of compounds is prerequisite for mastering the physical properties in solids. For this reason, extensive efforts are devoted to reach the breakthroughs in the field. In this paper, a stacked method with 2D building blocks combined with theoretical computation is proposed to design the ZrSiCuAs type layered compounds: LnOZnSb (Ln=La, Ce, Pr, Nd). Then, the design was confirmed by their syntheses and structure characterizations.

The tetragonal ZrSiCuAs type structure is relatively simple with ZrSi and CuAs layers stacked along c-axis with space group P4/nmm (as shown in Fig.1). A new set of "compounds" are constructed by replacing ZrSi and CuAs layers with LnO and ZnSb layers, respectively. The structures of LnOZnSb are subsequently optimized by means of quantum calculation methods and the electronic structure investigated using Castep code to understand their stability. Furthermore, LnOZnSb (Ln=La, Ce, Pr, Nd) are synthesized via three-step solid reaction and the optimized structures were confirmed by XRD (Fig.2). The results of simulation and experiment show that LnOZnSb (Ln=La, Ce, Pr, Nd) are narrow band-gap semiconductors.

Fig.1 Crystal structure of ZrSiCuAs

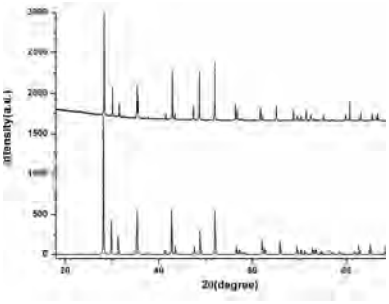

Fig.2 XRD pattern of NdOZnSb (the red line represents the simulation result)

References

1. Laurent Cario, Houria Kabbour, Alain Meerschaut, Chem. Mater. 17 (2005) 234.
2. R.Pöttgen and D.Johrendt, Z. Naturforsch. 63 **(**2008) 1135.

MS11-6 Cation···Cation Supramolecular Interactions in Zinc–Imidazole–Oxovanadate Compounds

Samroeng Krachodnok[1], Kenneth J. Haller[1], Ian D. Williams[2]
[1] *Institute of Science, 111 University Avenue, Muang, Nakhon Ratchasima, 30000, Thailand (ken.haller@gmail.com, dsk4610137@live.com)*
[2] *Hong Kong, University of Science and Technology, , Hong Kong, (chwill@ust.hk)*

Noncovalent interactions involving aromatic sections of molecules are ubiquitous, and particularly when acting in concert, rival the robustness of hydrogen bonds. Herein, we report the ability of an imidazole and its derivatives capable of both hydrogen bonding and aromatic interactions in three zinc–imidazole–oxovanadate compounds, namely $[Zn(Im)_4]_2[V_4O_{12}]$ (**1**), $[ImH]_2[\{Zn(Im)_3\}_2V_{10}O_{28}]\cdot 2H_2O$ (**2**), and $[2\text{-MeImH}]_2[Zn(2\text{-MeIm})_4]_2[V_{10}O_{28}]$ (**3**), to form extended concerted aryl interaction motifs. Cationic $[Zn(Im)_4]_2^{4+}$ dimers in **1** bind in two concerted $(EF)_2$ embrace motifs and further bind to neighboring zinc complexes to form 2D supramolecular layers perpendicular to the *c* axis. Adjacent layers are held together by two FF π···π interactions to form a 3D supramolecular network. The tetrahedral zinc complexes in **2** form two EF C–H···π hydrogen bond interactions in 1D herringbone fashion to generate 2D nets and further interact with pillared imidazolium dimers to construct a 3D supramolecular framework. Two different EF C–H···π hydrogen bond interactions in **3** link cationic $[Zn(Im)_4]_2^{4+}$ dimers with imidazolium dimers to form 1D –Zn–Zn–ImH–ImH– chains.

MS11-7 Synthesis and X-ray Structures of Diorganotin Complexes with *Tris*{(hydroxymethyl)aminomethane Schiff base

See Mun Lee, Hapipah Mohd Ali and Kong Mun Lo
Chemistry Department, University of Malaya, 50603 Kuala Lumpur, Malaysia (smlee@um.edu.my)

Tris(hydroxymethyl)aminomethane (THAM) and its derivatives are known to display a variety of biological activities such as antibiotic, anticancer, antihistamine, antifungal, anti-inflammatory and many others. In this study, two THAM Schiff bases, namely t*ris*{(hydroxymethyl)-[5-bromosalicylideneiminate]} and *tris*{(hydroxymethyl) aminomethane [5-chlorosalicylideneiminate]} were prepared. The Schiff bases were reacted with diorganotin starting materials to form the diorganotin complexes, *bis*[1-hydroxy-2-hydroxymethyl-2-(5-bromo-2-oxidobenzylideneamino)-3-oxidomethylpropane]dimethyltin(IV), **C1**, [1-hydroxy-2-hydroxymethyl-2-(5-chloro-2-oxido-benzylideneamino)-3-oxido-methylpropane]dimethyltin(IV), **C2**, [1-hydroxy-2-hydroxymethyl-2-(5-bromo-2-oxido-benzylideneamino)-3-oxidomethylpropane]diphenyltin(IV), **C3** and [1-hydroxy-2-hydroxymethyl-2-(5-chloro-2-oxido-benzylideneamino)-3-oxidomethylpropane]-diphenyltin(IV), **C4**. The complexes were characterized by using various spectroscopic methods and their X-ray structures were determined.

The compound **C1** crystallises in the monoclinic, $P2_1/n$ space group. Its molecular structure shows that the ligand, *tris*{(hydroxymethyl)aminomethane[5-bromosalicylideneaminate]} is tridentate in which the one hydroxymethyl oxygen, one phenoxy oxygen and an imino nitrogen atoms are involved in coordination with the tin atom. The same hydroxylmethyl oxygen is also involved in the coordination with the adjacent molecule to form a dimer with a central Sn_2O_2 stannoxane ring. Whereas, the X-ray structure of **C2** which contains a chloro-substituted Schiff base is monomeric. Compounds **C3** and **C4** are also monomeric, probably due to the steric effect as a result of the presence of bulky phenyl organic groups.

MS12-1 Precise Structure Analysis of Ceramic Materials up to 1830 K

Masatomo Yashima
Department of Materials Science and Engineering, Interdisciplinary Graduate School of Science and Engineering,, Tokyo Institute of Technology, Nagatsuta-cho 4259-J2-61, Midori, Yokohama, 226-8502, Japan (yashima@materia.titech.ac.jp)

We review our recent works on the visualization of diffusional pathway of mobile ions and chemical bonding in ceramic materials through synchrotron and neutron powder diffraction experiments, which would be useful for the design of ceramic materials. Crystal structure and electron-density distribution of α-silicon nitride (α-Si_3N_4, space group: $P31c$) have been investigated by a combined technique of Rietveld method, maximum-entropy method (MEM) and MEM-based pattern fitting (MPF) of high-resolution synchrotron powder diffraction data. In combination with density functional theory (DFT) calculations, the present experimental electron-density distribution of the α-Si_3N_4 indicates covalent bonds between Si and N atoms

and the charge transfer from the Si to N atom. The present work suggests that the high bulk modulus of the α-Si_3N_4 is attributable to the high minimum electron density of the Si-N bond. Tantalum oxynitride (TaON) is investigated by neutron and synchrotron diffraction analysis to clarify the structural and electronic features responsible for the visible-light activity of this material. In combination with DFT calculations, the present measurements confirm the TaON photocatalyst to be monoclinic with space group $P2_1/c$. Bond valence sums for the oxygen and nitrogen atomic sites are calculated to be 2.1 and 3.2, respectively. Electron density analyses based on synchrotron data in combination with DFT calculations reveal covalent bonds between Ta and O atoms and between Ta and N atoms. The hybridization of anion 2p and Ta 5d orbitals attributed to the covalent bonds between Ta and O or N atoms results in increased dispersion of the valence band, raising the top of the valence band and leading to a visible-light response. Our group has developed new high-temperature neutron and high-resolution synchrotron diffraction techniques to study the precise crystal structures, nuclear and electron density in inorganic materials up to 1900 K. These techniques enabled precise structural analysis leading to diffusion path and structural disorder in ionic conductors. Here we review our recent works on the positional disorder and diffusion path of oxide ions in Bi_2O_3, $(La_{0.8}Sr_{0.2})(Ga_{0.8}Mg_{0.15}Co_{0.05})O_{2.8}$, CeO_2, $Bi_{1.4}Yb_{0.6}O_3$, $Ce_{0.93}Y_{0.07}O_{1.96}$, and $La_{0.64}(Ti_{0.92}Nb_{0.08})O_3$ at high temperatures. We also describe the diffusion path of Li cations in Li-doped lanthanum titanate perovskite $La_{0.62}Li_{0.16}TiO_3$ at room temperature and of Cu cations in copper iodide CuI at 760 K. These were studied through the nuclear/electron density distribution obtained by a combined technique including a Rietveld refinement and a maximum-entropy method (MEM)-based pattern fitting of the neutron-powder-diffraction data. We found that the mobile ions in fluorite-type ionic conductors have a complicated disorder spreading over a wide area and shift to the <111> directions from the ideal fluorite site at high temperatures. The fast oxide-ion conductors $Bi_{1.4}Yb_{0.6}O_3$ and $Ce_{0.93}Y_{0.07}O_{1.96}$ exhibited a curved diffusion pathway along the <100> direction. The Cu cation conductor has also a fluorite-type structure and curved diffusion pathway along the <100> direction. The curve feature would be common for various ionic conductors. We have demonstrated that the diffusion path of mobile oxide ions in the lanthanum gallate-based compound was not along the straight line between the ideal positions, but exhibited an arc shape away from the B-site cation ($Ga_{0.8}Mg_{0.15}Co_{0.05}$). The diffusion pathway forms a three-dimensional network. The double perovskite-type $La_{0.64}(Ti_{0.92}Nb_{0.08})O_3$ exhibits a curved diffusion pathway at high temperatures. The diffusion pathway in the $La_{0.64}(Ti_{0.92}Nb_{0.08})O_3$ forms a two-dimensional network. We also report for the first time the diffusional path of oxide ions in a K_2NiF_4-type mixed conductor $(Pr_{0.9}La_{0.1})_2(Ni_{0.74}Cu_{0.21}Ga_{0.05})O_{4+\delta}$, through a high-temperature neutron powder diffraction study.

MS12-2

Zeolite Structure Analysis by Powder X-ray Data

Yingxia Wang[1], Jie Su[1], Jianhua Lin[1], Hermann Gies[2]
[1]State Key Laboratory of Rare Earth Materials Chemistry and Application, College of Chemistry and Molecular Engineering, Peking University, Beijing, 100871, China (wangyx@pku.edu.cn)
[2] Inst. Geologie, Mineralogie und Geophysik, Ruhr-Universität Bochum, 44780 Bochum, Germany

Zeolites have attracted considerable attention due to their use in industrial applications as catalysis, ion exchange, adsorption, and separation. As metastable phases with microporous framework structures, zeolites are often obtained as polycrystalline products from hydrothermal reaction systems. Then powder X-ray diffraction is a powerful technique for the structure determination or the framework confirmation. Zeolite frameworks are built on the basis of vertex sharing tetrahedra. Conventionally zeolites are silicates/aluminosilicates. The combination modes of SiO_4 groups as well as the corresponding structural parameters, such as Si-O bond length (~1.61 Å), Si-O-Si angle (~145°) and Si…Si distance (~3.0 Å) are helpful in the analysis of new structures. On the basis of structural principle, we can apply every kind of methods by the aid of suitable programs to puzzle out the structures.

1. Ab intio structure determination

1) Model building: It is a straight way to have the structure visible, which involves the reasonable use of the known structure building units. RUB-41, the condensation product of a layered hydroxyl silicate RUB-39, is a microporous silica. After indexing the powder X-ray profile, the lattice constants are obtained[1]. By searching the database of zeolite structures, we found the resemblance of RUB-41 with HEU framework [2, 3]. Accordingly the same layer is built, but linked in a different way from that of HEU to meet the demand of the lattice constant along b direction. Five unique Si positions are read out directly from the model and O atoms are obtained by tetrahedral geometric relations. The structure is finally refined by Rietveld method. As the precursor of RUB-41, the layer in the structure of RUB-39 is similar to that of RUB-41, then a rigid body is defined, one additional O atom is revealed using TOPAS by simulated annealing method. The SDA molecules are located during the structure refinement process.
2) Solving the structure from powder X-ray data: RUB-43 is a microporous germinate. It crystallizes in a c-centered monoclinic lattice with unit cell parameters of a=13.9340(4)Å, b=33.016(1)Å, c=11.6808(3)Å and β=127.5210(12°) and space group *C2/m*. Five germanium atom-positions were revealed by EXPO using direct method[4]. The missing germanium atoms were located by Fourier techniques. The positions of O, N and C atoms were found in the course of the Rietveld refinement using TOPAS[5].

2. Confirmation of the known framework topology by structure refinement

We shall discuss two examples. PKU-11 is a silicate synthesized by a simple quarternary ammonium SDA. A comparison with the Atlas indicates that the XRD profile is similar to that of framework STF. A set of electron diffraction patterns related to one grain in different tilting angles were taken. The indexing result of ED patterns reveals a triclinic lattice with the constants of a=11.56 Å, b=11.30Å, c=7.30 Å, α=94.7°, β=97.7°, and γ =103.9 °, which are consistent with the framework parameters of STF. The Rietveld refinement of the calcined

product was performed by TOPAS, using the structure data from SSZ-35 as initial setting. The other example is a silicogermanate (PKU-12) with CLO- framework type. CLO- framework contains 20-rings，which is the largest pore size among all known zeolite frameworks. It was firstly obtained as a gallium phosphate, named as Cloverite. Much work has been done on the synthesis of new materials with this topology; however, the reported compounds were all phosphates. As a silicogermante, the framework structure of PKU-12 has been confirmed to be isostructural to CLO- by Rietveld analysis.

References (selected)

[1] C. Dong, J Apply Crystallogr., 32(1999) 838.
[2] M. M. J. Treacy, J. B. Higgins, Collection of Simulated XRD Powder Patterns for Zeolites, 5th,2007
[3] Ch. Baerlocher, L. B. McCusker, D. H. Olson, *Atlas of Zeolite Framework Types, 6th*, **2007**
[4] A. Altomare, M.C. Burla, G. Cascarano, C. Giacovazzo, A.Guagliardi, A.G.G. Moliterni, G. Polidori, J. Appl. Crystallogr. 28(1995) 842.
[5] TOPAS V3: General profile and structure analysis software for powder diffraction data, Bruker AXS, Karlsruhe (Germany)

Spinner-Scan Method for Evaluation of Particle Statistics in Powder Diffractometry

MS12-3

Takashi Ida[1], Taishi Goto[1], Hisashi Hibino[2]
[1] *Omohi college, Graduate School of Engineering, Nagoya Institute of Technology, Gokiso, Showa-ku, Nagoya, 466-8555, Japan (ida.takashi@nitech.ac.jp)*
[2] *Ceramics Research Laboratory, Nagoya Institute of Technology, Asahigaoka, Tajimi, Gifu, 507-0071, Japan)*

The uncertainty in measured diffraction intensities caused by particle statistics, which originates from the limited number of crystallites satisfying the diffraction condition, has been evaluated by a step-scan measurement about the rotation angle of a specimen spinner attached to a laboratory powder X-ray diffractometer.

Particle statistics for a standard Si powder (NIST SRM640c) and three size fractions (nominally 3-7, 8-12 and 18-22 μm in Stokes diameter) of quartz powder separated by a sedimentation method have been analysed by scanning electron microscopy (SEM) and the spinner-scan method using a powder X-ray diffractometer (Rigaku RAD-2C). The effective particle sizes of Si and three fractions of quartz powder have been estimated at 5.6, 7.1, 12, 25 μm by analyzing the SEM images.

The observed spinner-scan intensity profile of the Si 111 reflection is shown in Fig. 1. Periodic drift in the observed intensity profile is modeled by Fourier expansion up to the second order. The residual statistical variance, after subtraction of the periodic drift and variance caused by counting statistics, has been assigned to the variance caused by particle statistics. It has been found that the effective numbers of diffracting crystallites evaluated for different reflections well correspond with the multiplicities of reflection, which confirms that particle statistics has certainly been evaluated by this method. Crude values of the effective diameter D'_{eff} estimated for each reflection by applying the theoretical formula of Alexander *et al.* (1948) are shown in Fig. 2. A calibration curve has been derived assuming the effective diameter of 5.6 μm determined by the SEM image analysis and slight

modification of the formula.

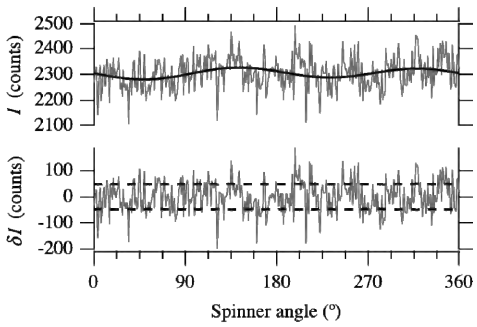

Fig. 1 Spinner-scan profile of Si 111 reflection. The upper panel shows raw intensity (grey line) and assumed drift profiles (black line). The lower panel shows the residuals (grey line) and counting errors (broken lines).

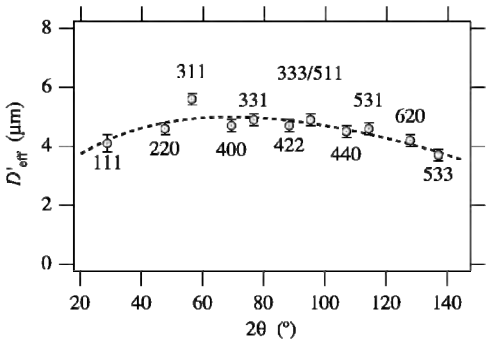

Fig. 2 Effective diameter D'_{eff} of Si powder calculated with assumed instrumental parameters (circles) and the calibration curve (broken line).

The spinner-scan X-ray diffraction intensity data of quartz powder samples were similarly collected. The effective diameters of three fractions of quartz powder have been estimated at 6.5(2), 11.7(2) and 22.8(2) μm, by analyzing the spinner-scan profiles applying the above calibration curve. The results show that the statistical variance assigned to particle statistics can be quantitatively evaluated by this method, and estimation of crystallite size over a range of several μm, which is practically impossible to be evaluated by conventional methods based on line-broadening analysis, has been achieved at considerable accuracy.

MS12-4 Structural and magnetic properties of doped wide bandgap semiconductors

Gang Wang[1], Bo Song[1,2], Hui Li[1], Liangbao Jiang[1], Xiaolong Chen[1], Wenjun Wang[1], Wanyan Wang[1]

[1] *Beijing National Laboratory for Condensed Matter Physics, Institute of Physics, Chinese Academy of Sciences, P.O. Box 603, Beijing, 100190, China (gangwang@aphy.iphy.ac.cn)*

[2] *Academy of Fundamental and Interdisciplinary Sciences, Harbin Institute of Technology, Harbin, 150080, China*

Diluted magnetic semiconductors (DMSs) represent the most promising candidates for spintronics simultaneously manipulating charge and spin of electrons.[1] Theoretical work has predicated that III-V and II-VI DMSs possess Curie temperatures (T_Cs) exceeding room temperature,[2] which is crucial for the proposed spintronic applications. Many experiments based on thin films have been carried out to verify such hypotheses.[3-5] However, much debate existing over second phase segregation and intrinsic defects in these films originating from the non-equilibrium epitaxial growth process make argument for the origin of high temperature ferromagnetism in the materials.

Here we report on the structural and magnetic properties of doped wide bandgap semiconductors AlN, SiC synthesized by solid state reaction and physical vapor transport techniques. Especially, in order to exclude the effect of magnetic second phase, nonmagnetic element Al is adopted to make the compounds magnetic besides transition metals Ni, Mn, and

so on. Ferromagnetism with T_Cs above 300 K is observed in the homogenous polycrystals, whiskers and single crystals confirmed by structural analyses. Obviously, current models, such as superexchange, carrier-mediated exchange and magnetic polarons, seem not applicable for the formation of the ferromagnetic order in these high resistive samples. The origin of the magnetic interactions responsible for T_Cs higher than room temperature by doping less than 1 at.% needs to be further explored. Our work demonstrates the potential for the spin moments controlling by doping in wide bandgap semiconductors and for the development of wide bandgap semiconductor based spintrosic devices.

References

[1] H. Ohno, *Sicence* **1998**, 281, 951.
[2] T. Dietl, H. Ohno, F. Matsukura, J. Cibert, D. Ferrand, *Science* **2000**, 287, 1019.
[3] M. L. Reed, N. A. El-Masry, H. H. Stadelmaier, M. K. Ritums, M. J. Reed, C. A. Parker, J. C. Reberts, S. M. Bedair, *Appl. Phys. Lett.* **2001**, 79, 3473.
[4] M. E. Overberg, C. R. Abernathy, S. J. Pearton, N. A. Theodoropoulou, K. T. McCarthy, A. F. Hebard, *Appl. Phys. Lett.* **2001**, 79, 1312.
[5] M. C. Park, K. S. Huh, J. M. Myoung, J. M. Lee, J. Y. Chang, K. I. Lee, S. H. Han, W. Y. Lee, *Solid State Commun.* **2002**, 124, 11.

MS12-5 Vanadium substituted potassium tungsten bronzes – its synthesis and characterization

A. M. Abdullah[1], A. Hussain[2]
[1] *Bangladesh Council of Scientific and Industrial Research (BCSIR) Laboratories, Chittagong – 4220, Bangladesh, (abdullah059@yahoo.com)*
[2] *Department of Chemistry, University of Dhaka, Dhaka – 1000, Bangladesh, (altaf@univdhaka.edu)*

Polycrystalline samples with nominal compositions $K_xV_yW_{1-y}O_3$ ($x = 0.3$, $y \leq 0.3$ and $x = 0.5$, $y \leq 0.3$) were synthesized by conventional solid state method at 800°C using appropriate amount of WO_3, WO_2, V_2O_5, and K_2WO_4. The samples were characterized with XRD, SEM/EDX and optical spectroscopy. Analysis of X-ray powder patterns reveal that single phase of vanadium substituted potassium hexagonal tungsten bronzes (K-HTB) could be prepared for nominal composition $x = 0.30$, $y \leq 0.15$. For further increase in nominal vanadium content (y), an additional phase appears as a second phase. Structure refinement of pure K-HTB samples using Rietveld fitting procedures reveal a decrease in *a* and an increase in *c* lattice parameters with increasing nominal V content. The elemental compositions of the pure samples were determined by SEM/EDX analysis and show an increase in V content with increasing y. The samples with nominal composition $K_{0.5}V_yW_{1-y}O_3$ show pure tetragonal tungsten bronze (TTB) type structure up to $y = 0.05$. Investigations of the optical reflectivity and the infrared absorption spectra of powder $K_{0.3}V_yW_{1-y}O_3$ (HTB) samples indicate a decreasing polaron concentration with increasing V content.

MS12-6

Charge Density study from high-resolution powder diffraction data

Eiji Nishibori[1], Shinobu Aoyagi[1], Hiroshi Sawa[1]
Department of Applied Physics, Nagoya University, Nagoya, 464-8603, Japan (o47271a@cc.nagoya-u.ac.jp)

The electron density distribution in materials determines their properties and functions. The structure factors from x-ray diffraction give information of total electron density distribution including both the core and the valence electrons. Required accuracy of structure factors for accurate charge density study is much higher than that of normal crystallographic structural study in atomic level, where main concern is atomic arrangement.

The accuracy of powder diffraction data has been considered to be much poorer than that of the single crystal diffraction method due to the following reasons. Firstly, the measured integrated Bragg intensities are relatively weak. Secondly, it is difficult to obtain the individual integrated Bragg intensities due to peak overlaps and some other relatively minor reasons. Therefore, it has been considered that the powder diffraction data is not appropriate for accurate charge density studies.

Recent progress of synchrotron powder x-ray diffraction technique including the third generation synchrotron x-ray source such as SPring-8, detector, measurement system and analytical method provides us a possibility to obtain accurate structure factors for charge density studies. We have recently developed the both experimental and analytical techniques based on multi-powder diffraction data[1)] for an improvement of the accuracy of the data. The method have been successfully applied charge density studies of silicon, diamond, and $CoSb_3$[2)] by Maximum Entropy Method (MEM). The MEM provides total charge density of material from experiment. For an observation of valence electrons from experiment, additional analytical techniques are required.

Recently, we have carried out various types of accurate structural studies, the multi-pole refinement, anharmonic thermal factor refinement, and Bader topological analysis, of several kinds of inorganic materials from multi-powder diffraction data. Furthermore, we have developed a new method for the determination of the experimental valence charge density by a combination of the MEM and the multi-pole refinement. The experimental valence charge densities of some inorganic materials from high resolution (d>0.2Å) multi-powder data will be presented.

References

1. Nishibori E., Sunaoshi E., Yoshida A., Aoyagi S., Kato K., Takata M., Sakata M., Acta Crystallographica, A63 (2007) 43-52
2. Ohno, A,, Sasaki, S, Nishibori,E., Aoyagi, S., Sakata,M., Iversen, B. B. Physical Review B76. (2007) 064119.

MS12-7

Interplay between the crystalline and magnetic structures in lightly Cr-doped $Bi_{0.37}Ca_{0.63}Mn_{0.96}Cr_{0.04}O_{2.9}$

Wen-Hsien Li[1],.Chun-Chuen Yang[1], Chun-Ming Wu[1], Jirong Sun[2], Jeffrey W. Lynn[3]
[1] *Center for Neutron Beam Applications and Department of Physics, National Central University, Jhongli, 32001 Taiwan (whli@phy.ncu.edu.tw)*
[2] *State Key Laboratory for magnetism, Institute of Physics and Center for Condensed Matter Physics, Chinese Academy of Science, Beijing, 10008 China. (jrsun@g203.iphy.ac.cn)*
[3] *NIST Center for Neutron Research, National Institute of Standards and Technology, Gaithersburg, MD 20899, USA (Jefrey.Lynn@nist.gov)*

The strong interplay between the crystalline structure, electrical transport and spin magnetism has generated a large variety of interesting properties in hole-doped perovskite manganese oxides $(Ln_{1-x}A_x)(Mn_{1-y}B_y)O_3$, where *Ln* is a lanthanide ion, *A* is an alkaline-earth metal and *B* is a transition metal. It is known that the physical properties of this class of materials are sensitive to A-site as well as B-site doping. Generally speaking, *A*-site doping creates a Mn^{3+}/Mn^{4+} mixed-valence state that not only affects the carrier density but also significantly influences the colossal magnetoresistance exhibited by this class of material. *B*-site doping, on the other hand, disrupts the electrically and magnetically active Mn-O-Mn network, weakening the double exchange (DE) interaction, and is believed to be detrimental to the conduction mechanism. Here, we report on the results of studies made on the interplay between the crystalline and magnetic structures of a 4% Cr-doped $Bi_{0.37}Ca_{0.63}Mn_{0.96}Cr_{0.04}O_{2.99}$ by ac magnetic susceptibility, electrical resistivity, and neutron diffraction measurements. The compound crystallizes into a monoclinic $P2_1/m$ symmetry, where Mn-trimers are formed along the [101] and $[10\bar{1}]$ crystallographic directions. A Jahn-Teller distortion occurs at 280 K. The thermal behavior of charge transport may be described by a three-dimensional variable range hopping conduction. Strong interplay between the localized magnetic electrons and the itinerant electrons are clearly revealed as the localization length increases by 20% when the Mn spins become ordered. The Mn spins order at 85 K, but short range magnetic correlations persist up to 160 K. Exchange integrals favor a magnetic structure with the moments pointing in the [101] direction, which agrees well with the magnetic structure proposed based on the neutron magnetic diffraction patterns. Both the Jahn-Teller transition and the magnetic ordering temperature are substantially reduced with Cr doping compared to the undoped system.

MS13-1

The structure of rat liver vault

Hideaki Tanaka,[1]Koji Kato,[1] Eiki Yamashita,[1] Tomoyuki Sumizawa,[2] Yong Zhou,[3] Min Yao,[3] Kenji Iwasaki,[1] Masato Yoshimura,[4] and Tomitake Tsukihara[1,5]

[1]*Institute for Protein Research, Osaka University, 3-2 Yamada-oka, Suita, Osaka 565-0871, Japan,*

[2]*University of Occupational and Environmental Health, 1-1 Iseigaoka, Yahatanishi, Kitakyushu, Fukuoka 807-8555,*

[3]*Faculty of Advanced Life Sciences, Graduate School of Life Sciences, Hokkaido University, Sapporo, Hokkaido 060-0810, Japan,*

[4]*National Synchrotron Radiation Research Center, 101 Hsin-Ann Road, Hsinchu Science Park, Hsinchu 30076, Taiwan,*

[5]*Department of Life Science, University of Hyogo, 3-2-1 Koto, Kamighori, Akoh, Hyogo 678-1297, Japan. (e-mail: tsuki@protein.osaka-u.ac.jp)*

Vaults are large barrel-shaped ribonucleoprotein particles that are highly conserved in a wide variety of eukaryotes. Though several functions have been proposed for vaults since their first discovery in 1986, including roles in multidrug resistance, cell signaling and innate immunity, their cellular function remains unclear. Most vault particles are present in the cytoplasm, but a few of them localize to the nucleus. Rat liver vault comprises a small untranslated RNA consisting of 141 bases (vRNA) and three proteins. The sequences of these proteins are known for the human vault. The 99-kDa major vault protein (MVP) is the major structural protein and can self-assemble to form vault-like particles, the 193-kDa vault poly(ADP-ribose)polymerase presumably ribosylates substrates, and the 290-kDa telomerase-associated protein 1 is important for stabilization of vRNA.

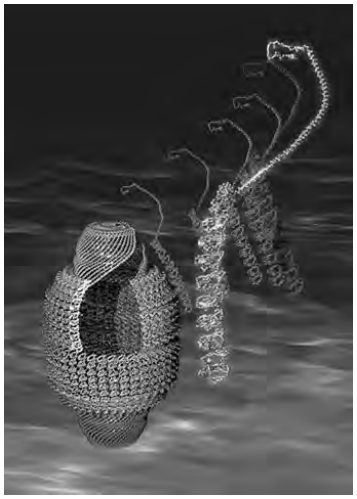

On the basis of the X-ray structure, which was of an empty vault built from a cysteine-tagged construct of MVP (termed cpMVP vaults), cpMVP vault was proposed to comprise 96 MVP molecules each folding into 14 domains. 48 MVP molecules were proposed to extend between the middle and each tip of the vault, so that the cpMVP vault exhibited 48-fold dihedral symmetry(1). However, our crystallographic analysis of rat liver vault, at 10 Å resolution, demonstrated that the particle exhibits 39-fold dihedral symmetry instead of 48-fold dihedral symmetry (2).We have determined the X-ray structure of rat liver vault at 3.5 Å resolution (3) and show that the cage structure consists of a dimer of half vaults, with each half vault comprising 39 identical major vault protein (MVP) chains (Figure). Each MVP monomer folds into 12 domains; nine structural repeat domains, a shoulder domain, a cap-helix domain and a cap-ring domain. Interactions between the 42-turn long cap-helix domains are key to stabilizing the particle. The shoulder domain is structurally similar to a core domain of stomatin, a lipid-raft component in erythrocytes and epithelial cells.

References

1. D. H. Anderson, V. A. Kickhoefer, S. A. Sievers, L. H. Rome, D. Eisenberg, *PLoS Biol*. **5**, e318 (2007).
2. Koji Kato, Hideaki Tanaka, Tomoyuki Sumizawa, Masato Yoshimura, Eiki Yamashita, Kenji Iwasaki and Tomitake Tsukihara, *Acta Crystallogr.* D **64**, 525-531 (2008).
3. H. Tanaka, K. Kato, E. Yamashita, T. Sumizawa, Y. Zhou, M. Yao, K. Iwasaki, M. Yoshimura and

T. Tsukihara, Science, **323**, 384-388 (2009).

MS13-2 Recognition of Nuclear Export Signal by CRM1

Xiuhua Dong, Anindita Biswas, Katherine Suel, Laurie Jackson, Hongmei Gu, Rita Martinez, Yuh Min Chook
Dept. of Pharmacology, UT Southwestern, 6001 Forest Park, Dallas, TX 75390-9041, USA (yuhmin.chook@utsouthwestern.edu)

CRM1 (also known as XPO1 and exportin 1) mediates nuclear export of hundreds of proteins through the recognition of the leucine-rich nuclear export signal (LR-NES). Here we present the 2.9 Å structure of CRM1 bound to snurportin 1 (SNUPN). Snurportin 1 binds CRM1 in a bipartite manner by means of an amino-terminal LR-NES and its nucleotide-binding domain. The LR-NES is a combined a-helical-extended structure that occupies a hydrophobic groove between two CRM1 outer helices. The LR-NES interface explains the consensus hydrophobic pattern, preference for intervening electronegative residues and inhibition by leptomycin B. The second nuclear export signal epitope is a basic surface on the snurportin 1 nucleotide-binding domain, which binds an acidic patch on CRM1 adjacent to the LR-NES site. Multipartite recognition of individually weak nuclear export signal epitopes may be common to CRM1 substrates, enhancing CRM1 binding beyond the generally low affinity LR-NES. Similar energetic construction is also used in multipartite nuclear localization signals to provide broad substrate specificity and rapid evolution in nuclear transport.

MS13-3 NEMO regulates NF-κB activation by specific recognition of linear ubiquitin chains

Simin Rahighi[1,2], Fumiyo Ikeda[3], Masato Kawasaki[1,2], Masato Akutsu[1,2,4], Nobuhiro Suzuki[1], Ryuichi Kato[1,2], Tobias Kensche[3], Tamami Uejima[1], Stuart Bloor[4], David Komander[4], Felix Randow[4], Ivan Dikic[3] and Soichi Wakatsuki[1,2]
[1]SBRC, PF, IMSS, High Energy Accelerator Research Organization (KEK), Tsukuba, Ibaraki 305-0801, Japan (simin@post.kek.jp), (soichi.wakatsuki@kek.jp)
[2] Graduate University for Advanced Studies, Hayama, Kanagawa 240-0193, Japan
[3] Institute of Biochemistry II, Goethe University School of Medicine, Theodor-Stern-Kai 7, D-60590 Frankfurt (Main), Germany
[4]MRC Laboratory of Molecular Biology, Hills Road, Cambridge CB2 0QH, UK

Modification of proteins by ubiquitin is critical for regulation of multiple cellular functions. NEMO (NF-κB essential modulator) as a regulator of the NF-κB signaling is in turn regulated by binding to ubiquitylated substrates. This study reveals that NEMO UBAN (ubiquitin binding in ABIN proteins and NEMO) motif specifically recognizes linear (head-to-tail) ubiquitin chains and this specific recognition is required for NF-κB activation by TNF-α and other agonists *in vivo*. NEMO UBAN motif itself adopts a homo-dimer coiled-coil structure which forms a hetero-tetrameric complex with linear diubiquitins. Each NEMO dimer symmetrically accommodates two linear diubiquitin molecules, one on either side of the structure. In each diubiquitin the distal ubiquitin is recognized through the canonical Ile44 surface and the proximal one through a novel surface which is adjacent but not overlapping

with the hydrophobic surface. The linker of the two ubiquitin moieties formed by the C-terminal tail of the distal ubiquitin provides interaction core with the UBAN motif. Interactions made to all four ubiquitin moieties are essential for efficient activation of NF-κB signaling by NEMO explaining the detrimental effects of mutations in UBAN leading to X-linked ectodermal dysplasia and immunodeficiency.

MS13-4 The atomic structure of granulovirus polyhedrin at 1.8Å resolution

Elaine Chiu[1], Shin-Mei Yeh[1], Richard Bunker[1], Clemens Schulze-Briese and Peter Metcalf[1]

[1] *School of Biological Sciences, University of Auckland, Thomas Building 110, 3A Symonds Street, Auckland, New Zealand (peter.metcalf@auckland.ac.nz)*

[2] *Swiss Light Source at Paul Scherrer Institute, Villigen 5232, Switzerland (clemens.schulze@psi.ch)*

Granulovirus (Cydia pomonella betabaculovirus, CpGV) sprays are widely used as specific biological control agents to control codling moth in apple orchards. The environmental stability of CpGV is a result of a unique 70nm thick crystalline surface layer surrounding the membrane of each virus particle. This crystalline layer consists mainly of the 248 amino acid protein CpGV polyhedrin, 50% identical to the amino acid sequence of the polyhedrin produced by *Autographa Californica* Multicapsid Nucleopolyhedrovirus (AcMNPV), the type specific baculovirus. In AcMNPV and other alphabaculoviruses, polyhedrin in the nucleus of infected cells forms larger cubic crystals, which contain numerous virus particles. CpGV are about 400nm long and contain only a few thousand unit cells surrounding a single virus particle. In spite of the small size, CpGV diffract X-rays to at least 3.2Å resolution in powder experiments. We expressed CpGV polyhedrin in insect cells obtaining intracellular micro-crystals, which were used to determine the atomic structure at 1.8Å resolution. The talk will describe the structure of crystalline surface layer of granulovirus, determined using both single crystal micro-crystallography and powder methods.

MS13-5 Crystal structure of human REV7 in complex with REV3 fragment

Kodai Hara[1], Toshiyuki Shimizu[1], Yoshiki Murakumo[2], Shunsuke Kobayashi[3], Toshiaki Kogame[3], Satoko Akashi[1], Satoru Unzai[1], Tomo Hanafusa[4], Haruo Ohmori[4], Shunichi Takeda[3], Mamoru Sato[1], Hiroshi Hashimoto[1]

[1] *Yokohama City University, Graduate School of Nanobioscience, 1-7-29 Suehiro-cho, Tsurumi-ku, Yokohama 230-0045, Japan (hash@tsurumi.yokohama-cu.ac.jp)*

[2] *Nagoya University, Graduate School of Medicine, 65 Tsurumai-cho, Showa-ku, Naogya 466-8550, Japan*

[3] *Kyoto University, Graduate School of Medicine, Konoe Yoshida, Sakyo-ku, Kyoto 606-8501*

[4] *Kyoto University, Institute of Virus Research, 53 Shogoin, Kawara-cho, Sakyo-ku, Kyoto 606-8507, Japan*

Trans-Lesion DNA synthesis (TLS) is one strategy of DNA damage tolerance mechanisms to allow continuation of DNA synthesis at damaged template. TLS consists of two major

processes, nucleotide insertion at the lesion site and extension. DNA polymerase ζ (Polζ) is one of key player in TLS and it acts as both inserter and extender. Polζ is composed of catalytic REV3 and regulatory REV7 subunits. Furthermore, REV7 also interacts with REV1, which is also a key DNA polymerase in TLS. In addition, REV7 involves in multiple protein-protein interactions in various cellular functions including transcription and cell-cycle check point. For instance, REV7 interacts with ELK1 and a phosphorylated form of JNK in response to DNA damage and cell stress. Several studies also suggest that REV7 can inhibit the anaphase promoting complex (APC) through interactions with CDH1 in G2/M phase. Recently, it has been reported that a *Shigella* effector IpaB interferes the inhibition of APC by interacting with REV7, thereby causing cell-cycle arrest. Although REV7 plays a role of an adopter protein in various cellular functions, the mechanism of those interactions by REV7 still unknown. Here we report the crystal structure of human REV7 in complex with human REV3 fragment. The structure of REV7-REV3 complex revealed that the C-terminal region of REV7 wrapped the REV3 fragment, thereby adopting a knot structure. Furthermore, we performed the pull down assay by using REV7 mutants and REV3 and revealed the mechanism of the interaction of REV7 with REV3.

MS14-1

High-Pressure Synthesis and Superconducting Properties of Oxygen-deficient Oxypnictide Superconductors *Ln*FeAsO$_{1-y}$

H. Eisaki[1,5], K. Miyazawa[1,2], M. Nakajima[1,3,5], S. Ishida[1,3,5], M. Ishikado[1,4,5], K. Kihou[1,5], P. M. Shirage[1], C. H. Lee[1,5], N. Takeshita[1,5], R. Kumai[1,5], Y. Tomioka[1,5], H. Kito[1,5], K. M. Kojima[3,5], T. Ito[1,5], S. Shamoto[4,5], S. Uchida[3,5], A. Iyo[1,2, 5]

[1]*National Institute of Advanced Industrial Science and Technology (AIST), 1-1-1 Central 2, Umezono, Tsukuba, Ibaraki, 305-8568, Japan. (h-eisaki@aist.go.jp)*

[2] *Department of Applied Electronics, Tokyo University of Science, 2641 Yamazaki, Noda, Chiba 278-3510, Japan.*

[3]*Dept. of Physics, University of Tokyo, 7-3-1 Hongo, Bunkyo-ku, Tokyo 113-0033, Japan*

[4]*Quantum Beam Science Directorate, Japan Atomic Energy Agency, Tokai, Naka, Ibaraki, 319-1195, Japan.*

[5] *JST, Transformative Research-Project on Iron Pnictides (TRIP), 5, Sanbancho, Chiyoda, Tokyo 102-0075, Japan.*

We have synthesized a series of oxygen-deficient, fluorine-free oxypnictide superconductor, *Ln*FeAsO$_{1-y}$ (Ln: rare-earth) using high-pressure technique. Superconductivity shows up by introducing oxygen deficiency and sharp superconducting transition with their transition temperature higher than 50K is observed for heavier *Ln*'s (Nd, Sm, Gd, Tb, and Dy). The effects of oxygen deficiency, variation of Ln ions, and the external pressure on Tc indicate the strong influence of the crystal structure on the superconducting properties of the oxypnictide superconductors.

MS14-2 Diffraction study on the Fe-based high temperature superconductors

Wei Bao
Department of Physics, Renmin University of China, 59 Zhongguancun Ave., Haidian District, Beijing, 100872, China (wbao@ruc.edu.cn)

High temperature superconductivity has been discovered recently in the ZrCuSiAs, $ThCr_2Si_2$ and PO structures, with the FeAs(Se) antifluorite layer as the common structural building block [1]. We will present our neutron diffraction study on crystal and magnetic structures of NdFeAs(O,F) [2], $BaFe_2As_2$ [3] and Fe(Se,Te) [4] superconductor systems. The NdFeAsO and $BaFe_2As_2$ share the same in-plane magnetic structure. But the rare-earth magnetic ion Nd alters the interlayer magnetic moment alignment from antiparallel to parallel. Such a result was also later found to be the case for Ce or Pr materials of the ZrCuSiAs family. The FeTe has a very different in-plane magnetic order than that for the previous two systems. Since all three systems have the similar Fermi surface geometry, the prevailing spin-density-wave nesting Fermi surface mechanism proposed for antiferromagnetic order in these materials does not look as convincing as before our results of FeTe was reported. And localized magnetism mechanism should deserve a better evaluation.

Combined x-ray and neutron diffraction techniques, we demonstrate for the first time the coexistence of antiferromagnetic order and superconductivity in the $ThCr_2Si_2$ family of materials, using $(Ba,K)Fe_2As_2$ as samples [5]. This differs from cuprate high temperature superconductors, for which long-range antiferromagnetic order and superconductivity exist side-by-side. The coexistence would provide constraint on the possible superconducting order parameter. Our result has been since confirmed in other Ni or Co doped $BaFe_2As_2$ systems by other groups.

References

[1] Y. Kamihara et al., *J. Am. Chem. Soc.* **130**, 3296 (2008); M. Rotter et al., *Phys. Rev. Lett.* **101**, 107006 (2008); F.-C. Hsu et al., *PNAS* **105**, 14262 (2008).
[2] Y. Qiu et al., *Phys. Rev. Lett.* **101**, 257002 (2008).
[3] Q. Huang et al., *Phys. Rev. Lett.* **101**, 257003 (2008).
[4] W. Bao et al., *Phys. Rev. Lett.* **102**, 247001 (2009).
[5] H. Chen et al., *Europhys. Lett*., **85**, 17006 (2009).

MS14-3 Electric Polarization Flop and Magnetic Phase Transition Induced by Magnetic Field in Multiferroic RMn_2O_5 (R = Tm, Yb)

Hiroyuki Kimura[1], Yuma Sakamoto[1], Mamoru Fukunaga[1], Yukio Noda[1], Nobuyuki Abe[1], Kouji Taniguchi[1], Taka-hisa Arima[1], Shuichi Wakimoto[2], Kazuhisa Kakurai[2]
[1] *Institute of Multidisciplinary Research for Advanced Materials, Tohoku University, Katahira 2-1-1, Aoba, Sendai 980-8577, Japan (kimura@tagen.tohoku.ac.jp)*
[2] *Japan Atomic Energy Agency*

Multiferroic RMn_2O_5 (R = rare-earth, Bi, Y) is well known as an antiferromagnetic, ferroelectric material showing a colossal magnetoelectric (CME) effect. This system has a rich variety of dielectric responses induced by the application of magnetic field, of which

behaviors strongly depend on the type of rare-earth ions. Recently, we have found that in $TmMn_2O_5$, electric polarization flops from *b*-axis to *a*-axis with decreasing temperature under zero-magnetic field [1]. Previous report on $TmMn_2O_5$ shows that the polarization along *b*-axis was induced by applying magnetic field [2]. These facts indicate that the polarization flop from *a*-axis to *b*-axis can be induced by magnetic field in this material. To confirm this polarization flop, we conducted polarization measurement under magnetic field, resulting that the polarization flop occurs around $H = 0.6$ T as magnetic field is applied parallel to *c*-axis. We also found the electric polarization flop from *b*-axis to *a*-axis in $YbMn_2O_5$, which occurs at $T = 4.2$ K under $H = 1.75$ T as well as at $T = 5.5$ K under $H = 0$ T. Neutron diffraction measurements for $TmMn_2O_5$ and $YbMn_2O_5$ showed that the magnetic phase transition concomitantly takes place at the transition of polarization flop. We also discovered the Microscopic magnetic phase boundaries completely agree with dielectric phase boundaries in temperature-Magnetic field phase diagram, suggesting that the flop of electric polarization is triggered by magnetic phase transition.

This work has been supported by a Grant-In-Aid for Scientific Research (A), No. 21244051, and Grant-In-Aid for Scientific Research on Priority areas ``Novel States of Matter Induced by Frustration", No. 19052001, from the Ministry of Education, Culture, Sports, Science and Technology.

MS14-4 Effect of Ga^{3+} Substitution for Mn^{3+} on Magnetic and Dielectric Properties in Multiferroic YMn_2O_5

Yuma Sakamoto[1], Hiroyuki Kimura[1], Satoru Horio[1], Arno Fey[1], Mamoru Fukunaga[1], Ryoji Kiyanagi[1], Yukio Noda[1], and Hiraka Haruhiro[2]

[1] *Institute of Multidisciplinary Research for Advanced Materials, Tohoku University, Katahira 2-1-1, Aoba, Sendai 980-8577, Japan (yuma@mail.tagen.tohoku.ac.jp)*

[2] *Institute of Materials Research, Tohoku University Katahira 2-1-1, Aoba, Sendai 980-8577, Japan*

Multiferroic RMn_2O_5 (R = rare-earth, Bi, Y) shows ferroelectric and antiferromagnetic ordering simultaneously and a colossal magnetoelectric effect (CME). This suggests strong correlation between the magnetism and dielectricity. The magnetic phases of YMn_2O_5 include a two-dimensional incommensurate (2D-ICM) phase, a 1D-ICM phase, a commensurate (CM) phase and another low temperature 2D-ICM (LT2D-ICM) phase. The ferroelectric (FE) phase is first realized in the CM phase, and then changes to the so-called weak ferroelectric (WFE) phase in the LT2D-ICM phase. We revealed that a transverse spin spiral structure of $Mn^{4+}O_6$ octahedron chains along the c-axis is established in the CM phase [1] and in the LT2D-ICM phase [2], and then two independent $Mn^{4+}O_6$ chains are connected by $Mn^{3+}O_5$ pyramid. From the $\mathbf{S}_i \times \mathbf{S}_{i+1}$ mechanism, this chiral spin structure along the c-axis produces macroscopic electric dipolemoment along the b-axis. On the other hand, antiferromagnetic interaction in the ab-plane plays another possible origin to produce the electric dipolemoment due to the so-called magnetoelastic coupling.

In order to understand the roles of the magnetic moments of Mn^{4+} and Mn^{3+} ions, non-magnetic ions, Ga^{3+}, were introduced at the site of Mn^{3+} ($YMn^{4+}(Mn_{1-x}Ga_x)^{3+}O_5$), diluting the mean magnetic moment at that site. Thus, we expect the nonmagnetic Ga^{3+} ion

will disconnect the interaction between $Mn^{4+}O_6$ octahedron chains. In turn, the role of $Mn^{4+}O_6$ octahedron chains becomes clear.

Neutron diffraction and electric measurements show steep decrease of the FE and CM phase as the concentration of Ga^{3+} increases. Meanwhile the phase transition temperature of LT2D-ICM remains almost unchanged. Therefore the Ga-doping was found to suppress the FE and CM phase. This means that the FE and CM phase is produced by the interaction between $Mn^{4+}O_6$ octahedron chains, while the WFE and LT2D-ICM phase is produced by the chiral spin structure of $Mn^{4+}O_6$ octahedron along the c-axis.

This work has been supported by a Grant-In-Aid for Scientific Research (A), No. 21244051, and Grant-In-Aid for Scientific Research on Priority areas ``Novel States of Matter Induced by Frustration", No. 19052001, from the Ministry of Education, Culture, Sports, Science and Technology.

References

[1] Y. Noda, H. Kimura, Y. Kamada, T. Osawa, Y. Fukuda , Y. Ishikawa, S. Kobayashi, Y. Wakabayashi, H. Sawa, N. Ikeda and K. Kohn, Physica B 385-386 (2006) 119-1122.
[2] J.-H. Kim, S.-H. Lee, S. I. Park, M. Kenzelmann, A. B. Harris, J. Schefer, J.-H. Chung, C. F. Majkrzak, M. Takeda, S. Wakimoto, S. Y. Park, S-W. Cheong, M. Matsuda, H. Kimura, Y. Noda, and K. Kakurai, Phys. Rev. B78(2008) 245115(10pp).

MS15-1 Electron Microscopy of Low-Dimensional Nanomaterials

Fangfang Xu
Shanghai Institute of Ceramics, Chinese Academy of Sciences, 1295 Dingxi Road, Shanghai, 200050, China (ffxu@mail.sic.ac.cn)

Crystallography in micro- or nano-scale could be resolved via electron microscopy (EM) taking advantages of its high spatial resolution, variety of electron diffraction (ED) techniques, and local chemical information. Revealing the micro-crystallography can bring about a lot of useful informations of materials including the formation mechanism, growth habit, and specifically, the nature of properties. Here, we present our work during the past few years on the EM of low-dimensional nanomaterials which have exhibited promising applications in nanoelectronics, nanophotonics and biotechnology.

The researches to be introduced include a new tubular structure of graphite-type nanotubes[1,2], new polytypes of graphitic BN[3], crystallography of Co@BN nanocables[4], growth mechanism of one-dimensional (1D) nanomaterials generated without any catalysts or templates[5], and defect structures in niobate nanosheets[6]. Electron diffractions discovered a new tubular structure of hexagonal BN showing an Archimedes spiral geometry (Fig.1). Complete structural models have been established for this new tubular form, taking into account of disclination angles, coincidence site lattices and centers of disclination operation. The specific conical helix structures of BN nanotubes have been found to exhibit some interesting structural and mechanical properties, i.e. the structural parameters could be tailored via heat treatment and the nanotubes behaved like a metallic spring. New polytype structures of graphitic BN, i.e. 12R and 24R, have been observed in BN fibers as revealed by EDs and high

resolution electron microscopy (HREM). EM of Co@BN nanocables figured out the crystallography of Co-B phase inside the small volume of nanotubes and the structural relations between the metal core and tubular shell. HREM and structural modeling revealed 1D growth of crystals dominated by pseudo-screw packing of polyhedral growth units in a vapor-phase (VP) kinetics (Fig.2). Crystallography of niobate nanosheets have been studied focusing on the defect and surface structures. Dynamics of defects have been examined via in-situ EM, induced by either heating or electron irradiation. These researches proved that EM should be a powerful and effective tool for the analysis of crystallography in very small scale.

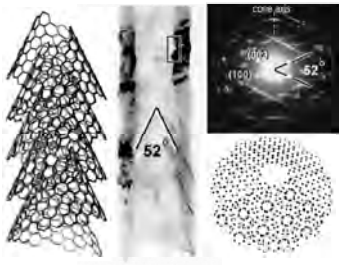

Fig. 1 Structures of tubular conical helix.

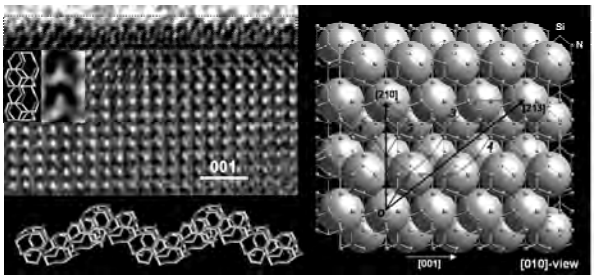

Fig. 2 1D growth mechanism in VP processes.

References

1. F. F. Xu, Y. Bando, R. Ma, D. Golberg, Y. Li and M. Mitome, *J. Am. Chem. Soc*., **125** (*26*) 8032-8038 (2003).
2. F. F. Xu and Y. Bando, *Acta Crystallogr. A*, **59**, 168-171 (2003).
3. F. F. Xu, Y. Bando and M. Hasegawa, *Chem. Commun*., **14**, 1490-1491 (2002).
4. F. F. Xu, Y. Bando, D. Golberg, M. Hasegawa and M. Mitome, *Acta Mater*., **52** (*3*) 601-606 (2004).
5. F. F. Xu, L. L. Zhang, X. F. Du and Y. C. Zhu, *Cryst. Growth Des.*, **8** (*7*) 2574-2580 (2008).
6. F. F. Xu, Y. Ebina, Y. Bando and T. Sasaki, *J. Phys. Chem. B*, **107** (*28*) 6698-6703 (2003), **107** (*36*) 9638-9645 (2003).

3 Dimensional Coherent Electron Difractive Imaging of Nanoparticle

MS15-2

Fu-Rong Chen[1,2], Roman Dronyak,[1,2], Keng S. Liang[2]
[1] *Department of Engineering and System Science, National Tsing Hua University, Hsinchu 30013, Taiwan (frchen@ess.nthu.edu.tw)*
[2] *National Synchrotron Radiation Research Center, Hsinchu 30076, Taiwan (dronyak@nsrrc.org.tw)*

The electron diffraction pattern from a faceted MgO nanoparticle was phased using coherent diffractive imaging (CDI) technique. The primary limitations of the accurate and reproducible inversion of the electron diffraction pattern are due to the difficulty in treating experimental noises, substrate scattering and partial spatial coherence of the incident beam. Furthermore, the reconstruction of the complex-valued exit wave function requires sufficiently tight boundary of the sample called "support". In this work, we present the phase recovery procedure that utilizes guided hybrid input-output (GHIO) algorithm with dynamic support to reconstruct the stable and reproducible solution by optimizing feedback parameter of the algorithm and threshold value for dynamic support. To quantify the spatial accuracy of recovered result the deviation map was obtained as a relative standard deviation of the

averaged solution. The result shows that the reproducible solution can be deduced from diffraction patterns only, without information from TEM image [1-2].

Figure 1 shows recovered shape and exit wave of the sample with their deviation maps. The contrast decay at the edges and corners of the sample is due to the thickness decrease of the faceted nanoparticle. The region of low accuracy in the exit wave is comparable with the resolution of the recovered shape function. It may be due to the large amount of missed weak scattering signals in the recorded diffraction patterns. Therefore, it complicates imaging the local structure at atomic resolution, such as for single-atom defects. The optimization analysis and effects of the incident illumination on the phase recovery technique will be discussed in detail.

Tree dimensional diffraction data around Bragg peak of {020} were recorded by rotating nano-particle along [220] axis every 0.1 degree. As shown in Fig. 2, the 3 dimensional CDI exit wave was reconstructed using from 34 diffraction data spanned 3.4 degree. The reconstruction algorithm and result will be discussed in detail.

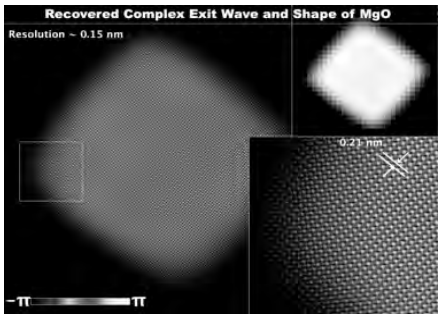

Fig.1 the reconstructed exit wave of MgO nanoparticle

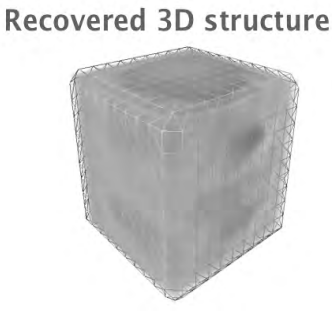

Fig.2 the 3-D reconstructed EW

References

[1] R. Dronyak, C.-K. Feng, K. S. Liang and F.-R. Chen. Electron diffractive imaging of the MgO nano-particle: towards atomic-resolution. XXI IUCr Congress and General Assembly, Osaka. Acta Cryst. A64, C130 (2008).
[2] This work was supported by the National Science Council (NSC 97-2112-M-213-001 and NSC 95-2221-E-007-093) and the Thematic Project of Academia Sinica of Taiwan.

MS15-3 High-resolution Structural Analysis of Membrane Proteins by Electron Crystallography

Kaoru Mitsuoka
Biomedicinal Information Research Center (BIRC), National Institute of Advanced Industrial Science and Technology (AIST), 2-41-6 Aomi, Koto-ku, Tokyo, 135-0064, Japan (kaorum@ni.aist.go.jp)

Transmission electron microscopy at low temperatures, cryoEM, of biological specimens provides several unique possibilities such as obtaining a very broad spatial information interval reaching from cellular to atomic dimensions, understanding functionally relevant conformational changes from heterogeneous samples and localization of individual components in large systems. It is also possible to study biomolecules in a close to natural environment, e.g. membrane proteins in a lipid bilayer. The branch of cryoEM that is using

periodically assembled biomolecules in the form of two-dimensional (2D) crystals is termed electron crystallography and can provide structural information at a resolution level which allows building of atomic models.

The superfamily of proteins called Membrane Associated Proteins in Eicosanoid and Glutathione metabolism (MAPEG) are relatively small membrane-bound enzymes. The substrates of these proteins are in most cases hydrophobic molecules and the active sites are located in the lipid embedded parts of the polypeptide chains. Thus, in order to obtain a detailed understanding of the mechanism and to determine interactions with substrates and inhibitors it is of fundamental importance that the enzymes are located in a lipid bilayer environment during experiments. Electron crystallography is thought to be a suitable method because of this reason.

We have chosen to study MAPEG members and their interaction with small molecules because of human health relevance in general and particularly since several of these proteins constitute potential drug targets against common diseases. Moreover, we know from previous work that they are prone to form 2D crystals suitable for high-resolution electron crystallographic analysis. The detoxification enzyme microsomal glutathione transferase 1, MGST1, was the first MAPEG structure to be determined (1). The structure of rat MGST1, at 3.2 Å resolution, solved in complex with glutathione, defines the active site location and a cytosolic domain involved in enzyme activation.

More recently we have also obtained an atomic model of microsomal prostaglandin E synthase 1, MPGES1 (2). This MAPEG member is of particular importance in medicine since it is the inducible, terminal enzyme in the cascade of events that leads to the formation of prostaglandin E2, a potent mediator of pain, fever and inflammation. Together with results from site-directed mutagenesis and activity measurements, we can thereby demonstrate the role of specific amino acid residues. Glutathione is found to bind in a U-shaped conformation at the interface between subunits in the protein trimer. It is exposed to a site facing the lipid bilayer, which forms the specific environment for the oxidoreduction of PGH2 to PGE2 after displacement of the cytoplasmic half of the N-terminal transmembrane helix. Hence, insight into the dynamic behavior of MPGES1 and homologous membrane proteins in inflammation and detoxification is provided.

In addition, we will discuss about our recent efforts to improve the resolution of structural analysis of aquaporin 1, a water channel, whose atomic model was first determined by electron crystallography (3).

References

1. Holm, P. J., Bhakat, P., Jegerschold, C., Gyobu, N., Mitsuoka, K., Fujiyoshi, Y., Morgenstern, R., Hebert, H. (2006) *J. Mol. Biol*. **360**, 934-945.
2. Jegerschöld, C., Pawelzik, S. C., Purhonen, P., Bhakat, P., Gheorghe, K. R., Gyobu, N., Mitsuoka, K., Morgenstern, R., Jakobsson, P. J., Hebert, H. (2008) *Proc. Natl. Acad. Sci. USA*. **105**, 11110-11115.
3. Murata, K., Mitsuoka, K., Hirai, T., Walz, T., Agre, P., Heymann, J. B., Engel, A., Fujiyoshi, Y. (2000) *Nature*, **407**, 599-605.

Strain mapping near Si/SiGe interfaces using HOLZ line CBED patterns

MS15-4

Koh Saitoh[1], Maiko Hamabe[2], Nobuo Tanaka[1]
[1] *EcoTopia Science Institute, Nagoya University, Furo-cho, Chikusa-ku, Nagoya 464-8603, Japan (saitoh@esi.nagoya-u.ac.jp)*
[2] *Department of Crystalline Materials Science, Nagoya University, Furo-cho, Chikusa-ku, Nagoya 464-8603, Japan*

Lattice strain is one of the important parameters, which influences the physical properties of crystalline materials, especially in the modern semiconductor industry. Convergent-beam electron diffraction (CBED) may provide one of the best solutions for such industrial requirements, due to its high spatial-resolution and accuracy. In the lattice parameter determination by CBED, the positions of higher-order Laue zone (HOLZ) lines in the 000 disc are fitted between the experimental and simulated patterns. However, the splitting of HOLZ lines, which are often observed in CBED patterns taken at a vicinity to interfaces and surfaces, prevents the conventional technique (Fig. 1). It has been reported that the splitting of HOLZ lines is caused by a bending distortion of the lattice and can be determined by the fitting of intensity profiles across the HOLZ lines in experimental CBED patterns to dynamical simulations. Such dynamical simulations, however, are unsuitable for practical use because of its huge calculation cost.

In the present study, we propose a simple method to determine the bending strain of a lattice together with lattice constants on the basis of the kinematical diffraction theory and the Hough transform technique. The method is applied to determine bending strains in a Si substrate region close to a Si/SiGe interface.

Fig. 2 shows a schematic diagram of a lattice with a bending strain. Each lattice point is displaced in the x-direction, whose displacement magnitude depends on the z-coordinate (the direction of incident electron). It is found that the scattering amplitude, which is originally peaked at the reciprocal lattice points in the non-bended lattice, shows a split of the peaks in the k_z-direction, resulting in the splitting of HOLZ lines. We confirmed that the width of the splitting is approximately proportional to $|\mathbf{g}\bullet\mathbf{R}|$, inner product of the lattice displacement vector **R** and the reciprocal lattice vector **g**. Figs. 3(a) and 3(b) show simulations of the Si [320] HOLZ line pattern without a bending strain and with a bending strain with **R**//[001], respectively. By a fitting of the experimental and simulated patterns using the Hough transform technique for a series of HOLZ line patterns taken from a region near the Si/SiGe interface, a two-dimensional strain distribution is visualized.

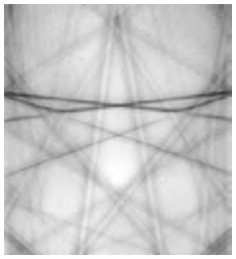

Fig.1: Si [320] HOLZ line pattern taken from a region near a Si/SiGe interface.

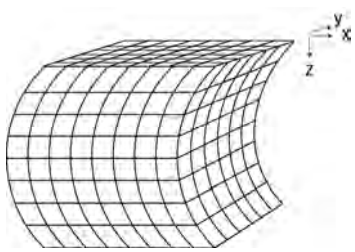

Fig.2: Model of a lattice with a bending strain.

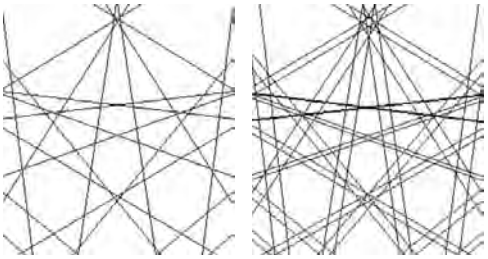

Fig.3 HOLZ line patterns simulated from lattices without a bending strain (a) with a bending strain (b).

Visualization of the orbital-ordered state of $FeCr_2O_4$ using the CBED method

MS15-5

Daisuke Morikawa, Kenji Tsuda, Shintaro Ohtani and Takahisa Arima
Institute of Multidisciplinary Research for Advanced Materials, Tohoku University, Japan, 2-1-1 Katahira, Aoba-ku, Sendai, 9808577,Japan
(morikawa@mail.tagen.tohoku.ac.jp)

A structure analysis method using convergent-beam electron diffraction (CBED), which was developed by Tsuda and Tanaka[1,2], enables us to directly determine the electrostatic potential from a nanometer-scale specimen area. The electron density distribution can be also obtained from the electrostatic potential through the Poisson's equation. We have applied the method to a spinel oxide $FeCr_2O_4$, which undergoes a structural phase transformation at 135K from a cubic spinel structure of the high-temperature phase to a tetragonal structure of the low-temperature phase with Jahn-Teller (JT) distortion [3]. A ferro-type orbital-ordering of 3d electrons of the Fe atoms is expected to occur in the low-temperature phase [4].

$FeCr_2O_4$ single crystals were grown by the chemical vapor transport (CVT) method. Energy-filtered CBED patterns of the low-temperature phase were obtained at specimen temperature of 90K using an energy-filter transmission electron microscope (EFTEM) JEM-2010FEF with an accelerating voltage of 100kV. Atom positions, Debye-Waller factors and low-order structure factors were refined by nonlinear least squares fitting between the experimental CBED patterns and dynamical diffraction calculations using analysis software MBFIT [1]. The electrostatic potential and electron density distributions were reconstructed from the refined parameters.

Figure (a) shows the result of the present CBED analysis, the $4e/Å^3$ isosurface of the electron density colored with electrostatic potential at the Fe-O tetrahedron. Clear anisotropy of the electrostatic potential has been found in the *c*-direction, being attributed to the ferro-type $3z^2\text{-}r^2$ orbital ordering.

For comparison, the electrostatic potential and electron density of the orbital-ordered state has been simulated using non-spherical scattering factors for the Fe $3z^2\text{-}r^2$ orbital [5]. The non-spherical scattering factors were applied to the same low-order structure factors as those determined in the CBED experiments. It is seen that the simulated result of Fig. (b) shows very good agreement with the experimental one.

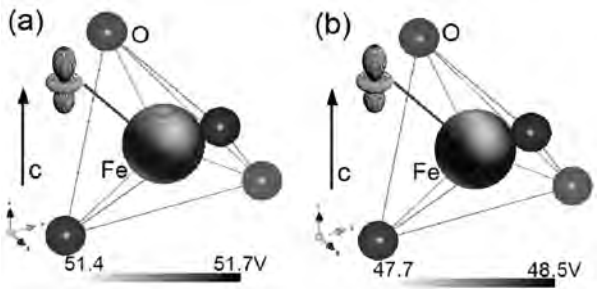

Figures (a) and (b): 4e/Å3 isosurfaces of electron density colored with electrostatic potential at Fe-O tetrahedral, obtained from (a) the present CBED analysis and (b) the simulation using non-spherical scattering factors.

References

[1] K. Tsuda & M. Tanaka, *Acta Cryst*. **A55**, 939-954 (1999).
[2] K. Tsuda *et al*., *Acta Cryst*. **A58**, 514-525 (2002).
[3] G. Shirane & D. E. Cox, *J. Appl. Phys*. **35**, 954 (1964).
[4] T. Arima *et al*., *J. Magn. Magn. Mat*. **310**, 807 (2007).
[5] R. J.Weiss & A. J.Freeman, *J. Phys. Chem. Solids.* **10**, 147 (1959)

RS-1 Synthesis, structures and properties of modulated fresnoites

Patryck K. K. Allen, Siegbert Schmid
School of Chemistry, University of Sydney, NSW 2006, Australia

In response to the negative environmental impact of lead-based materials, recent European Union and Japanese legislation has introduced severe restrictions on the use of hazardous substances in electronic equipment, creating a demand for lead-free electronic materials, particularly piezoelectrics [1, 2]. A comprehensive understanding of the relationship between the structural chemistry and physical properties is vital for the design and development of new, environmentally friendly electronic materials.

The fresnoite family of modulated structures, $A_2TiM_2O_8$ (A = Ba, Sr; M = Si, Ge), has been shown to exhibit excellent piezoelectric properties [3, 4], making them one of several possible alternatives to replace PZT and other lead-based electroceramic materials. A wide range of techniques including synchrotron X-ray diffraction, neutron powder diffraction, electron diffraction, and differential scanning calorimetry have been used to investigate the structural behaviour of selected members of the $Ba_{2-2x}Sr_{2x}TiSi_2O_8$ solid solution, including temperature and compositionally induced phase transitions.

This contribution will discuss a variety of the diverse aspects of this ongoing project, including the non-trivial synthesis of the $Ba_{2x}Sr_{2-2x}TiSi_2O_8$ series, the use of a modulated structure approach to characterise powder diffraction data using Jana2006, and new evidence of the phase transition that removes the structural modulation in $Ba_2TiSi_2O_8$.

Recent evidence for the coexistence of two incommensurately modulated $Sr_2TiSi_2O_8$ phases at room temperature and results from variable temperature X-ray powder diffraction (Figure 1) will also be presented.

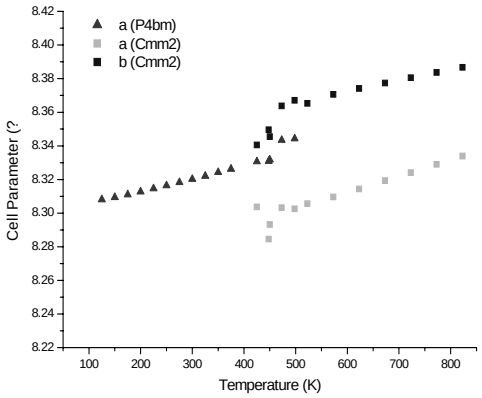

Figure 1: Change in cell parameters a and b in $Sr_2TiSi_2O_8$ when heated from 125–823 K.

References

1. Y. Li, K. S. Moon, C. P. Wong, *Science*, **2005**, 308, (5727), 1419-1420.
2. Y. Saito, H. Takao, T. Tani, T. Nonoyama, K. Takatori, T. Homma, T. Nagaya, M. Nakamura, *Nature*, **2004**, 432, (7013), 84-87.
3. Asahi, T. Osaka, J. Kobayashi, S. C. Abrahams, S. Nanamatsu, M. Kimura, *Phys. Rev. B*, 63, **2001**, (9), 1-13.
4. Halliyal, A. S. Bhalla, S. A. Markgraf, L. E. Cross, *Ferroelectrics*, **1985**, 62, 27-38.

RS-2

Structural and Spin Phase Transitions in the Polymeric Hybrid Organic-Inorganic Materials

Kittipong Chainok[1,2], Stuart R. Batten[3], Keith S. Murray[3], A. David Rae[4], Ian D. Williams[5], Kenneth J. Haller[1]

[1] *School of Chemistry, Institute of Science, Suranaree University of Technology, Nakhon Ratchasima 30000, Thailand (ken.haller@gmail.com)*

[2] *Department of Chemistry, Faculty of Science, Rangsit University, Pathumtani 12000, Thailand (Kittipong.C@rsu.ac.th)*

[3] *School of Chemistry, Institute of Science, Monash University, Clayton, Victoria 3800, Australia (Keith.Murray@sci.monash.edu.au, Stuart.Batten@sci.monash.edu.au)*

[4] *Research School of Chemistry, Australian National University, Canberra, ACT 0200 Australia (rae@rsc.anu.edu.au)*

[5] *Department of Chemistry, Hong Kong University of Science and Technology, Clear Water Bay, Kowloon, Hong Kong, P. R. China (chwill@ust.hk)*

Phase transitions in polymeric hybrid organic-inorganic materials are present. The order-disorder structural phase transition was observed in the polymeric isomorphous compounds of formula $[M(Im)_4V_2O_6]_\infty$, where M = Mn, Co, Ni, Im = imidazole.[1] The phase transition was studied by single crystal X-ray diffraction between 100 and 295 K. It was observed that the room temperature $P4_2/n$ disordered phase is reversibly transformed to the $I4_1/a$ ordered phase below 281 K for Mn and 175 K for Co. The ordered phase of Ni was found to have space group $P2/n$ at 100 K. The phase transition mechanisms of these compounds were affected by a change of the hydrogen bond connectivity. Another particularly interesting phase change is the magnetic spin-crossover (SCO) behavior found in the 3-D framework of formula $[Fe(AIBN)_3](MCl_4)_2$ where M = Fe^{III} and In^{III}, AIBN = 2,2'-azobisisobutyronitrile.[2] The SCO transitions were characterized by use of temperature dependent magnetic susceptibility (2−300 K) and Mössbauer effect spectral measurements (4.2, 77 and 295 K) together with single crystal X-ray crystallography (103 and 233 K). The data revealed that the AIBN compounds exhibit incomplete "half" SCO phenomena with no accompanying crystallographic phase change. Taking into account for the solid state phase transition, in the cases of formal $[M(Im)_4V_2O_6]$ and the later $[Fe(AIBN)_3](MCl_4)_2$ compounds are considered to be crystallographic first order phase transition and magnetic spin transition between two electronic states (high spin → low spin) in molecular chemistry, respectively, as evidence through careful investigation on such methods mentioned above. In addition, a review on X-ray crystal structures of another hybrid materials that have formed in attempts to bridge different aspects of solid state supramolecular chemistry and molecular crystal engineering, and also to understand their magnetostructure correlations are also proud to describe.[3,4]

References

1. Chainok, K.; Haller, K. J.; Rae, A. D.; Willis, A. C.; Williams, I. D. Investigation of the structure and phase transitions of the polymeric organic-inorganic hybrids: $[M(Im)_4V_2O_6]_\infty$, M = Mn, Co, Ni, Im = imidazole. To be submitted to *Acta Cryst. B*., 2009.
2. Chainok, K.; Neville, S. M.; Moubaraki, B.; Batten, S. R.; Murray, K. S.; Forsyth, C. M.; Cashion, J. D.; Haller, K. J. Synthesis, structures and spin crossover properties of infinite 3-D framework iron(II) containing organodinitrile bridging ligands. To be submitted to *Dalton Trans*., 2009.
3. Chainok, K.; Neville, S. M.; Moubaraki, B.; Batten, S. R.; Murray, K. S.; Haller, K. J. Antiferromagnetic coupling in 3-D network Ni^{II}–Ni^{II} cyanide-bridged homometallic compounds of $[Ni(CN)_4Ni(en)]\cdot 2H_2O$ and $[Ni(CN)_4Ni(tn)]\cdot H_2O\cdot MeOH$. To be submitted to *Dalton Trans*., 2009.

4. Chainok, K.; Neville, S. M.; Moubaraki, B.; Batten, S. R.; Murray, K. S.; Forsyth, C. M.; Cashion, J. D.; Haller, K. J. Synthesis, structures and magnetic properties of novel cyanide-bridged Fe^{II}–M^{II} heterometallic compounds, M^{II} = Mn, Ni, Cu. To be submitted to *Inorg. Chem*., 2009.

RS-3 Charge Density Study on Metal Complexes with Non-Innocent Ligand

Yu-Chun Chuang[1], Chou-Fu Sheu[1], Gene-Hsiang Lee[2], Yu Wang[1,2]
[1] *Department of Chemistry, National Taiwan University, Taipei, Taiwan (d94223006@ntu.edu.tw)*
[2] *Instrumentation Center, National Taiwan University, Taipei, Taiwan*

High resolution X-ray diffraction experiments and atom-specific X-ray absorption experiments are combined to investigate a series of square planar complexes containing M-S bonds. Studies on complexes of $(pyH)_z[M(mnt)_2]^{-z}$, where M = Ni or Cu and z= 2 and 1, $pyH=C_5NH_6^+$, mnt= $S_2C_2CN_2^{2-}$, are undertaken to identify the site of one electron oxidation-reduction to be at either the metal or the ligand due to the non-innocent character of the mnt (maleonitriledithiolate) ligand. Interestingly it is nicely demonstrated that the one electron redox reaction of Ni and Cu series is a ligand-based and a metal-based respectively. The metal K-, L-edge and the S K-edge X-ray absorption spectroscopy unambiguously indicate the site of oxidation and also provide some bonding characters of the M-S bond. The differences in geometries and in bonding characters in terms of topological properties associated with the bond critical points will be discussed between the oxidized form (2-) and the reduced form(1-). In the case of Ni complexes, the formal oxidation state of Ni remains as Ni(II) and each mnt ligand carries 2- in the $[Ni(mnt)_2]^{2-}$; but only one of the mnt is reduced in the $[Ni(mnt)_2]^{1-}$. On the contrary, in the case of Cu complexes, the mnt remains as 2- in both $[Cu(mnt)_2]^{2-}$ and $[Cu(mnt)_2]^{1-}$, but the formal oxidation state of Cu is Cu(II) and Cu(III) respectively. Bond characterizations and d-orbital populations will be presented in a combined study of experiment and theory. The complimentary results of XAS, XRD and DFT calculations are to be discussed. The conclusion on the redox behavior will be firmly established; the accompanied changes in M-L bonding will be illustrated.

RS-4 Topological features of short Cl…Cl contacts via experimental and theoretical charge density analysis

Venkatesha R. Hathwar, T. N. Guru Row
Solid State and Structural Chemistry Unit, Indian institute of Science Bangalore 560012, India (venkatesh@sscu.iisc.ernet.in)

Studies on halogen…halogen contacts in organic compounds using *ab initio* calculations[1] and crystallographic studies[2] show that these interactions are controlled by electrostatics. Indeed, these are represented as $C\text{-}X_1\cdots X_2\text{-}C$ moieties (where θ_1=C- $X_1\cdots X_2$ and $\theta_2=X_1\cdots X_2$-C; $R_{ij}=X_1\cdots X_2$ distance). Cl…Cl contacts are directive and are either attractive or repulsive based on the geometry of contact [2]. In order to decipher the specific interaction profiles of Cl…Cl contacts in the presence of other weak O-H…N, C-H…N and C-H…O hydrogen bonds, charge density analysis of 2-chloroquinolin-3-yl methanol and 2-chloro-3-

chloromethyl-8-methylquinoline have been carried out using high resolution X-ray diffraction data (resolution, $\sin\theta/\lambda = 1.08$ Å^{-1}) collected on good quality crystals at 100 K.

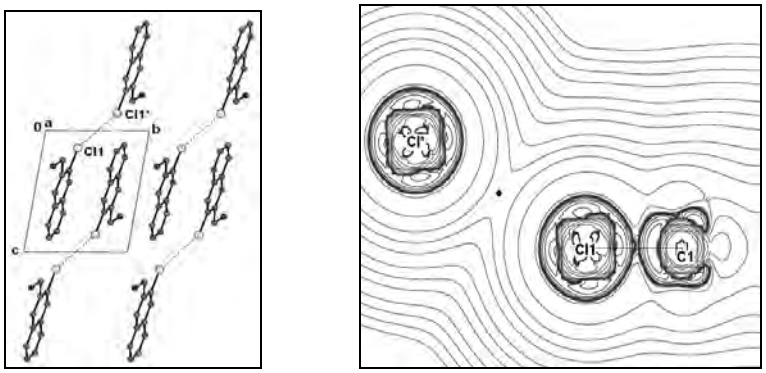

Figure1. Packing diagram highlighting Cl..Cl contacts along with the Laplacian map depicting the (3, -1) bond critical point.

The intermolecular interactions were analyzed based on Bader's QTAIM theory[3] incorporated in XD2006 package[4]. Theoretical calculations of charge density analysis were carried out using CRYSTAL06[5] for the comparison of observed results. The Cl…Cl short contact is observed as a 'closed shell' van der Waals interaction with the (3, -1) bond critical point (Figure 1) for 2-chloroquinolin-3-yl methanol displaying Type I interaction. On the other hand, 2-chloro-3-chloromethyl-8-methylquinoline displays a type II contact and the topological features suggest a nucleophile-electrophile interaction as observed earlier[6]. Further, the topological features associated with one electron properties were analyzed in both the compounds.

References

1. F. F. Awwadi, R. D. Willett, K. A. Peterson and B. Twamley, *Chem. Eur. J.* **2006**, 12, 8952.
2. (a) K. Gnanaguru, N. Ramasubbu, K. Venkatesan, and V. Ramamurthy, *J. Org.*Chem., **1985**, 50, 2337. (b) G. R. Desiraju and R. Parthasarathy, *J. Am. Chem.Soc.* **1989**, 111, 8725. (c) N. Ramasubbu,
3. R. Parthasarathy, and P. Murray-Rust, *J. Am. Chem. Soc.*, **1986**, 108, 4308.
4. R. F. W. Bader, *Atoms in Molecules-A Quantum Theory*, Oxford: Clarendon, **1990**.
   Volkov, P. Macchi, L. J. Farrugia, C. Gatti, P. Mallision, T. Richter and T. Koritsanszky, *XD2006,* **2006**.
5. R. Dovesi, V. R. Saunders, C. Roetti, R. Orlando, C. M. Zicovich-Wilson, F. Pascale, B. Civalleri, K. Doll, N. M. Harrison, I. J. Bush, Ph D'Arco and M. Linuell, *CRYSTAL06*, University of Torino, **2006**.
6. T. T. Thu Bui, S. Dahaoui, C. Lecomte, G. R. Desiraju, E. Espinosa, *Angew. Chem. Int. Ed.* **2009**, 48, 3838.

RS-5 Three-dimensional structures of Gram-positive bacterial pilins

Hae Joo Kang[1], Neil G. Paterson[1], Ton-That Hung[2], Edward N. Baker[1]
[1] *Maurice Wilkins Centre for Molecular Biodiscovery and School of Biological Sciences, University of Auckland, Private Bag 92019, Auckland, New Zealand (ted.baker@auckland.ac.nz)*
[2] *Department of Microbiology and Molecular Genetics, University of Texas Health Science Center, 6431 Fannin St., Houston, TX 77030, USA*

Bacterial pili are filamentous appendages that are critically involved in adhesion to host cells, leading to colonization of host tissues and establishment of infections. They are built from protein subunits called pilins; the backbone of the pilus is formed by hundreds of copies of a major pilin, while several minor pilins with specialized functions are associated with the

backbone. While pili of Gram-negative bacteria such as *E. coli* have been extensively studied, the pili on Gram-positive organisms have only recently discovered and are fundamentally different in that the pilins are held together by covalent isopeptide (amide) bonds formed by sortase enzymes.

We previously determined the first atomic structure of a Gram-positive major pilin, Spy0128 from *Streptococcus pyogenes* (Group A Streptococcus; GAS) (1). The crystal structure of Spy0128 showed an elongated molecule comprising two Ig-like domains. This structure also revealed a previously unknown mechanism for stabilizing proteins, in the form of self-generated isopeptide (amide) bonds. This brought significantly new understanding of the assembly of Gram-positive bacterial pili. The major pilins of different Gram-positive bacteria show wide variations in size and sequence, however, making it difficult to predict whether the structural principles seen in Spy0128 apply also to other Gram-positive pili. Here we present the high resolution crystal structure of a major pilin from *Corynebacterium diphtheriae*. This reveals a similar modular structure of Ig-like domains, yet with several variations from Spy0128. Two of its domains contain internal Lys-Asn isopeptide bonds which are somewhat different from those found in Spy0128. These are strategically located to give strength and stability to the pilin subunits and also facilitate proper assembly of pilus. We also confirm, by mass spectrometry of native pili, the identity of the residue used in pilus polymerization and note a pilus-like assembly of this *C. diphtheriae* pilin molecules in the crystal. These results point to a likely common architecture for the shafts of many Gram-positive pili, with several variations that can account for their functional differences.

Reference

Hae Joo Kang, Fasséli Coulibaly, Fiona Clow, Thomas Proft and Edward N. Baker (2007), Stabilizing isopeptide bonds revealed in Gram-positive bacterial pilus structure, *Science*, 318, 1625-1628.

RS-6 Crystal Structure determination of a non-Pfam protein AF1514 by S-SAD using a Cr X-ray source

Yang Li, Neil Shaw,Gaojie Song,Chongyun Cheng ,Jie Yin, Zhi-Jie Liu
National Laboratory of Biomacromolecules, Institute of Biophysics, Chinese Academy of Sciences, Beijing, China

Most of the targets selected by many structure genomics centres are from Pfam protein families. Many Pfam sequences have significant biological meaning, while the functions of most non-Pfam sequences are unknown to date. However, this does not mean that non-Pfam sequences are biologically less meaningful. Some non-Pfam sequences and structures are predicted to play important roles for the uniqueness of these organisms. The present work describes the structure determination of AF1514, a non-Pfam protein from ***Archeoglobus fulgidus*** with unknown function, solved at 1.8 Å resolution by using anomalous signal of sulphur atoms generated by chromium X-rays (wavelength = 2.29Å).

New Water Clusters Hosted by Diamondoid MOFs

RS-7

Mohammad Hedayetullah Mir, Jagadese J Vittal
National University of Singapore, Department of Chemistry, 3 Science Drive 3, Singapore 117543, Singapore (g0600472@nus.edu.sg)

Water constitutes the most abundant compound on the earth, covering 71% of the planet's surface, mostly in oceans and other large bodies of water. Water is essential for living organisms as it plays an important role in many biological and chemical systems. It exhibits a wide spectrum of physical and chemical properties in various forms. Although scientists have studied the structure of water extensively, the structure of bulk water is understood poorly. The presence of water molecules in solid-state structures can play an important role in stabilising some supramolecular structures. A number of discrete water clusters have been structurally characterised with varying numbers of water molecules from 3 to more than 30 in a variety of inorganic and organic crystal hosts. However, in the discrete water clusters, the structure of cyclic water heptamer was elusive. The electron-water heptamer is one of the magic numbers in the mass spectra of electron-water clusters.

We discovered the structure of discrete cyclic water heptamer at 296 K in the 3D metal organic framework (MOF) having daimondoid topology. When the single crystal is cooled to 223 K, it undergoes Single-Crystal to Single Crystal (SCSC) phase transition from monoclinic C2/c to $P2_1/c$ space group accompanied by structural transformation from cyclic $(H_2O)_7$ to bicyclic water heptamer containing edge sharing pentamer and tetramer rings (Fig. 1 Left). When the anion is changed from BF_4^- to ClO_4^- anion, the cyclic water heptamer transforms to another heptamer composed of cyclic pentamer ring buttressed by an acyclic dimer via SCSC transformation. Interestingly, a small change in the structure of the backbone of the MOF from 1,10-phenanthroline to 2,2'-bipyridine ligand transforms the cyclic water heptamer to a new acyclic form of water aggregate, *viz.*, *helicate* $(H_2O)_7$ which has been trapped between the ClO_4^- anions in the diamondoid channels (Fig. 2 Right). Our studies provide new insights into the properties and behavior of bulk water where the water molecules interact with the surface of the containers through weak interactions.

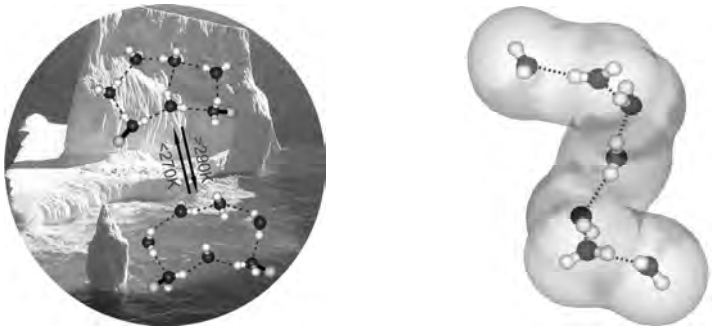

Fig. 1. Structural transformations of water heptamer (left). Structure of water helicate (right)

References

1. M. H. Mir and J. J. Vittal, *Angew. Chem. Int. Ed.* **2007**, *46*, 5925–5928.
2. M. H. Mir and J. J. Vittal, *Cryst. Growth Des.* **2008**, *8*, 1478–1480.
3. M. H. Mir, L. Wang, M. W. Wong and J. J. Vittal, *Chem. Commun.*, **2009**, 4539 - 4541.

RS-8 Laser assisted deposition of $AgInSe_2$ films on Si(100)

Dinesh Pathak[1], R. K. Bedi[1] and Davinder Kaur[2]
[1]*Material Science Laboratory, Department of Physics, Guru Nana k Dev University, Amritsar – 143005, India.*
[2]*Department of Physics and Centre of Nanotechnology*
(dineshpathak80@gmail.com)

Laser ablation has attracted special interest for the formation of thin films Compared with other formation technique . A distinctive feature of laser ablation is that it allow high quality and stochiometry of films of even very complex element material. In this presentation laser ablation of $AgInSe_2$ chalcopyrite semiconductor will be discussed in which it is difficult to maintain stochiometry by conventional method. High Quality $AgInSe_2$ (AIS) films were grown on Si(100) substrates by the ultra-high-vacuum pulsed laser deposition technique from the AIS target synthesized from high-purity materials. The X-ray diffraction studies of the films show that films are textured in (112) direction. .The substrate temperature appears to influence the properties of films. Increase in substrate temperature results in more order structure .Compositional analysis has been carried out by EDAX. It is observed that compositional stochiometry is maintained to the more extent by PLD technique than other traditional methods like thermal evaporation. The optical studies of the films show that the optical band gap is about 1.20 eV.

RS-9 New Structural Model of Malaria Pigment

Ratchadaporn Puntharod[1,2], Bayden R. Wood[3], Evan G. Robertson[3], Kenneth J. Haller[1]
[1] *School of Chemistry, Suranaree University of Technology, Nakhon Ratchasima, 30000, Thailand, (ratchada_aim@hotmail.com)*
[2] *Department of Chemistry, Maejo Unviersity, Chiangmai 50290, Thailand.*
[3] *Biospectroscopy Centre, Monash University, Clayton, Victoria, 3800, Australia.*

The crystal structure of five-coordinate high-spin iron(III) Fe(OEP)picrate has been studied as a model system for malaria pigment due to intense interest the molecular structure of malaria pigment (hemozoin) which is indistinguishable with β-hematin. To examine the conformation of porphyrin plane and ethyl groups substituted in *beta*-pyrrole positions with a picrate as axial ligand was studied by single crystal X-ray crystallography and resonance Raman spectroscopy. The macrocyclic porphyrin structure is the out-of-plane normal deformations of the saddle-shaped. The axial ligand orientation is the role in controlling the unequal distance of Fe–N bond (2.040(2), 2.028(2), 2.055(2), and 2.053(2) Å). The distance of axial Fe–O bond is 1.93(2) Å. The Fe(OEP)picrate molecules interact in pairs via π–π stacking interaction and nitro-nitro interaction. Fe(OEP)picrate exhibits the enhancement of totally symmetric oxidation state marker band, ν_4 at 1370 cm^{-1} for ν(pyr half ring) when using near-IR excitation laser and the characteristic bands of *beta* substituted hemes in the ranges of 1621–1639 for $\nu(C_\alpha C_m)_{asym}$ and 750–756 cm^{-1} for ν(pyr breathing) similar with β-hematin.

Crystal data for Fe(OEP)picrate: $C_{42}H_{46}FeN_7O_7$, monoclinic space group *C*2/c, a = 26.3997(20), b = 13.7806(18), c = 25.4126(20) Å, β = 119.955(9)°, V = 8010.2(14) $Å^3$, Z = 8 at 298 K.

RS-10 Structural insight into acute intermittent porphyria

Gaojie Song[1], Yang Li[1], Chongyun Cheng[1], Yu Zhao[1], Ang Gao[1], Rongguang Zhang[2], Andrzej Joachimiak[2], Neil Shaw[1], Zhi-Jie Liu[1]
[1]*National Laboratory of Biomacromolecules, Institute of Biophysics, Chinese Academy of Sciences, Beijing 100101, China.*
[2]*Structural Biology Center, Advanced Photon Source, Argonne National Laboratory, IL 60439 USA.*

Acute intermittent porphyria (AIP), an inherited disease of heme biosynthesis, is one of the most common type of the porphyrias. Reduced activity of the enzyme porphobilinogen deaminase (PBGD), which catalyses the sequential condensation of 4 molecules of porphobilinogen to yield preuroporphyrinogen, has been linked to the symptoms of AIP. We have determined the three dimensional structure of human PBGD at 2.2 Å resolution. Analysis of the structure revealed a dipyrromethane cofactor molecule covalently linked to Cys261, sitting in a positively charged cleft region. In addition to the critical catalytic Asp99, a number of other residues are seen hydrogen bonded to the cofactor and play a role in catalysis. Sequential entry of 4 pyrrole molecules into the active site is accomplished by movement of the domains around the hinges. Interestingly, some of the mutations of the human PBGD documented in patients suffering from AIP are located far away from the active site. The structure provides insights into the mechanism of action of PBGD at the molecular level and could aid the development of potential drugs for the up-regulation of PBGD activity in AIP.

Keywords: human porphobilinogen deaminase, X-ray structure, heme biosynthesis, porphobilinogen，hinge

RS-11 Accurate measurements of anomalous dispersion effect shows there is no chloride ion between Fe and Cu ions in the reduction site of oxidized Cytochrome *c* Oxidase

Michihiro Suga[1], Kazumasa Muramoto[2], Eiki Yamashita[1], Masao Mochizuki[2], Kazunori Maeda[2], Kyoko Ito-Shinzawa[1], Shinya Yoshikawa[2] and Tomitake Tshukihara[1, 2]
[1] *Institute of Protein Research, 3-2, Yamadaoka, Suita, Osaka, 565-0871, JAPAN (m-suga@protein.osaka--u.ac.jp)*
[2] *Department of Life Science, University of Hyogo, 3-2-1 Koto, Kamighori, Akoh, Hyogo 678-1297, JAPAN*

Cytochrome *c* oxidase (C*c*O) is a key component of the respiratory chain that catalyzes dioxygen reduction coupled with a proton-pumping process. The O_2 reduction site includes a high-spin heme A (heme a_3) and a copper ion (CuB) with 3 histidine imidazoles as the ligand. An existence of peroxide bridge between Fe and Cu ions in the reduction site of the fully oxidized C*c*O was reported [H., Aoyama, et al. Proc. Natl. Acad. Sci. USA 106:2165-2169 (2009)]. However, other groups insist that a chloride ion exists in the dioxygen reduction site. It is true that if Cl^- ion binds to heme a3 or CuB with occupancy of 0.5 each, the electron

number would be fitted. To overcome this possibility, we performed an X-ray experiment.

We collected the dataset using X-rays of 1.7470Å wavelength, where f''_{Fe}=0.47, f''_{Cu}=0.74, f''_{P}=0.55, f''_{S}=0.70 and f''_{Cl}=0.88. The data were collected on the beamline BL44XU at the SPring-8. In order to reduce the deterioration of peroxide structure by the X-ray irradiation, the experiment was carried out at 40K temperature using the He cryostat, and four crystals were used. A dataset was collected at 3.0Å resolution with R_{merge} value of 18.4, a completeness 100.0%, and averaged redundancy of 31.4, and I/sigma(I) of 34.4 in the highest 3.03 - 3.00Å resolution shell. To improve the accuracy of the Bijvoet difference, the intensity data were collected in the inverse-beam mode, which records Friedel pairs on two consecutive images to reduce the influence of radiation damage on the Bijvoet difference. For accurate phase determination, reference data was also collected using X-ray at 0.9Å wavelength with an isomorphous crystal.

In the anomalous Fourier map, most of the Sulfur atoms in the Met and Cys residues exhibited electron distribution at higher than 5.0 sigma, and some phosphorus atoms in the lipids were also observed. One the other hand, no prominent peaks were observed in the reduction center. This result excluded the possibility that a chloride ion exists between CuB and heme a_3.

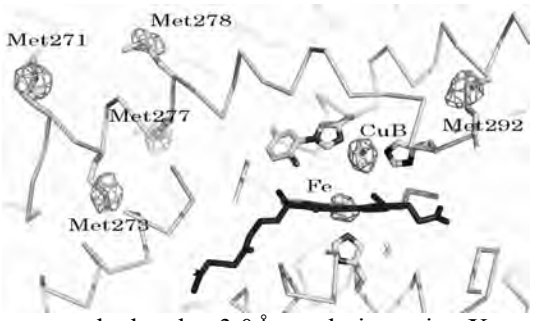

Anomalous difference Fourier map calculated at 3.0Å resolution using X-rays of 1.7470Å wavelength and contours were drawn at 4.0σ. (1σ=0.0048e^-/Å^3)

RS-12

Perakine Reductase, The First AKR Superfamily Member Involved In Indole Alkaloids Biosynthesis : Characterization, Crystallization And X-Ray Analysis

Lianli Sun[1,2*], Meitian Wang[3], Santosh Panjikar[4], Joachim Stöckigt[1,2*]

[1] *Institute of Materia Medica, College of Pharmaceutical Sciences, Zhejiang University, 388 Yu Hang Tang Road, Hangzhou, Zhejiang Province, 310058, P.R. China (lianlisun80@yahoo.com.cn)*

[2] *Department of Pharmaceutical Biology, Institute of Pharmacy, Johannes Gutenberg-University Mainz, Staudinger Weg 5, D-55099 Mainz, Germany (stoeckig@uni-mainz.de)*

[3] *Swiss Light Source PX III, Paul Scherrer Institute, CH-5232 Villigen, Switzerland*

[4] *European Molecular Biology Laboratory, Hamburg Outstation Deutsches Elektronen-Synchrotron, Notkestrasse 85, D-22603 Hamburg, Germany*

Perakine reductase (PR) catalyzes an NADPH-dependent conversion of perakine to raucaffrinoline (Figure), representing a side-branch of the biosynthetic pathway of the antiarrhythmic alkaloid ajmaline in plant cell suspension cultures of the Indian medical plant

Rauvolfia serpentina [1].

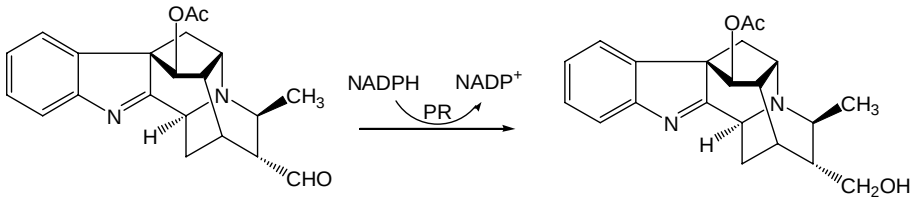

Perakine Raucaffrinoline

Figure. Perakine reductase catalyzes the enzymatic reaction from perakine to raucaffrinoline in presence of the reduced cofactor NADPH.

PR was functionally expressed in *Escherichia coli* as the N-terminal His_6-tagged enzyme and was purified to homogeneity. Sequence alignments studies define PR as a novel member of the aldo-keto reductase (AKR) superfamily, exhibiting the conserved catalytic tetrad Asp52, Tyr57, Lys84, His126. Site-directed mutagenesis of each of these functional residues to an alanine residue results in > 97.8% loss of enzyme activity. PR represents the first example of the large AKR-family which is involved in the biosynthesis of plant –derived monoterpenoid indole alkaloids. In addition to a new esterase, PR significantly extends the Rauvolfia alkaloid network to the novel group of peraksine alkaloids. Surprisingly, PR displays also an unusual broad substrate acceptance, reducing small benzaldehyde analogs, medium cinnamic aldehyde derivatives, up to bulky indole alkaloids. The relatively low substrate specificity and delivering de-toxified alcohols from compounds with reactive aldehyde groups also suggests a chemical defence and self-protecting function of PR [2].

The best crystals of methylated His_6-tagged PR were obtained by the hanging-drop vapor-diffusion technique. The crystals diffracted to 2.30 Å and belong to space group $C222_1$, one asymmetric unit cell contains one molecule. The final 3D-structure elucidation of PR is presently under progress.

References

1. Ruppert M, Ma X, Stöckigt J. Alkaloid biosynthesis in *Rauvolfia* – cDNA cloning of major enzymes of the ajmaline pathway *Curr. Org. Chem.,* **2005**, 9, 1431-1444.
2. Sun L, Ruppert M, Sheludko Y, Warzecha H, Zhao Y, Stöckigt J. Purification, cloning, functional expression and characterization of perakine reductase – the first example from the AKR enzyme family, extending the alkaloidal network of the plant *Rauvolfia*. *Plant Mol. Biol.,* **2008**, 67, 455-467.

RS-13

3-D Structure and Enzymatic Mechanism of Polyneuridine Aldehyde Esterase: from C_{10}- to C_9-Skeleton in Ajmaline Biosynthesis

Liuqing Yang[1,2], Marco Hill[2], Meitian Wang[3], Santosh Panjikar[4], Joachim Stöckigt[1,2,*]

[1], *Institute of Materia Medica, College of Pharmaceutical Sciences, Zhejiang University, 383 Yu Hang Tang Road, Hangzhou, Zhejiang Province, 310058, P.R. China (yangliuqing1984@hotmail.com)*

[2], *Department of Pharmaceutical Biology, Institute of Pharmacy, Johannes Gutenberg-University Mainz, Staudinger Weg 5, D-55099 Mainz, Germany (Hill@uni-mainz.de)*

[3], *Swiss Light Source PX III, Paul Scherrer Institute, CH-5232 Villigen, Switzerland (meitian.wang@psi.ch)*

[4], *European Molecular Biology Laboratory, Hamburg Outstation Deutsches Elektronen-Synchrotron, Notkestrasse 85, D-22603 Hamburg, Germany (panjikar@embl-hamburg.de)*

[*] *Corresponding author: joesto2000@yahoo.com*

Polyneuridine aldehyde esterase (PNAE , EC 3.1.1.78) plays a central role in the biosynthesis of alkaloids in the Indian medicinal plant *Rauvolfia serpentina* (L.) Benth. ex Kurz. PNAE is localized in the middle of the pathway transforming polyneuridine aldehyde to epi-vellosimine, which is a precursor for the synthesis of the monoterpenoid indole alkaloid ajmaline (an important therapeutic to treat antiarrhythmic heart disorders). The enzyme catalyses the following reaction:

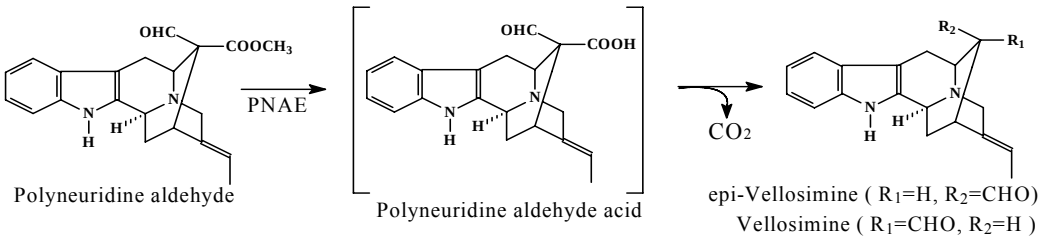

Figure : Transformation of polyneuridine aldehyde catalyzed by PNAE.

After heterologous expression of PNAE-cDNA in *Escherichia coli* , the N-terminal His_6-tagged PNAE was purified to homogeneity and crystallized for the first time. Sequence alignment and the 3D structure placed the enzyme as a new member into the α/β hydrolase superfamily.

PNAE exhibits an extraordinary high substrate specificity. In order to provide a structural evidence of this specificity and to analyze the structure of the binding site, cDNA of a knock-out mutant (His224Ala) was expressed in *E.coli*. The mutant enzyme was crystallized and soaked with its substrate polyneuridine aldehyde. The generated enzyme-product complexes were investigated by X-ray analysis. The results reveal now the complex enzymatic mechanism and explain the biosynthesis of C_9- from the C_{10}-monoterpenoid alkaloids stage.

Since the cap domain and the architecture of the binding pocket of PNAE determining which compound is accepted, low substrate specificity can probably be attained due to the rational structure-based redesign of PNAE, and the generation of novel alkaloids can be used in future for biological screening.

References

1. E. Dogru, H. Warzecha, F. Seibel, S. Haebel, F. Lottspeich, J. Stöckigt, *Eur. J. Biochem.* **2000**. *267*, 1397-1406.
2. E. Mattern-Dogru, X. Ma, J. Hartmann, H. Decker, J. Stöckigt, *Eur. J. Biochem.* **2002**. *269*, 2889-2896.
3. L. Yang, M. Hill, M. Wang, S. Panjikar, J. Stöckigt, *Angew. Chem. Int. Ed.* **2009**. (in press).

RS-14

Structural Basis and Catalytic Mechanism for the Dual Functional Endo-*β*-N-Acetylglucosaminidase A

Jie Yin[1], Lei Li[2], Neil Shaw[1], Yang Li[1], Lai-Xi Wang[3], Peng Wang[3], Zhi-Jie Liu[1]

[1] *National Laboratory of Biomacromolecules, Institute of Biophysics, Chinese Academy of Sciences, Beijing, China* (yinjie@moon.ibp.ac.cn)

[2] *Departments of Biochemistry and Chemistry, The Ohio State University, Columbus, Ohio, United States of America*

[3] *Institute of Human Virology and Department of Biochemistry and Molecular Biology, University of Maryland School of Medicine, Baltimore, Maryland, United States of America*

Endo-β-N-acetylglucosaminidases (ENGases) are dual specificity enzymes with an ability to catalyze hydrolysis and transglycosylation reactions. Recently, these enzymes have become the focus of intense research because of their potential for synthesis of glycopeptides. We have determined the 3D structures of an ENGase from Arthrobacter protophormiae (Endo-A) in 3 forms, one in native form, one in complex with Man3GlcNAc-thiazoline and another in complex with GlcNAc-Asn. The carbohydrate moiety sits above the TIM-barrel in a cleft region surrounded by aromatic residues. The conserved essential catalytic residues - E173, N171 and Y205 are within hydrogen bonding distance of the substrate. W216 and W244 regulate access to the active site during transglycosylation by serving as "gate-keepers". Interestingly, Y299F mutation resulted in a 3 fold increase in the transglycosylation activity. The structure provides insights into the catalytic mechanism of GH85 family of glycoside hydrolases at molecular level and could assist rational engineering of ENGases.

Keywords: Endo-A / X-ray structure / glycoprotein / $Man_3GlcNAc$-thiazoline / GlcNAc-Asn

References

Yin J *et al*. (2009) Structural Basis and Catalytic Mechanism for the Dual Functional Endo-β-N-Acetylglucosaminidase A. PLoS ONE 4(3): e4658.

P-1 Structural insights into the chemotactic pathway in *Helicobacter pylori*

Kwok Ho LAM[1], Thomas King Wah LING[2] and Shannon Wing Ngor AU[1]
[1]*Centre for Protein Science and Crystallography, Department of Biochemistry and Molecular Biotechnology Program, Faculty of Science, The Chinese University of Hong Kong, Hong Kong.*
[2]*Department of Microbiology, The Chinese University of Hong Kong, Hong Kong. (shannon-au@cuhk.edu.hk)*

Helicobacter pylori is a gram negative microaerophilic bacterium that colonizes human stomach and is related to gastritis, peptic ulcer, adenocarcinoma and gastric cancer. The chemotactic pathway is an important virulence trait in *H. pylori* and is featured with four additional CheY-like containing proteins - one CheY2 and three CheVs. CheY2 modulates the level of phosphor-CheY1 in retrophosphorylation while the roles of CheVs are unknown. All CheY-like proteins are phosphorylated by CheA, but the rate of phosphotransfer is in the order of CheY1 > CheY2 > CheVs.

Here we report the crystal structures of CheY1 in complex with $SO4_2^-$ and BeF_3^- from *H. pylori.* Interestingly, the sulfate-bound form mimics the transient state of phosphorylation and further suggests the functional significance of Thr84 in the phospotransfer reaction. On the other hand, interaction of CheA-P2 domain with CheY1, but not other CheY/CheV proteins underlines the preferential recognition to CheY1 by CheA in phosphotransfer reaction. Pull down assay, qualitative surface plasmon resonance and size exclusion chromatography analysis demonstrated that only CheY1 interacted with CheA-P2 domain, indicating that the differential phosphotransfer was attributed by the P2 domain. Homology modeling of CheV1 and CheY2 suggested that the distinctive characteristics at the α4β5α5 surface were responsible for the specific CheA-CheY interaction. Our result has provided the first structural insight into the features of chemotactic system in epsilon proteobacteria and further our knowledge on how the bacterium evolved to different chemotactic pathway.

P-2 Solid-liquid interface method (SLIM): A new crystallization method for proteins

Erik Brostromer,[a, §] Jie Nan,[a, §] Lan-Fen Li [a] and Xiao-Dong Su [a,b*]
[a]*National Laboratory of Protein Engineering and Plant Genetic Engineering, College of Life Sciences, Peking University, Beijing 100871, People's Republic of China,*
[b]*Shenzhen Graduate School of Peking University, Shenzhen 518055, People's Republic of China*

Despite impressive advances in theories, methods and technologies, crystallization still remains a serious bottleneck in structural determination of macromolecules. Here we present a novel solid-liquid interface method (SLIM) for protein crystallization, based on the pre-adding and drying of a crystallization reagent, and thereafter the dispensing of a protein solution to the dried media to initiate crystallization from the solid-liquid interface. Not only quick and easy to perform, the method also allows for a less concentrated protein solution for setting up crystallization trials.

P-3 Structural Basis for the Nucleotide-dependent Domain Rearrangement of 70-kDa Heat Shock Proteins

Yi-Wei Chang[1,2], Yuh-Ju Sun[2], Chung Wang[1], Chwan-Deng Hsiao[1]
[1] *Institute of Molecular Biology, Academia Sinica, Taipe 11529i, Taiwan (yiwei@imb.sinica.edu.tw, mbcw@gate.sinica.edu.tw, hsiao@gate.sinica.edu.tw)*
[2] *Institute of Bioinformatics and Structural Biology, National Tsing Hua University, Hsinchu 300, Taiwan (yjsun@life.nthu.edu.tw)*

The 70-kDa heat shock proteins (Hsp70s) are highly conserved ATP-dependent molecular chaperones composed of an N-terminal nucleotide binding domain (NBD) and a C-terminal protein substrate binding domain (SBD) in a bilobate structure. Interdomain communication and nucleotide-dependent structural motions are critical for Hsp70 chaperone functions. Our understanding of these functions remains elusive due to insufficient structural information on intact Hsp70s that represent the different states of the chaperone cycle. We report here the crystal structures of DnaK from *Geobacillus kaustophilus HTA426* bound with ADP-Mg^{2+}-Pi at 2.37 Å and the 70-kDa heat shock cognate protein from *Rattus norvegicus* bound with ADP-Pi at 3.5 Å. The NBD and SBD in these structures are significantly separated from each other, and they might depict the ADP-bound conformation. Moreover, a Trp reporter was introduced at the potential interface region between NBD and the interdomain linker of GkDnaK to probe environmental changes. Results from fluorescence measurements support the notion that substrate binding enhances the domain-disjoining behavior of Hsp70 chaperones.

P-4 Complex structure of tarocystatin-papain and characterization of tarocystatin proposed the role of C-terminal domain of group-2 phytocystatin

Ming-Hung Chu[1], Kai-Lun Liu[1], Kai-Wun Yeh[1] and Yi-Sheng Cheng[1,2]
[1] *Institute of Plant Biology, National Taiwan University, Taipei, 106 Taiwan*
[2] *Department of Life Science, National Taiwan University, Taipei, 106 Taiwan (chengys@ntu.edu.tw)*

Tarocystatin (CECPI) is a member of group-2 phytocystatin. It shared a conserved N-terminal cystatin (CY) domain with group-1 phytocystatin, but composed of an extended C-terminal domain. The complex structure of tarocystatin-papain has been resolved at a resolution 2.03Å. Interestingly, the C-terminal domain cannot be observed in the complex structure with only N-terminal domain in complex of papain. For further characterizing the tarocystatin, three segments of tarocystatin, including full length (FL), N-terminal domain (NtD) and C-terminal domain (CtD), were prepared to analyze the domain-domain interaction and inhibitory property. The domain-domain interaction by glutaraldehyde cross-linking and yeast two hybrid were carried out and showed the results that a weak interaction could be observed between NtD and CtD. The tarocystain also could form homodimer via the interaction of NtDs. In the inhibitory activity assay, the GST-fused FL showed the best inhibitory activity, and GST-NtD and FL showed almost the same inhibitory property. On the contrary, GST-CtD showed an enhanced activation activity of papain than CtD or GST, respectively. It means

that the inhibitory activity of CY domain could be enhanced by fused GST or CtD. Consequently, structural models of tarocystatin with the intermolecular interaction of NtD and NtD to form homodimer, or the intramolecular interaction of NtD and CtD to form latexin-like were proposed.

P-5 Study on Structural Biology in Disease/structure-based Drug Design

Ki Joon Cho[1], Ji-Hye Lee[2], Intekhab Alam[2], Yi Ho Park[2], and Kyung Hyun Kim[2]
[1] *School of Life Sciences & Biotechnology, Korea University, Seoul 136-701, Korea (c-azna@korea.ac.kr)*
[2] *Department of Biotechnology & Bioinformatics, College of Science & Technology, Korea University, Chungnam 339-700, Korea (jihyelee@korea.ac.kr; Intekhab@korea.ac.kr; ballashe@naver.com; khkim@korea.ac.kr)*

Helicobacter pylori is the causative agent of chronic gastritis, duodenal ulcer, gastric carcinoma and gastric lymphoma. Iron is essential for the survival of the bacteria and proteins involved in iron metabolism are suggested as the major determinants of virulence. Among those proteins, ferritin has a role in storage of up to 4,500 irons inside the protein shell. In order to get a structural insight of the mechanism of iron uptake and release, crystal structures of *H.pylori* ferritin have been solved at resolutions 1.3Å-2.1Å as apo, low-iron bound, intermediate, and high iron bound states. As the iron content increased, significant conformational changes have been observed at the 4-fold symmetry channel in intermediate and high iron bound states, while no such change was observed in low and apo states. At high magnetic fields, the magnetic moment of the high-iron bound state was approximately 10 times higher than that of the low-iron state. Exposure of the crystals to a magnetic field of as high as 3 Tesla triggered the conformational change at the 4-fold channel at the apo and low-iron structures, identical to that found at the intermediate and high-iron structures. Our results provide the structural evidence of the translocation of Fe ions through the 4-fold channel and magnetic properties of ferritin in the presence of a magnetic field are described.

P-6 Crystal Structure of Carboxynorspermidine Decarboxylase from *Helicobacter pylori*

Chen-Hsi Chu, Chin-Yi Chen, and Yuh-Ju Sun
Institute of Bioinformatics and Structural Biology, National Tsing Hua University, 101, Section 2 Kuang Fu Road, Hsinchu 30013, Taiwan (d928216@oz.nthu.edu.tw)

Carboxynorspermidine decarboxylase (CANSDC) belongs to group IV pyridoxal 5'-phosphate (PLP)-dependent decarboxylase. CANSDC catalyzes the decarboxylation of carboxynorspermidine to norspermidne in polyamine biosynthesis. The cofactor, PLP, makes a covalent bond with the catalytic lysine residue to form a Schiff base. CANSDC from *Helicobacter pylori* (*Hp*CANSDC) has been overexpressed and purified with the endogenous PLP. The binding of *Hp*CANSDC and norspermidine was characterized by a CD and UV/Vis spectrum. The *Hp*CANSDC crystal structure was determined by multiwavelength anomalous dispersion (MAD) method at 2.1 Å resolution. *Hp*CANSDC functions as a dimer in solution

and folds as a head-to-tail dimer in crystal. The overall structure of *Hp*CANSDC contains an N-terminal TIM-like β/α barrel domain and a C-terminal β-barrel domain. The binding pocket of *Hp*CANSDC is built by the active site loop (loop β6α6) and a specificity element (α10). Loop β6α6 situates a rather "down" conformation and it might protect the substrate/product from solvent to be bound in the active site. The α10 is at the relatively backward position in order to accommodate the longer substrate, carboxynorspermidine.

P-7

Crystallographic Studies of Manihot esculenta hydroxynitrile lyase mutants

Charles B.C. Cielo[a], Mohammad Dadashipour[b], Tatsuo Hikage[c], Atsuo Suzuki[a], Tsunehiro Mizushima[a,d], Hidenobu Komeda[b], Yasuhisa Asano[b], Takashi Yamane[*a]

[a]*Department of Biotechnology, School of Engineering, Nagoya University, Chikusa-Ku, Nagoya 464-01, Japan (yamane@nubio.nagoya-u.ac.jp)*

[b]*Department of Biotechnology, Faculty of Engineering, Toyama Prefectural University, Toyama 939-0398, Japan*

[c]*High Intensity X-ray Laboratory, Nagoya University, Chikusa-Ku, Nagoya 464-01, Japan*

[d]*Present address; Department of Structural Biology and Biomolecular Engineering, Graduate School of Pharmaceutical Sciences, Nagoya City University, Nagoya 467-8603, Japan*

Cassava (*Manihot esculenta*) is a major root crop that contains potentially toxic levels of cyanogenic glycosides that provide the plant with protection from herbivory as well as function in amino acid catabolism. Free *Manihot esculenta* hydroxynitrile lyase (*Me*HNL) catalyzes the stereospecific production of (S)-ketone cyanohydrins, an industrially important intermediate for fine chemicals and pharmaceuticals. The effective production of *Me*HNL via *Escherichia coli* expression systems has previously been demonstrated. However, improvements in protein yield are necessary for its feasible industrial application. Several *Me*HNL mutants have demonstrated significantly increased enzyme solubility and yield. It is the aim of this study to establish structural bases for this improvement.

We solved the structure of the *Me*HNL mutant K176P via molecular replacement using wild type *Me*HNL (*wtMe*HNL) as the molecular search model (PDB ID: 1E8D). Although the crystals of the K176P mutant and the wild-type enzyme are non-isomorphous, no major deviations in structure were observed between the two enzymes. It was of particular interest to note that crystals of two *Me*HNL mutants (K176P, H103M) formed under identical crystallization conditions producing isomorphous crystals. In contrast with *wtMe*HNL, 4 molecules were assigned to a single asymmetric unit for K176P, suggesting a tetrameric quarternary structure. Furthermore, in K176P, 2 glycerol molecules were found in the monomer-monomer interface located in essentially identical positions and in proximity of the mutated residue in the two dimers found in the asymmetric unit of the crystal.

We propose that the mutations contribute to improving protein solubility by affecting quarternary structure formation.

P-8 The Effects of UV Irradiation of Protein Crystals

Angela R. Criswell, Pierre LeMagueres, Bret Simpson
Rigaku Americas Corp, 9009 New Trails Dr., The Woodlands, TX 77381 USA
(angela.criswell@rigaku.com)

Automation of crystallization experiments enables sampling of large crystallization spaces by coarse and fine screening. The result is an increased number of crystallization experiments that require visual inspection. Consequently, crystallographers further rely on automation to monitor crystal growth and to identify crystals for additional diffraction screening. Compared to visible light inspection alone, ultraviolet (UV) image inspection has proven useful for protein crystal identification through exploitation of the fluorescence responses of aromatic amino acid residues such as tryptophan. Results show UV imaging to be an efficient method to single out protein crystals from other non-protein solid materials within crystallization drops.

Due to the increased use of UV irradiation there is greater attention given to the impact of UV irradiation on crystallographic samples. To date, little is known about the effects of UV irradiation on protein crystals and even less is known about the effects on crystallization experiments. This work examines the effects of UV irradiation on protein crystals in drops and in loops. Experiments show that one can detect and measure trends in both X-ray diffraction experiments and in the 3-dimensional protein structure of crystals. As expected, the trends are more observable as the UV exposure time increases. These experiments also investigate the effects of UV exposure at different stages during crystallization to examine the impact on crystal formation and nucleation.

P-9 Excitation coupling in bioluminescence: combined X-ray and NMR determination of the clytin-GFP topology

Yingang Feng[1], Maxim Titushin[1,2], Yang Li[1], Jinfeng Wang[1], Eugene Vysotski[2], Zhi-Jie Liu[1]
[1]*National Lab of Biomacromolecules, Institute of Biophysics, Chinese Academy of Sciences, Beijing 100101, China*
[2]*Institute of Biophysics, Russian Academy of Science, Siberian Branch, Krasnoyarsk 660036, Russia*

Bioluminescence in medusa *Clytia gregarium* is Ca^{2+}-induced and involves two distinct proteins, clytin and green fluorescent protein (GFP). Clytin contains one tightly bound coelenterazine molecule, which becomes available for reaction with O_2 only subsequent to Ca^{2+} binding. Clytin belongs to the EF-hand super-family of Ca^{2+}-binding proteins and contains three "EF-hand" Ca^{2+}-binding sites. When clytin is in the excited state, the energy is transferred to GFP through so called "bioluminescence resonance energy transfer (BRET)" mechanism. But how these two molecules interact and facilitate the energy transfer is unknown. This study reports the crystal structure determination of clytin and GFP by X-ray crystallography method and the identification of protein-protein interaction surfaces by NMR method. The energy transfer mechanism at atomic level will be discussed as well.

References

1. Stepanyuk, G.A., Liu, Z.J*, Vysotski, E.S., Lee, Rose, J. and Wang, B.C. (2009). Structure based mechanism of the Ca^{2+}-induced release of coelenterazine from the *Renilla* binding protein. Proteins, 74(3):583-93
2. Liu, Z.J., Stepanyuk, G.A., Vysotski, E.S., Lee, J., Markova, S.V., Malikova, N.P., and Wang, B.C. (2006). Crystal structure of obelin after Ca2+-triggered bioluminescence suggests neutral coelenteramide as the primary excited state. Proc Natl Acad Sci *103*, 2570-2575.
3. Deng, L., Markova, S.V., Vysotski, E.S., Liu, Z.J., Lee, J., Rose, J., and Wang, B.C. (2004). Crystal structure of a Ca2+-discharged photoprotein: implications for mechanisms of the calcium trigger and bioluminescence. J Biol Chem 279, 33647-33652.
4. Liu, Z.J., Vysotski, E.S., Chen, C.J., Rose, J.P., Lee, J., and Wang, B.C. (2000). Structure of the Ca^{2+}-regulated photoprotein obelin at 1.7 A resolution determined directly from its sulfur substructure. Protein Sci 9, 2085-2093.

P-10 Structural study of FIH with CQ, HQ inhibitor complex

Sojung Han, Hyunjin Moon, Jungwoo Choe
University of Seoul, Siripdae-gil 13(jeonnong-dong 90), Daongdaemun-gu, Seoul 130-743 KOREA (jchoe@uos.ac.kr)

Mammalian cells have their own mechanism to survive the condition of low oxygen concentration (hypoxia) by turning on hypoxic transcriptional factors. HIF (hypoxia-inducible factor) is an $\alpha\beta$-heterodimeric-transcription factor that induces the expression of genes, such as EPO (erythropoietin) and VEGF (vascular endothelial growth factor), under hypoxic conditions. And the activity or the expression level of HIF is regulated by hydroxylases which belong to 2OG (Oxoglutarate)- and Fe(II)- dependent dioxygenase superfamily, and are also categorized into cellular oxygen sensors. FIH (factor inhibiting HIF) is one of that hydroxylases and play an important role in controlling the HIF activity under hypoxia.Structural studies of FIH have shown that it forms a homodimer, and each of its subunit has the double-stranded β-helix core, a jellyroll-like-barrel embracing the conserved Fe(II)-binding triad region, featuring it belonging to the 2OG dependent dioxygenase superfamily. NOG (*N*-Oxalylglycine) and its pro-form dimethyl *N*-oxalylglycine (DMOG) are known as inhibitors of FIH. Structure of FIH with inhibitor complexes has been solved. These inhibitors, however, are not appropriate to be used as drug, because they create negative charges. So we focused on quinol family, such as Clioquinol, and Hydroxy quinol, which have similar structural feature and coordination with NOG, but are neutral in charge. Here we made a structural an analysis with FIH and CQ, HQ complex crystals. And we defined the structure with 2.6Å resolution.

P-11 Structure of Maleylacetate Reductase from *Rhizobium* sp. strain MTP-10005

Yasuo Hata[1], Tomomi Fujii[1], Masahiro Yoshida[2], Tadao Oikawa[2]
[1] *Institute for Chemical Research, Kyoto University, Uji, Kyoto 611-0011, Japan (hata@scl.kyoto-u.ac.jp)*
[2] *Kansai University, Suita, Osaka 564-8680, Japan, (oikawa@ipcku.kansai-u.ac.jp)*

Maleylacetate reductases play a crucial role in the aerobic microbial degradation of aromatic

compounds. In fungi and yeasts, the enzymes are involved in the catabolism of very common compounds, such as phenol, tyrosine, benzoate, 4-hydroxybenzoate and resorcinol. In bacteria, the enzymes contribute to the degradation of resorcinol, 2,4-dihydroxybenzoate (β-resorcylate) and 2,6-dihydroxybenzoate (γ-resorcylate), via hydroxyquinol and maleylacetate. Maleylacetate reductases catalyze the NADH- or NADPH-dependent reduction of maleylacetate or 2-chloromaleylacetate to 3-oxoadipate or of substituted maleylacetates to substituted 3-oxoadipates.

Maleylacetate reductase from *Rhizobium* sp. strain MTP-10005 (GraC) catalyzes the reduction of maleylacetate to 3-oxoadipate and plays an important role in the catabolic pathway of the resorcinol produced through decarboxylation of 2,6-dihydroxybenzoate. The polypeptide chain of the enzyme consists of 351 amino acid residues with a mass of 36,405. The structure of the present enzyme is expected to reveal structural features that may be common to maleylacetate reductases from other aerobic microorganisms. Here, we report the X-ray structure of maleylacetate reductase from *Rhizobium* sp. strain MTP-10005.

Expression and purification of the C-terminally His-tagged protein were performed according to the method of Yoshida *et al*. Initial crystallization experiments were performed by the hanging-drop vapour-diffusion method using Crystal Screens (CSs) (Hampton Research, CA, USA) at 293 K. Small crystals were obtained after several days using 8 mg ml^{-1} protein solution (50 mM Tris-HCl buffer, pH 8.0) and the reservoir solution CS II #32. The crystallization conditions were optimized based on those of the CS II #32 solution in conjunction with Additive Screen (Hampton Research). The final conditions produced rhombohedron-shaped crystals with approximate dimensions of 0.25 × 0.20 × 0.1 mm at 293 K in 3 d using the sitting-drop vapour-diffusion method. Drops prepared by mixing 1 μl protein solution at 6 mg ml^{-1} (in 50 mM Tris-HCl buffer, pH 8.0) and 1 μl reservoir solution were equilibrated against 500 μl reservoir solution consisting of 1.3 M ammonium sulfate, 0.1 M sodium chloride, 2% (w/v) benzamidine HCl, and 0.1 M NaHEPES (pH 7.5). The drops were microseeded with the original crystals grown in CS II#32 before crystallization.

Data collection was performed at beamline BL-6A, Photon Factory, Tsukuba, Japan. Before data collection, each crystal was soaked into a cryoprotectant solution consisting of 1.4 M ammonium sulfate and 25%(v/v) glycerol for less than one minute, and flash-cooled in a nitrogen stream at 100 K. The native data set was collected up to 1.96 Å resolution, and the 3 Å MAD data sets with four different wavelengths for a Hg-derivative crystal. All diffraction images were processed with the program *HKL2000*. The crystal belongs to space group *C*2, with unit-cell parameters a = 56.85, b = 121.13, c = 94.09 Å, β= 101.48°. The V_M value is 2.18 $Å^3$ Da^{-1} for four dimeric molecules in the unit cell. An initial electron density map was obtained at 3 Å resolution using MAD phases and interpreted with the help of the structure of lactaldehyde reductase (PDB ID=1RRM) which is homologous in sequence to GraC. The structure was refined at 1.96 Å resolution up to R=0.165 and Rfree=0.216.

GraC is dimeric in the crystal. Its subunit consists of two domains: the N-terminal NAD-binding domain adopting an α/β structure and the C-terminal α-helical domain. The active site is located in the cleft between the domains of the subunit. The two subunits (Sub A & Sub B) have a little bit different structures from each other in the present crystal. Sub A

binds 2 SO_4^{2-} ions, 1 benzamidine molecule, and 1 glycerol molecule, and has a closed conformation, whereas Sub B binds no ligand except 1 SO_4^{2-} ion and has an open conformation. Thus, the present crystal structure of GraC reveals the structures of maleylacetate reductase both in the substrate-binding state and in the ligand-free state.

P-12 Current status and developments of macromolecular crystallography beamlines at the Photon Factory

Masahiko Hiraki, Leonard Chavas, Yusuke Yamada, Naohiro Matsugaki, Noriyuki Igarashi and Soichi Wakatsuki
Structure Biology Research Center, Photon Factory, Institute of Materials Structure Science, High Energy Accelerator Research Organization (KEK), Oho 1-1, Tsukuba, Ibaraki, 305-0801, Japan (masahiko.hiraki@kek.jp)

Structural Biology Research Center at the Photon Factory is currently operating five macromolecular crystallography beamlines (Table 1). BL-5A, BL-17A, AR-NW12A and AR-NE3A are insertion device (ID) beamlines, while BL-6A is a conventional bending magnet beamline. Among these ID beamlines, major purpose of the beamlines, BL-5A, AR-NW12A and AR-NE3A is high-throughput. The new beamline AR-NE3A was constructed for fully-automated data collection [1] supported by Astellas Pharma Inc. and has been opened in April, 2009. A micro-focus beamline BL-17A was designed for micro-crystal structure analysis. In addition, the lower energy beam at around 6 keV is used for structure determination by SAD phasing with light atoms.

We are now building a new micro-focus beamline BL-1A supported by Targeted Protein Research Program C of the Ministry of Education, Culture, Sports, Science and Technology of Japan. The aim of BL-1A is to deliver brilliant lower energy beam at around 4-5 keV dedicated to sulphur SAD experiments and more photon flux at around 12 keV than that of BL-17A. BL-1A will be opened to users in April, 2010.

For further high-throughput protein crystallography, we facilitate automation of beamline operation, with developments of sample exchange robots PAM [2], automated sample centering system and unified beamline control software. These developments based on stable beamlines and reliable network will allow for the goal of fully-integrated structure determination pipeline.

Table 1 PF macromolecular crystallography beamlines

	-	High-throughput beamlines			Micro-focus beamline
Beamline	BL-6A	BL-5A	AR-NW12A	AR-NE3A	BL-17A
Wavelength range (Å)	0.7-1.9	0.9-1.3	0.7-1.9	0.7-1.9	0.95-1.33 1.6-2.2
Energy reso. (ΔE/E)	$1x10^{-3}$	$2.5x10^{-4}$	$2.5x10^{-4}$	$2.5x10^{-4}$	$2.5x10^{-4}$
Photon flux (phs./sec)	$1.0x10^{10}$ @1.0A	$1.5x10^{11}$ @1.0A	$2.0x10^{11}$ @1.0A	$1.3x10^{12}$ @1.0A	$6.6x10^{9}$ @1.0A $1.3x10^{10}$ @2.0A
Slit size (mm)	0.23 x 0.15	0.2 x 0.2	0.2 x 0.2	0.2 x 0.2	0.02 x 0.02
Detector	Q4R	Q315r	Q210r	Q270	Q270
Typical data collection time (min)	120	14	14	24	24
Sample exchanger	-	PAM	PAM	PAM	PAM

References

1. Yusuke Yamada, *et al*., Fully automated data collection system at the macromolecular crystallography beamlines in the Photon Factory, *AsCA2009.*
2. Masahiko Hiraki, *et al*., *J. Synchrotron Rad.* (2008) 15, 300-303.

P-13

A new beamline at SPring-8 dedicated to protein micro-crystallography

Kunio Hirata[1], Go Ueno[1], Atsushi Nisawa[1], Nobutaka Shimizu[1,2], Takashi Kumasaka[1,2], Yoshiaki Kawano[1], Takaaki Hikima[1], Takashi Tanaka[1,2], Sunao Takahashi[1,2], Kunikazu Takeshita[1,2], Hirokatsu Yumoto[2], Haruhiko Ohashi[1,2], Shunji Goto[1,2], Hideo Kitamura[1], Toru Ohata[1,2], Yukito Furukawa[1,2], Masaki Yamamoto[1]

1. RIKEN/SPring-8 Center, (hirata@spring8.or.jp)

2. JASRI/SPring-8

Structure determinations of proteins are often hindered by the small size of the available crystals. However, proteins involved in recent target of crystallography, such as membrane proteins or protein complexes, tend to show difficulties in growing their crystal size. Thus, demands for achieving protein micro-crystallography are getting larger and larger. A new undulator beamline at SPring-8 dedicated to protein micro-crystallography, BL32XU, has been constructing.

In order to realize the protein micro-crystallography, we designed a micro-focus beamline at SPring-8. The beamline should provide spatially brilliant and small beam of the order of a few or several micro-meters. A ray trace simulation based on our optical design shows achievable beam size at sample position corresponds to 1 x 1 μm^2 with 6 x 10^{10} photons/sec/μm^2. The beam size will be changeable up to the maximum size of 20 x 20 μm^2 according to size of sample crystals or experimental conditions. Design concepts of a sample environment suppressing background noise and a mirror chamber stabilizing both intensity and position of the micron-sized beam at sample position will be presented.

Possible ways to utilize the micro beam not only for micro-crystals but for 'low-quality' ones will also be introduced. One of them is probing single-crystal volumes from a heterogeneous protein crystal using the micro-beam. In exchange of such kind of spatial advantages, radiation damage of crystals should be considered more carefully when micro beam is utilized. Both of the expert system for data collection strategy and the 'on-the-fly' monitoring system of radiation damage are also under development.

Some experimental results of R&D for high-precision diffractometer, highly efficient CCD detector, and hopefully, the first result of commissioning of the beamline will be presented.

The new beamline will largely benefit users by cutting off their time to optimize crystallization conditions especially for smaller and lower quality crystals. The beamline will be operated mainly for the National Project, named "Targeted Proteins Research Program", from 2010.

P-14 Molecular Interplay Between Replicative Helicase DnaC and Its Loader DnaI from *Geobacillus kaustophilus*

Chwan-Deng Hsiao[1], Kuang-Lei Tsai[1,2], Yu-Hua Lo[1,2], Yuh-Ju Sun[2]
[1] *Institute of Molecular Biology, Academia Sinica, Taipei, 115, Taiwan (hsiao@gate.sinica.edu.tw)*
[2] *Institute of Bioinformatics and Structural Biology, National Tsing Hua University, Hsinchu, 300, Taiwan*

Helicase loading factors are thought to transfer the hexameric ring-shaped helicases onto the replication fork during DNA replication. However, the mechanism of helicase transfer onto DNA remains unclear. In *Bacillus subtilis*, the protein DnaI, which belongs to the AAA+ family of ATPases, is responsible for delivering the hexameric helicase DnaC onto DNA. Here we investigated the interaction between DnaC and DnaI from *Geobacillus kaustophilus HTA426* (*Gk*DnaC and *Gk*DnaI) and determined that *Gk*DnaI forms a stable complex with *Gk*DnaC with an apparent stoichiometry of *Gk*DnaC$_6$-*Gk*DnaI$_6$ in the absence of ATP. Surface plasmon resonance analysis indicated that *Gk*DnaI facilitates loading of *Gk*DnaC onto single-stranded DNA (ssDNA) and supports complex formation with ssDNA in the presence of ATP. Additionally, the *Gk*DnaI C-terminal AAA+ domain alone could bind ssDNA, and binding was modulated by nucleotides. We also determined the crystal structure of the C-terminal AAA+ domain of *Gk*DnaI in complex with ADP at 2.5 Å resolution. The structure not only delineates the binding of ADP in the expected Walker A and B motifs but also reveals a positively charged region that may be involved in ssDNA binding. These findings provide insight into the mechanism of replicative helicase loading onto ssDNA.

P-15 Crystal structure of CRN-4: implications for domain function in apoptotic DNA degradation

Yu-Yuan Hsiao*[1,2] and Hanna S. Yuan[2, 3]
[1]*Institute of Bioinformatics and Structural Biology, National Tsing Hua University, (hanna@sinica.edu.tw)*
[2]*Institute of Molecular Biology, Academia Sinica,*
[3]*Graduate Institute of Biochemistry and Molecular Biology, National Taiwan University, Taipei, Taiwan*

Programmed cell death (apoptosis) is an essential biological process for the development and maintenance of appropriate cell number and for the defense against virus infection. One of the major biochemical features of apoptosis is chromosome DNA fragmentation. Cell death related nuclease 4 (CRN-4) is one of the apoptotic nucleases involved in DNA degradation in *Caenorhabditis elegans*. CRN-4 contains an N-terminal DEDDh exonuclease domain and a C-terminal domain of unknown function. To reveal the molecular basis of DNA fragmentation in apoptosis, we analyzed CRN-4's biochemical properties and determined its crystal structures in apo-form, Mn^{2+}-bound active form and Er^{3+}-bound inactive form. CRN-4 is a dimer with both metal-dependent DNase and RNase activities. It prefers to cleave double-stranded over single-stranded DNA, with optimal DNase activity in apoptotic salt conditions and pH ranges. Comparison of the Mn^{2+}-bound and Er^{3+}-bound CRN-4 structures revealed the geometry of the functional nuclease active site in the N-terminal DEDDh domain.

The C-terminal domain bound to a structural zinc ion, termed the Zn-domain, is folded into a novel mixed α/β structure, containing basic surface residues ideal for RNA/DNA recognition. Site-directed mutagenesis further confirmed the catalytic residues in the N-terminal DEDDh domain and the DNA-binding residues in the Zn-domain. The structural comparison of CRN-4 to a number of dimeric DEDDh family nucleases, PARN, TREX2 and RNase T, further demonstrated that CRN-4 both dimerizes and interacts with DNA in a unique way. Combining all these data, we suggest a structural model where DNA is bound at the Zn-domain and cleaved at the DEDDh nuclease domain in CRN-4 when the cell is triggered for apoptosis.

P-16

The Crystal Structures of 2-aminobenzothiazole-based Inhibitors in Complexes with the Urokinase-type Plasminogen Activator

Longguang Jiang[1,2] , Haiyang Yu[3], Cai Yuan[1], Jundong Wang [3], LiQing Chen [4] , Edward J.Meehan[4], Zixiang Huang [1], Mingdong Huang [1]

[1]*Fujian Institute of Research on the Structure of Matter, The Chinese Academy of Sciences, Fuzhou, Fujian 350002, China (mhuang@fjirsm.ac.cn)*

[2]*Graduate School of the Chinese Academy of Sciences, Beijing 100039, China (jianglg07@gmail.com)*

[3]*University of FuZhou, FuZhou, 350108, China(yhyang198@gmail.com)*

[4] *University of Alabama in Huntsville, Huntsville, AL 35899, USA(chenlq@uah.edu)*

Urokinase-type plasminogen activator (uPA) plays a crucial role in the regulation of plasminogen activation, tumor cell adhesion and migration[1]. The inhibition of uPA activity is a promising mechanism for anti-cancer therapy[2]. Most current uPA inhibitors employ a highly basic group (either amidine or guanidine group) to target the S1 pocket of uPA active site, which leads to poor oral bioavailability[3]. Here we study the possibility to use less basic 2-aminobenzothiazole (ABT) as S1 pocket binding group. We report the crystal structures of the complexes of uPA with ABT or with 2-amino-benzothiazole-6-carboxylic acid ethyl ester (ABTCE). The inhibitory constants of these two inhibitors were measured by a chromogenic competitive assay, and it was found that ABTCE is a better inhibitor for uPA (K_i = 656μM) than ABT (K_i = 5.03mM). This work shows that the 2-amniobenzothiazole can be used as P1 group which may have better oral bioavailability than the commonly used amidine or guanidine group. We also found the ethyl ester group occupies the characteristic oxyanion hole and contacts to uPA 37- and 60-loops. These works provides structural information for further improvements of potency and selectivity of this new class of uPA inhibitor.

References

1. Fazioli, F. and F. Blasi, Urokinase-type plasminogen activator and its receptor: new targets for anti-metastatic therapy? Trends Pharmacol Sci, 1994. **15**(1): p. 25-9.
2. Andreasen, P.A., *et al*., The urokinase-type plasminogen activator system in cancer metastasis: a review. Int J Cancer, 1997. **72**(1): p. 1-22.
3. Rockway, T.W. and V.L. Giranda, Inhibitors of the proteolytic activity of urokinase type plasminogen activator. Curr Pharm Des, 2003. **9**(19): p. 1483-98.

P-17 Structural and biochemical characterization of yeast monothiol glutaredoxin Grx6/YDL010W

Ming Luo[1], Yong-Liang Jiang[1], Xiao-Xiao Ma[1], Ya-Jun Tang[1], Yong-Xing He[1], Jiang Yu[1], Rong-Guang Zhang[2], Yuxing Chen[1] and Cong-Zhao Zhou[1]
[1] *Hefei National Laboratory for Physical Sciences at Microscale and School of Life Sciences, University of Science and Technology of China, Hefei, Anhui, 230027, People's Republic of China*
[2] *Structural Biology Center, Argonne National Laboratory, 9700 South Cass Avenue, Argonne, IL 60439 USA*

Glutaredoxins (Grxs) represent a ubiquitous family of proteins which could reduce the disulfide bonds of their substrate proteins with reduced glutathione. *Saccharomyces cerevisiae* Grx6 is a monothiol Grx whose active-site sequence (CSYS) is reminiscent of CPYC active-site sequence of classic dithiol Grxs. Grx6 contains an N-terminal signal sequence (M1-I36) and localizes at the endoplasmic reticulum and Golgi compartments. We found that Grx6 is able to dimerize through its N-terminal domain (K37-T110) and could further be bridged by a putative [2Fe-2S] cluster to form tetramer. We also demonstrate that Grx6 is the first monothiol Grx showing both glutathione-disulfide oxidoreductase activity and glutathione S-transferase activity. In the crystal structure of Grx6 C-terminal domain (K111-N231) we solved, a novel two-stranded antiparallel β-sheet motif was revealed besides the classic Grx domain. This novel motif is unique among all known structures of Grxs, which may characterize a novel Grx subfamily. Moreover, we suggest an active site motif without tryptophan and proline residues which could lead to the identification of further Fe-S cluster binding Grxs.

P-18 Structure and Interaction of Ubiquitin-Associated Domain of Human Fas Associated Factor 1

Joon Kyu Park[1,2], JinSue Song[3], Jae-Jin Lee[4], Yun-Seok Choi[3], Kyoung-Seok Ryu[3], Jae-Hong Kim[2], Kong-Joo Lee[4], Young-Ho Jeon[3] and Eunice EunKyeong Kim[1*]
[1]*Life Sciences Division, Korea Institute of Science and Technology, 39-1, Hawolgok-dong, Sungbuk-gu, Seoul, Korea 136-791; (Eunice@kist.re.kr)*
[2]*School of Life Sciences and Biotechnology, Korea University, Anam-dong, Sungbuk-gu, Seoul, Korea 136-701;*
[3] *Korea Basic Science Institute, 804-1 Yangchung-Ri, Ochang, Chungbuk, Korea 363-883;*
[4] *College of Pharmacy and Division of Life & Pharmaceutical Sciences, Ewha Womans University, Seoul, Korea 120-750;*

Fas associated factor 1 (FAF1) is a multi-domain protein that was first identified as a member of the Fas death-inducing signaling complex, but later found to be involved in various biological processes. Although the exact mechanisms are not clear, FAF1 appears to play an important role in cancer, asbestos-induced mesotheliomas, and Parkinson's disease. It interacts with poly-ubiquitinated proteins, Hsp70, p97/VCP in addition to the proteins in the Fas-signaling pathway. We have determined the crystal structure of the ubiquitin associated domain of human FAF1 (hFAF1-UBA) and examined its interaction with ubiquitin and ubiquitin-like proteins using NMR. The hFAF1-UBA revealed a canonical three-helical bundle, and it selectively binds to mono- and di-ubiquitin (Lys48-linked), but not to SUMO-1

and NEDD8. The interaction between the hFAF1-UBA and di-ubiquitin involves the hydrophobic interaction accompanied by a transition in the di-ubiquitin conformation. These results provide structural insight into the mechanism of polyubiquitin recognition by hFAF1-UBA

***Acknowledgements**: This work was supported by grants from the Functional Proteomics Center, the 21C Frontier Research & Development Program of the Korea Ministry of Science and Technology, the Korea Institute of Science and Technology Institutional Program Grant.*

P-19 New design platform for malonyl-CoA-acyl carrier protein transacylase

Seung Kon Hong, Kook Han Kim, and Eunice EunKyeong Kim
Life Sciences Division, Korea Institute of Science and Technology, 39-1, Hawolgok-dong, Sungbuk-gu, Seoul, Korea 136-791;
(eunice@kist.re.kr)

The biosynthesis of fatty acids is a fundamental component of the cellular metabolic pathway, since fatty acids are the essential building blocks for membrane phospholipid formation. Since most bacteria and plants synthesize fatty acids using a discrete and highly conserved group of enzymes called the type II fatty acid synthase (FAS II) system that is different from yeast and animal which utilize the type I fatty acid synthase (FAS I), type II FAS system have been receiving enormous attention as possible antibiotic targets. Among them is malonyl-CoA-acyl carrier protein transacylase (MCAT; FabD; EC2.3.1.39) which is responsible for transferring the malonyl group from malonyl-CoA to the holo acyl carrier protein (ACP). We have obtained the crystal structure of MCAT from *Streptococcus aureus* and *S. pneumoniae* which are major pathogens at 1.46 and 2.0Å resolution, respectively. The data obtained could be used in aiding the process of novel inhibitor design.

***Acknowledgements**: This work was supported by grants from the Functional Proteomics Center, the 21C Frontier Research & Development Program of the Korea Ministry of Science and Technology, the Korea Institute of Science and Technology Institutional Program Grant.*

P-20 Structural Studies of Two PHP-like Tyrosine Phosphatases, CpsB from *Streptococcus pneumoniae* and YwqE from *Bacillus subtilis*

Hyoun Sook Kim[1], Sang Jae Lee[1], Do Jin Kim[1], Hye-Jin Yoon[1], Soon-Jong Kim[3], and Se Won Suh[1,2]
[1] *Department of Chemistry, College of Natural Sciences, Seoul National University, 151-747, Seoul, Korea (sewonsuh@snu.ac.kr)*
[2] *Department of Biophysics and Chemical Biology, College of Natural Sciences, Seoul National University, 151-747, Seoul, Korea (sewonsuh@snu.ac.kr)*
[3]*Department of Chemistry, Mokpo National University, 534-729, Mokpo, Korea (sjkim@mokpo.ac.kr)*

CpsB from *Streptococcus pneumoniae* and YwqE from *Bacillus subtilis* are the representatives of the novel bacterial manganese-dependent protein tyrosine phosphatases

(PTPs), which are different from Cys-based eukaryotic and prokaryotic PTPs including low-molecular-weight phosphotyrosine protein phosphatases. Influencing on pneumococcal virulence and invasive disease of *S. pneumoniae*, CpsB regulates capsular polysaccharide biosynthesis with CpsC and CpsD via tyrosine phosphorylation of CpsD, its cognate protein tyrosine kinase. Recent reports show that YwqE acts toward various substrates including single-stranded DNA-binding proteins and is involved in diverse functions such as bacterial DNA metabolism or UDP-glucuronate biosynthesis. To gain insight into function at the molecular level, we have purified and crystallized CpsB and YwqE. X-ray diffraction data were collected to high resolution, 2.0 Å and 1.6 Å, respectively. Two proteins are folded into a TIM-barrel motif with a binuclear metal center. Our structural analyses support the classification of these novel PTPs into the PHP (DNA polymerase and histidinol phosphate)-related amidohydrolase superfamily and allows us to propose a reaction mechanism of these enzymes.

P-21 Crystal structure and functional implications of the human Rad9-Hus1-Rad1 DNA damage checkpoint complex

Jin Seok Kim, Sun Young Sohn, Gwang Hyeon Gwon and Yunje Cho
National Creative Initiatives for Structural Biology and Department of Life Science, Pohang University of Science and Technology, Hyo-ja dong, San31, Pohang, KyungBook, South Korea (yunje@postech.ac.kr)

Three evolutionarily conserved proteins, Rad9, Hus1, and Rad1, form a heterotrimeric 9–1–1 complex that plays critical roles in cellular responses to DNA damage by activating checkpoints and by recruiting DNA repair enzymes to DNA lesions. We have determined the crystal structure of the human Rad9 (residues 1–272)–Hus1–Rad1 complex at 2.5 Å resolution. The 9^{1-272}–1–1 complex forms a closed ring, with each subunit having a similar structure. Despite its high level of similarity to proliferating cell nucleus antigen in terms of overall structure, the 9^{1-272}–1–1 complex exhibits notable differences in local structures, including interdomain connecting loops, H2 and H3 helices, and loops in the vicinity of the helices of each subunit. These local structural variations provide several unique features to the 9–1–1 heterotrimeric complex—including structures of intermolecular interfaces and the inner surface around the central hole, and different electrostatic potentials at and near the interdomain connecting loops of each 9–1–1 subunit—compared to the proliferating cell nucleus antigen trimer. We propose that these structural features allow the 9–1–1 complex to bind to a damaged DNA during checkpoint control and to serve as a platform for base excision repair. We also show that the 9^{1-272}–1–1 complex, but not the full-length 9–1–1 complex, forms a stable complex with the 5′ recessed DNA, suggesting that the C-terminal tail of Rad9 is involved in the regulation of the 9–1–1 complex in DNA binding.

P-22 Structural Basis for the Substrate Specificity and Reaction Mechanism of Bacterial Aminopeptidase

Kyeong Kyu Kim[1], Minh Hai Ta[1], HyeJin Park[1], Sangho Lee[2]
[1]*Department of Molecular Cell Biology, Sungkyunkwan University School of Medicine, Suwon 440-746, Korea (kkim@med.skku.ac.kr)*
[2]*Department of Biological Science, Sungkyunkwan University, Suwon 440-746, Korea.*

Aminopeptidases play an important role in diverse physiological processes including the cleavage of N-terminal methionine and the catabolic turnover of peptides into amino acids. Their substrate specificities must be tightly regulated because unnecessary peptide cleavages can result in the loss of essential cellular functions and cell death. PepS, a key metallopeptidase in the protein turnover, shows specificity towards small peptides possessing arginine or aromatic amino acids at the N-terminus, however, the mechanisms underlying this specificity and reaction are not clearly understood.

Using crystal structures of PepS and its complexes with substrate or inhibitors, we are able to elucidate how PepS differentiates its substrates from other functional proteins and how it hydrolyzes them. PepS consists of two domains and depending on their relative movements, the conformation can be closed or open. The closed conformation of PepS prevents the substrate entry, but the open conformation accommodates the substrates into its binding pocket that is a hole with 20 Å depth and 10 Å width. However, the enzyme can be fully activated only in the closed conformation since the catalytic residues are rearranged into active configuration in the close state. Taken these structural data together, we propose that PepS alternates between open and closed conformations by domain movements during each catalytic cycle; opening for swallowing the substrates, closing for the hydrolysis of the bound substrates, and opening again for product release.

P-23 Structural study of Enhanced Intracellular Survival protein, Eis protein from *Mycobacterium tuberculosis*

Kyoung Hoon Kim[1], Ji Young Yoon[1], Hyoun Sook Kim[1], Sang Jae Lee[1], Do Jin Kim[1], Hye-Jin Yoon[1], and Se Won Suh[1,2]
[1]*Department of Chemistry, College of Natural Sciences, Seoul National University, Seoul 151-742, Korea (sewonsuh@snu.ac.kr)*
[2]*Department of Biophysics and Chemical Biology, College of Natural Sciences, Seoul National University, Seoul 151-742, Korea (sewonsuh@snu.ac.kr)*

Mycobacterium tuberculosis, the causative agent of tuberculosis, is one of the oldest pathogens known to human and is responsible for the death of over 1.8 million people every year. The pathogenic mycobacteria have developed strategies to circumvent the major killing mechanisms employed by macrophages and take advantage of the enclosed environment within its host cell to avoid humoral and cell-mediated immune responses. Secretory proteins play a major role in host-pathogen interactions. The eis gene of Mycobacterium tuberculosis has been shown to play a role in the survival of the avirulent *Mycobacterium smegmatis* within the macrophage. Eis is present in cytosolic and cell envelope fractions of *M. tuberculosis*. It is released into culture supernatants and into the cytoplasm of infected macrophages. In one study, sera from 40% of pulmonary tuberculosis patients were positive

for anti-Eis antibody, indicating that the protein is antigenic. Eis reduces TNF-alpha and IL-4 production by mitogen-stimulated human T-cells, indicating that Eis affects T-cell function. However, the eis mutant shows no growth defect in a macrophage cell line or in mice. Bioinformatic analyses suggest that Eis is an acetyltransferase. Additional evidence indicates that it modulates the host immune response but the precise function of Eis is unclear.

To gain insight into the Eis protein function at the molecular level, we have purified and crystallized Eis protein. X-ray diffraction data were collected to 2.85 Å using synchrotron X-rays. The native crystal belongs to the monoclonal space group $P2_1$, with unit cell parameters of a = 108.13 Å, b = 150.19 Å, c = 184.38 Å, and $\alpha = \gamma = 90°$, $\beta = 103.05°$. The asymmetric unit contains twelve monomers, giving a crystal volume per protein mass (Vm) of 2.53 $Å^3$ Da^{-1} and a solvent content of 51.5%. The structure was solved by single-wavelength anomalous diffraction method and has been refined to crystallographic R_{work} and R_{free} values of 22.8% and 28.2%, respectively.

P-24 Study on Structural biology in disease

Myung-Il Kim, Woo-Suk Jung, Sangkee Rhee
School of Agricultural Biotechnology, Seoul National University, Seoul, Korea (mikim01@snu.ac.kr)

Amylosucrase from *Neisseria polysaccharea* (NpAS) is a transglucosidase of family 13 glycoside hydrolase which catalyzes the synthesis of amylase-like polymer by hydrolase and glucosyltransferase activity using sucrose as a substrate. Recently, a novel enzyme from *Xanthomonas axonopodis* pv. glycines, with a high sequence similarity of 57% with that of NpAS, was characterized as a member of the newly defined carbohydrate utilization locus which regulates the utilization of plant sucrose in phytopathogenic bacteria. Interestingly, the enzyme named sucrose hydrolase (SUH) exhibits exclusively the hydrolase activity not a glucosyltransferase activity. In order to elucidate structural and functional features of SUH, we carried out crystallographic and site-directed mutagenesis. Four different crystal structures of SUH, including the free enzyme, SUH-sucrose complex, and SUH-glucose complex, reveal structural snapshots along the catalysis. Structural comparisons with NpAS provide that an overall structure of SUH is essentially identical with that of NpAS, and that the active site of SUH in the SUH-sucrose for the Michaelis complex is a pocket-type formed by conformational change, while NpAS has a tunnel-type active site with no indication of the conformational changes by the binding of sucrose. Site-directed mutagenesis was performed such that the active site residues in SUH were replaced with residues crucial for a glucosyltransferase activity in NpAS. Our structural and functional analysis suggests that a pocket-shaped active site and the identity of residues in the vicinity of the active site of SUH are designed to be optimal for the unique hydrolytic activity of sucrose.

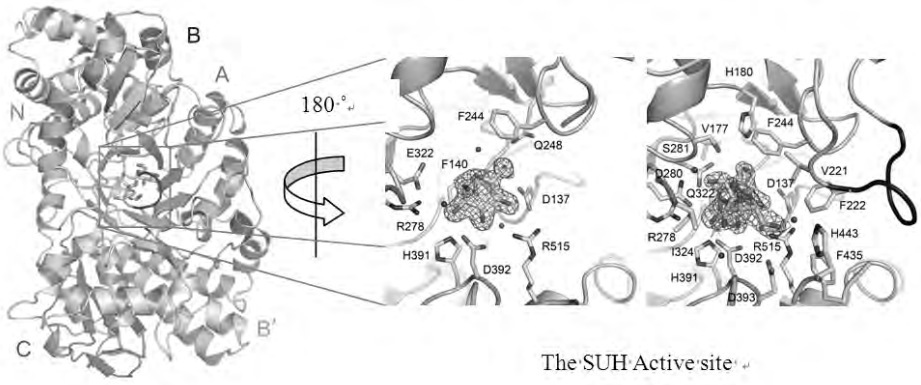

Overall structure

The SUH Active site

P-25

Structural insights into TDP-43, a new player in neurodegenerative diseases

Pan-Hsien Kuo[1,2], Lyudmila G. Doudeva[2], Yi-Ting Wang[1,2,3], Che-Kun James Shen[2] and Hanna S. Yuan[2,3,4,*]

[1]*Institute of Bioinformatics and Structural Biology, National Tsing Hua University,*
[2]*Institute of Molecular Biology, Academia Sinica,*
[3]*Taiwan International Graduate Program, Chemical Biology and Molecular Biophysics, Academia Sinica,*
[4]*Graduate Institute of Biochemistry and Molecular Biology, National Taiwan University, Taipei, Taiwan*

TDP-43 is a pathogenic protein: its normal function in binding to UG-rich RNA is related to cystic fibrosis, and inclusion of its C-terminal fragments in brain cells is directly linked to frontotemporal lobar degeneration (FTLD) and amyotrophic lateral sclerosis (ALS). We determined the crystal structure of the C-terminal RRM2 domain of TDP-43 in complex with a single-stranded DNA at a resolution of 1.65 Å. We show that TDP-43 is a dimeric protein with two RRM domains, both involved in DNA and RNA binding. The crystal structure reveals the basis of TDP-43's TG/UG preference in nucleic acids binding. It also reveals that RRM2 domain has an atypical RRM-fold with an additional β-strand involved in making protein-protein interactions. This self association of RRM2 domains produced thermal-stable RRM2 assemblies with a melting point greater than 85°C as monitored by circular dichroism at physiological conditions. These studies thus characterize the recognition between TDP-43 and nucleic acids and the mode of RRM2 self association, and provide molecular models for understanding the role of TDP-43 in cystic fibrosis and the neurodegenerative diseases related to TDP-43 proteinopathy.

P-26 Pushing low-resolution data to the limit - the structure of the third component of the ligand binding site of the human insulin receptor

John G. Menting, Brian J. Smith, Colin W. Ward, Michael C. Lawrence
The Walter and Eliza Hall Institute of Medical Research, 1G Royal Parade, Parkville, Victoria 3052, Australia (lawrence@wehi.edu.au)

Despite the structure of insulin being known for over forty years[1], the structural detail of the manner in which it binds to its receptor and effects signalling remains elusive. Our crystal structure[2] of the *apo*-form of the human insulin receptor ectodomain homodimer at 3.8 Å resolution revealed that the ligand binding site is formed by a juxtaposition of the first leucine rich-repeat domain (L1) of one monomer with the first and second fibronectin domains of the alternate monomer. Such a mode of assembly of the ligand binding site was, in particular, consistent with the symmetric, alternative cross-linking model of insulin binding to its receptor and thus provided the first structural basis for the negative cooperativity of ligand binding displayed by the receptor[3].

However, absent from the resolved structure was the C-terminal region of the receptor α-chain. This segment of sixteen residues (the "αCT peptide", residues 704-719) lies within a disordered segment of the receptor and is known to be absolutely essential for ligand binding[4]. Strikingly, addition of this peptide in exogenous form is able to restore ligand binding ability to certain domain-minimised receptor fragments that are otherwise devoid of such ability[5]. The crystal structure of the *apo*-form of the receptor did, however, contain a tube-like segment of difference electron density lying on the insulin-binding surface of L1 and at the time resisted all attempts at interpretation, though we surmised that it might have arisen from the αCT peptide[2].

We have now devised techniques that have led to a clear interpretation of the electron density segment as arising from residues within the C-terminal region of the receptor α-chain (see Figure).

Figure Schematic view of the C-terminal segment of the insulin receptor α-chain

We thus have obtained the first view of the mode of assembly of all three components of the insulin binding site. The implications are profound. (1) The structure creates an entirely new paradigm about how insulin might bind to its receptor. (2) Combined with our isothermal titration calorimetry data, the structure explains the mode of binding of the so-called Site 1 class of insulin mimetic peptides which have been developed to bind to the insulin receptor with high affinity[6]. (3) The findings carry over directly to the type 1 insulin-like growth factor receptor system, suggesting that the αCT peptide binding site on L1 may in fact be a target for anti-cancer therapeutics.

References:
[1]. Harding, M.M., et al., J. Mol. Biol. 16, 212-26 (1966).
[2]. McKern, N.M. et al., Nature 443, 218-21 (2006).
[3]. De Meyts, P. Diabetologia 37 Suppl. 2, S135-48 (1994).
[4]. Ward, C.W. & Lawrence, M.C. Bioessays 31, 422-34 (2009).
[5]. Kristensen, C., et al., J. Biol. Chem. 277, 18340-5 (2002).
[6]. Schäffer, L. et al. PNAS 100, 4435-9 (2003).

P-27

Crystal structures of aprotinin and its complexs

Ji-Hye Lee[1], In Seok Yang[1], Ki Joon Cho[2], Intekhab Alam[1], Yi Ho Park[1], and Kyung Hyun Kim[1]
[1] Department of Biotechnology & Bioinformatics, College of Science & Technology, Korea University, Chungnam 339-700, Korea (jihyelee@korea.ac.kr; graduate@korea.ac.kr; Intekhab@korea.ac.kr; ballashe@naver.com; khkim@korea.ac.kr)
[2] School of Life Sciences & Biotechnology, Korea University, Seoul 136-701, Korea (c-azna@korea.ac.kr)

Aprotinin has been shown to decrease heparin binding to platelets. Heparin which is a highly sulfated glycosaminoglycan is an anticoagulant produced by mast cells. In addition, heparan sulfate is known to be able to facilitate formation of the protofilament for amyloid fibrillogenesis. The crystal structures of aprotinin complexed with sucrose octasulfate (SOS) and Val-Phe-Phe (VFF) were determined at 1.7 and 1.6 Å resolutions, respectively. The crystal structure of aprotinin complexed with SOS, a polysulfated heparin analog, showed three aprotinin molecules per one SOS in the asymmetric unit. However, five aprotinins seem to be randomly arranged to form a complex with one SOS molecule. The sulfate groups of SOS interact with positively charged residues Lys and Arg, from which a binding mode of heparin to aprotinin is described. A tripeptide VFF was accidently observed at the monomer-monomer interface in a decameric form of aprotinin at acidic pH, which was confirmed by cocrystallization with a synthesized VFF tripeptide. Although there is no direct evidence for the origin of VFF, a hydrophobic region including VFF in amyloid beta is known to play a critical role in nucleation of amyloid formation. The interaction of aprotinin with the tripeptide is described.

P-28

Crystal Structure of the Glycosyltransferase Domain of Cholesterol-α-Glycosyltransferase from *Helicobacter pylori*

Sang Jae Lee[1], Hyoun Sook Kim[1], Do Jin Kim[1], Kyoung Hoon Kim[1], Ji Young Yoon[1], Jun Young Jang[1], Hye-Jin Yoon[1], Se Won Suh[1,2]
[1] Department of Chemistry, College of Natural Sciences, Seoul National University, 151-747, Seoul, Korea (sewonsuh@snu.ac.kr)
[2] Department of Biophysics and Chemical Biology, College of Natural Sciences, Seoul National University, 151-747, Seoul, Korea (sewonsuh@snu.ac.kr)

Helicobacter pylori infection causes gastric pathology such as ulcer and carcinoma. *H. pylori* follows a cholesterol gradient and extracts the lipid from plasma membranes of human stomach epithelial cells for subsequent glucosylation by cholesterol-α-glycosyltransferase.

Cholesterol-α-glycosyltransferase abrogates phagocytosis of *H. pylori* and subsequent T cell activation. Thus the development of antibiotics could be possible based on the inhibition of cholesterol glucosylation. To provide the structural basis for inhibitor discovery, we have determined the crystal structure of the glycosyltransferase domain of cholesterol-α-glycosyltransferase from *H. pylori*. X-ray diffraction data were collected to 1.5 Å using synchrotron X-rays. The native crystals are triclinic, belonging to the space group P_1, with unit-cell parameters a = 35.79 Å, b = 40.71 Å, c = 53.74 Å, and α = 101.44°, β = 94.87°, γ = 90.58°. The asymmetric unit contains two monomers, giving a crystal volume per protein mass (V_M) of 1.91 $Å^3$ Da^{-1} and a solvent content of 35.7%. The structure was solved by multi-wavelength anomalous diffraction method and has been refined to crystallographic R_{work} and R_{free} values of 19.2% and 23.3%, respectively.

P-29 A Novel 'in situ' Inhibitor Elongation Strategy Produces a Stable Covalent Intermediate With Human Pancreatic Alpha-Amylase

Chunmin Li[1], Ran Zhang[2], Leslie K. Williams[1], Brian P. Rempel[2], Stephen G. Withers[2], Gary D. Brayer[1]

[1] *Department of Biochemistry and Molecular Biology, University of British Columbia, Vancouver, BC V6T 1Z3, Canada (chunmin.li@gmail.com)*

[2] *Chemsitry Department, University of British Columbia, Vancouver, BC V6T 1Z1, Canada*

Human pancreatic α-amylase (HPA) is a key endoglycosidase involved in the digestion of dietary starch in the gut. Control of the activity of HPA thus provides a valuable therapeutic approach for diseases such as diabetes and obesity. Despite extensive mechanistic studies of HPA, determination of a detailed structure of a trapped covalent glycosyl-enzyme intermediate has proven elusive. To remedy this situation we have developed a new in situ strategy for trapping and subsequent structural elucidation of HPA glycosyl-enzyme intermediates. In particular, our structural studies unambiguously show the covalent attachment of a 5-fluoro-α-L-idosyl moiety in the chair conformation to the side chain of the catalytic nucleophile D197. The elongated versions of this intermediate complex are found to bind in the high affinity -2 and -3 binding subsites, where they form extensive hydrogen bonding interactions. Comparison of these structural results with the related non-covalent complex formed by acarbose highlights the structural rigidity of the enzyme surface and the key role that substrate conformational flexibility plays during catalysis. Collectively, our structural results provide insight into several key catalytic steps.

P-30 Crystallization and preliminary X-ray crystallographic studies of *O*-methyltransferase from the *Anabaena Pcc 7120*

Guoming Li [1,3], Zhenting Tang[1,2], Geng Meng[1,2], Kesheng Dai[3], Jindong Zhao[1,2], Xiaofeng Zheng[1,2*]
[1]*National Laboratory of Protein Engineering and Plant Genetic Engineering,* [2]*Department of Biochemistry and Molecular Biology, College of Life Sciences, Peking University, Beijing, 100871, .China,*
(gml_1002@yahoo.com.cn, xiaofengz@pku.edu.cn)*
[3]*School of Biological Science and Medical Engineering, Beihang University, Beijing 100191, P.R.China.*

O-methyltransferase (OMT) is a ubiquitous enzyme that exists in bacteria, plants and humans, which catalyzes a methyl transfer reaction using *S*-adenosyl-L-methionine-(AdoMet) as a methyl donor and a wide range of phenolics as acceptor. To investigate the structure and function of OMTs, *omt* from the *Anabaena Pcc 7120* was cloned into expression vector pET21 and expressed in soluble form in *Escherichia coli* strain BL21(DE3). The recombinant OMT protein was purified to homogeneity through a two-step strategy. A preliminary crystal image of OMT was provided using hanging-drop vapor diffusion method. The crystals of OMT diffracted to a resolution of 2.4 Å and belong to $C222_1$ space group. The unit cell parameters are *a*=131.620 Å, *b*=227.994 Å, *c*=150.777 Å, α=β=γ=90°. There may be 8 molecules per asymmetry unit.

P-31 Crystallographic study of NQO2 and structure-based ligand design

Yazhuo Li, Cristina de Matteis
School of Pharmacy, Center for Biomolecular Sciences, The University of Nottingham, University Park, Nottingham, NG7 2RD, UK. (paxyl1@nottingham.ac.uk)

NQO2, which is one of flavoprotiens also known as QR2, was discovered decades ago[1-3]. Its sequence and tissue distribution has been studied widely, and results suggest that distribution depends on the species. The role of NQO2 has also been investigated, and current opinion is that NQO2 is one of the detoxifying enzymes in Phase II; it shows a sequence identity with its analogue NQO1, another detoxifying enzyme, of about 49% and it also functions to carry out two-electron transfer to reduce quinones to stable intermediates such as hydroquinones [3. However, this was challenged by experimental data obtained when menadione was tested in both wild type and NQO2 knocked out mice. Menadione which is supposed to undergo one-electron reduction to produce semiquinone to damage tissues appeared to be not toxic in the absence of NQO2 in the knocked out model. We know a little about the structure of NQO2 until its apo-structure was published in 1999. But the understanding of binding mode of its substrates and inhibitors with enzyme is still very limited.

Protein-ligand complexes have been successfully co-crystallized, including substrates and inhibitors. High-resolution datasets have been collected at Synchrotron. Atomic structures of complexes have been built to reveal the binding mode of the ligands. Density map indicated

the presence of ligands in the binding pockets, and the orientations and positions of the ligands are quite clear. On the other hand, because NQO2 is one of the heated targets for cancer therapy, the NQO2 structure-based ligand design was carried out through screening chemical database in order to find novel inhibitors or substrates of NQO2 on the basis of modes interpreted from the crystal structure since its ambiguity on function. One of the high resolution crystal structures (PDB entry: 1SG0) from Brookhaven database was used as the target model, the docking suite GOLD and Gold scoring function were adopted to screen the library to identify the compound as candidates to cure cancer and other diseases, the active site was refined by molecular dynamic simulation. In addition, preliminary enrichment of its natural inhibitors was done; one of its predicted modes has been confirmed by its crystal structure. Sub library was built, which the potential substrates or inhibitors were filtered by physical or chemical properties. Their bioactivities need to be measured as to categorize in the future.

References

1. Liao, S. and H.G. Williams-Ashman, Inhibition of the enzymic oxidation of some dihydropyridines by polycyclic aromatic hydrocarbons. Biochemical Pharmacology, 1961. 6(1-2): p. 53-54.
2. Liao, S. and H.G. Williams-Ashman, Enzymatic oxidation of some non-phosphorylated derivatives of dihydronicotinamide. Biochemical and Biophysical Research Communications, 1961. 4(3): p. 208-213.
3. Liao, S., J.T. Dulaney, and H.G. Williams-Ashman, Purification and Properties of a Flavoprotein Catalyzing the Oxidation of Reduced Ribosyl Nicotinamide. 1962. p. 2981-2987.

P-32

Insights into the Alkyl Peroxide Reduction Pathway of *Xanthomonas campestris* Bacterioferritin Comigratory Protein from Trapped Intermediate/Ligand Complex Structures

Shu-Ju Liao[1], Chao-Yu Yang[1], Ko-Hsin Chin[3], Andrew H.-J. Wang[2] & Shan-Ho Chou[1, 3]

[1] *Institute of Biochemistry, National Chung-Hsing University, Taichung, 40227, Taiwan*
[2] *Institute of Biological Chemistry, Academia Sinica, Nankang, Taipei, Taiwan*
[3] *National Chung Hsing University Biotechnology Center, Taichung, 40227, Taiwan, (shchou@nchu.edu.tw)*

Considerable insights into the alkyl peroxide oxidoreduction activity of *Xanthomonas campestris* bacterioferritin comigratory protein (*Xc*BCP) have been obtained from trapped intermediate/ligand complex structures determined by X-ray crystallography. Multiple sequence alignment and enzyme assay indicated that *Xc*BCP belongs to a subfamily of atypical 2-Cys peroxiredoxins (Prxs), containing a strictly conserved peroxidatic cysteine (C_P48) and an unconserved resolving cysteine residue (C_R84). Crystals at different states, i.e. Free_SH state, Intra_SS state, and Inter_SS state, were obtained by screening the *Xc*BCP proteins from a double C48S/C84S mutant, a wild-type, and a C48A mutant, respectively. A formate or an alkyl analog with two water molecules that mimic an alkyl peroxide substrate was found close to the active site of the Free_SH or Inter_SS state, respectively. Their global structures were also found to contain a novel substrate binding pocket capable of accommodating an alkyl chain no less than 16 carbons. In addition, in the Intra_SS or

Inter_SS state, substantial local unfolding or complete unfolding of the C_R-helix was detected, with the C_P-helix remaining essentially unchanged, which is in sheer contrast with the observation before that the C_P-helix exhibits local unfolding during disulfide bond formation in typical 2-Cys Prxs. These rich experimental data have enabled us to draw a pathway on how *Xc*BCP carries out its oxidoreduction activity through the alternate opening and closing of the substrate entry channel and the disulfide-bond pocket.

References

Liao S-J, Yang C-Y, Chin K-H, Wang AH-J, Chou S-H. Insights into the Alkyl Peroxide Reduction Pathway of Xanthomonas campestris Bacterioferritin Comigratory Protein from Trapped Intermediate/Ligand Complex Structures. J Mol Biol 2009; in press

P-33 Crystal Structure of the Cytoplasmic Domain of the Type II Secretion System Component EpsL of *Vibrio parahaemolyticus*

Li-Ying Lin[1], Nien-Tai Hu[1], and Nei-Li Chan[1, 2]
[1]*Institute of Biochemistry, College of Life Sciences, National Chung Hsing University, Taichung, Taiwan.(sparklingstonelin@gmail.com)*
[2]*Institute of Biochemistry and Molecular Biology, College of Medicine, National Taiwan University, Taipei, Taiwan. (nlchan@ntu.edu.tw)*

The type II secretion system (T2SS) is used for the translocation of fully folded extracellular proteins across the outer membrane of Gram-negative bacteria. At least 12 distinct protein components are required for the functioning of T2SS by forming a secretion nano-machine that spans both the outer and inner membranes, providing a direct connection between the cytoplasm and outer membrane. Such a trans-envelop assembly couples ATP hydrolysis, taking place exclusively in the cytoplasm, to protein translocation. In T2SS, the cytosolic secretion ATPase EpsE is recruited to the membrane-associated secretion complex by interacting with the cytoplasmic membrane proteins EpsL. Therefore, EpsL serves as a critical link between ATP utilization and exoprotein secretion. To provide a structural understanding of this critical interaction, we have determined the crystal structure of cytoplasmic domain of EpsL from *V. parahaemolyticus* at 2.6 Å resolution by the multiwavelength anomalous diffraction (MAD) method. The analysis of the structure will be presented during the meeting.

P-34 Crystal Optimization of a Secondary Transporter Membrane Protein to 4.5 Å Resolution

Xiangyu Liu[1,2], Pontus Gourdon[1], Xiaodong Su[2], Poul Nissen[1]
[1] *Center of Structural Biology, Department of Molecular Biology, Aarhus University, Science Park, Gustav Wieds Vej 10C, 8000 Aahus, Denmark (xyliu@bioxray.au.dk)*
[2] *School of Life Sciences, Peking University, Beijing100871, China*

Integral membrane proteins represent about 20–30% of the total proteins of various organisms. Despite their important physiological roles, they are highly underrepresented in the protein data bank (PDB), due to the difficulties in overproducing, purifying, stabilizing and crystallizing them. This is mainly due to their amphipathic character; the existence of a

hydrophobic surface requires detergent micelles to make them soluble in an aqueous solution, but frequently this treatment also adversely affects their activity (due to e.g. loss of cofactors, lipids or subunits) as well as the chances to acquire well-diffracting crystals (due to e.g. hindrance of potential crystal contacts).

The formate transporter FocA, which belongs to the formate-nitrite transporter (FNT) family, exists in several bacteria, archaea and yeasts. In general, FocA homologs are 250-300 residues in length with 6 putative transmembrane helices and they share no apparent similarity with any structures in the PDB. The first FocA protein was found in E.coli and it is believed to be involved in formate influx and/or efflux while using protons as the symport counter ions (Suppmann B & Sawers G., 1994, Mol Microbiol. 11(5): 965-82). As such, FocA may be a key protein in regulating the intracelullar formate concentration during cell anaerobic growth. Pyruvate formate-lyase (PFL) converts pyruvate to formate and acetyl CoA under anaerobic conditions (Becker A & Kabsch W, 2002, J Biol Chem. 277(42): 40036-42). Hence the levels of these products have to be tightly controlled; the concentration of formate is also important as the substance may trigger various transcription regulators (such as FHLA) and its accumulation could furthermore result in cytoplasmic acidification and an uncoupled proton gradient (R.G. Sawers, 2005, Biochem Soc Trans, 33, 42). A high resolution model of FocA would help to elucidate the substrate binding and transport mechanism of the entire FNT family.

We have cloned and expressed a bacterial FocA. Specific truncations were made to prevent spontaneous degradation and a His-tag was added to facilitate purification. The solubilization detergent and concentration was optimized, and the protein was purified with Ni^{2+} affinity and Superdex 200 size-exclusion chromatography. For the subsequent crystallization experiments, the most suitable protein buffer and detergent, as judged by multiple Superdex 200 PC gel filtration runs, was selected after a relatively large screen of conditions. Initial crystallization hits were obtained following screening with several detergents, but the size and diffraction properties were limited. Optimized crystals grew to larger size (0.2 mm * 0.15 mm * 0.1mm) and the best ones diffracted to 4.5 Å at MAXLAB (Sweden). However, the crystals still suffer from anisotropy, and display diffuse scattering and high mosaicity. We will report on the subtle modifications of the preparation protocol that enabled the initial crystals to form. In addition, the careful and systematic approach to optimize these crystals from the first small diffracting entities to the current resolution will be presented. We will also show how we wish combat the existing diffraction obstacles and improve the resolution beyond 4.5 Å in the near future. We believe that several of these approaches may be of general interest for other projects where crystals of membrane proteins are sought for.

P-35 The crystal structure of a replicative hexameric helicase DnaC and its complex with single-stranded DNA

Yu-Hua Lo[1,2], Kuang-Lei Tsai[1,2], Yuh-Ju Sun[2], Wei-Ti Chen[1], Cheng-Yang Huang[1] and Chwan-Deng Hsiao[1]
[1]*Institute of Molecular Biology, Academia Sinica, Taipei, 115, Taiwan (d948227@oz.nthu.edu.tw)*
[2]*Institute of Bioinformatics and Structural Biology, National Tsing Hua University, Hsinchu, 300, Taiwan*

DNA helicases are motor proteins that play essential roles in DNA replication, repair, and recombination. In the replicative hexameric helicase, the fundamental reaction is the unwinding of duplex DNA; however, our understanding of this function remains vague due to insufficient structural information. Here, we report two crystal structures of the DnaB-family replicative helicase from *Geobacillus kaustophilus* HTA426 (*Gk*DnaC) in the apo-form and bound to single-stranded DNA (ssDNA). The *Gk*DnaC-ssDNA complex structure reveals that three symmetrical basic grooves on the interior surface of the hexamer individually encircle ssDNA. The ssDNA-binding pockets in this structure are directed toward the N-terminal domain collar of the hexameric ring, thus orienting the ssDNA towards the DnaG primase to facilitate the synthesis of short RNA primers. These findings provide insight into the mechanism of ssDNA binding and provide a working model to establish a novel mechanism for DNA translocation at the replication fork.

P-36 Structures of yeast glutathione S-transferase Gtt2 reveal a new catalytic type of GST family

Xiao-Xiao Ma, Yong-Liang Jiang, Yong-Xing He, Rui Bao, Yuxing Chen and Cong-Zhao Zhou*
Hefei National Laboratory for Physical Sciences at Microscale, and School of Life Sciences, University of Science and Technology of China, Hefei, Anhui, 230027, People's Republic of China (zcz@ustc.edu.cn)

Glutathione S-transferases (GSTs) are ubiquitous detoxification enzymes which catalyze the conjugation of electrophilic substrates to glutathione (GSH). Here we solved the three-dimensional structures of Saccharomyces cerevisiae Gtt2 in apo- and two ligand-bound forms at 2.23, 2.20 and 2.10 Å, respectively. Despite sharing a similar overall structure to other GSTs, lack of any classic catalytic essential residues (Tyr, Ser and Cys) distinguishes this first fungal GST structure from all cytosolic GSTs of known structures. Subsequent site-directed mutagenesis in combination with activity assays reveal that a water molecule stabilized by Ser129 and His133 works as the deprotonator towards GSH sulfur atom instead of the classic catalytic residues. Moreover, due to the stereo-hindrance between helix α1 and GSH, only glycine and alanine are permitted at the N-terminus of helix α1. Taken together, yeast Gtt2 represents a novel atypical-type of cytosolic GSTs which are dominantly distributed in lower organisms.

P-37

Fragment-based screening by X-ray crystallography: discovery of novel inhibitors targeting the adrenaline-synthesising enzyme

Jennifer L Martin[1], Nyssa Drinkwater[1], Gary Grunewald[2] and Michael McLeish[3]
[1]*Institute for Molecular Bioscience, University of Queensland Brisbane QLD 4072;*
[2]*Kansas University Lawrence Kansas USA;*
[3]*IUPUI Indiana USA*

Fragment-based lead discovery is a relatively new approach to drug design that involves screening libraries of compounds that are significantly smaller (typically 120-250 Da) than drug molecules (typically up to 500 Da) [1-3]. The rationale is that "drug-like" fragments represent individual binding epitopes whereas larger "drug-like" compounds found in conventional high throughput screen (HTS) libraries represent combinations of binding epitopes. Drug-like fragments that bind would have lower affinities than drug-like compounds, but would be more "efficient" ligands – and therefore better starting points for lead development - because a greater proportion of atoms are involved in favourable receptor contacts.

A major advantage of fragment-screening is that it more efficiently samples chemical space than traditional screening approaches [4-5] and therefore requires significantly fewer compounds to be screened. For example, a library of 400 fragments screened on a two sub-site receptor samples chemical space as efficiently as a library of drug-like compounds containing all possible linked combinations of the fragments (400x400 or 160,000 compounds). Consequently, fragment libraries typically contain a few hundred fragments, whereas HTS libraries may contain hundreds of thousands of compounds.

Hits from a fragment library have K_d values lower than those of hits from HTS libraries, and typically in the range of 1 mM-10 μM [3, 5]. As a consequence they would often not register as hits in the functional assays used for HTS. Therefore fragment-screening approaches use highly sensitive techniques, such as X-ray crystallography, that can detect low-affinity binding and which can directly identify the binding site, the binding orientation and favourable interactions formed by the fragment. This level of detail is exploited in subsequent steps to optimise potency and selectivity using standard medicinal chemistry techniques.

We have used fragment-based screening by X-ray crystallography to identify fragments that bind to PNMT, the adrenaline-synthesising enzyme. Inhibitors of PNMT have the potential to be used in the treatment of hypertension and will also represent novel pharmacological tools to probe the role of adrenaline in the central nervous system. We screened a commercial library of 384 compounds, as cocktails of 4 compounds. and identified 12 hits (ie drug-like fragmetns that bound to PNMT). Nine of these hits were further characterised by ITC and found to have dissociation constants in the micromolar to sub-millimolar range. The binding affinity of the remaining three hits was too low to be detected by ITC. Using simple medicinal chemistry modifications we were able to improve the binding affinity of the best hits by 10-fold whilst maintaining a high ligand efficiency. The inhibitory effect of the modified compounds on PNMT enzyme activity was also investigated using a standard radio-assay. The efficiency and speed of the fragment-based screening approach for discovery and development of new drug leads is highlighted by the fact that all of the research - spanning

protein expression to crystallography, ITC, medicinal chemistry and enzyme kinetics - was performed by one PhD student over a period of 18 months.

References

1. Lesuisse, D. et al. J Med Chem 45, 2379-87 (2002).
2. Hartshorn, M. J. et al. J Med Chem 48, 403-13 (2005).
3. Rees, D. C., Congreve, M., Murray, C. W. & Carr, R. Nat Rev Drug Discov 3, 660-72 (2004).
4. Andrews, P. R., Craik, D. J. & Martin, J. L. J Med Chem 27, 1648-57 (1984).
5. Carr, R. A., Congreve, M., Murray, C. W. & Rees, D. C. Drug Discov Today 10, 987-92 (2005).

P-38 Crystal structure of PACSIN 1 F-BAR domain reveals a novel membrane curvature sensing mechanism

Geng Meng[1,2], Xiaoyun Bai[1,2],Guoming Li[2], Yong Liu[1,2], Ming Luo[3], Xiaofeng Zheng[1,2*]

[1]National Laboratory of Protein Engineering and Plant Genetic Engineering,
[2]Department of Biochemistry and Molecular Biology, College of Life Sciences, Peking University, Beijing, 100871, .China, (mengg@pku.edu.cn, xiaofengz@pku.edu.cn)*
[3]Department of Microbiology, University of Alabama at Birmingham, Birmingham, Alabama, 35294,USA.

Protein kinase C and casein kinase 2 substrate in neurons (PACSIN), also named sydapin, is a protein family involved in the vehicle transportation and endocytosis. The characteristic of this family is the Fer-CIP4 homology-BAR (F-BAR) domain in the N terminus with a subsequent SCH domain. F-BAR (FCH-BAR) domain proteins have been found with membrane-deforming properties and could form membrane invaginations or tubulation through the dimerized crescent-shaped molecules. The curvature of the membrane tubules depends on the BAR domain structure and the oligomerization of the proteins. Unlike any other F-BAR domain that generates low curvature tubules, PACSIN protein could not only generate the common tubules but also lead to high curvature tubules and tubules fission. In order to investigate the novel tabulation mechanism of the PACSINs, we crystallized and solved the structure of the F-BAR domain of PACSIN 1. The structure reveals a unique loop extrudes from the protein surface and influences the curvature of membrane bending mediated by the protein. This extruded loop lead to the small tubules' formation and suggests the profound function of PACSINs in vesiculation and endocytosis difference with other F-BAR domain proteins.

P-39 Stabilization mechanism by Hyp-Thr-Gly sequence in collagen-helix

Keita Miyama[1], Tatsuya Morimoto[1], Koichi Masakiyo[1], Tatsuya Kawaguchi[1], Kenji Okuyama[1], Kazunori Mizuno[2], Hans Peter Bächinger[2]

1 Department of Macromolecular Science, Graduate School of Science, Osaka University, Toyonaka 560-0043, JAPAN (okuyamak@chem.sci.osaka-u.ac.jp)
2 Shriners Hospital for Children, Research Department, Portland, Oregon 97239, USA

Collagen is the most abundant protein found in animals. It has a charactistic amino acid sequence; Gly at every third position and high content of imino acid (Pro and Hyp). Therfore,

its amino acid sequence has been designated by $(Xaa\text{-}Yaa\text{-}Gly)_n$, where the X and Y positions are frequently occupied by Pro and Hyp, respectively. Because of this sequence constraint, collagens adopt a triple-helical structure. For the last two decades, it was believed that only the Hyp residues in the Y position stabilize the collagen-helix. However, it was shown recently that the Hyp residues in the X position also stabilize the triple-helical structure in the Hyp-Hyp-Gly and Hyp-Thr-Gly sequences. Especially, the latter sequence seems to be utilized for the stabilization of cuticle collagen of *Riftia pachyptila* [1]. To understand the stabilization mechanism of this sequence, we analyzed high resolution structures of host-guest peptides, $(Pro\text{-}Pro\text{-}Gly)_4$-Hyp-Yaa-Gly- $(Pro\text{-}Pro\text{-}Gly)_4$ (hereafter, OYG) (Yaa = Thr, Val, Ser).

Crystals of OTG, OVG and OSG peptides were obtained by a hanging- or sitting-drop vapor diffusion method. The diffraction data were collected at SPring-8 (BL41XU and BL44XU) at 100K. Crystals of OTG and OVG peptides exhibited pseudo-merohedral twinning, while the OSG peptide grew as a single crystal with similar lattice parameters as those of other two. Structures of these peptides were obtained by the molecular replacement method and refined by SHELXL at high resolution (< 1.2 Å).

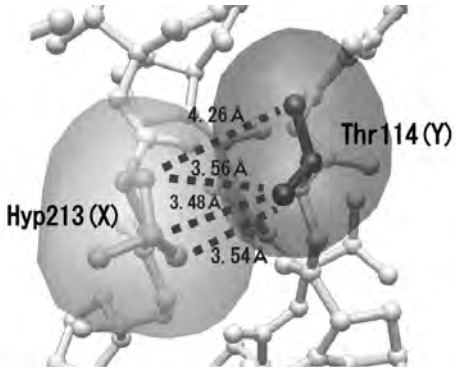

Fig.1 Inter-atomic distances between Hyp213 (X) and Thr114 (Y) of the OTG peptide

Detailed structures in the guest regions revealed the importance of interaction between Hyp in the X position and Yaa of the adjacent strand in the same molecule (Hyp(X):Yaa stacking pair). As an example, Hyp(X):Thr (Y) stacking pair is shown in Fig.1. By adopting *gauche*$^+$ conformation, the plane of Thr side chain defined by C_α, C_β, C_γ and O_δ atoms faced the ring plane of imino acid with van der Waals contacts between them. Similar interaction was also observed in the OVG crystal. This interaction seems to be important for the stabilization on the triple-helical structure in these peptides.

Reference

K. Mann et al. *J. Mol. Biol.*, 261, 255(1996)

P-40

Protein Function Annotation from Sequences and Structures with Tools at PDBj

Daron M. Standley[1], Mieszko Lis[2], Akira R. Kinjo[3], Haruki Nakamura[4]
[1] *Immunology Frontier Research Center, Osaka University, 3-2 Yamadaoka, Suita, Osaka 565-0871, Japan (standley@ifrec.osaka-u.ac.jp)*
[2] *MIT Computer Science and Artificial Intelligence Laboratory, 32 Vassar street, Cambridge, MA, USA (mieszko@csail.mit.edu)*
[3] *PDBj, Institute for Protein Research, Osaka University, 3-2 Yamadaoka, Suita, Osaka 565-0871, Japan (akinjo@protein.osaka-u.ac.jp)*
[4] *PDBj, Institute for Protein Research, Osaka University, 3-2 Yamadaoka, Suita, Osaka 565-0871, Japan (harukin@protein.osaka-u.ac.jp)*

The aim of structural genomics is to characterize protein function at the residue and atomic levels for target proteins without known function. More and more new protein sequences continue to appear with the rapid development of genome analysis methods, and prediction of function from only sequence information is highly desirable. We have developed a pipeline system to annotate protein function from sequences (and, when available, structural information), and make it available to the public from the PDBj web site[1] (http://www.pdbj.org).

SFAS (Sequence to Function Annotation Server, http://www.pdbj.org/sfas/) is a web-based tool for predicting the function of an amino acid sequence, using our new homology modeling service, *Spanner* (http://www.pdbj.org/spanner/). Alternatively, *Spanner* can build models from the results produced by the sequence-structure multiple-alignment system, *MAFFTash* (http://www.pdbj.org/ MAFFTash.3/), as well as several other external programs for sequence alignment and threading. The resulting 3D model is then used as an input template structure of *SeSAW*[2] (http://www.pdbj.org/ SeSAW/). *SeSAW* is based on sequence-weighted structure alignments to protein folds, and uses sequence profiles for both the template and the query to weight the structurally aligned residue pairs. The combination of sequence profiles and structure alignments makes it possible to reliably detect functional similarities while dealing with very distant homology. *GIRAF*[3] (http://giraf.pdbj.org/) is an efficient search method for atomic alignments of possible ligand binding sites and protein-protein interfaces. It is not constrained by sequence homology, sequence order or protein fold, and hence is applicable to the cases where no structural homologs can be found.

Both *SeSAW* and *GIRAF* have been used to annotate structural genomics targets with unknown functions[2]. The most functionally similar proteins are often found not to be the most structurally similar ones, which highlights the importance of incorporating evolutionary information via sequence profiles. They were also used to predict the function of a new and essential protein sequence, which was later experimentally confirmed[4].

References

[1] Standley, D. M. et al. *Brief. Bioinf.* **9**, 276-285 (2008),
[2] Standley, D. M. et al., *PROTEINS* **72**, 1333-1351 (2008),
[3] Kinjo, A. R. & Nakamura, H. *Structure* **17**, 234-246 (2009),
[4] Matsushita, K. et al., *Nature* **458**, 1185-1190 (2009)

P-41 Structural insights into a pyridoxal 5'-phosphate-dependent fold-type Ⅰ racemase, α-amino-ε-caprolactam racemase from *Achromobacter obae*

Seiji Okazaki[a,b], Atsuo Suzuki[a], Koji Suzuki[a], Hidenobu Komeda[c], Yasuhisa Asano[c], Takashi Yamane *[a]

[a]*Department of Biotechnology, Graduate School of Engineering, Nagoya University, Nagoya 464-8603, Japan (yamane@nubio.nagoya-u.ac.jp)*

[b]*Present address: Structural Biology Research Center, Photon Factory, Institute of Materials Structure Science, High Energy Accelerator Research Organization (KEK), Tsukuba 305-0801, Japan (okazakis@post.kek.jp)*

[c]*Department of Biotechnology, Faculty of Engineering, Toyama Prefectural University, Toyama 939-0398, Japan (asano@pu-toyama.ac.jp)*

α-Amino-ε-caprolactam (ACL) racemase (ACLR, EC 5.1.1.15) is a 51 kDa enzyme that catalyzes the interconversion of L- and D-ACL. Recently, amino acid amide racemizing activity was found in ACLR [1], and the combined method of ACLR with D-stereospecific amino acid amidase has been developed for D-amino acid production from D, L-amino acid amide [2]. To clarify the structure-function relationships of ACLR, the crystal structures of the native and ε-caprolactam complex of ACLR were determined at 2.3 and 2.4 Å resolutions, respectively [3]. This is the first structural report of racemase which belongs to fold-type Ⅰ.

The structure of ACLR is composed of three segments; (1) an N-terminal segment (residues 1 to 43), (2) a large, pyridoxal phosphate (PLP) binding domain (residues 44 to 319) and (3) a C-terminal domain (residues 320 to 436). The C4' in PLP covalently bonded to the ε-amino group of Lys267 forming the internal aldimine. The substrate-binding site is assigned between Trp49 and Tyr137 by the location of ε-caprolactam in the complex structure. For identifying the catalytically important residues, the energy-minimized model of the L-ACL-PLP external aldimine intermediate was produced. The carboxyl group of Asp210 is a reasonable candidate that recognizes the nitrogen atom of lactam or amide in the substrate. From structural comparison with fold-typeⅢ alanine racemase, Tyr137 of ACLR plausibly plays as acid/base catalytic residue which is essential for two-base mechanism in racemization.

References

1. Asano, Y. & Yamaguchi, S. (2005). *J. Mol. Catal. B. Enzym.* **36**, 22-29.
2. Asano, Y. & Yamaguchi, S. (2005). *J. Am. Chem. Soc.* **127**, 7696-7697.
3. Okazaki, S., Suzuki, A., Mizushima, T., Kawano, T., Komeda, H., Asano, Y. and Yamane, T. (2009). *Biochemistry* **48**, 941-950.

P-42 Fluorescence-Based Screening for Soluble Human Proteins by POET in Baculovirus-infected Insect Cells for Structural Studies

Songying Ouyang, Zhijie Liu

Institute of Biophysics, Chinese, 15 Datun Road, Chaoyang District, Beijing, 100101, China (ouyangsy@moon.ibp.ac.cn)

Production of structure-grade soluble proteins in substantial quantities takes a critical role in protein structure research. Unfortunately, this has been impeded because a variety of proteins

were found insoluble, unstable or can not be purified in bacterial expression system. Baculovirus expression vector system is a eukaryotic expression system and thus uses many of the protein modification, processing, and transport systems present in higher eukaryotic cells and usually provide very high levels of foreign gene production. The baculovirus/insect cell expression system is a very attractive and powerful tool for the production of heterogeneous gene products, especially expression of recombinant eukaryotic proteins. This article describes an improved pooled open reading frame (ORF) expression technology (POET) that uses recombinational cloning and Liquid Chromatography Tandem mass spectrometry (LC/MS) to identify proteins that yield high levels of soluble, purified protein expressed in insect cells. Twenty-two human gene ORFs/fragments were subcloned into baculovirus expression vector and positive recombinant bacmids were constructed, purified, and transfected into Sf9 insect cells. After bulk expression and purification, 2 proteins were identified as soluble protein with higher expression level. By using this improved POET method described here allows the expression characteristics of proteins to be quickly determined in only once experiment in baculovirus expression system.

Keywords: POET; baculovirus; soluble protein

P-43

Crystal Structure of the Periplasmic Region of MacB, a Noncanonic ABC Transporter

Sun-Hee Park, § Yongbin Xu,§ Se-Hoon Sim,# Ki Hyun Nam,^ Xiao Ling Jin,§ Hong-Man Kim,# Kwang Yeon Hwang,^ Kangseok Lee,# and Nam-Chul Ha

§College of Pharmacy and Research Institute for Drug Development, Pusan National University, Busan 609-735, Republic of Korea,
#Department of Life Science, Chung-Ang University, Seoul 156-756, Republic of Korea, and ^Division of Biotechnology and Genetic
Engineering, College of Life and Environmental Sciences, Korea University, Seoul 136-791, Republic of Korea

MacB is a noncanonic ABC-type transporter within Gram-negative bacteria, which is responsible both for the efflux of macrolide antibiotics and for the secretion of heat-stable enterotoxin II.

In Escherichia coli, MacB requires the membrane fusion protein MacA and the multifunctional outer membrane channel TolC to pump substrates to the external medium.

Sequence analysis of MacB suggested that MacB has a relatively large periplasmic region.

To gain insight into how MacB assembles with MacA and TolC, we determined the crystal structure of the periplasmic region of Actinobacillus actinomycetemcomitans MacB.

Fold matching program reveals that parts of the MacB periplasmic region have structural motifs in common with the RND-type transporter AcrB.

Since it behaved as a monomer in solution, our finding is consistent with the dimeric nature of full-length MacB, providing an insight into the assembly in the tripartite efflux pump.

P-44 Structure of an eIF4A - PDCD4 complex provides insight into the inhibition of translation

Young Bong Park, Jihye Lee, Jeong Ho Chang and Yunje Cho
National Creative Initiatives for Structural Biology and Department of Life Science, Pohang University of Science and Technology, Hyo-ja dong, San31, Pohang, KyungBook, South Korea (yunje@postech.ac.kr)

Tumor suppressor programmed cell death protein 4 (PDCD4) inhibits the translation initiation factor eIF4A, an RNA helicase that catalyzes the unwinding of secondary structure at the 5' untranslated region (5' UTR) of mRNAs, and controls the initiation of translation. Here we determined the crystal structure of the human eIF4A and PDCD4 complex. The structure reveals that one molecule of PDCD4 binds to the two eIF4A molecules through the two different binding modes. While the two MA3 domains of PDCD4 bind to one eIF4A molecule, only the C-terminal MA3 (cMA3) domain of the same PDCD4 interacts with another eIF4A molecule. The eIF4A-PDCD4 complex structure suggests that the MA3 domain(s) of PDCD4 binds perpendicular to the interface of the two domains of eIF4A, preventing the domain closure of eIF4A and blocking the binding of RNA to eIF4A, both of which are required events in the function of eIF4A helicase. The structure, together with biochemical analyses, reveals insights into the inhibition mechanism of eIF4A by PDCD4, and provides a framework for designing chemicals that target eIF4A.

P-45 Crystal Structure of Bacterial Lysozyme Inhibitor MliC, Complexed with c-type Lysozyme

Shunfu Piao, Soohwan Yum and Nam-Chul Ha
College of Pharmacy and Research Institute for Drug Development, Pusan National University, Room #311, Pharmacy Building, Jangjeon-dong Geumjeong-gu, Busan 609-735, Republic of Korea (hnc@pusan.ac.kr)

Lysozymes are an important component of the innate immune system of animals that hydrolyze peptidoglycan, the major bacterial cell wall constituent. Many bacteria have contrived various means of dealing with this bactericidal enzyme, one of which is to produce lysozyme inhibitors. Recently, a novel family of bacterial lysozyme inhibitors was identified in various Gram-negative bacteria, named MliC (membrane bound lysozyme inhibitor of C-type lysozyme). Here, we report the crystal structure of *Pseudomonas aeruginosa* MliC in complex with chicken egg white lysozyme. Combined with mutational study, the complex structure demonstrates that the invariant loop of MliC plays a crucial role in the inhibition of the lysozyme by its insertion to the active site cleft of the lysozyme, where the loop forms hydrogen and ionic bonds with the catalytic residues. Since MliC family members have been implicated as putative colonization or virulence factors, the structures and mechanism of action of MliC will be of relevance to the control of bacterial growth in animal hosts.

P-46 Structural Basis of Transport of Lysophospholipids by Human Serum Albumin

Shihui Guo[1,2], Xiaoli Shi[1,2], Mingdong Huang[1,2]
1. State Key Laboratory of Structural Chemistry, Fujian Institute of Research on the Structure of Matter, The Chinese Academy of Sciences, 155 Yang Qiao Xi Lu, Fuzhou, Fujian, 350002, China (sxl_sharly@fjirsm.ac.cn)
2. Graduate School of Chinese Academy of Sciences, The Chinese Academy of Sciences, Beijing 10039, China

Lysophospholipids play important roles in cellular signal transduction, and are implicated in many biological processes, including tumorigenesis, angiogenesis, immunity, atherosclerosis, arteriosclerosis, cancer, and neuronal survival. The intracellular transport of lysophospholipids is through fatty acid binding protein. Lysophospholipids are also found in extra cellular space. However, the transport mechanism of lysophospholipids in extracellular space is unknown. Human serum albumin (HSA) is the most abundant carrier protein in blood plasma and plays important role in determining the absorption, distribution, metabolism, and excretion of drugs. In this study, lysophosphatidylethanolamine (LPE) was used as the ligand for analysis of the interaction of lysophospholipids with HSA by fluorescence quenching and crystallography. Fluorescence measurement showed that LPE binds to HSA with a dissociation constant (Kd) of 5.6 μM. The presence of fatty acid (myristate) reduces this binding affinity (Kd of 12.9 μM). Despite the relatively large size of this lysophospholipid, the binding affinity between LPE and HSA is comparable to that of fatty acid. Moreover, we determined the crystal structure of HSA in complex with both a fatty acid (myristate) and LPE, and showed that LPE binds at Sudlow site1 located in subdomain IIA. LPE occupies two of three subsites in Sudlow site 1 with the LPE acyl chain occupying the hydrophobic bottom of Sudlow site 1 and the polar head group located at Sudlow site 1 entrance region pointing to solvent. This orientation of LPE in HSA suggests HSA is capable to accommodate other lysophospholipids and phospholipids. This study provides structural information on HSA-lysophospholipids interaction and may facilitate the understanding of the transport and distribution of lysophospholipids.

P-47 Inactivation of Nucleoside Diphosphate Kinase-A through a Conformational Change of the C-terminal Loop Induced by Oxidation

Mi-Sun Kim, Dong-Hae Shin
Department of Pharmacy, Division of Life and Pharmaceutical Sciences, Ewha Womans University, Seoul, Korea 120-750 (dhshin55@ewha.ac.kr)

Nucleoside diphosphate kinase (NDK) catalyzes the transfer of the γ-phosphoryl group from a nucleoside triphosphate (NTP) to a nucleoside diphosphate (NDP) by using ATP as a major phosphate donor through a conserved histidine residue. NDP kinases play a primary role not only in maintaining cellular pools of all NTPs but also in the regulation of important cellular processes. NDK-A (NM23-H1) acts as a metastasis suppressor for some tumor types. The oxidation of NDK-A with 5 mM H_2O_2 for 1 hour nullify enzyme activity. We present here the crystal structure of oxidized human NDK-A determined at 2.8 Å resolution. The crystals

belong to the cubic space group $P2_13$ with cell parameters a = b = c = 106.77 Å and the asymmetric unit contains a dimer. The overall structure is a hexamer, which can be viewed as a trimer of three dimers in this oxidation form. In the native form, Cys145 locates on the equatorial surface of the hexamer and is close to a neighboring Cys145 from another subunit. However in the oxidation form, Cys145 makes a disulfide bridge with Cys4. This disulfide bridge induces a large conformational change of C-terminal domain, which may result in inactivation of NDK-A. Here we also describe the enzyme activation and inactivation mechanism based on the crystal structures.

P-48 Crystal Structure of *Stenotrophomonas maltophilia* FeoA complexed with Zinc: A Unique Procaryotic SH3 Domain-like Protein Possibly Acts as a Bacterial Ferrous Iron Transport Activating Factor

Yi-Che Su[1], Ko-Hsin Chin[1], Andrew H.-J. Wang[2] & Shan-Ho Chou[1, 3]
[1] *Institute of Biochemistry, National Chung-Hsing University, Taichung, 40227, Taiwan*
[2] *Institute of Biological Chemistry, Academia Sinica, Nankang, Taipei, Taiwan*
[3] *National Chung Hsing University Biotechnology Center, Taichung, 40227, Taiwan, (shchou@nchu.edu.tw)*

Iron is vital to the majority of prokaryotes, which, have therefore developed a variety of iron transport pathways to compete with the host for their iron supplies. The most common pathways employed by bacteria appear to be those that transport ferric complexes, such as ferric-siderophores, ferric-transferrin, ferric-citrate etc. However, ferrous iron is believed to be the preferred form for iron uptake due to its much better solubility (0.1 M for Fe^{2+} vs. 10^{-18} M for Fe^{3+} at pH 7). Interestingly, the major route for bacterial ferrous iron uptake was found to be via a Feo (*Fe*rro*u*s iron transport) system that differs considerably from the ferric iron transport systems. Surprisingly, relatively little research was done on this important and novel system. Nevertheless, the Feo system is now known to comprise three genes, which likely form an operon of *feo*ABC: FeoA is a small protein of approximately 75 residues with unknown function; FeoB is a large protein of 773 residues with an integral membrane domain and is likely to act as a ferrous permease; and FeoC is another small protein containing a Fe-S cluster and possibly serves as a transcriptional regulator for the *feo*ABC operon.

Stenotrophomonas maltophilia (Sm) has emerged as an important opportunistic pathogen in the immunodepressed hosts. Recently, it has been described as a "superbug" that can resist any antibiotics, which has caused tremendous difficulty in treating its infections. However, structural study of proteins encoded by this bacterium is still scarce. Here we report the tertiary structure of *Sm*FeoA determined to a resolution of 1.7 Å from a Selenium-Methionine single-wavelength anomalous dispersion (Se-SAD) approach. It bears weak similarity to the C-terminal SH3 domain of bacterial DtxR (diphtheria toxin regulator protein) and Iron-dependent regulator (IdeR). Although no clear sequence identity with eukaryotic SH3-domain proteins can be found, the final structure of *Sm*FeoA is indeed found to adopt a SH3-domain fold similar to those of the eukaryotic proteins. Since eukaryotic SH3-domain is well known for its capability to mediate protein-protein interactions, this has led to the suggestion that FeoA may interact with FeoB to regulate the FeoB-dependent ferrous iron

uptake activity. In the current *Sm*FeoA, it was found to adopt a unique dimer cross-linked by two zinc ions coordinated by an aspartate residue, a histidine residue, and two chloride ions. Since FeoB was found to contain a G-protein like domain, there is thus a possibility that FeoA may interact with FeoB through the G-protein/SH3 domain interaction, with FeoA possibly acting as a ferrous ion transport activating factor.

P-49 Single-stranded DNA-binding protein complex from *Helicobacter pylori* suggests an ssDNA-binding surface

Yuh-Ju Sun and Kun-Wei Chan
Institute of Bioinformatics and Structural Biology and [2]Institute of Biotechnology National Tsing Hua University, Hsinchu 300, Taiwan (yjsun@life.nthu.edu.tw)

Single-stranded DNA-binding protein (SSB) plays an important role in DNA replication, recombination, and repair. SSB consists of an N-terminal single-stranded DNA-binding domain with an oligonucleotide/oligosaccharide binding fold and a flexible C-terminal tail involved in protein-protein interactions. SSB from *Helicobacter pylori* (*Hp*SSB) was isolated, and the ssDNA-binding characteristics of *Hp*SSB were analyzed by fluorescence titration and electrophoretic mobility shift assay. Tryptophan fluorescence quenching was measured as 61%, and the calculated cooperative affinity was 5.4×10^7 M^{-1} with an ssDNA binding length of 25-30 nucleotides. The crystal structure of the C-terminally truncated protein (*Hp*SSBc) in complex with 35-mer single-stranded DNA [*Hp*SSBc-$(dT)_{35}$] was determined at a resolution of 2.3 Å. The *Hp*SSBc monomer folds as an OB-fold with a Y-shaped conformation. The ssDNA wrapped around the *Hp*SSBc tetramer through a continuous binding path comprising five essential aromatic residues and a positively charged surface formed by numerous basic residues.

P-50 A novel pharmaceutical protein, crystal structures of an anti-HIV actinohivin from an actinomycete, and its complex with mannobiose

Masaru Tsunoda[1], Kaoru Suzuki[1], Tsubasa Sagara[1], Atsushi Takahashi[1], Junji Inokoshi[2], Satoshi Omura[2], Takeshi Sekiguchi[1], Haruo Tanaka[1] and Akio Takénaka[1]
[1] *Iwaki-Meisei University, 5-5-1 Chuodai-Iino, Iwaki, 970-8551, Japan (atakenak@iwakimu.ac.jp)*
[2] *Kitasato University, 5-9-1 Shirokane, Minato-ku, Tokyo, 108-8641, Japan*

Actionohivin (AH) has been isolated as a lectin from actinomycete *Longispora albida* K97-0003T [1]. This protein inhibits HIV viral entry to human susceptive cells. As compared with cyanovirin-N, AH binds more specifically to the high mannose-type saccharide chains (HMTG) of HIV gp120 protein. AH is a small protein of 114 amino acid residues, being arranged in a unique sequence repeated by three times tandemly. To reveal the structure of the specific binding, X-ray analyses of the apo-form and its complex with mannobiose Man1-α(1-2)-Man2 have been performed at 0.90 and 1.80 Å resolutions, respectively. In the apo-form crystal, the protein structure is composed of the three modules similar to each other,

as speculated from the tandem repeats in the sequence. Each module consists of a β-sheet of four β-strands, a long loop and a π-helix. The three modules are associated with a pseudo three-fold symmetry, in which the three β-sheets form a triangular barrel. Inside of the barrel, hydrophobic residues form a stable core. On the outer surface, a long loop with a π-helix in each module is running from the top to the bottom of the barrel. This loop and the preceding two β-strands containing the carbohydrate-binding motifs LD-QXW form a valley with a pocket for carbohydrate-binding. In the three sites of the complex-form, three mannobioses are bound, respectively. In the first pocket of the module 1, the carboxyl group of Asp15 bridges between the two hydroxyl groups (OH3 and OH4) attached to the C3 and C4 atoms of Man2, through hydrogen bonds. At the same time, OH3 forms another hydrogen bond with the amide group of Asn28 and OH4 forms another hydrogen bond with the hydroxyl group of Tyr23. In addition, the mannose ring of Man2 is sandwiched between Leu25 and Tyr32 by hydrophobic interactions. To stabilize the pocket formation, Gln33 forms double hydrogen bonds with the main chain amide group at Asn28 and the carbonyl group at Ala27. In the second and the third pockets, the mannobioses are also bound in the similar ways. The structural features are completely consistent to the results of mutation experiments of these amino acid residues. The Man1 group which is largely bent by the α(1-2) bond is protruded into the solvent region. In this pocket, the mannobiose end of D1 branch of HMTG could be accommodated in a way similar to the geometry described above, and the end of D2 or D3 branch might contact with a valley. Therefore, it is possible to speculate that each pocket accepts the D1 and D2/D3 branches of HMTG. The three pockets are located to form an almost regular triangle at a distance of 17 Å between the pockets. This separation might be possible to accept three HMTGs on a gp120 at the same time.

Reference

Tanaka H, Chiba H, Inokoshi J, Kuno A, Sugai T, Takahashi A, Ito Y, Tsunoda M, Suzuki K, Sekiguchi T, Takenaka A, Umeyama H, Hirabayashi J, Omura S (2009) Action mechanism of the highly specific and potent anti-HIV property of actinohivin, a microbial lectin with three sugar-binding pockets. *PNAS* **106**, in press.

P-51

The SARS-unique domain of SARS-CoV contains two macrodomains that bind G-quadruplexes

Jinzhi Tan[1], Clemens Vonrhein[2], Oliver S. Smart[2], Gerard Bricogne[2], Michela Bollati[1,4], Yuri Kusov[1], Guido Hansen[1], Jeroen R. Mesters[1], Christian L. Schmidt[1], Rolf Hilgenfeld[1,3]

[1]*Institute of Biochemistry, Center for Structural and Cell Biology in Medicine, University of Lübeck, Germany, (jztan@biochem.uni-luebeck.de)*

[2]*Global Phasing Ltd., Cambridge, UK, (gb10@globalphasing.com)*

[3]*Laboratory for Structural Biology of Infection and Inflammation, c/o DESY, Hamburg, Germany, (Hilgenfeld@biochem.uni-luebeck.de)*

[4]*on leave from Dept. of Biomolecular Sciences & Biotechnology, University of Milan, Via Celoria, 26, 20133 Milano, Italy (michela.bollati@unimi.it)*

The SARS coronavirus (SARS-CoV) is much more pathogenic for humans than any other coronavirus. Therefore, protein domains encoded by the SARS-CoV genome that are absent in other coronaviruses are of particular interest, because they may be responsible for the extraordinary virulence. The most prominent such domain has been identified by

bioinformatics as part of non-structural protein 3 (Nsp3) of the virus and appropriately named the "SARS-unique domain" (SUD) [1]. Through the efforts of several laboratories around the world, the structures of a number of non-structural proteins of the SARS coronavirus replicase/transcriptase complex have been determined. However, the SUD has escaped all attempts at crystallizing it because of its instability.

After construction of many fragments, we have managed to obtain the core of the SUD in a crystalline form, and determined its X-ray structures at 2.2 and 2.8 Å resolution, respectively. This revealed that SUD_{core} contains two copies of the so-called macrodomain. Furthermore, we have shown that each of these, as well as the entire SUD_{core} and full-length SUD, specifically bind to G-quadruplexes, both in the DNA and RNA form [2,3]. G-quadruplexes occur in the 3'-nontranslated regions of mRNAs coding for several host-cell proteins involved in apoptosis or signal transduction. By mutational studies, we could show that replacement of pairs of lysine residues on the C-terminal subdomain of SUD_{core} abolished binding of G-quadruplexes completely.

There is also a link to poly(ADP-ribose) polymerase (PARPs), as the structure of the SUD subdomains show some distant similarity to the catalytic domain of these enzymes, and other macrodomains have been shown to bind ADP-ribose (whereas SUD does not). Further, PARP-1 also binds G-quadruplexes and PARP domains exist in the antiviral protein ZAP, which is active against viruses containing a macrodomain (e.g. alphaviruses and coronaviruses). We speculate that SARS-CoV could inactivate ZAP by competing with it for G-quadruplex regions in RNA, suggesting a way for the SARS virus to fight the innate immune system of the host cell.

References

1. Snijder E.J., Bredenbeek P.J., Dobbe J.C., Thiel V., Ziebuhr J., Poon L.L.M, Guan Y., Rozanov M., Spaan W.J.M., Gorbalenya A.E. *J. Mol. Biol.*, **331,** 991-1004 (2003).
2. Tan J., Kusov Y., Mutschall D., Tech S., Nagarajan K., Hilgenfeld R., Schmidt C.L. *Biochem. Biophys. Res. Commun.* **364**, 877-882 (2007).
3. Tan J., Vonrhein C., Smart O.S., Bricogne G., Bollati M., Kusov Y., Hansen G., Mesters J.R., Schmidt C.L., Hilgenfeld R. *PLoS Path.*, **5**, e1000428 (2009).

P-52

A crystallographic study of $Tic110_C$ protein from *Cyanidioschyzon merolae*

Jia-Yin Tsai and Chwan-Den Hsiao
[1] *Institute of Molecular Biology, Academia Sinica. 128 Sec. 2, Academia Rd, Nankang, Taipei 115, Taiwan, (jytsai@imb.sinica.edu.tw)*

Tic110 (translocan of the inner envelope membrane) is an intergral membrane protein containing a short N-terminal membrane anchor and a hydrophilic region (~98 kDa) that extends into the plastid stroma. Here, the crystallization and preliminary analysis of the C-terminal domain (659-1007) of Tic110 protein hydrophilic region from *Cyanidioschyzon merolae* Tic110 ($cmTic110_C$) are reported. The $cmTic110_C$ has been crystallized at 293 K using PEG 400 as precipitant. The crystal structure has been determined by x-ray MAD method. These crystals belong to the hexagonal space group $P6_522$, with unit-cell parameters

a = b = 122.7, c = 243.2 Å. A 99.8% complete native data set from a frozen crystal has been collected to 3.7 Å at 100 K with an overall Rmerge of 6.0%.

P-53 Crystal structure of the human FOXO3a-DBD/DNA complex suggests the effects of post-translational modification

Kuang-Lei Tsai[1,2], Yuh-Ju Sun[2], Cheng-Yang Huang[1], Jer-Yen Yang[3], Mien-Chie Hung[3] and Chwan-Deng Hsiao[1,*]
[1]*Institute of Molecular Biology, Academia Sinica, Taipei, 115, Taiwan (d948243@oz.nthu.edu.tw)*
[2]*Institute of Bioinformatics and Structural Biology, National Tsing Hua University, Hsinchu, 300, Taiwan*
[3]*Deaprtment of Molecular and Cellular Oncology, The University of Texas M. D. Anderson Cancer Center, Houston, Texas 77030, USA*

FOXO3a is a transcription factor of the FOXO family. The FOXO proteins participate in multiple signaling pathways, and their transcriptional activity is regulated by several post-translational mechanisms, including phosphorylation, acetylation, and ubiquitination. Because these post-translational modification sites are located within the C-terminal basic region of the FOXO DNA-binding domain, it is possible that these post-translational modifications could alter the DNA-binding characteristics. To understand how FOXO-mediated transcriptional activity, we report here the 2.7 Å crystal structure of the DNA-binding domain of FOXO3a (FOXO3a-DBD) bound to a 13-bp DNA duplex containing a FOXO consensus binding sequence (GTAAACA). Based on a unique structural feature in the C-terminal region and results from biochemical and mutational studies, our studies may explain how FOXO-DBD C-terminal phosphorylation by protein kinase B (PKB) or acetylation by cAMP-response element binding protein (CBP) can attenuate the DNA-binding activity and thereby reduce transcriptional activity of FOXO proteins. In addition, we demonstrate that the methyl groups of specific thymine bases within the consensus sequence are important for FOXO3a-DBD recognition of the consensus binding site.

References

1. FoxOs at the crossroads of cellular metabolism, differentiation, and transformation. Cell (2004) 117:421–426.
2. Crystal structure of the human FOXK1a–DNA complex and its implications on the diverse binding specificity of winged helix/forkhead proteins. J. Biol. Chem. (2006) 281:17400–17409.

P-54 Novel crystal structure of *Helicobacter pylori* neutrophil-activating protein (HP-NAP)

Osamu Tsuruta, Naoya Akao, Hideshi Yokoyama, Satoshi Fujii
University of Shizuoka , 52-1 Yada, Suruga-ku, Shizuoka-shi, Shizuoka-ken, 422-8526, Japan (d09205@mail.u-shizuoka-ken.ac.jp)

Background *Helicobacter pylori* is a pathogen associated with gastric diseases, including gastric ulcers and stomach cancers. *Helicobacter pylori* neutrophil-activating protein (HP-NAP) is a major 17 kDa antigen of *H. pylori*. This protein activates neutrophils and

produces reactive oxygen species. Thus, it is thought that HP-NAP is a cause of gastric cancer. HP-NAP is a ferritin-like iron storage protein. Crystal structure of HP-NAP was solved in 2002 at 2.5 Å resolution (Giuseppe Zanotti *et al.*)[1]. According to the study, HP-NAP forms a hollow spherical dodecamer and contains 12 ferric ion binding sites in the dodecamer. In order to understand the mechanism of iron uptake and elimination, we have determined the novel crystal structure of HP-NAP. We obtained the metal-free crystal with different amino-acid sequence. Moreover, because a new crystal is high symmetry and a high resolution, several structural bases of the accumulation of the metal will be able to be elucidated by the comparison with Zanotti's structure.

Method HP-NAP was expressed as a His-tag fused protein and crystallized using the hanging drop vapor diffusion method at 20 °C. To prevent the protein from aggregation, 0.1 M L-arginine was used during the purification and crystallization. Crystals were grown against 500 μl of a reservoir solution containing 25% ethylene glycol. Crystallization drops were prepared by mixing 2 μl of 8.3 mg ml^{-1} of protein solution in 50 mM Tris-HCl (pH 8.8) and equal amount of the reservoir solution. A crystal (0.1 x 0.2 x 0.5 mm) was flash-frozen at -178 °C under a nitrogen-gas stream with the cryoprotectant solution containing 50% ethylene glycol. X-ray diffraction data were collected at beam-line BL5A of the Photon Factory in Japan. Diffraction data integration, scaling, and merging were performed using HKL2000. Structure determination and refinement were performed by the molecular replacement method using MOLREP and REFMAC in the CCP4 package. Zanotti's structure was used as a search model. Modeling was carried out with COOT.

Results and Discussion We determined the structure of HP-NAP at 2.2 Å resolution higher than that of the Zanotti's one. The space group of our crystal was *F*432 and that of Zanotti's one is $P2_1$. Thus, we have obtained the crystal that has higher symmetry and gives higher resolution data. Additionally, our crystal has a high water content of 65.9% and does not contain iron atom. By the comparison with Zanotti's structure, several new evidences including the big structural changes of three amino-acid residues by the metal coordination were obtained (His37, Asp52 and Glu56). There were two different pores formed at 3-fold rotational axes and metal ions may pass through each of them. To understand the iron uptake and elimination mechanisms, more structural information such as mobility and charge distribution will be elucidated. Due to its high water content, the new crystal is also suitable for soaking experiment.

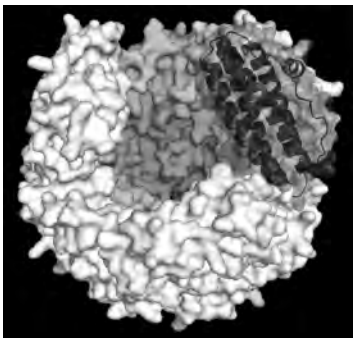

Structure of the HP-NAP dodecamer. It forms a sphere of 90 Å in diameter and has a large hollow space of 50 Å in diameter. Its inner surface is negatively charged and thus HP-NAP is reported to accommodate up to 500 iron atoms per dodecamer. To show the hollow structure, top and front subunits are removed. One subunit is shown as a ribbon diagram and the others are shown as a surface representation view.

Reference

Giuseppe Zanotti, Elena Papinutto, William G. Dundon et al., Structure of the Neutrophil-activating Protein

from *Helicobacter pylori*, *J. Mol. Biol.*, **323**, 125-130 (2002).

P-55 Structural and function researches on human glutathione transferase kappa

Bing Wang, Yingjie Peng, Jianping Ding
Institute of Biochemistry and Cell Biology, Shanghai Institutes for Biological Sciences, Chinese Academy of Sciences, 320 Yue-Yang Road, Shanghai 200031, China (wangbing@sibs.ac.cn)

Glutathione transferases (GST) are a family of multifunctional proteins involved in the cellular detoxification of cytotoxic and genotoxic compound. The function of GST is to versatile and catalyze the nucleophilic addition of the thiol of reduced glutathione to a wide variety of hydrophobic electrophiles. GST kappa is a unique class of this family for its cellular localization and structure, which plays roles not only in detoxification but also in diabetes demonstrated recently.

We solved the structure of human GST kappa in apo form and the complex structure of *h*GSTk and its inhibitor S-Hexylglutathione (GTX) at high resolution. The complex structure of *h*GSTk and its inhibitor may imply some hints for anti-cancer drug design. Compared with the complex structure of *h*GSTk and GSF, the loop consisted of 52-62 residues changed its conformation and formed an α-helix to interact with GSH directly. This result could be confirmed by steady state kinetics parameters for *h*GSTk.

References

1. Morel, F., Rauch, C., Petit, E., Piton, A., Theret, N., Coles, B., and Guillouzo, A. (2004) Gene and protein characterization of the human glutathione S-transferase kappa and evidence for a peroxisomal localization. J Biol Chem. **279(16):**16246-53.
2. Jane E. Ladner, James F. Parsons, Chris L. Rife, Gary L. Gilliland, and Richard N. Armstrong. (2004) Parallel Evolutionary Pathways for Glutathione Transferases: Structure and Mechanism of the Mitochondrial Class Kappa Enzyme rGSTK1-1. Biochemistry. **43 (2)**: 352-361
3. Li, J., Xia, Z., and Ding, J. (2005) Thioredoxin-like domain of human k class glutathione transferase reveals sequence homology and structure similarity to the y class enzyme. Protein Science. **14**:2361–2369
4. Liu, M., Zhou, L., Xu, A., Lam, K.S., Wetzel, M.D., Xiang, R., Zhang, J., Xin, X., Dong, LQ., and Liu, F. (2008) A disulfide-bond A oxidoreductase-like protein (DsbA-L) regulates adiponectin multimerization. Proc Natl Acad Sci U S A. **105(47)**:18302-7.

P-56 HCV Membrane Protein Purification, Characterization and Crystallization

Liping Wang, Randy Bledsoe, William Burkhart, Annie Hassell, Robert Reid, Derek Parks, Warren Rocque, Michael Thomson, Shawn Williams
GlaxoSmithKline, 5 Moore Drive, RTP, NC 27709, USA (liping.8.wang@gsk.com)

Although almost half of drug discovery targets are membrane proteins, crystallography support on these projects is rare. Historically, the difficulty expressing, purifying active protein, and obtaining structures required a long time span that was incompatible with drug discovery. Because of the increasing number of membrane protein structures, including some

at high resolution, we started to explore the crystallization of a HCV membrane protein at GSK. The protein purification, biochemical and biophysical characterization and protein crystallization efforts will be described and discussed.

P-57 An Intramolecular Self-Activation Mechanism of Human Caspase-6

Xiao-Jun Wang[1], Xiang Liu[1], Kai-Tuo Wang[1], Wei Mi[1], Yan Zhang[2], Lan-Fen Li[1], Andrea C. LeBlanc[3], Xiao-Dong Su [1,4]
[1]*National Laboratory of Protein Engineering and Plant Genetic Engineering and*
[2]*College of Life Science, Peking University, Beijing 100871, People's Republic of China*
[3]*Department of Neurology and Neurosurgery, McGill University, Lady Davis Institute for Medical Research, 3755 Ch. Côte Ste-Catherine, Montreal, Quebec, Canada*
[4]*Peking University Shenzhen Graduate School, Shenzhen 518055, People's Republic of China*

Caspases represent a family of cysteinyl proteases involved in inflammation and apoptosis. The short pro-domain effector Caspase-6 (Casp6) is activated early in cognitive impairment and in Alzheimer disease (AD), and is associated with neurodegeneration and axonal pruning. To understand the mechanism of Casp6 activation, we have determined the crystal structures of catalytically inactive Casp6 lacking its pro-domain (Δpro-Casp6C163A) and Ac-VEID-CHO inhibited active Casp6. The Δpro-Casp6C163A structure shows unexpectedly that the intersubunit linker cleavage site ^{190}TEVD^{193} fits well into the active site as a β strand, and the D193 is positioned readily to be attacked by the nucleophile C163. We have confirmed biochemically that this intra-molecule-cleavage is a prerequisite condition for casp6 self activation and further demonstrated that this unique intramolecular cleavage is dependent on the length of the L2 loop since deletion of only 4 amino acid residues from the linker or substitution of the Casp6 linker by the shorter Casp3 linker is sufficient to abolish self-cleavage. These results show that unlike other effector caspases, which are activated through exo-caspase proteolytic processing, Casp6 can activate by intramolecular self-cleavage.

P-58 Redesign of a non-specific endonuclease to yield better DNA-binding activity and altered DNA sequence cleavage preference

Yi-Ting Wang[1,2,3], Jon D. Wright[4], Lyudmila G. Doudeva[1], Hua-Ci Jhang[1], Carmay Lim[4] and Hanna S. Yuan[1,2]
[1] *Institute of Molecular Biology, Academia Sinica, Taipei, Taiwan*
2 Institute of Chemical Biology and Molecular Biophysics, Taiwan International Graduate Program, Academia Sinica
3 Institute of Bioinformatics and Structural Biology, National Tsing Hua University
4 Institute of Biomedical Sciences, Academia Sinica, Taipei, Taiwan

It is of crucial importance to elucidate the underlying principles that govern the binding affinity and selectivity between proteins and DNA. Here we use the nuclease domain of Colicin E7 (nColE7) as a model system to generate redesigned nucleases with improved DNA-binding affinities and altered sequence cleavage preferences. ColE7 is an *Escherichia*

coli toxin, bearing a nonspecific endonuclease domain with a preference for hydrolyzing DNA phosphodiester bonds at the 3' O-side after thymine.

Using systematic computational screening, six nColE7 mutants were predicted to fold and bind DNA. Fluorescence kinetic assays confirmed that all of the six designed mutants were well-folded active enzymes, and three of the six mutants, D493N, D493Q and K497R, had 3 to 5-fold higher DNA binding affinity than wild-type nColE7. Footprint assays further showed that D493N and D493Q digested DNA with an increased preference for guanine at -1 and +3 sites, as compared to the wild-type enzyme. To elucidate the observed higher DNA-binding affinity and altered sequence preference in cleavage, the crystal structure of the nColE7 mutant, D493Q, in complex with an 18-bp DNA was determined, and free energy decomposition calculations were performed. In summary, these results show that a combination of crystal structural analysis and computational screening is a useful means for generating redesigned nucleases with higher DNA-binding affinities and altered sequence preferences in DNA cleavage.

P-59 Trapping of Silica Nanoparticles at the Air-Water Interface by Proteins

Joo Chuan Ang, Jhih-Min Lin, Peter N. Yaron and John W. White*
Research School of Chemistry, Australian National University, Canberra 0200, Australia

We have observed the formation of protein-nanoparticle complexes at the air-water interface from three different methods of presenting the nanoparticles to proteins. The structures formed resemble the "protein-nanoparticle corona" proposed by Lynch et al.[1,2] in relation to a possible route for nanoparticle entry into living cells. To do this the methods of X-ray and neutron reflectivity (with isotopic contrast variation between the protein and nanoparticles) have been used to study the structures formed at the air-water interface of β casein presented to silica nanoparticle dispersions. Whilst the silica dispersions showed no observable reflectivity, strong signals appear in the reflectivity when protein is present. Drop-wise spreading of a small amount of protein at the air-silica sol interface and presentation of the silica sol to an isolated monomolecular protein film (made by the "flow-trough"[3] method) give an immediate signal. Mixing the components in solution only produces a slow response but in all cases a similar structure is formed. The different responses are interpreted in structural and stoichiometric ways.

References

1. Lynch, I et al. The nanoparticle-protein complex as a biological entity: a complex fluids and surface challenge for the 21st century. *Adv in Colloid and Interface Science* 2007, 134-135, 167-174
2. Adam W. Perriman, Duncan J. McGillivray and John W. White. Reactions of Isolated Mono-Molecular Protein Films. *Soft Matter, 2008, 4, 2192 - 2198*
3. John. W. White*, Adam. W. Perriman, Duncan. J. McGillivray and Jin-Minh Lin -Protein Interfacial Structure and Nanotoxicology, *Nuclear Instruments and Methods in Physics Research* A600 (2009) 263-265
4. ntegrated Research into the nanoparticle- protein corona: a new focus for safe, sustainable and equitable development of nanomedicines T.A.Faunce, J.W.White and K. Matthaei , Nanomedicine (2008), 3(6) 859-866

5. Perriman, A. W., Henderson, M. J., Holt, S. A., White, J. W. – Effect of the Air–Water Interface on the Stability of beta–Lactoglobulin. *The Journal of Physical Chemistry. B* (2007), 111(48): pp. 13527–37.

P-60 Crystal structure of *Helicobacter pylori* urease accessory protein ureF

Yu Hang Fong[1], Yu Wai Chen[2], Kam Bo Wong[1]
[1]*Department of Biochemistry, The Chinese University of Hong Kong, Shatin, Hong Kong.(kbwong@cuhk.edu.hk)*
[2]*Randall Division of Cell and Molecular Biophysics, King's College London, London WC2R 2LS, United Kingdom. (yu-wai.chen@kcl.ac.uk)*

Urease is a nickel containing metalloenzyme that catalyses the conversion of urea into ammonia and carbon dioxide. Its activity is thought to be essential for the survival of *Helicobacter pylori* in the acidic environment in the stomach of the human host. UreF is one of the molecular chaperons involved in metallocenter assembly and activation of urease. Various roles have been proposed for ureF in the urease activation process. However, the exact function of ureF remained elusive. In our effort to elucidate the mechanism of urease activation, we have determined the crystal structure of ureF in *H. pylori.* Crystals of ureF were grown overnight in 24-28% PEG MME 5000 and 0.1M Bis-Tris pH 7.0. Diffraction data were collected on beamline I-04 at the Diamond Light Source. Crystal structure was phased with MAD and solved using PHENIX AutoSol to 2.0?. It was then followed by iterative cycles of model building and refinement with PHENIX.refine. The final crystal structure has a R_{free} of 0.232 and R_{work} of 0.191. Analysis of the crystal structure revealed that it belongs to C2 space group, with 3 asymmetric units per unit cell and cell dimenions of a = 135.16, b = 89.04, c =65.99. Our model of ureF consists of residue 25 to 233, forming a total of 9 alpha helices. UreF exists as a dimer in the crystal structure with a buried surface area of ~1600A, which corresponds to roughly 15% of the total surface area. Based on the structure, potential functional implications of ureF were discussed.

P-61 Structural and function researches on two α-isopropylmalate synthases from *Leptospira biflexa*, key enzymes in leucine biosynthesis

Jian Wu[1], Zilong Zhang[2], Wei Lin[2], Jun Ma[2], Peng Zhang[1], Guoping Zhao[2], Jianping Ding[1]
[1] *Institute of Biochemistry and Cell Biology, Shanghai Institutes for Biological Sciences, Chinese Academy of Sciences, 320 Yue-Yang Road, Shanghai 200031, China (wujian@sibs.ac.cn)*
[2] *Institute of Plant Physiology and Ecology, Shanghai Institutes for Biological Sciences, Chinese Academy of Sciences, 300 Feng-Lin Road, Shanghai 200032, China*

Leptospirosis, a spirochetal zoonosis and mainly caused by Leptospira interrogans, is a globally re-emerging infectious disease that has disseminated from its habitual rural base to become the cause of urban epidemics in poor communities of industrialized and developing nations. Leptospirosis has been recognized as a notifiable infectious disease in China since 1955. The trend of this disease has been steady for recent years but outbreaks occasionally occurred, especially in several southern provinces of China and potential risk factors may

exist in these areas. Similar with other micro-organisms, Leptospira biflexa, highly homologous to pathogenic L. interrogans, employs an IPM pathway to synthesize leucine and LbIPMSs (L. biflexa α-isopropylmalate synthases) catalyze the pivotal reaction of this pathway, which converts α-kiv (α-ketoisovalerate) and acetyl-CoA into α-ipm (α-isopropylmalate), thus making it an attractive target for the development of antibacterial agents. Two IPMS genes are expressed in Leptospira, one product is IPMS1 composed of catalytic-, sub1-, sub2-, and regulatory domains, and the other is IPMS2 containing the three former domains. We report here the crystal structure of the catalytic domain of IPMS2 and the complex structures of full-length IPMS2 with bound Zn^{2+} and α-kiv or α-ipm. The catalytic domain consists of an $(\alpha/\beta)_8$ TIM barrel flanked by sub1 domain, and the sub2 domain are mainly composed of three α-helixes. IPMS2 forms a homodimer and the active site is located at the centre of the TIM barrel near the C-terminal ends of the β-strands. Sequence alignments and biochemical data indicate that IPMS1 and IPMS2 share high similarity with each other and both prefer acetyl-CoA substrate, however, the kinetic and mutagenesis studies show that IPMS2 possesses relative low enzymatic activity but high specificity on α-kiv substrate, while IPMS1 have the opposite features, consistent with the results from the structural comparisons and analyses.

References

1. Vinetz, J. M. (2001) Leptospirosis. Curr. Opin. Infect. Dis. **14**, 527–538
2. Bharti, A. R., Nally, J. E., Ricaldi, J. N., Matthias, M. A., Diaz, M. M., Lovett, M. A., Levett, P. N., Gilman, R. H., Willig, M. R., Gotuzzo, E. et al. (2003) Leptospirosis: a zoonotic disease of global importance. Lancet Infect. Dis. **3**, 757–771
3. Koon, N., Squire, C. J. and Baker, E. N. (2004) Crystal structure of LeuA from Mycobacterium tuberculosis, a key enzyme in leucine biosynthesis. Proc. Natl. Acad. Sci. U.S.A. **101**, 8295–8300
4. Ma, J., Zhang, P., Zhang, Z., Zha, M., Xu, H., Zhao, G. and Ding, J. (2008) Molecular basis of the substrate specificity and the catalytic mechanism of citramalate synthase from Leptospira interrogans. Biochem. J. **414**, 45–56
5. Zhang, P., Ma, J., Zhang, Z., Zha, M., Xu, H., Zhao, G. and Ding, J. (2009) Molecular basis of the inhibitor selectivity and insights into the feedback inhibition mechanism of citramalate synthase from Leptospira interrogans. Biochem. J. **421**, 133–143

P-62

Structural basis for a Reciprocating Mechanism of Negative Cooperativity in Dimeric Phosphagen kinase Activity

Xiaoai Wu[1], Sheng Ye[2], Shuyuan Guo[3], Wupeng Yan[1], Mark Bartlam[4] and Zihe Rao[1,4,5]

[1] *Laboratory of Structural Biology, School of Medicine,Tsinghua University, Beijing, China (wuxa@xtal.tsinghua.edu.cn)*

[2] *Department of Biochemistry and Molecular Biophysics, Columbia University, and Howard Hughes Medical Institute, New York, NY, USA*

[3] *School of Life Science & Technology, Beijing Institute of Technology, Beijing, China*

[4] *College of Life Sciences & Tianjin Key Laboratory of Protein Science, Nankai University, Tianjin, China*

[5] *National Laboratory of Macromolecules, Institute of Biophysics, Chinese Academy of Sciences, Beijing, China (raozh@nankai.edu.cn)*

Phosphagen kinase (PK) family members catalyze the reversible phosphoryl transfer between phosphagen and ADP to reserve or release energy in cell energy metabolism. The structures of

classic quaternary complexes of dimeric creatine kinase (CK) revealed asymmetric ligand binding states of two protomers, but the significance and mechanism remain unclear. In order to further understand this negative cooperativity, we determined the first structure of dimeric arginine kinase (dAK), another PK family member, at 1.75 Å, as well as the structure of its ternary complex with AMPPNP and arginine. Further structural analysis shows that the ligand-free protomer in a ligand-bound dimer is opened more widely than the protomers in a ligand-free dimer, leading to three different states of a dAK protomer. The unexpected allostery of the ligand-free protomer in a ligand-bound dimer should be relayed from the ligand-binding-induced allostery of its adjacent protomer. Mutations that weaken the inter-protomer connections dramatically reduced the catalytic activities of dAK, indicating the importance of the allosteric propagation mediated by the homodimer interface. These results suggest a reciprocating mechanism of dimeric PK, which is shared by other ATP related oligomeric enzymes, e.g. ATP synthase.

Keywords: crystal structure, arginine kinase, creatine kinase, energy metabolism

P-63

Structural and Kinetic Analysis of Raucaffricine Glucosidase (RG) from the Medicinal Plant *Rauvolfia*

Liqun Xia[1,2*], Martin Ruppert[2], Meitian Wang[2], Santosh Panjikar[4], Joachim Stöckigt[1,2*]

[1] *Institute of Materia Medica, College of Pharmaceutical Sciences, Zhejiang University, 388 Yu Hang Tang Road, Hangzhou, Zhejiang Province, 310058, P.R. China (joesto2000@yahoo.com)*

[2]*Department of Pharmaceutical Biology, Institute of Pharmacy, Johannes Gutenberg-University Mainz, Staudinger Weg 5, D-55099 Mainz, Germany*

[3] *Swiss Light Source PX III, Paul Scherrer Institute, CH-5232 Villigen, Switzerland*

[4]*European Molecular Biology Laboratory, Hamburg Outstation Deutsches Elektronen-Synchrotron, Notkestrasse 85, D-22603 Hamburg, Germany*

Raucaffricine-O-β-D-glucosidase (RG) is an enzyme that takes part in the biosynthesis of monoterpenoid indole alkaloids from the medical plant *Rauvolfia serpentina* (L.) Benth. Ex Kurz. Based on initial sequence alignment studies, RG belongs unequivocally to the glycosyl hydrolase (GH) family 1. The sequence identity was up to 55% compared to strictosidine glucosidase (SG) which represents the gateway to the biosynthesis of the mentioned indole alkaloid family.The family consists of about 2000 members. The best substrate for recombinant RG was raucaffricine (K_M 0.85 mM, Vmax 20.37 μM/min).The glucosides secologanin and strictosidine at the beginning of ajmaline biosynthesis pathway were also hydrolyzed in contrast to SG, which accepts exclusively its natural substrate strictosidine. Site-directed mutagenesis of RG's functional residue Glu-186 to a Gln residue results in >99% loss of enzyme activity. Crystals of RG and its complexes of inactive mutant Glu186Gln (with secologanin and strictosidine, respectively) were obtained and survived X-ray measurements at room temperature. Complete data sets were collected to less than 2.5Å. Detailed three-dimensional information describing both, native RG and complexes of inactive mutant of RG, thus providing additional structural characterization and identification of the amino acids that occupy the active site surface of the enzyme. Structural analysis and site-directed mutagenesis experiments demonstrate the essential role of Glu-186

in catalysis. The data presented here will contribute to deciphering the structure-related substrate specificity and might allow a future structure-based rational re-engineering of substrate acceptance of the enzyme.

P-64

Structure and Functional Implications of the Human Rad9-Hus1-Rad1 Cell Cycle Checkpoint Complex

Min Xu, Lin Bai, Yong Gong, Wei Xie, Haiying Hang, Tao Jiang
Institute of Biophysics, Chinese, 15 Datun Road, Chaoyang District, Beijing, 100101, China (tjiang@ibp.ac.cn)

Cellular DNA lesions are efficiently countered by DNA repair in conjunction with delays in cell-cycle progression. Previous studies have demonstrated that Rad9, Hus1, and Rad1 can form a heterotrimeric complex (the 9-1-1 complex) that plays dual roles in cell cycle checkpoint activation and DNA repair in eukaryotic cells. Although the 9-1-1 complex has been proposed to form a toroidal structure similar to proliferating cell nuclear antigen (PCNA), which plays essential roles in DNA replication and repair, the structural basis by which it performs different functions has not been elucidated. Here we report the crystal structure of the human 9-1-1 complex at 3.2Å resolution. The crystal structure, together with biochemical assays, reveals that the interdomain connecting (IDC) loops of hRad9, hHus1, and hRad1 are largely divergent, and further cocrystallization study indicates that a PIP-box containing peptide derived from hFen1 binds tightly to the IDC loop of hRad1, providing the molecular basis for the damage-repair-specific activity of the 9-1-1 complex in contrast to PCNA. Furthermore, structural comparison with PCNA reveals other unique structural features of the 9-1-1 complex that are proposed to contribute to DNA damage recognition. Here we propose a damage sensing model. In this model, the clamp loader Rad17-RFC2-5 forms an ATP-dependent complex with the 9-1-1 sliding clamp in which Rad17 interacts with Rad1, and loads the 9-1-1 complex onto DNA via opening the Rad1-Rad9 interface. Sliding of the clamp/clamp loader along DNA will stop when certain types of DNA lesions are detected by some key residues inside the clamp. The detection of DNA lesions then leads to conformational changes that facilitate the ring closure and ATP hydrolysis, consequently stimulate the dissociation of Rad17-RFC2-5 clamp loader from the 9-1-1 clamp, and ultimately trigger further DNA repair. Collectively, our studies provide new insights into DNA damage sensing and repair, which provides a starting point for further investigations and development of new anticancer agents.

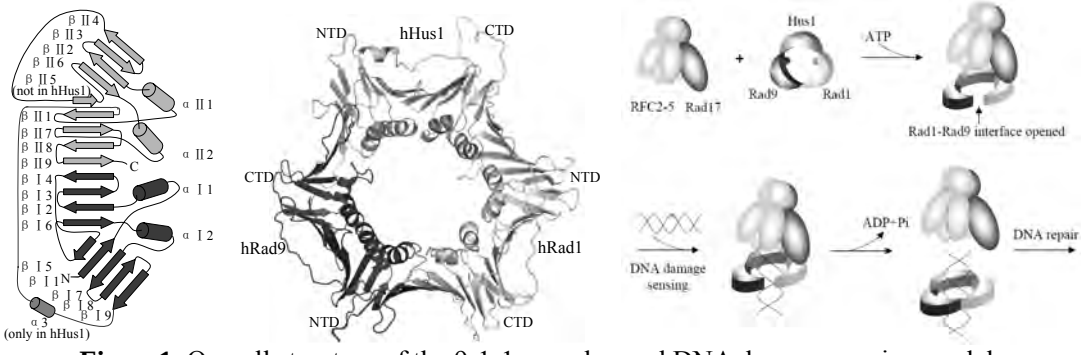

Figure1. Overall structure of the 9-1-1 complex and DNA damage sensing model.

References

1. Xu, M., Bai, L., Gong, Y., Xie, W., Hang, H., and Jiang, T. (2009) *J. Biol. Chem.* **284**, 20457-20461
2. Sancar, A., Lindsey-Boltz, L. A., Unsal-Kacmaz, K., and Linn, S. (2004) *Annu. Rev. Biochem.* **73**, 39-85
3. Lukas, J., Lukas, C., and Bartek, J. (2004) *DNA Repair (Amst)* **3**, 997-1007
4. Bermudez, V. P., Lindsey-Boltz, L. A., Cesare, A. J., Maniwa, Y., Griffith, J. D., Hurwitz, J., and Sancar, A. (2003) *Proc. Natl. Acad. Sci. U. S. A.* **100**, 1633-1638
5. Zou, L., Cortez, D., and Elledge, S. J. (2002) *Genes Dev.* **16**, 198-208
6. Rauen, M., Burtelow, M. A., Dufault, V. M., and Karnitz, L. M. (2000) *J. Biol. Chem.* **275**, 29767-29771

P-65

In situ proteolysis doubles the success rate in protein crystallization and structure determination

Xiaohui Xu[1,3], Aiping Dong[2], Hong Cui[1,3], Tatiana Skarina[1,3], Elena Evdokimova[1,3], Aled Edwards[1 2 3], Andrzej Joachimiak[3], Alexei Savchenko[1,3]

1.Ontario Center for Structure Proteomics, UHN, University of Toronto, 112 College St. RM24, Toronto, Ontario, M5G 1L6 Canada (xxu@uhnres.utoronto.ca, Alexei.savchenko@utoronto.ca)

2. The Structural Genomics Consortium (SGC), University of Toronto, 101 College St, Suite 700. Toronto, Ontario, M5G 1L7 Canada,(aled.edwards@utoronto.ca, a.dong@utoronto.ca)

3.Midwest Center for Structural Genomic (MCSG), Argonne National Laboratory,9700 South Case Ave, Chicago, IL U.S.A (andrzejj@anl.gov)

Obtaining well-diffracting crystals remains the main bottle-neck in protein crystallography. Analysis of large-scale structural genomics projects (http://targetdb.pdb.org) reports 13.5% success rate in obtaining the structure quality crystals from a given set of purified proteins. Thus vast majority of proteins submitted to conventional crystallization trials either do not crystallize or form poor quality crystals, which can not be used for structure determination. We present here a general rescue technique, named in situ proteolysis, allowing 15~20% increase in successful crystallization.

Our method is based on observation that trace amounts of protease present in the protein sample may lead to formation of hydrolyzed protein fragment prompt to crystallization. To test if addition of protease can be used as general crystallization technique we selected 55 bacterial protein samples from the pool of Midwest Centre for Structural Genomics targets. Of the 55 proteins, 20 had previously failed to crystallize and 35 had formed crystals that were unsuitable for structure determination. Addition of chymotrypsin protease to each protein sample prior crystallization trials (in 1:100 ratio) resulted in obtaining structure quality crystals for eight proteins. The Trypsin and subtilisin protease addition to the remaining protein samples allowed obtaining three additional structures.

The analysis of eleven solved structures demonstrated that in every case the polypeptide chain forming the crystal lattice was partially degraded by protease. The relative simplicity and significant increase in successful crystallization makes this method a prominent rescue technique in protein crystallization. Apply this technique to large scale crystal screening that can dramatically improve the quality of crystal and double the success rate in structure determination.

P-66 A functional Assembly of a Tripartite acrolide-specific Efflux Pump

Yongbin Xu[1, †], Hong-Man Kim[2], Kangseok Lee[2] and Nam-Chul Ha[1].
[1]*College of Pharmacy and Research Institute for Drug Development, Pusan National University, Busan 609-735, Korea (hnc@pusan.ac.kr)*
[2]*Department of Life Science, Chung-Ang University, Seoul 156-756, Korea (kangseok@cau.ac.kr)*

In Gram-negative bacteria, type I protein secretion systems and tripartite drug efflux pumps have a periplasmic membrane fusion protein (MFP) as an essential component. MFPs bridge the outer membrane factor and an inner membrane transporter, although the oligomeric state of MFPs remains unclear. The most characterized MFP AcrA connects the outer membrane factor TolC and the resistance–nodulation–division-type efflux transporter AcrB, which is a major multidrug efflux pump in *Escherichia coli*. MacA is the periplasmic MFP in the MacAB–TolC pump, where MacB was characterized as a macrolide-specific ATP-binding-cassette-type efflux transporter. Here, we report the crystal structure of *E. coli* MacA and the experimentally phased map of *Actinobacillus actinomycetemcomitans* MacA, which reveal a domain orientation of MacA different from that of AcrA. Notably, a hexameric assembly of MacA was found in both crystals, exhibiting a funnel-like structure with a central channel and a conical mouth. The hexameric MacA assembly was further confirmed by electron microscopy and functional studies *in vitro* and *in vivo*. The hexameric structure of MacA provides insight into the oligomeric state in the functional complex of the drug efflux pump and type I secretion system.

P-67 Homology Modeling of apo-CDK5 and Insights into Structure-Based Inhibitor Design

Kosaraju Vamsi Krishna, Seow Yi Lim, Feng Xue
Department of Chemistry, National University of Singapore 3 Science Drive 3, Singapore 117543 (chmxf@nus.edu.sg)

Cyclins and cyclin-dependent kinases (CDKs) play important roles in cell cycle regulation. CDKs are a class of evolutionarily conserved serine/threonine protein kinases, each CDK associates with a corresponding cyclin regulatory subunit to activate its phosphorylation activity [1]. Unlike most human CDKs that involved in cell division, the post-mitotic CDK5 is a crucial regulator of neuronal migration during the development of the central nervous system [2, 3]. Recent evidence indicates that deregulation of CDK5 is involved in the pathology of neurodegenerative diseases such as Parkinson's disease or Alzheimer's disease (AD), the leading cause of dementia and a increasing accelerated stochastically driven aging process.

The crystal structure of CDK5-p25 complex unveiled a number of key facts related to the activation and ligand binding [4]. However, CDK5 activation mechanism, which significantly differs from typical CDK activation, is still unclear due to lack of the structure of inactive CDK5 (apo-CDK5). We built a 3D model of apo-CDK5 based on the crystal structure of

apo-CDK2 (PDB: 1PW2) using homology modeling by spatial restraints implemented in MODELLER. The model was refined by molecular mechanics and the stereochemical quality was assessed by PROCHECK, ProsaII and Profiles-3D. Further molecular dynamic simulation was applied to ensure the stability of the model. Molecular docking studies were performed with known inhibitors to prove the suitability of the model for structure-based drug design. Inactive kinases have been recognized to be another possible avenue to achieve selectivity among kinase targets. Imatinib, a selective tyrosine kinase inhibitor, was docked into the binding site of apo-CDK5 to evaluate the possibility of novel inhibitors. Interestingly, the results showed that the inhibitor is capable of reaching the back floor of apo-CDK5 binding site, as well as reveals additional hydrophobic pocket created by T-loop.

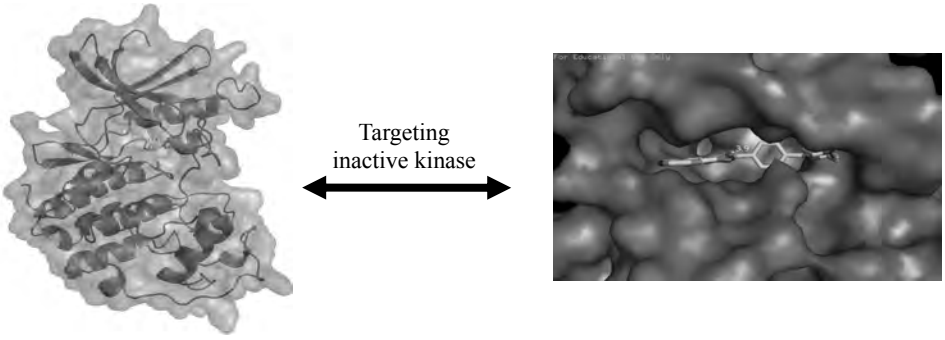

References

1. Morgan, D.O., *Cyclin-dependent kinases: engines, clocks, and microprocessors.* Annu Rev Cell Dev Biol, 1997. **13**: p. 261-91.
2. Bibb, J.A., *Role of Cdk5 in neuronal signaling, plasticity, and drug abuse.* Neurosignals, 2003. **12**(4-5): p. 191-9.
3. Paglini, G. and A. Caceres, *The role of the Cdk5--p35 kinase in neuronal development.* Eur J Biochem, 2001. **268**(6): p. 1528-33.
4. Tarricone, C., *et al.*, *Structure and regulation of the CDK5-p25(nck5a) complex*. Mol Cell, 2001. **8**(3): p. 657-69.

P-68

Xanthomonas campestris PqqD in the Pyrroloquinoline Quinone Biosynthesis Operon Adopts a Novel Saddle-Like Fold That Possibly Serves as a PQQ Carrier

Chao-Yu Yang[1], Tung-Yi Tsai[1], Andrew H.-J. Wang[2] & Shan-Ho Chou[1, 3]
[1]*Institute of Biochemistry, National Chung-Hsing University, Taichung, 40227, Taiwan*
[2] *Institute of Biological Chemistry, Academia Sinica, Nankang, Taipei, Taiwan*
[3] *National Chung Hsing University Biotechnology Center, Taichung, 40227, Taiwan, (shchou@nchu.edu.tw)*

Pyrroloquinoline quinone (4,5-dihydro-4,5-dioxo-1H-pyrrolo-[2,3-f]quinoline- 2,7,9-tricarboxylic acid, PQQ) is a novel heat-stable, water soluble redox cofactor present in a variety of bacterial alcohol and aldose dehydrogenases. It belongs to the third family of ortho-quinone cofactor following the well-known pyridine nucleotide- (such as NAD) and flavin-dependent (such as FAD) cofactors. Discovery of PQQ has elicited considerable interests due to its role as a growth-promoting factor both in animals and plants. Although the

structures and functions of many enzymes using PQQ as a cofactor has been elucidated, relatively little is known about the pathway leading to the biosynthesis of this intriguing cofactor. Recently six genes belonging to the *pqq*ABCDEF operon were found to be essential for the biosynthesis of PQQ, and the biosynthesis of PQQ were found to involve many unique synthesis steps. Structural studies of these genes are necessary to elucidate the synthesis mechanism. However, until now, only the structures of PqqB and PqqC have been determined. We now report the tertiary structure of PqqD from a plant pathogen *Xanthomonas campestris* (*Xc*) determined to a resolution of 1.66 Å using X-ray crystallography. The crystal structure of *Xc*PqqD was found to adopt a dimer of novel saddle-like fold that revealed considerable differences to the structure predicted *de novo* and carried out in the absence of suitable template. In addition, a phosphate ligand was found to be situated very well in the highly positively-charged central channel. Docking study of PqqD with PQQ located PQQ at the similar phosphate binding site as well, indicating that PqqD can possibly bind PQQ and serve as a PQQ carrier.

Reference

Tsai T-Y, Yang C-Y, Shih H-L, Wang AH-J, Chou S-H. *Xanthomonas campestris* PqqD in the Pyrroloquinoline Quinone Biosynthesis Operon Adopts a Novel Saddle-Like Fold That Possibly Serves as a PQQ Carrier. ***Proteins: Structure, Function and Bioinformatics*** 2009; in press.

P-69

Dual functions of an exosome component protein Rrp46/CRN-5 in RNA degradation and DNA fragmentation

Che-Chuan Yang[1,2], Yi-Ting Wang[2,3,4], Yu-Yuan Hsiao[2,4], Lyudmila G. Doudeva[2], and Hanna S. Yuan[1,2,3*]

[1] Graduate Institute of Biochemistry and Molecular Biology, National Taiwan University Taiwan

2 Institute of Molecular Biology, Academia Sinica

3 Institute of Chemical Biology and Molecular Biophysics, Taiwan International Graduate Program, Academia Sinica

4 Institute of Bioinformatics and Structural Biology, National Tsing Hua University, Hsinchu, Taiwan.

(hanna@sinica.edu.tw)

Rrp46 is one of the RNase PH family proteins, first identified as a component protein of the eukaryotic exosome, a protein complex involved in RNA turnover, surveillance and processing. The Rrp46 homolog, CRN-5, was subsequently characterized as a cell death-related nuclease, participating in DNA fragmentation during apoptosis in *C. elegans*.

Here, we compare the biochemical and structural properties of CRN-5 to its human homolog, hRrp46, and its rice homolog, oRrp46. The crystal structures of CRN-5 and oRrp46 were also determined at a resolution of 3.9 Å and 2.0 Å, respectively. We found that the recombinant and endogenous Rrp46/CRN-5 formed homodimers, and the dimeric oRrp46 had both phosphorolytic RNase and hydrolytic DNase activities, whereas hRrp46 and CRN-5 only bound to DNA with neither RNase nor DNase activity. Crystal structures of CRN-5 showed that the homo-dimeric assembly was similar to that of archaeal Rrp41-Rrp42. Site-directed mutagenesis of several residues in oRrp46 abolished its DNase and DNA/RNA binding

activities, confirming the critical importance of these residues in catalysis and substrate binding. CRN-5, although without any detectable DNase activity itself, interacted with the apoptotic nuclease CRN-4, and enhanced the DNase activity of CRN-4. Together, all these results strongly suggest that Rrp46 plays dual roles, functioning as an exosome component protein in RNA turnover in a healthy cell, and switching its role to participate in DNA fragmentation in apoptosis.

P-70 Preliminary X-ray analysis of human Frk kinase domain

Xiaoyan Yang[1], Takayoshi Kinoshita[1], Nao Miyano[1], Tetsuko Nakaniwa[1], Koichi Yokota[2], Masaki Gouda[2], Toshiji Tada[1]
1Department of Biological Science, Graduate School of Science, Osaka Prefecture University, Gakuen-cho 1-1, Sakai, Osaka 599-8531, Japan.
2Carna Bioscinences Inc. , KIBC 511, 5-2-2, Minatojima-Minatomachi ,Chuo-ku, Kobe 650-0047, Hyogo, Japan.

Frk is a member of Src family kinases and expressed especially in epithelial tissue. Developmental expression patterns and functional over-expression suggested that Frk had a crucial role in growth suppression and differentiation. Excess Frk activity is involved in type I diabetes via beta-cell destruction and numerous human cancers. We aimed to perform X-ray crystallography on Frk to elucidate the precise active-site structure for structure-based drug design. The C-terminal His-tagged Frk kinase domain was expressed by E. coli. Purification by the Ni-NTA affinity and anion-exchange chromatograms yielded three major peaks. The fractionized samples were characterized as Frk at the differential phosphorylation states by the SDS-PAGE, western blotting and activity measurement experiments. The unphosphorylated and mono-phosphorylated (in the activation loop) proteins were crystallized using the commercially available screening kits. Optimization of crystallization condition is currently in progress.

P-71 Crystal structures of human BTG2 and mouse TIS21 involved in suppression of CAF1 deadenylase activity

Xiuna Yang[1,2], Masahiro Morita[3], Hui Wang[1,2], Toru Suzuki[3], Wen Yang[1,4], Yunhai Luo[1], Cong Zhao[4], Yue Yu[5], Mark Bartlam[4], Tadashi Yamamoto[3,*] and Zihe Rao[1,2,4]
[1]Laboratory of Structural Biology, Tsinghua University, Beijing 100084, (yangxn@xtal.tsinghua.edu.cn)
[2]National Laboratory of Macromolecules, Institute of Biophysics, Chinese Academy of Sciences, Beijing 100101, China,(raozh@xtal.tsinghua.edu.cn)
[3]Division of Oncology, Institute of Medical Science, University of Tokyo, Minato-ku, Tokyo 108-8639, Japan,(tyamamot@ims.u-tokyo.ac.jp)
[4]College of Life Sciences & Tianjin State Laboratory of Protein Sciences, Nankai University, Tianjin 300071(bartlam@nankai.edu.cn)

BTG2 is the prototypical member of the TOB family and is known to be involved in cell growth, differentiation, and DNA repair. As a transcriptional co-regulator, BTG2 interacts with CCR4-associated factor 1 (CAF1) and POP2 (CALIF), which are key components of the general CCR4/NOT multi-subunit transcription complex, and which are reported to play

distinct roles as nucleases involved in mRNA deadenylation. Here we report the crystal structures of human BTG2 and mouse TIS21 to 2.3 Å and 2.2 Å resolution, respectively. The structures reveal the putative CAF1 binding site. CAF1 deadenylase assays were performed with wild-type BTG2 and mutants that disrupt the interaction with CAF1. The results reveal the suppressive role of BTG2 in the regulation of CAF1 deadenylase activity. Our study provides insights into the formation of the BTG2-CAF1 complex and the potential role of BTG2 in the regulation of CAF1.

Keywords: BTG2; TOB family; CAF1 binding; deadenylase activity; crystal structure

P-72 Crystal Structure of YqeH, a Circularly Permuted GTPase

Ji Young Yoon[1], Hye-Jin Yoon[1], Hyoun Sook Kim[1], Kyoung Hoon Kim[1], Do Jin Kim[1], Sang Jae Lee[1], Jun Young Jang[1], and Se Won Suh[1,2]
[1]*Department of Chemistry, College of Natural Sciences, Seoul National University, 151-747, Seoul, Korea (sewonsuh@snu.ac.kr)*
[2]*Department of Biophysics and Chemical Biology, College of Natural Sciences, Seoul National University, 151-747, Seoul, Korea*

Proteins containing circularly permutated G-domains are prevalent in bacteria (YlqF, YqeH, YjeQ, YawG, MJ1464), yeast, plants, and even humans (LSG1). YqeH is essential for the viability of *Bacillus subtilis*. YqeH participates in the biogenesis of the 30S ribosome subunit and assists in 50S ribosome assembly. The YqeH C-terminal domain contains some conserved residues that have been shown to be important for RNA binding by TRAP. YqeH probably acts as a G-protein that regulates nucleic acid recognition. To gain insight into the YqeH function at the molecular level, we have overexpressed and crystallized YqeH from *Thermotoga maritima* in complex with GDP. X-ray diffraction data were collected to 2.8 Å using synchrotron X-rays. The native crystal belongs to the tetragonal space group $P4_1$, with unit cell parameters of a = 81.62 Å, b = 81.62 Å, c = 146.00 Å, and $\alpha = \beta = \gamma = 90°$. The asymmetric unit contains two monomers, giving a crystal volume per protein mass (Vm) of 2.89 $Å^3$ Da^{-1} and a solvent content of 57%. The structure was determined using the multi-wavelength anomalous diffraction data from a crystal of the SeMet-substituted protein. The model has been refined to crystallograpic R_{work} and R_{free} values of 20.3% and 29.2%, respectively.

P-73 Structure and function study of the DUF55 domain of human thymocyte nuclear protein 1 and structure determination method study of twinning crystals

Feng Yu[1], Aixin Song[2], Chunyan Xu[1], Lihua Sun[1], Jian Li[1], Lin Tang[1], Hongyu Hu[2], Jianhua He[1*]
[1] *Shanghai Institute of Applied Physics, Chinese Academy of Sciences, Shanghai, China (hejh@sinap.ac.cn)*
[2] *The Institute of Biochemistry and Cell Biology, Chinese Academy of Sciences, Shanghai, China*

Human thymocyte nuclear protein 1 (hTHYN1), which is related with apoptosis, contains a unique DUF55 domain of 167 residues (55 - 221), but its cellular function is unclear.

The recombinant full-length hTHYN1 protein is unstable at high concentration and is therefore not well suited for structural analysis. DUF55 domain is a stable domain of hTHYN1 and suited for structural analysis. Crystals of DUF55 belong to the trigonal space group $P3_1$, and cell dimension is $a = b = 51.26$, $c = 122.40$ Å. Datasets to 2.3 Å resolution were collected. The intensity statistical analysis confirmed that the crystals of DUF55 domain were partially twinned by tetartohedry, and twin fractions were 0.424, 0.300, 0.134 and 0.142. The structure determination of DUF55 domain was very difficult and couldn't be achieved by previously reported approach, so an improved approach was developed and applied to it. After the structure was determined, only one twofold axis of rotational pseudosymmetry was found in the crystal structure, which was different from other tetartohedral twinning cases.

Using the *DALI* program, a YTH domain, which is a potential RNA binding domain from human YTH domain-containing protein 2, was identified to have the most similar three-dimensional fold to DUF55. It is implied that DUF55 might be a potential RNA-related domain.

P-74 Structure of Catalytic Domain of Matriptase in Complex with SFTI-1

Cai Yuan[1], Longguang Jiang[1], Liqing Chen[2], Mingdong Huang[1]
[1] *Fujian Institute of Research on the Structure of Matter, The Chinese Academy of Sciences, Fuzhou, Fujian 350002, China (yuancai@fjirsm.ac.cn)*
[2] *University of Alabama in Huntsville, Huntsville, AL 35899, USA (chenlq@uah.edu)*

Matriptase is a type II transmembane serine protease. It was demonstrated to be able to activate pro-uPA and pro-HGF/SF to their active forms [1], and thus play an important role in tumor invasion and metastasis. Here we report the structure of catalytic domain of matriptase in complex with sunflower trypsin inhibitor (SFTI-1), a potent inhibitor of matriptase with a Ki of 0.92 nM [2,3]. Our crystal structure at 2.0 Å shows that SFTI-1 binds in the active site of matriptase. Arg2, Thr4, Lys5, Ile7, and Phe12 of SFTI-1 play important roles in matriptase binding through hydrogen bonds and van der Waals interactions with the residues located in the active site of matriptase. Although the scissile bond between Lys5 and Ser6 of matriptase is oriented properly for nucleophilic attack, the electron density confirms the scissile bond is uncleaved within the ``average'' structure observed in the crystal, probably because that the distance between SFTI-1 Lys5 C and matriptase Ser195 O^{γ} is too long for effective chemical

reaction. This study provide insight to matriptase structure and may assist with design of specific inhibitors to matriptase.

References

1. Uhland K. Matriptase and its putative role in cancer. Cell Mol Life Sci 2006;63 (24):2968-78.
2. Long YQ, Lee SL, Lin CY, Enyedy IJ, Wang S, Li P, Dickson RB, Roller PP. Synthesis and evaluation of the sunflower derived trypsin inhibitor as a potent inhibitor of the type II transmembrane serine protease, matriptase. Bioorg Med Chem Lett 2001;11 (18):2515-9.
3. Korsinczky ML, Schirra HJ, Craik DJ. Sunflower trypsin inhibitor-1. Curr Protein Pept Sci 2004;5 (5):351-64.

P-75 Crystallization and preliminary X-ray crystallographic analysis of Escherichia coli CusB

Bo-Young Yun, Yongbin Xu and Nam-Chul Ha
A College of Pharmacy and Research Institute for Drug Development, Pusan National University, Jangjeon-dong, Geumjeong-gu, Busan 609-735, Republic of Korea,

Periplasmic membrane-fusion proteins (MFPs) are an essential component of multidrug and metal-efflux pumps in Gram-negative bacteria. However, the functional structure of MFPs remains unclear. CusCFBA, the CuI and AgI efflux system in Escherichia coli, consists of the MFP CusB, the OMF CusC and the RND-type transporter CusA. The MFP CusB bridges the inner membrane RND-type efflux transporter CusA and the outer membrane factor CusC and exhibits substrate-linked conformational changes which distinguish it from other MFP-family members. CusB from E. coli was overexpressed and the recombinant protein was purified using Ni–NTA affinity, Q anion-exchange and gel-filtration chromatography. The purified CusB protein was crystallized using the vapour-diffusion method. A diffraction data set was collected to a resolution of 3.1 A ˚ at 100 K. The crystal belonged to space group C222.

P-76 Crystallization and preliminary crystallographic analysis of a ribokinase from Staphylococcus aureus

Lin Wang[1,2], Haipeng Wang[1], Jianbin Ruan[1], Changlin Tian[1,2], Baolin Sun[1,2] and Jianye Zang[1]
[1] *School of Life Sciences, University of Science and Technology of China, 96 Jinzhai Road, Hefei, Anhui 230027, People's Republic of China (zangjy@ustc.edu.cn)*
[2] *Hefei National Laboratory for Physical Sciences at Microscale, University of Science and Technology of China, 96 Jinzhai Road, Hefei, Anhui 230027, People's Republic of China*

Ribokinase belongs to the PfkB carbohydrate kinase family and is found in both prokaryotes and eukaryotes (Bork et al., 1993). Ribokinase, which catalyzes the reaction of D-ribose and ATP to produce ADP and ribose-5-phosphate, plays a key role in the recycling of sugars produced from the metabolism of nucleotides (Anderson & Cooper, 1969; Lopilato et al., 1984). The catalytic activity of ribokinase is nearly completely dependent on the presence of pentavalent ions (PIV) such as phosphate (Maj & Gupta, 2001). Although there is a phosphate

ion present near the active site in the structure of *E. coli* ribokinase in complex with ribose and ADP (Sigrell et al., 1998), the exact role that PIV plays in activating ribokinase still remains elusive. In order to address this question, a ribokinase from *Staphylococcus aureus* named Sa239 was cloned, expressed, purified. And it was crystallized at 295 K under the condition consisting of 23% (w/v) PEG 3000, 0.1 M sodium citrate pH 5.6. A complete data set to 2.89 Å resolution was collected at 100 K on beamline 3W1A at BSRF and processed using HKL-2000 (Otwinowski & Minor, 1997). The R_{merge}s of the dataset are 10.2% and 40.6% for overall data and highest shell, respectively. And the crystal belongs to the hexagonal space group $P6_122$ or $P6_522$ with unit cell parameters a = b = 91.8Å, c = 160.7Å, α=β= 90º, γ= 120º. The calculated Matthews coefficient (V_M) of 3.01$Å^3$ Da^{-1}, with a solvent content of 59.2%, indicates the presence of one molecule in the asymmetric unit (Matthews, 1968). On the other hand, microcrystals of Sa239 in complex with phosphate were obtained too. The crystals of Sa239 and its complex with phosphate ions provide the basis of their structures solving and their structures will help in elucidating the mechanism by which phosphate ions activate ribokinase.

References

1. Anderson, A. & Cooper, R. A. (1969). Biochim. Biophys. Acta, 177, 163–165.
2. Bork, O., Sander, C. & Valencia, A. (1993). Protein Sci. 2, 31–40.
3. Lopilato, J. E., Garwin, J. L., Emr, S. D., Silhavy, T. J. & Beckwith, J. R. (1984). J. Bacteriol. 158, 665–673.
4. Maj, M. C. & Gupta, R. S. (2001). J. Protein Chem. 20, 139–144.
5. Matthews, B. W. (1968). J. Mol. Biol. 33, 491–497.
6. Otwinowski, Z. & Minor, W. (1997). Methods Enzymol. 276, 307–326.
7. Sigrell, J. A., Cameron, A. D., Jones, T. A. & Mowbray, S. L. (1998). Structure, 6, 183–193.

P-77

Nucleoside Monophosphate Complex Structures of the Endonuclease Domain from the Influenza Polymerase PA Subunit Reveal the Substrate Binding Site inside the Catalytic Center

Cong Zhao[1,$], Zhiyong Lou[1,$], Yu Guo[2], Ming Ma[3], Yutao Chen[3], Shuaiyi Liang[1], Liang Zhang[2], Shoudeng Chen[3], Xuemei Li[3], Yingfang Liu[3,*], Mark Bartlam[2] and Zihe Rao[1,2,3,*]

[1] *Structural Biology Laboratory, Tsinghua University, Beijing, 100084, China, (raozh@xtal.tsinghua.edu.cn).*

[2] *College of Life Sciences and Tianjin State Laboratory of Protein Science, Nankai University, Tianjin 300071, China*

[3] *National Laboratory of Macromolecules, Institute of Biophysics, Chinese Academy of Science, Beijing, 100101, China. (liuy@sun5.ibp.ac.cn)*

Highly pathogenic influenza strains currently in circulation pose the significant risk of a global pandemic. Following the reported crystal structure of the endonuclease domain from the avian influenza virus polymerase PA subunit, here we report the results of a systematic X-ray crystallographic analysis of its complex with adenosine, uridine and thymidine monophosphates (NMPs). Electron density corresponding to the monophosphate moiety of each nucleotide was apparent in each NMP complex and bound to the catalytic metal. A hydrophobic site was found to contribute to nucleoside binding. The NMPs complex

structures should represent the conformation of the bound product after nuclease cleavage. Moreover, one solvent molecule was found to occupy an equivalent position to the second reported Mn^{2+} ion where it mediates the interaction between bound NMPs and PAN in the presence of Mg^{2+} ion. The results presented here indicate a possible cleavage mechanism and identify a distinct nucleotide binding pocket. The identification of this binding pocket opens a new avenue for anti-influenza drug discovery targeting the cap-dependent endonuclease, in response to the world-wide threat of influenza.

P-78 From peptidic inhibitor leads to non-peptidic drugs: Making use of the reversible binding of peptide aldehydes to cysteine proteases in Dynamic Ligation Screening

Lili Zhu,[1] Jinzhi Tan,[1] Marco F. Schmidt,[2,3] Jörg Rademann[2,3] & Rolf Hilgenfeld[1]
[1] *Institute of Biochemistry, University of Lübeck, Ratzeburger Allee 160, 23538 Lübeck (zhu@biochem.uni-luebeck.de)*
[2] *Institute for Chemistry and Biochemistry, Free University Berlin, Takustr. 3, 14195 Berlin*
[3] *Leibniz Institute for Molecular Pharmacology (FMP), Robert-Rössle-Str. 10, 13125 Berlin*

In contrast to chloromethyl ketones, aldehydes bind reversibly to the active-site sulfhydryl of cysteine proteases [1]. We have developed a novel procedure that makes use of this property in the search for non-peptidic competitive inhibitors of these proteases. This procedure is called"Dynamic Ligation Screening" (DLS). We used the SARS coronavirus main proteinase (SARS-CoV M^{pro}) as an example to test the DLS concept [2]. First, a peptidic aldehyde inhibitor was reacted with the protease. This led to the formation of a covalent adduct between the active-site Cys145 and the inhibitor. Then, we screened a small library (234 compounds) of non-peptidic amines and other nucleophiles for compounds that would react with the protease-bound aldehyde and replace the active-site cysteine. The resulting imine was assumed to occupy subsites P5 to P2'. Subsequently, the compound discovered had its amine replaced by an aldehyde warhead. It was reacted with the native protease and formed a covalent adduct. The same library of nucleophiles was then screened for another non-peptidic compound that would replace Cys145 from the aldehyde. The ligation product discovered inhibited the enzyme with a K_i of 2.9 μM. Remarkably, this non-peptidic, competitive inhibitor was ligated from two halves each of which had no inhibitory activity on its own. These reactions will only work in the presence of the target enzyme. Thus, the reversibility of the covalent adduct formation between aldehydes and cysteine proteases can be used to discover non-peptidic inhibitors that block the target by non-covalent interaction. Recently, we determined three crystal structures of SARS-CoV M^{pro} in complex with peptide aldehydes (Ac-ESTLQ-H, Ac-NSFSQ, and Ac-NSTSQ-H), explaining the mechanism of aldehyde inhibitor binding to SARS-CoV M^{pro}. Co-crystallization experiments with the ligation imine product are underway and performing the reaction in the crystals is also being tested..

References

1. S.I. Al-Gharabli, S.T. Shah, S. Weik, M.F. Schmidt, J.R. Mesters, D. Kuhn, G. Klebe, R. Hilgenfeld, J.

Rademann, Chembiochem 7, 1048-1055 (2006).
2. M.F. Schmidt, A. Isidro-Llobet, M. Lisurek, A. El-Dahshan, J. Tan, R. Hilgenfeld, J. Rademann, Angew Chem Int Ed Engl 47, 3275-3278 (2008).

P-79

Co-crystallization of Valproic acid by Co-grinding and Structure Determination from Powder Diffraction Data

Masahide Aoki[1], Hidehiro Uekusa[1], Hiroyuki Kurobe[2], Etsuo Yonemochi[2], Katsuhide Terada[2]

[1] *Tokyo Institute of Technology, 2-12-1 Ookayama, Meguro-ku, Tokyo, 152-8551, JAPAN (aoki.m.ab@m.titech.ac.jp)*

[2] *Toho University, 2-2-1 Miyama, Funabashi-shi, Chiba, 274-8510, JAPAN*

Co-crystallization of pharmaceuticals with low molecular weight compounds is very effective to improve physical properties such as stability, solubility, and bioavailability. Valproic acid (oily liquid) is known as antiepileptic agent, and used as sodium valproate form (white crystalline powder) which is highly hygroscopic and deliquescent. In this study, valproic acid co-crylstals were explored to improve its hygroscopicity and the crystal structure was analyzed from PXRD.

As a result of vigorous screening, valproic acid and L-arginine co-crystal was obtained only by co-grinding at 1:1 molar ratio (Fig.1). L-arginine is an amino acid with relatively strong basicity, and known to form organic salts with acids in co-crystals. The hygroscopicity is greatly improved by co-crystallization, so the co-crystal is stable up to R.H. 70%. In contrast, sodium valproate transforms to hydrate form at R.H. 35% and deliquesces at R.H. 45%.

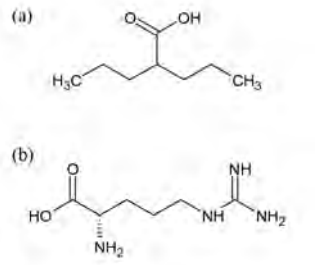

Fig.1 : (a) valproic acid (b) L-arginine

When valproic acid and L-arginine were crystallized from water solution, only amorphous materials were obtained, so it was difficult to prepare single crystals for X-ray structure analysis. Thus, the crystal structure was determined directly from powder diffraction data. The powder diffraction dataset was measured in SPring-8 (BL19B2) using large IP Debye-Scherrer camera. The structure solution was carried out by direct space method using a zwitter-ion form of L-arginine, and organic salt form of the complex as the model structure. The best solution was refined by Rietveld method using restraints (Fig.2).

Carboxylic anion group of valproic acid forms four O…H-N hydrogen bonds with L-arginine. In addition, L-arginine forms N-H…O hydrogen bond with another L-arginine. In the crystal, there are layers of valproic acid and L-arginine (Fig.3). Hydrophobic alkyl chains of valproic acid are inside of the valproic acid layer, on the other hand, hydrophilic carboxyl groups are exposed to the L-arginine layer and forming hydrogen bonds with L-arginine.

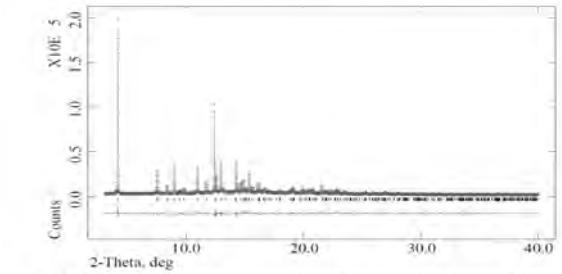

Fig.2 : Final Rietveld plot , cross:experimental , black solid:calculated , lower line:difference

Fig.3 : Crystal structure

The Design of New Bicyclo[3.3.0]octane Lattice Inclusion Hosts and Cocrystal Partner Molecules

P-80

Roger Bishop[1], Mohan M. Bhadbhade[2], Isa Y. H. Chan[1]
[1] *School of Chemistry, University of New South Wales, UNSW Sydney NSW 2052, Australia (r.bishop@unsw.edu.au)*
[2] *Analytical Centre, University of New South Wales, UNSW Sydney NSW 2052, Australia,(m.bhadbhade@unsw.edu.au)*

Vossen, working in Schroeter's laboratory, unexpectedly discovered a beautiful red salt of composition $(C_{16}H_{15}O_{10}Na).(CH_3OH)_2$ in 1910 [1]. A considerable amount of chemical detective work was necessary before the general structure of Schroeter and Vossen's red salt, a bicyclo[3.3.0]octane derivative, was reported by Yates and Bhat in 1954 [2]. However, details of the stereochemistry, metal co-ordination, and the role of the methanol guest molecules, remained unknown until we reported the crystal structure of (**1**).$(CH_3OH)_2$ in 2002 [3].

Reduction of the red salt with sodium amalgam yields a tetraester, shown by us to have the structure **2** [4]. Although compound **2** was a non-host molecule, our X-ray structure determination revealed that this simple V-shaped substance packed rather inefficiently by itself in the solid state.

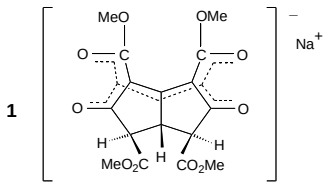

1

This characteristic is known to be one that often results in guest inclusion in order to achieve a denser and lower energy crystal structure. Therefore we were encouraged to prepare other bicycle [3.3.0]octane derivatives and explore their inclusion behaviour. It turns out that several very simple dialcohol derivatives of this ring system are excellent new host molecules. The properties of these compounds are being investigated systematically as part of a current Ph.D. project. The achiral dialcohol **3** is one example of these new alicyclic host molecules. Examples of lattice inclusion and cocrystal structures formed by **3** will be described in crystal engineering terms.

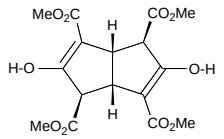

2

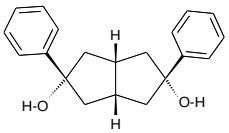

3

References

[1] G. Vossen, *Inauguraldissertation*, University of Bonn, Germany, 1910.
[2] P. Yates and G. Bhat, *Chem. Ind. (London)*, 1954, 1237.
[3] D. Djaidi, R. Bishop, D. C. Craig and M. L. Scudder, *New J. Chem.*, 2002, **26**, 614.
[4] D. Djaidi, Ph. D. thesis, The University of New South Wales, 2006.

P-81 Zintl Phase Compounds $Yb_{1-x}Ca_xCd_2Sb_2$ With Tunable Thermoelectric Properties Induced by Cation Substitution

Qigao Cao[1,2], Hui Zhang[1], Meibo Tang[1], Haohong Chen[1], Xinxin Yang[1], Xiangxin Guo[1], Jingtai Zhao*[1], Grin Yuri*[3]
[1] *Shanghai Institute of Ceramics Chinese Academy of Sciences, Chinese, 1295 Dingxi Road, Changning District, Shanghai, 200050, China (caoqigao@mail.sic.ac.cn)*
[2] *Graduate School of Chinese Academy of Sciences, Beijing, China*
[3] *Max-Planck-Institut für Chemische Physik fester Stoffe, Nöthnitzer Str. 40, 01187 Dresden, Germany*

It has been shown previously that the thermoelectric properties of the Zintl phase compound $YbCd_2Sb_2$ can be finely tuned via Zn substitution at the Cd-site in the anionic $(Cd_2Sb_2)^{2-}$ framework. Here we report the results of the investigation of isoelectronic substitution of Yb by Ca. The *p*-type $Yb_{1-x}Ca_xCd_2Sb_2$ ($0.2 \le x \le 0.8$) samples have been synthesized via a solid-state reaction followed by suitable cooling, annealing, grounding, and spark plasma sintering (SPS) densification processes. In samples with x=0.2, 0.4, 0.5, 0.6, 0.8, the electrical conductivity, Seebeck coefficient, and thermal conductivity measurements have been performed as a function of temperature from 300 to 650 K. It is found that the Ca substitution effectively lowers the thermal conductivity for all samples at high temperature, while it significantly increases the Seebeck coefficient. As a result, the best dimensionless figure of merit *ZT* of 0.96 has been attained at 650 K for x=0.4.

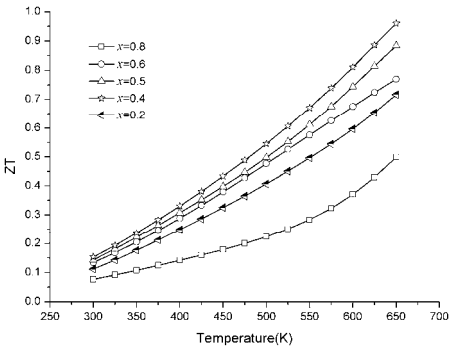

P-82 Molecular self-assembly – tweezers, forks, and boxes

Christine Cardin, Yu Gan, Zhixue Zhu and Howard Colquhoun
Department of Chemistry, university of Reading, Whiteknights, Reading, RG6 6AD, UK (c.j.cardin@rdg.ac.uk)

Intense current interest in the design of multi-component, nanoscale molecular assemblies has led to the exploitation of many types of intermolecular interaction, including π-stacking between aromatic donor and acceptor sites. This type of interaction has recently enabled the fabrication of nanoscale devices including light- and redox-driven switches and molecular logic-gates. In view of the relatively labile nature of the *N*-benzylpyridinium linkage on which much research into π-stacked molecular assemblies has so far depended, Professor **Colquhoun** has recently developed a new class of supramolecular materials based on aromatic poly (imide-sulfone) chemistry. Linear and macrocyclic materials of this type display extreme thermochemical stability and readily form π-stacked donor-acceptor complexes with polycyclic hydrocarbons such as pyrene.

Most importantly, sequence-selective complexation of the imide residues in aromatic *co*-polyimides by a pyrene-based molecular tweezer *enables monomer-sequence information to be read by the tweezer* and reported through sequence-dependent ^{1}H NMR complexation

shifts. These very significant discoveries in molecular information-processing have been crucially dependent on single-crystal X-ray analyses of tweezer-complexes with linear and cyclic oligo-imides (e.g. **2** and **3** above: hydrogens omitted for clarity). Tweezer-chain binding has thus been shown to arise not only from π-π stacking interactions but also from N-H...O and C-H...O hydrogen bonding, and from polymer chain-folding. Crystallographic data of this type are of the utmost importance for predictive computational modelling of tweezer-polymer interactions.

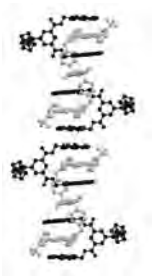

Recently we have refined in-house data on the elegant doubly-bound oligomer-tweezer ('zigzag') complex shown here. The crystal structure shown at right provides the first unequivocal model for chain-folding and small-molecule binding in any synthetic polymer system. Moreover, the supramolecular geometry found in the solid state is remarkably consistent with extensive NMR studies of tweezer-binding in solution. The crystal contains very large solvent cavities and both model building and structure-refinement required very high quality diffraction data. Using the in-house data from our Oxford Diffraction Enhance-Ultra source, with a data collection time of three days, a model has in fact now been built, with a current R factor of 13.2 %.

These and related examples of molecular self-assembly will be reported in this poster.

P-83

Metal Organic Frameworks from 3,3'-Biphenic Acid

Chun-Lung Choi[1], Herman H-Y. Sung[1], M. Gerry J. Lesley[2], Ian D. Williams[1]
[1] *Department of Chemistry, Hong Kong University of Science and Technology, Clear Water Bay, Kowloon, Hong Kong, China (chwill@ust.hk)*
[2] *Department of Chemistry, Southern Connecticut State University, New Haven, U.S.A..*

Biphenyl based carboxylates appear to have excellent characteristics for formation of open yet stable, crystalline metal-organic framework polymers (MOFs). Whilst 4,4'- and 2,2'-biphenic acids are commercially available and have been studied in depth, the 3,3' analogue is not and its potential for MOF formation virtually unexplored. The ligand was prepared by coupling of an arylbromide with phenylboronic acid by Miyaura-Suzuki catalyzed coupling. The coordination polymers of 3,3'-biphenic acid with variety of transition metals and lanthanides have been explored and about 10 new phase types are reported. Using 4,4'-bipyridine as a N-donor spacer ligand highly open frameworks [M(3,3'-biphenate)$(4,4'\text{-bipy})_{0.5}$] can be formed containing paddle-wheel tetracarboxylate metal dimers. These network structures triply interpenetrate. From hydrothermal synthesis conditions at high pH several novel open-framework hybrid solids containing 3,3'-biphenate and hydroxide can be formed, e.g. $[Zn_5(OH)_8(3,3'\text{-biphenate})]$ and $[Ln_3(OH)_6(3,3'\text{-biphenate})(OAc)]$. The structural stabilities and sorption properties of these novel MOF materials are under investigation

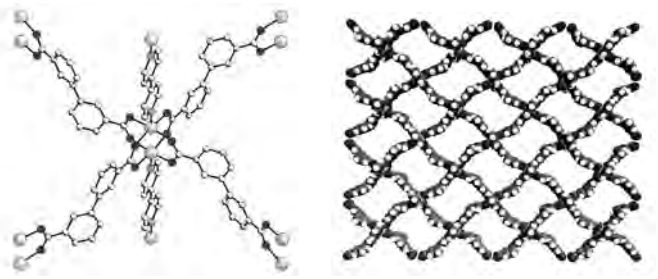

***Acknowledgements**: We are grateful to the Research Grant Council HK (603306) and HKUST for funding of this work and Connecticut State University for granting sabbatical leave for Prof. Lesley.*

P-84 On the quality of data necessary for performing 2nd & 4th moment method of evaluating crystallite size & dislocation density

Prabal Dasgupta[1] & Bholanath Mondal[2]
[1,2]Department of central Scientific services, Indian Association for the Cultivation of Science, Kolkata-700032,India (prabaldasgupta@hotmail.com)

With the advent of epoch-making paper by Borbely et al[1] ,renaissance of 2^{nd} & 4^{th} moment method of evaluating crystallite size has taken place. They reported that they have made use of high resolution XRD data.Present work aims to explores what quality of XRD data is essential to carry out such analysis.Background & instrumental broadening corrected, 111&200 profiles of XRD data of commercial grade metallic Cu & Ni (in step-scan mode), those were stripped of $K\alpha_2$ contribution(using Bruecker software), were subjected to such analysis.M_2 & M_4/q^2 plots suggest that peak broadening in these materials are mainly crystallite size-related broadening .Different step widths(ranging from .005 to .03deg) and scan speeds (0.2,0.5& 2.50sec per stepwidth)were chosen so as to ascertain the quality of data that yields more or less same crystallite size(within 3%) from the 2^{nd} & 4^{th} moment plot.It was revealed that stepwidth of 0.01deg or less with scan speed of at least 2.0 sec step $^{-1}$ yields satisfactory converegence.

Reference

I.A.Borbely,A. Revesz & I.Groma ,Zeit Krist. Suppl **23** (2006) 87-92

P-85 Crystal structure of organic compound ethyl-2-amino-5-bromothiazole-4-carboxylate

K.V.Arjuna Gowda[1], Ramakrishna Gowda[2] and I.A.Khazi[3]
[1]Department of Physics, Government First Grade College, K.R.Pura, Bangalore, INDIA
[2]Department of Physics, Government College for women, Kolar, INDIA
[3]Department of Chemistry, Karnataka University, Dharwad, INDIA
(arjunagowda@indiainfo.com)

The 2-amino-5-bromothiazole-4-carboxylate was required for the proposed synthesis of ethyl-2-amino-5-arylthiothiazole-4-carboxylates and ethyl-2-amino-5-arenesulfonyl thiazole4-

carboxylates by affecting SN2 reaction between suitably substituted thiophenoxide ions and 2-amino-5-bromothiazole-4-carboxylate, which are reported to have anti-bacterial, anti-tubercular, Chemotherapeutic and schistosomicidal activities.

The title compound grown by slow evaporation from aqueous ethanol pale yellow needle crystals obtained. The compound crystallizes as monoclinic system and cell parameters a=8.665(6)Å, b=9.903(7)Å, c=11.381(7)Å, α=96.777(11)° β=93.596(11)° and γ=109.321(10)°.

The structure has been solved by direct methods using SHELXS-97 and refined by a full-matrix least-square method using SHELXL-97 program. The final R-value is 0.0403. The title compound is under progress for publication.

P-86

Local Structure Analysis of an Automobile Catalyst $La_{1.02}Fe_{0.95}Pd_{0.05}O_3$ by Pd K-edge XAFS

Shoshi Higuchi[1], Daiju Matsumura[2], Yasuo Nishihata[2], Jun'iciro Mizuki[2], Hikaru Terauchi[1], Isao Takahashi[1], Masashi Taniguchi[3], Mari Uenishi[3], Hirohisa Tanaka[3], Kimiyoshi Kaneko[4]

[1] *Kwansei-Gakuin University, 2-1 Gakuen, Sanda Hyogo 669-1337, Japan, (czn29980@kwansei.ac.jp)*

[2] *Synchrotron Radiation Research Center, Japan Atomic Energy Agency, Sayo, Hyogo 679-5148, Japan*

[3] *Daihatsu Motor Co., Ltd., Gamo, Shiga 520-2593, Japan*

[4] *Hokko Chemical Industry Co., Ltd., Fine Chemical Reserch Laboratories, 2165, Toda, Atsugi-shi, Kanagawa 243-0023, Japan*

A $La_{1.02}Fe_{0.95}Pd_{0.05}O_3$(LFPO) catalyst has special feature which maintains high catalytic property even in long time use, while an alumina catalyst employs a sufficient excess of precious metals to ensure the activity. The reason of the long life catalyst is that the Pd particle goes in and out of the perovskite structure of the LFPO during oxidation and reduction processes in the exhaust gas. Because of this mechanism, the Pd particle size maintains effectively small. [1][2]

In this study, samples were prepared by the alkoxide method and coprecipitation method for the LFPO. We observed the local structural difference of these two samples by x-ray absorption fine structure (XAFS) at 15 K with transmission mode at BL14B1, SPring-8. The information by XAFS technique is different from long range structural information by x-ray diffraction technique. XAFS technique shows elementary selective local structure. Therefore, XAFS technique is very suitable to observe the local structure round Pd as a trace additive to arbitrary select.

Figure 1 shows extended x-ray absorption fine structure (EXAFS) function of the two samples. It is found that main oscillations from Pd-O bond for the each sample are similar. However some slight differences were found as shown in Fig.2 which shows an extended figure for the square in Fig.1. These differences are derived from short wavelength component. From the result of analysis, it is found that high coordination structure raises these differences. At conclusion, it is revealed that first coordination from Pd-O bond is similar between two samples, which were prepared by alkoxide method and coprecipitaton method, and minute

structure in higher coordination is different between them.

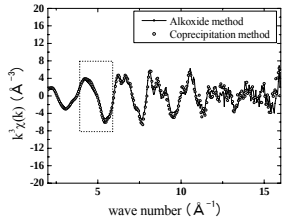

Fig.1 EXAFS function $k^3\chi(k)$ measured at 15 K

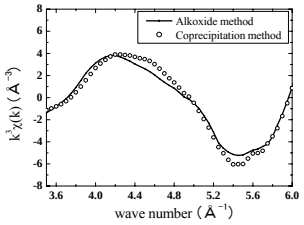

Fig.2 Close up of the EXAFS function in fig.1

References

[1] Y. Nishihata *et al*., Nature, 418, 164 (2002)
[2] H. Tanaka *et al*., Angew. Chem. Int. Ed, 5998, 45 (2006)

P-87 Regulation of Anthracene Arrangement and Photoluminescence Properties by Using Organic Salts

Tomoaki Hinoue, Norimitsu Tohnai, Ichiro Hisaki, Mikiji Miyata
Osaka University, 2-1, Yamadaoka, Suita-City, Osaka, 565-0871 Japan
(koriki@molrec.mls.eng.osaka-u.ac.jp)

Solid-state photoluminescent properties depend strongly on molecular arrangement as well as molecular structure of the constituent molecules. However, it is difficult to regulate the arrangements and therefore the relationships with solid-state photoluminescent properties have not been elucidated exactly. In this context, we have regulated the arrangement of fluorophores by employing organic salts composed of sulfonic acid bearing the fluorophores and aliphatic amines. This method afforded convenient regulation of packing manner of the fluorophores depending on the substituents of aliphatic amines. Here, we present the regulation of anthracene arrangement and concomitant solid-state photoluminescence by using ammonium anthracene disulfonate. Although unmodified anthracene molecule aggregate in only 2-dimensional herringbone arrangement, ammonium anthracene disulfonate afforded 1-dimentional and discrete monomer-like arrangement of anthracene moieties as well as herringbone arrangement. Discrete arrangement showed strong fluorescence due to the suppression of nonradiative deactivation, while 1-dimentional arrangement did weak but red-shifted fluorescence.

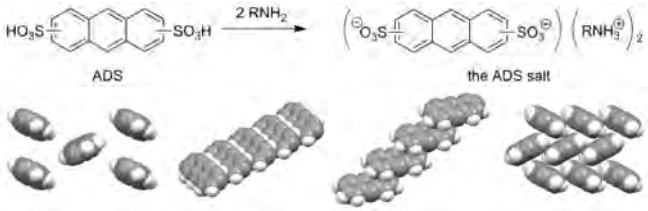

Figure 1. Organic salts composed of anthracene disulfonic acid and aliphatic amine (top), and molecular arrangement of anthracene moieties obtained by X-ray crystal structure analyses (bottom).

References

1. Mizobe, Y., Tohnai, N., Miyata, M., Hasegawa, Y., Chem. Commun. 2005, 1839–1841.
2. Mizobe, Y., Hinoue, T., Yamamoto, A., Hisaki, I., Miyata, M., Hasegawa, Y., Tohnai, N., Chem. Eur. J.,

in press.

P-88 X-ray structural study of intercalation compounds Bi_xTiS_2

Sho Ikeda , Takuro Kawasaki and Ken-ichi Ohshima
Institute of Materials Science ,University of Tsukuba, Tsukuba 305-8573,Japan

Intercalated compounds titanium disulfides M_xTiS_2 have various structures and peculiar physical properties depending on the kind or composition of M. Recently, Li et al. have reported that the resistivity and thermopower decreased as intercalated Bi content increased[1,2]. However, there are no systematic reports on the crystal structure analysis of Bi_xTiS_2.

Single crystals of Bi_xTiS_2 were grown in evacuated silica tubes by chemical vapor transport method using iodine as a transport gas.Fig.1 shows the SEM image of Bi_xTiS_2. Structures were investigated by single crystal X-ray diffraction method, where the data were collected using Imaging Plate (RAPID, Rigaku) at room temperature. The crystal structure was solved by charge flipping methods and refined by the program JANA2006. The space groups and lattice parameters of Bi_xTiS_2 change with increasing intercalated Bi.

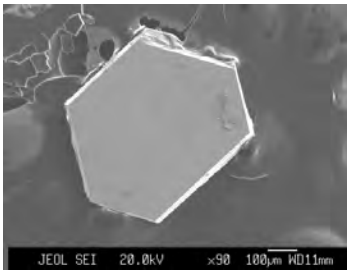

Fig.1 SEM image of Bi_xTiS_2

References

[1] D. Li, X.Y. Qin, Y.J. Gu (2006). Materials Research Bulletin 41, 282–290.
[2] D. Li, X.Y. Qin, J. Liu, H.S. Yang (2004). Phys. Lett. A 328, 493–499.

P-89 Crystal Structure of Tetracaine Hydrochloride Polymorphs

Sayaka Ina[1], Hidehiro Uekusa[1], Naoko Itoda[2], Etsuo Yonemochi[2], Katsuhide Terada[2]
[1] *Tokyo Institute of Technology, Japanese, 2-12-1 Ookayama, Meguro-ku, Tokyo, 152-8551, Japan (ina.s.aa@m.titech.ac.jp)*
[2] *Toho University, 2-2-1 Miyama, Funabashi-shi, Chiba, 274-8510, JAPAN*

Tetracaine hydrochloride (Fig. 1) is widely used local anesthetic drug. From thermal analysis, it has ten (pseudo-) polymorphic forms, i.e. six anhydrous, three hydrates (hemi-, mono-, and tetra-hydrates), and one amorphous form, in different temperature and R.H. range, however, only one crystal structure (Form 1) is known. Such pharmaceutical polymorphs should show different physical properties like bioavailability or solubility depending on their crystal

structures. In this study, the crystal structures of the polymorphic crystals including the hydrates are analyzed, and their characteristic properties are examined.

Stable crystals of hemihydrate were recrystallized from 9:1 mixture of ethanol and water. On the other hand, tetrahydrate crystals were obtained from anhydrous form (Form 1) at the high humidity conditions (> R.H. 85%) or in slurry, which were relatively unstable and transformed into mono- and then hemihydrates at ambient conditions. Crystal structure of hemihydrate crystal was determined by single crystal X-ray structure analysis. The crystallographic data are *monoclinic*, space group $P2_1$ with a=10.845(3), b=6.263(2), c=24.944(7)Å, β=94.695(6)°, and V=1688.5(9)å^3.

In the crystal structure, two tetracaine hydrochloride molecules and one water molecule were independent. As for these two independent molecules, the torsion angle of $-(CH_2)_2NMe_2$ groups are different. It has a layer structure along c-axis in the crystal, in which the molecules are packed as herringbone manner. The layers are connected by Cl^- and water molecule via $NH^+\cdots Cl^-$ and $OH\cdots Cl^-$ charge assisted hydrogen bondings, and also by carbonyl O…HN hydrogen bonding (Fig. 2). On the other hand, anhydrate form (Form1) has one independent molecule, and it has flatter layer structure, which is considerably different from hemihydrate, for example, each molecule has the same orientation in the same layer. The layers are also connected by $NH^+\cdots Cl^-$ hydrogen bonds similar to the hemihydrate.

The difference of these crystal structures may influence characteristic such as solubility and stability.

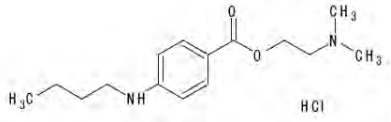

Fig 1. Tetracaine hydrochloride

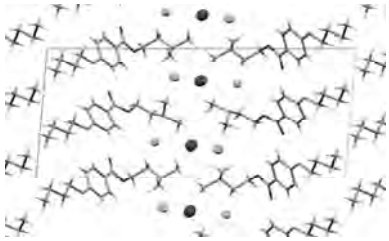

Fig 2. Crystal structure of hemihydrate viewed along b-axis

P-90 High Resolution X-ray Diffraction Analysis on $(Lu_{2.1},Bi_{0.9})Fe_5O_{12}$ Layers Grown on $Gd_3Ga_5O_{12}$ Substrate

Hong Ji *, Huaiwu Zhang , Qiye Wen
State Key Laboratory of Electronic Thin Films and Integrated Devices, University of Electronic Science and Technology of China, Chengdu 610054, China (jihong@uestc.edu.cn)

Epilayer composition, homogenous strain and surface morphology, which depend on process parameters, such as different doping, layer thickness, growth rate, etc. are of significant importance for the device applications of the rare earth iron garnets films. High resolution X-ray diffraction (HRXRD） is the most important non-destructive tool to obtain information about physical properties, including crystal structure, defect levels, composition and thickness of an epilayer and orientation relationship between the epilayer and its substrate. This paper introduces HRXRD analysis (measuring X-ray instrument: Bede D1 Four-circle

Diffractometer) on cubic $(Lu_{2.1},Bi_{0.9})Fe_5O_{12}$ thick films (~8um) grown on (111) $Gd_3Ga_5O_{12}$(GGG) single-crystal substrates (diameter size of 50 mm) by liquid phase epitaxy (LPE) method (growth rate of 0.39 nm/min), including observations of microstructural heterogeneity on the epilayers using a rocking curve measurement (or ω scan), including measurements of lattice constant on the epilayers using a ω/2θ scan. In the case of using a crystal analyzer , the (444) peak of $(Lu_{2.1},Bi_{0.9})Fe_5O_{12}$ is observed at the high-angle side of the $Gd_3Ga_5O_{12}$ (111) peak. The full width at half maximum intensity (FWHM) of rocking curve of the $(Lu_{2.1},Bi_{0.9})Fe_5O_{12}$ (444) peak is 14.16 arcsec. The calculated lattice constant of $(Lu_{2.1},Bi_{0.9})Fe_5O_{12}$ is 12.3732Å.

The purpose of this paper is to investigate the lattice constant of $(Lu_{2.1},Bi_{0.9})Fe_5O_{12}$ film layer. In general, the lattice constant of $(Lu_{2.1},Bi_{0.9})Fe_5O_{12}$ changes systematically with the Lu or Bi composition. In addition, it is understand that the crystal orientation direction of the $(Lu_{2.1},Bi_{0.9})Fe_5O_{12}$ epilayer is tilted with respect to the $Gd_3Ga_5O_{12}$ substrate because its mosaic structure, which will affect the measurement results. Therefore, a method for eliminating the effect of epilayer tilt is needed to obtain reliable the $(Lu_{2.1},Bi_{0.9})Fe_5O_{12}$ lattice constant. The derivative analysis technique for carefully corrected Bragg angle of the $(Lu_{2.1},Bi_{0.9})Fe_5O_{12}$ diffraction peak has been described in the paper. In some cases, we only need to measure the average angular difference (peak separation) $\Delta\theta_B$ to eliminate the effect of epilayer tilt (in an actual analysis, its $\Delta\theta_B$ value depends on lattice mismatch and the presence or absence of lattice relaxation). In the case for symmetric diffraction, from the $\Delta\theta_B$ between the 444 $_{sub}$ and 444 $_{film}$ reflections, we can calculate the lattice constant of the film (α_{film}) if the lattice constant of the substrate (α_{sub}) is known [in this example, $Gd_3Ga_5O_{12}$ substrate, α_{sub}= 12.3800 Å (cubic)]. In here, based on the $\theta_{epi} = \theta_{Bsub} + \Delta\theta_B$ and the $\alpha_{film} = [\sin(\theta_{Bsub}) / \sin(\theta_{epi})] \bullet \alpha_{sub}$ simple formulas, the lattice constant of $(Lu_{2.1},Bi_{0.9})Fe_5O_{12}$ can evaluated using a high-resolution out-of-plane measurement.

Study on Synthesis and Luminescence Properties of $LuBO_3:Ce^{3+}$

P-91

Teng-Teng Jin[1, 2], Jing-Tai Zhao[1] , Hao-Hong Chen[1], Xin-Xin Yang[1]
[1]*Key Laboratory of Transparent and Opto-Functional Inorganic Materials of Chinese Academy of Sciences, Shanghai Institute of Ceramics, Shanghai 200050, P.R. China(jtzhao@mail.sic.ac.cn)*
[2] *Graduate School of Chinese Academy of Science, Beijing, 100039, P.R. China*

Both calcite and vaterite phases of $LuBO_3:Ce^{3+}$ have been prepared through solid state reactions. Their X-ray and UV excited luminescence properties were investigated at room temperature. The as-obtained phosphor samples exhibit a strong and rapid near UV-blue emission, originating from the typical of the 5d→4f transitions of Ce^{3+}. The light yield of $LuBO_3:Ce^{3+}$ is much higher than that of the well-known BGO under the same conditions. The ultra fine powder of vaterite $LuBO_3:Ce^{3+}$ has been synthesized by hydrothermal and sol-gel method. However, due to the existence of the residual OH^-, the luminescence properties of these samples are not as good as that of solid state reactions. From the standpoints of luminescence efficiency and high density, $LuBO_3:Ce^{3+}$ is an attractive candidate of scintillating material. The single crystal growth of $LuBO_3:Ce^{3+}$ is under further investigation.

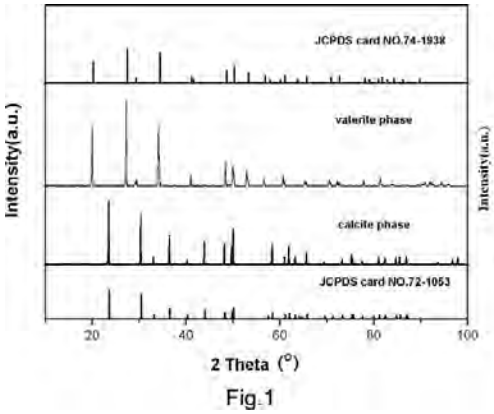

Fig.1

Fig.1.XRD patterns of $LuBO_3:Ce^{3+}$ samples.

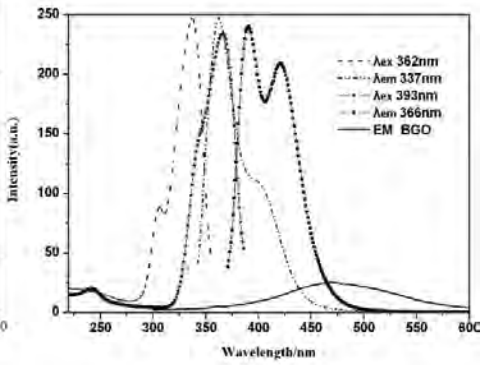

Fig.2

Fig.2. Excitation spectra and emission spectra of $LuBO_3:Ce^{3+}$ compared to BGO. calcite structure (λ_{ex}=362nm, λ_{em}=337nm) , vaterite structure (λ_{ex}=393nm, λ_{em}=366nm) .

References

[1] C.Mansuy, E.Tomasella, R.Mahiou, L.Gengembre, J.Grimblot, J.M.Nedelec, Thin Solid Films 2006, 515, 666.
[2] Yanping Li, Jiahua Zhang, Xia Zhang, Yongshi Luo, Shaozhe Lu, Xinguang Ren, Xiaojun Wang, Lingdong Sun, and Chunhua Yan, Chem. Matter. 2009, 21, 468.

P-92

Structure refinement and electron density distribution of trehalose dihydrate and anhydarate

Kunimitsu Kataoka, Shota Hasegawa, Takumi Tajima, Takuro Kawasaki and Ken-ichi Ohshima
Univ. of Tsukuba, 1-1-1 Tennodai, Tsukuba, Ibaraki, Japan

Trehalose dihydrate has been recently recognized to be an interesting sugar as substitutes for a part of function of water in the body of living things; an intracellular protectant or co-protectant against harsh conditoions, permitting to survive dehydration of freezing. Biopreservation of trehalose has been widely studied and the trehalose is much used in the handling of proteins, because of the stabilization it provides. However, there are few reports on the crystallographic investigation for the trehalose dihydrate[1,2] and anhydrate[3]. We have, therefore, determined the crystal structure and the electron density distributions (EDD) of trehalose diydrate and anhydrate using the single-crystal X-ray data for understanding of the structural characteristics.

The crystal structure of trehalose dihydrate was refined with the use of single-crystal X-ray and neutron diffraction data at room temperature and is shown in Fig. 1. Furthermore, in order to reduce an influence of atomic displacement parameters on the structure refinement, X-ray diffraction intensity has been measured at low temperature. The crystal structure of trehalose anhydrate was refined with the use of single-crystal X-ray diffraction data at room temperature and is shown in Fig. 2. All the refinement and MEM analysis were performed for obtaining the EDDs. From these results, the covalent bonding was confirmed to exist between the trehalose molecules and the internal water molecules about trehalose dihydrate and trehalose molecule and trehalose molecule about trehalose anhydrate. The EDDs, thus

obtained, was compared with that calculated using peseudopotentials and a planewave basis with the program ABINIT. Furthermore, the bond overlap population was calculated using a cluster model by the DV-Xα molecular orbital calculations model clusters

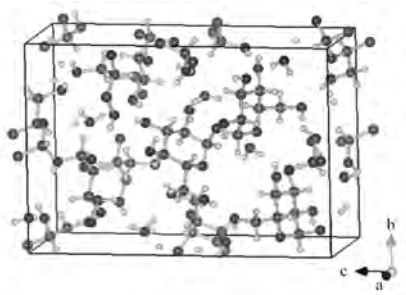

Fig. 1 Crystal structure of trehalose dihydaret

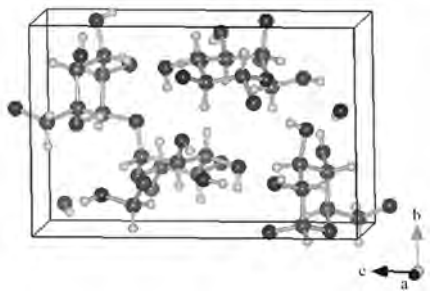

Fig. 2 Crystal structure of trehalose anhydrate

References

[1] G. M. Brown, D. C. Rohrer, B. Berking, C. A. Beevers, R. O. Gould and R. Simpson, *Acta Crystallogr. Sect. B,* **28**, 3145 (1972).
[2] T. Taga, M. Senma, and K. Osaki, *Acta Crystallogr. Sect. B,* **28**, 3258 (1972). [3] G. A. Jeffrey and R. Nanni, *Carbohydrate Research*, **137**, 21 (1985).

P-93

A single-crystal study of hollandite-type $Ba_xTi_8O_{16}$ and hexagonal $BaTiO_{3-x}$

Kunimitsu Kataoka[1,2,3], Norihito Kijima[1], Hiroshi Hayakawa[1], Junji Akimoto[1] and Ken-ichi Ohshima[2]
[1] *AIST, 1-1-1 Higashi, Tsukuba, Ibaraki, Japan*
[2] *Univ. of Tsukuba, 1-1-1 Tennodai, Tsukuba, Ibaraki, Japan*
[3] *Research Fellow of the Japan Society for the Promotion of Science*

The reduced titanium oxides form a class of compounds that can exhibit interesting electronic and magnetic properties such as an oxide superconductor in $LiTi_2O_4$ and a semiconductor-metal transition in Ti_2O_3, as well as their intriguing structure features. In the Ba-Ti-O system, several compounds including Ti^{3+} are reported in the literature until now. Hollandite-type $Ba_xTi_8O_{16}$ (x = 0.8-1.3)[1,2] are reported in three crystallographic symmetries; i) tetragonal system, ii) monoclinic system, and iii) a superstructure. On the other hand, reduced hexagonal $BaTiO_{3-x}$ are reported in a compositional range of $0 < x < 0.12$.[3] In the present study, we successfully synthesized single-crystal samples of hollandite-type $Ba_xTi_8O_{16}$ and hexagonal $BaTiO_{3-x}$, and determined the crystal structures and electron density distributions of these compounds using the single-crystal X-ray diffraction data.

$Ba_xTi_8O_{16}$ samples were synthesized at 1373 K using Fe crucibles. $BaTiO_{3-x}$ samples were synthesized at 1473 K using Ti tubes. The crystal structures of $Ba_xTi_8O_{16}$ and $BaTiO_{3-x}$ were refined using single-crystal X-ray diffraction data. Space group of $Ba_xTi_8O_{16}$ is determined as *I4/m* with the lattice parameters of a=10.145 Å, and c=2.968 Å, whose is shown Fig. 1. Space group of $BaTiO_{3-x}$ is determined as $P6_3/mmc$ with the lattice parameters of a = 5.731 Å, and c = 13.989 Å, whose is shown Fig. 2.

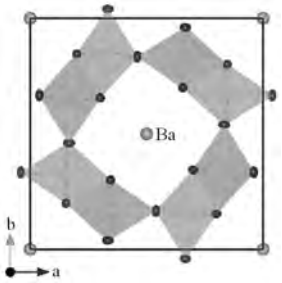

Fig. 1 Crystal structure of $Ba_xTi_8O_{16}$

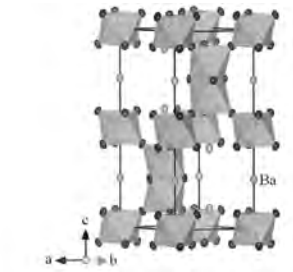

Fig. 2 Crystal structure of $BaTiO3_{-x}$

Acknowledgements*: This research was supported by the Research Fellowship of the Japan Society for the promotion of Science for Young Scientists (21・1415).*

References

[1] R. W. Cheary, *Acta Crystallogr. Sect. B,* **46**, 599 (1990).
[2] T. Höche, P. Olhe, R. Keding, C. Rüssel, P. A. van Aken, R. Schneider, H.-J. Kleebe, X. Wang, A. Jacobson and S. Stemmer, *Philosoph. Mag.*, **83**, 165 (2003).
[3] K. Kolodiazhnyi, A. A. Belik, S. C. Wimbush and H. Haneda, *Phys. Rev.*, B, **77**, 075103 (2008).

P-94

Ordered Arrangements of Nb Atoms in Layered Compounds Nb_xTiS_2

Takuro Kawasaki, Yuki Azuma, Ken-ichi Ohshima
Institute of Materials Science, University of Tsukuba, Tsukua 305-8573, Japan (Kawasaki@jb.bk.tsukuba.ac.jp)

It is well known that the transition metal disulfides MS_2 have a two dimensional layered structure, in which in-plane atoms have strong covalent bondings and that various atoms or molecules can be intercalated between the layers due to inter-layer weak van der Waals interaction. These intercalation compounds are of interest because of the low-dimensional properties and because of the application as high energy density batteries and thermoelectric materials.

Ordered arrangements of intercalated Ti atoms in self-intercalation compounds $Ti_{1+x}S_2$ are reported by Moret.[1] Because of long-range and short-range ordered arrangements of intercalated Ti atoms in the van der Waals gap layers of the compounds, superlattice reflection and diffuse scattering different according to x were appeared in the X-ray diffraction patterns.

In the present study, the layered compounds Nb_xTiS_2 with the nominal compositions x=0.20, 0.40, 0.60, 0.80 and 1.0 were prepared by chemical vapor transport technique using iodine as a transport gas. Electron diffraction patterns perpendicular to the c^* axis were obtained for the five specimens with the use of transmission electron microscope (JEOL JEM-2010). In x=0.20, honeycomb-like hexagonal diffuse scattering is appeared. In x=0.40, superlattice reflections are appeared at 1/3,1/3,0, 2/3,2/3,0 and their equivalent positions. In x=0.60, separated hexagonal diffuse scattering is appeared. In x=0.80, superlattice reflections at 1/2,1/2,0, 1/2,0,0, 0,1/2,0 and their equivalent positions are appeared. On the other hand, in x=1.0, superlattice reflection and diffuse scattering did not appear in the diffraction pattern. These revealed that the in-plane arrangements of intercalated Nb atoms are different according to the composition x in the compounds. The diffraction pattern of x=0.20 and the

schematic drawing are shown below. Further, from the result of X-ray diffraction measurements it is expected that stacking sequences of TiS_2 layer in the compounds are different from the sequence of pure 1T-type TiS_2.

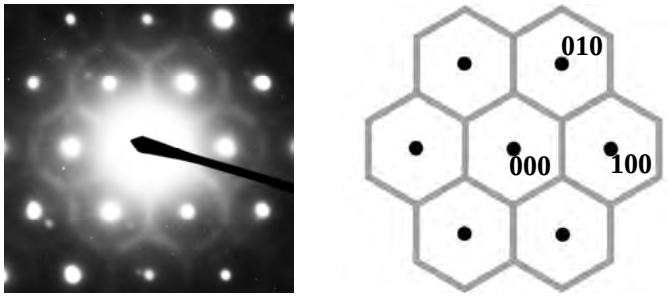

Electron diffraction pattern of $Nb_{0.20}TiS_2$

Reference

R. Moret, M. Huber, and R. Comes: Journal De Physique. **38** (1977) C7-202.

P-95 Structure Analysis of $CaMoO_4$ using Energy-filtered Precession Electron Diffraction

Jin-Gyu Kim, Sung-Woo Lee, Kyung Song, Youn-Joong Kim
Korea Basic Science Institute, 52 Eoeun-dong, Yuseong-gu, Daejeon, 305-333, Korea (jjintta@kbsi.re.kr)

Although X-ray crystallography is very useful for the structure analysis of large single or powder crystals (> 1 micron), there are several limitations for application to nano-crystalline materials. Electron diffraction is a more adequate method for structure determination in cases where X-ray diffraction is not applicable, such as multi-phase or nanometer-sized powders because of its higher interaction between electron and specimen. The dynamical effect of electron interaction, however, is the most serious problem for structure solving by electron diffraction. As a solution for this problem, the electron precession technique, first developed by Vincent and Midgley, is very useful to get intensities of electron diffraction reflections closer to kinematical characters [1].

Our electron precession unit, 'SPINNING STAR', was installed in Carl-Zeiss EM912 Ω (120kV, Ω Energy-Filter). To apply the precession technique for determining the crystal structure of $CaMoO_4$, we have calibrated and evaluated several parameters, such as precession semi-angle (φ), R_{ov} (usable diffraction radius), specimen thickness. First, precession semi-angle depends on the maximum beam tilt angle and objective lens type of electron microscope. In case of our precession system, we can use the precession angle up to ~ 2.9 degree. Second, R_{ov} is related to the wavelength of source and cell parameters of specimen. The lattice length of specimen should be smaller than 16 Å in our TEM (Transmission Electron Microscope). We experienced that it is possible to obtain quasi-kinematical diffraction data for thicker sample of a about 100 nm using precession technique.

We have performed the structure analysis of $CaMoO_4$ by using conventional SAED (Selected Area Electron Diffraction), PED (Precession Electron Diffraction), and EF-PED

(Energy-Filtered Precession Electron Diffraction). All PED patterns were acquired at precession angle of 2.7 degree and EF-PED patterns were obtained with 15 eV and 30 eV of slit widths for zero-loss and plasmon-loss filtering, respectively. As a result, EF-PED method turned out to be advantages for determining crystal structures and accurate cell parameters of $CaMoO_4$ crystal structure due to resolution enhancement, shaper peak shape as well as reducing inelastic scattering effect.

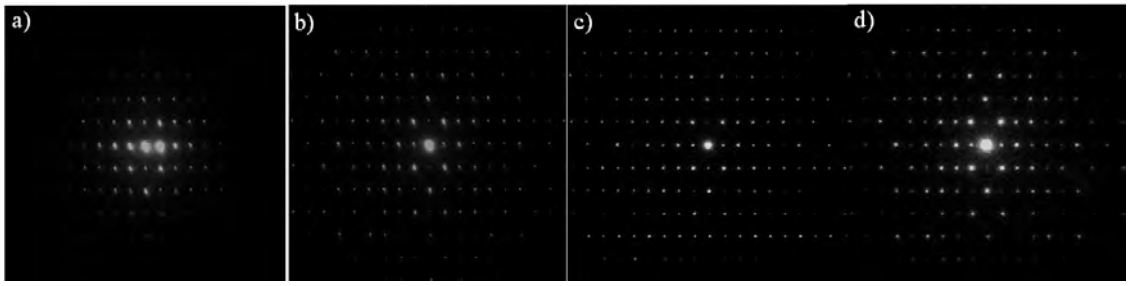

Fig. 1. Four different electron diffraction patterns for [110] zone axis of $CaMoO_4$ crystal: a) SAED pattern, b) PED pattern, c) Zero-loss filtered PED pattern, d) Plasmon-loss filtered PED pattern.

Reference

R. Vincent, P.A. Midgley, *Ultramicroscopy* **53** (1994) 271-282

P-96

Intermolecular interactions in two halogenated Imidazo [2,1-b] [1,3,4] thiadiazole derivatives

M K Kokila[1], G N AnilKumar[2], Puttaraja[1], S. S. Karki,[3] R. Vinayakumar,[3] S. Kumar[3],

[1]*Department of Physics, Bangalore University, Bangalore-560056, India (drmkkokila@hotmail.com)*

[2]*Department of Physics, M S Ramaiah Institute of Technology, MSRIT Post, Bangalore-560054, India, (anilkumargn@gmail.com)*

[3]*Department of Pharmaceutical Chemistry and Pharmacology, KLES College of Pharmacy, 2nd Block, Rajajinagar, Bangalore 560 010, India. (subhasskarki@gmail.com)*

Imidazo[2,1-b][1,3,4]thiadiazole with aryl substituted derivatives have been of interest to the medicinal chemists for many years because of their anticancer, antitubercular, antibacterial, antifungal, anticonvulsant, analgesic and antisecretary activities. Because the imidazo[2,1-b][1,3,4]thiadiazoles system is bioisosteric with imidazo[2,1-b]thiazole ring present in the well known immunomodulator. Recently in crystal engineering the study of interactions involving halogens, particularly fluorine is of major interest. Conventional hydrogen bonding is the significant interaction in many crystal structures but weak interactions involving halogens are of great importance. In the present study, we have analyzed the crystal and molecular structures of two Imidazo[2,1-b][1,3,4]thiadiazole derivatives with pharmacophoric substituents involving halogens such as bromine and fluorine with an intention of understanding the role of these halogens in stabilizing crystal structures.

Crystal structures of two compounds 2-benzyl-5-bromo-6-(4-fluorophenyl) imidazo [2,1-*b*] [1,3,4] thiadiazole(I), and 2-benzyl-5-bromo-6-(4-methylphenyl)imidazo[2,1-*b*] [1,3,4]

thiadiazole(II) were determined. It has been found that compound (I) crystallizes under Orthorhombic system, Pbca space group where as (II) crystallized under Monoclinic $P2_1/c$ spacegroup. In crystal packing of (I) is stabilized only by a number of C – H … pi interactions. A weak C – H … F interaction is also observed between the molecules. In (II) in addition to C – H …pi interaction there is also a rare C – Br …pi interaction that stabilized the molecular structure. A detailed discussion of packing & experimental results will be presented.

P-97 Crystal and molecular structure of 2-amino-*N*-(2-furylmethyl) -5,6-dihydro-4*H*-cyclopenta[*b*] thiophene-3-carboxamide'

M K Kokila[1], K. Chandra Kumar[2], Puttaraja[1], S. Mohan[3] and J. Saravanan[3]
[1]*Department of Physics, Bangalore University, Bangalore-560056, India (drmkkokila@gmail.com)*
[2] *Department of Engineering Physics, HKBK College of Engineering, Nagawara, Arabic College Post, Bangalore, Karnataka, 560045, India (chandru_mhk@rediffmail.com)*
[3] *PES College of Pharmacy, Hanumanthanagar, Bangalore, Karnataka, 560050, India.*

Thiophenes and their related derivatives containing amino and carboxyl functions have been found to exhibit broad spectrum of biological activities such as antiviral, antiinflammatory and antimicrobial activities. Specifically, 2-aminothiophene -3-carboxylates and carboxamides were recognized as allosteric enhancers for A1 adenosine receptors. In view of the above crystal structure of '2-amino-*N*-(2-furylmethyl) -5,6-dihydro-4*H*-cyclopenta[*b*]thiophene-3-carboxamide' has been presented.

The compound $C_{13}H_{14}N_2O_2S$, crystallizes under Monoclinic system, C2/c, space group, a = 21.6939(24) Å, b = 9.8547(11)Å, c = 15.1162(16) Å, β = 131.661(2)º, V = 2414.33(58) $Å^3$, Z = 8, D = 1.44 Mg m^{-3}. The data of the compound were corrected for LP factors and used for the structure solution. The structure was solved by direct methods using SIR92 program and refined using full matrix least squares on F^2 to an R value of 0.043 using SHELXL-97 program. The crystal is stabilized by intermolecular N – H … O and C – H … O hydrogen bonds.

P-98 Structures of bioactive compounds: substituted,3,2 –benzoxazaphosphinine derivatives

Krishnaiah . M[1] , Surendra Babu .V.H.H[1]and Vedavathi G.Puranik[2]
[1] *Department of Physics,Sri venkateswara University, Tirupati, 517502 India (profkrishnaiah.m@gmail.com)*
[2] *Centre for Material Characterization,National Chemical Laboratory,Pune, 411008 India (vg.puranik@ncl.res.in)*

The phosphorus heterocycles have recently attracted considerable attention owing to their unique physicochemical and potential biological properties. The oxazaphosphorine ring system bearing PO and PN units such as cyclophosmaide and its derivatives are known to be antitumor agents.

The molecular structures of 6-Bromo-3-(4-chlorophenyl)-2-(4-methoxyphenyl)-3,4-

dihydro-1,3,2-benzoxazaphosphinine 2-sulfide**[1],** 3-(3-Chloro-4-fluorophenyl)-2-(2-chlorophenoxy)-3,4-dihydro-2H-1,3,2-benzoxazaphosphorine 2-oxide**[2]** and 2-4 (-nitrophenoxy)-3,4-dihydro-6-bromo-3(1-phenylethyl)-2H-[1,3,2] benzoxazaphosphorine 2 – oxide**[3]** have been determined to study the effect of the substituents on heterocyclic moiety and their biological activity.

The six membered oxazaphosphinine ring exhibits a boat conformation with S atom in axial position in [1], a screw boat with phosphoryl O atom in axial position in [2] and a twist boat with phosphoryl O atom in equatorial position

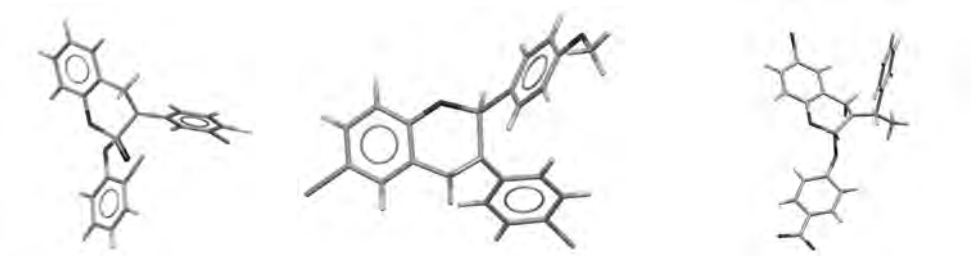

[1] **[2]** **[3]**

All the compounds show significant antimicrobial and insecticidalactivity. It has been seen that the phosphoninine group is responsible for this biological activity. The changes in conformation of the phosphoninine moiety and its effect on the activity will be discussed.

P-99 Critical evolution of surface morphology of Quartz (001) surface on alpha-incommensurate-beta structural phase transitions

Tsuyoshi Kumagai, Chibon Hyon, Yoshiki Ueno, Hikaru Terauchi and Isao Takahashi
Faculty of Science and Technology, Kwansei Gakuin University, Sanda 6691337, Japan (avl22854@kwansei.ac.jp)

SiO_2 is a ubiquitous material in the lithosphere and known to exhibit isomorphism under high temperature and pressure. Especially, structural phase transition between alpha quartz and beta quartz has attracted great attention for the decades owing to its reversibility and peculiar triangular domain structure (Dauphine twins) forming in alpha phase on cooling from hexagonal beta phase. Group theoretical considerations had predicted an incommensurate (IC) phase as an additional intermediate phase, subsequently confirmed. It is not surprising not to be reported till then, if relatively high transition temperature (T_c = 846 K) and narrow temperature range of the IC phase (ca. 1.3 K) are recalled. Although there are a lot of dielectric materials showing the Normal - IC – Commensurate (N-IC-C) phase successive phase transitions, we must regard quartz as a unique substance in which instability of acoustic phonon slightly away from the Gamma point in reciprocal space constructed by hexagonal symmetry plays an crucial role in developing the IC structure and responsible for the Dauphine twins formation. In spite of the understandings and amount of our knowledge on bulk structure on N-IC-C phase transitions, we must admit that less is known for surface structure and surface morphology when it undergoes the successive phase transitions. In the

present study, we investigated the surface structure of quartz with surface-sensitive-X-ray diffractions so as to give a novel insight into this phase transitions.

Sample was a (001) plane of synthesized quartz polished at room temperature with dimension of 20 mm x 20 mm x 1.5 mm. It was placed into a heater with a PID temperature controller mounted on an X-ray diffractometer (SmartLab, Rigaku). Sample temperature was controlled between room temperature and 950 K with a stability of 0.5 K where the sample was kept in air. Surface-sensitive X-ray diffractions we exploited were crystal truncation rod (CTR) scattering emanating from the 003 Bragg point and X-ray reflectivity (XR). Rocking curves (q_x scan) and longitudinal curves (q_z scan) of XR in 2theta range between 0 and 5-8 degrees were collected at each temperature.

In the alpha phase, a noticeable increase in width of specular XR (q_x scan) beyond the total reflection regime is reproducibly observed as the sample temperature T approaches T_c. Furthermore, specular XR in total reflection regime also shows an anomalous decrease in intensity. Both anomalies can well be fitted by $C/(T_c - T)$, indicating that the variation of surface morphology in alpha phase does accompany some critical features.

P-100 Synchrotron radiation X-ray characterization of epitaxial magnetic multilayers of yttrium iron garnet/gadolinium gallium garnet

Chih-Hao Lee[1,2], K.S. Laing[2], and M.Y. Chern[3]
1. Department of Engineering and System Science, National Tsing Hua University, Hsinchu, Taiwan. (chlee@mx.nthu.edu.tw)
2. National Synchrotron Radiation Research Center, Hsinchu, Taiwan (kslaing@nsrrc.org.tw)
3. Department Physics, National Taiwan University, Taipei, Taiwan. (mychern@phys.ntu.edu.tw)

Epitaxial magnetic multilayers of yttrium iron garnet/gadolinium gallium garnet (YIG(111)/GGG(111)) on GGG single crystal substrates using the laser ablation deposition method. In this work, X-ray reflectivity, in-plane and plane normal diffraction and truncation rod measurements were carried out to characterize in detail the epitaxial relations of the multilayer, noting that both YIG and GGG have the same cubic structure with a nearly identical lattice constant (0.03% difference). The perfection of the epitaxy can be best revealed in the observation of the in-plane forbidden (1-10) peak and truncation rod measurement. The reflectivity curves show the surface roughness is small than 1 nm. The longitudinal diffuse scattering curve as functions of two theta angle show the same pattern of oscillation as specular reflection, which indicates the thin film is in good conformation relation on each layer for the sample of YIG/GGG multilayer. The measurable intensity of the forbidden in-plane peak, YIG┌ or GGG, indicates that the structure of the YIG/GGG epitaxial film was slightly deformed. The truncation rod profile of (YIG(1)/GGG(1))12 shows a diffraction intensity of the superperiod of the sample which reveals a good in-plane solid on solid epitaxial relation.

Study on Simulation and Preparation of Spherical Diamond Film

P-101

Duosheng Li[1], Xianliang Zhou[1], Dunwen Zuo[2] , Xiaozhen Hua[1]
[1] *College of Material Science and Engineering , Nanchang Hangkong University, Nanchang 330034, China (ldsnuaa@nuaa.edu.cn)*
[2] *College of Mechanical and Electrical Engineering , Nanjing University of Aeronautics and Astronautics, Nanjing 210016, China*

Spherical diamond film has some excellent properties and is a good candidate for some applications[1-3]. FEM is a good method to simulate the fluid and temperature field of film.

Velocity, pressure and temperature fields of reaction chamber were simulated by FLUENT. Spherical diamond film was prepared on convex Mo substrate by DCPCVD, Internal quality and surface morphology were investigated by scanning electron microscopy (SEM), Raman spectroscopy. The total pressure was 46 Torr, and CH4 concentration was about 1.6%, and substrate temperature was about 1150K.The velocity, pressure and temperature fields of simulation are shown in Fig.1, Fig.2 and Fig.3 respectively.

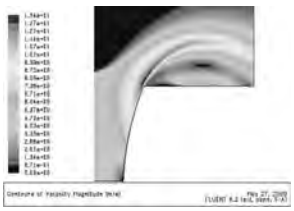

Fig.1 Velocity field of DC plasma

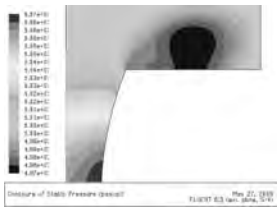

Fig.2 Pressure field of DC plasma

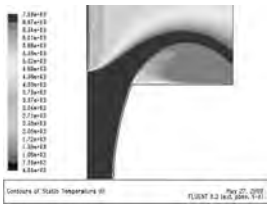

Fig.3 Temperature field of DC plasma

Fig.1 shows that plasma velocity field from the exit of anode nozzle was uniform. But the velocity field of near convex Mo substrate was not uniform, and it was much lower in center near substrate than that of the edge of substrate. Fig.2 shows that plasma velocity field fluctuates above spherical substrate, in center of plasma, the pressure is the biggest, and it tends to decrease with increasing of radius of the plasma，which is harmful to prepare high quality spherical diamond film. Fig.3 shows that there is a uniform temperature field on the substrate. It is necessary to successfully prepare spherical diamond film.

SEM micrographs of diamond films are shown in Fig.4 (a), (b) respectively.

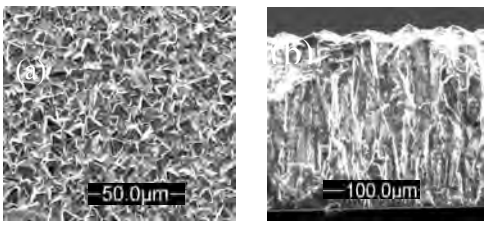

Fig.4. SEM of diamond film: (a) surface, (b) cross-section

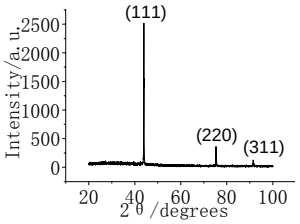

Fig.5. XRD of diamond film

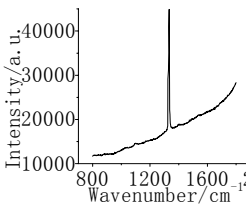

Fig.6. Raman of diamond film

Fig.4 (a) shows that the grain of spherical diamond film is uniform, compact. There were not non-diamond inclusions, and there are also not remarkable bigger gains in the film. Fig.4 (b) indicated that the columnar structure grains keep their columnar growth direction from the substrate surface to the growth surface. An average size of diamond crystal was about 15μm.Diamond (111), (220) and (311) peaks were found in Fig.5 by XRD, thus, diamond film is polycrystalline and (111) faces of diamond film are dominant. Fig.6. shows there is a sharp

diamond characteristic peak at 1332.0 cm-1 with FWHM, and characteristic peaks of polycrystalline graphite and amorphous graphite were not obviously observed. Thus, high quality spherical diamond film was prepared.

References

[1] Paul W. May, MATERIALS SCIENCE: The New Diamond Age, Science. 2008, 319(14), 1490
[2] D.S. Li, D.W. Zuo, R.F. Chen, Solid State Ionics, 179(2008), 1263
[3] I. Vlasov, O. I. Lebedev, V. G. Ralchenko, Advanced Materials, 2007, 19(22), 4058

The Topological Analysis of Minerals

P-102

Li Jia-Ju[1] Li Hui[2]
[1] *Institute of Geology and Geophysics Chinese Academy of Sciences Beijing 100029*
[1] *Shimadzu International Trading(Shanghai) Co. Limited Beijing Branch 100022*
(lijiaju_1@yahoo.com.cn) (bsljj@shimadzu.com.cn)
[2] *Beijing University of Technology, Beijing 100124 (huilicn@yahoo.com)*

The electron density distribution of Pyrite and Pyrrhotite were reconstructed with powder X-ray diffraction data in this research work. Meanwhile, the gradient of charge density and its Laplacian were also supplied. With these results, it shows obviously that the characters of bond critical points of Fe-S bond in these two minerals are different. This difference represented the bond type of Fe-S in Pyrite and Pyrrhotite and its characters of physics and chemistry.

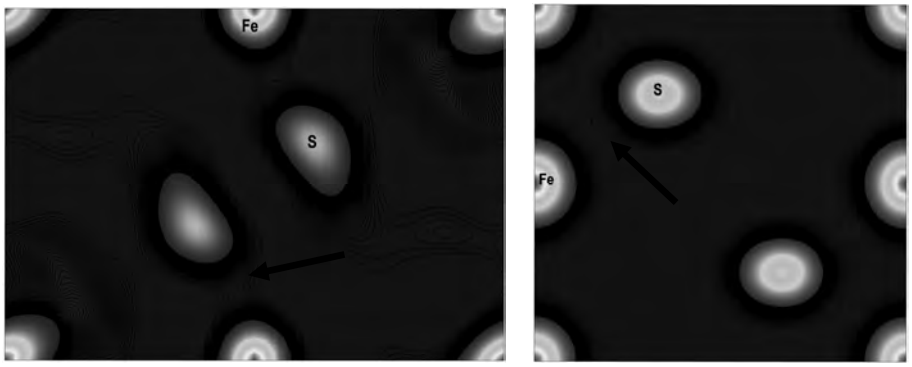

Fig. 1 The electron density of Pyrite (1-10) plane (*Left*) and Pyrrhotite (110) plane (*Right*). The charge density grids range from 0.2e/Å^3 to 3.0e/Å^3 intervals 0.05e/Å^3. The charge densities in bond critical points (Arrow) of Pyrite and Pyrrhotite are 0.335e/Å^3 and 0.25e/Å^3 respectively.

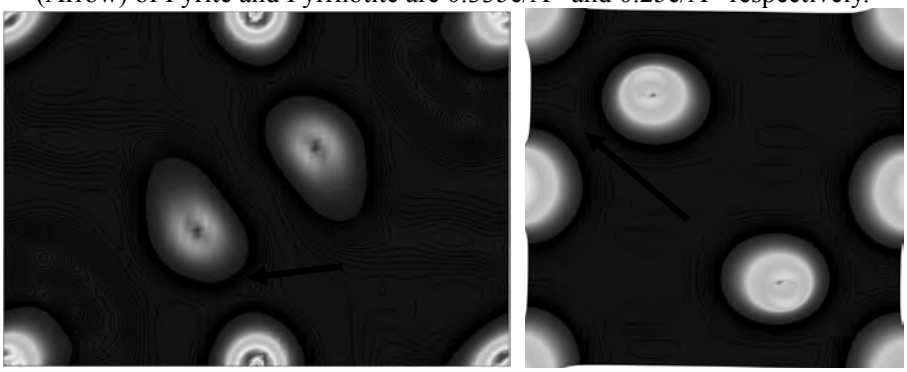

Fig. 2 The gradient of electron density of Pyrite (1-10) plane (*Left*) and Pyrrhotite (110) plane (*Right*). The grids range from 0.0e/Å^4 to 5.0e/Å^4 intervals 0.2e/Å^4. The gradient of electron density in bond critical points (Arrow) of Pyrite and Pyrrhotite equals to 0.0e/Å^4.

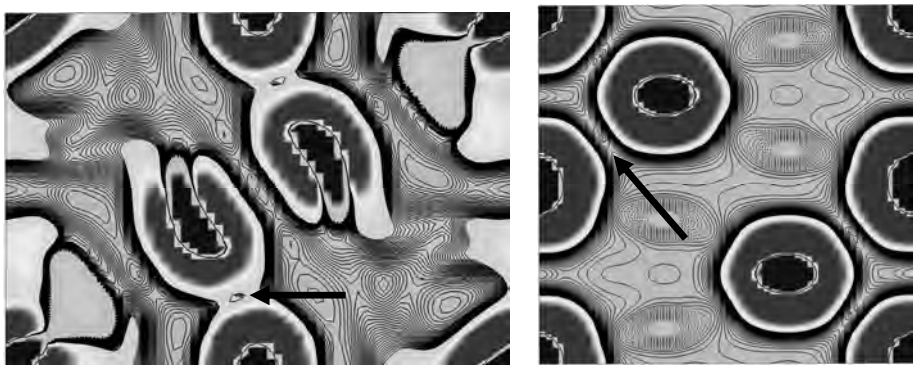

Fig. 3 The Laplacian of Pyrite (1-10) plane (*Left*) and Pyrrhotite (110) plane (*Right*). The grids range from -2.0e/Å^3 to 6.0e/Å^5 intervals 0.2e/Å^5. The Laplacian in bond critical points (Arrow) of Pyrite and Pyrrhotite are 5.4e/Å^5 and 2.0e/Å^5 respectively.

The electron density, gradient electron density and Laplacian distribution of Pyrite (1-10) plane and Pyrrhotite (110) plane show that the electron density values in BCP(bond critical point) are $\rho(r_c)_{\mathrm{ED}}$ = 0.335, 0. 25e/A^3, $\bigtriangledown\rho(r_c)_{\mathrm{GRD}}$ = 0. 0, 0. 0e/A^4 and $\bigtriangledown^2\rho(r_c)_{\mathrm{Lap}}$ = 5.4, 2.0e/A^5 respectively. The values of $\rho(r_c)_{\mathrm{ED}}$ for pyrite are higher than pyrrhotite. This means the bond strength of pyrite is higher and more stable than pyrrhotite. The bond length of Fe-S in pyrite and pyrrhotite are 2.259Å and 2.451Å respectively. It is well known, the pyrite is harder, more difficult to be oxidized and semi-conductance as germanium and diamond, while pyrrhotite having good conductibility, magnetism, easier to be oxidized and its hardness is lower.

References

1. G..V. Gibbs, R.T. Downs, D.F. Cox, et al., Z. Kristallogr., 2008, 223, 1-40.
2. K. Momma, F, Izumi, J. Appl. Cryst.., 2008, 41, 653.

P-103

XC6012 from *Xanthomonas campestris* Adopts a Novel Tetrameric PilZ Domain Structure Stabilized by a Central Parallel Four-Stranded Coiled-Coil

Tso-Ning Li[1], Ko-Hsin Chin[1], Andrew H.-J. Wang[2] & Shan-Ho Chou[1, 3]
[1]*Institute of Biochemistry, National Chung-Hsing University, Taichung, 40227, Taiwan*
[2] *Institute of Biological Chemistry, Academia Sinica, Nankang, Taipei, Taiwan*
[3] *National Chung Hsing University Biotechnology Center, Taichung, 40227, Taiwan, (shchou@nchu.edu.tw)*

Cyclic di-GMP (c-di-GMP) has emerged as an important secondary messenger, controlling a variety of cellular processes, mainly in biogenesis of extracellular components, flagella and pili, and exopolysaccharide synthesis in diverse bacteria. It is proposed to be a key regulator in bacterial evolution, during its transition from a single-cellular and motile entity to a multicellular and sessile entity. PilZ domain is found to be one of the key receptors for this important second messenger. Currently, many such PilZ domain-containing proteins have been identified, and several tertiary structures of PilZ domains capable of binding c-di-GMP with strong affinity have been determined. These include the receptor protein PA4608 from *Pseudomonas aeruginosa* (1YWU) that was determined by NMR method, and the receptor proteins VCA0042 from *Vibrio cholerae* O1 (1YLN) and PP4397 from *Pseudomonas putida*

KT2440 (2GJG) that were determined by X-ray crystallography. A co-crystal structure of the PilZ/c-di-GMP complex from *Vibrio cholerae* has also been reported (2RDE), providing more structural insights into the allosteric conformational changes triggered by the c-di-GMP binding. However, not every one of them can bind c-di-GMP tightly. PA2960 from *Pseudomonas aeruginosa* is one of such sequences, and is a protein required for type IV pilus-mediated twitching motility. However, it lacks a c-di-GMP switch loop, and the essential residues in the **D/N**x**S**xxG signature sequence required for c-di-GMP binding. It has therefore been suggested that PA2960 may represent an inactive form of the PilZ domain, or needs accessory protein domains such as PilZNR or PilZN to stabilize the bound c-di-GMP. There are thus more studies necessary to fully understand how these different PilZ domains interact with their receptors.

Xanthomonas campestris pv. *Campestris* genome was found to contain four PilZ domain-containing proteins (Xc0965, Xc2249, Xc2317, and Xc3221). Mutations of Xc2249 were found to lead to a significant reduction in the virulence of Chinese radish, a reduction in mobility, and the extracellular enzyme production. To better understand the pathogenic effect of Xc2249, we have used X-ray crystallography to determine the crystal structure of the Xc2249 homolog, XC6012 from *Xanthomonas campestris*. The final results indicate that it adopts a novel tetrameric PilZ-domain structure stabilized by a central parallel four-stranded coiled-coil, with the four PilZ domains pointing outward. Interestingly, the c-di-GMP signature motif for XC6012 is again only partially fulfilled, indicating it may need other cofactors to perform its functions.

References

Mccarthy Y, Ryan RP, O'donovan K, He Y-Q, Jiang B-L, Feng J-X, Tang J-L, Dow J. M. The role of PilZ domain proteins in the virulence of *Xanthomonas campestris* pv. *campestris*. ***Molecular Plant Pathology*** 2008;9:819-824.

New palladium-containing skutterudites $BaPd_4Sn_xSb_{12-x}$

P-104

Ying Liang[1, 2], Horst Borrmann[1], Walter Schnelle[1], Jing-Tai Zhao[2] and Yuri Grin[1]
[1] *Max-Planck-Institut für Chemische Physik fester Stoffe, Nöthnitzerstr. 40, 01187 Dresden, Germany(yliang@cpfs.mpg.de)*
[2] *State Key Lab of High Performance Ceramics and Superfine Microstructures, Shanghai Institute of Ceramics, Chinese Academic of Sciences, Dingxi Road 1295, Shanghai 200050, P.R.China(jtzhao@mail.sic.ac.cn)*

A new skutterudite $BaPd_4Sn_xSb_{12-x}$ has been synthesized and characterized. The lattice parameter refinement and the WDX analyses revealed a wide range of homogeneity for $2 \leq x \leq 7$. It is evident by the single crystal X-ray diffraction that the Sn and Sb atoms in random distribution share the framework site with different coordinate parameters caused by the difference in atomic size. The thermal electrical properties vary evidently with the tin-to-antimony ration.

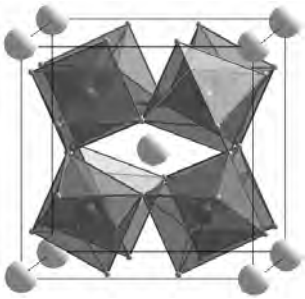

Figure 1. The crystal structure of $BaPd_4Sn_{7.3}Sb_{4.9}$. The palladium atoms (dark gray ball) are octahedrally coordinated by Sn/Sb atoms (light gray balls). The barium atoms (white ball) are icohedrally coordinated by 8 Pd atoms and 12 Sn/Sb atoms.

Table 1. Composition and lattice parameters of $BaPd_4Sn_xSb_{12-x}$

Starting Composition	Lattice parameter (Å)
$BaPd_4Sn_{7.3}Sb_{4.9}$ (crystal refinement)	9.4139(2)
$BaPd_4Sn_{6.0}Sb_{6.0}$	9.4165(7)
$BaPd_4Sn_{5.5}Sb_{6.5}$	9.4202(2)
$BaPd_4Sn_{5.0}Sb_{7.0}$	9.4246(2)
$BaPd_4Sn_{4.0}Sb_{8.0}$	9.4395(8)
$BaPd_4Sn_{3.0}Sb_{9.0}$	9.4500(8)
$BaPd_4Sn_{2.0}Sb_{10.0}$	9.4626(4)

P-105 Preparation and Characterization of Ammonium Polyphosphate with Crystal Form-V

Xinchun Liu, Wenyan Chen, Gousheng Liu
Engineering Research Center of Resources Process Engineering, Ministry of Education. East China University of Science and Technology, Shanghai 200237, China (gsliu@ecust.edu.cn)

As halogen-free and intumescent flame retardant, ammonium polyphosphate (APP) has been extensively applied in the field of flame retardant materials in recent decades. In the six different kinds of crystal forms from form-I to form-VI, more attentions have been paid to form-I and form-II at home and abroad. Except form-I and form-II, form-V APP has better stability. Until now, less study has been found for APP with crystal form-V.

In this study, APP with crystal form-V has been prepared. Ammonium phosphate is the main raw material, urea is the condensing agent. The two chemicals are mixed, heated and melted at high temperature under a dry ammonia atmosphere. Some effects, such as chemical ratio, heating temperature, time of heating and condensing, flow and pressure of dry ammonia atmosphere are investigated. Structural characterization of prepared product is carried out through XRD, SEM, and IR. Compared with the patterns of industrial-grade APP with crystal form-I, form-II, form-V and cited from literature, it is identified that the prep ared product is APP with crystal form-V. The optimal conditions are:n(ammonium phosphate salt):n($CO(NH_2)_2$）=1:1, thermal melting temperature 360~380℃, thermal melting time 50~60min, ammonia flow 1.2~1.5L/min, ammonia pressure 0.02~0.04Mpa and sustain 1h under such atmosphere.

Keywords: Ammonium polyphosphate, XRD, Structural characterization, Different crystal forms

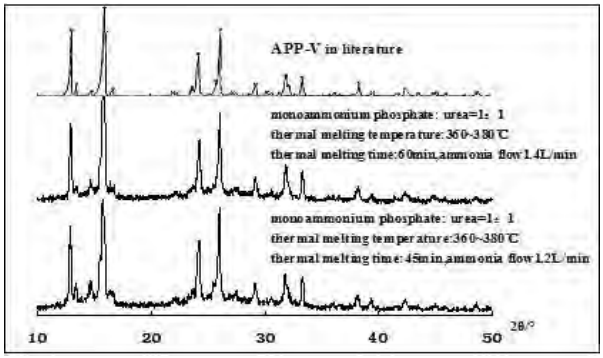

XRD spectra of prepared product and cited in literature

References

[1]Watanabe Makoto. Production of V type of Ammonium Polyphosphate[P]. JP 09235110，1997

[2]C. Y. Shen, et al. Preparation and Characterization of crystalline of long chain Ammonium Polyphosphates[J]. Am. Chem. Soc.1969, 91(1): 62~67

P-106 Acid-base approach to Valproic acid co-crystal and the crystal structure analysis

Takashi Miyamoto[1], Akiko Sekine[1], Hidehiro Uekusa[1], Etsuo Yonemochi[2], Katsuhide Terada[2]

[1] *Tokyo Institute of Technology, Japanese, 2-12-1, Oookayama, Meguro-ku, Tokyo, 152-8551, JAPAN (miyamoto.t.aa@m.titech.ac.jp)*

[2] *Toho University, 2-2-1 Miyama, Funabashi-shi, Chiba, 274-8510, JAPAN*

Valproic acid (2-*n*-Propylpentanoic acid, Fig.1) is used as an antiepilepsy drug. It is liquid in the ambient temperature and also its sodium salt has strong higroscopicity. In order to control the hygroscopic properties, organic salt co-crystal formation of valproic acid with organic base molecule would be an effective strategy. In this study, this kind of acid-base approach was examined and the crystal structures of valproic acid and organic base co-crystal were analyzed.

Through co-crystal screening experiments based on co-grinding method, co-crystal of valproic acid with 2-amino-3-hydroxypyridine (Fig.1) was successfully formed. The single crystal was obtained by recrystallization from methanol solution of equimolar amounts mixture. The X-ray structure analysis showed that it crystallized in the monoclinic space group $P2_1/c$ with cell parameters a = 12.2783(2), b =12.6185(2), c = 18.3943(3) Å and β =92.711(1)°. The asymmetric unit contains two valproic acids and two 2-amino-3-hydroxy-pyridine molecules. The major difference of two valproic acids is the conformation of propyl groups. Amino pyridine group and carboxylic group form a $[R_2^2(8)]$ heterosynthon via two N-H…O hydrogen bondings. Actually, charge interactions by the proton transfer from carboxylic acid to pyridine were observed. Also, each carboxylic oxygen atom forms hydrogen bond with the amino proton of a neighboring molecule. These hydrogen bonds form zigzag chains of valproate and 2-amino-3-hydroxypyridium ions along the a-direction (Fig.2). The chains are connected via hydroxyl OH…O hydrogen bonds to construct whole crystal structure.

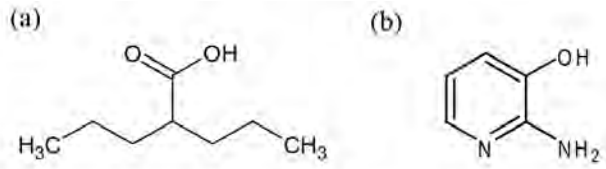

Fig.1 : (a) valproic acid (b) 2-amino-3-hydroxypyridine

Fig.2 Zigzag chain stryctyre along the a-direction

P-107 Hydrogen-bonded Network in Quaternary Ammonium Salts Used as Charge Control Agents

Jin Mizuguchi[1], Kazuya Uta[1], Yohei Sato[1], Osamu Yamate[2]
[1] *Graduate School of Engineering, Yokohama National University, 79-5 Tokiwadai, Hodogaya-ku, 240-8501 Yokohama, Japan (mizu-j@ynu.ac.jp)*
[2] *Orient Chemical Industries, Ltd., 541-0057 Osaka, Japan*

We have previously investigated the origin of the unusual high thermal stability of benzyltributylammonium-4-hydroxynaphthalene-1-sulfonate used as a charge control agent (P-51: Orient Chemical Industries, Ltd.) from the standpoint of the X-ray structure analysis. In anions of P-51, we found chains of OH···O intermolecular hydrogen-bonds between the OH group of one anion and the sulfonate O atom of the neighboring one. The present hydrogen-bond network is found to impart a polymer-like stability to P-51. In the present investigation, we extended our studies to seven derivatives of P-51, in which the cation remains the same while the anion part is modified. Among these, five derivatives are solid and possess various OH···O hydrogen-bond networks in anions: dimer, or one-dimensional, or two-dimensional network. These results lead us to conclude that the hydrogen-bond network is responsible for the high thermal stability of P-51 derivatives. On the other hand, the remaining two derivatives are found to be liquid at room temperature, probably because of the lack of intermolecular hydrogen bonds.

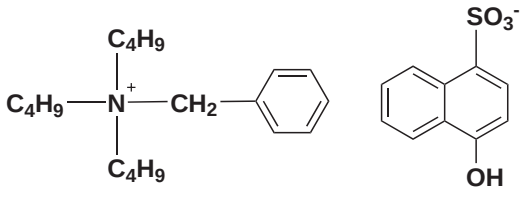

Structure of P-51

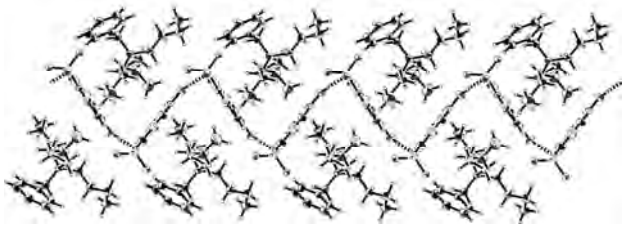

Molecular arrangement of P-51

P-108 Suppression of Pseudo-polymorphs by High Temperature Crystallization: Case Study of Oleanic Acid

Thanh-ha Nguyen[1], Alvin W-H. Siu[1],Herman H-Y. Sung[1], Henry H-Y. Tong[2], Ian D. Williams[1]
[1] *Department of Chemistry, Hong Kong University of Science and Technology, Clear Water Bay, Kowloon, Hong Kong, China (chwill@ust.hk)*
[2] *Macao Polytechnic Institute, Macau, China*

Oleanic acid ($C_{30}H_{48}O_3$) is a common chiral triterpenoid natural product found in certain Traditional Chinese Medicinal sources and, together with its derivatives, is of growing importance for treatment of a variety of ailments. It has low aqueous solubility, but can be recrystallized from many organic solvents. Commercial sources of the parent compound give a powder diffractogram consistent with a methanol solvate, which may be prepared from hot MeOH. A non-solvated form can be obtained from hot acetonitrile or acetone, whilst various alcohols yield different pseudo-polymorphs, containing the alcohol or water, several of which we have structurally characterized by single crystal diffraction. Use of solvothermal conditions, in which crystallization occurs at higher temperatures can lead to suppression of the various alcoholic pseudo-polymorphs and directly yield the non-solvated phase. The driving force behind this phenomenon, which is important for pharmaceutical processing, is the relative instability of pseudo-polymorphs at higher temperatures due to the increasing loss of entropy due to the trapped solvate molecules.

Acknowledgements*: We are grateful to RGCHK and HKUST (RPC07/08.SCI17) for financial support.*

P-109 Measurement using multiple diffraction with four-circle diffractometer

Koji Okada[1], Kiyoaki Tanaka[1], Yasuyuki Takenaka[2], Isao Kagomiya[1]
[1] *Nagoya Institute of Technology, Gokiso-cho, Showa-ku, Nagoya, Japan (Tanaka.kiyoaki@nitech.ac.jp)*
[2] *Hokkaidou University of Education, 1-2 Hachiman-cho Hakodata, Hokkaido, Japan, (bow@bussei.hak.hokkyodai.ac.jp)*

Introduction Multiple diffraction (MD) is a phenomenon observed when two or more reciprocal lattice points meet the diffraction requirement at the same time. We call the reflection being measured as the primary reflection($\mathbf{H}_1$) and the remaining one as the secondary reflection($\mathbf{H}_2$). By rotating the crystal around the scattering vector (ψ-rotation) of the primary reflection, the condition for MD to occur is surely fulfilled. In the present study a four-circle diffractometer equipped with the APD detector installed at PF14A was used. The Ψ-angles for large multiple diffraction (weakly primary beam and strong secondary beam) are observed for several primary reflections. Then the UB-matrix[(1)] were calculated by a least-squares method minimizing the sum of the differences between observed and calculated

psi-angles. In the present presentation the basic relationships and experimental results will be presented.

Calculate psi-angle $\mathbf{H}_2$ is rotated around $\mathbf{H}_1$ (Ψ-rotation) and is expressed as function of Ψ, $\mathbf{H}_2(\Psi)$. When $\mathbf{H}_1$ is on the reflection sphere with ω-2θ setting, which defines Ψ=0, the reciprocal point of $\mathbf{H}_2(0)$ locates at P_0 in Fig. 1. Then $\mathbf{H}_2(0)$ is rotated around $\mathbf{H}_1$ by Ψ_1 and Ψ_2 and cross the reflection sphere at P_1 and P_2, respectively. It also crosses the horizontal plane (x-y and x'-y' plane) at P_0' after the rotation Ψ_0. Since the absolute value of the Ψ-angles from P_0' to P_1 and P_2 are equal to Ψ', $\Psi_1 = \Psi_0 + \Psi$' and $\Psi_2 = \Psi_0 - \Psi$'. By using the relation that P_1 and P_2 are on the reflection, Ψ', $\mathbf{H}_1$ and $\mathbf{H}_2$ fulfill the following equation: $\cos\Psi' = \tan(\theta_1) \cdot (\mathbf{H}_{21} \cdot \mathbf{H}_2) / |\mathbf{H}_1 \times \mathbf{H}_2|$, where $\mathbf{H}_{21}=\mathbf{H}_1-\mathbf{H}_2$, θ_1 is the Bragg angle of $\mathbf{H}_1$. The four angles for two reflections $\mathbf{H}_1$ and $\mathbf{H}_2$ to fulfill the diffraction condition simultaneously are easily evaluated from eq. (1).

Experimental The four-angles (Ψ-angle) are measured experimentally about single crystal of Fe_3O_4 at PF14A and compared with those calculated by the above equation. Though the peak width is very narrow, significant differences were found for 25 pairs indicating the crystal orientation determined experimentally can be improved by utilizing the multiple diffraction.

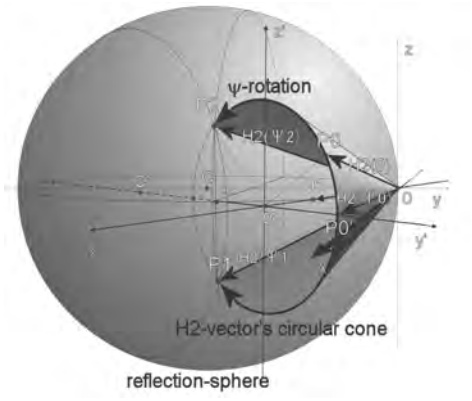

Fig.1. $\mathbf{H}_2(\Psi)$ with Ψ-rotation makes a circular cone and crosses reflection sphere

References

William R. Busing and Henri A. Levy (1967). Acta Cryst. 22, 457.

P-110 Electronic spectra of the 1:1 rhodamine B base with ethyl gallate in solution and in the solid state

Kazuyuki Sato, Hideki Shima, Jin Mizuguchi
Graduate School of Engineering, Yokohama National University, 79-5 Tokiwadai, Hodogaya-ku, 240-8501, Yokohama, Japan (d07sd201@ynu.ac.jp)

The electronic spectra of the 1:1 rhodamine B base (RBB: leuco dye) with ethyl gallate (EG: developer) have been studied in solution and in the solid state (*i.e.* in spin-coated films and in single crystals) on the basis of the crystal structure analysis. There are two crystalline phases in the 1:1 "RBB/EG" colorant at low (93 K) and room temperatures. In solution, the maximum color intensity occurs with the 1:1 molar ratio of RBB with HCl, giving an

absorption band at about 556 nm. In the solid state of spin-coated RBB/EG layers, an absorption band appears around 577 nm due to the ring opening caused by the hydrogen-bond formation between RBB and EG. However, the color intensity is found to be limited to about 80% of the maximum available value. This has been attributed to a residual fraction of RBB molecules whose lactone-ring is still closed due to steric hindrance. In addition, the polarized reflection spectra measured on single crystals of RBB/EG exhibit a drastically different spectrum (*i.e.* absorption maximum: about 480 nm) from that of spin-coated films of the amorphous state. This suggests that strong excitonic interactions of the H-aggregate type are operative in single crystals of RBB/EG that displace significantly the absorption band toward shorter wavelengths.

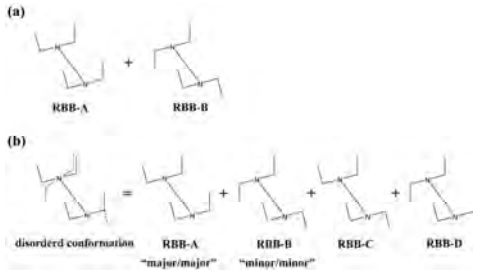

Schematic illustration of the molecular conformation: (a) 93 K and (b) RT.

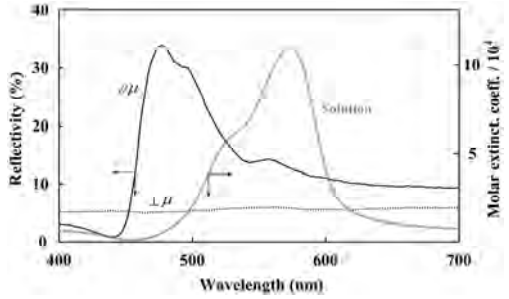

Polarized reflection spectra together with solution spectrum measured on the (010) plane of RBB/EG single crystals.

P-111 Crystal Structures and Photochromism of Indandione derivatives

Akiko Sekine[1], Yuji Karakane[1], Hidehiro Uekusa[1], Masashi Yokoyama[2], Yuki Nakai[2], Koichi Tanaka[2]

[1] *Department of Chemistry and Materials Science, Tokyo Institute of Technology, Tokyo, 152-8551, Japan (asekine@chem.titech.ac.jp)*

[2] *Department of Life Science and Biotechnology, Kansai University, Osaka, 564-8680, Japan*

It has been reported that trans-biindenylidenedione derivatives show photochromism in the solid state as evidenced by color change, from yellow to red, upon irradiation with UV and visible light [1].

The direct observation of the photoproduct and photoreactant by the single crystal X-ray analysis revealed that the photochromic reaction was caused by a Norrish Type II intra-molecular hydrogen transfer.

Recently, new indandione derivatives that have related skeleton to trans-biindenylidenedione were synthesized and found to show photochromic reaction. In this paper, we investigated the relationship between crystal structure and photochromic mechanism.

Five indandione derivatives (Fig.1) have different sizes of cycloalkanes (five- (**3**,**4**), six- (**1**,**2**), and seven- (**5**) membered ring) to modify the intra- and inter-molecular configuration. Among them, crystals of **1**, **2**, and **5** showed photochromism (yellow to orange, colorless to dark green, and colorless to green, respectively) by the photo-irradiation (>300nm) and the ESR signals were observed.

On the other hand, for both **3** and **4**, the photochromism and the ESR signals were not observed. The crystal structure analysis shows that there are no strong intermolecular interactions in crystals of **1**-**5**. The observed ESR signals indicated the mechanism would be a hydrogen subtraction by carbonyl oxygen, so the nearest H…O distances were examined.

For **1**, **2** and **5** crystals which show photochromism, the distances were 2.283(2)Å, 2.222(2)Å, and 2.221(2)Å. However, for **3** and **4** crystals which doesn't show the photochromism, the distance were between 2.601(2)Å and 2.9682(2)Å which are significantly longer than the photochromic crystals. Therefore, it is considered that new photochromism of the indandione derivatives was also caused by the Norrish Type II intra-molecular hydrogen transfer reaction same as trans-biindenylidenediones.

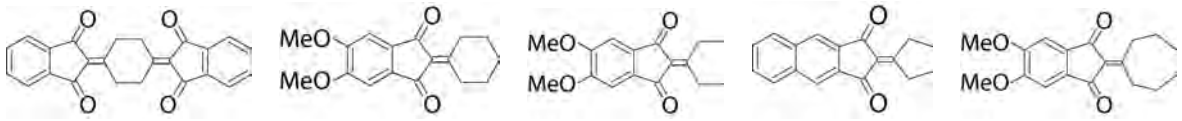

1 **2** **3** **4** **5**

Fig. 1 Indandione derivatives

Reference

Koichi Tanaka et al., *CryslEngComm.*, 2004, **6**(2), 1-4

P-112

Structural and Functional Analysis of Nup120 Suggests Ring Formation of the Nup84 Complex

Hyuk-Soo Seo, Yingli Ma, Erik W. Debler, Daniel Wacker, Stephan Kutik, Günter Blobel, André Hoelz

Laboratory of Cell Biology, Howard Hughes Medical Institute, The Rockefeller University, 1230 York Ave, New York, NY 10065, USA (hseo@rockefeller.edu)

The Nup84 complex constitutes a key building block in the nuclear pore complex (NPC). Here, we present the crystal structure of one of its seven components, Nup120, which reveals a β-propeller and an α-helical domain representing a novel fold. We discovered a previously unidentified interaction of Nup120 with Nup133 and confirmed the physiological relevance *in vivo*. Since mapping of the individual components in the Nup84 complex positions Nup120 and Nup133 at opposite ends of the heptamer, our findings indicate a head-to-tail arrangement of elongated Nup84 complexes into a ring structure, consistent with a fence-like coat for the nuclear pore membrane. The attachment site for Nup133 resides at

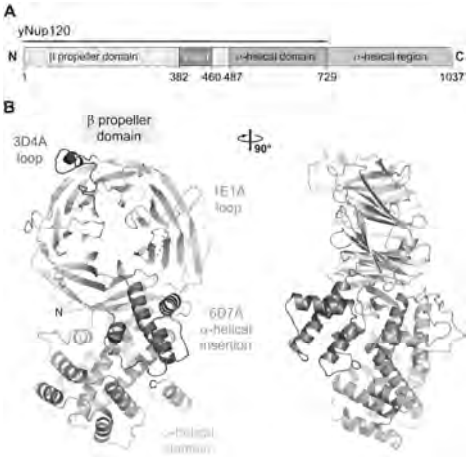

the very end of an extended unstructured region, which would allow for flexibility in the diameter of the Nup84 complex ring. These results illuminate important roles of terminal unstructured segments in nucleoporins for the architecture, function, and assembly of the NPC.

P-113 Gas Pores Formation in Laser Induced Ti Melts for Implant Prototyping

A. A. Shaikh[1], S. Dudziak[2], O. Meier[2] and T. M. Gesing[3]
[1]*Department of Chemistry, University of Dhaka, Dhaka 1000, Bangladesh (aftab74@yahoo.com)*
[2]*Laser Zentrum Hannover e. V. Hollerithallee 8, 30419 Hannover, Germany (S.Dudziak@lzh.de)*
[3]*Department of Crystallography, Institute of Geosciences, University of Bremen, Germany (gesing@uni-bremen.de)*

Ti based materials have been extensively used as implants for artificial hard-tissue replacement because of their excellent biocompatibility, superior corrosion resistance, high specific strength and low density. Although the Young's modulus of pure Ti (110 GPa) is relatively low compared to other conventional implant materials (210 GPa for stainless steel), there is a huge difference in elasticity between the Ti implant and its surrounding tissues. However, critical problems arisen by the mismatch of Young's modulus between implant and surrounding tissues are still unsolved. An alternative to improve the mechanical property mismatch is to reduce elastic modulus of pure Ti by introducing pores, thereby minimizing stress shielding effect between implant and bone where inserting. A number of biocompatible foaming agents have been developed by our research group which allows a laser induced Ti foaming without leaving the toxic degradation products in the Ti matrix. The porous samples were analysed regarding the total porosity, the allocation and the size and shape of pores by taking optical and electron micrographs together with micro-CT imaging and analysis. The porous Ti structure with maximum total porosity of 57.0% could be generated in this laser induced foaming process. The porous Ti sample with this amount of porosity is predictable to reduce the stiffness of pure Ti material. Therefore, this porous material could have high potentiality to use as implant material for hard-tissue replacement.

P-114 A Study of Tantalum Substituted Potassium Tungsten Bronzes

Md. Mahbubur Rahman Shakil[1], Altaf Hussain[2]
[1] *Department of Chemistry, Dhaka University of Engineering & Technology, Gazipur-1700, Bangladesh, (mrshakildu@yahoo.com)*
[2] *Department of Chemistry, University of Dhaka, Dhaka -1000, Bangladesh, (altaf@univdhaka.edu)*

Tungsten bronzes are non-stoichiometric ternary metal oxides having general formula A_xWO_3 where A is electropositive element and $0 < x < 1$. Because of their interesting physical and chemical properties, pure potassium tungsten bronzes have been studied extensively [1]. However, there are very few reports available on tantalum substituted potassium tungsten

bronze [2]. Therefore, attempts were made to prepare a series of compounds in the system $K_xTa_yW_{1-y}O_3$ with x = 0.30, $0.00 \leq y \leq 0.30$ and x = 0.55, $0.00 \leq y \leq 0.10$ by conventional solid state synthesis method.

The samples were characterized with XRD, SEM/EDX and optical spectroscopy. X-ray powder patterns reveal that the samples with nominal compositions x = 0.30, $y \leq 0.30$ show hexagonal tungsten bronze (HTB) type pure phase and the samples with x = 0.55, $0.02 \leq y \leq 0.10$ show a mixture of two phases (K-HTB and tetragonal potassium tungsten bronze, K-TTB). Structure refinements of K-HTB samples using Rietveld fitting procedures reveal a decrease in *a* and an increase in *c* lattice parameters with increasing nominal Ta content. The elemental compositions of the crystals determined by SEM/EDX analysis also show an increase in Ta content with increasing y. Investigations of the optical reflectivity and the infrared absorption spectra of powder $K_{0.3}Ta_yW_{1-y}O_3$ samples indicate a decreasing polaron concentration with increasing Ta content.

References

[1] Ph. Labbe, Key Engineering Materials 68 (1992) 293-339.
[2] A. Deschanvres, M. Frey, B. Raveau, J. C. Thorhazeau, Bull. Soc. Chim. Fr. 9 (1968) 3519.

P-115 Stability and tinctorial strength of black leuco-colorants as viewed from the crystal structure of a phenolic developer

Hideki Shima, Kazuyuki Sato, and Jin Mizuguchi
Graduate School of Engineering, Yokohama National University; 79-5 Tokiwadai, Hodogaya-ku, 240-8501 Yokohama, Japan (d09gd230@ynu.ac.jp)

2-[(4-Hydroxyphenyl)sulfonyl]-phenol (BPS) is a well-known developer for black leuco-dyes (for example, 6'-(diethylamino)-3'-methyl-2'-(phenylamino)-spiro[isobenzofuran-1(3H),9'-[9H]-xanthen)-3-one]: ODB) in thermosensitive papers. Although BPS is a small molecule (molecular weight: about 250), it is thermally stable as characterized by a high melting point of about 184 °C. Furthermore, BPS is also known to stabilize the 1:1 "ODB/BPS" system. Because of this, structure analysis of BPS has been carried out in order to elucidate the stability of BPS itself as well as its "leuco/developer" system. Then, we found that one BPS molecule is hydrogen-bonded to four different neighboring ones, forming an OH···O two-dimensional hydrogen-bond network. This ensures a high thermal stability of BPS. On the other hand, in the "ODB/BPS" system, only one of the four hydrogen bonds in BPS is used for the formation of the 1:1 "ODB/BPS" colorant while the remaining three hydrogen bonds keep the network. As for the tinctorial strength in spin-coated ODB/BPS, the color intensity is found to be limited to about 70 % of the maximum available value. This is because there is a fraction of ODB molecules whose lactone-ring is still closed due to the steric hindrance.

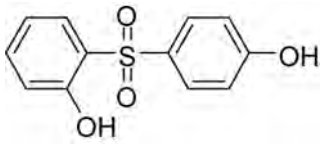

Molecular structure of BPS

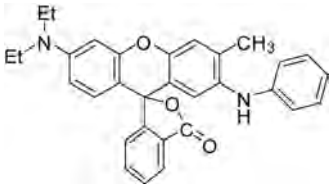

Molecular structure of ODB

P-116

Crystallographic statistical studies of the decavanadate anion: toward a prediction of the non-covalent interactions

Anne Spasojević – de Biré[1] , Nada Bosnjaković-Pavlović
[1] *Laboratoire "Structures Propriétés et Modélisation des Solides", UMR 8580 du CNRS, Ecole Centrale Paris, 92295 Châtenay-Malabry, France (anne.spasojevic@ecp.fr)*
[2] *Faculty of Physical Chemistry, University of Belgrade, P.O.Box 47, 11001 Belgrade, Serbia (nadab@ffh.bg.ac.rs)*

More than 100 structures containing the $[V_{10}O_{28}\ H_x]^{6-x}$ anion has already been published. From a geometric point of view, the decavanadate anion $[V_{10}O_{28}]^{6-}$ appears very rigid with really small variations in interatomic distances or bond angle values.

We have retrieved from the organic-organometallic database (CSD), the protein data base (PDB) and an extensive bibliographic search 30 different crystalline structures, which imply 600 contacts for which the structure is of excellent crystalline quality. In a previous study, we have experimentally determined the electron and electrostatic properties of two decavanadate based compound $Na_3V_{10}O_{28}(C_4N_3OH_5)_3(C_4N_3OH_6)_3 \cdot 10H_2O$ and $(NH_4)_6\ [V_{10}O_{28}]\ .\ 6H_2O$. From these results we have predicted the preferential non-covalent interactions (figure 1a) with the different oxygen atoms of the decavanadate anion. These predictions are confirmed, in this statistical study. The non-covalent interactions are strongly different depending on the oxygen atom type. The Ob and Oc oxygen atoms, for which the electrostatic potential in the vicinity have the lowest value, are involved mainly in the strong O-H…O, N-H…O while Of or Og are mainly involved in weakest hydrogen bonds such as C-H…O or cation interactions. (figure 1b).

These results are important in the context of the various biological applications of the decavanadate such as, for example, inhibition of the Ca^{2+} ATPase, myosin ATPase, and new development in insulin mimetic.

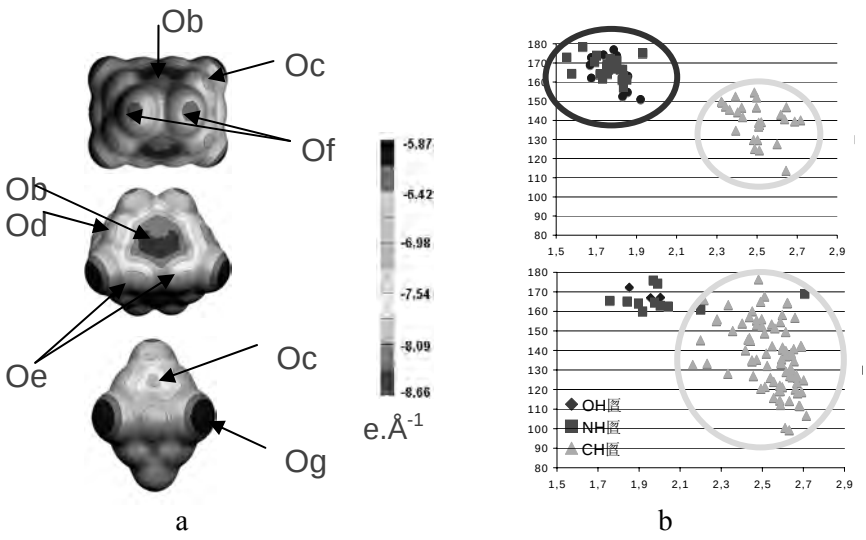

Figure 1. a) Molecular surface of the decavanadate anion colored by the experimental electrostatic potential values. b) Distribution of the hydrogen bonds observed between an OH, NH or CH moiety and an oxygen of the decavanadate anion ; x axis : H…O distance (Å) ; y axis DH…O angle (°) ; top Ob, bottom Og.

P-117

Non Photochemical Light Induced Nucleation. A tool to crystallize polymorphs on demand ? Application to carbamazepine.

David Miret[1,2], Janice Aber[2], Bruce Garetz[2], Philippe Scouflaire[3], Anne Spasojević – de Biré[1]

[1] *Laboratoire "Structures Propriétés et Modélisation des Solides", UMR 8580 du CNRS, Ecole Centrale Paris, 92295 Châtenay-Malabry, France (anne.spasojevic@ecp.fr)*

[2] *Department of Chemistry, Polytechnic Institute of New York University, New York, USA (bgaretz@duke.poly.edu)*

[3] *Laboratoire EM2C, UPR 288 du CNRS, Ecole Centrale Paris, 92295 Châtenay-Malabry Cedex, France (philippe.scouflaire@em2c.ecp.fr)*

There is tremendous pressure on the pharmaceutical industry to understand the polymorphism of drugs in order to control and produce the most stable and effective polymorphs. There is a growing awareness of the effects of polymorphism and pseudo-polymorphism on the properties of drugs, such as their physical and chemical stability, solubility, dissolution rate, bio-availability, and mechanical properties, and their consequences on the manufacturing process. We have developed a fundamental approach to study polymorphism, which combines high-resolution X-ray diffraction and ab initio theoretical calculations. That would enable us to study the consequences of drug polymorphism on the physical and chemical properties of drugs. Ideally, the experimental study of polymorphism requires the possibility to crystallize the desired polymorphic forms "at will" and to obtain new, yet uncharacterized phases.

Garetz and Myerson have invented an original nucleation method, termed NPLIN, "Non-Photochemical Light-Induced Nucleation" that makes it possible to control the nucleation process. We have already implemented this method at Ecole Centrale Paris and tested it successfully on glycine.

Carbamazepine is anti-epileptic drug, a highly polymorphic compound (4 true polymorphs, more than 20 hydrates or solvates) generally studied as a model compound for studying polymorphism. It represents a suitable compound for the demonstration of the feasibility of the NPLIN method for drug compound.

The polymorphs obtained after crystallization under NPLIN method will be discussed according to the hypothesis that the optical Kerr effect is involved in the NPLIN mechanism.

a b

Figure 1. a) Schematic representation of the NPLIN method. b) Dimer of carbamazepine molecules involved in the 4 thrue polymorphs.

P-118

Investigation of Lattice dynamics and Anharmonicity of Raman modes in $BaWO_4$ crystal

J. Suda[1], P. G. Zverev[2], O. Kamishima[3], J. Kawamura[3] and T.Hattori[4]
[1] *Department of Electric Engineering, Kushiro National College of Technology, Otanoshike-nish, kushiro, 084-0916, Japan, (suda@kushiro-ct.ac.jp)*
[2] *A M Prokhorov General Physics Institute Russian Academy of Sciences, 38 Vavilov Street, Moscow 119991, Russia,(pgz2000@yandex.ru)*
[3]*Institute of Multidiscpilinary Research for Advanced Materials, Tohoku University, Katahira, Aobaku, Sendai 980-8577, Japan*
[4]*Department of Applied Physics, Faculty of Science, Tokyo University of Science, Tokyo 162-8601, Japan*

The phonon-dispersion relations (Fig. 1) of $BaWO_4$ crystal are calculated using the Lattice dynamical calculations approach described earlier [1]. Spontaneous Raman spectra (Fig. 2) in the $BaWO_4$ were measured in the temperature range 10-295K for a body-centered tetragonal phase [2]. The temperature dependence of linewidth of the Eg (72 cm^{-1}) and the SRS-active Ag (926 cm^{-1}) were analyzed using TDOS (Fig. 3) due to cubic term. The calculated results well describe the observed ones in this temperature range in Fig. 4. Also, the variation of linewidth of the 72cm^{-1} peak is also about 1.8 times greater than those for the 926cm^{-1} peak. The scattering of a thermal phonon by observed phonons dominates phonon-phonon interactions on the lower-frequency mode [the Eg (72 cm^{-1})]. Phonon-phonon interactions on the higher mode [the Ag (926 cm^{-1})] are dominated by the decay of the observed phonons into two phonons having lower energies. We found that this originates in a clearly large phonon band gap (Fig. 1) in the PDOS (phonon density of states) that produces a difference in anharmonic effects on each peak's channels. This result is similar to that in the high-temperature phase in the case of $LaGaO_3$ [3].

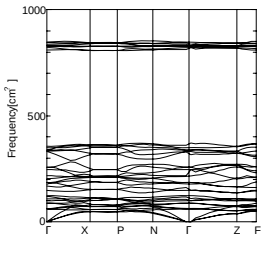

Fig.1

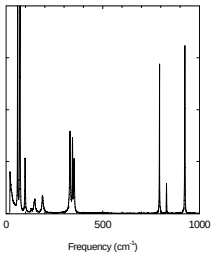

Fig.2

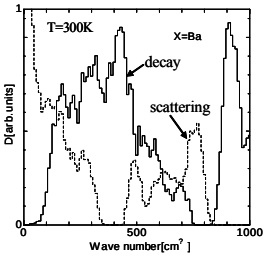

Fig.3

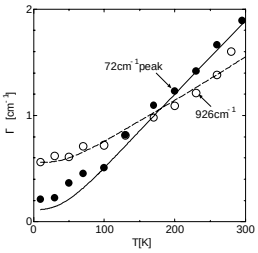

Fig.4

References

[1] J. Suda and T. Sato, *J. Phys. Soc. Japan.* **66**, 1707(1997).
[2] T. T. Basiev, A. A. Sobol, Yu. K. Voronko, P. G. Zverev, Optical Materials, **15**, 205 (2000).
[3] J. Suda *et al.*, *J. Phys. Conf. Ser* **92**, 012148(2007).

P-119 Absolute Structure Determination of Organic Compounds: an Update

Herman H-Y. Sung[1], Thanh-ha Nguyen[1], Zoltan Gal[2], Ian D. Williams[1]
[1] *Department of Chemistry, Hong Kong University of Science and Technology, Clear Water Bay, Kowloon, Hong Kong, China (hermans@ust.hk)*
[2] *Oxford Diffraction Ltd., Abingdon, United Kingdom.*

There has been a renaissance in the use of copper X-radiation for small molecule structures, in part due to the advent of dual wavelength diffractometers. One advantage for pure light atom organic molecules is the larger anomalous scattering terms for softer Cu-Kα radiation offers realistic prospects for absolute structure determination. The classical method of careful measurement of strongly differentiated Friedel pairs is not readily attempted with modern CCD diffractometry. In this paper we report a summary of absolute structure determination for a range of synthetic and natural product organics. Even with a data set of reasonable quality the Flack x parameter is typically indeterminate since its esd is often 0.15-0.20. Results are compared using a new approach using Bayesian statistics (the Hooft y parameter) available in the PLATON program package. The new method appears slightly more robust and has the advantage of quantifying the probability of chirality determination. Attempts to solve organic absolute structures using Mo-Kα data are also reported, including use of multi-pole refinement.

***Acknowledgements**: The Research Grants Council of Hong Kong and HKUST are gratefully acknowledged for funding of this work through grant RPC07/08.SCI17.*

P-120 Crystal structure and phase transition of a lead-based inorganic-organic perovskite ($C_5H_{10}NH_2$) $PbBr_3$

Kota Takano , Munehiko Nakatsuma , Miwako Takahashi and Ken-ichi Ohshima
Institute of Materials Science, Unviersity of Tsukuba, Japan
(takano@jb.bk.tsukuba.ac.jp)

Organic-inorganic hybrid perovskites have been synthesized and widely studied. They are low-dimensional compounds and exhibit unique physical properties like anisotropic

conductivity and structural phase transitions due to a structural instability. Lead-halide perovskites $(C_5H_{10}NH_2)PbX_3$ (X=I, Br, Cl) are one-dimensional semiconductors consisting of one-dimensional chains of face-sharing lead-halide octahedra and barrier parts of $C_5H_{10}NH_2^+$ molecules. For $(C_5H_{10}NH_2)PbI_3$, structure and physical properties have been extensively studied. It has a structure of orthorhombic $C222_1$ (No.20) and undergoes temperature induced successive phase transitions and a pressure-induced transition. For $(C_5H_{10}NH_2)PbBr_3$ on the other hand, there are very few studies[1] and its precise structure has not been determined yet. In this research, we synthesized single crystals of $(C_5H_{10}NH_2)PbBr_3$ and investigated its crystal structure using single crystal X-ray diffraction (XRD*)*. The structure at room temperature is determined to be monoclinic $P2_1$ space group (No.4). The phase transition in $(C_5H_{10}NH_2)PbBr_3$ was also studied using Differential Scanning Calorimetry (DSC) and XRD for a temperature range of 100K ~ 420K. We found a phase transition occurs at around 380K-410K and the structure transforms to orthorhombic $C222_1$ in high temperature phase.

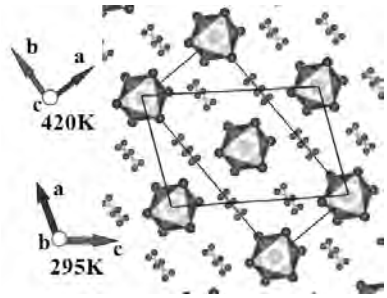

Fig.1. Crystal structure at room temperature and 420K.

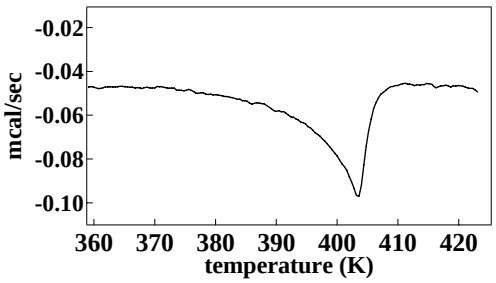

Fig.2. The DSC curve of $(C_5H_{10}NH_2)PbBr_3$.

Reference

A. Bonamartini Corradi *et al*.: Inorganica Chimica Acta **254** (1997) 137-143.

P-121

Super accurate structure factor measurement ad PF14A

Kiyoaki Tanaka[1], Yasuyuki Takenaka[2], Terutoshi Sakakura[1], Shirou Fanahashi[1], Koji Okada[1]

[1] *Nagoya Institute of Technology, Gokiso-cho, Showa-ku, Nagoya, Japan (Tanaka.kiyoaki@nitech.ac.jp)*

[2] *Hokkaidou University of Education, 1-2 Hachiman-cho Hakodata, Hokkaido, Japan, (bow@bussei.hak.hokkyodai.ac.jp)*

Introduction We have been investigated the 4f-electron density distribution[1)] and realise that the accuracy of the structure-factor measurement with the laboratory X-ray source and diffractometer is very close to its limit and more accurate data should be collected. Thus, the research aiming to measure structure factors of all reflections with the accuracy of 0.1 % was started.

Experimental Since more than 2.5x105 photon counts are necessary to reduce the statistical counting error less than 0.1% and since the multiple diffraction should be avoided with ψ-scan, the four-circle diffractometer equipped with the APD detector installed at PF14A was used. Since high order reflections of CeB_6 (space group pm-3m, a=4.1407A) is still strong (the largest ratio of the structure factors is 9.8.), 5800 reflections in the full space were

measured with the statistical counting error less than 0.1% in five days. When reflections deviated more than 2% from the mean of the symmetry related reflections they were measured again. The reference reflections which were measured to see the stability of the experiment were not fluctuated more than 1% after the intensity normalization using the monitor counts measured by the ionic chamber (IC). This is due to the top-up operation recently started at PF. The ψ-rotation was made possible for the diffractometer at BL14 and the multiple diffraction were avoided though it can't be avoided for some reflections even with the parallel SR beams[2]. When the secondary reflection comes on the Ewald sphere after the primary reflection, the intensity of which is measured, with the delay angle of 1.5 times of the sum of the FWHM's (full width at half maximum) of the two reflections, 1010 secondary reflections were judged to be affected by the MD effect. FWHM of five reflections was averaged to be 0.0126°and used to evaluate MD.

Refinement Starting from the final parameters of our previous refinement at room temperature[3], the scale factor, atomic parameters and type I extinction parameters were refined. R factors without and with the reflections affected by MD are 0.00610 and 0.00606. After the XO analysis R factor was reduced to 000433. This indicates the measurement with the SR gave reliable results. The difference density after the spherical-atom refinement clearly revealed peaks of 0.25eÅ^{-3} due to 4fj=5/2Γ_8. After the XAO analysis[4] these peaks were deleted. However the differences between the observed and calculated structure factors of low-order strong reflections are still large. They are more than 10 times of their statistical counting errors.

Discussion Judging from the very low R factors the measurement was successful. The intensity of the incident beams was monitored with the IC. However it is easily influenced by the Xe gas pressure passing the IC. Actually the monitor counts varied sometimes more than 5%. However the structure factors of the reference reflections which were normalized using the monitor counts were stable indicating the correction by the monitors was successful. Thus if more reliable monitor is used, the accuracy of the measurement will be enhanced. The large differences between the observed and calculated structure factors remained in the low order strong reflections indicating the anisotropic extinction correction is not good enough.

References

1) R. Makita et al. (2007) *Acta Cryst*. B**63**, 683-692.
2) Y. Takenaka et al. (2008). *Acta Ceryst*. A**64**, C566.
3) K. Tanaka & Y. Onuki (2002). *Acta Cryst*. B**58**, 423-436.
4) K. Tanaka, et al (2008). *Acta cryst.* A**64**, 437-439.

P-122 Surface Morphology and Crystallinity of Poly(hydroxybutyrate)/Poly(L-lactic acid) Blends

Akihisa Tokuda, Takashi Asano, Yusuke Oji, Yukihiro Ozaki, Hikaru Terauchi, and Isao Takahashi
Faculty of Science and Technology, Kwansei Gakuin University, Sanda 6691337, JAPAN (adl28058@kwansei.ac.jp)

For past decades, biodegradable polymers have attracted a lot of attention due to the

world-wide concern on environmental problem and preservation of fossil fuels. Polymers are often used as films and fibers where surface properties become more and more important than those of bulk. Even for biodegradable polymer thin films and fibers, controlling surface morphology and structure is a critical issue for practical usage in near future. Polymer blend (polymer alloy) is a widely-accepted effective technique for improving the physical properties of polymeric materials. However, we must admit that little is known for ultrathin films of blended biodegradable polymers. In the present study, we study crystallization and morphology of the biodegradable polymer blends with surface-sensitive X-ray diffraction techniques.

Poly(hydroxybutyrate)[PHB] is a biodegradable crystalline polymer which is transparent, good odor and indicates decent thermo-plasticity, biocompatibility and relatively high melting point. All of such properties make PHB a promising biodegradable polymer. Therefore, controlling the crystallinity in the surface region and thin films also affecting the surface morphology becomes an essential technique for delicate fabrications in near future.

In the present study, we study thin films of PHB blended with another biodegradable polymer, Poly(L-lactic acid) [PLLA] to investigate how PLLA affects the surface structure and morphology of PHB film with thickness of several nm. The spin-coated polymer blends were prepared on Si(100). X-ray reflectivity (XR) and grazing incident X-ray diffraction (GIXD) were chosen as tools for investigation of surface morphology and crystallinity in the surface region, respectively. Atomic force microscopy was also used to observe surface morphology. From weight ratio dependence and molecular weight dependence of PLLA on crytallinity and morphology, we found that a small amount of PLLA (ca. 10wt%) effectively retards the crystallization of PHB and makes the surface sufficiently flat in PHB/PLLA films, which we never have had corresponding results for bulk samples. We confirm that PLLA is an appropriate material which affects the surface morphology of ultrathin PHB without deteriorating its biodegradability.

P-123 Status Report on Super High Resolution Powder Diffractometer at J-PARC

Shuki Torii[1], Takashi Kamiyama[1], Takashi Muroya[1], Setsuo Sato[1], Hidenori Sagehashi[1], Ryoko Oishi[1], Takahiro Morishima[1], Teguh Panca Putra[1], Junrong Zhang[1], Kenji Iwase[2], Masao Yonemura[2], Akinori Hoshikawa[2], Toru Ishigaki[2], Susumu Ikeda[1]

[1] *High Energy Accelerator Research Organization, KEK Tokai Campus, 2-4 Shirakata Shirane, Tokai, Naka, Ibaraki 319-1195, Japan, (torii@post.kek.jp)*

[2] *Ibaraki University, Ibaraki Quantum Beam Research Center, 162-1 Shirakata, Tokai, Naka, Ibaraki 319-1106, Japan,*

At the end of May in 2008, the first neutron was produced successfully from a spallation neutron source in Japan Proton Accelerator Research Complex (J-PARC). High resolution Bragg reflections were obtained using the *Sirius* diffractometer chamber at Super High Resolution Powder Diffractometer (SuperHRPD) beam line at Materials and Life Science Experimental Facility (MLF). We divide and consider the project of SuperHRPD in two phases. In the "Phase-I" of our project, we started up quickly by using the existing *Sirius*

chamber. Simultaneously, we were carrying out basic study to design and construct a new SuperHRPD chamber, and the *Sirius* chamber will be exchanged for new one in summer of 2009. We have succeeded in achieving the best resolution among all the neutron powder diffractometers in the world, a part of detector pixels of SuperHRPD has achieved $\Delta d/d$ = 0.035 %. Currently, about 300 detectors have been installed in the backward detector bank (2θ = 150º ~ 175º), and several standard samples including Si (NIST SRM640c) have been measured. As the result, a chi-square value of 2.08 was obtained from a refinement of the Si powder data using a Z-Code developed by our group. In the "Phase-II", we will install a new chamber to improve *S*/*N*, and achieve better resolution as well as intensity. In the design of a new chamber, a detector solid angle is increased, *d*-range / *Q*-range is expanded, and also has options of high-intensity mode and high-resolution mode with incident collimations.

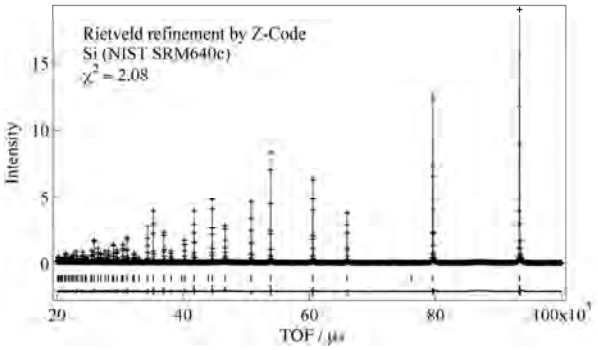

Fig.1 The fitting result using a Z-Code

Crystal Structure Comparisons of Tetrakis(4-hydroxyphenyl)alkane Inclusion Crystals

P-124

Kazuyuki Toyota[1], Hidehiro Uekusa[1], Natsuki Amanokura[2], Masami Kaneko[2], and Hiroshi Suzuki[2]

[a] *Department of chemistry and materials science, Tokyo Institute of Technology, 2-12-1 Ookayama, Meguro-ku, Tokyo, JAPAN*

[b] *Nippon Soda Co.Ltd, JAPAN*

Inclusion crystals have unique characteristics such as controlled guest solubility or temperature dependent guest releasing, which are relevant to the structure of host framework enclosing guest molecules. Hence it is of great importance to investigate and develop host frameworks to design new functional materials. 1,1,2,2-tetrakis (4-hydroxyphenyl)ethane, TEP (*Fig.1*), has four phenyl groups in different directions to build various types of hydrogen bonding host frameworks corresponding to the types of guest molecules. In our previous study, three kinds of host frameworks accommodating different kinds of guest molecules via hydrogen bonds were analyzed to show TEP has well-qualified ability as an inclusion host molecule.

In this study, new host molecules are synthesized as the modification of TEP, and their inclusion crystal structures are analyzed to compare the host frameworks. By making the central alkane chain longer, new host molecules, TBP and TPP, (*Fig.1*) were synthesized to make inclusion crystals with small organic molecules. In contrast to practically rigid TEP molecule, their longer alkane chains give more conformational flexibility so as to form new

host frameworks that are different from TEP inclusion crystals.

TBP-THF-H_2O inclusion crystal is an example of new host frameworks (*Fig.2*). In the channel structure of TBP host framework, THF molecules are aligned in 1-dimentional manner. Because new hosts should form larger channel in the framework by utilizing their flexibility, larger organic molecule guests which could not be accommodated to the TEP frameworks are employed as guests in order to demonstrate the inclusion ability of new hosts.

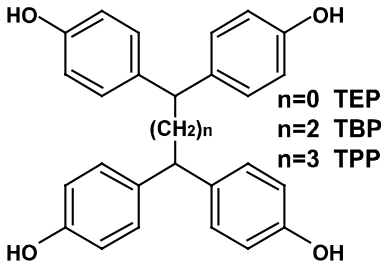

Fig.1 Molecular structures of hosts. n=0,2,3 corresponds to TEP, TBP, TPP, respectively.

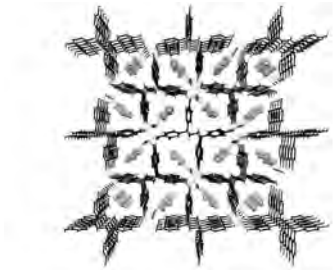

Fig.2 The crystal structure of TBP-THF-H_2O projected from a-axis.

P-125

Pharmaceutical Polymorphs and their Phase Transitions Investigated by *Ab Initio* Structure Determination from Powder Diffraction Data

Hidehiro Uekusa[1], Etsuo Yonemochi[2], Katsuhide Terada[2]
[1] *Tokyo Institute of Technology, Ookayama 2, Meguro-ku, Tokyo 152-8551, JAPAN (uekusa@cms.titech.ac.jp)*
[2] *Toho University, 2-2-1 Miyama, Funabashi-shi, Chiba, 274-8510, JAPAN*

Many pharmaceutical organic crystals show polymorphism including hydrate or solvate crystals. As their physicochemical properties such as stability, solubility, and bioavailability differ from each other depending on the crystal structures. Also by a mechanical treatment or during storage, unexpected phase transition among (pseudo-) polymorphs is sometimes observed. Thus, in order to utilize the pharmaceutical polymorphic crystals as API, structural investigation of phase transition phenomena is essential. However, after the phase transition, a single crystalline form usually tends to degrade and becomes powdery crystal. In such case, *ab initio* structure determination from powder diffraction data (SDPD) is efficient technique to analyze the crystal structure from PXRD.

In this study, crystal structures and phase transitions of pharmaceutical polymorphs are investigated by SDPD technique.

1. Thermal transformation of Tolbutamide polymorphic crystals

Tolbutamide (Fig. 1) is a hypoglycemic agent, and has four polymorphic forms. From the heat of solution measurement, it was found that the stability of Form III decreased above 303K due to the thermal phase transition to a new form. The crystal structure was determined from high resolution PXRD using synchrotron radiation by SDPD technique. In the new form of crystal, tolbutamide molecule shows a twist in the terminal chain orientation, and the molecular packing is almost similar [1].

2. Two step dehydration process of Lisinopril dihydrate

Pharmaceutical hydrates are well used as API (Active Pharmaceutical Ingredients) and often show dehydration phenomena. Lisinopril (Fig. 2) is used as an anti-hypertension drug in the dihydrate form. A DSC-PXRD measurement indicated that water molecules were released at 373K and 383K to form monohydrate and anhydrous form, respectively. Both crystal structures were successfully analyzed from high resolution PXRD. The dehydration mechanism is illustrated as the two step water molecule releasing from two different channel structures in order. During the process, terminal phenylethyl group turns to close the empty channel and to stabilize the structure.

3. Pharmaceutical co-crystal formation by co-grinding

Co-grinding of pharmaceutical compound with co-crystal former sometimes gives a new co-crystal having favorable properties. Co-crystal of valproic acid and L-arginine (Fig. 3) was obtained only by this method to resolve the hygroscopicity of API. Because the ground co-crystal was powdery crystal, the crystal structure was analyzed by SDPD technique to reveal unique layer structure and very stable crystalline form even under high R.H. conditions.

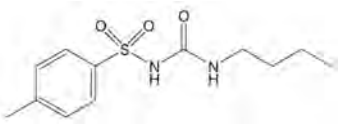

Fig.1 Tolbutamide

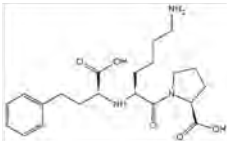

Fig.2 Lisinopril

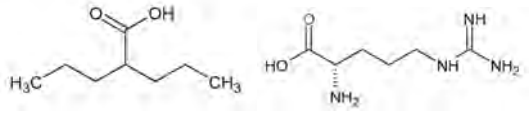

Fig. 3 Valproic acid and L-arginine

Reference

H. Hasegawa et al., *International Journal of Pharmaceutics*, **369**, 12-18(2009).

P-126 Molecular ordering and orientation in surface region of natural cocoa butter and its constituent oils, POP, SOS and POS revealed by X-ray Diffraction

Yoshihito Uozaki, Kimihiko Nozaki, Mai Uenaka, Hikaru Terauchi and Isao Takahashi

Faculty of Science and Technology, Kwansei Gakuin University, Sanda 6691337, Japan (zm28987@kwansei.ac.jp)

Cocoa butter exhibits six polymorphisms characterized by the type of molecular stacking and orientation. Cocoa butter consists of various oils and fats, e.g., POP (sn-1,3-dipalmitoyl -2-oleoylglycerol), SOS (sn-1,3-dipalmitoyl-2-stearoyl-glycerol) and POS (1,3-rac-palmitoyl-stearoyl-2-oleoylglycerol). The properties of these oils and fats are similar to each other; POP, SOS, POS and other fats has five (or six) similar polymorphisms and show successive transformations from quasi-stable form to stable form like cocoa butter.

We recently studied surface-induced preferred orientation of natural cocoa butter ultrathin films with surface-sensitive X-ray diffractions, and found a novel double-layer to single-layer transition reminiscent of transitions seen in smectic liquid crystals. [1] In the present study, we expand the research on the surface structure of each principal constituent oils, POP, SOS and POS, and their bulk structures. The techniques adopted here are X-ray reflectivity (XR)

and Grazing incident X-ray diffraction (GIXD) with a supplementary use of AFM and optical microscopy. Since the typical diffraction angles of XR correspond to that of small angle X-ray scattering (SAXS), XR enables us to determine the surface morphology and distribution of electron density in a wide range of scale between sub microns to several nano meters. On the other hand, GIXD is quite sensitive to the molecular orientations in the surface region of materials to a depth of several nanometers to microns. For POP, a quasi-stable pseudo- ' form revealed to be fairly stable in the double-layer of spin-coated thin films, which has never been attained for the bulk structure. We consider that either confined effect or dimensionality affects the configuration of local minima in energy landscape of this material.

Reference

Y. Hayashi et. al., Transactions of the Materials Research Society of Japan, Vol. 33[3] (2008) 641-644.

INTER MOLECULAR INTERACTIONS IN 2 AMINO AND SCHIFF BASES OF THIOPHENES

P-127

Vasu Sriranga [a] and Deepak Chopra [b]
[a] *Vivekananda Degree College, Bangalore-560055 , India (asusriranga@rediffmail.com)*
[b] *Solid State Structural Chemistry Unit, IISc., Bangalore560012, India (deepakcryst@gmail.com)*

Probing intermolecular interactions in functionalized thiophenes has been carried out to understand the influence of various substituents on the bond parameters and the conformation. The research work reported describes the crystal structure and onformation.

The research work reported describes the crystal structure and conformational studies of 2-amino thiophenes, and Schiff bases of thiophenes, which serve as starting materials for number of intermediate derivatives. These compounds are antibacterial, antitubercular, antifungal, anti-inflammatory and antitoxic. The crystallographic studies throw light on molecular structure which helps in understanding the activities of the biological molecules. The X-ray structure determination of 17 compounds has been carried out in the above family.

The structural comparisons of all the thiophene compounds are as follows. There are certain similar and dissimilar molecular and crystal packing features are described amont 2-amino thiophene derivatives and Schiff bases of thiophne derivatives. The thiophene moiety is planar in all the compounds. It is noticed that from the half-chair conformation with different substituents. Strong intra-molecular interactions which locks the molecular conformation is observed in all the compounds. In addition to this the presence of intermolecular interactions within the crystal lattice is influencing the packing of the molecules which modifies the properities. Interesting details will be presented at the time of conference.

P-128 Organo-chelated Borates as Anions for Crystallization and Chiral Resolution

Lawrence W-Y. Wong, Jack W-H.Kan, Pokka K-C. Pang, Alex S-F. Au Yeung, Thanh-ha Nguyen, Herman H-Y. Sung, Ian D. Williams
Department of Chemistry, Hong Kong University of Science and Technology, Clear Water Bay, Kowloon, Hong Kong, China (chwill@ust.hk)

Boron may be chelated by a variety of dianionic ligands such as diolates, catecholates, salicylates and mixed alkoxy-carboxylates, such as tartrate, lactate and mandelate. The resulting molecular species have one negative charge per tetrahedrally coordinated boron centre. In this respect these species are analogs of tertrafluoroborate $[BF_4]^-$ and tetraphenylborate $[BPh_4]^-$ which have been extensively used as crystallizing counter-anions, with low coordinative ability. Herein we report the facile synthesis of several familes of organo-chelated borates, along with some representative crystal chemistry. The use of asymmetric chelates such as salicylate creates a stereogenic center at boron. The chiral borabis(salicylates) $[BSal_2]$ have been resolved using quninium or sparteinium cations. Solution CD spectra indicate the chirality at boron has a half-life of an hour at RT. Such compounds may be useful crystallizing agents but are not helpful for chiral resolution. The use of chiral chelating ligands, such as R- or S-mandelate, offer help in this repect. Use of R-mandelic acid affords exclusively $[B_S(R\text{-}Man)_2]$ ions in 15 solid state structures to-date and has allowed successful chiral separation of Traditional Chinese Medicinal components from racemic mixtures.

***Acknowledgements**: The Research Grants Council of Hong Kong is gratefully acknowledged for funding of this work through grant 603307.*

P-129 A Unique Approach to Precisely Dispense Chemicals with Diverse Properties

Jian Xu and Matthew Lundy
Rigaku Automation Inc., 5999 Avenida Encinas, Suite 150, Carlsbad, CA 92008

A common challenge researchers are faced with in many different laboratory techniques is the consistent handling of liquids that have varying physical properties, such as viscosity and volatility. In order to address this need, Rigaku has created the Alchemist™ II, which employs a unique approach to liquid handling and stock management [1] and excels at precisely dispensing volumes ranging from 1 microliter up to 10 milliliters. Using Tapper™ technology, viscosity dependent dispensing parameters, and three different sized positive displacement

syringes, the Alchemist II dispenses a wide range of viscosities, ranging from low viscosity solutions such as alcohols to high viscosity polymer solutions such as 30% polyethylene glycol 20,000, with a high degree of precision, without requiring touch-off on the target plate. We report herein the dispense precision achieved by the Alchemist II when dispensing several diverse chemical stocks, measured using a quantitative volumetric dispense assay. The results of the study demonstrate the Alchemist II's ability to dispense chemicals with differing physical properties consistently over a wide range of volumes.

1. Alchemist II information available at http://www.rigaku.com/automation/alchemist.html

P-130 Reversible Transformation and Fluorescent Properties in Polymorphic Crystals of n-Butylammonium 2-Naphthalenesulfonate

Atsushi Yamamoto, Masaaki Matsumoto, Tomoaki Hinoue, Yuji Mizobe, Ichiro Hisaki, Mikiji Miyata, Norimitsu Tohnai
Department of Material and Life Science, Graduate School of Engineering, Osaka University, 2-1 Yamadaoka, Suita, Osaka, 565-0871, Japan,
(yamamoto@molrec.mls.eng.osaka-u.ac.jp)

Organic luminescent materials have been extensively researched. In particular, dynamic tuning or switching system of solid-state luminescence has been much attention for their potential application to optoelectronic devices. For the purpose of construction of these systems, we have been modulated molecular arrangements by using organic salts.

Recently, we have reported organic salts composed of anthracene- 2,6-disulfonic acid with primary amines exhibited a static change of crystal structures and fluorescence intensity in the solid-state[1-2]. Here we report an organic salt of 2-naphthalenesulfonic acid and *n*-butylamine **(Scheme 1)** showed a dynamic change of crystal structures by mechanical stimuli and heating. And these phenomena induced modulation of fluorescence colours.

Organic salt of *n*-butylammonium 2-naphthalenesulfonate yielded two polymorphic crystals: the block-like Form A and the plate-like Form B. The former was obtained from polar solvents such as 1-propanol, while the latter was obtained from non-polar solvents such as *m*-xylene.

As a result of X-ray crystallographic studies, Form A has π-π interactions among naphthalene rings and hydrogen-bonding network involving two oxygen atoms of sulfonate group. So, this form exhibited excimer luminescence. On the other hand, Form B has CH-π interactions and the network involving three oxygen atoms. Luminescence from Form B which has edge-to-edge interaction of naphthalene rings was monomeric.

Interestingly, Form A was transformed to From B by mechanical grinding. Moreover, Form A was recovered by heat treatment at 120 ˚C **(Figure 1)**. At the same time, luminescent properties were changed between them because of drastic change of structures[3].

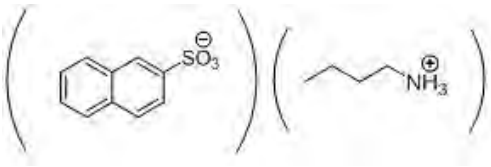

Scheme 1

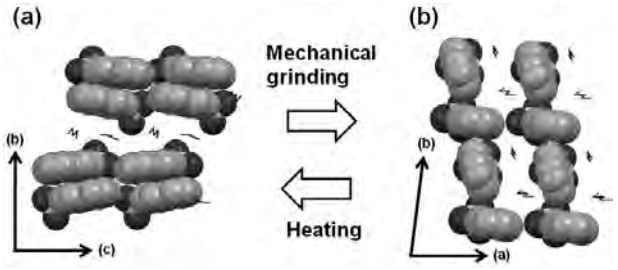

Figure 1. Reversible structure change between two polymorphic crystals: Form A**(a)** and Form B**(b)**composed of 2-naphthalenesulfonic acid and *n*-butylamine.

References

1) Y. Mizobe, N. Tohnai, M. Miyata, and Y. Hasegawa, *Chem. Commun*., **2005**, 1839-1841.
2) Y. Mizobe, H. Ito, I. Hisaki, M. Miyata, Y. Hasegawa, and N. Tohnai, Chem. Commun., **2006** 2126-2128.
3) A. Yamamoto, M. Matsumoto, T. Hinoue, Y. Mizobe, I. Hisaki, M. Miyata and N. Tohnai, Synth. Met., ***2009**, 905-909.*

P-131

$NaVO_2(IO_3)_2(H_2O)$: A New 1D Vanadyl Iodate With Very Strong Second Harmonic Generation

Bing-Ping Yang, Jiang-Gao Mao*
State Key Laboratory of Structural Chemistry, Fujian Institute of Research on the Structure of Matter, Chinese Academy of Sciences, Fuzhou 350002 (mjg@fjirsm.ac.cn)

The search of new second-order nonlinear optical (NLO) material is of current interest and great importance owing to their applications in photonic technologies.[1] Metal iodates such as α-$LiIO_3$ which also contain a lone-pair cation I^{5+} in an asymmetric coordination geometry have been reported to show wide transparency region, large second-harmonic generation (SHG) coefficients, high optical damage thresholds as well as good thermal stability.[2] Vanadium(V) is apt to form a vanadyl moiety (*cis*-VO_2^+) in acidic aqueous media. When four additional ligands bind the vanadyl moiety, the resultant VO_6 octahedron strongly distorted because of the bent nature of the O=V=O bond angle (≈107°). The combination of iodate with distorted VO_6 octahedron may result in new compounds with excellent SHG properties. Guided by this idea, we have successfully obtained a new type of polar material, $NaVO_2(IO_3)_2(H_2O)$, with a very large SHG response of about 20 x KDP. Herein we report its crystal structure, and NLO properties.

$NaVO_2(IO_3)_2(H_2O)$ crystallizes in the acentric space group $P2_1$ (No.4). Its anionic structure may be considered to be one-dimensional, composed of $[VO_2(IO_3)_2]^{1-}_{\infty}$ zig-zag chains, these chains run down the *b*-axis, are separated by Na^+ cations. These chains are constructed from five-coordinate V(V) atoms that are bound by two terminal oxo atoms to create a *cis*-VO_2^+ moiety and by one monodentate and two bridging iodate anions to create a distorted trigonal bipyramidal geometry. I^{5+} cations are in asymmetric coordination environment attributed to the SOJT effects. I^{5+} cations are in distorted trigonal-pyramidal environments, being coordinated by three oxygen atoms. I-O bond distances range from 1.773(6) Å to 1.873(5) Å. The polarizations of all of the IO_3 anions are toward the -b direction. The Na^+ cations is

surrounded by six oxygen atoms from one aqua molecule and two IO_3 groups in a unidentate fashion and three vanadyl oxygen atoms with Na–O distances in the range of 2.385(7) - 2.587(7) Å.

Optical diffuse reflectance spectrum indicates an optical band gap of 2.54 eV. $NaVO_2(IO_3)_2(H_2O)$ is stable up to 218 ºC. The SHG measurements on the sieved powder samples (80-100 mesh), using 1064 nm radiation, revealed that $NaVO_2(IO_3)_2(H_2O)$ exhibits a very large SHG response of about 20 x KDP (KH_2PO_4). Furthermore, the compound was found to be phase-matchable. The extremely large SHG efficiency can be attributed to the synergic effect of the polarizations of the IO_3^- anions.

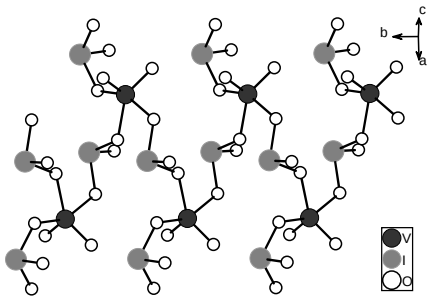

Fig.1. 1D chain $[VO_2(IO_3)_2]^{1-}_{\infty}$ in $NaVO_2(IO_3)_2(H_2O)$

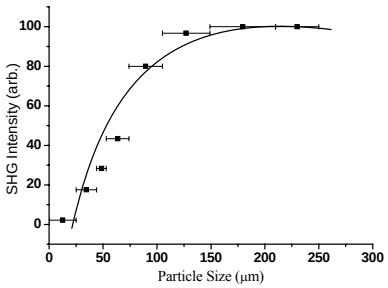

Fig.2.Phase-matching curve for $NaVO_2(IO_3)_2(H_2O)$.

References

1. (a) Chen, C.; Liu, G. *Annu. Rev. Mater. Sci.* **1986**, *16*, 203. (b) Ok, K. M.; Halasyamani, P. S. *Chem. Soc. Rev.* **2006**, *35*, 710. and references cited therein.
2. (a) Chang, H.-Y.; Kim, S.-H.; Halasyamani, P. S.; Ok, K. M. *J. Am. Chem. Soc.* **2009,** *131*, 2426. (b) C.-F. Sun, C.-L. Hu, J.-B. Ling, T. Hu, F. Kong, X.-F. Long, J.-G. Mao, *J. Am. Chem. Soc.* **2009,** In press**.**

***Acknowledgments**: We thank the Nation Natural Science Foundation of China (No. 20825104, 20731006) for the financial support.*

P-132

Critical narrowing of glass transition in supported ultrathin polystyrene films

Chunming Yang, Naoki Koyasu, Kohei Ishimoto, Hikaru Terauchi, Isao Takahashi
Faculty of Science and Technology, Kwansei Gakuin University, Gakuen 2-1, Sanda 669-1337, Japan (yangchunming@126.com)

Most materials form the crystalline sate as a minimum free-energy state of given external conditions, but not a few materials are known to favor noncrystalline states. The glass forming materials are ubiquitous and even crucial in our civilization. In the past decades, a lot of studies have dedicated to the properties and peculiar dynamics of glass forming materials placed in highly confined circumstances, such as a nano-pore structures and ultra thin films. The dynamics in such a confined system will strongly be affected by boundary conditions. The broadening phenomenon of glass transition would be one of the most representative interface effects, in which the glass transition ranging in the temperature increases with decreasing the thickness.

In the present study, we perform precise measurements on X-ray reflectivity (XR) of thin

polystyrene (PS) films under various heating rates. Atactic PS thin layers were prepared by spin-coating method with Si substrates. Before the XR measurements, samples were annealed above bulk glass transition temperature T_g for 12 h. Film thickness investigated ranges from 4 nm and 70 nm, comparable to the radius of gyration. The broadening of transition temperature is most distinctively observed under the fast heating condition (0.50 ^{o}C/min), which is consistent with previous studies [1, 2]. Furthermore, a narrowing of transition temperature is also found with the PS films with decreasing thickness under the slowest heating condition (0.01^{o}C/min). Since the broadening in thin films reflects the heterogeneity and local dynamics which depends on the distance from the free surface [3], the narrowing of transition might be some homogeneity of dynamics in ultrathin films developing with the time interval.

References

[1] S. Kawana, R.A.L. Jones, Phys. Rev. E 63, 021501 (2001)
[2] Zahra Fakhraai and James A. Forrest, Phys. Rev. Lett. 95, 025701 (2005)
[3] James A. Forresta, Kari Dalnoki-Veressb, Advances in Colloid and Interface Science, 94, 167(2001)

P-133 Zeolitic Imidazolate Framework (ZIF) Compounds using Asymmetric Imidazoles

Fion T-Y. Yeong, Fanny L-Y. Shek, Herman H-Y. Sung, Ian D. Williams
Department of Chemistry, Hong Kong University of Science and Technology, Clear Water Bay, Kowloon, Hong Kong, China (chwill@ust.hk)

Metal imidazolides of formula [MIm_2] are a highly robust family of metal organic framework materials. Variable temperature pXRD studies show stabilities up to 400^{o}C. Many of these phases have been prepared from polar organic solvents such as dialkyl-formamides under basic conditions. Metal dications, such as Zn, Co or Cd are tetrahedrally coordinated and the imidazolide anions act as bent bridging ligands, Thus topologically they are analogues of SiO_2 and aluminosilicate zeolites. Since the organic imidazole and crystallization conditions can be varied greatly, a diverse family of open frameworks are possible. One interesting aspect we explore in this paper is the case of asymmetric imidazoles, such as 4-methyl-imidazole, 4-nitro-imidazole, 4-phenyl-imidazole and 2-ethyl-4-methyl-imidazole. These introduce an asymmetry into each Im bridge and could lead to three outcomes; amorphous phases, crystalline phases with 4,5-positional disorder or fully ordered crystalline phases. In general lower temperatures give amorphous or poorly crystalline phases, whilst higher crystallization temperatures (160^{o}C) can lead to fully ordered systems. We are now exploring possible high temperature solid-state phase transitions of the amorphous materials.

***Acknowledgements**: We are grateful to the Research Grant Council HK (603307) and HKUST for funding of this work.*

Modulated structure feature in over-doped manganese oxides

P-134

Xiuzhen Yu[1], YasuhideTomioka[2], Yoshio Kaneko[3], Toru Asaka[4], Koji Kimoto[1], Taka-hisa Arima[5], Yoshinori Tokura[3,6], and Yoshio Matsui[1]

[1] *Advanced Electron Microscopy Group, ANCC, National Institute for Materials Science, Tsukuba, 305-0044, Japan (Yu.xiuzhen@nims.go.jp)*

[2] *Nanoelectronics Research Institute, National Institute of Advanced Industrial Science and Technology, Tsukuba 305-8562, Japan*

[3] *Multiferroic Project, ERATO, Japan Science and Technology Agency, Tokyo 113-8656, Japan*

[4] *Japan Fine Ceramics Center (JFCC), 2-4-1 Mutsuno, Atsuta-ku, Nagoya, 456-8587, Japan*

[5] *Institute of Multidisciplinary Research for Advanced Materials, Tohoku University, Sendai 980-8577, Japan*

[6] *Department of Applied Physics, University of Tokyo, Tokyo 113-8656, Japan*

In half-doped perovskite manganese oxide $RE_{1-x}Ca_xMnO_3$ (x = 0.5) (*RE*: rare earth elements), the charge/orbital ordering (CO/OO), being responsible for the ordering of Mn^{3+}/Mn^{4+} with 1/1 accompanied by the e_g-orbital ordering, are associated with the modulated crystal structure with modulation vector $\boldsymbol{Q}$ = (0, 1/2, 0) [1]. Accordingly, the CO/OO structure feature can be certainly defined by analyzing the modulated crystal structure[2-3]. Different to stable CO/OO structure observed in $RE_{0.5}Ca_{0.5}MnO_3$ with pseudo-cubic structure and small quenched disorder, the CO/OO structure in over-doped $RE_{1-x}Sr_xMnO_3$ (x>0.5) and layered perovskite $RE_{1-x}Ca_{1+x}MnO_4$ (x>0.5) should be complex due to unbalance of Mn^{3+}/Mn^{4+} or layered structure, and hence multi-phase competition[4]. It is therefore desirable to study the modulated structure of over-doped manganites in CO/OO state.

In this study, the modulated structures of $Sm_{1-x}Sr_xMnO_3$ (x>0.5) and layered perovskite $Pr_{1-x}Ca_{1+x}MnO_4$ (x>0.5) have been systematically investigated by low-temperature transmission electron microscopy (TEM). In $Sm_{1-x}Sr_xMnO_3$ (x>0.5) with relatively large quenched disorder, the commensurate CO/OO structure with modulation vector $\boldsymbol{Q}$ = (0, 1/3, 0) was observed above the A-type antiferromagnetic transition temperature (T_{NA} ~ 180 K) [4]. This modulation structure changes to an incommensurate one below T_{NA}. In layered perovskite $Pr_{1-x}Ca_{1+x}MnO_4$ with small quenched disorder, the incommensurate CO/OO is independent on temperature, and the modulation wavenumber linearly decreases with increasing *x*.

These results reveal that in $Sm_{1-x}Sr_xMnO_3$ (x>0.5) the commensurate CO/OO structure with $\boldsymbol{Q}$ = (0, 1/3, 0) is fluctuated as it competes with A-type [4] antiferromagnetic structure, while in layered perovskite $Pr_{1-x}Ca_{1+x}MnO_4$, the stable incommensurate CO/OO is seen, being analogous to that observed in $RE_{1-x}Ca_xMnO_3$ (x > 0.5) [5].

References

1. "*Colossal Magnetoresistive Oxide*s" edited by Y. Tokura, Gorden and Breach Scirnce Publisher, (2000).
2. X. Z. Yu, R. Mathieu, T. Arima, Y. Kaneko, J. P. He, M. Uchida, T. Asaka, T. Nagai, K. Kimoto, Y. Matsui and Y. Tokura, Phys. Rev. B **75**, (2007) p. 174441.
3. X. Z. Yu, Y. Tomioka, T. Asaka, K. Kimoto, T. Arima, Y. Tokura and Y. Matsui, Appl. Phys. Lett. **94**, 082509 (2009).
4. Y. Tomioka, X. Z. Yu, T. Ito, Y. Matsui and Y. Tokura, Phys. Rev. B, in press.
5. G. C. Milward, M. J. Calderon and P. B. Littlewood, Nature **433**, 607 (2005).

P-135

Structural Studies of Ba_2LaIrO_6 and La_2ZnIrO_6 – Two Monoclinic Perovskites With Different Space Groups

Qingdi Zhou, Brendan J. Kennedy
School of Chemistry, The University of Sydney, Sydney, NSW 2006 Australia
(q.zhou@chem.usyd.edu.au)

For well over half a century the structural chemistry, electronic and magnetic properties of ABO_3 perovskites including the $A_2BB'O_6$ double perovskites, in which two different ions are regularly ordered at the octahedral *B*-site have been of interest. The enormous flexibility of perovskites allows the possibility of forming materials with highly tailored compositions, and hence structures and ultimately properties. The solid-state chemistry of mixed-metal oxides containing ruthenium or iridium has attracted a great deal of recent research reflecting the diverse range of structures and electronic properties displayed by such oxides. For example, the perovskite $SrRuO_3$ is ferromagnetic below 160 K [1] and the layered perovskite Sr_2RuO_4 is a superconductor below 1 K [2].

Despite the strong correlation between structure and properties in perovskites accurate and precise structures of numerous well studied examples are not available. Ba_2LaIrO_6 is a case at point. This oxide was apparently first prepared by Thumm et al [3] who concluded that it was cubic with ordering of the La and Ir cations. Ramos et al [4] reported the material was actually orthorhombic without ordering of the La and Ir cations. In 1999 Wakeshima et al [5] also reported ordering of the cations but suggested the true symmetry was monoclinic in $P2_1/n$. Most recently Fu and IJdo [6] concluded the symmetry was actually rhombohedral in space group $R\bar{3}$, this space group allowing ordering of the two *B*-site cations. Whist differences in preparative methods occasionally result in different symmetries; it is more common that the high pseudo symmetry and weakness of selected diagnostic reflections leads to uncertainty in the choice of space group. This is especially true when the structures are determined by powder X-ray diffraction methods utilising un-monochromated Cu radiation on laboratory based diffractometers as employed in the above four experimental studies. Xiang et al [7] concluded from density functional theory calculations that the most likely structure of Ba_2LaIrO_6 was rhombohedral.

The continuing interest in Ba_2LaIrO_6 prompted us to re-examine the structure of this oxide using both synchrotron X-ray and neutron powder diffraction. Accurate and precise structures for the two oxides La_2ZnIrO_6 and Ba_2LaIrO_6 are presented. The structure of La_2ZnIrO_6 is monoclinic in space group $P2_1/n$ in which both in-phase and out-of-phase tilting co-exist with the rock-salt like ordering of the Zn and Ir cations. Careful analysis of the synchrotron diffraction profile of Ba_2LaIrO_6 suggests that, at room temperature, this exists as a mixture of monoclinic $I2/m$ and rhombohedral $R\bar{3}$ phases, both of which are characterised by out-of-phase tilting of the cation ordered BO_6 octahedra. The pure rhombohedral phase is obtained by heating the sample to 375 K, with further heating resulting in the loss of the tilting of the octahedra, the structure being in $Fm\bar{3}m$. Cooling the sample induces an

additional phase transition to a triclinic structure in $I\bar{1}$.

References

1. J. M. Longo; P. M. Raccah; J. B. Goodenough, *J. Appl. Phys.* **39** (1968) 1327.
2. Y. Maeno; H. Hashimoto; K. Yoshida; S. Nishizaki; T. Fujita; J. G. Bednorz; F. Lichtenberg, *Nature* **372** (1994) 532.
3. I. Thumm; U. Treiber; S. Kemmlersack, *J. Solid State Chem.* **35** (1980) 156.
4. E. M. Ramos; I. Alvarez; R. Saezpuche; M. L. Veiga; C. Pico, *J. Alloys Compounds* **225** (1995) 212.
5. M. Wakeshima; D. Harada; Y. Hinatsu, *J. Alloys Compounds* **287** (1999) 130.
6. W. T. Fu; D. J. W. Ijdo, *J. Alloys Compounds* **394** (2005) L5.
7. H. P. Xiang; X. J. Liu; X. F. Hao; J. Meng; Z. J. Wu, *J. Alloys Compounds* **457** (2008) 571.

SMART BREEZE - The affordable high-quality solution for Chemical Crystallography

P-136

Eric Hovestreydt[1], Michael Ruf[2], Holger Ott[1]
[1] *Bruker AXS GmbH, Oestliche Rheinbrueckenstrasse 49, D 76181 Karlsruhe, Germany (info@bruker-axs.de)*
[2] *Bruker AXS Inc., E. Cheryl Parkway 5, MADISON, WI 53711-5373, United States of America (info@bruker-axs.com)*

An exceptionally easy to operate solution for users in chemical crystallography has become available. The SMART BREEZE offers automated molecular 3D structure analysis at affordable costs.

The air-cooled BREEZE 4K CCD detector sets the SMART BREEZE apart from traditional water-cooled CCD systems. Nevertheless, the BREEZE offers the same or even higher data quality when compared to most conventional water-cooled CCD cameras due to the extremely low electronic noise of its CCD chip. Examples will be shown.

Despite of the moderate price the highly versatile fixed-chi goniometer is accurate and precise and built for durability.

APEX2 software offers a high level of automation, is extremely easy to use, and provides feedback with modern graphics. The highly intuitive software opens the field of crystallography to synthetic chemists and novice crystallographers, giving access to fast and reliable structure determination. Publication-ready reports which are generated automatically in various formats and HTML reports will be shown and discussed.

Ready, set, screen: X8 PROSPECTOR

P-137

Eric Hovestreydt[1], Matt Benning[2], Marianna Biadene[1]
[1] *Bruker AXS GmbH, Oestliche Rheinbrueckenstrasse 49, D 76181 Karlsruhe, Germany (info@bruker-axs.de)*
[2] *Bruker AXS Inc. E. Cheryl Parkway 5, MADISON, WI 53711-5373, United States of America(info@bruker-axs.com)*

The key for success in solving a protein structure is finding the best crystal. When screening a myriad of candidates, it is important to have a highly reliable no-nonsense system, one that keeps working day and night.

The only way to find out how well your crystal diffracts is to put it in the X-ray beam. Why

waste your valuable synchrotron time screening crystals? The X8 PROSPECTOR is a system designed to serve the demand for efficient screening, economical and reliable. It tells you everything about your crystals prior to going to the beamline With its compact design and small footprint, it can be placed in any laboratory. The source is completely air-cooled and therefore requires no external plumbing. It also uses regular, single-phase power, so it requires no special electrical wiring. A microfocus sealed tube delivers X-rays equivalent in intensity to a traditional 300 micron rotating anode generator. Coupled with the QUAZAR optics, this source delivers a highly stable beam.

The rock-solid, most sensitive, fourth generation APEX II CCD detector is coupled with this powerful source.

The X8 PROSPECTOR not only speeds up your screening work, it also takes you by the hand through the whole process. The PROTEUM2 software controls the hardware and analyzes the results to give quick and reliable answers to your questions.

A couple of examples will be presented showing how easily the X8 PROSPECTOR finds the jewels from your crystallization plates. Furthermore, we will discuss examples of a complete structural data collection on proteins, peptides and pharmaceutical compounds.

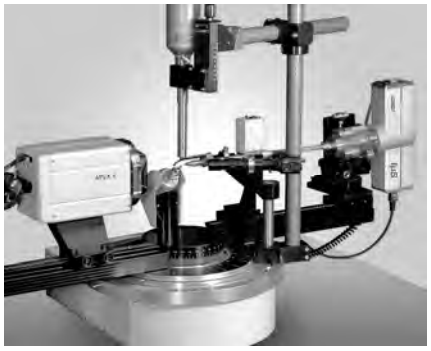

P-138 Focusing Effects in Parabolic Shaped Multi-Plate Crystal Cavity for X-rays

Y.-Y. Chang[1], S.-Y. Chen[1], M.-T. Tang[2], Yu. Stetsko[2], M. Yabashi[3], S.-C. Weng[1], C.-H. Chu [1], B.-Y. Shew[2], and S.-L. Chang[1]
[1] Department of Physics, National Tsing Hua University, Hsinchu,Taiwan,300 (d947301@oz.nthu.edu.tw)
[2] National Synchrotron Radiation Research Center, Hsinchu, Taiwan, 300
[3] Spring-8/RIKEN Mikazuki, Hyogo, Japan

The Fabry-Perot type multi-plate crystal cavities consisting of compound refractive lenses (CRL) on silicon wafers are prepared by using micro-electronic lithographic techniques. Each refractive lens is a parabolic shaped concave lens. The crystal orientation of this X-ray optical device is the same as that of the two-plate x-ray resonators reported (Phys. Rev. Lett. 94, 174801, 2005). Experimentally, the transmitted X-ray beam size of the (12 4 0) back diffraction through these monolithic silicon crystal devices is measured with a fine knife-edge. The measurements show enhanced focusing effect from the CRL due to X-ray back diffraction. Also observed is the energy-dependent focusing. Detailed analysis on cavity

interference and beam focusing will be discussed.

P-139 Bringing the power of synchrotron crystallography to the chemical community

William Clegg, Ross W Harrington, Luca Russo
School of Chemistry, Newcastle University, Newcastle upon Tyne NE1 7RU, UK (w.clegg@ncl.ac.uk)

Between 2001 and 2008 the synchrotron component of the U.K. National Crystallography Service, run from Newcastle, made extensive and frequent use of station 9.8 at Daresbury's Synchrotron Radiation Source, successfully and efficiently generating a large collection of structures from difficult samples submitted by groups engaged in a wide range of chemical and materials research. Station 9.8 had been constructed in a Newcastle-led project during 1994–1997 and established a reputation as the most productive facility of this kind in the world, with a major international impact including serving as a model for other facilities developed subsequently. Following the closure of the SRS, the service has transferred to beamline I19 at Diamond Light Source and we have been among the first users to be allocated time there, as part of the ongoing commissioning phase of the new facility.

Our in-depth experience with challenging samples at Daresbury has enabled us to contribute substantially to the development of the equipment and software of I19, identifying features for improvement. By the time of the AsCA Meeting we will have made 8 visits to collect data (6 already by June), with significant improvements already noted and more expected each time; we have now reached what can almost be considered as normal productivity operation rather than commissioning and development. A variety of new structures have been determined, and we have addressed interesting problems including twinning, major disorder, superstructures, and compounds of which the true chemical identity was quite unexpected.

We will give an account of some of the main features of the beamline from a users' point of view, describe some of our experiences, and present a selection of new results to demonstrate what can be achieved with this facility, even in its early days. Funding for continuation of the National Service is currently being sought. There are useful lessons here for other facilities.

P-140 Optimization of parameters for new rotation function

Wei Ding [1],FanJiang [2]
[1] *Institute of Physics, Chinese Academy of Sciences, No.8 South Third Street ZhongGuanCun, Haidian District, P.O.Box603, Beijing, 100190, China (wding@bio.iphy.ac.cn)*
[2] *Institute of Physics, Chinese Academy of Sciences, Beijing, 100190, China (fjiang@aphy.iphy.ac.cn)*

A new rotation function calculated by matching the search model directly with the Patterson vector map had been described by our recent works (Jiang, 2008). The results of that work were encouraging but the parameters seemed to be dependent on the specific models and

crystal structures, so designing a way of optimizing or screening for a best set of parameters is necessary. In this work, we consider that the correct solutions are the signal and the random ones are the noise. We first demonstrate that the signal-to-noise ratio is a valid criterion in parameters choice. But when the correct solution is unknown, the value of signal can not be calculated. However, we further verify that the value of noise is a suitable criterion too. According to the second criterion, we get the optimized parameters, and our final works show that the satisfactory test results can be deduced by them.

Reference

Jiang, F. (2008). *Acta Cryst.* D**64**, 561-566.

P-141

The current status of versatile neutron diffractometer iMATERIA at J-PARC

Toru Ishigaki[1], Akinori Hoshikawa[1], Masao Yonemura[2], Kenji Iwase[1], D. S. Adipranoto[1], Hidetoshi Oguro[1], Takahiro Morishima[3], Takashi Kamiyama[3], Ryoko Oishi[3], Kazuhiro Mori[4], Ryoji Kiyanagi[5], Kazuya Aizawa[6], Makoto Hayashi[7]

[1] *Frontier Research Center for Applied Nuclear Sciences, Ibaraki University, Tokai, Naka, Ibaraki, 319-1106, JAPAN (toru.ishigaki@j-parc.jp)*

[2] *Institute of Applied Beam Science, Ibaraki University, Hitachi, Ibaraki, JAPAN*

[3] *Neutron Science Laboratory, KEK, Tsukuba, Ibaraki, JAPAN*

[4] *KUR, Kyoto University, Kumatori, Osaka, JAPAN*

[5] *IMRAM, Tohoku University, Sendai, Miyagi, JAPAN*

[6] *J-PARC Center, JAEA, Tokai, Naka, Ibaraki, JAPAN*

[7] *Ibaraki prefecture, Mito, Ibaraki, JAPAN*

Ibaraki prefecture, the local government of the area where J-PARC sites in Japan, has decided to build a versatile neutron diffractometer (IBARAKI Materials Design Diffractometer, iMATERIA) to promote industrial applications for neutron beam in J-PARC. iMATERIA is planned to be a high throughput diffractometer so that materials engineers and scientists can use this diffractometer like the chemical analytical instruments in their materials development process. It covers the d in range $0.18 < d$ (Å) < 5 with $\Delta d/d = 0.16$ % at high resolution bank, and $5 < d$ (Å) < 800 with the resolution changing gradually at three detector banks of 90 degree, low angle and small angle. It takes several minutes to obtain a 'Rietveld-quality' data for the X-ray laboratory sized sample measured at 1MW. Currently, the beam power is limited for tuning the accelerator, so that the standard measuring time is about one to two hours. To promote industrial applications, a utilization system of this diffractometer is required. Since several tens to thousands experiments will be carried out in one year, we have to prepare an automatically sample exchange system and special large numbers of sample holders. The analysis software is also very important for powder diffraction data, so that we prepare a software package consisting of combination of several powder-diffraction software, structural databases and visualization. The construction of iMATERIA was completed as one of the day-one instruments at J-PARC and the beam-on commissioning was started since May 2008. The recent data of iMATERIA will be reported.

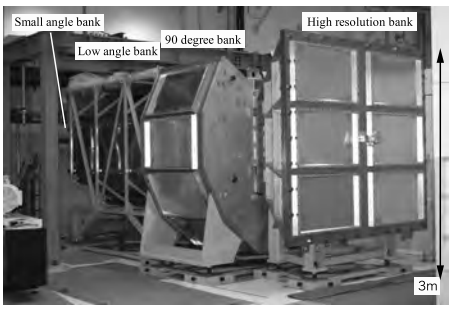

Fig.1 IBARAKI Materials Design Diffractometer, iMATERIA without detector for each bank and instrument shieldings. High-resolution bank, special environment bank (90 degree bank), low angle bank, can be seen from right to left. and small angle detector bank, which are not shown in picture, are situated in the low angle vacuum chamber (left hand of the picture).

P-142 Study on membrane chain-chain packing by grazing incident X-ray diffraction

Ming-Tao Lee
National Synchrotron Radiation Research Center, Taiwan (mtlee@nsrrc.org.tw)

Membrane structure is very important issue for cell. Membrane is not only the "wall" for protecting cell but also the interface for exchanging signal, ions and molecules. Many evidences show that membrane protein will fold to functional structure by associating with suitable membrane structure. Lipid chain-chain packing is one of important structures and will affect membrane thickness, lipid lateral diffusion and membrane domain formation. We will use grazing incident X-ray diffraction to probe lipid chain-chain packing. The 12keV X-ray light source in BL13A beam line of NSRRC and home-made humidity-temperature controlled chamber will be applied in the measurements. The ion channel peptide Gramicidin A and cholesterol will be used to interact with model membrane to study their effect on chain-chain packing.

P-143 Imposition of multiple *F* constraints in the maximum entropy method

Koichi Momma and Fujio Izumi
Quantum Beam Center, National Institute for Materials Science, 1-1 Namiki, Tsukuba, Iaraki 305-0044, Japan (MOMMA.Koichi@nims.go.jp), (IZUMI.Fujio@nims.go.jp)

The maximum entropy method (MEM) is used for reconstruction of the least-biased distribution of electron or nuclear densities from X-ray or neutron diffraction data by maximizing the information entropy S under some constraints. Because the errors of observed structure factors, $F_o(\boldsymbol{h}_i)$, for reflec- tions $\boldsymbol{h}_i$ should have Gaussian distribution ideally, the so-called F constraint is usually imposed on calculated structure factors $F(\boldsymbol{h}_i)$:

$$C_F = \frac{1}{N}\sum_i \left[\frac{|F_o(\boldsymbol{h}_i) - F(\boldsymbol{h}_i)|}{\sigma(\boldsymbol{h}_i)}\right]^2 - 1 = 0, \quad (1)$$

where N is the total number of reflections, and $\sigma(\boldsymbol{h}_i)$ is the standard uncertainty of $|F_o(\boldsymbol{h}_i)|$. However, the above constraint has a serious disadvantage that the distribution of the normalized residuals of the structure factors, $\Delta F(\boldsymbol{h}_i)/\sigma(\boldsymbol{h}_i) = [|F_o(\boldsymbol{h}_i)| - |F(\boldsymbol{h}_i)|]/\sigma(\boldsymbol{h}_i)$, tend to deviate from the expected Gaussian distribution. The Gaussian distribution of the errors is a

prerequisite for Eq. (1), which, however, does not always ensure the Gaussian distribution of $\Delta F(\boldsymbol{h}_i)/\sigma(\boldsymbol{h}_i)$.

In order to improve the histogram of $\Delta F(\boldsymbol{h}_i)/\sigma(\boldsymbol{h}_i)$, Palatinus and van Smaalen [1] proposed the generalized F constraint defined as

$$C_{Fn}=\frac{1}{N m_n}\sum_i\left[\frac{|F_o(\boldsymbol{h}_i)-F(\boldsymbol{h}_i)|}{\sigma(\boldsymbol{h}_i)}\right]^n-1=0, \tag{2}$$

where m_n is the even n-order central moment of the normalized Gaussian distribution. C_{F2} corresponds to constraint (1). Although C_{Fn} constraints with n = 4–8 provide us with better histograms of $\Delta F(\boldsymbol{h}_i)/\sigma(\boldsymbol{h}_i)$ with less artifacts in reconstructed electron densities, none of the constraints are sufficient to constrain the histogram to the Gaussian shape.

In this study, a new computer program has been written in C++ to impose a set of multiple F constraints with different orders of n. The normalized electron density, ρ_k, with the maximum S under the multiple constraints C_{Fn} (n = 2, 4, 6, ···) is given by

$$\rho_k=\frac{\tau_k\exp\left[\sum_n\lambda_n\frac{\partial C_{Fn}}{\partial\rho_k}\right]}{\sum_{k'}\tau_{k'}\exp\left[\sum_n\lambda_n\frac{\partial C_{Fn}}{\partial\rho_{k'}}\right]}, \tag{3}$$

where the suffixes k and k' denote positions in the unit cell, and λ_n is the Lagrangian multiplier. Equation (3) cannot be solved analytically because both sides of Eq. (3) contain ρ_k. Our new program adopts 0-th order single pixel approximation [2] to solve Eq. (3) by iterative calculations with λ_n values dynamically adjusted in every cycle. Simultaneous imposition of two or three F_n constraints with different n led to artifact suppression in the resulting electron densities. The number of iterations required for the convergence of MEM analysis is also reduced, even when convergence is hardly achieved by imposing the classical F constraint.

Some examples of applying the new methodology of MEM to single-crystal and powder diffraction data will be presented.

References

[1] Palatinus, L. & van Smaalen, S. (2002). *Acta Cryst.* A**58**, 559–567.
[2] Kumazawa, S., Takata, M. & Sakata, M. (1995). *Acta Cryst.* A**51**, 47–53.

P-144

Synchrotron Radiation Beamline for Macromolecular Assemblies Operated by the IPR at SPring-8 (BL44XU)

Eiki Yamashita[1], Masato Yoshimura[1,2], Mamoru Suzuki[1], Kazuya Hasegawa[3], Yukito Furukawa[3], Toru Ohata[3], Takashi Kumasaka[3], Go Ueno[4], Masaki Yamamoto[4], Shinya Yoshikawa[5], Tomitake Tsukihara[1,5], Atsushi Nakagawa[1,*]

[1] *Institute for Protein Reseach, Osaka University, 3-2 Yamadaoka, Suita, Osaka 565-0871, Japan (*atsushi@protein.osaka-u.ac.jp)*

[2] *Taiwan NSRRC, Taiwan Beamline Office at SPring-8, 1-1-1 Kouto, Sayo-cho, Sayo-gun, Hyogo 679-5148, Japan*

[2] *JASRI/SPring-8, 1-1-1 Kouto, Sayo-cho, Sayo-gun, Hyogo 679-5198, Japan*

[3] *RIKEN/SPring-8, 1-1-1 Kouto, Sayo-cho, Sayo-gun, Hyogo 679-5148, Japan*

[4] *Graduate School of Life Science, University of Hyogo, 3-2-1 Kouto, Kamigori-cho, Ako-gun, Hyogo 678-1297, Japan*

Biological macromolecular assemblies play significant roles in many biological reaction systems, such as energy transfer, protein synthesis, signal transduction, molecular motors and so on. Detailed understanding of the functions of the macromolecular assemblies requires information derived from three-dimensional atomic structures. X-ray crystallography is one of the most powerful techniques to determine the three-dimensional structures of macromolecular assemblies at atomic level.

It is usually be known that biological macromolecular assembles are difficult to be crystallized or grown to larger size crystals. In addition, the unit cells of these crystals are quite large. Because of these features of the crystals of biological macromolecular assemblies, it is usually very difficult to obtain good diffraction data. The difficulties of diffraction data collection of biological macromolecular assembles are as follows; extremely weak diffraction power, narrow space between diffraction sports, x-ray radiation sensitive etc. High brilliance and highly paralleled synchrotron radiation from the undulator is an extremely powerful tool for diffraction data collection from macromolecular assembly crystals with large unite cell.

The Institute for Protein Research (IPR) of Osaka University is operating a beamline for crystal structure analysis of biological macromolecular assemblies at SPring-8 (BL44XU). This beamline is specially designed to collect high quality diffraction data from biological macromolecule assembly crystals with large unit cells. The light source of this beamline is a SPring-8 standard type in-vacuum undulator. Liquid nitrogen cooled double crystal monochromator and horizontal focusing mirror are used as the optical components. A newly designed high precision diffractometer combined with a specially designed large image-plate detector, DIP6020, is installed. Recently, BSS (Beamline Scheduling Software), which is SPring-8 protein crystallography beamline standard GUI, is installed to unify user operation throughout protein crystallography beamlines in the SPring-8. Diffraction data from crystals of biological macromolecular assemblies with large unit cell (over 700 angstrom) has been collected higher than 3.5 Å resolution.

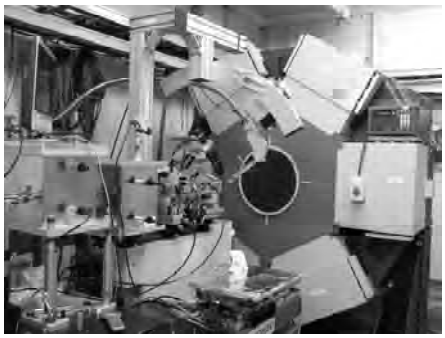

Present status and the future plan of the beamline will be discussed.

P-145 X-ray diffraction from crystals in crystallization plates

Tadeusz Skarzynski
Oxford Diffraction Ltd., Oxford Industrial Park, Yarnton, Oxfordshire, OX5 1QU, United Kingdom. (tadeusz.skarzynski@oxford-diffraction.com)

The PX Scanner is a unique instrument from Oxford Diffraction enabling the identification and characterization of protein crystals with X-rays, in-situ, in the crystallization plate. The PX Scanner addresses the bottleneck in high-throughput crystallization allowing a quantitative evaluation of the diffraction properties of crystals without having to manually extract crystals from the crystallization plate. Combining an optical imaging system with a powerful, micro-focus Cu X-ray source, highly sensitive CCD detector and intuitive software provides an essential laboratory resource for crystallographers involved in difficult structural biology projects.

The PX Scanner is now further enhanced with new software named CrystalEyes which expands the functionality of the instrument, utilizing new algorithms to improve the acquisition and quality of the optical and X-ray images. Furthermore, new database access capabilities allow the data to be easily output from the PX Scanner and integrated with a 'LIMS' style lab data management system.

We will show how the PX Scanner can be used as a powerful tool providing valuable information at all stages of macromolecule crystallization, including differentiating salt from protein crystals in initial screens, selecting the best crystals for synchrotron X-ray data collection, optimizing harvesting, cryo-protecting and soaking conditions, and determining crystal lattice parameters.

P-146 Electrostatic potential as an experimental or a theoretical tool for a better understanding of drug interactions

Anne Spasojević – de Biré[1] and Nour Eddine Ghermani[2]
[1] *Laboratoire "Structures Propriétés et Modélisation des Solides", UMR 8580 du CNRS, Ecole Centrale Paris, 92295 Châtenay-Malabry, France (anne.spasojevic@ecp.fr)*
[2] *Laboratoire Physico-chimie, Pharmacotechnie, Biopharmacie, UMR 8612 du CNRS, Paris-Sud, Faculté de pharmacie, 92296 Châtenay-Malabry, France (noureddine.ghermani@u-psud.fr)*

High-resolution X-ray diffraction and theoretical calculations allow a fine characterization of these electronic and electrostatic properties in crystals, which is essential to the understanding and prediction of the interaction of drugs with the biological targets (pharmacology) and excipients (formulation). This fundamental approach can have important consequences for practical applications in the areas of drug design or drug delivery.

Our collaborative work has enabled us to answer several questions posed by medicinal

chemists or galenists, in particular relative to the following topics:

- Electronic and electrostatic properties of racemic ibuprofen
- Electronic and electrostatic properties of a complex of zinc aspirin
- Understanding of the crystallization of busulfan, a pediatric cancer chemotherapeutic drug, and development of a new formulation (encapsulation in a cyclodextrine derivate)
- Experimental and theoretical electrostatic properties of styrylquinoline-based compounds as new inhibitors in the integrase of the HIV-1 (figure 1a)
- Understanding of the reactivity toward nucleophile agent: a putative intermediary product in the total synthesis of cephalotaxine (antileukemic agent) (figure 1b)
- Electronic and electrostatic properties of co-crystal of decavanadate – cytosine, compound implied in the activity or inhibition of various enzymes (phosphotransferases, Ca^{2+} ATP-ase, adenylate kinase, …)
- Experimental and theoretical electrostatic properties of salicyladehyde thiosemicarbazone, a pharmacophore of trombopoietin mimics, one of the simplest ligands in the thiosemicarbazone family.

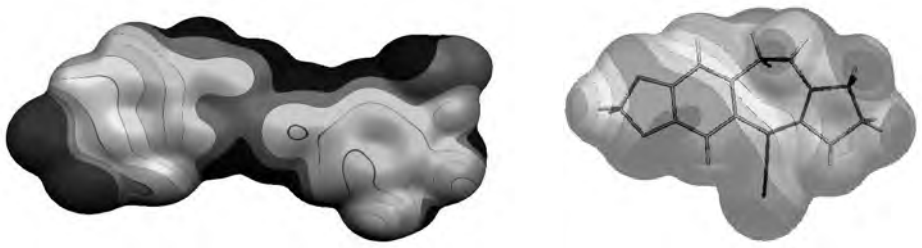

a b

Figure 1. a) Molecular surface of a styryl-quinoline based compound colored by theoretical electrostatic potential values. b) Molecular surface of cephalotaxine colored by experimental electrostatic potential values.

The Effect of Disk Chopper Phasing on Neutron Beam Spectrum of SuperHRPD at J-PARC

P-147

Teguh Yulius Surya Panca Putra[1,2], Shuki Torii[2], Junrong Zhang[2], Takashi Muroya[2], Setsuo Sato[2], Takashi Kamiyama[2]

[1] *The Graduate University for Advanced Studies (SOKENDAI), SOKENDAI-KEK Office, 1-1 Oho, Tsukuba 305-0801, Japan (panca@post.kek.jp)*

[2] *High Energy Accelerator Research Organization, KEK Tokai Campus, 2-4 Shirakata Shirane, Tokai, Naka, Ibaraki 319-1195, Japan*

Experimental results on various phasing of disk chopper at Super High Resolution Powder Diffractometer (SuperHRPD) BL08 of J-PARC are reported. SuperHRPD is a neutron powder diffractometer at Materials and Life Science Facility (MLF), Japan Proton Accelerator Research Complex (J-PARC). SuperHRPD looks at a decoupled poisoned hydrogen moderator and within approximately 100 m total flight path, SuperHRPD is characterized by its world best resolution $\Delta d/d = 0.03\%$ at $d < 4$ Å with d-range $0.5 < d$ [Å] < 60. Identification of individual intensities of Bragg reflection can be more easily conducted with this high resolution of SuperHRPD. It will also enable the study of more complicated structure resulting in better reliability in obtained structure parameters.

Three disk choppers are used to select the desired wavelength range of the neutron beam from the source, whose repetition rate of 25 Hz. First disk chopper (DC1) was installed at 7.1 m from the moderator, while DC2 and DC3 installed at 12.725 m and 12.775 m, respectively. During the experiment, DC1 were kept rotated at frequency of 8.33 Hz, while DC2 and DC3 were open stopped. Phasing of DC1 was varied from -50^o until +30^o in 5^o increment, relative to the position of neutron beam guide tube. Fig. 1 shows that pashing configurations of the disk chopper gave different neutron beam spectrums. Disk chopper phasing in this experiment selected an area from the initial neutron spectrum leaving the moderator with different wavelength width. For example, DC1 phasing at +10^o (in Fig. 1) will limit the wavelength until 4.58 Å as shown in path-time diagram in Fig. 2. Disk chopper phasing, therefore, enable us to pick out any incident wavelength that we choose. The result from this experiment will be useful in selecting the wavelength width of neutron for experiments with different purposes.

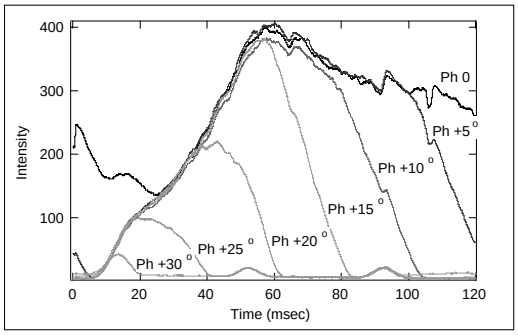

Figure 1. Neutron spectrum resulted showing the effect of disk chopper phasing.

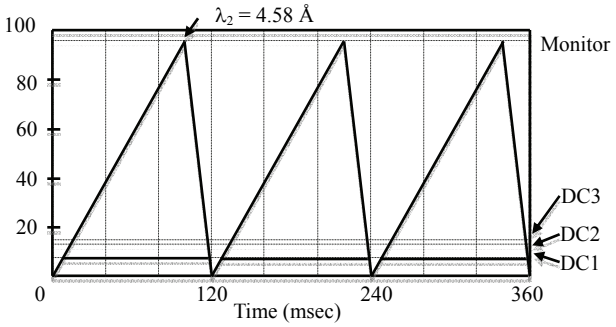

Figure 2. Path-time diagram showing DC1 phasing +10^o as shown in Fig. 1.

References

1. R.M. Brugger, Mechanical and Time-of-flight Techniques, in: P.A. Egelstaff (Ed.), Thermal Neutron Scattering, Academic Press, New York, 1965 (Chapter 2)
2. C.G. Windsor, Pulsed Neutron Scattering, Taylor & Francis Ltd., London, 1981
3. J.R.D. Copley, Nucl. Instr. and Meth. in Physics Research A 273 (1988) 67
4. J.R.D. Copley, Nucl. Instr. and Meth. in Physics Research A 303 (1991) 332
5. T. Ishigaki et.al., Journal of Neutron Research 13 (1-3) 2005

P-148

A Novel Mounting Tool Using Adhesive for Protein Crystals

Tomoya Kitatani[1,2], Tomokazu Hasegawa[3], Shigeru Sugiyama[1,2], Kensaku Hamada[3], Hiroaki Adachi[1,2,4], Hiroyoshi Matsumura[1,2,4], Satoshi Murakami[2,4,5], Tsuyoshi Inoue[1,2,4], Yusuke Mori[1,2,4], Kazufumi Takano[1,2,4]

[1] *Graduate School of Engineering, Osaka University, Suita, Osaka 565-0871, Japan (ktakano@mls.eng.osaka-u.ac.jp)*
[2] *CREST JST, Suita, Osaka 565-0871, Japan*
[3] *PharmAxess Inc., Ibaraki, Osaka 567-0085, Japan*
[4] *SOSHO Inc., Osaka 541-0053, Japan*
[5] *Graduate School of Bioscience and Biotechnology, Tokyo Institute of Technology, Yokohama 226-8503, Japan*

We have developed a novel mounting tool, Crystal Catcher, for protein crystals that directly captures a crystal from a drop with an adhesive (Kitatani et al., 2008, 2009). This tool has a loop-free structure and can reduce the amount of solution around the captured crystal in

comparison with conventional loop-based mount tools. The crystal caught by the Crystal Catcher is immediately mounted in a stream of nitrogen gas held at 100K for XRD measurement. We have developed Crystal Catchers CT-100, CT-200, CT-300 and CT-400, which adopt different types of adhesive and nozzle materials. CT-100 and CT-300 are suitable for fragile crystals and crystals in aqueous solutions. CT-200 and CT-400 are appropriate for extracting a protein crystal from high-viscosity or organic solutions. CT-300 and CT-400 enable the capture of small crystals 50μm in size. We are now able to manipulate crystals of various sizes and in various conditions using the series of the Crystal Catcher devices.

The extra solution around captured crystal not only degrades the quality of data-collection statistics but also disturbs the initial phase determination by the sulfur single-wavelength anomalous diffraction (SAD) method. The effect of reducing the solution in this tool is helpful in the sulfur SAD method. We have evaluated the effects of our tool on a quality and crystallographic data in the sulfur SAD method using Co Kα radiation.

References

1. Kitatani et al. (2008) Appl. Phys. Express 1, 037002.
2. Kitatani et al. (2009) Jpn. J. Appl. Phys. 47, 8995.

P-149 New Possibilities for X-ray Diffractometry: Brighten Up Your Home-Lab

J. Wiesmann, T. Samtleben , B.Hasse, J. Graf, C.Michaelsen
Incoatec GmbH, Max-Planck-Straße 2, D-21502 Geesthacht, Germany
(administration@incoatec.de)

The latest developments in new X-ray microfocus sources lead to new possibilities in X-ray diffractometry. Using the new Incoatec Microfocus Source (IμSTM) with the latest kind of two dimensional focussing Montel optics, the so called QuazarTM optics, in combination with a two dimensional detector allows high quality diffractometry measurements with very good resolution of very small and weakly scattering samples in the home-lab in short time.

Foto of Incoatec Microfocus Source:

The advantages of the new 30 W air cooled IμS with a focal spot size below 50 μm are presented. The use of IμS is as easy as for all sealed tube systems and the performance exceeds typical combinations of traditional rotating anodes with multilayer optics. With a focussing optics IμS achieves in a single crystal diffraction set-up a flux above 3•10E08 cps in a 250 μm spot with Cu-K or a flux above 10E07 cps in an 110 μm spot for Mo-Ķ radiation.

For SAXS experiments there is also an IμS available with a 2 dimensional collimating optics.

Various examples of new application measurements on different X-ray samples are shown, like proteins, small molecules and SAXS, proving the broad field of applicability of the IμS.

P-150 Desktop Minstrel UV™: A Novel Protein Crystal Monitoring Automation System Using UV Fluorescence Microscopy

Jian Xu, Craig Sterling and Michael Willis
Rigaku Automation, 5999 Avenida Encinas, Suite 150, Carlsbad, CA 92008

Identifying protein crystals in crystallization droplets has long been considered a challenging step in the field of protein crystallography. Although there are numerous automated crystallization robots readily available, none have been able to successfully monitor crystal growth by distinguishing protein crystals from non-protein crystals and detecting crystals from drops that are otherwise difficult to see with visible light. In order to fulfill this critical need, Rigaku has developed a novel protein crystal monitoring automation system, the Desktop Minstrel UV™, which uses UV fluorescence microscopy. The system includes an ultraviolet microscope with at least one ultraviolet light emitting diode, providing illumination with the wavelength matching the absorption of the fluorescing amino acids, such as tryptophan. To greatly decrease photo-damage to the protein crystals, the fluorescing light illuminated on the sample is reduced to the minimum and is then digitally recorded by a camera with a CCD sensor. We have conducted crystallization experiments with various proteins in order to evaluate this system. The resulting UV images from these experiments clearly reveal the protein crystals from non-protein crystals, such as salts. In addition, this UV crystal monitoring system is built upon the platform of Rigaku's state-of-art imaging automation technology, the Desktop Minstrel™, which makes the evaluation of a large number of crystallization experiments possible. The Desktop Minstrel UV enables researchers to accurately harvest protein crystals for data collection or design follow-up experiments.

P-151 SAXS/WAXS Experiments with a Single Detector

Naoto YAGI[1,2] and Noboru OHTA[1]
[1]*Japan Synchrotron Radiation Institute, SPring-8, 1-1-1 Kouto, Sayo, Hyogo 679-5198, Japan. (yagi@spring8.or.jp)*
[2] *RIKEN SPring-8 Center, 1-1-1 Kouto, Sayo, Hyogo 679-5198, Japan.*

There is an increasing demand to record the wide-angle X-ray scattering/diffraction (WAXS) in small-angle X-ray scattering/diffraction (SAXS) experiments. For this purpose, it is common to use two detectors, each one for SAXS and WAXS. However, this method has drawbacks: (1) The region between the two detectors, medium-angle region, cannot be recorded. (2) The WAXS detector tends to be a linear detector which is unsuitable for a complicated oriented diffraction patterns. (3) Sometimes it is hard to match exposures of the two detectors. It is obviously ideal to cover a large range of the scattering with a single detector.

For this reason, we have been trying large-area detectors for SAXS/WAXS measurements. One detector is RIGAKU RAXIS-VII image plate detector at BL40B2 in SPring-8. This detector has an area of 300mm x 300mm with a 100umx100um pixel. In a diffraction pattern from a lipid, a series of reflections in the small-angle region and the reflections at about 0.41 nm-1 that appears at around 0.24 nm-1. The former is from the lamellar structure, and the latter from the lateral packing of the lipid molecules in the bilayer.

Another detector we are using is RIGAKU Jupiter210 at BL45XU. The detector was previously used for protein crystallography data collection. The hutch B of this beamline was converted to the SAXS/WAXS station by bringing a bench for small-angle scattering. The typical sample-to-detector distance is 500 mm. The X-ray wavelength of 0.09 nm is usually used. The beam stop is 2mm in diameter, which enables us to measure the small-angle region up to 1/30 nm-1. Jupiter210 comprises of four CCDs with tapered fibers. The area is 210mmx210mm. By placing the beam stop at the lower area of the detection area, it is possible to cover down to 1/0.25 nm-1 in the wide-angle region. Since the readout of Jupiter210 (<10 sec) is faster than that of RAXIS-VII (>60 sec) and the flux of BL45XU (undulator beamline) is higher than that of BL40B2 (bending magnet beamline), this system is suitable for scanning SAXS/WAXS experiments.

It is clear that a detector with a larger area and fast readout is ideal for SAXS/WAXS experiment. A example of such a detector is ADSC Quantum-315 or MAR MX-325. Another technique required is a large vacuum window. The design of the entrance "nose" of the vacuum chamber that does not block WAXS is also important.

P-152 Fully automated data collection system at macromolecular crystallography beamlines in the Photon Factory

Yusuke Yamada, Naohiro Matsugaki, Masahiko Hiraki, Leonard M.G. Chavas, Noriyuki Igarashi and Soichi Wakatsuki
Structural Biology Research Center, Photon Factory, Institute of Materials Structure Science, High Energy Accelerator Research Organization, 1-1 Oho, Tsukuba, Ibaraki, 3050801, Japan (yusuke.yamada@kek.jp)

Structural biology research center in the Photon Factory has pursued the enhancements of synchrotron beamlines for macromolecular crystallography [1]. Recently, we have constructed a new beamline, AR-NE3A, which is dedicated for a high-throughput data collection required in pharmaceutical application. At AR-NE3A, we could obtain the highest photon flux at the sample position among high-throughput beamlines at the Photon Factory. In the experimental hutch, a high precision diffractometer, a fast-readout and high-gain CCD detector, and a sample exchange system able to handle more than two hundred cryo-cooled samples stored in a Dewar, have been installed. Consequently, data set collection from a large number of samples can be carried out within a day. To facilitate high-throughput data collection required for pharmaceutical researches, fully automated data collection and processing systems have been developed.

In this system, a user prepares a file describing a experimental schedule and data collection

condition of each sample. In each cycle, a sample is exchanged by the sample exchange system and centered by recognizing a shape of the loop. After the centering of the sample, data set collection is carried out based on a user pre-defined condition. Once the data set is collected, this data set is automatically submitted to data reduction software. Finally, all cycles are completed, a brief summary containing pictures of a sample after the centering, diffraction image and data reduction statistics is reported.

This system is operated since April 2009 and utilized in actual pharmaceutical research during beam time term April-June 2009. In the presentation, some results and statistics during this beam time term will be shown.

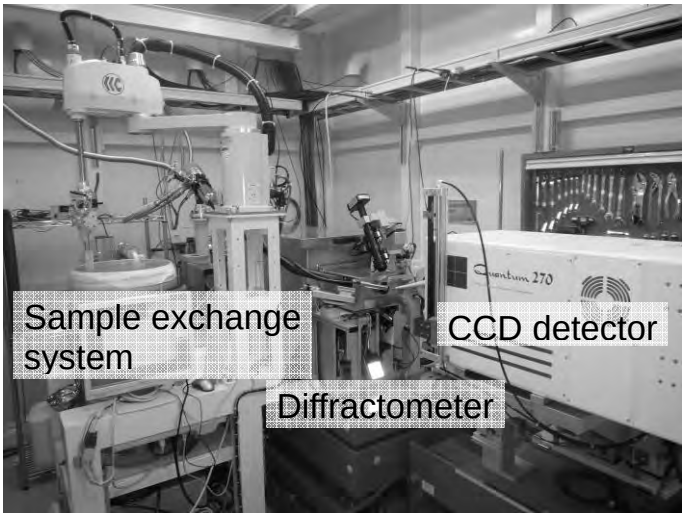

Figure. Experimental apparatus in the end station of AR-NE3A

Reference

Hiraki *et al.* "Current status and developments of macromolecular crystallography beamlines at the Photon Factory" Joint Conference of the Asian Crystallographic Association and Chinese Crystallographic Society Oct. 22nd –25th , 2009, Beijing, China

P-153

Development of a New Rietveld Code as Powder Diffraction Analysis Suite, Z-Code

Masao Yonemura[1], Takahiro Morishima[2], Ryoko Oishi[2], Dyah Sulistyanintyas[3], Hidetoshi Oguro[3], Kenji Iwase[3], Akinori Hoshikawa[3], Toru Ishigaki[3], Kazuhiro Mori[4], Ryoji Kiyanagi[5], Junrog Zhang[2], Teguh Panca[2], Shuki Torii[2], and Takashi Kamiyama[2]

[1] *Institute of Applied Beam Science, Ibaraki University, 4-12-1 Nakanarusawa, Hitachi, Ibaraki, 316-8511 Japan (yonemura@mx.ibaraki.ac.jp)*

[2] *Institute of Materials Structure Science, High Energy Accelerator Research Organization, 1-1 Oho, Tsukuba, Ibaraki, 305-0801 Japan*

[3] *Frontier Research Center for Applied Atomic Sciences, Ibaraki University, 162-1 Shirakata, Tokai, Naka, Ibaraki, 319-1106 Japan*

[4] *Kyoto University Research Reactor Institute, Kumatori, Sennan, Osaka, 590-0494 Japan*

[5] *Institute of Multidisciplinary Research for Advanced Materials, Tohoku University, 2-1-1 Katahira, Aoba, Sendai, Miyagi, 980-8577 Japan*

New Japanese Spallation Neutron Source (JSNS), Materials and Life Science Facility (MLF) in Japan Proton Accelerator Research Complex (J-PARC) has been inaugurated. Four different powder diffractometers (Super High Resolution(S-HRPD), High Throughput (iMATERIA), Engineering(TAKUMI), Total Diffraction(NOVA)) have already put out the first great data. Furthermore, two more diffractometers have been proposed. In this situation, new powerful and useful analysis software for powder diffraction data is desired. Since 2004, the powder diffraction group in J-PARC has started to develop a new powder diffraction analysis suite, Z-Code (code-name for the development), which was presented in previous AsCA and IUCr. Fig.1 shows the overview of Z-Code. It is the integrated environment for finding out crystal structures using various analysis methods from powder diffraction data. For example, It has the general functions of Indexing, Peak Searching, Structure Matching from a Data Base, and Conventional Rietveld analysis. Z-Code also supports Texture analysis, Profile analysis, Fourier synthesis, and Maximum Entropy Method as the advanced analysis components.

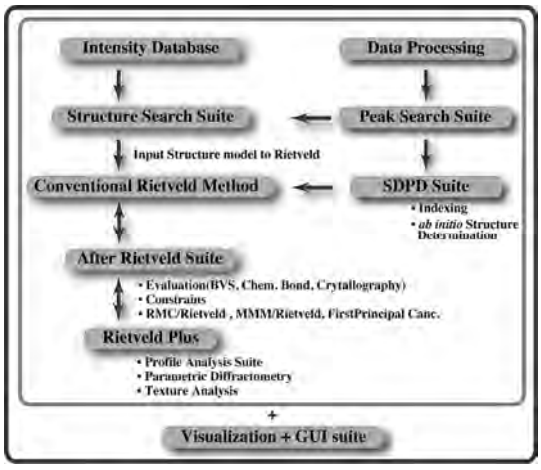

Fig. 1 The overview of Z-Code. Z-Code is still under development for both professional and beginners.

We just released and began to test the new Rietveld analysis software called "Z-Rierveld" with the first users of the powder diffractometers in J-PARC. Z-Rietveld is the one component of Z-Code. It has a Graphical User Interface (GUI) and many powerful features for the refinement of crystal structures. Z-Rietveld has demonstrated nice refinements of a complicated structure models using multiple data sets, such as x-ray and neutron ones. In this

presentation, more features and details of Z-Rietveld will be discussed.

P-154 Study of Time Rebinning for Super High Resolution TOF Neutron Diffraction

Junrong Zhang, Shuki Torii, Teguh Panca Putra, Takashi Muroya, Takahiro Morishima, Ryoko Oishi, Takashi Kamiyama
Institute of Materials Structure Science, High Energy Accelerator Research Organization, 2-4 Shirakata Shirane, Tokai, Ibaraki 319-1195, Japan
(jrzhang@post.kek.jp)

High resolution becomes increasingly important for studying tiny structural changes and subtle microstructures of materials. SuperHRPD@J-PARC is the world highest resolution neutron powder diffractometer of its type, with the resolution of $\Delta d/d$ = 0.03% in the backscattering detector. However the high resolution is gained at the cost of intensity, by increasing the neutron flight path. Hence, it is significantly useful to rebin the TOF data on the high-precision structure refinements.

The calibration run of NIST Silicon was performed at SuperHRPD. Only the data collected on the backscattering bank were used for Rietveld analysis. The neutron diffraction pattern is plotted in Fig.1, where the data have been corrected for incident spectrum including the contribution of holder and empty. Due to the low statistics in some measurements, the time channel rebinning routine is utilized to enhance the typical 'Rietveld-quality' data. Rebinning across the whole TOF spectrum is carried out in the bin groupings of like 8 or 16, etc, by the summation of points with increasing steps or weights. (The schemes of weight are shown as stepwise curves in Fig.1.) It will reduce the estimated standard deviation on each point. The well-defined instrumental line shape and extremely sharp peaks can be obtained. As indicated in Fig.2(a), all features are preserved in bin grouping of 8, and however there is clearly a loss of information in Si (311) peak using a bin grouping of 16. That is the price for time rebinning. Therefore careful consideration must be paid in case of peak overlap and reflection splitting. In addition, it can be seen from Fig.2(c) that the statistic fluctuation in the background is suppressed largely.

More importantly, time rebinning can decrease the number of points across the diffraction profile. The data were analyzed with the Rietveld method using the Z-Code, GSAS, and FullProf software. It was concluded that refinement procedure could be speeded up dramatically, and the convergence was easier to be approached. High reliable fits and good background subtraction were achieved, that R_p factors given by GSAS are 11.01%, 8.87%, and 7.97% for data with no binning and in bin groupings of 8 and 16, respectively. Additionally, we also found that different bin groupings have subtle effects on the structure and profile function parameters. In summary, the time rebinning is proved to be very effective for Rietveld refinement of high resolution TOF diffraction data.

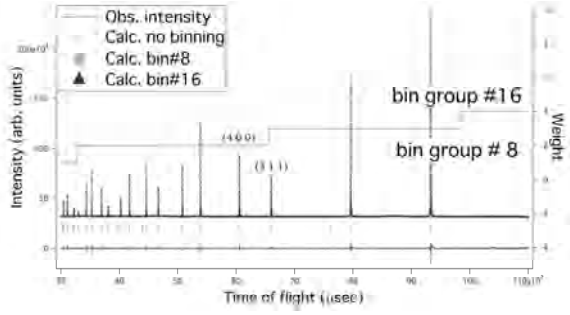

Fig.1 The observed and calculated diffraction patterns and their differences, with no binning and in bin groupings of 8 and 16, respectively. The lower and upper stepwise curves illustrate the schematic representations for bin groupings of 8 and 16, respectively.

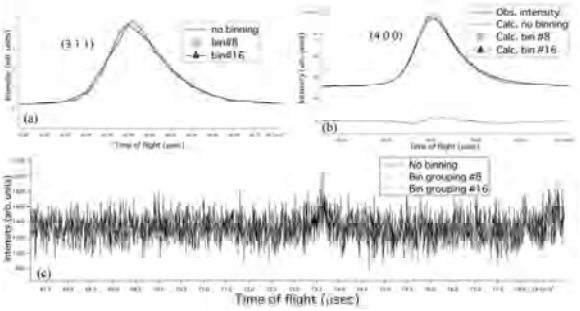

Fig.2 a), b), and c) are observed Si (311) peak, calculated Si (400) reflection, and background, with no binning and in bin groupings of 8 and 16, respectively.

P-155 Echidna High-Resolution Neutron Powder Diffractometer at OPAL: one year of experience and experiments

Maxim Avdeev, James Hester
Bragg Institute, Australian Nuclear Science and Technology Organisation, PMB 1, Menai, 2234 NSW, Australia (Maxim.Avdeev@ansto.gov.au)

A new high-resolution neutron powder diffractometer "Echidna"* is now fully operational at the OPAL reactor (Australian Nuclear Science and Technology Organisation) and has been open to the international community since mid-2008. Access is via calls for proposals twice a year (May/November) and a "mail-in" service** for rapid turnaround.

The instrument is well suited for studying a wide variety of materials, ranging from those with a high degree of structural disorder to materials with long-period magnetic lattices. This flexibility arises from the combination of Ge{hhl} monochromators with a continuously variable take-off angle (90-140º) providing access to wavelengths from 1 Å to 3.2 Å and a d-spacing range of 0.5 to 30 Å.

Selection of 5' or 10' primary and secondary collimators, in addition to the natural $\alpha 1$ and $\alpha 2$ horizontal divergence options (~12'-38' and ~20'-40' depending on the wavelength used, respectively), adds considerable flexibility in adjusting the "intensity/resolution" balance. This enables the instrument configuration to be matched to sample complexity. If required, Echidna may be configured to reach a resolution of $\Delta d/d \sim 5 \times 10^{-4}$.

Variable vertical focusing of the monochromator and a large array of 128 position-sensitive ^{3}He detectors results in data collection times that are relatively short for a high-resolution 2θ scanning powder diffractometer. Depending on the selected instrument configuration, sample composition, and sample size these times are typically between 1 and 6 hours. An extra gain in peak/background ratio is achieved by using a custom-built vacuum chamber for room temperature experiments.

The details of design and data treatment software and recent experimental results will be presented.

* www.ansto.gov.au/research/bragg_institute/facilities/instruments/echidna/specifications
** www.ansto.gov.au/research/bragg_institute/users

P-156 WebCSD – on-line access to the Cambridge Structural Database and applications in chemical education

Gary M. Battle
Cambridge Crystallographic Data Centre (CCDC), 12 Union Road, Cambridge CB2 1EZ, UK (battle@ccdc.cam.ac.uk).

The Cambridge Structural Database (CSD) serves as the worldwide repository of small-molecule organic and metal-organic crystal structure data. As such, this unique database of one-half million molecules is a crucially important resource for chemical education.

However, despite this abundance of experimental data, many aspects of structural chemistry are still taught using 2-D drawings, or idealized 3-D models.

The CSD is provided with a range of sophisticated search and analysis tools. Whilst these tools enable crystallographers, structural chemists and the drug design community to extract vital structural knowledge, the requirement to install and become familiar with an extensive suite of software can be a barrier for the non-expert user.

WebCSD is a new web-based interface to the CSD, offering fast and simple access to crystal structure data using only a standard web-browser. This talk will describe this on-line tool and how, through a Discovery Corps Senior Fellowship (DCF) from the National Science Foundation, the use of crystal structure data has been integrated into the undergraduate chemistry curriculum in more than 30 institutions in the US.

***Acknowledgements**: This work is supported is by the Cambridge Crystallographic Data Centre and the United States National Science Foundation under Grant No. 0725294.*

P-157 Enhancing Stability of Enzymes through Modulation of Inter-domain Interactions: A Case Study

Debi Choudhury, Sumana Roy, Sampa Biswas and J. K. Dattagupta
*Crystallography and Molecular Biology Division, Saha Institute of Nuclear Physics, 1/AF Bidhannagar, Kolkata-700064, India, (*sampa.biswas@saha.ac.in*)*

Inter-domain interactions are known to play a major role in the stabilization of multidomain proteins. So engineering higher inter-domain interactions can be a justified approach to increase the stability of a protein. However, inter-domain motion in a multidomain protein is related to protein function like enzyme catalysis and thus engineering inter-domain interactions sometimes may lead to a loss of protein function. Aim of this study was to rationally design mutant(s) with enhanced thermostability for multidomain enzymes retaining their full activity. Papain is an archetype enzyme of the papain family which has two interacting domains and the active-site cleft lies at the interface between these domains. We therefore chose papain as a model protein for enhancing stability which may also be of benefit for industry. From the three dimensional X-ray structures of three thermostable proteases of the papain family, Ervatamins A, B and C, we could identify three residues which were thought to be responsible for higher inter-domain interactions in these enzymes and we carried out replacement of these three amino acids at the corresponding positions of papain through SDM. In the process, we were able to generate a double and a triple mutant of papain which were found to be experimentally more thermostable than the wild type. The optimum temperature of activity of these mutants increased by 10-12 ºC and their half-life of activity at 65 ºC was 20-30 min longer than the wild type. The kinetic experiments on these two mutants also confirmed that catalytic efficiency has not significantly changed. In-silico molecular simulation studies and normal mode analysis on the mutants were carried out to establish the molecular and structural basis for the changed properties. Such an approach for enhancing stability can be extended for other multidomain proteins.

Wide-Angle incidence Waveguides Using X-Ray Diffraction

P-158

S.-L. Chang[1] , C.-J. Huang[1], L.-S. Cai[1], H.-Y. Chen[1], C.-H. Chu[1], M.-T. Tang[2], Yu. P. Stetsko[2], B.-Y. Shew[2]
[1] *Department of Physics, National Tsing Hua University, Hsinchu,Taiwan, 300. (slchang@phys.nthu.edu.tw)*
[2] *National Synchrotron Radiation Research Center, Hsinchu, Taiwan, 300.*

We report on the diffraction phenomena of X-rays in nano-scale waveguides in the wide-angle incidence geometry. This type of waveguides is different from the conventional types where grazing incidence or normal incidence of X-rays is adopted. In order to bend a wide-angle incident beam along the crystal surface, the (113) reflection of silicon at the 8.8785keV is used. The waveguides are prepared on a [001] Si wafer of 6 inches in diameter and 675 um in thickness. The designed waveguides are along [110] direction. The sizes of the waveguides are 5mm long and 700, 450, 400, and 350 nm wide, respectively. The sample wave guides are prepared by using microelectronic lithographic techniques to etch out the Si wafer by 1 um in depth. The waveguides are then plated with gold for about 150 nm in thickness on the top, the left and right surface and 300 nm for the bottom. Detailed analysis on the interference among the existing eight modes of wave propagation in this waveguide will be discussed.

Study on Structural Biology

P-159

Ko-Hsin Chin[a, b] & Shan-Ho Chou[a, b, *]
[a] *Institute of Biochemistry*
National Chung-Hsing University, Taichung, 40227, Taiwan
[b] *National Chung Hsing University Biotechnology Center*
National Chung-Hsing University, Taichung, 40227, Taiwan

C-di-GMP controls the transition between pathogenicity and biofilm formation in eubacteria, yet not much is known about how this nucleotide exerts its action in cells. In the plant pathogen Xanthomonas campestris, the expression of a number of pathogenicity genes is regulated by the levels of c-di-GMP and also by the CAP-like protein XcCLP. In this manuscript, we report the structural insights into the interaction between c-di-GMP and XcCLP in gene regulation. We have determined the crystal structure of an active XcCLP variant using X-ray crystallography, and have shown using EMSA and Biacore experiments that XcCLP binds target promoter DNA with sub-mmolar affinity in the absence of any ligand. Detailed structural comparisons of XcCLP with constitutively active CRP variants from Escherichia coli showed that changes of several crucial residues in XcCLP culminate in a substantial structural transition leading to the formation of an active conformation suitable for DNA binding. Competitive EMSA experiments of the XcCLP/DNA complex titrated with c-di-GMP indicated that c-di-GMP inhibits XcCLP from binding cognate DNA. Modeling studies of XcCLP/c-di-GMP complex indicated that c-di-GMP interposes between the XcCLP dimerization and DNA-binding domains, reorienting the DNA-contacting helix. These results strongly suggest that XcCLP is a c-di-GMP responsive transcriptional regulator adopting an intrinsically active DNA-bound conformation, yet its DNA-binding capability is abrogated when bound with c-di-GMP. XcCLP is therefore the first transcription factor in the CRP/FNR superfamily observed to regulate *Xcc* pathogenicity genes expression in a manner negatively

controlled by c-di-GMP.

P-160 The Structural analysis of the FAS1 domain 4 of βig-h3 for relationship with corneal dystrophy.

Jiho Yoo[1], Jongsoo Jeon[1], Kuglae Kim[1], Eugkweon Kim[3], Jongsun Kim[2], Hyun-Soo Cho[1]*.
[1] *Department of Biology, college of Life Science and Biotechnology, Yonsei Uviversity, 134 Shinchon-dong, Seodaemun-gu, Seoul 120-749, Republic of Korea. (hscho8@yonsei.ac.kr)*
[2] *Department of Microbiology and Brain Korea 21 Project of Medical Sciences*
[3] *Department of Biochemistry and Molecular Biology, Yonsei University college of Medicine, Seoul, Republic of Korea*

The βig-h3 is a kind of extracellular matrix proteins and involved in cell adhesions. It has been reported that mutations on the βig-h3 gene cause amyloid deposits and induce a corneal dystrophy disease in human eyes. In order to elucidate the molecular basis of the βig-h3 for inducing amyloid deposits and a corneal dystrophy, we determined the crystal structure of the βig-h3 FAS1 domain 4. It shows a canonical FAS1 domain structure which consists of six α-helices and six β-strands. Interestingly, R555 residue of which the mutations are the ones of the frequently founded in corneal dystrophy patients is exposed outward. On the other hand, most other mutations for a corneal dystrophy are found inside of the protein suggesting the mutations would induce folding problems. Along with results of molecular dynamics simulations and CD spectrums, the crystal structure of the βig-h3 FAS1 domain 4 suggests that R555 mutations cause a local structural change especially in the a5-a6 loop resulting in disturbance of the protein-protein interactions and gives us the insight for the molecular mechanism for a corneal dystrophy.

P-161 Structural analysis of a prokaryotic Kir channel captured in multiple conformations

Oliver B. Clarke[1,2], Alessandro T. Caputo[1,2], Brian J. Smith[1], Jacqueline M. Gulbis[1]
[1] *Walter and Eliza Hall Institute of Medical Research, 1G Royal Pde, Parkville 3052, Melbourne, Victoria, Australia (clarke@wehi.edu.au; jgulbis@wehi.edu.au)*
[2] *Department of Medical Biology, University of Melbourne, Parkville 3052, Victoria, Australia*

Inward rectifiers (Kir; IRK) are a family of ligand-gated K^+ channels with diverse roles in the physiology of higher organisms. They stabilise the resting membrane potential, and are crucial in the regulation of cardiac [1] and pancreatic [2] function. We are carrying out a systematic study of gating in inward rectifier K^+ (Kir) channels, utilising the prokaryotic channel KirBac3.1 as a model system to obtain insights into the function and regulation of mammalian Kirs. The recently reported crystal structure of a chimeric channel comprising the pore of the prokaryotic KirBac1.3 and the cytoplasmic regions of mouse Kir3.1 revealed seamless integration of mammalian and prokaryotic segments [3]. Their physical accord established the validity of using prokaryotic channels for investigating molecular aspects of the mammalian system.

We have recently solved several new crystal structures of a prokaryotic inwardly rectifying

potassium channel, KirBac3.1. In comparison with previously solved structures of both KirBac3.1 and KirBac1.1, our structures reveal intriguing differences.

Most strikingly, the cytoplasmic assembly is rotated with regards to the transmembrane domain, forming a novel interface between the cytoplasmic assembly and the amphipathic slide helices of the transmembrane region. This interface is stabilized by a salt-bridge between a highly conserved aspartate on the slide helix and an arginine contributed by the cytoplasmic domain of an adjacent subunit.

Rearrangement of the cytoplasmic subunit interfaces is observed in some of the structures, including reconfiguration of a functionally important salt bridge, disruption of which is implicated in the genesis of Andersen's syndrome.

The implications of these structures for current models of the gating process in Kir channels will be discussed.

References

[1] F. M. Gribble, S. J. Tucker, S. Seino, F. M. Ashcroft, *Diabetes*.
[2] F. M. Ashcroft, S. J. Ashcroft, D. E. Harrison, *The Journal of Physiology* **400**, 501
[3] M. Nishida, M. Cadene, B. T. Chait, R. MacKinnon, *EMBO J* **26**, 4005.

P-162 Crystallization and Preliminary X-ray analysis of PNP 4-mono-oxygenase from *Pseudomonas putida* DLL-E4

Zhongli Cui, Weidong Liu , Wenjing Shen
College of Life Sciencess,Nanjing Agricultural University, 6 Tongwei Road, Nanjing, 210095 P.R.China (czl@njau.edu.cn)

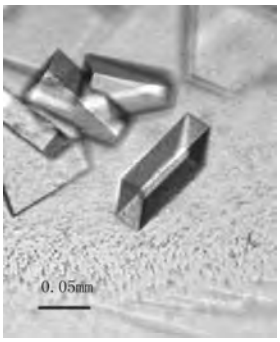

p-nitrophenol (PNP, also known as 4-nitrophnol or 4-NP), is the most common and important in terms of quantities manufactured and extent of environmental contamination. It is used for synthesis of medicines, dyes, explosives, leather colouring, wood preservatives, and rubber chemicals (Uberio, 1997).The strain Pseudomonas putida DLL-E4 (Liu Zhi 2003) degrading methyl parathion (MP) was isolated from soil polluted by MP for long term, and it can use PNP as sole carbon and nitrogen sources. We successfully cloned pnpA gene(genbank accession number: FJ376608) from a DNA fragment which exhibits PNP 4-monooxygenase activity from Pseudomonas putida DLL-E4, we expressed pnpA in Escherichia coli with a C-terminal 6-his tag and purified it to homology by Ni-NTA column.

Crystallization conditions were performed by Hampton Research Crystallization Kits(Hampton Research). Diffraction-quality oblique parallelepiped shape crystals were obtained with hanging drop vapor diffusion method performed at 293 K by mixing 3µl 10 mg/ml protein with 3µl reservoir solution and equilibrated against 500 µl mother liquor, the mother liquor contains 20 mM HEPES (pH 7.0), 15% PEG 4000, and 15% isopropane. The crystals reached dimensions of up to 0.025 x 0.1 x 0.1mm(figure in topright) after 2 days.

Diffraction data were collected from a single crystal at the beam line BL17U of Shanghai Synchrotron Radiation Facility (Shanghai, P.R. China) using a MAR 225 CCD area detector (MAR Research). The diffraction data for the crystal were integrated and scaled using HKL-2000 (Otwinowski & Minor, 1997)The collected data has 97.9% completeness and with an overall R-merge of 7.8 % on intensity, and the space group of the crystal belongs to the orthorhombic P212121 with unit-cell parameters a = 54.47, b = 77.56, c = 209.17. Based on the subunit Molecular Weight is 47.3 kDa (including six histidine residues), there were two molecules in the asymmetric unit and the Matthews coefficient VM was 2.33 Å3 Da-1, corresponding to a solvent content of 47.35% (Matthews, 1968), the estimated mosaicity of the data is 0.117°. Further attempts to solve the structure by multiwavelength anomalous diffraction (MAD) method (Hendrickson et al., 1990) using selenomethionine-substituted protein are currently under way.

References

1. Uberio, V. & Bhattacharya, S. K. (1997). *Water Environment Research*, **69**, 146-156.
2. Liu, Z., Hong, Q. & Zhang X. Z. (2003). *China Environmental Science*, **23**, 435-439.
3. Otwinowski, Z. & Minor, W. (1997). *Methods Enzymol*. **276**, 307-326.
4. Matthews, B. W. (1968). *J. Mol. Biol*. **33**, 491-497
5. Hendrickson, W. A., Horton, J. R. & LeMaster, D. M. (1990). *EMBO J*. **9**, 1665-1672.

P-163

How to interpret the quarterly charged $[Ni(dmit)_2]^{-1/4}$? — Structure and electrical conductivity of (n-Bu_4N)$[Ni(dmit)_2]_4$MeCN

Qi Fang [1,*], Wen-Tao Yu [1], Chun-Li Guo [1], Wei Xu [2]
[1] *State Key Laboratory of Crystal Materials, Shandong University, Jinan 250100, China, (fangqi@sdu.edu.cn)*
[2] *Institute of Chemistry, Chinese Academy of Sciences, Beijing 100080, China*

$Z[M(dmit)_2]_x$ (Z is mono-cation) type conductive and super-conductive complexes have received great attentions. Here we report the structure and conductivity of the new (n-Bu_4N)$[Ni(dmit)_2]_4$ MeCN.

We grew the crystal *in situ* of the reaction: $4[Ni(dmit)_2]^- + 3Ag^+ \rightarrow 3Ag + 4[Ni(dmit)_2]^{-1/4}$. The X-ray diffraction data were collected on a Bruker P4 diffractometer by Mo K_α radiation at 293 K. Crystal data: *P*-1 space group; *a*, *b*, *c* = 12.029(1), 14.795(2), 23.076(3) Å; α, β, γ = 102.85(1), 103.82(1), 96.31(1)°; V = 3829.8(7) Å^3; and R_1, wR_2 = 0.0476, 0.0881 ($I > 2\sigma(I)$); S = 1.002; $\Delta\rho_{max}$, $\Delta\rho_{min}$ = 0.358, -0.295 e/Å^3.

As shown in Fig. 1, the Lnσ of the single crystal (σ is conductivity) has a linear dependence on T^{-1}, indicating a semi-conductive behavior with a low activation energy being E_a = 0.12 eV. The planar coordination anions are parallel arranged in tetras (see Fig. 2). Within a tetrad $\{4[Ni(dmit)_2]^{-1/4}\}$, the interplanar distance is 3.56 Å and the Ni…Ni distances are 4.05, 4.06, and 4.08 Å. Between tetrads, the interplanar distance (3.63 Å) and Ni…Ni distance (4.91 Å) are larger.

As shown in Fig.3, the IR spectra of (n-Bu_4N)$[Ni(dmit)_2]_4$MeCN shows two C=C peaks at 1349 and 1265 cm^{-1} with the intensity ratio of 1:3. Meanwhile, the IR C=C peaks of

(n-Bu_4N)[Ni(dmit)$_2$] and [Ni(dmit)$_2$] are located at 1349 and 1266 cm^{-1}, respectively. This indicates that the tetrad {4[Ni(dmit)$_2$]$^{-1/4}$} may consist of one mono-anion [Ni(dmit)$_2$]$^-$ and three neutral [Ni(dmit)$_2$].

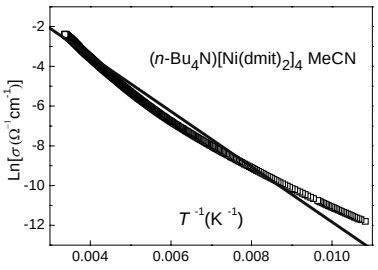

Fig. 1 Lnσ~T^{-1} curve (σ is conductivity)

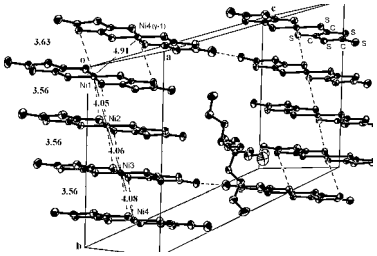

Fig. 2 Crystal structure of (n-Bu_4N)[Ni(dmit)$_2$]$_4$MeCN

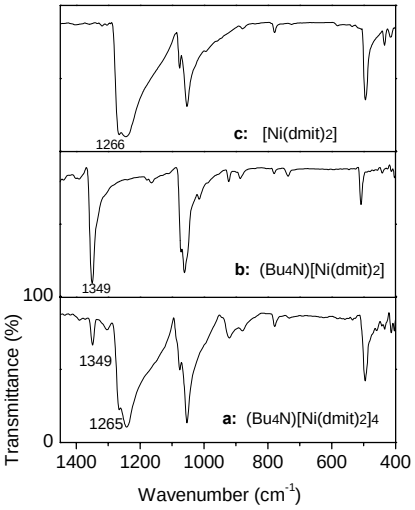

Fig. 3 IR spectra of several complexes

P-164 The structure of the ribosome with elongation factor G trapped in the post-translocational state

Yong-Gui Gao, Maria Selmer[1], Christine M. Dunham[1], Albert Weixlbaumer[1], Ann C. Kelley and V. Ramakrishnan

MRC Laboratory of Molecular Biology, Hills Road, Cambridge CB2 0QH, United Kingdom (yggao@mrc-lmb.cam.ac.uk)

Elongation factor G (EF-G) is a GTPase that plays a crucial role in the translocation of tRNAs and mRNA during translation by the ribosome. We report a crystal structure refined to 3.6 Å resolution of the ribosome trapped with EF-G in the post-translocational state using the antibiotic fusidic acid. Fusidic acid traps EF-G in a conformation intermediate between the GTP and GDP forms. The interaction of EF-G with ribosomal elements implicated in stimulating catalysis, such as the L7/L12 stalk and the L11 region, and of domain IV of EF-G with P-site tRNA and mRNA shed light on various aspects of EF-G function in catalysis and translocation. The stabilization of the mobile stalks of the ribosome also results in a more complete description of its structure. As the first ribosome GTPase structure, the present research also paves way for study on other GTPase bound to ribosome.

Keywords: Elongation factor G, EF-G, ribosome, translation, translocation, fusidic acid

Growth and Characterization of α and γ-glycine single crystals

P-165

T.P.Srinivasan[1,2], S.Anandhi[1] and R.Gopalakrishnan[1]
[1]*Department of Physics, Anna University Chennai, Chennai – 600 025, Tamil Nadu, India.(krgkrishnan@yahoo.com and krgkrishnan@annuniv. edu)*
[2]*Deparment of Physcis, K.L.N. College of Engineering, Madurai , Tamil Nadu, India.(tps176@yahoo.com)*

Complexes of amino acids with inorganic salts have been of interest as materials for optical second harmonic generation (SHG), and all amino acids except glycine contain chiral carbon atoms and perhaps crystallize in the non-centrosymmetric space group [1]. Dipolar molecules possessing an electron donor group and an electron acceptor group contribute to large second order optical nonlinearity arising from the intramolecular charge transfer between the two groups opposite nature. Due to this dipolar nature, amino acids have been considered as potential candidates for NLO applications [1]. Although the salts of amino acids like L-Arginine [2], L-Histidine [3] and L-Proline [4] are reported to have NLO properties; the complexes of glycine with inorganic salts are not explored for optical SHG so far, since glycine, the simplest amino acid, does not possess the asymmetric carbon, it is NLO inactive. Out of the number of semi organic single crystals of glycine that have been already reported, most of them are not NLO active [5-7]. Glycine has three polymorphic crystalline forms α, β, γ [8,9]. Both α and β forms crystallize in centrosymmetric space groups ruling out the possibility of optical second harmonic generation. But γ-glycine crystallizes in non-centrosymmetric space groups $P3_1$ making it a possible candidate for NLO applications and it is difficult to grow the γ-glycine crystals [10,11]. The thermodynamic stabilities of the three polymorphs of glycine at room temperature are in the order γ > α > β [12]. It has recently been reported that complexes of the γ- glycine can be efficient in optical SHG with inorganic salt sodium nitrate [1]. Ferroelectrocity was discovered for glycine silver nitrate [13]. It was also reported that glycine combines with $CaNO_3$ [14] and $LiNO_3$ [15] to form single crystals but none of these are reported to have nonlinear optical property. To the best of the knowledge of the authors there is no report available on the growth and characterization of pure and γ- glycine.

The nonlinear optical single crystals of α-glycine and γ-glycine were grown by the slow evaporation solution growth method from aqueous solution as shown in figure 1(a) and 1 (b). The title compound was synthesized and purified by repeated recrystallization process. From the single crystal XRD analysis it is confirmed that the grown α-glycine crystallizes in monoclinic system with space group $P2_1/n$ and γ-glycine crystallizes in hexagonal with space group $P3_1$[16]. The determined lattice parameter values of α-glycine and γ-glycine crystals are in-line with the literature. In the FT-IR spectrum, the peak observed at 3167.51cm^{-1} of α-glycine and 3171.36cm^{-1} of γ-glycine is assigned to NH_3 asymmetric stretching mode which is related to the hydrogen bond strength. The bands at 1329cm-1 in the IR spectra are more reasonably assignable to NO_3^- ion in γ-glycine [17]. The range and percentage of optical transmission were ascertained by recording UV–Vis–NIR spectrum. It is observed that the lower cut-off wavelength of α-glycine and γ-glycine are 233nm and 257nm respectively. In γ-glycine, 100% transparency is observed in the wavelength region between 330nm and 800nm. It is to be noted that the optical transparency below 330nm in the UV region is the

most desirable characteristics for any nonlinear optical application such as second harmonic generation. Its second harmonic generation relative efficiency was measured by Kurtz and Perry powder technique using Nd:YAG laser and was observed to be 135mV for γ-glycine and to 95mV for potassium dihydrogen orthophosphate. Group theoretical analysis of the fundamental modes of α-glycine crystal predicts that there are 120 vibrational optical modes and are seen to decompose into $\Gamma_{117} = (30A_g+29A_u+30B_g+28B_u)$ apart from three acoustic modes $1A_u+2B_u$. γ -glycine crystal predicts that there are 90 vibrational optical modes and are seen to decompose into Γ_{90} = (44A + 43E) apart from three acoustic modes 1A+2E. The factor group analysis for α-glycine and γ-glycine crystals was performed by following the procedures outlined by Rousseau et al.[18]. Dielectric and thermal characteristics of low temperature solution grown single crystals of α-glycine and γ-glycine have been carried out. The dielectric constant and dielectric loss have been measured as a function of frequency in the range 50Hz – 5MHz and temperature range between 311K, 323K and 373K. It is found that dielectric constant decreases with increasing frequency for both α and γ -glycine crystals. Dielectric constant and dielectric loss are low for the γ -glycine compared to α glycine[19].

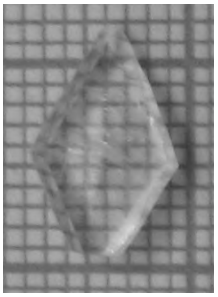

Figure 1(a).As grown γ- glycine

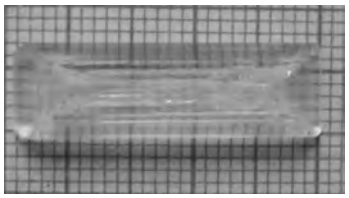

Figure 1(b). As grown α-glycine

References

[1] M.N. Bhat, S.M. Dharmaprakash, J. Cryst. Growth 235 (2002) 511.
[2] D. Eimert, S. Velsko, L. Davis, F. Wang, G. Loiaceono, G. Kennedy, IEEE J. Quantum Electron 25 (1989) 179.
[3] M.D. Aggarwal, J. Choi, W.S. Wang, K. Bhat, R.B. Lal, A.D. Shield, B.G. Penn, D.O. Frazier, J. Cryst. Growth 204 (1999) 179.
[4] R.D.A. Hudson, A.R. Manning, J.F. Gallagher, M.H. Garcia, Tetrahedron Lett. 43 (2002) 8375.
[5] B. Brezina, Mat. Res. Bull. 6 (1971) 401.
[6] J.K.M. Rao, M.A. Vishwamitra, Acta Cryst. B 28 (1972) 1484.
[7] S. Natarajan, J.K.M. Rao, Z. Kristallogr. 152 (1984) 179.
[8] G. Albrecht, R.B. Corey, J. Am. Chem. Soc. 61 (1939) 1087.
[9] E. Fischer, Ber. Dtsch. Chem. Ges. 38 (1905) 2917.
[10] Y. Iitaka, Acta Crystallogr. 11 (1958) 225.
[11] Y. Iitaka, Acta Crystallogr. 14 (1961) 1.
[12] I. Weissbuch, V. Yu. Torbeev, L. Leiserowitz, M. Lahav, Angew. Chem. Int. Ed. 44 (2005) 3226.
[13] R. Pepinsky, Y. Okaya, D.P. Eastman, T. Mitsui, Phys. Rev. 107 (1957)1538.
[14] S. Natarajan, K. Ravikumar, S.S. Rajan, Z. Kristallogr. 168 (1984) 75.
[15] J.Baran, M.Drozd, A. Pietraszko, M. Trzebiatowska, H. Ratajczak, J. Polish. Chem. 77 (2003) 1561.
[16].Yochi Iitaka, Acta Cryst. (1961),14,1.
[17] J.Baran, A.J.Barnes, H.Ratajczak,Spectrochim. Acta Part A: Mol. Biomol. Spectrosc.51A(1995) 197.
[18] D.L. Rousseau, R.P. Bauman, S.P.S. Porto, Journal. Raman Spectrosc. 24 (1993) 91.
[19] C.P.Smyth, Dielectric Behaviour and Structure, McGraw Hill, New York 1995.

P-166 Unusual arrangement of EF hand motifs in Calcium binding protein-1 of *Entameoba histolytica* and its functional implications

Shivesh Kumar, Ruchi Jain and S. Gourinath
School of Life Sciences, Jawaharlal Nehru University, New Delhi – 110067

Calcium plays a pivotal role in the pathogenesis of amoebiasis, a major disease caused by *Entamoeba histolytica*. A repository of EF-hand containing calcium-binding proteins (CaBPs) from *E. histolytica* share a high sequence similarity, they bind to different target proteins in a Ca^{2+} dependent manner, leading to regulation of different functional pathways. The crystal structure of the *Entamoeba histolytica* Calcium Binding Protein-1 (EhCaBP1) has been determined at 2.4 Å resolution. Only two out of the four expected EF-hand motifs could be modelled into the electron density map. Unlike CaM, the first two EF-hand motifs in EhCaBP1 are connected by a long helix and form a dumbbell shaped structure. Owing to domain swapping oligomerization, three EhCaBP1 molecules interact in a head-to-tail manner to form a triangular trimer. Three glycine residues in the central linker region connect the two domains of the protein that imparts flexibility and is the major cause of the disorder of the C-terminal of the protein. The oligomeric state of EhCaBP1 imparts reduced flexibility between domains and may be responsible for the limited target reorganisation. To understand the mode of target binding, co-crystallisation of EhCaBP1 with Phenylalanine shows that Phe binds to the hydrophobic pocket of the assembled-domain. The Phe bound assembled domain shows only 1.23Å RMS deviation with the N-terminal domain of CaM, bound to hydrophobic IQ-motif of cardiac Ca^{2+} channel. The hydrophobic residue Phe of the peptide (bound to CaM N-terminal domain) and Phe bound to EhCaBP1 assembled-domain are located at the similar regions. Functional studies clearly show the involvement of N-terminal domain as the functional domain of EhCaBP1 in activating kinase and localization in phagocytic cup. To validate the full-length structure, the initiatives have been taken to determine the structures of the individual domains. The crystal structure of N-terminal domain has been determined at 2.5 Å resolution. The structure is similar to the N-terminal domain of the full-length protein with the extended conformation of the EF-hand motifs connected with a long central helix. These studies clearly demonstrate that the N-terminal domain in trimeric form has most of the functions in comparison to the full length EhCaBP1 and N-terminal domain also has calcium dependent target binding activity.

P-167 Crystal structure of human Bfl-1 in complex with BAK BH3 peptide

Rongjin Guan[1], Rong Xiao[1], Li Zhao[1], Eileen White[2], Celine Gelinas[2], Guy Montelione[1]
[1]*Center for Advanced Biotechnology and Medicine (CABM), Rutgers, The State University of New Jersey*
[2]*Robert Wood Johnson Medical School, UMDNJ, 679 Hoes Lane West, Piscataway NJ 08854*

The Bcl-2 family proteins are crucial regulators of apoptotic pathways and are therefore considered important therapeutic targets in anticancer therapies. Bfl-1, or A1, is a pro-survival

member of the Bcl-2 family. Bfl-1 is a transcriptional target of nuclear factor-kB (NF-kB) that is overexpressed in many human tumors and is a means by which NF-kB inhibits apoptosis. Recently we have expressed and purified human Bfl-1 with its C-terminal 24 amino acids removed, after tremendous efforts on expressing the full-length protein without any success. We mixed the Bfl-1 protein with a 16 aa BH3 peptide of human BAK and further purified the complex, which was then crystallized. The X-ray diffraction data were collected on beamline X4C at Brookhaven. The complex structure was determined by molecular replacement and refined to 2.2 Å resolution. Bfl-1 adopts the canonical bcl-2 family fold which comprises 8 α-helices. The BAK peptide was half buried in a primarily hydrophobic groove in Bfl-1, which is formed by helices α5 and α8 (bottom of the groove) and those from α2, α3, α4 and the α4-α5 loop (sides of the groove). The BAK peptide forms seven hydrogen bonds and numerous vdW contacts with Bfl-1 residues from helices 4, 5, 8 and 4- 5 loop. We compared these interactions with those found in Bfl-1: Bim complex structure reported recently. Analysis the features of the drug targeting groove in Bfl-1 and Mcl-1 also explained why ABT-737 (a potential anti-cancer drug mimic BH3 domains of BH3-only proteins) can bind to Bcl-x_L but can not engage Bfl-1 and Mcl-1. This provides important structural information for designing new anti-cancer drugs targeting Bfl-1.

P-168 Secondary Extinction and Diffraction Behaviors in Single Crystals

Hua-Chen Hu
China Institute of Atomic Energy, Beijing102413, China, (hchu3310@gmail.com)

The X-ray and neutron diffraction processes in mosaic crystals with different shapes such as plane, cylinder and sphere are systematically investigated and solved within the framework of Darwin's transfer equations.

Plane and Deformed Crystals Universal expressions for the secondary extinction factor in X-ray and neutron crystallography are developed for the first time[1-2], based on a general solution of the power transfer equations from plane crystals. The vital key to the successful explanation of the solution of Darwin's equations, with a clear physical interpretation, is the introduction of a parameter ξ, the ratio of absorption cross section μ to diffraction cross section σ. As a result of these new development, the author was invited to rewrite chapter 6.4，Vol.C of the *International Tables of Crystallography* (*ITCr*)(2004) since the existing formulae of the integrated reflecting power ratio (*IRPR*) for asymmetrical Bragg and Laue geometry given in the *ITCr* (2001) are only the limiting cases of the present generalized formulae for $\xi_0 \rightarrow \infty$. The maximum reduced depth of radiation penetration as well as the optimal reduced thickness for both Bragg and Laue geometry are given in the paper[1]. They are important parameters for monochromator design. An unique method "layer coupling model" [3] was developed for the calculation of *IRPR* from bent or gradient mosaic crystal. It is now accepted internationally as "the discrete form of Darwin's equations".

Cylindrical and Spherical crystals During the past four decades, the essence of the diffraction geometry for a cylindrical crystal, which is the key for determining the *IRPR* of spherical crystals (the most common shape of sample used in experiment), remains obscure.

As a result, the previously published theory was valid only within a small region (μR< 2.5). By analyzing the power ratio distribution, an exact and unique description of the diffraction geometry for a cylindrical crystal was obtained for the first time[4-5]. When μR>4, the diffraction geometry is essentially that of the Bragg-Bragg case, almost restricted to the **fg** region, but with a continuously varying asymmetry parameter (Fig.1). This explanation of diffraction geometry is universal, and it should be of importance to the further investigation of all kinds of cylindrical crystals in the future, even for ideal crystal, etc. The construction of a series of extensive extinction factor tables corresponding to a wide range of θ, σR and μR values ($0.05 \leq \sin\theta \leq 0.9$, $0 < \sigma R \leq 30$, $0 \leq \mu R \leq 30$) and its 4D fitting formulae for cylindrical and spherical crystals with several kinds of mosaic distributions are underway.

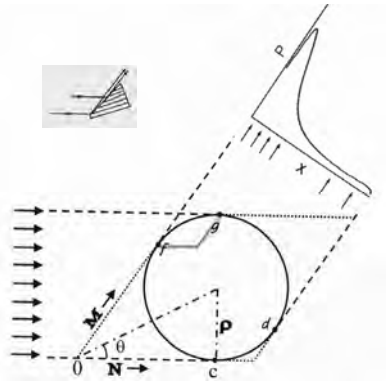

Figure 1 Diffraction Geometry and reflection profile for a cylindrical crystal with $\xi = 0.5$, $\sigma R = 0.5$, $\mu R = 1.25$.

References

[1] Hu, H. C. *Acta Cryst.* A**53**, 484-492, (1997).
[2] Hu, H. C. *Acta Cryst.* A**53**, 493-504, (1997).
[3] Hu, H. C. *J. Appl. Cryst.* **25,** 731-736. (1992).
[4] Hu, H. C. *Acta Cryst.* A**59**, 493-297-310, (2003).
[5] Hu, H. C.， Yang, Z. *Acta Cryst.* A**60**, 562-564, (2004).

P-169 The Development of A "Unified" Microfluidic Technology for Protein Crystallization

Jiang Huang
GN Biosystems, Inc., 25495 Whitesell St., Hayward, California 94545, U.S.A.
(jiang.huang@gnbiosystems.com)

Dialysis protein crystallization is a well-established and effective method for protein crystallization. However, it is labor-intensive, time-consuming, cost-prohibitive (due to large protein consumption) and difficult to automate. The disposable XZ™ dialysis crystallography plate has been developed to specifically address these issues. With the XZ™ microfluidic dialysis technology, 96 dialysis protein crystallization trials as low as 15nL/reaction can be setup in 4 minutes. Other advantages of the XZ™ plates are: high-throughput setup and imaging compatibility, clear path to structure due to directly scalable and easy crystal retrieval designs and it's compatibility with in-situ x-ray diffraction data collection, and simple sample/reagent loading protocols. Furthermore, with minor changes in protocol or design, vapor diffusion, microbatch and interface diffusion crystallization methods can all be carried out using the XZ™ plates. Large volume (4μl/dialysis chamber, 96 well plate) XZ™ plate

design is also developed to facilitate high throughput 2-D membrane protein crystallization.

P-170 ProSeed: A General Method to Introduce Beneficial Nuclei to Promote Protein Crystallization

Jeff E. Habel[1], Liwei Hung[1,2]
[1] *Lawrence Berkeley National Lab , Berkeley, CA 94720, USA (jhabel@lbl.gov)*
[2] *Los Alamos National Lab, Los Alamos, NM 87545, USA (lwhung@lanl.gov)*

After over a decade of high-throughput technology development, crystallization remains one of the most crucial bottlenecks in protein structure determination. Figures taken from recent Protein Data Bank indicate that the success rate from purified proteins to diffraction quality crystals is only 18%. Most of the disappointment can be attributed to failure in obtaining initial crystallization leads. Various techniques have been reported to help solve this critical problem. Nevertheless, these practices tend to be protein specific and are often case dependent. Development remains a hit-and-miss process.

Two factors are essential to effective crystallization events: phase transition, and nucleation. Although the former can often be extrapolated from initial screening experiments, the latter continues to be a semi-random process. While careful observations of screening experiments may help identify potential crystalline targets for seeding experiments, it remains less than practical when throughput and automation become factors of consideration. To solve these problems we developed a universal method to introduce beneficial nuclei into crystallization process helping to eliminate the nucleation factor. In our test case, after nuclei were introduced into a set of 282 'failed' conditions, 82 new conditions yielded crystals. While a set of control experiments demonstrated other factors contributed to crystal formation (dilution, precipitant synergy, etc.), the results suggest that a significant number of failures in crystallization were due to lack of nucleation. Our method is general and semi-automated with a script designed for the Art Robbins PHOENIX robot. This method may not only improve success rates for high-throughput crystallization projects, but also for those whose successes are critical. Current ongoing research salvaging our structural genomics targets will also be presented.

P-171 Automated Ligand Identification in PHENIX

Liwei Hung, Thomas C. Terwilliger
Los Alamos National Lab, Los Alamos, NM 87545, USA (lwhung@lanl.gov)

Over 60% macromolecular structures in the Protein Data Bank (PDB) contain bound small molecule ligands. In the case where there is no knowledge about the bound ligand, to interpret the unknown electron density is a rather difficult task in crystallographic model building.

We have implemented an automated ligand identification strategy in the framework of the PHENIX software suite using the RESOLVE ligand identification algorithm. The Resolve_ligand_identification task carries out fitting of a library of ligands to a given electron density map. Subsequently it conducts statistical analysis and ranking of the ligand fitting

results. The Resolve_ligand_identification task works with the ligand library provided with PHENIX suite by default. This library contains the 200 most frequently observed ligands in the PDB. The program is also capable of fitting and ranking ligands in a custom ligand library provided by the users. The current version takes advantage of multi-threading computing environment, and provides a mechanism for users to incorporate biological knowledge in the process of identifying potential ligands in their protein structures.

P-172 Crystal Structure of the TNF-α Inducing Protein (Tipα) from *Helicobacter pylori*: Insights into its DNA Binding Activity

Jun Young Jang[1], Hye-Jin Yoon[1], Ji Young Yoon[1], Hyoun Sook Kim[1], Sang Jae Lee[1], Kyoung Hoon Kim[1], Do Jin Kim[1], and Se Won Suh[1,2]
[1] *Department of Chemistry, Seoul National University, 151-747, Seoul, Korea (sewonsuh@snu.ac.kr)*
[2] *Department of Biophysics and Chemical Biology, Seoul National University, 151-747, Seoul, Korea (sewonsuh@snu.ac.kr)*

Helicobacter pylori infection is one of the highest risk factors for gastroduodenal diseases including gastric cancer. TNF-α is one of the essential cytokines for tumor promotion and thus a *H. pylori* protein which induces TNF-α is believed to play a significant role in gastric cancer development in humans. The *HP0596* gene product of *H. pylori* strain 26695 was identified as the TNF-α inducing protein (Tipα). Tipα is secreted from *H. pylori* as dimers and enters the gastric cells. It was shown to have a DNA binding activity. Here we have determined the crystal structure of Tipα from *H. pylori.* Its monomer consists of two structural domains ("mixed domain" and "helical domain"). Tipα exists as a dimer in the crystal and the dimeric structure represents a novel scaffold for DNA binding. The surface electrostatic potential of Tipα dimer and the docking calculations suggest that a positively charged surface patch that is formed across the two monomers by the loop between helices α1 and α2 may be important in DNA binding.

P-173 Determination of structural and magnetic phase diagram of solid solution of $BiFeO_3$-$BaTiO_3$ system

Ryoji Kiyanagi[1], Tadashi Yamazaki[1], Yuma Sakamoto[1], Hiroyuki Kimura[1], Yukio Noda[1], Kenji Ohoyama[2]
[1] *Institute of Multidisciplinary Research for Advanced Materials, Tohoku University, Sendai 980-8577, Japan (kiyanagi@tagen.tohoku.ac.jp)*
[2] *Institute of Material Research, Tohoku University, Sendai 980-8577, Japan*

$BiFeO_3$ (BFO) is known as a perovskite-type multiferroic material with ferroelectricity (T_C ~ 1000 K) and antiferromagnetism (T_N ~ 650 K). Solid solutions of BFO with other perovskite materials have been intensively studied for the exploration of better multiferroicity. $BaTiO_3$ (BTO) is a well-known ferroelectric material (T_C = 406 K) with the perovskite structure. Dielectric measurements on BFO-BTO solid solutions ((1-*x*)BFO+*x*BTO) showed enhancement of spontaneous polarization. Furthermore, the material exhibits a weak ferromagnetism. Structural studies so far reported are based on X-ray powder diffraction at

room temperature. The result suggested that the material changes its structure at $x = 0.33$ from hexagonal to cubic. However, the spontaneous polarization, according to the dielectric measurement, persists in the concentration of $x > 0.33$. In order to elucidate the inconsistency between the structure and the dielectric property and to draw a phase diagram of (1-x)BFO+xBTO system, structural investigation was conducted by means of neutron and X-ray powder diffraction.

The diffraction patterns, especially the neutron powder diffraction patterns, clearly showed the existence of the hexagonal phase in a wide range of x. The hexagonal phase coexists with the cubic phase in $0.2 < x < 0.6$ and with the tetragonal phase in $0.6 < x < 0.8$. The spontaneous polarization observed in the dielectric measurement probably arises from the coexisting hexagonal phase.

Variation of T_N with respect to x was examined by monitoring the intensity of a magnetic reflection, and the structural phase transition temperature (T_S) was estimated from the variation of the intensity of a hexagonal-phase-specific reflection. Both temperatures were found to decrease as x increases. The decrease of T_N can be attributed to decrease of the magnetic moment of Fe^{3+}, and the change in T_S may be caused by a small distortion induced by the surrounding cubic or tetragonal structure.

***Acknowledgements**: This work has been supported by a Grant-In-Aid for Scientific Research (A), No. 21244051, and Grant-In-Aid for Scientific Research on Priority areas ``Novel States of Matter Induced by Frustration", No. 19052001, from the Ministry of Education, Culture, Sports, Science and Technology.*

Development of laboratory SAXS spectrometer

P-174

Seok-Gn Ryu[1], Chang-Hee Lee[2], Myungkook Moon[2], Jongkyu Cheon[2], Hyun Hoon Song[1],Woon Bo Shim[1]
[1]Department of Advanced Materials, Hannam University, Daejeon, Korea (songhh@hnu.kr)
[2]HANARO Center, Korea Atomic Energy Research Institute, 150 Deokjin-dong, Yuseong-gu, Daejeon 305-353, Korea (leech@kaeri.re.kr)

Small angle X-ray scattering is well known classical technique and recently it has renaissance in some sense in structural biology in addition to widely used nano-scale studies because SAXS requires neither crystals nor special sample preparation, and is not limited by molecular mass but applicable under nearly physiological conditions. Even SAXS permits quantitative analysis of kinetic processes like assembly and disassembly, and allows one to study structural transitions and conformational changes on which biological function often relies.

Though SAXS beamlines at synchrotron are very powerful and produces high quality data, home-made SAXS machine using laboratory source could play a lot of roles from education and training to advanced researches, too. Based on 2-dimensional position-sensitive gas detector technology which has been developed at HANARO center, we have built home-made SAXS machine using the unused port of an already running rotating anode source for X-ray diffractometer and Osmic mirror. Most of the components are of off-the-shelf parts and

developed in-house and it, therefore, is very flexible under measuring conditions and is relatively cheap to construct. We report here our experience of home SAXS machine development and early results with several improvement points, too.

Fig.1 home-made SAXS spectrometer

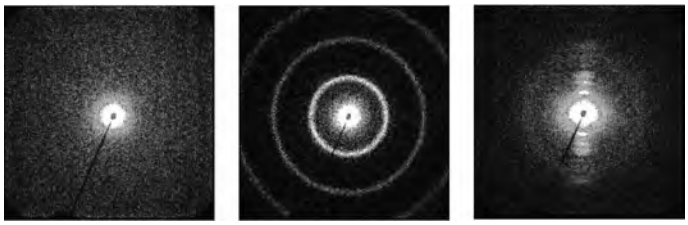

Fig.2 Background, silver behenate and chicken tendon patterns

P-175 Coordination Polymers of *N*-(7-hydroxy-4-methyl-8-coumarinyl)-amino acids: Fabrication of Crystalline, Gel and Fiber Materials

Wei Lee Leong, Jagadese J. Vittal
Department of Chemistry, National University of Singapore, Singapore 117543. (chmjjv@nus.edu.sg)

Considerable efforts have been devoted to study the rational design, properties, function and applications of crystalline materials while the discovery of gels has been largely serendipitous at the initial stage and, currently, evolve to design and understanding of the gelation process. Development of coordination polymers from crystalline materials to soft materials such as gels and fibers would provide a new insight in studies and applications of functional materials.

Recently, we found that metal complexes of *N*-(7-hydroxy-4-methyl-8-coumarinyl)-amino acids can be fabricated into crystalline, gel and fiber materials by interplay of metal ions, solvent and intermolecular interactions (Scheme 1). The Cu(II), Ni (II) and Zn (II) complexes have been shown to display fascinating structures including heptanickel hexagonal cluster, heterobimetallic metallocrown, pentanickel cluster, helical and zigzag coordination polymers. It may be noted that variation of metal ions has facilitated the assembly of such diverse structural architectures. Interestingly, Zn(II) and Mg(II) coordination polymers can self-assemble into gel materials in the absence of long chain hydrophobic groups. The 1D coordination polymeric strands aggregate and further self-assemble into a 3D network structure through noncovalent interactions to entrap water molecules. The most striking finding is that the dramatic enhancement of fluorescence properties of coumarin chromophore upon the formation of coordination polymeric hydrogel. Furthermore, Mg(II) coordination polymer can be obtained as random cross linking gel and well-aligned nanofiber by changing the chirality of amino acid backbone and pH of the solution. Our studies provide more insight into the self-assembly process of crystalline and amorphous materials that demand widespread of practical applications.

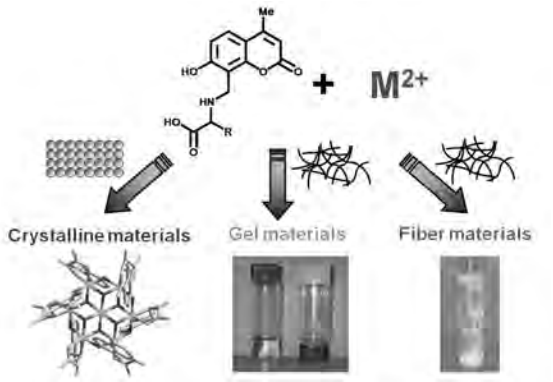

References

1. W. L. Leong, A. Y.-Y. Tam, S. K. Batabyal, L. W. Koh, S. Kasapis, V. W.-W. Yam, J. J. Vittal, *Chem. Commun.*, **2008**, 3628.
2. W. L. Leong, S. K. Batabyal, S. Kasapis, J. J. Vittal, *Chem. Eur. J.*, **2008**, 14, 8822.
3. W. L. Leong, S. K. Batabyal, S. Kasapis, J. J. Vittal, submitted.

P-176

RainbowMEM: A New Maximum Entropy Analysis Package

Hui LI[1], Jiaju LI[2], Xiaolong CHEN[3] and Ze ZHANG[1]
1 Beijing University of Technology, 100124, Beijing, China (huilicn@yahoo.com)
2 Institute of Geology and Geophysics, CAS, 100029, Beijing, China
3 Institute of Physics, CAS, 100080, Beijing, China

A new maximum entropy analysis package, RainbowMEM, was developed. This package is written with Visual Basic (VB) language, which has graphic interface (GUI) and runs under Windows operation system (OS). This package contains three modules: maximum entropy charge density calculation module, molecule topology analysis module and 3D charge density gradient display module. In this package, mixed radix fast Fourier transforms (MRFFT) algorithm was adopted. Therefore, the calculation efficiency of RianbowMEM is quite high. The maximum grid amount which RainbowMEM can deal with is 27,000,000. This amount is big enough to deal with most inorganic and organic crystal materials.

1. Maximum Entropy Charge Density Module

Example: $K_2Al_2B_2O_7$

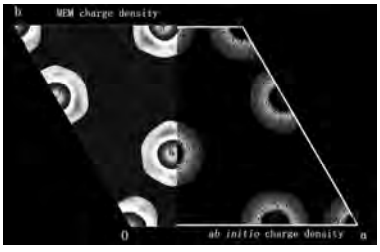

Fig.1 The comparison of the maximum entropy charge density (the left part) and the *ab initio* calculation charge density (the right part, CASTEP[1]) of $K_2Al_2B_2O_7$. This figure shows the K atoms layer, whose bond type is an ion bond basically. The charge density grids range from 0.5e/Å^3 to 2.5e/Å^3 intervals 0.038e/Å^3.

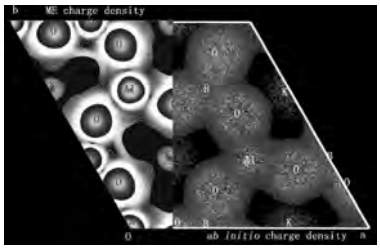

Fig.2 This figure shows the Al-O and B-O layer, whose bond type is a covalence ion mixed bond. The charge density grids range from 0.5e/Å^3 to 2.5e/Å^3 intervals 0.038e/Å^3.

Fig. 3. The 3D maximum entropy charge density of GaN. (a) Calculated by RainbowMEM program. (b) Calculated by MEED[2] program. The isosurface value is 1.25e/Å^3.

2. Molecule Topology Analysis Module

In this module, the critical point position, charge density value, Hessian matrix and eigenvalue can be supplied.

Fig.4 The interface and calculation result of molecule topology analysis module

3. 3D charge density gradient display module

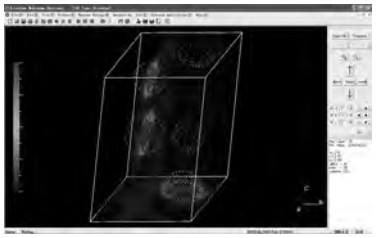

Fig.5 The interface of 3D charge density gradient display module

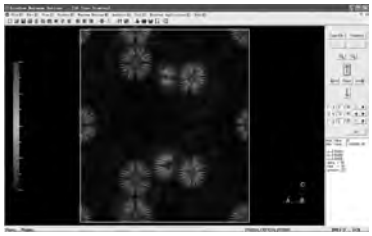

Fig. 6 Bond critical point (Arrow) of Al-O bond in $K_2Al_2B_2O_7$

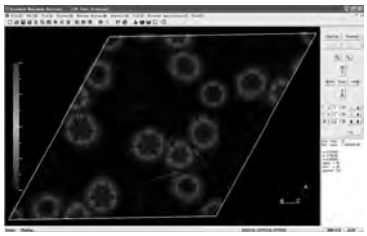

Fig. 7 Bond critical point (Arrow) of B-O bond in $K_2Al_2B_2O_7$

Conclusion

With the charge density information, the physical and chemical properties of the materials can be analyzed more directly. Restoring the accurate charge density with experimental diffraction data became a promising research field in the crystallography. In this work, the authors developed a new X-ray charge density maximum entropy analysis program, RainbowMEM, which can deal with either powder or single crystal X-ray diffraction data. This program also supplied the molecule topology analysis and 3D charge density gradient display function which is convincing to the charge density analysis.

***Acknowledgements**: This work is financial supported by the National Natural Science Foundation of China (NSFC) Project 10704004.*

References

[1] M. D. Segall, P. J. D. Lindan, M. J. Probert, C. J. Pickard, P. J. Hasnip, S. J. Clark, and M. C. Payne, *J. Phys.:Cond. Matt.*, **14(11)**, 2717-2743, (2002)

[2] M. Sakata and M. Sato, *Acta Cryst*., **A46**, 263-270, (1990)

P-177 Crystallization Force: A Density Functional Theory Concept for Characterizing Molecular Packing in Organic Crystals

Tonglei Li
Department of Pharmaceutical Sciences, University of Kentucky, 725 Rose Street, Lexington, KY 40536, U.S. (tonglei@uky.edu)

Because of the rich diversity in functional groups and the flexibility in molecular configuration and conformation, organic compounds are inclined to polymorphic formation in solid state, which can be greatly affected by the selection of solvent and other crystallization conditions. Intermolecular interactions are typically of weak forces such as van der Waals and stronger short-range ones including hydrogen bonding that determine the spatial packing of organic molecules during the crystallization process. In order to uncover the underlying mechanism that drives a molecule to have various packing motifs in solid state, an electronic concept or function within the framework of conceptual density functional theory (DFT) is developed, namely, crystallization force. The concept aims to describe the local change in electronic structure as a result of the self-assembly process of crystallization in order to quantify the locality of intermolecular interactions that directs the molecular packing in crystal.

Crystallization force stems from how the electronic structure of a molecular system responds to a perturbation to the number of electrons in the system. Conceived within the framework of DFT, it is developed in our laboratory as the following:

$$\mathbf{G}_\alpha = \mathbf{\Phi}^+_\alpha \frac{dq_\alpha}{f^+_\alpha} \qquad \text{when } dq_\alpha > 0$$

$$\mathbf{G}_\alpha = \mathbf{\Phi}^-_\alpha \frac{dq_\alpha}{f^-_\alpha} \qquad \text{when } dq_\alpha < 0$$

where $\mathbf{\Phi}^+_\alpha$ and $\mathbf{\Phi}^-_\alpha$ are the nucleophilic and electrophilic nuclear Fukui functions of atom α and $f^+(\mathbf{r})$ and $f^-(\mathbf{r})$ are the nucleophilic and electrophilic electronic Fukui functions at position $\mathbf{r}$, respectively. The change in atomic charge (or, equivalently, the negative of the change in atomic population) of atom α because of the molecular packing of crystallization is dq_α. As such, the crystallization force, $\mathbf{G}_\alpha$, can be regarded as the inherent nuclear Fukui function associated with crystallization. Due to its physical nature as Hellmann-Feynman force, a $\mathbf{G}_\alpha$ may thereby quantify the local binding force in a crystal.

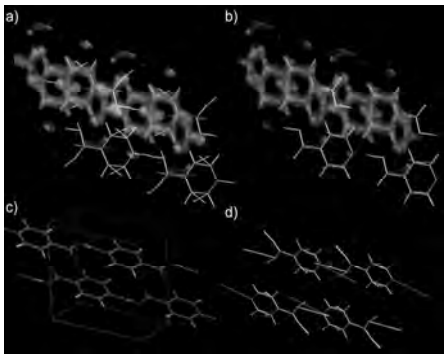

Figure 1. Isosurfaces of electron density (in gray) and electronic Fukui functions of isonicotinic acid with nucleophilic in red (a) and electrophilic in blue (b); nuclear Fukui functions are illustrated as arrows. For simplicity, not all electronic structures are drawn. Hydrogen bonds are shown in pink dash lines (c). Crystallization forces are represented as arrows (d).

Figure 1 shows one example of crystallization forces calculated of isonicotinic acid. The calculations were done with Crystal 06 by using the basis set of B3LYP/6-21G**. The molecules form hydrogen bonds in the crystal between the –OH and N. Large nucleophilic Fukui functions are located mainly at the –COOH while large electrophilic at the ring. Because some atoms gain electrons and others lose when the molecule "moves" from the gas or liquid phase to the crystalline phase, the crystallization force provides a unified expression to embody these Fukui functions. The crystallization forces nicely depict the hydrogen bonds in both directionality and magnitude (Figure 1d).

P-178

Crystal structure of a lead(II) complex with furan-2-ylmethylene salicyloyl hydrazine

Ying-Ying Zhang, Shi-Xiong Liu*
Department of Chemistry, Fuzhou University, Fuzhou 350002, P.R. China
(shixiongliu@yahoo.com)

A lead(II) complex with furan-2-ylmethylene salicyloyl hydrazine, $[Pb(C_{12}H_9N_2O_3)_2]_n$ (**1**), has been synthesized and structurally characterized. Complex **1** crystallizes in tetragonal, space group $P\,4_12_12$, with a = 9.477(3) and c = 26.352(6) Å, V = 2367(1) Å^3, Z = 4, D_c = 1.868 g/cm^3, $F(000)$ = 1280, μ = 7.176 mm^{-1}, S = 1.084, the final R = 0.0344 and wR = 0.0524 for 2286 observed reflections with $I > 2\sigma(I)$.

The lead complex possesses C_2 point symmetry and is located on a twofold crystallographic axis 2[110]. The Pb atom is coordinated by six oxygen donors and two nitrogen ones from four hydrazine ligands L_1, in which there are two kinds of Pb-O bond distances. The bond lengths of Pb1-O2 (carbonyl), Pb1-O2A, Pb1-N2 (hydrazine), and Pb1-N2A (carbonyl) are 2.310(4), 2.310(4), 2.544(4) and 2.544(4) Å, respectively, which are in the normal Pb-O and Pb-N bond distance range. At the same time, interatomic distances of Pb1-O3 (furfural), Pb1-O3A, Pb1-O1B(phenol) and Pb1-O1C are 2.976(5), 2.976(5), 2.909(4) and 2.909(4) Å, respectively. Therefore, lead atom in the title complex is in a holodirected eight-coordinated polyhedron.

Every lead complex molecule $[Pb(C_{12}H_9N_2O_3)_2]$ connects four adjacent complex mole cules by four hydrazine ligands L_1. Every hydrazine ligand L_1 acts as a biconnectors to coordinate to two lead atoms of two lead complex molecules. Therefore, complex **1** features a 3D coordination network.

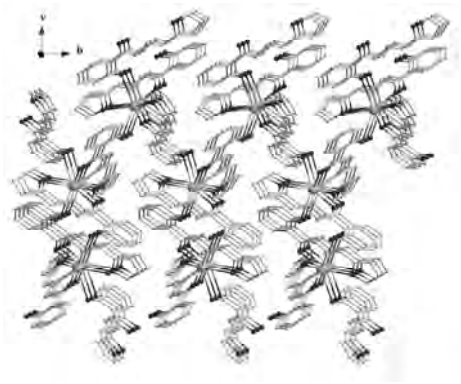

***Acknowledgements**: This project was financially supported by the Natural Science Foundation of China ((No. 20431010 and 20171012), the Natural Science Foundation of Fujian Province, China (E0110010).*

P-179

Structures, Luminescence of Lanthanide-Organic Frameworks

Tian-Fu Liu[1], Rong Cao*[1], Wen-Hua Sun*[2]
[1]*State Key Laboratory of Structural Chemistry, Fujian Institute of Research on the Structure of Matter, Chinese Academy of Sciences, Fujian, Fuzhou, 350002, P. R. China. (Liutiafu@fjirsm.ac.cn)*
[2]*Key Laboratory of Engineering Plastics, Institute of Chemistry, Chinese Academy of Sciences,Beijing, 100080, People's Republic of China. (whsun@iccas.ac.cn)*

A series of coordination polymers $[Ln_2(Hcbmp)(ox)_3(H_2O)_2]$ (Ln = Sm (1), Eu (2), Gd (3) H_2cbmp = 2-(carboxylic acid)-6-(2-benzimidazolyl)pyridine, ox = oxalic acid) has been hydrothermally synthesized and structurally characterized. Single-crystal X-ray analysis reveals that they are isostructural and crystallize in C2/c space group. Oxalate ligands and Ln ions compose an infinite bi-layer structure. The water molecules，both solvated and coordinated，are arranged between the layer. The Hcbmp ligands distribute on both sides of the layer chelating with Ln metal ions. So the resulting configuration shows *a* perfect sandwich structure in the *b* direction (Figure 1). Meanwhile, the luminescent properties were investigated at room temperature. Complex 1 and 2 exhibit strong fluorescent emissions in the visible and near-infrared region. As shown in Figure 2, transitions from the excited $^4G_{5/2}$ state to different J levels of the lower $^6H_{2/9}$ state were observed in the emission spectrum of complex 1. The complex 2 gave typical Eu emission spectrum containing the expected sequence of $^5D_0$-^7F_J (J=0,1,2,3,4.) (Figure 3). Thus, these complexes could be anticipated as good candidates for efficient luminescent materials and fluorescent probes.

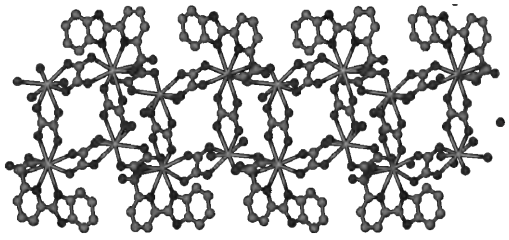

Figure 1

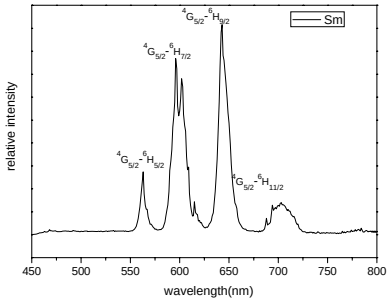

Figure 2

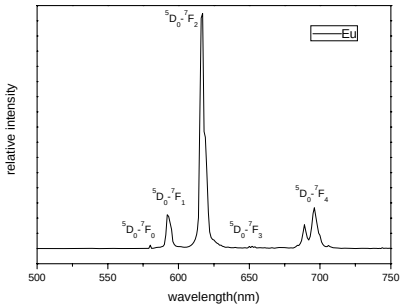

Figure 3

P-180 Cubic Lipid Phase & Bicelle Crystallization of Membrane Proteins

Hartmut Luecke

Cubic Lipid Phase (CLP): The CLP method for membrane protein crystallization has been refined to allow large-scale screening of various membrane proteins. The various parameters (CLP lipid, water content, bilayer lipid additive, pH, ionic strength, precipitating agent etc.) can be varied. Three distinct seven-transmembrane proteins where crystallized and their high-resolution structures determined.

Bacteriorhodopsin (BR): High-resolution maps from X-ray diffraction of bacteriorhodopsin crystal obtained in CLP and some of its photointermediates have yielded insights to how the isomerization of the bound retinal drives ion transport. Although some important mechanistic details are still undecided, the events of the photochemical cycle are now understood to reflect changes in specific hydrogen bonds of protein groups and bound water molecules in response to motions of the retinal chain. A nearly complete lipid bilayer is also present in the x-ray-derived atomic model.

Sensory Rhodopsin (SR): Atomic resolution structures of a phototaxis receptor in haloarchaea, the first sensory member of the widespread microbial rhodopsin family, have yielded insights into spectral tuning and the interaction face with its membrane-embedded transducer. Spectral differences between the sensory rhodopsin and light-driven proton pump bacteriorhodopsin depend largely on the repositioning of a conserved arginine residue in the chromophore-binding pocket. Information from the structures combined with biophysical and biochemical analysis have established a model for receptor activation and signal relay involving light-induced helix tilting in the receptor transmitted to the transducer by lateral transmembrane helix-helix interactions.

Anabaena SR (ASR): The structure of a sensory rhodopsin from the cyanobacterium *Anabaena* has been determined to 1.9 Å resolution. This represents the first eubacterial rhodopsin structure. In comparison to the archaeal rhodopsins BR and SR there are many striking rearrangements and shifts in hydrogen bonding patterns on both the extracellular and the cytoplasmic half of the receptor. Also, the cytoplasmic face, which is thought to interact with the soluble transducer, is structurally well defined and very different from that of the archaeal rhodopsins. The structure of the soluble transducer of this photoreceptor (ASRT) has

also been determined - it forms a C4 tetramer with a new all-beta fold. Studies characterizing the interaction between transmembrane photoreceptor and soluble transducer are underway.

Xanthorhodopsin (XR): a light-driven ion pump from the halophilic eubacterium *Salinibacter ruber* found in saltern crystallizer ponds of Spain, contains a blue-absorbing carotenoid that functions as a light-harvesting antenna for its retinal chromophore. In addition to the adaptations to bind and accurately position the carotenoid antenna for efficient excited-state energy transfer to the retinal, XR exhibits major structural differences to the previously studied microbial pumps and photoreceptors, in particular near the initial proton acceptor, Asp-96 (Asp-85 in BR), which forms a salt bridge with a histidine conserved in proteorhodopsin, as well as in the region of Arg-93 (Arg-82 in BR) and in the BC loop. The rearrangement of the latter causes the formation of a large aqueous pocket, which is accessible to the bulk solvent, in a region where the proton release group of bacteriorhodopsin (Glu-194, Glu-204, ordered waters) is located.

P-181 New Inorganic Second-order NLO Materials Based on Lone Pair Cations

Jiang-Gao Mao, Ting Hu, Yong Zhou, Chuan-Fu Sun and Fang Kong
State Key Laboratory of Structural Chemistry, Fujian Institute of Research on the Structure of Matter, Chinese Academy of Sciences, Fuzhou 350002, P. R. China (mjg@fjirsm.ac.cn)

The search of new second-order nonlinear optical (NLO) materials is of current interest and great importance owing to their applications in photonic technologies. Currently, the most widely used such materials are inorganic crystals based on borates such as β-BaB_2O_4 (BBO) and LiB_3O_5 (LBO) and phosphates such as KH_2PO_4 (KDP) and $KTiOPO_4$ (KTP).[1] It is reported that systems contain a lone pair cation such as Se(VI), Te(IV) and I(V) are apt to form non-centrosymmetric structures (NCS) with good second-order NLO properties.[2] Our group has been working on NLO materials based on lone pair cations for many years. Some compounds showing good second-order NLO properties are summarized below.

1. Combinations of borate and selenite.

The combination of B-O and Se(IV)-O bonds led to a new type of second-order NLO compound, $Se_2B_2O_7$ with a SHG efficiency of 2.2xKDP. Its structure features a 3D network composed of $B_2O_7^{8-}$ anions made of two corner-sharing BO_4 groups which are further bridged by lone pair containing Se(IV) cations in an asymmetric SeO_3E(E is lone pair) geometry. It is stable up to 350 °C.

2. Combinations of two types of lone pair cations.

A serial of noncentrosymmetric (NCS) mixed metal iodates, namely, $Ln_3Pb_3(IO_3)_{13}(\mu$-O) (Ln = La, Ce, Pr, Nd), have been synthesized by hydrothermal reactions of Ln_2O_3 (Ln = La, Ce, Pr, Nd), $PbCl_2$, I_2O_5 and H_2O at 200 °C.

All four isostructural compounds exhibit a three-dimensional crystal structure that consists of

LnO_9 polyhedra that are connected by asymmetric IO_3 group with the Pb^{2+} inserted into the voids of the thus formed network via Pb-O bonds. SHG measurements on the La, Pr and Nd compounds indicate that they display SHG responses of 2×KDP, 1×KDP and 0.8×KDP, respectively. The La, Pr and Nd compounds are also thermally stable up to 500, 500 and 420 ^oC, respectively.

3. Combinations of d^0-Transition metal ion and a lone pair cation.

By incorporation of Mo(VI) and Te(IV), $Ag_2Mo_3Te_3O_{16}$ with a large SHG response of 8xKDP was obtained. Its structure features one-dimensional $[Mo_3Te_3O_{16}]^{2-}$ anionic chains composed of $[Mo_3O_{14}]^{10-}$ clusters interconnected by $[Te_3O_8]^{4-}$ anions via corner-sharing, such 1D chains are further interconnected by Ag^+ ions into a 3D network.

By combination of V(V) and Te(IV) we obtained $Cd_4V_2Te_3O_{15}$ with a moderate strong SHG efficiency of about 1.4 times of KDP. Its structure features a 3D network in which the cadmium tellurite layers are bridged by "isolated" VO_4 tetrahedra and 1D vanadium oxide chains of corner-sharing VO_4 tetrahedra. It is thermally stable up to about 840 ºC and transparent in the IR region. Furthermore, its large crystal crystals could be grown from the stoichiometric melts theoretically.

By the combination of Nb^{5+} cation with d^0 electronic configuration and lone pair containing iodate anion, a new SHG material, $BaNbO(IO_3)_5$ has been prepared. Its anionic structure can be considered to be "zero-dimensional", composed of an axially distorted NbO_6 octahedron linked with five IO_3^- groups and one terminal O^{2-} anion with the Ba^{2+} cations acting as spacers between these anions. It exhibits a very large SHG signal of about 14 x KDP and is phase-matchable. It has also high thermal stability and wide transparent region.

References

1. *P.* Becker, *Adv. Mater.* **1998**, *10*, 979-992.
2. Chang, H.-Y.; Kim, S.-H.; Halasyamani, P. S.; Ok, K. M. *J. Am. Chem. Soc.* **2009,** *131*, 2426.
3. (a) Kong, F.; Huang, S.-P.; Sun, Z.-M.; Mao, J.-G.; Cheng, W.-D. *J. Am. Chem. Soc.* **2006**, *128*, 7750-7751; (b) Jiang, H.-L.; Huang, S.-P.; Fan, Y.; Mao, J.-G.; Cheng, W.-D. *Chem. Eur. J.* **2008**, *14*, 1972; (c) Hu, T.; Qin, L.; Kong, F.; Zhou, Y.; Mao, J.-G. *Inorg. Chem.* **2009**, *48*, 2193; (d) Zhou, Y.; Hu, C.-L.; Hu, T.; Kong, F.; Mao, J.-G. ***Dalton Trans***. **2009**, Advanced Papers; (e) Sun, C.-F.; Hu, C.-L.; Xu, X.; Ling, J.-B.; Hu, T.; Kong, F.; Long, X.-F., Mao, J.-G. *J. Am. Chem. Soc.* **2009**, Articles ASAP.

P-182 Crystal structure and phase transitions in $C_5H_{10}NH_2PbI_3$

Munehiko Nakatsuma, Miwako Takahashi, Kota Takano, Takuro Kawasaki, Kunimitsu Kataoka and Ken-ichi Ohshima
Institute of Materials Science, University of Tsukuba, Japan
(nakatsuma@jb.bk.tsukuba.ac.jp)

The lead-halide perovskites material $C_5H_{10}NH_2PbI_3$ is one-dimensional semiconductor. In the crystal, semiconducting parts of one-dimensional chains of face-sharing lead-iodide octahedra are separated by barrier parts of $C_5H_{10}NH_2^+$ molecules. The crystal structure at room temperature is orthorhombic with space group of $C222_1$ (No.20) [1]. It has been shown by Raman scattering, DSC and optical absorption measurements that the structure undergoes

temperature-induced successive phase transitions: phase I above 284.5 K, phase II for 255.5 K to 284.5 K, phase III for 250 K to 255.5 K, and phase IV below 250 K. The transitions are found to involve rotational/orientational ordering of the $C_5H_{10}NH_2^+$ molecules [2], but precise structure at each phase has not been determined yet. In order to determine the structures for low temperature phases, we have performed single crystal X-ray diffraction measurements.

Single crystals of $C_5H_{10}NH_2PbI_3$ were grown by solution method. The integrated intensities were collected with Rigaku R-AXIS RAPID. Data collections for phase II and III were carried out at 275K and 265K, respectively. The structures in phase II is determined to be monoclinic $P2_1$ (No.4) with lattice parameters a= 10.110(3)Å, b= 8.149(2)Å, c= 15.923(3)Å, β= 99.980 (8)º and volume V= 1292.06(53) Å^3 (Fig.1). In the phase III, the structure is identified to be $P2_1$ with lattice parameters a= 17.310(26)Å, b= 8.205(12)Å ,c= 20.091(25)Å, β= 115.829(60)º, and V= 2568.49(22) Å^3, which is twice as large as that of phase I (Fig.2). It is found that displacement and distortion of lead-iodide octahedra play an important role in the phase transitions.

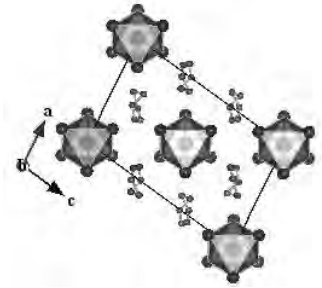

Fig. 1

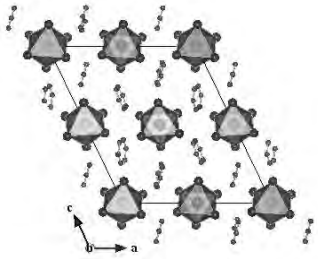

Fig. 2

References

1. G.V.Gridnova, E.A.Ziger, V.M.Kkoshkin,S.V.Lindemann,Yu.T.Struchkov,V.E.shklover: Doklady Akademii Nauk 278(1984)414
2. S. Oishi, K. Matsuishi and S. Onari: private communication.

P-183

Crystallographic structure and luminescence properties of $Y(Ta,Nb)O_4:Eu^{3+},Tb^{3+}$ phosphors

Mihail Nazarov, Do Young Noh, Su Woong Lee
Department of Materials Science and Engineering, Gwangju Institute of Science and Technology, 1 Oryong-dong, Buk-gu, Gwangju 500-712, Republic of Korea (Nazarov@gist.ac.kr)

Crystallographic analysis plays an essential role in luminescence investigations of phosphors. The detailed X-ray diffraction (XRD) analysis, energy dispersive spectroscopy (EDS), Electron probe micro analysis (EPMA), Infrared and Raman spectroscopy as well as photoluminescence (PL), cathodoluminescence (CL) and X-ray luminescence (XL) were carried out in order to enlarge the understanding of the radiative processes in yttrium tantalate ($YTaO_4$) and niobate ($YNbO_4$) phosphors activated by europium and terbium. However, to the best of our knowledge, no work has been reported using doubly activators for $Y(Ta,Nb)O_4$ phosphors.

Three types of host lattices with double activation by rare earth elements Eu^{3+} and Tb^{3+} were

prepared by solid state reaction method. General formula of the investigated phosphors is $Y_{1-x-y}Eu_xTb_yTa_{1-z}Nb_zO_4$, denoted as $Y(Ta,Nb)O_4:Eu^{3+},Tb^{3+}$. For the samples we measured, x = 0.025, y = 0.025 and z = 0; 0.15 or 1.

The crystalline structure and order degree of phosphor samples were evaluated on the basis of Synchrotron X-ray Diffraction (SR-XRD) patterns and FT-IR spectra. The high resolution and the excellent detectors for SR-XRD (Pohang Accelerator Laboratory, Korea) permit the identification and quantification of trace phases not possible use other means especially for double activated phosphors. The results show that the compound $YTaO_4$ has a fergusonite (distorted sheelite) structure with $I2\text{-}C_2^3$ space group symmetry and site symmetry C_2 for the molecular TaO_4. Monoclinic M' structure of $YTaO_4$ is differ from monoclinic M-structure of $YNbO_4$. FT-IR spectra put in evidence that the vibrations corresponding to NbO_4^{3-} groups and TaO_4^{3-} groups are different. The shape of FT-IR spectra in the domain of MO_4 group vibrations (where M = Ta, Nb) illustrates the change of the metal-oxygen bonds number: six in octahedron coordination $YTaO_4$ and four in tetrahedral coordination $YNbO_4$. In $M'\text{-}YTaO_4:Eu^{3+},Tb^{3+}$, the Y atoms are surrounded by 8-coordinated oxygen atoms forming a distorted cube. From our calculations the Y-O averaged distance is 2.37Å. The Ta atoms are in a distorted octahedral coordination with four shorter Ta-O bonds at 1.96Å and 1.87Å and two longer at 2.23Å. The total amount of atoms inside of the M'-YTaO4 structure is: 2 yttrium atoms, 2 tantalum and 8 oxygen atoms. Following the same procedure, we calculated and drew the crystallographic structure of $YNbO_4:Eu^{3+},Tb^{3+}$. The Y atoms are also surrounded by 8-coordinated oxygen atoms forming a distorted cube. The Y-O averaged distance is 2.35Å. The Nb atoms are in a distorted octahedral coordination, with four shorter Nb-O at 1.94Å and 1.83Å and two longer at 2.43Å. Adding Eu^{3+} and Tb^{3+} appears to have negligible effect on the crystallographic structure and on the shape of infrared spectra in low activator concentrations, but terbium activation decreases the absorbance in $YNbO_4$.

PL, CL and XL illustrate very high intensity of Eu emission in both matrixes, whereas Tb incorporation is very effective only in $YTaO_4$. Contribution of both rare earth activators is observed in the all spectra, from this, we can vary the concentration of these activators and get a broad variation of visible photoluminescence colors. These phosphors may be applied to the X-ray intensifying screens for medical diagnosis, cold cathode lighting and in many different optoelectronic devices.

P-184 Structural Membrane Proteomics – X-ray Structure of Sulfide:Quinone Oxidoreductase on The Hyperthermophilic Eubacteria *Aquifex aeolicus*

Guohong Peng, Marco Marcia, Ulrike Wedemeyer, Ye Gao, Tao Wang, Tanja Hedderich, Chuli Zhang & Hartmut Michel
Max Planck Institute of Biophysics Frankfurt am Main60439, Germany, (guohong.peng@mpibp-frankfurt.mpg.de)

Proteins from hyperthermophilic organisms are considered to be more stable and more rigid than their mesophilic counterparts. Therefore, the possibility of obtaining stable, homogeneous and crystallizable membrane protein complexes should be better with complexes from thermophilic organisms than with complexes from mesophilic ones. Thus, we

have purified and characterized a number of proteins and protein complexes from native membranes of *Aquifex aeolicus* using conventional biochemical techniques, identified these proteins by mass spectrometry, and followed by crystallization trials. For those originally annotated as hypothetical or putative proteins in *Aquifex* genome, we try to determine their functions. So far we are able to identify 72 protein chains which belong to 38 membrane proteins/protein complexes. All of protein complexes that we have purified to homogeneity in sufficient amount, have yielded diffracting crystals. Two structures of these protein complexes had been determined. One of them is sulfide:quinone oxidoreductase. Surprisingly it is a trimeric, periplasmic intergral monotopic membrane protein involving into energy conversion process. The X-ray structure of this enzyme reveals basic mechanisms of sulfide respiration and detoxification.

P-185 Kinetics of Crystalline-Non-Crystalline Phase Transition in Sucrose

Son Van Phung [1], Taro Fujita[2], Miwako Takahashi[1] and Ken-ichi Ohshima[1]
[1] *Institute of Materials Science, University of Tsukuba, Tsukuba 305 -8573, Japan, (ohshima@bk.tsukuba.ac.jp)*
[2] *Microphase Co.., Ltd., Tsukuba 300 – 2651, Japan, (fujita@bk.tsukuba.ac.jp)*

Sucrose is one of the most important ingredients in foods and has great potentialities for new functional materials. Melting points among sucrose crystals with high purity are different from each other, which were reported as in a temperature range between 433 and 464K[1)]. The measurements were used by macroscopic techniques, e.e. differential scanning calorimeter and thermal gravimetry-differential thermal analysis (TG-DTA). Though there are several proposals for understanding of different melting points based on the content of the impurity, different preparation and so on, no detailed structural studies have been performed for such big difference of melting points. It is helpful to try the time-dependent data collection of the melting points at the fixed temperature for clearing the inconsistency.

The in-situ X-ray diffraction measurements in sucrose have been performed for investigating the kinetics of crystalline-non-crystalline phase transition. The characteristic time until the integrated intensity of (111) Bragg reflection becomes half was observed in a temperature range between 413 to 433K from analyzing time-dependent X-ray diffraction intensity data. The time called as incubation time is interpreted with the use of Avrami's idea.

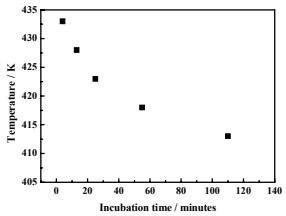

Fig 1. Temperature vs. incubation time

References

M. Okuno, S. Kishihara, M. Otsuka, S. Fujii and K. Kawasaki : Int. Sugar J. 105 (2003) 29.

P-186 Metal Coordination Polymers containing tetrapyridyl based Ligands

Abdul Malik Puthan Peedikakkal[1], Jagadese J. Vittal*[1]
Department of Chemistry, National University of Singapore, 3 Science Drive 3, Singapore 117543 (chmjjv@nus.edu.sg)

Coordination polymers or Metal-organic frameworks are an interesting class of molecule-based on metal-connecting nodes and bridging ligands. They have received considerable attention due to their potential applications in hydrogen storage, CO_2 separation, heterogeneous catalysis and having interesting magnetic, optical, electronic properties. Nitrogen based ligands are important in constructing such materials. Here we have shown various structural motifs with specific topologies can be synthesized from 1,2-bis(4-pyridyl)ethylene, 4,4'-bpe(**L1**) and (1,2,3,4-tetrkis (4-pyridyl)cyclobutane, 4,4'-tpcb (**L2**) ligands using transition metal ions. **L2** was synthesized from **L1** using photochemical [2+2] cycloaddition and isomerization reaction. **L1** acts as a linear spacer in forming the networks with metal-connecting nodes. On the other hand, one of the cyclobutane isomers of **L2**, namely, *rtct*-4,4'-tpcb acts as an excellent four connecting tetrahedral node that have been utilized in fabricating three dimensional framework structures. The formation of multidimensional frameworks including linear, zig-zag, ladder, interpenetrated and non-interpenetrated networks with interesting topologies will be discussed during the talk.

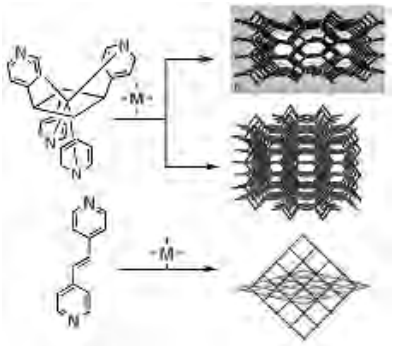

Fig. 1, A perspective view of three dimensional network structures with specific topologies formed by **L1** and **L2** using metal ions (Zn(II) and Co(II).

References

1) Peedikakkal, A. M. P.; Lip. L. Koh.; Vittal, J. J. *Chem Communications*, **2008**, 441-443.
2) Peedikakkal, A. M. P.; Vittal, J. J. *Chem-A European Journal,* **2008**, 14, 5329-5334.
3) Peedikakkal, A. M. P.; Vittal, J. J. *Crystal Growth & Design*, **2008**, 8, 375-377.

P-187 Structural basis for the mechanism of respiratory complex I

Leonid Sazanov, John Berrisford
MRC Mitochondrial Biology Unit, Cambridge, UK (sazanov@mrc-mbu.cam.ac.uk)

Complex I of respiratory chains plays a central role in cellular energy production, but the mechanism of this highly efficient enzyme is currently unknown. Dysfunction of complex I is

implicated in many human neurodegenerative diseases and aging. Previously, we have solved the first structure of the hydrophilic domain of complex I [1,2]. The domain represents the catalytic core of the complex and consists of eight different subunits of 280 kDa total mass. It contains all known redox centres of the enzyme – 9 Fe-S clusters and the primary electron acceptor flavin mononucleotide.

Here, we present several X-ray structures of the oxidized and reduced hydrophilic domain of complex I from *Thermus thermophilus*, which were determined at up to 3.1 Å resolution. They reveal the mode of interaction with substrate NADH and conformational changes in the complex upon reduction. Fe-S cluster N2 is the electron donor to quinone and is coordinated by unique motif involving two consecutive (tandem) cysteines. An unprecedented "on/off switch" (disconnection) of coordinating bonds between the tandem cysteines and this cluster was observed upon reduction. Comparison of structures suggests a novel mechanism of coupling between electron transfer and proton translocation, which will be discussed.

References

[1] Hinchliffe, P., and Sazanov, L. A. (2005) *Science* 309, 771-774
[2] Sazanov, L. A., and Hinchliffe, P. (2006) *Science* 311, 1430-1436

Structural basis for translational inhibition by the tumour suppressor Pdcd4

P-188

Portia G Loh[1], Hsin-Sheng Yang[2], Haiwei Song[1]
[1] *Institute of Molecular and Cell Biology, Proteos, Singapore (haiwei@imcb.a-star.edu.sg)*
[2] *Graduate Center for Toxicology and Markey Cancer Center, College of Medicine, University of Kentucky, Lexington, KY, USA*

Programmed cell death protein 4 (Pdcd4) is a novel tumor suppressor protein, which functions as an inhibitor of translation initiation and consequently prevents neoplastic transformation and tumour invasion. Loss of Pdcd4 expression is correlated to tumor progression in lung, colon, prostate, and breast cancers. The inhibition of translation initiation by Pdcd4 is achieved through specific interactions of its two tandem MA3 domains with the eukaryotic translation initiation factors eIF4A. We have solved the crystal structures of an N-terminal-truncated Pdcd4 in free form and in complex with eIF4A. Upon binding to eIF4A, Pdcd4 undergoes a marked conformational change to form a heterotrimeric complex with eIF4A, with one Pdcd4 binding to two eIF4A molecules in two different modes. The binding of Pdcd4 to eIF4A is required to inhibit the enzymatic activity of eIF4A, translation initiation, and AP-1-dependent transcription. Both MA3 domains are required to efficiently compete with the C-terminal domain of eIF4G (eIF4Gc) for binding to eIF4A whereas a single MA3 is sufficient to inhibit translation. Our structural and mutational analyses reveal that Pdcd4 inhibits translation initiation by trapping eIF4A in an inactive conformation, and blocking its incorporation into the eIF4F complex. These results may help design drugs that mimic the action of Pdcd4 to treat cancers which have lost Pdcd4 expression.

P-189 Exploring the Bond topological and Electrostatic properties of Benzimidazole molecule via Experimental and Theoretical Charge Density Study

Arputharaj David Stephen,[a] Reji Thomas,[b] Vijayan Narayayanasamy[c] and Poomani Kumaradhas[a]
[a]*Department of Physics, Periyar University, Salem-636 011, India (davidstephen_dav@yahoo.co.in)*
[b]*Chemistry and Physics of Materials Unit, Jawaharlal Nehru Centre for Advanced Scientific Research, Jakkur, Bangalore-560 064, India*
[c]*National Physical Laboratory, Dr. K.S. Krishnan Road, NewDelhi-110 012, India*

The experimental electron density distribution of Benzimidazole has been determined from multipole refinement model using accurate high resolution X-ray diffraction intensity data collected at 100K. The theoretical charge density distribution was calculated from high level *ab initio* and Density functional theory calculations, using MP2 and B3LYP methods with the basis set 6-311G**. The bond topological analysis of the experimental electron density shows the difference of charge density distribution in the homo and heteroatomic bonds. The molecular charge density difference between theory and experiment explicitly reveals the influence of crystal field effect in the experimental electron density distribution. The isosurface electrostatic potential shows the electro positive and negative regions in the molecule. A large negative potential found at the vicinity of nitrogen atom. The bond topological analysis on intermolecular hydrogen bond confirms the strength of interaction from ρ_{bcp} and $\nabla^2\rho_{bcp}$ values.

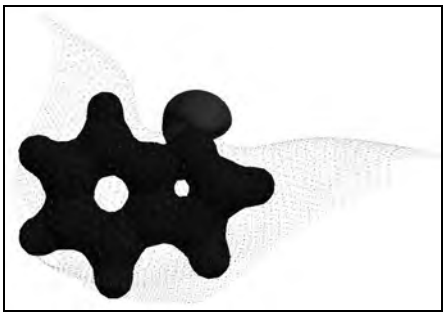

Isosurface representation of experimental electrostatic potential of Benzimidazole molecule
Blue: positive potential (+0.5 eÅ^{-1}), red: negative potential (-0.2 eÅ^{-1})

P-190 X-Ray Based Enzyme Design for Alkaloid Libraries

Joachim Stoeckigt
College of Pharmaceutical Sciences, Institute of Materia Medica, Zhejiang University, 383 Yu Hang Tang Road, Hangzhou, Zhejiang Province, 310058, P.R. China. (joesto2000@yahoo.com)

Medicinal plants are a rich source of natural products with high pharmacological and therapeutic value. It is estimated that less than 10% of higher plants from rain forests are well investigated for the occurrence of biological active compounds and remaining 90% of the plants are unexplored. Because of drastic environmental changes, a higher demand of palm oil production and climate influences, rain forests are shrinking world wide dramatically. This results in irreversible loss of still unknown secondary metabolites, loss of their enzymes of

biosynthesis and loss of the corresponding genes.

The lecture will summarize enzymatic and genetic approaches for generation of novel libraries of biologically important alkaloids based on the biosynthesis of alkaloids of the plant *Rauvolfia serpentina,* an Indian medicinal plant from Ayurvedic medicine. In particular the following points will be discussed :

- detection, purification and partial sequencing of the new enzymes
- heterologous enzyme expression in *E. coli* and crystallization
- x-ray analysis and exploration of enzyme mechanisms
- rational enzyme re-design and generation of new alkaloid libraries

Recently obtained structural results are illustrated in the following network of *Rauvolfia* alkaloids :

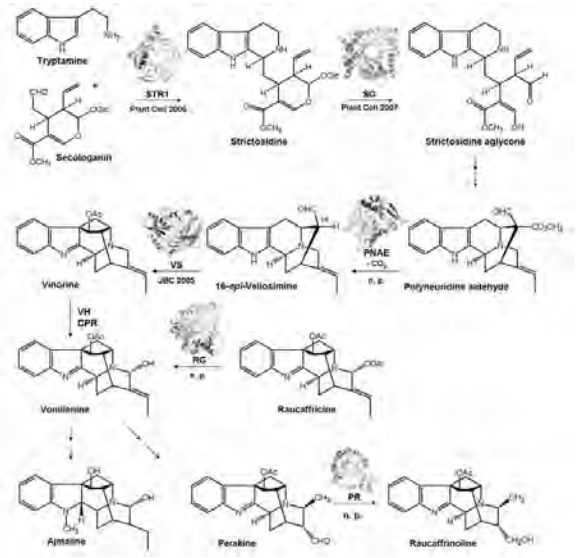

References

1. Yang, L., Hill, M., Wang, M., Panjikar, S., Stoeckigt, J. *Angew. Chemie.* **2009**, (in press).
2. Stoeckigt, J., Panjikar, S. *Nat. Prod. Rep*. **2007**, *24*, 1382-1400.
3. Barleben, L., Panjikar, S., Ruppert, M., Koepke, J., Stöckigt, J. *Plant Cell.* **2007**, *19*, 2886-2897.
4. Loris, E., Panjikar, S., Ruppert, M., Barleben, L., Unger, M., Schubel, H., Stöckigt, J. *Chem. Biol.* **2007**, *14*, 979-985.

P-191 Crystal Structure of Porcine Reproductive and Respiratory Syndrome Virus (PRRSV) Leader Protease Nsp1α

Yuna Sun[1, $], Fei Xue[2, $], Yu Guo[3], Ming Ma[1], Ning Hao[1], Xuejun C. Zhang[1], Zhiyong Lou[2,*], Xuemei Li[1, *], and Zihe Rao

[1] *National Laboratory of Macromolecules, Institute of Biophysics, Chinese Academy of Science, Beijing, 100101, China, (lixm@sun5.ibp.ac.cn)*

[2] *Structural Biology Laboratory, Tsinghua University, Beijing, 100084, China, (louzy@xtal.tsinghua.edu.cn)*

[3] *College of Life Sciences and Tianjin State Laboratory of Protein Science, Nankai University, Tianjin 300071, China*

Porcine Reproductive and Respiratory Syndrome Virus (PRRSV), a positive strand RNA virus that belongs to the *Arteriviridae* family of *Nidovirales*, has been identified as the causative agent of porcine reproductive and respiratory syndrome (PRRS). Nsp1-alpha is the amino (N)-terminal protein in a polyprotein encoded by the PRRSV genome and is reported to be crucial for subgenomic (sg) mRNA synthesis, presumably by serving as a transcription factor. Before functioning in transcription, nsp1-alpha proteolytically releases itself from nsp1-beta. However, the structural basis for the self-releasing and biological functions of nsp1-alpha remains elusive. Here we report the crystal structure of nsp1-alpha of PRRSV (strain XH-GD) in its naturally self-processed form. Nsp1-alpha contains a zinc finger domain (which may be required for its biological function), a papain-like cysteine protease (PCP) domain with a zinc ion unexpectedly bound at the active site (which is essential for proteolytic self-release of nsp1-alpha), and a carboxyl-terminal extension (which occupies the substrate binding site of the PCP domain). Furthermore, we determined the exact location of the nsp1-alpha self-processing site at Cys-Ala-Met180//Ala-Asp-Val, from crystallographic data and N-terminal amino acid sequencing. The crystal structure also suggested an *in cis* self-processing mechanism for nsp1-alpha. Furthermore, nsp1-alpha appears to have a dimeric architecture both in solution and as a crystal, with a hydrophilic groove on the molecular surface that may be related to nsp1-alpha's biological function. Compared with existing structure and function data, our results suggest that PRRSV nsp1-alpha functions differently from other reported viral leader proteases, such as FMDV L^{pro}.

P-192 Structure and guest release behavior comparison of inclusion crystals of 1,1,2,2- tetrakis (4- hydroxy phenyl) ethane and imidazole derivatives

Takenori Takeda[1], Akiko Sekine[1], Hidehiro Uekusa[1], Natsuki Amanokura[1], Masami Kaneko[2] and Hiroshi Suzuki[2]

[1] *Department of chemistry and materials science, Tokyo Istitute of Technology, 2-12-1, Ohokayama, Meguro-ku, Tokyo, 152-8551, Japan (takeda.t.ab@titech.ac.jp)*

[2] *Nippon Soda Co.Ltd, 2-1-2-chome, Ohtemachi, Chiyodaku, Tokyo 100-8165, Japan*

1,1,2,2-tetrakis(4-hydroxyphenyl)ethane, TEP (Fig.1) is a tetrapodal host molecule which has four hydroxyl phenyl groups in different directions to form different types of hydrogen bonding host frameworks. Inclusion compound of TEP and imidazole derivative (Fig.2), an anionic polymerization initiator of epoxy resin, is an industrial material that has controlled

polymerization initiation temperature depending on the guest release temperature [1]. In this study, a series of inclusion crystal structures were analyzed to reveal the relationships between the guest release temperature and crystal structure.

Seven analyzed inclusion crystals have the guest release temperatures within the range of 160-220°C. In both imidazole (166°C) and 2-phenylimidazole (220°C) inclusion compounds (**1** and **7**), guests are stacked in similar channel structure parallel to *a*-axis (Fig.3). These guests were connected with hosts by **1**: OH…N, **7**: OH…N and NH…O hydrogen bondings. The reason why **7** has the highest guest release temperature of the seven can be explained that the guest release motion from the channel was prevented by a bulky substituent.

4-methylimidazole and 1-methylimidazole have the same molecular weight, but quite different thermal stability (mp. -60°C and 46°C). It is interesting that their inclusion crystals (**3** and **4)** were isomorphs. Guests were arranged in the layer parallel to bc plane, and connected to the hosts by OH...N hydrogen bonding, and also NH…π and CH…π interaction, respectively. In spite of the different stability of the guest imidazoles, they have similar guest release temperature indicating that the stability of the guest in the inclusion crystal depends on the crystal structure. 2-methylimidazole, 2-*n*-propylimidazole, and 2-*i*-propylimidazole inclusion compound (**2**, **5**, and **6**) were the ethyl acetate solvates, and the thermogravimetry measurements showed the release of the ethyl acetate and imitazole occur in two stages.

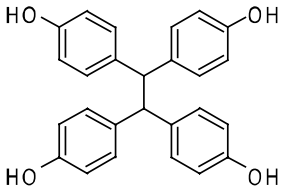

Fig.1:TEP

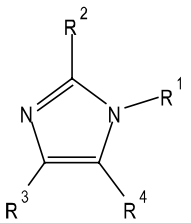

Fig.2:imidazole derivative

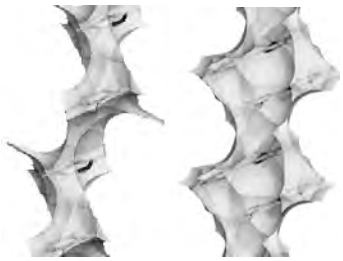

Fig.3: Channel structure
1 (left, b axis projection) **7** (right, c axis projection)

Reference

N. AMANOKURA et al. Polymer Journal, Vol. 39, No. 8, pp. 845–852 (2007)

Calcium binds to LipL32, a lipoprotein from pathogenic *leptospira*, and modulates fibronectin binding

P-193

Jung-Yu Tung[1], Shao-Wen Chou[1], Chien-Chih Lin, Yi-Ching Ko[2], Chih-Wei Yang[2], and Yuh-Ju Sun[1]
[1]*Institute of Bioinformatics and Structural Biology, National Tsing Hua University, Hsinchu, Taiwan (d934605@oz.nthu.edu.tw)*
[2]*Kidney Institute and Graduate Institute of Clinical Medical Science, Chang Gung Memorial Hospital, Taiwan*

Tubulointerstitial nephritis is a cardinal renal manifestation of leptospirosis. LipL32, a virulence factor of pathogen *Leptospira*, is the major lipoprotein of outer membrane proteins.

LipL32 recognizes extracellular matrix components and adheres to the host cell to evade an immune response. The crystal structure of Ca^{2+}-bound LipL32 was determined at 2.3 Å. LipL32 consists of a novel polyD sequence with a cluster of seven aspartate residues to form a continuous acidic surface patch for Ca^{2+} binding. A significant conformational change was induced when Ca^{2+} bound to LipL32. The binding of fibronectin F30 to LipL32 was monitored by Stains-all dye and which interaction is associated with Ca^{2+}. Based on the Ca^{2+}-bound LipL32 crystal structure and the Stains-all circular dichroism results, a LipL32-F30 complex model was proposed. The fibronectin-binding site of LipL32 is near to the polyD region, and LipL32 interacts with F30 through significant electrostatic interactions. The Ca^{2+} binding to LipL32 might be important for extracellular matrix interaction with the host cell in *Leptospira*.

P-194 Purification, crystallization and preliminary data analysis of Proteorhodopsin

Ning Wang, Tingting Ran, Weiwu Wang
Nanjing Agricultural University, 1 Weigang Road, Xuanwu District, Nanjing, Jiangsu, 210095, China (wwwang@njau.edu.cn)

Proteorhodopsins (PRs), are seven TM light-driven proton pumps using retinal as chromophore, which genes were isolated from marine micro-plankton(1-3). Sequence analysis shows that PRs share less than 30% identity with all other microbial rhodopsins, such as bacteriorhodopsin (Br), sensory rhodopsin (SR), anabaena rhodopsin.

To understand the light driven proton pumping mechanism of PRs, PRs were overexpressed in *E. coli* and purified by IMAC, the protein purity was then analyzed by SDS PAGE. The purified protein was crystallized by vapor diffusion method with MPD as precipitant. The crystal grew to full size (0.02X0.02-0.04X0.2 mm) within a few days. The X-ray diffraction data were collected to 3.3 Å by using synchrotron radiation at SLS (Swiss Light Source). Preliminary x-ray diffraction data analysis has shown that the crystal belongs to orthorhombic space group P21212, with 5-6 PR molecules in the asymmetric unit; the unit cell parameters were a=161, b=169 and c=64 Angstrom. Using molecular replacement to solve the structure did not success due to the low sequence similarity with its homologs, the selenomethionine crystal deravitive and heavy atom deravitives are in preparation.

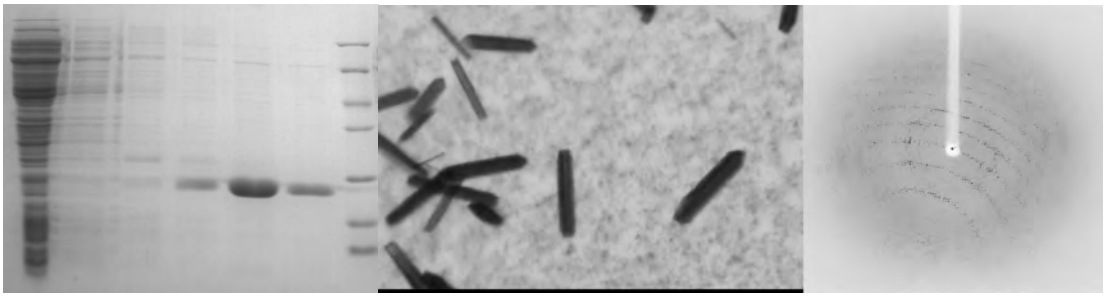

A. Purification of PR B. Crystallization of PR C. The diffraction pattern of PR crystal

Keywords: Proteorhodopsins (PRs), Crystallization, Protein purification

References

1. Béjà O, et. Al. Bacterial rhodopsin: evidence for a new type of phototrophy in the sea. Science. 289(5486):1902-6. (2000)
2. Béjà O, et. Al. Proteorhodopsin phtotrophy in the ocean. Nature. 411(6839):786-9. (2001)
3. Venter JC, et. Al. Environmental genome shotgun sequencing of the Sargasso Sea. Science. 304(5667):66-74. (2004)
4. Rusch DB, et. Al. The Sorcerer II Global Ocean Sampling expedition: northwest Atlantic through eastern tropical Pacific. PLoS Biol. 5(3):e77. (2007)

P-195 Structure, mechanistic action, and essential residues of laminaripentaose-producing β-1,3-glucanase

Wen-Ching Wang[1], Hsin-Mao Wu[1], Sheng-Wen Liu[2], Ming-Tsung Hsu[1], Jong-Yih Lin[3], and Yaw-Kuen Li[2],
[1] *Institute of Molecular and Cellular Biology & Department of Life Science, National Tsing Hua University, Hsinchu, Taiwan;*
[2] *Department of Applied Chemistry, National Chiao Tung University, Hsinchu, Taiwan;*
[3] *Department of Mechanical Engineering, National Chung Hsing University, Taichung, Taiwan*

Laminaripentaose-producing β-1,3-glucnase (LPHase), a member of glycoside hydrolase family 64, cleaves a long-chain polysaccharide β-1,3-glucan into specific pentasaccharide oligomers. We have solved the crystal structure of LPHase from *Streptomyces matensis* DIC-108 to 1.62 Å resolution using multiple-wavelength anomalous dispersion methods. The LPHase structure shows a barrel domain and a mixed (α/β) domain, forming a wide-open groove between the two domains. The liganded crystal structure was also solved to 1.80 Å, showing an overall identical conformation with the native enzyme. Within the wide groove, a laminaritetraose molecule is found to sit in an electronegatively charged central region and is proximal to several conserved residues including two carboxylates (Glu^{154} and Asp^{170}) and four other sugar-binding residues (Thr^{156}, Asn^{158}, Trp^{163}, and Thr^{167}). Molecular modeling using a laminarihexaose as a substrate suggests roles for Glu^{154} and Asp^{170} as acid and base catalysts, respectively, whereas the side chains of Thr^{156}, Asn^{158}, and Trp^{163} demarcate subsite +5. Site-directed mutagenesis of Glu^{154} and Asp^{170} confirms that both carboxylates are essential for catalysis. Together, our results suggest that LPHase uses a direct displacement mechanism involving Glu^{154} and Asp^{170} to cleave a β-1, 3-glucan into specific α-pentasaccharide oligomers.

P-196 A novel (4,8)-connected 3D metal-organic framework based on *in situ* ligand

Peng Li, Jiaying Lou, Yaming zhou, Linhong Weng*
Shanghai Key Laboratory of Molecular Catalysis and Innovative Materia1, China. Department of Chemistry, Fudan Unviersity, Shanghai 200433, China, (lhweng@fudan.edu.cn)

Design and construction of metal-organic frameworks (MOFs) whose topological paradigms consistent with those of natural minerals, have attracted considerable due to its potential application for these materials.[1, 2] However, there is an unfavorable lack of investigation of

binodal high-connected structures, such as (4,8)-connected framework. Previous examples of (4,8)-connected frameworks are reminiscent of binary inorganic compounds fluorite CaF_2 (flu),[3, 4] one of the most important and frequently encountered structure type in minerals, and $PoCl_2$ (scu)[5] which is built from square-planar and cubical nodes.

Here in this report, one 3D MOF $[Zn_3(bdc)_2(4\text{-bph})]_n \cdot 2n(H_2O)$ (**1**) (H_2bdc = 1,4-benzenedicarboxylic acid, 4-bph = N,N'-bis(4-picolinoyl) hydrazine) was isolated by hydrothermal method, the 4-bph was synthesized *in situ* via the hydrolysis of 2,5-bis(4-pyridyl)-1,3,4-oxadiazole) (4-bpo) with the aid of acid. Compound **1** is constructed from a distorted planar four-connected node and a distorted eight-connected node, and each four-connected node connects four eight-connected nodes, while each eight-connected node links four four-connected nodes and four eight-connected nodes. Consequently, the net of **1** defines a new type of (4, 8)-connected topological framework which is unobserved and different from the known flu and scu network topologies (Fig. 1).

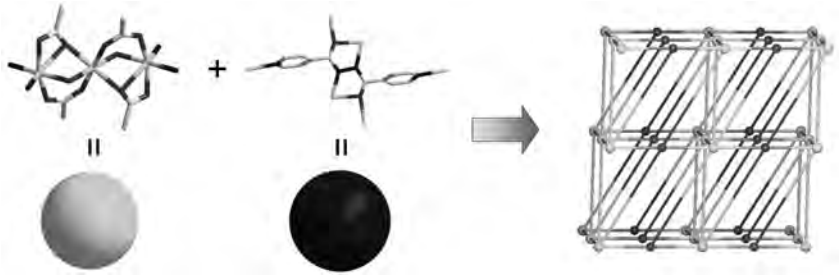

Fig. 1 A scheme of novel (4,8)-connected network structure constructed of a trimetalilc cluster (cyan pellet) and a planar four-connected 4-bph building block (blue pellet).

References

1. Rosi, N. L.; Kim, J.; Eddaoudi, M.; Chen, B. L.; O'Keeffe, M.; Yaghi, O. M. *J. Am. Chem. Soc.* **2005,** 127, (5), 1504-1518; Mueller, U.; Schubert, M.; Teich, F.; Puetter, H.; Schierle-Arndt, K.; Pastre, J. *J. Mater. Chem.* **2006,** 16, (7), 626-636.
2. Chun, H.; Kim, D.; Dybtsev, D. N.; Kim, K. *Angew. Chem.-Int. Edit.* **2004,** 43, (8), 971-974; Zou, R. Q.; Zhong, R. Q.; Du, M.; Kiyobayashi, T.; Xu, Q. *Chemical Communications* **2007**, (24), 2467-2469.
3. Ma, L. Q.; Mihalcik, D. J.; Lin, W. B. *J. Am. Chem. Soc.* **2009,** 131, (13), 4610-4612.

P-197 Solvent-Dependent Assembly of Ni(II) Coordination Polmers: Structural Variation from 1D to 2D

Jiaying Lou, Peng Li, Yaming Zhou, Linhong Weng*
Shanghai Key Laboratory of Molecular Catalysis and Innovative Materia1, China. Department of Chemistry, Fudan Unviersity, Shanghai 200433, China, (lhweng@fudan.edu.cn)

The assembly of coordination polymers by design is one aim of crystal engineering because their structures are intimately related to their outstanding bulk properties.[1,2]

Two coordination polymers $\{[Ni(3\text{-bpo})_2(p\text{-BDC})(H_2O)_2]\cdot(H_2O)_2\}_n$ (**1**) and $\{[Ni(3\text{-bpo})(p\text{-BDC})]\cdot(H_2O)_4\}_n$ (**2**) based on mixed ligands, where *3*-bpo = *2,5*-bis(*4*-pyridyl)-*1,3,4*-oxadiazole and *p*-BDC = *1,4*-benzenedicarboxylic acid, have been synthesized under solvothermal reactions by different solvent system. Compound **1,** synthesized from CH_3OH, forms a infinite 1-D chain structure (Fig. 1) and **2**, synthesized

from *2*-BuOH, shows a 2-D layered structure bridged by both ligands *3*-bpo and *p*-BDC with a square cavity of 9.82×10.68 $Å^2$ (Fig. 2). Their structures range from a 1D chain to a 2D network, showing the solvent effect on the structures of the complexes.

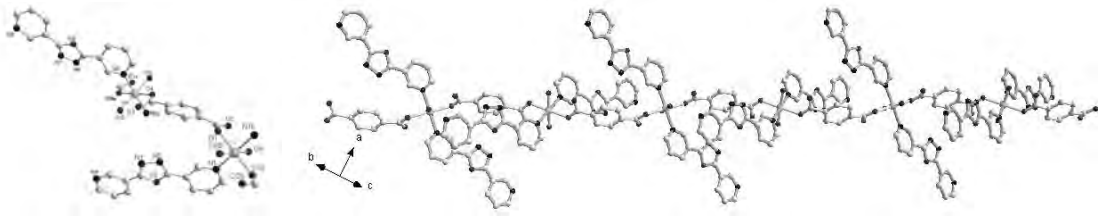

a) b)

Fig. 1 a) A portion view of **1** with atom labels of the asymmetric unit. Hydrogen atoms are omitted for clarity; b) The 1D chian for compound **1**. Ni, cyan; C, grey; O, red; N, blue.

a) b)

Fig. 2 a) A portion view of **2** with atom labels of the asymmetric unit. Hydrogen atoms are omitted for clarity; b) The 2D grid network (4, 4) net construction for compound **2**. Ni, cyan; C, grey; O, red; N, blue. The green rods stand for 3-bpo, the yellow rods stand for p-bdc.

References

[1] J. Lee, O. K. Farha, J. Roberts, K. A. Scheidt, S. T. Nguyen, J. T. Hupp, Chem. Soc. Rev. 38 (2009) 1450-1459.

[2] P. Horcajada, C. Serre, G. Maurin, N. A. Ramsahye, F. Balas, M. Vallet-Regi, M. Sebban, F. Taulelle, G. Ferey, J. Am. Chem. Soc. 130 (2008) 6774-6780.

Structural basis for the inhibition of human MTHFS by N10-substituted folate analogues

P-198

Dong Wu[1], Yang Li[1], Gaojie Song[1], Chongyun Cheng[1], Rongguang Zhang[2], Andrzej Joachimiak[2], Neil Shaw[1], and Zhi-Jie Liu[1]

[1]*National Laboratory of Biomacromolecules, Institute of Biophysics, Chinese Academy of Sciences, Beijing 100101, China.(wudong@moon.ibp.ac.cn)*

[2]*Structural Biology Center, Argonne National Laboratory, IL 60439 USA.*

5,10-Methenyltetrahydrofolate synthetase (MTHFS) regulates the flow of carbon through the one-carbon metabolic network, which supplies essential components for the growth and proliferation of cells. Inhibition of MTHFS in human MCF-7 breast cancer cells has been shown to arrest the growth of cells. Absence of the three-dimensional structure of human MTHFS (hMTHFS) has hampered the rational design and optimization of drug candidates.

Here, we report the structures of native hMTHFS, a binary complex of hMTHFS with ADP, hMTHFS bound with the N5-iminium phosphate reaction intermediate, and an enzyme-product complex of hMTHFS. The N5-iminium phosphate captured for the first time in our crystal structure unravels a unique strategy used by hMTHFS for recognition of the

substrate and provides structural basis for the regulation of enzyme activity. Binding of N10-substituted folate analogues places Y152 in the middle of the channel connecting ATP binding site with the substrate binding pocket, precluding the positioning of ;-phosphate for a nucleophilic attack. Using the structures of hMTHFS as a guide, we have probed the role of residues surrounding the active site in catalysis by mutagenesis. The ensemble of hMTHFS structures and the mutagenesis data yield a coherent picture of the MTHFS active site, determinants of substrate specificity, and new insights into the mechanism of inhibition of hMTHFS.

References

1. Appling, D. R. (1991) Compartmentation of folate-mediated one-carbon metabolism in eukaryotes. *FASEB J.* 5, 2645-2651
2. Fox, J. T., Stover, P.J. (2008) Folate-mediated one-carbon metabolism. *Vitam Horm.* 79, 1-44
3. Field, M. S., Szebenyi, D.M., Perry, C.A., Stover, P.J. (2007) Inhibition of 5,10-methenyltetrahydrofolate synthetase. *Arch Biochem Biophys.* 458, 194-201
4. Jolivet, J. (1997) Human 5,10-methenyltetrahydrofolate synthetase. *Methods Enzymol.* 281, 162-170
5. Jolivet , J., Dayan, A., Beauchemin, M., Chahla, D., Mamo, A., Bertrand, R. (1996) Biochemical and Molecular Studies of Human Methenyltetrahydrofolate Synthetase *Oncologist.* 1, 248–253
6. Field, M. S., Szebenyi, D.M., Stover, P.J. (2006) Regulation of de novo purine biosynthesis by methenyltetrahydrofolate synthetase in neuroblastoma. *J Biol Chem.* 281, 4215-4221

P-199

High-resolution crystal structure and functional analysis of a truncated thylakoid lumen protein AtTLP18.3 reveal its novel phosphatase activity

Hsin-Yi Wu[1], Mao-Sen Liu, Tsan-Piao Lin[1], and Yi-Sheng Cheng[1,2]

[1]*Institute of Plant Biology, National Taiwan University, No. 1, Sec. 4, Roosevelt Road, Taipei, 10617 Taiwan, (chengys@ntu.edu.tw)*

[2]*Department of Life Science, National Taiwan University, Taipei, Taiwan*

AtTLP18.3 is an 18.3 kDa thylakoid lumen protein with 285 amino acids. The protein can be divided to three regions based on sequence analysis: a chloroplast transit peptide, a domain of unknown function (DUF477) and a transmenebrane α-helix(TMH). Previous studies indicated that the AtTLP18.3 protein is an auxiliary protein of photosystem II (PSII) repair cycle.(Sari et al., 2007) In order to clarify the possible molecular function of the AtTLP18.3 protein, the crystal structures of the truncated AtTLP18.3 without targeting signal and TMH were resolved. Since there is no any methionine residue in the truncated AtTLP18.3 protein, L127M and L157M were introduced for MAD method by site-directed mutagenesis. The crystals of native and double mutated AtTLP18.3 shows isomorphous in space group $P2_12_12_1$ with unit-cell parameters a = 46.9, b = 49.8, c =76.7 Å, α=β=γ=90°. Finally, the structure of mutant was resolved at a resolution 2.6 Å using single-wavelength anomalous dispersion (SAD) method, and the native structure was resolved at 1.6 Å resolution. For further structural comparison, the native structure of truncates AtTLP18.3 was submitted to the DALI and CATH database to search similar folding of protein with known function. The results showed that the structure of AtTLP18.3 resembled to various inorganic pyrophosphatase. The enzymatic activity of AtTLP18.3 was further identified by alkaline/acid phosphatase assay. Therefore, we proposed that the function of AtTLP18.3 will act as phosphatase to remove the phosphate group from

damage protein for repair cycle.

References

1. Mulo, P., Sirpio, S., Suorsa, M., and Aro, E.M. (2008). Auxiliary proteins involved in the assembly and sustenance of photosystem II. Photosynth Res 98, 489-501.
2. Sari, S., Allahverdiyeva, Y., Suorsa, M., Paakkarinen, V., Vainonen, J., Battchikova, N., and Aro, E.-M. (2007). TLP18.3, a novel thylakoid lumen protein regulating photosystem II repair cycle. Biochem J 406, 415-425.

P-200 Crystallization processes of inorganic functional materials: both experimental and theoretical studies

Dongfeng Xue* and Congting Sun
Department of Materials Science and Chemical Engineering, School of Chemical Engineering, Dalian University of Technology, Dalian 116012, China
(dfxue@chem.dlut.edu.cn)

Crystallization represents a kind of phase transition, which can be regarded as a process related to bond formation and breaking [1]. Some basic relations were quantitatively derived on the basis of energy viewpoint, starting from both thermodynamics and kinetics. According to the chemical bonding characteristics of constituent atoms, relative growth rate of all crystallographic planes can be quantitatively determined by the particular distribution of valence electrons, which is called as the chemical bonding theory of single crystal growth [2-4]. The ideal morphology of some important functional crystals such as ferroelectric and piezoelectric ZnO, Cu_2O, KH_2PO_4, and $LiNbO_3$, has been successfully predicted by using the chemical bonding theory, which consists well with our experimental results. Some observations concerning the morphology evolution can also be kinetically simulated by the present theory [5,6]. The obtained results indicate that the microscopic constituent chemical bonds can help us to comprehensively understand the crystallization mechanism on the basis of quantitative calculations of growth rate in different crystal faces. The chemical bonding theory builds up a link between the crystallographic structure, growth morphology and microscopic chemical bonds of crystal materials, which provides us a useful microscopic tool to quantitatively understand single crystal growth behaviors.

References

[1] **http://www.serialspublications.com/journals1.asp?jid=445&jtype=1**
[2] C. Sun, D. Xue, *Chemical Bonding Theory of Single Crystal Growth: a Crystallographic Viewpoint*, Astrophysics and Condensed Matter (Horizons in World Physics, Volume 262)**,** Nova Science Publishers, Ed. Thomas G. Hardwell, 2008, Chapter 8, pp. 215-234.
[3] X. Yan, D. Xu, D. Xue, Acta Materialia 55(17) (2007) 5747-5757.
[4] D. Xu, D. Xue, J. Crystal Growth 310 (2008) 1385–1390.
[5] J. Liu, D. Xue, Adv. Mater. 20 (2008) 2262-2267.
[6] J. Liu, H. Xia, D Xue, L. Lu, J. Am. Chem. Soc. 131 (2009) 12086-12087.

P-201 Chemical Bonding Characteristics and Structural Formability of Perovskite Compounds

Na Li, Dongfeng Xue*
Department of Materials Science and Chemical Engineering, School of Chemical Engineering, Dalian University of Technology, 158 Zhongshan Road, Dalian 116012, China (dfxue@chem.dlut.edu.cn)

The crystallographic structure of perovskite compounds has long been a hot topic that attracts much attention in the materials science community, particularly, quantitative studies of perovskite structures may lead to the findings of novel functional materials, and can further enhance various performances especially relevant to ferroelectricity, superconductivity, catalysis, colossal magnetoresistance and so on. Even numerous theoretical models have been proposed, the accurate prediction of perovskite structures still remains many challenges in both fundamental and applied aspects. With the aid of advanced computer techniques, we may develop some useful theoretical models or methods to effectively analyze and tentatively predict perovskite structures, which may combine the geometric configurations with the chemical bonding characteristics of constituent elements. In this chapter, we review recent theoretical studies of perovskite materials and structures, and their applications to predict new compounds. In particular, we introduce some new advances on the chemical bonding method and artificial neural networks modeling method in predicting the structural stability and formability of ABO_3-type perovskites, and identify some opportunities for continued research and specific areas where significant advancement are highly demanded.

P-202 Structural basis of nucleotide exchange and clients binding by a novel hsp70-cochaperone bag2

Zhen Xu, Richard C Page, Saurav Misra
The Cleveland Clinic Foundation,9500 Euclid Ave, Cleveland, Ohio 44195 USA (misras@ccf.org)

Molecular chaperones such as Hsp70 are required to assist most proteins to fold into precise three-dimensional conformations and to fulfill their biological functions. The relatively recently identified chaperone-associated ubiquitin ligase CHIP (C-terminus of Hsp70 interacting protein) can alter chaperone activity from protein folding to protein degradation. In contrast, the co-chaperone Bag2, which has previously been classified as a member of the Bag domain family of Hsp70 nucleotide exchange factor (NEF), carries out nucleotide exchange, substrate binding, and inhibition of CHIP-mediated protein degradation. Here we report the structural basis of Bag2 function. The free and Hsp70-bound crystal structures of the so-called BNB domain of Bag2 show that Bag2 is structurally distinct from other known Bag family of Hsp70 NEFs. NMR-based mapping demonstrates that the Bag2 substrate binding sites overlap with the Hsp70 interaction sites, suggesting that Hsp70 may directly displaces substrates from Bag2 onto its own substrate binding domain. Preliminary data suggests that a novel interaction between Bag2 and ubiquitin plays a role in Bag2-mediated inhibition of CHIP. Our structural data begin to elucidate how Hsp70, CHIP and Bag2 coordinate with each other to regulate the fate of unfolded proteins.

P-203

Structure of st0929, a putative glycosyl transferase from *Sulfolobus tokodaii*

Charles B.C. Cielo[a], Seiji Okazaki[a], Tatsuo Hikage[b], Atsuo Suzuki[a], Tsunehiro Mizushima[a], Ryoji Masui[c], Seiki Kuramitsu[c], Takashi Yamane *[a]

[a]*Department of Biotechnology, Graduate School of Engineering, Nagoya University, Nagoya 464-8603, Japan (yamane@nubio.nagoya-u.ac.jp)*

[b]*High Intensity X-ray Laboratory, Nagoya University, Nagoya 464-8603, Japan*

[c]*Department of Biological Sciences, Graduate School of Science, Osaka University, Osaka 560-0043, Japan*

Trehalose (α-D-glucopyranosyl α-D-glucopyranoside), is a naturally occurring, non-reducing disaccharide used industrially as a food additive, artificial sweetener, and chemical stabilizer for cosmetics and pharmaceuticals. A novel two-enzyme system was reported for the efficient production of trehalose from starch.[1)] This enzyme system involves the sequential action of maltooligosyl trehalose synthase (MTSase, EC: 5.4.99.15) and maltooligosyl trehalose hydrolase (MTHase, EC 3.2.1.141). MTSase catalyzes the conversion of the maltose α-1,4-glucosidic bond into the trehalose α-1,1-glucosidic bond.

The 704-residue hypothetical glycosyl transferase, st0929, was recently isolated from *Sulfolobus tokodaii*. In order to elucidate its function, the structure of st0929 was determined at 1.9 Å resolution utilizing the molecular replacement method. *Sulfolobus acidocaldarius* maltooligosyl trehalose synthase[2)] (SaMTSase), which has 52% sequence identity with st0929, was used as a search template. The overall structure of st0929 is essentially identical to that of SaMTSase. Likewise, the st0929 putative active site contains highly conserved residues that comprise the MTSase active site, including the catalytic triad and various subsites. It was of particular interest to note that the subsite +1 architecture of the putative active site is essentially identical to the unique subsite +1 architecture found in SaMTSase. The st0929 putative subsite +1 is formed by a cluster of tyrosine residues reported to be required for efficient glycosyl transferase activity. It also has sufficient dimensions to enclose the reducing end of a putative oligosaccharide substrate. We therefore propose that st0929 also plays a role in the synthesis of trehalose on the basis of the close sequence and structural resemblance between st0929 and SaMTSase.

References

1. Kubota, M., Sawatani, I., Oku, K., Takeuchi, K. and Murai, S. (2004). *J.Appl. Glyosci.* **51**, 63-70.
2. Kobayashi M., Kubota, M. and Matsuura, Y. (2003). *J. Appl. Glycosci.* **50**, 1-8.

P-204 Dimerization is important for the GTPase activity of chloroplast translocon components atToc33 and psToc159

Yi-Hung Yeh[1], Muppuru M. Kesavulu[1], Hsou-min Li[1], Shu-Zon Wu[1], Yuh-Ju Sun[2], Emadeldin H.E Konozy[1] and Chwan-Deng Hsiao[1]
[1] *Institute of Molecule biology, Academia Sinica, Taipei, Taiwan 115,*
[2] *Institute of Bioinformatics and Structural Biology, National Tsing Hua University, Hsinchu, Taiwan 300,*

Arabidopsis Toc33 (atToc33) is a GTPase and a member of the Toc (translocon at the outer-envelope membrane of chloroplasts) complex that associates with precursor proteins during protein import into chloroplasts. By inference from the crystal structure of psToc34, a homologue in pea, the arginine at residue 130 (Arg130) has been implicated in formation of the atToc33 dimer and inter-molecular GTPase activation within the dimer. Here we report the crystal structure at 3.2 Å resolution of an atToc33 mutant, atToc33(R130A), in which Arg130 was mutated to alanine. Both in solution and in crystals, atToc33(R130A) was present in its monomeric form. In contrast, both wild-type atToc33 and another pea Toc GTPase homologue, pea Toc159 (psToc159), were able to form dimers in solution. Dimeric atToc33 and psToc159 had significantly higher GTPase activity than monomeric atToc33, psToc159 and atToc33(R130A). Molecular modeling using the structures of psToc34 and atToc33(R130A) suggests that, in an architectural dimer of atToc33, Arg130 from one monomer interacts with the β-phosphate of GDP and several other amino acids of the other monomer. These results indicate that Arg130 is critical for dimer formation, which is itself important for GTPase activity. Activation of GTPase activity by dimer formation is likely to be a critical regulatory step in protein import into chloroplasts.

P-205 Synthesis, Structure and Properties of $Ba_8Au_5Ge_{40}$

Hui Zhang[*1,2], Walter Schelle[1], Michael Baitinger[1], Mei-Bo Tang[2], Zhen-Yong Man[2], Hao-Hong Chen[2], Xin-Xin Yang[2], Jing-Tai Zhao[2], Yuri Grin[1]
[1] *Max-Planck-Institute for Chemical Physics of Solids, Nöthnitzer str. 40, 01187 Dresden, Germany, (huizhang@cpfs.mpg.de)*
[2] *Key Laboratory of Transparent Opto-Functional Inorganic Materials, Chinese Academy of Sciences (Shanghai Institute of Ceramics), 1295 Dingxi Road Shanghai, 200050, China.*

$Ba_8Au_5Ge_{40}$ is prepared by reaction of BaGe, Au and Ge by induction furnace in an Ar filled glove box and plate cooling. Its composition, crystal structure and physical properties are investigated. Rietveld refinement revealed $Ba_8Au_5Ge_{40}$ crystallized in Clathrate I-type structure (Fig.left) with unit cell parameter a = 10.8004(1) Å. The profile reliable (R) factors are R = 2.76, R_w = 4.72, R_{ex} = 2.34, chi^2 = 4.07, respectively. The refined XRD pattern of $Ba_8Au_5Ge_{40}$ is given in Fig. right. The low temperature heat capacity, magnetic properties and thermoelectric properties will be discussed.

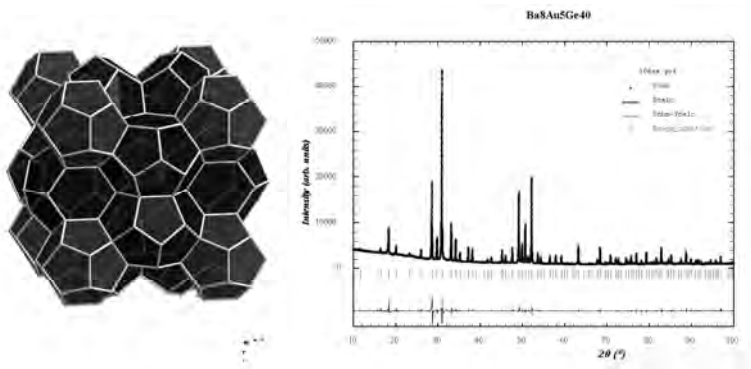

The crystal structure (left) and refined XRD pattern (right) of $Ba_8Au_5Ge_{40}$

P-206

Purification, crystallization and preliminary X-ray diffraction analysis of human THRSP

Wenzheng Zhang[1],Wei Peng[2],Weihong Zhou[1], Mark Bartlam[1], Zonghao Zeng[2] and Zihe Rao[1,2,3]

[1]*College of Life Sciences and Tianjin State Laboratory of Protein Sciences, Nankai University, Tianjin 300071, China (zhangwzh@nankai.edu.cn)*

[2]*National Laboratory of Biomacromolecules, Institute of Biophysics (IBP), Chinese Academy of Sciences, Beijing 100101, China*

[3]*Laboratory of Structural Biology, Tsinghua University, Beijing 100084, China (raozh@@nankai.edu.cn)*

THRSP（Spot 14，S14) is a small (about 17 kDa) acidic (pI 4.68) nuclear protein with no sequence similarity to other functional motifs. It initially came to attention in 1982 through its marked and rapid induction by thyroid hormone. The S14 gene encodes a protein that is predominantly expressed in lipogenic tissues, such as the liver, white and brown adipose tissues and the lactating mammary glands, where its expression is rapidly regulated by hormones and dietary constituents. It recently showed that S14 acts at the transcriptional level in the transduction of signals for increased expression of genes encoding lipogenic enzymes.These result suggest that the THRSP is a transcriptional fator of the lipogenic enzymes and could function in the regulation of lipid synthesis.

In humans, the S14 locus resides in the chromosome region 11q13, which is frequently amplified in breast tumours, and as a result, it has been suggested that this protein could play a role in the metabolism and growth of these kinds of tumours. The S14 gene is amplified in some breast cancers and is strongly expressed in most. Thus, S14 is a marker for aggressive breast cancer and a potential target as well. Future effort will center on validation of S14 as a therapeutic target and producing antagonists of its action.

Now, we have finished the purification, crystallization and preliminary X-ray diffraction analysis of human THRSP. This result has established a good foundation for the study of structure and function of human THRSP.

Structure of main protease from a global infectious human coronavirus, HCoV-HKU1

P-207

Qi Zhao1, Shuang Li1, Fei Xue1, Yilong Zou1, Cheng Chen1, Mark Bartlam1,2 & Zihe Rao1,2,3

1 Tsinghua-Nankai-IBP Joint Research Group for Structural Biology, Tsinghua University, Beijing 100084, China.

2 College of Life Sciences, Nankai University, Tianjin 300071, China.

3 National Laboratory of Biomacromolecules, Institute of Biophysics (IBP), Chinese Academy of Sciences, Beijing 100101, China.

Human coronavirus HKU1 (HCoV-HKU1) is a new coronavirus that was first identified in Hong Kong in 2005. Infection by HCoV-HKU1 occurs worldwide and causes syndromes such as common cold, bronchitis and pneumonia. The coronavirus main protease (Mpro), which is a key enzyme in viral replication via a cascade of proteolytic processing of replicase polyproteins, has been recognized as an attractive target for rational drug design. In this study, we report the structure of HCoV-HKU1 Mpro in complex with a Michael acceptor based inhibitor N3. The structure of HCoV-HKU1 serves as a high quality model for group 2A coronaviruses, which differ from group 2B coronaviruses such as SARS-CoV. The structure together with activity assays supports the relative conservation at the P1 position discovered in genome sequencing. Combined with structural data from other Mpros, this Structure provides insights into both substrate preference and antiviral-design against coronaviruses.

Reference

Zhao, Q., S. Li, F. Xue, Y. Zou, C. Chen, M. Bartlam, and Z. Rao. 2008. Structure of the main protease from a global infectious human coronavirus, HCoV-HKU1. J Virol.

Expression，Purification, Crystallization and Preliminary X-ray Analysis of Cytochrome P450 153C1 from *Novosphingobium aromaticivorans* DSM12444

P-208

Weihong Zhou[1], Wen Yang[1], Stephen G. Bell[4], Mark Bartlam[1], Luet-Lok Wong[4] and Zihe Rao[1,2,3]

[1]College of Life Sciences and Tianjin State Laboratory of Protein Sciences, Nankai University, Tianjin 300071, China (zhouwh@nankai.edu.cn)

[2]National Laboratory of Biomacromolecules, Institute of Biophysics (IBP), Chinese Academy of Sciences, Beijing 100101, China

[3]Laboratory of Structural Biology, Tsinghua University, Beijing 100084, China

[4] Department of Chemistry, University of Oxford, Inorganic Chemistry Laboratory, South Parks Road, Oxford OX1 3QR, UK

Cytochrome P450 enzymes constitute a large family of hemoproteins that catalyze the monooxygenation of a great variety of endogenous and exogenous organic compounds. They have been found throughout the biosphere from bacteria to higher plants and animals and participate in the biosynthesis of physiologically important compounds such as steroids and hormones, in fatty acid oxidation as well as detoxification of exogenous compounds from the environment. They play an important role in medicine, agriculture, detection and protection of environment, chemosynthesis and so on.

Novosphingobium aromaticivorans DSM12444 (*Novosphingobium aromaticivorans* F199) is a gram-negative bacte-rium which is known to degrade a range of hydrocarbons. The bacterium contains a high proportion of genes encoding proteins involved in the catabolism and transport of aromatic compounds including many oxygenase enzymes.

CYP153C1 from *Novosphingobium aromaticivorans* DSM12444 was observed to bind several substrates, especially linear alkanes, such as heptane, octane and nonane which are highly pollution to the environment. CYP 153C1 has potential biotechnological applications such as the degradation of linear alkanes compounds. The three-dimensional structure will provide valuable information on substrate binding and electron transfer，and structure basis for its application in protein engineering.

The recombinant CYP153C1 was highly expressed in Escherichia coli and purified; well-diffracting crystals were obtained by the hanging-drop vapor diffusion method. Crystals suitable for X-ray crystallography have been obtained and diffraction data were collected in-house to 2.7 Å resolution from a single crystal. The crystals belong to the space group *P321* with unit-cell parameters a =86.2 Å, b =86.2 Å, c =123.9 Å. The structure determination and substrates soaking are on the way.

References

1. Nelson, D. R. Mining database for cytochrome P450 genes. Methods Enzymol. 2002, 357, 3-15
2. Mansuy, D.; Renaud J. –p., Heme-thiolate proteins different from cytochrome P450 catalyzing monoxygenations. in Cytochrome P450 Structure, Mechanmism and Biochemistry Ortiz de Montellano, P. R. ed Plenum Press: New York and London, 1995; pp. 537-574
3. Stephen G. Bell, Luet-Lok Wong, P450 enzymes from the bacterium Novosphingobium aromaticivorans BBRC， 2007，360，666-672

Author Index

A

B

C

D

E

F

G

H

I

J

K

L

M

N

O

P

R

S

T

U

V

W

X

Y

Z